ICCT

INTERNATIONAL CONFERENCE
ON CHEMICAL TECHNOLOGY

8th International Conference on Chemical Technology

May 3 – 5, 2021

ČSPCH ČESKÁ SPOLEČNOST PRŮMYSLOVÉ CHEMIE

SCHP ČR

ÚSTAV CHEMICKÝCH PROCESŮ AV ČR
INSTITUTE OF CHEMICAL PROCESS FUNDAMENTALS OF THE ASCR

Univerzita Pardubice
Fakulta chemicko-technologická

STU FCHPT

ORLEN UniCRE

VYSOKÁ ŠKOLA CHEMICKO-TECHNOLOGICKÁ V PRAZE

proceedings

MAIN PARTNER

ORLEN Unipetrol

PARTNER

teva

SPONSORS

dekonta

DEZA®

Metrohm

SHIMADZU
Excellence in Science

euro support

MEDIA PARTNERS

Chemické listy

CHEMAGAZÍN

Proceedings of the 8th International Conference on Chemical Technology

1st edition, September 2021

EDITORS

Martin Veselý
University of Chemistry and Technology, Prague
Technická 5
166 28 Prague 6, Czech Republic

Zdeněk Hrdlička
University of Chemistry and Technology, Prague
Technická 5
166 28 Prague 6, Czech Republic

Jiří Hanika
Institute of Chemical Process Fundamentals of the CAS, Prague
Rozvojová 1/135
165 02 Prague 6, Czech Republic

Jaromír Lubojacký
Jistebník 242
742 82 Jistebník, Czech Republic

All communications submitted were duly reviewed by the scientific committee.

PUBLISHED AND DISTRIBUTED BY

Czech Society of Industrial Chemistry
Novotného Lávka 5
116 68 Prague, Czech Republic

in cooperation with
Czech Chemical Society
Novotného Lávka 5
116 68 Prague, Czech Republic

ISBN 978-80-88307-08-2

SCIENTIFIC COMMITTEE

Assoc. Prof. Ing. Jaromír Lederer, Ph.D. | UniCRE Litvínov (President)
Prof. Ing. Jiří Hanika, Ph.D. | ICPF of the CAS, Prague (Vice-President)
Prof. Dr. Ing. Karel Bouzek | UCT Prague
Prof. Dr. Fabio Fava | Department of Civil, Chemical, Environmental and Materials Engineering, University of Bologna
Assoc. Prof. Ing. Tomáš Hlinčík, Ph.D. | UCT Prague
Prof. Ing. Milan Hronec, Ph.D. | STU Bratislava
Prof. Ing. Ľudovit Jelemenský, Ph.D. | STU Bratislava
Prof. Ing. Tomáš Jirout, Ph.D. | CTU in Prague
Prof. Ing. Jan John, Ph.D., FJFI, CTU in Prague
Prof. Ing. Petr Kalenda, Ph.D. | FCHT University of Pardubice
Prof. Elena Korotkova | Tomsk Polytechnic University
Assoc. Prof. Ing. Milan Králik, Ph.D. | VUChT Bratislava
Prof. Flavia Marinelli | University of Insubria, Varese, Italy
Dr. Agustín Martínez | Universidad Politécnica de Valencia
Prof. Ing. Petr Mikulášek, Ph.D. | FCHT University of Pardubice
Ing. Jozef Mikulec, Ph.D. | VÚRUP Bratislava
Prof. Dimitry Murzin | Åbo Akademi University, Turku, Finland
Prof. Ing. Lucie Obalová, Ph.D. | VŠB TU Ostrava
Prof. Ing. Josef Pašek, Ph.D. | UCT Prague
Prof. Dr. Ing. Petra Patáková | UCT Prague
Ing. Ivan Souček, PhD. | Association of Chemical Industry of the Czech Republic
Prof. Ing. Ján Šajbidor, Ph.D. | FCHPT STU Bratislava
Prof. RNDr. Pavel Šajgalík, DrSc. | Slovak Academy of Sciences, Bratislava
Prof. RNDr. Jitka Ulrichová, Ph.D. | UP Olomouc
Prof. Ing. Kamil Wichterle, Ph.D. | VŠB TU Ostrava
Prof. Ing. Petr Zámostný, Ph.D. | UCT Prague

PROGRAM COMMITTEE

Ing. Jaromír Lubojacký, MBA | Ixa Consulting Jistebník (President)
Assoc. Prof. Ing. Jaromír Lederer, Ph.D. | UniCRE Litvínov (Vice-President)
Prof. Ing. Jiří Hanika, Ph.D. | ICPF of the CAS, Prague (Vice-President, Best Poster Award)
Prof. Ing. Petr Zámostný, Ph.D. | UCT Prague (Petrochemicals and Organic Technology)
Assoc. Prof. Ing. Karel Ciahotný, Ph.D. | UCT Prague (Gas, Coal, Fuel)
Prof. Dr. Ing. Karel Bouzek | UCT Prague (Inorganic Technology)
Prof. Dr. Ing. Petra Patáková | UCT Prague (Biotechnology)
Ing. Barbora Branská, Ph.D. | UCT Prague (Biotechnology)
Prof. RNDr. Bohumil Kratochvíl, DSc. | UCT Prague (Pharmaceutical Technology)
Ing. Miloslav Slezák, Ph.D. | FCHT University of Pardubice (Waste Processing, Air and Water Protection, Technologies for the Decontamination of Soils)
Prof. Ing. Lucie Obalová, Ph.D. | VŠB TU Ostrava (Waste Processing, Air and Water Protection, Technologies for the Decontamination of Soils)
Prof. Ing. František Babinec, Ph.D. | RISCO Brno (Secure Management Processes, Accidents Prevention, etc.)
Prof. Dr. Ing. Dalibor Vojtěch | UCT Prague (Material Engineering)
Ing. Ivan Souček, PhD. | Association of Chemical Industry of the Czech Republic (Economy of Chemical Industry)
Prof. Ing. Tomáš Jirout, Ph.D. | CTU in Prague (Chemical Processes and Devices)
Ing. Hugo Kittel, Ph.D., MBA I UCT Prague (Oil, Petrochemicals, Biofuels)
Assoc. Prof. Ing. Antonín Kuta, Ph.D. | UCT Prague (Polymers, Composites)

CONTENTS

OIL, PETROCHEMICALS, BIOFUELS

UTILIZATION OF SYNERGIES BETWEEN TRADITIONAL OIL REFINERIES AND BIOREFINERIES AS AN IMPORTANT FACTOR IN THEIR FURTHER DEVELOPMENT
Kittel H.

CO-PYROLYSIS OF FISCHER-TROPSCH WAX VACUUM RESIDUE WITH HYDROCRACKING PRODUCT
Karaba A., Rozhon J., Filip L., Zámostný P.

PARTIAL HYDROGENATION OF DOUBLE BONDS IN POLYUNSATURATED FATTY ACID METHYL ESTERS
Slezáčková M., Mikulec J., Blaško J.

MODELING OXYGEN PRODUCTION VIA CRYOGENIC AIR SEPARATION
Poláková N., Variny M.

ALTERNATIVE USAGE OF MSCR TEST FOR EVALUATION OF TYPE AND CONTENT OF THE USED POLYMER
Jíša P., Černý R.

COMPATIBILITY OF MARINE FUELS CONTAINING ALTERNATIVE MATERIALS
Schlehöfer D., Vráblík A.

CO-PROCESSING OF PYROLYSIS PRODUCTS
Dlasková Jaklová K., Zbuzková B., Vráblík A.

HYDROGEN PRODUCTION OPTIMIZATION IN REFINING INDUSTRY
Cibulka T., Variny M.

GAS, COAL, FUEL

INDUSTRIAL COMBINED HEAT AND POWER PLANT REPOWERING PROPOSAL
Kšiňanová M., Variny M.

MATERIAL ENGINEERING

PHONOLITE. AN AVAILABLE, NATURAL CZECH RESOURCE FOR PRODUCING NOVEL VALUABLE MATERIALS
Hidalgo-Herrador J.M., Tišler, Z., Frątczak J., de Paz Carmona H., Velvarská R., Kocík J.

DECARBONISATION OF THE CHEMICAL INDUSTRY IN LIGHT OF GREEN DEAL
Souček I.

CHITIN-CAFFEINE MODELS IN BIOCIDAL WOOD COATINGS
Kobetičová K., **Böhm** M., Ďurišová K., Nábělková J., Černý R.

BINDING INTERACTIONS OF METHYLXANTHINES TO BEECH WOOD
Kobetičová K., **Böhm M.**, **Černý R.**

COMBINED EFFECTS OF ADSORPTION AND PHOTOCATALYSIS ON MODEL DYE AO7 REMOVAL FROM AQUEOUS MEDIA USING TIO$_2$-LDH NANOCOMPOSITES
Starukh H., Petryk I., Matějová L., Martaus A.

SUBSTITUTION OF HAZARDOUS SUBSTANCES IN PYROTECHNIC COMPOSITIONS
Olšovský M., Krištof M., Kuna P.

ORGANIC TECHNOLOGY

THE EFFECT OF WATER AND SUBSTITUENTS OF AROMATIC RING ON ITS HYDROGENATION OVER A COBALT CATALYST
Valeš R., Dvořák B., Krupka J.

HYDROGENATION OF BUTYL SORBATE USING METAL COMPLEXES WITH Ru, Rh AND Ir AS CENTRAL ATOMS
Kotova M., Hrdličková R., Vyskočilová E., Červený L.

SELECTIVE MEERWEIN-PONNDORF-VERLEY REDUCTION OF CINNAMALDEHYDE OVER Al-CONTAINING CATALYSTS
Paterová I., Vyskočilová E., Gorlova O. and Červený L.

THE EFFECT OF TEMPERATURE AND CONCENTRATION OF WATER ON OXIDATION OF DICYCLOHEXYLAMINE WITH AIR
Valeš R., Kukučková A., Dvořák B., Krupka J.

POLYMERS, COMPOSITES

DEACIDIFICATION AND PRESERVATION OF CELLULOSIC OBJECTS OF CULTURAL HERITAGE
Králik M., Horváth B., Vizárová K., Vajová I., Gašparovičová D., Danielik V., Jurišová J.

AMINE-FUNCTIONALIZED POROUS POLYMERS FOR SELECTIVE CO_2 ADSORPTION
Setnickova K. , Jerabek K., Strasak T., Soukup K.

ECONOMICS OF CHEMICAL INDUSTRY

THE CURRENT TRENDS IN THE CHEMICAL INDUSTRY OF THE CZECH REPUBLIC – COVID 19 IMPACT
Souček I.

TECHNO-ECONOMIC OPTIMIZATION OF STEAM CRACKER'S STEAM NETWORK
Hanus K., Variny M.

DIGITAL WELLBEING FOR HIGHLY SKILLED STAFF
Dvorakova Z.

PERSONAL AND TRANSVERSAL COMPETENCIES IN BIO-BASED ECONOMY
Botek M., Diaz M.

CONSUMER ATTITUDES TOWARDS HOUSEHOLD WASTE SORTING
Frohlich A., Branska L., Patak M., Pecinova Z.

SYSTEM MODEL OF MAITENANCE DYNAMICS
Vytlačil D.

LIMITS AND BARRIERS TO PRODUCT LIFE CYCLE MONITORING FOR CHEMICALS – A CASE STUDY
Vavra J., Hemelikova M.

GREEN HUMAN RESOURCE MANAGEMENT IN COMPANIES OF CZECH CHEMICAL INDUSTRY
Bednarikova M., Kostalova J.

SUSTAINABLE PACKAGING INNOVATIONS FOR COSMETIC PRODUCTS
Škraňková P., Paták M., Branská, L., Pecinová, Z.

IDENTIFICATION OF FACTORS INFLUENCING OIL AND GAS PRICES AND THEIR MUTUAL CORRELATIONS
Košťálek J., Koťátková Stránská P.

SYNTHESIS AND PRODUCTION OF DRUGS

RHEOLOGICAL PROPERTIES OF POWDER MIXTURES AS A FACTOR OF HARD-GELATIN CAPSULE FILLING PERFORMANCE
Komínová P., Havelková P., Zámostný P.

TABLET MICROSTRUCTURE EVOLUTION DURING THE COMPACTION PROCESS
Römerová S., Dammer O., Zámostný P.

APPLICATION OF HANSEN SOLUBILITY PARAMETERS IN THE PHARMACEUTICAL INDUSTRY
Petříková E., Hriňová E., Čerňová M., Dammer O., Krejčík L., Patera J.

CERAMIDE LIPOSOMES: FORMULATION OF STRATUM CORNEUM LIPIDS FOR SKIN BARRIER RECOVERY
Vovesná A., Zbytovská J.

MORPHOLINE DERIVATIVES: NOVEL SUBSTANCES FOR MODULATING THE PERMEABILITY OF THE SKIN BARRIER
Dvořáková K., Štěpánek P., Zbytovská J.

IMPROVING DISSOLUTION RATE OF POORLY SOLUBLE DRUGS BY MILLING AND CO-MILLING TECHNIQUE
Slámová M., Beránek J., Patera J., Zámostný P.

DISSOLUTION KINETICS OF COMMERCIALLY AVAILABLE TABLETS USING AN OPTICAL MICROSCOPY TECHNIQUE
Bittner R., Zámostný P.

MONITORING THE ROLL COMPACTION PROCESS VIA RIBBON STIFFNESS MEASUREMENT
Petr J., Stasiak P., Zámostný P.

TECHNIQUE OF PHARMACEUTICAL POWDER COMPRESSIBILITY MEASUREMENT FOR UTILIZATION IN PREDICTIVE MATHEMATICAL MODELLING OF COMPACTION PROCESSES
Marinko N., Krpelan T., Zamostný P.

WASTE TREATMENT, WATER PROTECTION

POZOLAN ACTIVITY OF CALCINED CLAYS AND OTHER POZZOLANS USING THE FRATTINI TEST
Rak P., Šídlová M., Doležal T., Šulc R., Formáček P.

RESISTANCE OF MIXTURES PREPARED FROM DIFFERENT CZECH FLY ASHES TO FREEZING AND THAWING
Pulcová K., Šídlová M., Rak P., Šulc R., Formáček P.

AIR PROTECTION, TECHNOLOGIES FOR SOIL DECONTAMINATION

INNOVATIVE TECHNOLOGY PLASMICAT FOR HAZARDOUS AIR TREATMENT
Kroužek J., Mašín P., Rippelová V., Škarohlíd R.

PHOTOCATALYTIC DECOMPOSITION OF N_2O OVER S MODIFIED GRAPHITIC CARBON NITRIDE
Kočí K., Šihor M., Reli M. and Praus P.

BIOTECHNOLOGY AND BIOREFINERY

BIOSYNTHESIS OF METAL NANOPARTICLES USING VITIS VINIFERA EXTRACT AND THEIR ANTIMICROBIAL ACTIVITY
Miškovská A., Michailidu J., Čejková A.

GENUS *MONASCUS* AND ITS SECONDARY METABOLITES
Husakova M., Patakova P.

ANTIMICROBIAL AND ANTIVIRULENCE ACTIVITY OF PTEROSTILBENE, METHOXYLATED DERIVATIVE OF RESVERATROL
Kašparová P., Maťátková O.

CHITOSAN NANOPARTICLES AS A PROMISSING ANTIMICROBIAL AGENT
Maršík D., Masák J., Ulbrich P.

OPERON STRUCTURE INFERENCE IN *CLOSTRIDIUM BEIJERINCKII* NRRL B-589 USING RNA-SEQ
Schwarzerova J., Musilova J., Jureckova K., Branska B., Provaznik I., Patakova P., Sedlar K.

EFFECTS OF FURAN DERIVATIVES AND PHENOLIC COMPOUNDS ON ABE PRODUCTION BY *CLOSTRIDIUM BEIJERINCKII*
Heřmanová K., Branská B.

BIODIVERSITY OF PROKARYOTES FROM RADON SPRINGS IN JÁCHYMOV
Timkina E., Kolouchová I., Maťátková O.

ISOLATION OF FERULIC ACID FROM WHEAT BRAN USING VARIOUS ADSORBENTS
Nábělek J., Pořízka J., **Diviš, P.**

PRODUCTION AND ANALYSIS OF CRUDE BIOCHAR PRODUCED FROM WHEAT BRAN
Pořízka J., Švec J., Diviš P., Zouharová K., Sedláček P., Enev V., Hajzler J., Mravcová L., Trudičová M.

CIRCULAR BIODIESEL DOWNSTREAM SIDE-PRODUCTS UTILIZATION FOR UPSTREAM BIODIESEL VALORIZATION
Ondrejíčková P., Kafková V., Holíčková M., Cyprichová V., Gyuranová D., Krasňan V., Rebroš M.

CHEMICAL PROCESSES AND DEVICES

HOW DOES UNCERTAINTY OF THERMAL CONDUCTIVITY IMPACT MEASUREMENTS OF POOL BOILING HEAT TRANSFER COEFFICIENT?
Vajc V., Dostál M.

INORGANIC TECHNOLOGY

USE OF THE MSO TECHNOLOGY FOR THE TETRACHLORETHYLENE DISPOSAL
Galek V., Černá A., Pražák P., Hadrava J., Mastný L.

GEOPOLYMERS: THE INFLUENCE OF ALKALINE ACTIVATOR CATIONS ON EFFLORESCENCE
Novotná M., Polonská A., Šídlová M., Perná I.

SUSCHEM

THE ROADMAP OF SUSCHEM CZ IN CONTEXT OF THE NEW EU LEGISLATION

Mlčoch A., **Novák L.**, Šilhan M.

OIL,
PETROCHEMICALS,
BIOFUELS

UTILIZATION OF SYNERGIES BETWEEN TRADITIONAL OIL REFINERIES AND BIOREFINERIES AS AN IMPORTANT FACTOR IN THEIR FURTHER DEVELOPMENT

Kittel H.

University of Chemistry and Technology, Technická 1905, 166 28 Prague
hugo.kittel@vscht.cz

Abstract

The number of traditional oil refineries is declining in Europe, because petroleum products are considered a significant GHG source. The concept of biorefineries was developed in the last decades as an alternative to the traditional oil refineries. Although the terms “oil refinery” and “biorefinery” sound similar, they are not. There are big differences between them as well as significant synergies. Despite the fact that every traditional oil refinery has already been partially transformed into a biorefinery, processing bioethanol, FAME, eventually producing ETBE, HEFA, HVO, green propane, etc., and certain traditional oil refineries were transformed into biorefineries, this will not be enough to meet the goals of a circular economy. Therefore, the possible synergies between these two businesses are discussed in this paper. These synergies lie in the processing of similar biofeeds by different technologies, in the use technologies that have matured in the traditional oil refineries, in the high capacity of these technologies, existing infrastructure, logistic systems, and experienced staff. Synergies also consist of co-processing mineral and biocomponents to better quality products and to new products. The share in the production of petrochemical intermediates and chemicals from the traditional oil refineries will grow. Moreover, retrofitting the idling traditional oil refineries to biorefineries can reduce CAPEX for future investors.

Introduction

Traditional oil refineries (TORs) are industrial complexes processing crude oil to commodity products that are crucial to all types of road, rail, air, and maritime transport, for the chemical industry, and for the supply of electric power and energies. TORs are an excellent example of economy of scale – well established, well-positioned, logistically integrated, with a high processing capacity (typically >5 mil $t \cdot y^{-1}$ of crude oil). They operate very complex, sophisticated, optimized, and matured technologies with respect to yields, quality of final products, energy efficiency, and HSE protection (1). They operate based on BAT and BREF that are strict as never before (2). The majority of outputs have recently been reformulated into clean products, reducing content of sulfur and aromatics significantly and utilizing new blending components. However, the processed mineral feedstock – crude oil, containing about 85 % wt. of carbon – is the central problem of TORs from the perspective of a sustainable economy. The number of TORs is declining in Europe (3).

Biorefineries are a new type of refineries. This business can be defined as “the sustainable processing of biomass into a spectrum of biobased products (chemicals, materials, food, and animal feeds) and bioenergies (biofuels, power and heat)” (4), (5). Another important role of biorefineries is that they add value to products and co-products. The International Energy Agency (IEA) is responsible for supervision, development, and generalization of the biomass and bioenergy concept through so-called “tasks.” Task 42 specifically addresses the concept of biorefineries. It is accompanied by a number of satellite tasks, which signalizes that the problem is very complex in nature. The concept of biorefineries consists of four central notions – feeds, platforms, conversion processes, and products and energies:

- Various feeds are used, often specific to biorefineries.
- The platforms are key intermediates connecting different biorefinery feed sources and their processes. The most important platforms are biogas (methane), syngas (a mixture of carbon monoxide and hydrogen), clean hydrogen, organic solutions, pyrolytic liquids, diverse oils, glycerol, pure cellulose, lignin, and C_5/C_6 sugars. The number of involved platforms is an indication of biorefinery complexity.
- The processes are divided into mechanical (the chemical structure of the feed remains unchanged; pressing, milling, separation, distillation, extraction, absorption, adsorption) and chemical (the chemical structure changes). These processes are purely chemical (under mild conditions; hydrolysis/solvolysis, transesterification, hydrogenation, oxidation, and pulping), thermo-chemical (under severe conditions, high temperature and pressure; direct liquefaction – pyrolysis and hydrothermal conversion or indirect liquefaction – various gasification technologies with the Fischer-Tropsch synthesis downstream), electrochemical (water electrolysis), and biochemical (enzymatic or microbial, aerobic and anaerobic).

These processes can be combined in a technology scheme of an individual biorefinery. Similar feedstocks can be processed and similar products can be produced by various technologies. The technologies that can handle feedstocks of highly variable quality and are closely related to a cogeneration of electric power and steam are the most promising ones – pyrolysis and gasification.

- The two central biorefinery outputs are various specific products (chemicals – various alcohols, ethers, aldehydes; materials – phenol-formaldehyde resins, terpenes, gum rosins, tall oil, lignosulfonates; foods – xylitol, sugar syrup; animal feeds – lysine, and organic fertilizers) and energies (fuels, electric power, and heat). Based on the number of downloaded references, DOE has ranked twelve most cited biobased molecules, which are often closely related to the outputs of biorefineries (6). Biorefineries focusing on production of chemicals, materials, food, and animal feeds are called "product-driven." Biorefineries focusing on the production of biofuels and energies are called "energy-driven."

The pulp and paper industry is considered the first industrialized biorefinery system.

The following facts selected from a regular SWOT analysis of the concept, role, and current business of biorefineries are important in considering possible synergies with TORs (4). Biorefineries:

- Make a significant contribution to sustainable development on international basis.
- Maximize biomass conversion efficiency and added value.
- Produce a spectrum of biobased products and energies necessary for the biobased economy.
- Offer opportunities to many sectors and strengthen the economic position of sectors such as agriculture, forestry, chemistry, and energy production.

However,

- It is difficult to bring together key stakeholders that normally operate in different market sectors to discuss biorefinery-related topics, to promote necessary R&D activities, and to accelerate the deployment of new biotechnologies.
- There are alternative concepts of biomass utilization. The conflict between foods, chemicals, and energies production is fundamental. Therefore, biomass availability will be limited.
- The sustainability of biomass production is questioned.
- Energy density and the quality of biomass vary significantly.
- It is not yet clear what the best available processes and technology schemes are and they must be developed, designed, engineered, and proved.
- It is not yet clear what the most promising biomass value chains are and they must be defined and described.
- High CAPEX for pilot and demonstration projects is difficult to find.
- In contrast to the concept of biorefineries, the goals of the end users are often focused upon a single product.
- The long-term profitability in a real market environment has not been sufficiently proven.

The following examples of implemented projects of biorefineries pioneering certain feeds and technologies, listed in IEA document (4), can be mentioned:

- Tembec, Canada (7), (8): It is a pulp mill with a long history, a global leader in specialty cellulose. Cellulose wastes (pulping liquor) represent a feed to biotechnologies. The production of commercial ethanol started in 1982 via fermentation and distillation. Thereafter, an anaerobic wastewater reactor was installed in 2006 to produce biogas. The products are 16,000 $m^3 \cdot y^{-1}$ of ethanol, 170 $kt \cdot y^{-1}$ of lignosulfonates, 600 $TJ \cdot y^{-1}$ of biogas, acetic acid, and phenol-formaldehyde resins. It represents an early biorefinery project and serves as an example of the pioneering role of the pulp industry in the biorefineries concept.
- DAKA Biodiesel, Losning, Denmark (9), (10): It processes animal fats from slaughterhouses as a sole feed. As the content of free fatty acids in fats is generally higher than in vegetable oils, a two-step "EcoMotion" transesterification technology (11) was implemented. The first step is pre-esterification utilizing sulfuric acid as a liquid catalyst followed by alkaline re-esterification. The reaction product is distilled. It was a grass-root project, under the contract with BDI, Austria (12). The capacity of the facility is 50 $kt \cdot y^{-1}$ of biodiesel (EN 14214) and 5 $kt \cdot y^{-1}$ of glycerol. Other products are heavy bioheating oil and potassium sulfate. The facility started up in Apr. 2008. The project is interesting because of the processed feed (the animal fat) and the implemented technology (two-step transesterification).

- Biovalue, Biodiesel Plant Eemshaven, Netherland (13): The feed is a range of different raw materials – vegetable oils, UCOs, and animal fat. The technology consists in transesterification with an upstream vegetable oils press. The capacity of the facility is 66 kt·y^{-1} of feed. It was a grass-root, turn-key project, contractor "Christof Industries" (14). The central product is 50 kt·y^{-1} of biodiesel (EN 14214), 5 kt·y^{-1} of glycerin, and organic fertilizer. The plant started up in 2007, originally on virgin rapeseed oil. The new owner, Biooil (15), redesigned the plant on UCOs. The project is interesting because of the processed mixture of recycled feeds.
- ENSYN Côte-Nord, Canada (16): The feeds are agricultural and wood residues. The heart of the technology is the Envergent RPT rapid pyrolysis. The feed is heated to 500 °C, at ambient pressure, and then after 2 secs rapidly cooled to generate high yields of a light, pourable liquid biooil. The capacity is 66 kt·y^{-1} of the dry feed. It was engineered by Honeywell/UOP through a contract signed with Envergent Technologies (17). CAPEX was 103.9 million US$. The products include biocrude oil (40,000 m^3·y^{-1}), which can be used for power generation, renewable transportation fuels (36 kt·y^{-1} biogasoline, bio JET, and biodiesel), and a range of chemicals (for example flavors, adhesive resins, and charcoal). The unit was commissioned in 2018. The project is interesting because of the use of non-oil feed and for the selected promising technology.
- Next Renewable Fuels Inc., Port Westward, US (18), (19): Virgin seed oils, UCOs, animal fats, and greases will be used as feeds, however, no palm oil. BP, p.l.c., will supply the feeds through its feedstock aggregation and sourcing network. The "Ecofining" technology was selected (20). The capacity will be 2,000 kt·y^{-1} of renewable feedstocks. The products will be biodiesel and green propane. Shell will participate in the sale of the products. It is a grass-root-project with planned CAPEX of 1 billion US$. The contractor, Triten IAG, will manage design, engineering and construction (21). The start-up is planned in 2021. The project is interesting because of its huge capacity challenging the feeds supply and because of involving two oil giants, BP and Shell, at the same time.

Concerning BP´s strategic shift to renewables, see more (22). Hundreds of other similar biorefinery projects have been implemented around the world in the two last decades (23), (24).

Certain important steps to exploit the synergies resulting from the biorefinery concept were already taken in TORs. Implementing biocomponents in motor fuels in low concentration (up to 10% vol.), primarily bioethanol, ETBE, and FAME, reduced the crude oil inputs and carbon dioxide emissions from the consumption of motor fuels significantly, also with respect to the large volume produced and in the comparison with the generally low capacities of biorefineries. However, blending of these components is limited by quality standards. Therefore, TORs are now striving to increase the share of biocomponents converting certain oily feeds processed originally by biorefineries into hydrocarbons with properties similar to petroleum hydrocarbons, such as HEFA, SAF, HVO, synthetic gasoline, and waxes. Processes such as Bio-Verno, Ecofining, NexBTL, Vegan, etc. are used (25), (26). As the next step, certain idling and low complex TORs are converted to biorefineries. They partially or completely eliminate crude oil processing and mirror the activities of energy-based biorefineries. TORs pioneering this approach include:

- ENI, Porto Marghera, Venice, Italy (27), (28): The original crude oil capacity was 3.5 million t·y^{-1}. It was a low complexity refinery. Now palm oil (50 % wt. of feed diet), UCOs (about 50 % wt. available in Italy, thanks to agreements with consortia and municipal companies that deal with the collection of urban waste), by-products from processing of vegetable oils, soap pastes, and animal fats (tallow) are processed. The "Ecofining" technology is used to hydrotreat the feeds, with capacity of 230 kt·y^{-1}. In Jun. 2018, a purification plant started up there, which allows processing of crude used oils instead of pre-treated ones, to increase the amount of UCOs and animal fats processed. From 2024, an upgrade is planed to 560 kt·y^{-1} of feeds and approx. 420 kt·y^{-1} of biodiesel. The overall CAPEX of the transformation was rather huge, namely 500 million €, including R&D and other costs. The project was commissioned in 2014 and it is interesting because it was the world's first TOR conversion to a biorefinery.
- ENI, Gela, Italy (29), (30): The original crude oil capacity was 5 million t·y^{-1}. Now the facility processes vegetable oils, animal fats (tallow), regenerated UCOs, by-products from vegetable oils production, and algae oil. The technology was designed for treating advanced (RED II) and unconventional feeds of up to 100 % wt. of the design capacity. The two existing desulfurization units were modified to the "Ecofining" technology with a total capacity of 750 k·y^{-1} of biodiesel. A new steam reformer was built to produce hydrogen. Additionally, a pilot "waste-to-fuel" plant is operated in Gela, transforming organic wastes into biooil and biomethane since Dec. 2018. A lot of existing infrastructure will be demolished, including tanks, shelters, facilities for gas recovery, and gasoline blending. All petrochemical plants built in Gela since 1962 were mothballed. CAPEX of the conversion to a biorefinery was 294 million €. ENI planned to invest another 73 million € in pretreating of biofeeds, to be completed by 2020. Products

are biodiesel and EniDiesel+ with 15% vol. of HVO (31). The conversion began in Apr. 2016 and the facility was commissioned in Aug. 2019. The project is interesting because of its utilization of retrofitted desulfurization units, because of how the production of hydrogen was resolved and because the 3rd generation algae biofeed is utilized.

- Total, Le Méde (Châteauneuf-les-Martigues), France (32), (33): The original crude oil capacity was 7.55 million $t \cdot y^{-1}$. Feeds of the biorefinery section are 60-70% wt. virgin vegetable oils (rapeseed, sunflower, soybean, palm oil, corn and also new plants such as carinata) and 30-40 % wt. treated wastes (UCOs, animal fats, vegetable oil residues, etc.). Total has pledged to process max. 300 $kt \cdot y^{-1}$ of palm oil in a strictly controlled manner as concerns sustainability and respect to human rights, i.e. less than 50 % wt. of the total volume of feeds needed, and at least 50 $kt \cdot y^{-1}$ of French-grown rapeseed. The technology was developed by IFP Énergies Nouvelles and marketed by its affiliate Axens and called "Vegan". The capacity of the facility is 500 $kt \cdot y^{-1}$ of biodiesel. The project included plans to develop the production of Avgas from the continued operation of the reforming unit, which continues to supply the local petrochemical industry and provide the necessary hydrogen to the biorefinery. The products are bio JET, biodiesel, Avgas (non bio; Total is France's sole producer of Avgas), and AdBlue (non bio, 50 kt). The biorefinery includes a logistics and storage hub and a solar farm (8 MW). CAPEX was 200 €. The transformation took place from 2015 to Jun. 2019. Production was started-up in Jul. 2019. The project is interesting for synergy of TOR technology with the new biorefinery and for a progressive concept of an operational and logistic hub.
- Phillips 66, San Francisco, Rodeo, US (34), (35): The original crude oil capacity was 6 million $t \cdot y^{-1}$. The project will reconfigure the existing refinery to produce renewable fuels. A mix of feeds will be processed – soybean oil, UCOs, animal fats, and greases, however, no crude oil. A new pre-treatment unit will be constructed and the existing hydrocracking units retrofitted to process biofeeds. With the input capacity of 2,420 $kt \cdot y^{-1}$, it will be the world's largest facility of its kind. The start-up is planned for 2024. The products will be biogasoline, JET, and diesel. The project is interesting for its huge capacity challenging the feeds supply.

It can be stated that the converted TORs were not small in terms of capacity, but sometimes uncompetitive due to their low complexity.

The following question is important in this context – Can the progressive concept of biorefineries facilitate the necessary changes of TORs to stay in business, or will biorefineries fully substitute the current role of TORs in the future? This will be discussed in the next part of this paper.

Discussion

The concept of a biorefinery is characterized by a great variety of feedstocks, technologies, and co-products. When considering the future operation of TORs, it is important to understand which and how of these characteristics of the biorefineries can be exploited in further operation of TORs. The complexity of the biorefinery concept is much larger than the relatively conservative concept of TORs. However, the complexity of an individual biorefinery is obviously much lower than that of a TOR. TORs need to derive their long-term strategies from the biorefinery concept, but then optimize the specific synergies resulting from these synergies at the local level. Synergies between these both concepts can be found in the feed diet, processing of intermediates, technologies (including the design of apparatuses, catalysts, additives, etc.), technological infrastructure (supply and production of energies, utilities, waste water treatment, etc.), supply and dispatch logistic schemes, staff qualification, HSE area, and also in related CAPEX and OPEX.

With regard to the mineral origin of crude oil, TORs must at least change the feed diet to be able to stay in business. TORs are well adapted to process liquids characterized by high energy density. They are not ready to process feeds such as grasses, starch, sugar, lignocellulosic crops, and residues like biorefineries do. Therefore, for TORs the best strategy will be to look for those synergies based on liquid platforms, as per IEA concept, e.g., biooils, pyrolytic liquids, and organic solutions, but not based on C_5 and C_6 sugars. Each TOR is designed and optimized to process a certain crude oil quality and is very sensitive to any change in this quality (sulfur, organic chlorine, and naphthenic acids content). In contrast, liquids considered in IEA platforms are totally different and of highly variable quality. This will affect all aspects of their processing in TORs – unloading, storing, process parameters, yields, material compatibility, treatment of wastes, quality monitoring and control, etc. Each individual TOR must be retrofitted in advance to process any such feed. This will also require far more flexibility. Recently, the TORs have started to compete with biorefineries for oily feeds. TORs utilize more advanced and high capacity hydrogenation technologies rather than transesterification ones. They are not limited as concerns HVO blending. Due to the high capacity of technologies in TORs, they can be short as concerns oily feeds. Thus, a virgin vegetable oil has to be imported, for example the palm oil, which apparently contradicts the principles of sustainability (RED II). On the other hand, biorefineries have better capability to get virgin vegetable oils, to collect UCOs, animal fats, pre-treat these feeds, and to deal with oil wastes. However, blending or sale of FAME produced in biorefineries is limited. Processing oily feeds provides a good basis for cooperation at the local level.

It is clear that the next conversions of TORs to biorefineries must focus more on platforms other than biooil and it will require cooperation of both sectors. As concerns C_5 and C_6 sugar platform, TORs process what is referred to as "product" in IEA biorefinery concept, i.e. alcohols. Blending bioalcohols and mineral hydrocarbons into mogas is an excellent example of a synergy of components of different origin. Another synergy lies in the conversion of alcohols to ethers, which is a good example of how TORs can add extra value to the product of a biorefiery, i.e., an activity which is in line with the concept of biorefineries.

TORs are not well adapted to process gases as a feed. This means that the projects based on IEA gaseous platforms (syngas, biogas, and hydrogen) in order to supply raw materials to TORs have to pre-convert gases into synthetic crude oil or methanol that can be then easily processed in TORs.

A range of technologies which matured in TORs or represent certain base petrochemical processes (pyrolysis), were successfully tested to process biofeeds. However, the most promising ones are hydrogen based technologies, such as hydrogenation, hydrotreating, or hydrocracking, because they are capable to improve the quality of processed biofeeds across all IEA platforms to the quality required in motor fuels or chemicals. Retrofitted facilities can perform this task well. Additional new technologies will be involved in the TORs technology scheme, for example, pretreatment of UCOs, or related to hydrogen production. In TORs, hydrogen production traditionally based on catalytic reforming must be redesigned. It will be an excellent opportunity to incorporate "green" hydrogen, obtained by electrolysis of water, exploiting the excess of renewable electricity.

Certain biofeeds, intermediates, or products can be advantageously co-processed in TORs on existing or slightly retrofitted facilities, in comparable amounts and with minimal additional CAPEX (vegetable oils and alcohols) in comparison to biorefineries.

Processing of biofeeds will change material balance of TORs – it will increase the consumption of hydrogen, the content of oxygen dioxide in sour gases, and reduce sulfur production. The current surplus of sulfur may turn into a significant shortage. This can threaten inorganic chemical industry, as sulfur from refineries is now practically the only source of this element. Processing of biofeeds will also change the production of wastes from TORs. For example, waste water production will increase and the quality will deteriorate. Biofeeds will also negatively affect the quality and possible processing of slops in TORs.

TORs use a sophisticated technological infrastructure, ensuring the supply of various energies (electricity of various voltages, fuels of various composition, water steam of various pressure), auxiliary gases (compressed air, nitrogen, oxygen), chemicals and materials (additives and sorbents), water for various applications, central cooling systems, process loops of sour water and water condensate, treating of rain water, waste water treatment, protection of ground water, etc. To operate this infrastructure, vast experience is necessary. These systems can be well adapted and retrofitted to the processing of new biofeeds.

TORs are primarily focused on production of motor fuels (about 70 % wt. in a product portfolio). If they aspire to stay in this line of business and face the booming electromobility, they must blend more biocomponents and also offer clean biofuels. Blending biocomponents, such as HEFA, HVO, biomethanol, bioethanol, ETBE, maybe also DME, tetrahydrofuran, etc., TORs can offer advanced or new sustainable fuels (green propane, high cetane number diesel, low aromatics mogas, SAF, low sulfur marine fuels, etc.) and new chemicals. The share of petrochemical intermediates from TORs will definitely increase. Moreover, the chemicals based on biofeeds are characterized by multiple sustainability, because, unlike fuels, they can be recycled. To operate TOR as a hub, exploiting logistic systems can also significantly contribute to the abovementioned synergies.

Based on published data, the new biorefineries have CAPEX per $t \cdot y^{-1}$ approx. five times higher than TORs, partly because the capacity of these biorefineries is 5 to 25 times smaller than that of a TOR and these projects are not matured enough. However, transforming a TOR into a biorefinery, the costs of retrofitting the exploited facilities and mothballing, dismantling, and decommissioning the rest of the facilities has to be also considered.

New "spin-off" and "start-up" companies are increasingly involved in R&D, pilot testing, and scaling up ideas corresponding to the abovementioned synergies, making it easier to raise funds and acquire venture capital and accepting more risks than standard licensors would normally do. On the other hand, deployment of these ideas is often week, which is in contrast to TORs projects, which are almost always successful. For new projects dealing with these synergies, it seems to be critical to implement them repeatedly, because of variability and limited feed resources.

Conclusions

Today, biorefineries are a rapidly developing business concept. They offer a range of new intermediates and products based on sustainable feeds, which competes with the established business of traditional oil refineries. To manage this threat and to stay in business, traditional oil refineries should mobilize their assets, experience, seniority, and be inspired by this progressing concept to look proactively for possible forms of cooperation and exploit possible synergies to a maximum extent. Specific sources of these synergies have been discussed. These consist of processing similar biofeeds in traditional oil refineries and in biorefineries and adding extra value to intermediates and products of biorefineries. The platforms in the concept of biorefineries, as defined by IEA, can be important starting-points for these synergies. The technologies developed and matured in traditional oil refineries, primarily the hydroprocessing ones, and their complex infrastructure will be a significant part of these synergies. Processing, co-processing, and blending biocomponents, traditional oil refineries can produce premium quality motor fuels, new types of sustainable fuels and chemical products. These products can be easily distributed to the established customers exploiting the existing logistics systems. New biorefineries are extremely CAPEX demanding; therefore, significant CAPEX savings can be achieved by exploiting the existing facility, infrastructure, and position of the traditional oil refineries. Working on these synergies provides an interesting business opportunity for new venture entrepreneurs, creates a number of interesting topics for R&D and engineering companies, and facilitates communication and cooperation among the many stakeholders involved in the concept of sustainable economy.

Acknowledgement

The paper was supported by the Ministry of Education, Youth and Sports of the Czech Republic from the institutional support of the research organization (CZ60461373).

List of abbreviations

BAT .... Best Available Techniques
BREF .... Reference Document on Best Available Techniques
CAPEX.......... Capital Expenditures
DOE .... The U.S. Department of Energy
DME .... Di-Methyl Ether
ETBE .... Ethyl terc. Butyl Ester
FAME .... Fatty Acid Methyl Ester
GHG .... Greenhouse Gas
HEFA .... Hydrogenated Esters and Fatty Acids
HSE .... Health, Safety, and Environment
HVO .... Hydrogenated Vegetable Oil
IEA .... International Energy Agency
OPEX .... Operating Expenditures
SAF .... Sustainable Aviation Fuel
TOR .... Traditional Oil Refinery
UCO .... Used Cooking Oil

References

1. Kittel H. Strategic Challenges ahead for current oil refineries. Mikulov: ICCT Conference proceedings, pp. 147 (2019).
2. Barthe P., Chaugny M., Roudier S., Sanchco, L.D., Best Available Techniques (BAT) Reference Document for the Refining of Mineral Oil and Gas. JRC Science and Policy Reports. European Commission, 2015 [Online] 2015. http://eippcb.jrc.ec.europa.eu/reference/BREF/REF_BREF_2015.pdf.
3. George B.: Europe´s refineries face losses, capacity closures. Argus. [Online] Nov. 20, 2020. [Cited: Mar. 21, 2021.] https://www.argusmedia.com/en/news/2161918-europes-refiners-face-losses-capacity-closures.
4. Brown A.: Biorefineries: adding value to the sustainable utilization of biomass. IEA Bioenergy. [Online] Jan. 2009. [Cited: 30 Nov. 2020.] https://www.ieabioenergy.com/wp-content/uploads/2013/10/Task-42-Booklet.pdf.
5. Biorefining in a Circular Economy. IEA. [Online] 2020. [Cited: Dec. 14, 2020.] https://task42.ieabioenergy.com/.

6. Lane J.: The DOE´s 12 Top Biobased Molecules - what became of them. BiofuelsDigest. [Online] 30 Apr. 2015. [Cited: 30 11 2020.] https://www.biofuelsdigest.com/bdigest/2015/04/30/the-does-12-top-biobased-molecules-what-became-of-them/.
7. Williamson M.: A biorefiner ahead of its time. [Online] Apr. 2013. [Cited: 14 Dec. 2020.] https://www.scribd.com/document/188240333/Tembec-Biorefinery-Ipw-Final-PDF.
8. Wellisch M.: IEA Bioenergy, Task 42. Country report Canada. iea-bioenergy.task42-biorefineries.com. [Online] Nov. 2014. [Cited: Apr. 22, 2021.] https://www.iea-bioenergy.task42-biorefineries.com/upload_mm/b/d/a/693dd766-af57-4b76-ae26-747775393379_Canada_2014_Country_Report_IEA_Bioenergy_Task42.pdf.
9. Craymer L.: DAKA opens new 50 kt/yr Denmark biodiesel plant. [Online] 4 Apr. 2008. [Cited: 5 Sep. 2020.] https://www.icis.com/explore/resources/news/2008/04/04/9113569/daka-opens-new-50ktyr-denmark-biodiesel-plant/.
10. Sustainable Fuel for Now and the Future. Daka Denmark A/S. [Online] 2021. [Cited: Apr. 22, 2021.] http://www.dakaecomotion.dk/en/dkbd/the-company/.
11. Innovative technology to help combat climate change. [Online] 2021. [Cited: Apr. 20, 2021.] https://www.ecomotion.de/en/eco/technology-and-the-environment/.
12. Bioenergy International, GmbH. [Online] 2021. [Cited: Apr. 19, 2021.] https://www.bdi-holding.com/en/.
13. Biodiesel Plant Eemshaven. [Online] 2021. [Cited: Apr. 22, 2021.] https://www.christof.com/en/reference/biodiesel-plant-eemshaven/.
14. Christof Industries. 360° Industrial Solutions for a Sustainable Circular Economy. [Online] 2021. [Cited: Apr. 19, 2021.] https://www.christof.com/en/.
15. Collection of used cooking oil. [Online] 2021. [Cited: 19 Apr. 2021.] https://bio-oil.biz/from-waste-to-energy/?lang=en.
16. Construction begins on Ensyn’s Cote-Nord biocrude plant. [Online] 20 Jul. 2016. [Cited: 14 Dec. 2020.] https://www.pulpandpapercanada.com/construction-begins-on-ensyns-cote-nord-biocrude-plant-1100000324/.
17. Honeywell. RTP™ Technology: Biomass to Renewable Fuels. [Online] 2021. [Cited: 22 Apr. 2021.] https://uop.honeywell.com/en/industry-solutions/renewable-fuels/rtp-biomass-conversion.
18. BP to supply Next Renewable Fuels with renewable diesel feedstock. Biodiesel Magazine. [Online] May 28, 2019. [Cited: Sep. 12, 2020.] BP to supply Next Renewable Fuels with renewable diesel feedstock.
19. Kennedy H. T.: Where is Next Renewable Fuels going next and why we want them as a neigbor. biofuelsdigest.com. [Online] Jun 9, 2019. [Cited: 04 22, 2021.] https://www.biofuelsdigest.com/bdigest/2019/06/09/where-is-next-renewable-fuels-going-next-and-why-we-want-them-as-a-neighbor/.
20. Honeywell Introduces Simplified Technology to Produce Renewable Diesel. [Online] Jan. 12, 2021. [Cited: Apr. 22, 2021.] https://uop.honeywell.com/en/news-events/2021/january/honeywell-uop-ecofining-single-stage-process.
21. Our clients are agile, strategic, and smart. They make big bets. We make sure they win. IAG. [Online] 2019. [Cited: Apr. 22, 2021.] https://www.triteniag.com/.
22. Hirs E.: BP´s Strategic Shift To Renewables. Forbes. [Online] 5 Sep. 2020. https://www.forbes.com/sites/edhirs/2020/08/05/bps-strategic-shift-to-renewables/#3b3371ccdeb1.
23. Biorefinery Tool Map Gallery. [Online] 2021. [Cited: 21 Apr. 2021.] https://www.usda.gov/energy/maps/html/gallery.htm.
24. Map of 224 European biorefineries published by BIC and nova-Institute. [Online] Nov. 27, 2017. [Cited: Apr. 21, 2021.] https://news.bio-based.eu/map-of-224-european-biorefineries-published-by-bic-and-nova-institute/.
25. Šimáček P., Souček I., Pospíšil M., Vrtíška D., Kittel H.: Impact of hydrotreated vegetable Oil and Biodiesel on Properties in Blends with mineral Diesel Fuel. Thermal Science. 23, 1769 (2019).
26. Kittel H.: Licensoři a technologické licence pro čistou mobility a jejich možné uplatnění v České republice. Czech Chemical Society Symposium Series. 18, 203 (2020).
27. The Venice biorefinery. [Online] 2020. [Cited: 14 Dec. 2020.] https://www.eni.com/en-IT/operations/italy-venice-biorefinery.html.
28. Porto Marghera Venice Refinery. [Online] Jul. 17, 2014. [Cited: Apr. 22, 2021.] http://abarrelfull.wikidot.com/porto-marghera-venice-refinery.
29. Eni opens its bio-refinery in Gela. [Online] 2019. [Cited: 14 Dec. 2012.] https://www.eni.com/en-IT/media/press-release/2019/09/eni-opens-its-bio-refinery-in-gela.html.
30. Gela Refinery. [Online] 14 Jul. 2014. [Cited: 21 Apr. 2021.] http://abarrelfull.wikidot.com/gela-refinery.

31. ENI Diesel +. [Online] 2021. [Cited: 23 Apr. 2021.] https://oilproducts.eni.com/en_GB/products/fuels/automotive/diesel/eni-diesel.
32. Total. La Méde – A Facility for the energies of tomorrow. [Online] 2020. [Cited: 14 Dec. 2020.] https://www.total.com/energy-expertise/projects/bioenergies/la-mede-a-forward-looking-facility.
33. Total Le Mede. [Online] Jul. 14, 2014. [Cited: Apr. 22, 2021.] http://abarrelfull.wikidot.com/provence-refinery.
34. Phillips 66 to convert San Francisco refinery to renewable fuels. [Online] Aug. 14, 2020. [Cited: Sep. 5, 2020.] http://biomassmagazine.com/articles/17275/phillips-66-to-convert-san-francisco-refinery-to-renewable-fuels.
35. San Franciso Refinery. [Online] Jul. 14, 2014. [Cited: Apr. 22, 2021.] http://abarrelfull.wikidot.com/san-francisco-refinery.

CO-PYROLYSIS OF FISCHER-TROPSCH WAX VACUUM RESIDUE WITH HYDROCRACKING PRODUCT

Karaba A.[1,2], Rozhon J.[1], Filip L., Zámostný P.[1]

[1]*University of Chemistry and Technology Prague, Technická 5, 166 28 Prague 6 – Dejvice, Czech Republic*
[2]*Unipetrol Centre for Research and Education, Revoluční 1521/84, Ústí nad Labem, Czech Republic*
adam.karaba@vscht.cz

Abstract

The presented study deals with the assessment of the traditional feedstock co-pyrolysis possibility with the wax fraction produced via Fischer–Tropsch (FT) synthesis. The samples of wax fraction (FT wax) coming from experimental pilot-plant Fischer–Tropsch unit plant were studied. The vacuum distillate from the hydrocracking process (HCVD) was used as the traditional feedstock. The yields of individual products and fractions from pyrolysis and co-pyrolysis of the wax fraction with traditional HCVD feedstock were measured using the laboratory micro-pyrolysis technique, which was carried out at 815 °C peak temperature and 0.2 s residence time. The experimental study showed the FT wax yields being superior in the valuable lighter olefinic products in comparison to the traditional HCVD feedstocks providing for example as much as 43 % wt. of ethylene. The mixing effects of co-pyrolysis were not significant, and the yields of most products were proportional to the FT wax content in the co-pyrolysed feedstock.

Introduction

The FT synthesis process was named for the discoverers Franz Fischer and Hans Tropsch in 1922 (1). The FT synthesis is the key industrial process for utilization of the synthesis gas (2). It is a highly exothermic collection of catalyzed polymerization reactions converting the mixture of H_2 and CO from synthesis gas into the large number of product species. The spectrum of FT products consists of wide range of saturated, unsaturated, aromatic hydrocarbons and certain amount of oxygenated compounds such as aldehydes, ketones, alcohols etc. (1, 3). Nevertheless, the saturated hydrocarbons with various length from C_1 to C_{100}+ carbon atoms and 1-olefins are the main products of FT synthesis (4, 5). This array of output compounds can be fractionated into three main commercial cuts (5): FT Naphtha, FT Diesel, and FT Wax. The lightest naphtha fraction contains hydrocarbons ranging from C_5 to C_{11} carbon atoms. The diesel fraction contains hydrocarbons between C_9 and C_{22}, and the heaviest wax consist of hydrocarbons $>C_{20}$. Although the compositions of FT products are different from the petroleum, the specific downstream processes can be used for the FT products with minimum changes required. This is true especially for the naphtha and diesel fractions which can be incorporated into fuel processing pathways. Currently, the wax fraction is further refined primarily by hydrocracking, which allows the selective production of additional diesel fuel (6). The petroleum chemistry utilization of those waxes via steam cracking presents an attractive alternative because the high content of saturated, mostly linear, hydrocarbon chains promises abundant yields of valuable products. The FT feedstocks are comparatively less abundant than the traditional petroleum-based ones and thus their co-processing of mixtures of both feedstock types is a preferred way of utilization. Therefore, the aim of this study was to evaluate the possible product yields obtainable from FT wax via laboratory pyrolysis technique and compare them to those obtained from HCVD, which represent a compatible feedstock for blending.

Materials and methods

This study included FT wax vacuum residue fraction (boiling at 360 C+) obtained from the MOBSU plant situated in Findland. The HCVD representing a traditional steam-cracking feedstock was obtained from the Unipetrol RPA (Czech Republic) as the residue after vacuum distillation of hydrocracking products.

The apparatus for laboratory study of hydrocarbon pyrolysis was compiled from a standard pyrolysis unit Pyr-4A Shimadzu and on-line dual gas chromatography unit (2 x GC 17A Shimadzu). The pyrolysis pulse quartz tube reactor (3 mm i.d. x 5 mm o.d. x 180 mm long, 0.2 s average residence time in the hot zone) is a standard component of the pyrolysis unit Pyr-4A Shimadzu. Reactor is heated by the electric furnace achieving the reaction mixture temperatures up to 820 °C. The hot reaction of peak temperature zone is about 10 mm long, bordered by steep temperature ramps in the pre-heating and the cooling zones. The detailed description of the experimental technique was published elsewhere (7).

Experiments were conducted at peak operating temperature 815 °C (in relative accordance with the plant outlet coil temperature for given cracked feedstock), nitrogen carrier gas flow rate 65 $ml.min^{-1}$ and 300 kPa pressure gauge. Pyrolysis samples included pure FT Wax and HCVD and blended samples. The blended samples were prepared in molten state by differential weighing of individual components into 10 ml vials and contained 10, 20, 30 and 50 wt. % of FT wax in HCVD. Samples of 0.2 µL volume were injected into the pyrolysis reactor and the product yields were recorded by the on-line attached chromatographic system and recorded on FID detectors. The hydrogen yield was calculated using element balance.

Results and discussion

All results of separate pyrolysis and co-pyrolysis of FT wax and HCVD are summarized in Fig. 1-3.

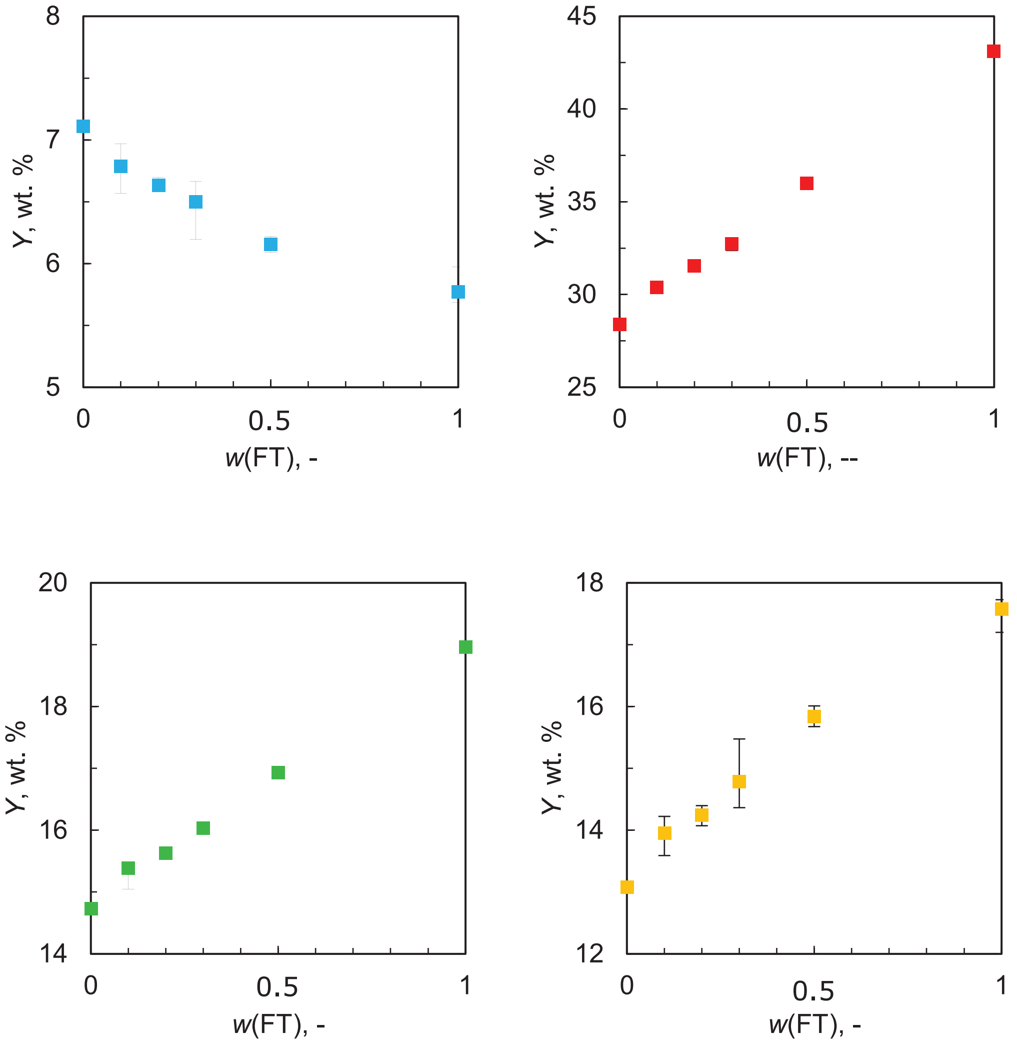

Figure 1. Methane (🟦), ethylene (🟥), propylene (🟩) a C_4-fraction (🟨) yields for different mass fraction of FT wax in HCVD at 815 °C peak pyrolysis temperature and 65 Nml·min^{-1} carrier gas flow rate.

A study of HCVD co-pyrolysis with an FT wax found that the addition of an FT wax to the HCVD increased the yields of ethylene, propylene, C_4-fraction and butadiene. The sum of C_4 hydrocarbons also includes butadiene, which is also plotted separately. The highest yield values of these substances and fractions were observed in the pyrolysis of pure FT wax, which corresponds to its highly paraffinic character. This is because paraffins are easily cleaved to radicals through β-scission and provide high yields of the desired light pyrolysis products.

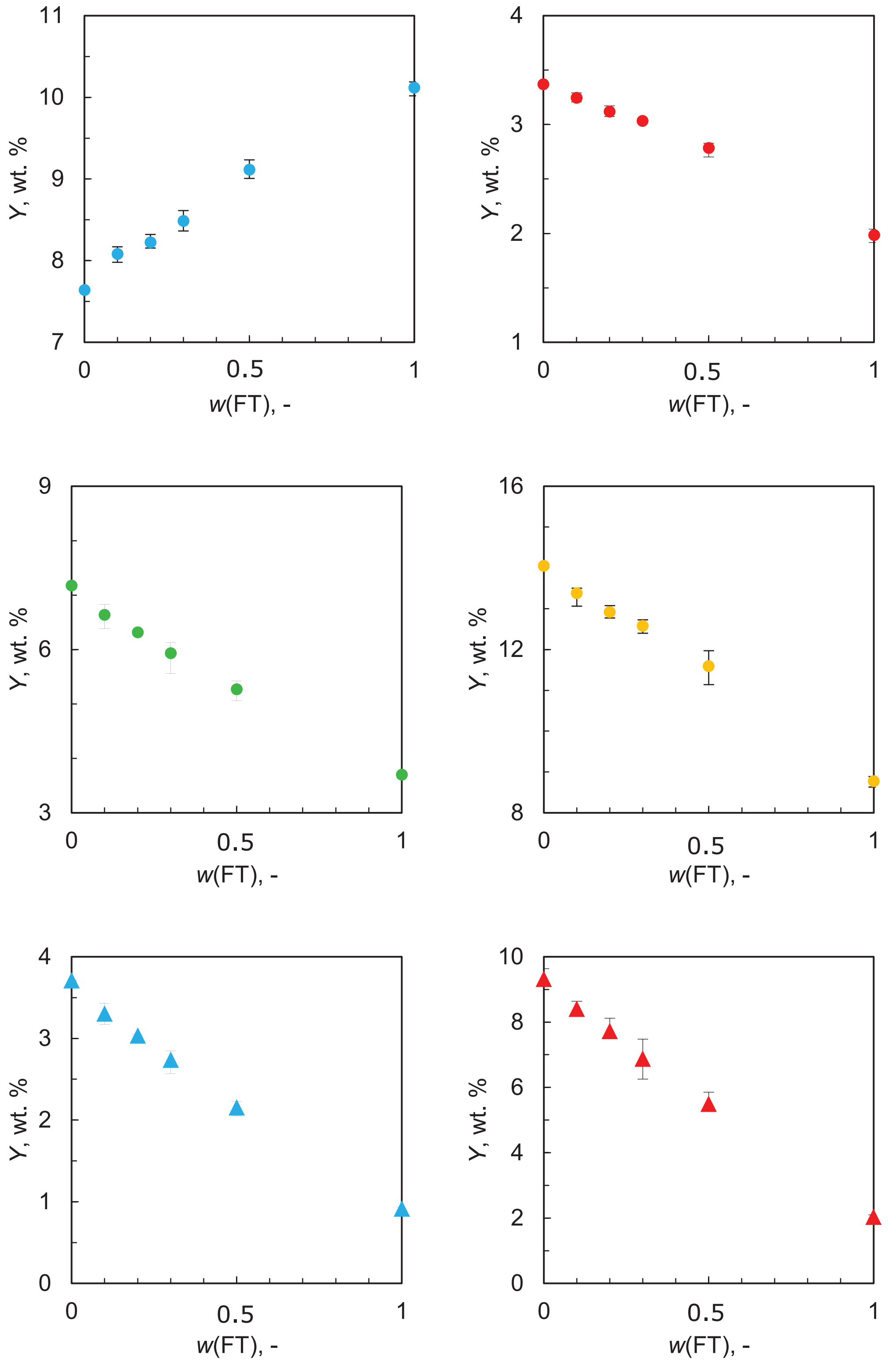

Figure 2. Butadiene (●), isoprene+cyclopentadiene (●), benzene (●), other C5-C6 (●), toluene (▲) and other C$_7$-C$_{12}$ (▲) yields for different mass fraction of FT wax in HCVD at 815 °C peak pyrolysis temperature and 65 Nml·min^{-1} carrier gas flow rate.

On the contrary, a decrease in methane, cyclopentadiene, isoprene, benzene, C5-C6 hydrocarbon fraction, toluene, C7-C12 hydrocarbon fraction, and pyrolysis oil yields with increasing content of FT wax in the feedstock.

This fact probably corresponds to the composition of HCVD products, which contain much more aromatics and cycloalkanes than the products from FT synthesis.

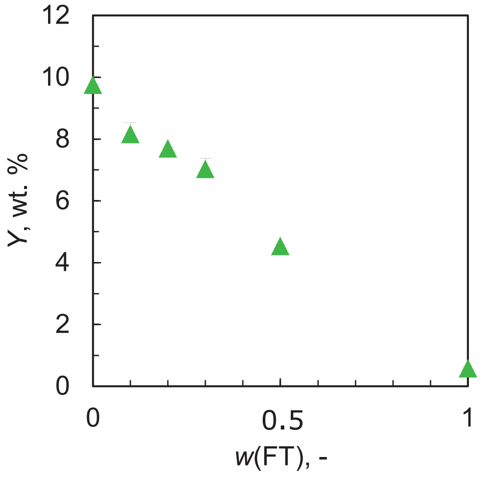

Figure 3. Pyrolysis oil (▲) yields for different mass fraction of FT wax in HCVD at 815 °C peak pyrolysis temperature and 65 Nml·min^{-1} carrier gas flow rate.

The decrease in pyrolysis oil yields leads to values close to zero in case of pyrolysis of the pure FT wax (Figure 3). While pure HCVD yielded as much as 9.8 wt. % of oil, FT wax yielded only 0.6 wt. %. In general, it can be stated that with increasing content of FT distillation residue in HCVD, yields of light products (ethylene, propylene, C4 fraction and butadiene) increase and yields of methane and heavy products decrease. As it is obvious from the figure 1 and 2, the most of trends is monotonic and approximately linear, there Is no obvious non-linearity in these trends except the yield of oi. The yields of C4 and isoprene+cyclopentadiene may be also partially curved. Most of the dependencies of the yields of co-pyrolysis are linear, which indicates that no significant co-pyrolysis effects exist between the two raw materials.

Conclusion

This study quantified the yields of main products obtained by the pyrolysis of FT wax confirming the FT wax as extremely good potential feedstock for steam cracking. The cumulative ethylene and propylene yield from FT wax increased by more than one third than that of the standard HCVD. Moreover, the products of FT wax co-pyrolysis include only low yields of pyrolysis oil and aromatics and thus they are likely to exhibit low coke formation in industrial processing. Also, the sample preparation procedure as well as the results showed good compatibility of both feedstocks which is promising for blended processing.

Acknowledgement

The publication is a result of the project COMSYN. This project has received funding from the European Union's Horizon 2020 research and innovation programme under grant agreement No 727476. The project COMSYN has been integrated into the National Sustainability Programme I of the Ministry of Education, Youth and Sports of the Czech Republic (MEYS) through the project Development of the UniCRE Centre, Project Code LO1606. The result was achieved using the infrastructure of the project Efficient Use of Energy Resources Using Catalytic Processes (LM2015039) which has been financially supported by MEYS within the targeted support of large infrastructures.

References

1. Dalai, A. K.; Davis, B. H., Fischer–Tropsch synthesis: A review of water effects on the performances of unsupported and supported Co catalysts. Applied Catalysis A: General 2008, 348 (1), 1-15.
2. Pendyala, V. R. R.; Jacobs, G.; Bertaux, C.; Khalid, S.; Davis, B. H., Fischer–Tropsch synthesis: Effect of ammonia on supported cobalt catalysts. Journal of Catalysis 2016, 337, 80-90.

3. Ail, S. S.; Dasappa, S., Biomass to liquid transportation fuel via Fischer Tropsch synthesis – Technology review and current scenario. Renewable and Sustainable Energy Reviews 2016, 58, 267-286.
4. van der Laan, G. P.; Beenackers, A. A. C. M., Intrinsic kinetics of the gas–solid Fischer–Tropsch and water gas shift reactions over a precipitated iron catalyst. Applied Catalysis A: General 2000, 193 (1), 39-53.
5. van de Loosdrecht, J.; Botes, F. G.; Ciobîcă, I. M.; Ferreira, A.; Gibson, P.; Moodley, D.; Saib, A.; Visagie, J.; Weststrate, C.; Niemantsverdriet, H., Fischer–Tropsch Synthesis: Catalysts and Chemistry. 2013; Vol. 7, p 525-557.
6. Komvokis, V. G.; Karakoulia, S.; Iliopoulou, E. F.; Papapetrou, M. C.; Vasalos, I. A.; Lappas, A. A.; Triantafyllidis, K. S., Upgrading of Fischer–Tropsch synthesis bio-waxes via catalytic cracking: Effect of acidity, porosity and metal modification of zeolitic and mesoporous aluminosilicate catalysts. Catalysis Today 2012, 196 (1), 42-55.
7. P. Zamostny, Z. Belohlav, L. Starkbaumová, Chem. Biochem. Eng. Q. 2007, 21 (2), 105-113.

PARTIAL HYDROGENATION OF DOUBLE BONDS IN POLYUNSATURATED FATTY ACID METHYL ESTERS

Slezáčková M.[1], Mikulec J.[1], Blaško J.[2]

[1]VÚRUP, a.s., Vlčie hrdlo, 820 03, Bratislava, Slovak republic
[2]Comenius University in Bratislava, Faculty of Natural Sciences, Iľkovičova 6, 842 15 Bratislava, Slovak republic
martina.slezackova@vurup.sk

Abstract

Some non-food oils contain a high proportion of polyunsaturated acids. This determines their oxidative stability and limited use in the production of FAME. One such raw material is oil from the plant *Camelina sativa*, L. (Crantz). It is necessary to technologically reduce the iodine value below the standard value of 120 mg I_2/g while maintaining other beneficial properties to the maximum extent. One possible solution is the partial hydrogenation of unsaturated bonds with minimal skeletal isomerization of cis-trans. Cu-based catalysts were prepared as hydrotalcites, which were converted to mixed oxides (450 °C) by annealing. Catalysts with a high dispersion of Cu have been shown to be effective selective catalysts for the hydrogenation of polyenes to monoenes in the hydrogenation of camelina oil and its methyl esters. The iodine value of the partially hydrogenated linseed oil was reduced from 153 to 101 mg I_2/100 g of sample.

Introduction

Triacylglycerides (TAG) and free fatty acids, which are found in various types of oilseeds and animal fats, are used to produce renewable fuel components for diesel engines. A common method for the production of biodiesel is the transesterification of triacylglycerides with methanol in the presence of a basic catalyst. One of the possibilities for the rapid introduction of advanced second-generation biofuels is the cultivation and use of the non-food plant. Oils extracted from *Camelina sativa*, belong to this group. They can also be grown on soils with lower fertility and quality, as well as on damaged soils. It has a shorter growing season, is more resistant to drought than oilseed rape. The plant is a known accumulator of heavy metals and can also be used to remediate soils with their high concentration. They are not suitable for food use due to the above-limit content of erucic acid.

The proportion of oil in the seed of camelina oil is in the range of 35 – 42 % by weight. Its properties are more similar to linseed oil, but its thermal stability is much higher. Camelina oil, compared to rapeseed oil, belongs to the group of oils which contain a high proportion of polyunsaturated fatty acids and are, therefore (even their methyl esters) very oxidatively unstable. It is necessary to technologically reduce the iodine value below the standard value of 120 mg I_2/g while maintaining other beneficial properties to the maximum extent.

A number of publications have addressed the oxidative stability of FAME produced from polyunsaturated feedstocks by partial hydrogenation[1-7]. Oxidation of unsaturated bonds in the fatty acid chain is a complex process where its course is influenced not only by oxygen but also by light, elevated temperature, the presence of certain metals, peroxides, antioxidants, and the size of the oil/ester-air interface. Oxidation is activated in the presence of metal contaminants such as Cu, Mn, Fe, Co, Ni, even at low concentrations. Therefore, it is necessary to completely remove them from the products and use metal passivators in combination with antioxidants.

One possible solution of oil/FAME instability is the partial hydrogenation of part of the unsaturated bonds with minimal skeletal isomerization of cis-trans because trans isomers have a higher solidification temperature than cis isomers.

The hydrogenation of plant oils in the food industry is a known process in which Ni catalysts are used in the particular formation of trans isomers must be minimal (health restriction). In the presence of conventional nickel catalysts, unsaturated vegetable oils are hydrogenated non-selectively to saturated fatty acids. Isomerization is used as a side effect in the hydrogenation, and undesired trans isomers of fatty acids are also formed.

In the case of the hydrogenation stabilization of polyunsaturated oils and/or their methyl esters for use in fuels, a compromise is required in the degree of saturation of the double bonds and the minimization of cis-trans isomerization. Pd (less Ru, Pt, Co) catalysts in combination with various activators on various types of catalytic supports were most often tested. Pd catalysts are very effective but do not selectively hydrogenate to Cx: 1 acid, but precise control of the reaction conditions (time, temperature, partial pressure, hydrogen) is required to avoid complete hydrogenation to Cx: 0 products.

Selective partial hydrogenation of polyunsaturated fatty acids can be achieved on Cu catalysts, which preferably takes place over the cis Cx: 1 isomer[4,8-10]. The addition of metal promoters (Ag, Pd) significantly reduces the content of trans Cx: 1 acid in the products[11]. Their disadvantage is the high sensitivity to deactivation.

High-activity Cu catalysts for the hydrogenation of polyunsaturated oils are only present if the copper is strongly dispersed on a support having a broad-pore structure to minimize the mass transfer limit[12]. The activity of the catalyst and its stability depends on the degree of dispersion of the copper on the surface of the support and its structure[12].

The aim of this work was to compare the selective partial hydrogenation of camelina oil and camelina oil methyl ester on Cu/SiO_2, Cu-hydrotalcite and Cu-Co hydrotalcite catalysts.

Experimental

Feedstock preparation and analysis

C. sativa var. Smilowska provided by Research and Breeding station at Vígľaš-Pstruša (Slovak republic) was grown in testing open field in spring season 2019. Mechanically pressed camelina oil from the Smilowska variety was used in the tests. Prior to the transesterification and hydrogenation process, oil refining is necessary to remove unwanted phospholipids as well as to reduce the metal content present in the oil. The crude pressed camelina oil was degummed with citric acid, deacidified with NaOH, refined with bleaching earth and silica gel. Degumming is necessary to prevent the deactivation of the catalyst; the procedure was very efficient. Camelina oil methyl ester was prepared by homogeneous transesterification with sodium methanolate (BÜCHI glass stirred reactor, 60 °C, methanol:oil molar ratio 6:1; 600 rpm). Table I compares the properties of crude and degummed camelina oil.

Table I
Comparison of crude pressed and degummed camelina oil

Oil properties	Unit	Raw oil	Degummed oil
Acid number	mg KOH/g	0.86	0.55
Iodine number	g I_2/100 g	153	152
Content of FFA	% C18:1	-	0.28
Density (20 °C)	g/dm^3	922.2	922.2
Kinematic viscosity (20 °C)	mm^2/s	64.9	65.75
P	mg/kg	13.16	<3
Ca	mg/kg	6.19	<1
Mg	mg/kg	2.51	<1
Na	mg/kg	<1	<1
K	mg/kg	2.85	<1
S	mg/kg	13.65	<5
Water content	wt. %	0.06	0.05

The properties of the products were evaluated by measuring the refractive index, iodine value and GC (after conversion to methyl esters in the case of oils) and GC-MS. Iodine number was evaluated by titration by using the STN EN 14111: 2003 standard.

Hydrogenation produces cis- and trans-isomers and therefore the available pure standard fatty acids had to be used for identification. Samples were directly analysed by high-performance gas chromatography on an Agilent, 6890N gas chromatograph. 0.2 µl of partially hydrogenated oil was dosed in split mode and separated on a ULTIMETAL column 8.5 m × 0.53 mm (ID) × 0.17 µm (Chrompack, Middelburg NL) with a temperature program from 80 °C to 380 °C with a temperature gradient of 10 °C/min at a constant pressure of 0,08 bar helium. The distribution of fatty acids in camelina oil (raw material) is in Table II.

Table II
Distribution of fatty acids in camelina oil (raw material)

Fatty acid	% wt.	Fatty acid	% wt.	Fatty acid	% wt.
C12:0	0.01	C18:2	18.78	C22:0	0.26
C14:0	0.07	C18:3	34.45	C22:1	1.79
C16:0	5.91	C20:0	1.28	C23:0	0.03
C16:1	0.10	C20:1	12.37	C24:0	0.15
C17:0	0.06	C20:2	1.66	C24:1	0.58
C18:0	2.76	C20:3	1.23		
C18:1	17.85	C20:4	0.02		

The camelina oil (CO) belongs to the group of vegetable oils that contain a high proportion of polyunsaturated fatty acids and therefore have low oxidative stability.

Synthesis of the catalysts

Three Cu-containing catalysts were prepared. 8 % Cu/SiO_2 was prepared by adding SiO_2 support to complex $[Cu(NH_3)_4]^{2+}$, and then the slurry was slowly diluted with demi water. The solid was separated by filtration, washed with water, dried at 120 °C and calcined in air at 450 °C for 4 hours.

Cu and Cu-Co catalysts were prepared through intermediate stages of hydrotalcite and mixed oxide. The synthesis of Cu hydrotalcites was performed by precipitation from Cu, Co, Mg and Al nitrates with Na_2CO_3 at pH=10. The synthesis was run at 23 °C with vigorous stirring and high dilution for 3 hours. Co-precipitation was followed by a 16 hour maturation process. The hydrotalcite precipitate was washed to pH=7 and filtered. The prepared Cu/HT and CuCo/HT catalyst were dried at 80 °C, activated by annealing at 450 °C for 4 hours to a mixed oxide. The composition (as mixed oxides) of the prepared catalyst is in Table III (ICP-OES).

Table III
Composition of Cu catalyst

Sample	Cu, % wt	Co, % wt	Mg, % wt	Al, % wt
Cu/SiO_2	8.1	-	-	-
Cu/HT	15.4	-	7.1	13.7
CuCo/HT	12.1	41.1	5.0	11.3

The XRD spectrum of the sample was measured to confirm the formation of a layered structure of Cu/HT and Cu-Co/HT that is characteristic of hydrotalcites. The X-ray diffraction spectrum of the obtained sample corresponds to the published data for Cu-containing hydrotalcites (Table IV).

Table IV
Parameters calculated from XRD pattern of hydrotalcite

	d_{003}, Å	D_{006}, Å	d_{110}, Å	D, nm	a, Å	c, Å
Cu/HT	7.45	3.74	1.51	23.67	3.01	22.34
CuCo/HT	7.60	3.80	1.54	21.65	3.02	22.60

Reduction of Cu precursors (oxides or mixed oxides) was performed at a temperature of 270 °C, a hydrogen pressure of 20 bar in n-C_{12} medium for two hours. After separation of the solvent, the catalyst was used. It is very important that the reduced catalyst does not come into contact with air.

Two commercial catalysts were also used as catalysts: 5 % Pd/C Degussa type E105CA/W and 5% Ru/Al_2O_3 reduced Aldrich.

Catalytic tests

The camelina oil and camelina oil methyl ester partial hydrogenation tests were carried out in a stirred Parr Instruments autoclave in the range of hydrogen pressures 6 - 16 bar, temperatures 130 - 180 °C, stirring 600 rpm, 200 mL oil and 1 g reduced catalyst, test duration 60 - 120 minutes. Separation of the product from the catalyst was performed by centrifugation and by filtration.

The catalyst was used repeatedly 4 times. Tests were performed on the partial hydrogenation of the linseed oil and subsequent homogeneous transesterification at 60 °C with sodium methanolate, methanol/oil molar ratio 6:1, stirring 600 rpm, reaction time 1 hour. The reverse procedure was also performed, in which the methyl ester was prepared in the intermediate phase and subsequently partially hydrogenated.

Results and discussion

Partial hydrogenation of camelina oil methyl ester

The main unsaturated fatty acids in camelina oil are linolenic (C18:3) and linoleic acid (C18:2). Reduction of the degree of unsaturation and thus adjusting the oxidative stability is a key factor in its use as a biocomponent in fuels. The content of polyunsaturated fatty acids also depends on the specific variety and growing conditions. The average number of double bonds of camelina oil is 1.77, the molar mass 903 and is higher than that of rapeseed or soybean oil. We examined both the possibilities of stabilizing camelina oil and camelina oil methyl ester.

The Pd/C catalyst was very active in the hydrogenation of camelina oil, but was non-selective. At temperatures above 150 °C and higher hydrogen partial pressures, complete hydrogenation of the double bonds to stearic acid occurred. A similar, slightly lower activity was observed for the Ru/Al_2O_3 catalyst. For both catalysts, a partial hydrogenation of camelina oil to monoenes (C18:1) was achieved at a hydrogen partial pressure of up to 4 bar and a temperature of up to 100 - 120°C.

Conversely, a copper catalyst are excellent catalysts partial hydrogenation of olefin, however, they are unstable and easily deactivated. According to published data, the deactivation of Cu catalysts is mainly due to the sintering of Cu atoms, the formation of carbon at the active centers of the catalyst and the leaching of Cu (reaction with free fatty acids). According to more recently published data, the size of the active centers of the catalyst is important.

The Cu/SiO_2 catalyst confirmed the published data on susceptibility to easy deactivation. On the other hand, the selective partial hydrogenation of camelina oil was effective when the catalyst handled correctly. Partial hydrogenation reduced the iodine value from 152 to 103 mg I_2/g, C18:3 content from 32.72 % wt to 0.94 % wt and the C18:2 content also decreased slightly from 18.47 to 12 % wt. The C18:1 content increased from 16.44 to 42.62 % wt. while the stearic acid content changed slightly from 2.54 to 3.62 wt %. The average number of double bonds decreased from 1.77 to 0.93.

The results of the partial hydrogenation of camelina oil with Cu catalysts prepared via hydrotalcites are shown in Table V. Cu catalysts prepared by this procedure were more active and less sensitive to deactivation than Cu/SiO_2. The camelina oil hydrogenation reaction also took place at a lower temperature (140 – 180 °C). The average number of double bonds decreased significantly from 1.77 to 0.93 - 0.95. The activity of the catalyst decreased slightly with repeated use, which was reflected in the need for an increased hydrogenation temperature. In the case of the CuCo/HT catalyst, the cis-trans isomerization proceeded minimally, in the case of the Cu/HT the proportion of trans isomers reached 19.6 %.

Table V

Results of the partial hydrogenation of camelina oil with Cu/HT and CuCo/HT catalysts

Parameter	Unit	Feed	Cu/HT	CuCo/HT
C18:0	% wt	2.54	3.05	6.67
C18:1	% wt	16.44	40.54	51.99
C18:2	% wt	18.47	17.2	5.34
C18:3	% wt	32.72	0.19	0
Iodine number	mg I_2/g	152	101	90
Average number double bonds	-	1.77	0.95	0.93

The hydrogenation of fatty acids that contain multiple double bonds takes place in a consecutive way. The behaviour of hydrogenation of triacylglycerides and/or FAME is limited by the low solubility of H_2, adsorption of hydrogen on the catalyst surface and thus interfacial mass transport limitations[14]. The prepared Cu/HT catalyst was more selective in the partial hydrogenation of camelina methyl ester, which may be related to the smaller ester molecule when adsorbed on the active center of the catalyst. The results confirm the possibility that isomerization is thermodynamically favorable but can be kinetically controlled during the process of FAME hydrogenation on Cu metal on mixed-oxide surfaces.

Oxidation stability of the camelina oil/FAMEs

Oxidation of fatty acid methyl esters is a complex process and takes place by various mechanisms[2]. The prediction of oxidative stability is complicated by the fact that it is influenced by several factors in addition to the composition. The composition of methyl esters has a significant effect on oxidative stability. Various indices have been introduced for the prediction of oxidative stability, based on the composition of methyl esters - iodine value, oxidazibility[13]. We can confirm the data from the source[3], that there is only a weak correlation between these indices and the oxidative stability determined by the Rancimat method. In addition to the composition, the oxidative stability is also affected by the content of natural antioxidants, the presence of some metals that accelerate autoxidation, temperature and also the concentration and composition of synthetic antioxidants.

Oxidizability was calculated after[13]:

$$Ox = [0.02 * \%\ wt\ oleic\ acid + \%\ wt\ linoleic\ acid + 2 * \%\ wt\ linolenic\ acid]/100$$

Table VI
Oxidizability and oxidation stability of the products

Catalyst	Oxidizability	Oxidative stability Rancimat method, hour
-	0.842	0.5
Cu/SiO_2	0.107	10
Cu/HT	0.184	37.5*
CuCo/HT	0.066	15

** 500 ppm antioxidant*

The oxidative stability of partially hydrogenated products was significantly influenced by the leached copper. In this case, the oxidative stability was extremely low and the copper showed its catalytic effect on the oxidation even at very low concentration. Conversely, exceptional oxidative stability has been achieved by removing copper and/or adding an antioxidant in combination with a metal passivator (Table VI).

Conclusions

Cu catalysts with a high dispersion of Cu have proven to be effective selective catalysts for the hydrogenation of polyenes to monoenes in the hydrogenation of camelina oil and camelina oil methyl esters. In this way, it is possible to control the content of saturated fatty acids and thus the relatively good low-temperature properties. A critical factor in the partial hydrogenation of camelina oil using Cu catalysts is its leaching.

The partially hydrogenated camelina oil methyl ester has excellent oxidative stability after antioxidant addition. The selective partial hydrogenation of polyunsaturated oils increase their oxidative stability during storage and is an unconventional raw material for biodiesel production.

Acknowledgements

This work was supported by projects APVV-16-0097 and APVV-16-0051.

References

1. Thunyaratchatanona Ch., Luengnaruemitchaia A., Chollacoop N., Chen S-Y., Yoshimura Y.: Fuel Process. Technol. *179*, 422 (2018).
2. Knothe G.: Fuel Process. Technol., *88*, 669 (2007).
3. Pullen J., Saeed K.: Fuel Process. Technol. *125,* 223 (2014).
4. Pecchia P., Galasso I., Mapelli S., Bondioli P., Zaccheria F., Ravasio N.: Ind. Crops Prod. *51*, 306 (2013).
5. Adu-Mensah D., Mei D., Zuo L., Zhang Q., Wang J.: Fuel, *251,* 660 (2019).
6. Falk O., Meyer-Pittroff R.: Eur. J. Lipid Sci. Technol*. 106,* 837 (2004).
7. Zuleta E.C., Baena L., Rios L.A., Calderón J.A.: J. Braz. Chem. Soc., *23(12)*, 2159 (2012).
8. Zaccheria F., Psaro R., Ravasio N., Bondioli P.: Eur. J. Lipid Sci. Technol., *114*, 24 (2012).
9. Zaccheria F., Psaro R., Ravasio N.: Green Chem., *11*, 462 (2009).
10. Zaccheria F., Ravasio N., Chan-Thaw C.E., Scotti N., Bondioli P.: Top Catal. *55*, 631 (2012).
11. Zhao Y., Ren Y., Zhang R., Zhang L., Yu D., Jiang L., Elfalleh W.: Food Biosci., *22*, 91 (2018).
12. Trasarti A.F., Segobia D.J., Apesteguía C.R., Santoro .F, Zaccheria F., Ravasio N.: J. Am. Oil Chem. Soc., *89,* 2245 (2012).
13. McCormick R.L., Ratcliff M., Moens L., Lawrence R.: Fuel Process. Technol., *88(7)*, 651 (2007).
14. Hu Ch., Creaser D., Siahrostami S., Gronbeck H., Ojagh H., Skoglund M.: Catal. Sci. Technol., *4(8)*, 2427 (2014).

MODELING OXYGEN PRODUCTION VIA CRYOGENIC AIR SEPARATION

Poláková N.[1], Variny M.[1]

[1] *Department of Chemical and Biochemical Engineering, Faculty of Chemical and Food Technology, Slovak University of Technology in Bratislava, Radlinského 9, 812 37 Bratislava, Slovak Republic*
miroslav.variny@stuba.sk

Abstract

Industrial-scale oxygen production is vital for many industrial branches. Current technologies exhibit a rather large specific power consumption, exceeding 150 kWh per ton of pure oxygen. With several of them being mature for decades, while others being still in development, possibilities for further energy consumption decrease should be exploited, to make the oxygen production via air separation more sustainable. With this long-term goal a model Cryogenic Air Separation Unit (ASU) is considered as a case study. First, its performance as a stand-alone plant is modeled and verified. Second, options for its improvement are identified and discussed, including heat recovery option from hot compressed air. The considered heat recovery project can be economically feasible, with the expected simple payback period of 6 to 13 years. The presented case study and its results contribute to sustainable industrial-scale oxygen production goal, while retaining a favorable production economy and exploiting the potential of carbon footprint reduction.

Introduction

Oxygen is the second most used gas in industry. It is used in food, chemical, oil industry, pharmacy, and others, with varying purity, state, and quantity requirements. Industrial praxis appreciates its contribution to carbon footprint lowering in oxycombustion application[1,2] whether in power and heat production sector[3,4], or in light metals melting and processing[5,6]. Its use in those applications offers at the same time potential for better process control[7] and for carbon capture and storage[8,9.]

To separate individual components of air, most air must be liquified. Gas can only be liquified at temperatures and pressures below its critical point; critical point of air is at T_c = 132.5 K and pressure P_c = 37.7 bar. Two liquefaction cycles are known, namely Linde and Kapica cycle.

There are two different ways of producing oxygen: non-cryogenic and cryogenic production route[10,11]. Non-cryogenic separation methods include membrane processes and pressure swing adsorption, both operated at ambient temperature.

Study objectives

Several goals are defined in this work.

- Design a process scheme based on literature research
- Determination of the required theoretical stages
- Enthalpy and material balance of system
- Calculation of the duty of the heat exchangers, expander, condenser/vaporiser
- Estimation of heat recuperation potential from hot compressed air

Air Separation Unit (ASU) description

Cryogenic separation method is based on different boiling points of mixture components. This method was invented by Carl von Linde and was first used in industry in the 20th century. Distillation columns used for the separation are placed in “cold boxes’’ where the temperature is very low. Thermodynamic minimal work of oxygen separation from air is equal to 53.1 kWh per ton of oxygen. In 2015, the most efficient ASU exceeded the minimum energy three times[12].

The designed scheme according to Figure 1 can be divided into three sections. The first section provides air compression and water removal. In this work, air is considered as a three-component mixture composed of nitrogen, oxygen, and water vapor. Due to the process layout, it has to be compressed to the pressure of 6 bar which is done by two-stage compression, with an intercooler and final cooler, both serving as partial condensers of water vapor at the same time. The rest of the water vapor is removed in an adsorber. Air leaving the adsorber is divided into two streams, in a ratio to be estimated.

Both streams enter the main heat exchanger, where they are pre-cooled by process effluents. One fraction of air proceeds through the expander, where it expands to the pressure of 1.5 bar and flows to the upper column. The second stream flows directly to the lower column.

The third section includes a separation column and a secondary heat exchanger. The column consists of a low-pressure column (LPC) which is the upper column, and a high-pressure column (HPC). Condenser of nitrogen vapors in HPC serves as the LPC reboiler. A part of the condensed nitrogen is used as a reflux for HPC. The main product is oxygen, obtained in the lower part of LPC. The secondary heat exchanger serves as a pre-cooler for streams that serve as refluxes for LPC.

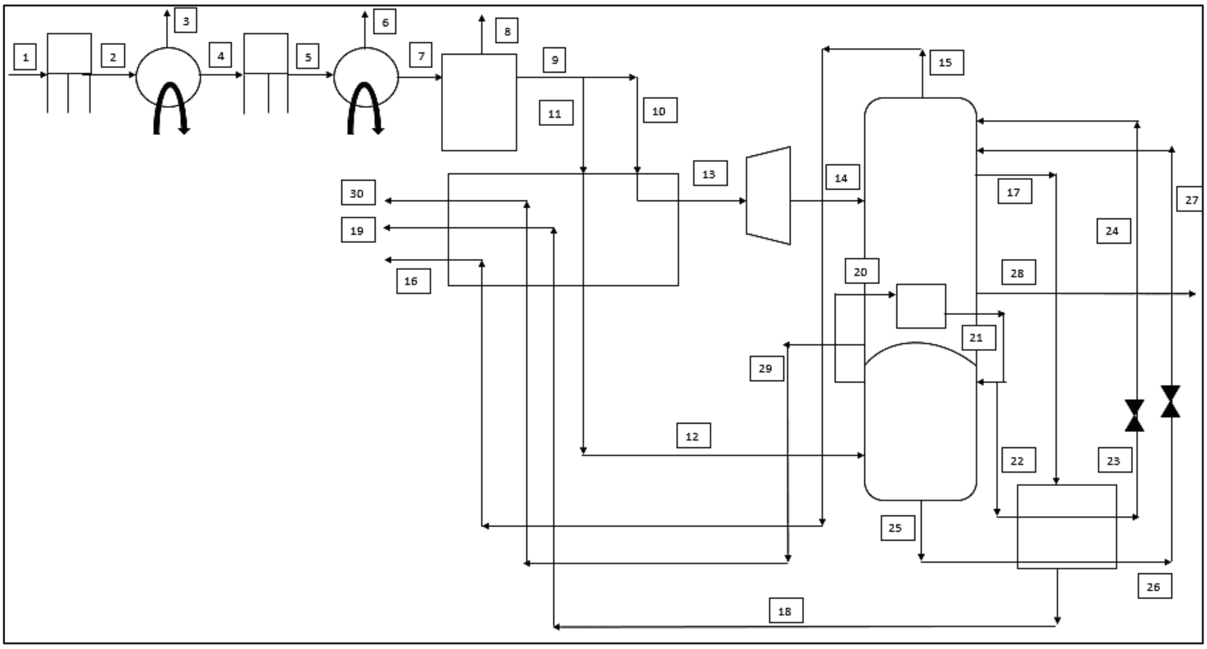

Figure 1. Designed scheme of cryogenic air separation

Model assumption and equations

Real equilibrium data are obtained by the Peng-Robinson thermodynamic model in AspenPlus software. Isobaric X-y equilibrium diagrams were constructed, and the number of theoretical stages required was determined using the McCabe-Thiele method[13].

The first section involving compression and removal of water vapor is calculated by a set of equations. Mass flow of dry air, $\dot{m}_G$, is calculated by equation (1)

$$\dot{m}_G = \frac{\dot{m}_1}{1+\overline{Y_1}} \tag{1}$$

where, $\dot{m}_1$ is the mass flow of air (kg.h^{-1}), and $\overline{Y_1}$ is the relative mass fraction of water vapor (kg.kg^{-1}). Since air is compressed by two-stage compression, it is necessary to estimate the optimal pressure ratio, β, employing equation (2)

$$\beta = \sqrt{\frac{P_{fin}}{P_0}} \tag{2}$$

where, P_0 is the initial pressure (Pa), and P_{fin} is the final pressure (Pa). Compressor power input is calculated by equation (3)

$$P_n = \frac{R\cdot T\cdot\left(\frac{\dot{m}_G}{M_G}+\frac{\dot{m}_G\cdot\bar{Y}}{M_{H_2O}}\right)\cdot\frac{n}{n-1}\cdot\left(\beta^{\frac{n-1}{n}}-1\right)}{\eta_c} \tag{3}$$

where, R is the molar gas constant (8.314 J.mol^{-1}.K^{-1}), T is temperature (K), M_G is the molar mass of dry gas (kg.mol^{-1}), M_{H_2O} is the molar mass of water (kg.mol^{-1}), n is the polytropic coefficient, and η_c is the overall compression efficiency.

Air cooling after compression carries away nearly all energy supplied by the compressor; thus, it would be beneficial to recover a part of it[10,14]. In this sense, heat recovery for hot water production is devised by means of installing an additional heat exchanger upstream of each water cooler. The water is heated from a temperature of 60 °C to 80 °C, it being assumed that this water temperature will ensure its year-round use. After the first heat exchanger air I assumed to cool down to 65 °C. The assumed pressure loss was 2 % of the air pressure at the inlet to the device. The reference state was chosen for the balance of the compression part: 0 °C, g, 100 kPa. The enthalpy balance of intercoolers in which water does not condense is as follows (4)

$$\dot{H}_{input} - \dot{H}_{outlet} = m_{\dot{H_2O}} \cdot c_p \cdot \Delta T \tag{4}$$

where $\dot{H}_{input}$ is the enthalpy flow of the stream entering the intercooler and $\dot{H}_{outlet}$ is the enthalpy flow of the stream leaving the intercooler, $m_{\dot{H_2O}}$ is the mass flow of cooling water, c_p is specific heat capacity and ΔT is the temperature difference at the outlet and inlet to the heat exchanger.

The enthalpy balance of intercoolers in which water does condense is provided by equation (5)

$$\dot{H}_{input} - \dot{H}_{outlet} - \dot{H}_{H_2O} = m_{\dot{H_2O}} \cdot c_p \cdot \Delta T \tag{5}$$

where $\dot{H}_{input}$ is the enthalpy flow of the stream entering the intercooler and $\dot{H}_{outlet}$ is the enthalpy flow of the stream leaving the intercooler and $\dot{H}_{H_2O}$ is the enthalpy flow of the condensed water.

The heat exchanger parameters in which heat is recovered were calculated for the summer period. It has been considered that the cold medium, the water, flows in the tubes. For the hot medium, a forced flow was assumed when bypassing the bundle of tubes arranged one behind the other in a direction perpendicular to the axis of the tubes in the inter-tube space of the heat exchanger without compartments.

The price of a new heat exchanger C_E is calculated according to the equation (6)

$$C_E = C_B \cdot \left(\frac{K}{K_B}\right)^M \cdot CEPCI_{HX} \cdot \frac{€}{\$} \tag{6}$$

where C_B is the price of the basic heat exchanger in the reference year, K_B basic capacity, K is the capacity of the new heat exchanger, $CEPCI_{HX}$ is the ratio of the values of the CEPCI (The Chemical Engineering Plant Cost Index) indices in year X and in the reference year[13].

The total investment costs of C_F are calculated according to the equation (7)

$$C_F = C_E \cdot \left(f_M \cdot f_T \cdot f_P \cdot (1 + f_{PIP})\right) + C_E \cdot (f_{ER} + f_{INST} + f_{ELEC} + f_{UTIL} + f_{OS} + + f_{BUILD} + f_{SP} + f_{DEC} + \\ + f_{CONT} + f_{WC}) \tag{7}$$

where f_M is material factor, f_P is pressure factor, f_T is temperature factor, f_{PIP} is piping factor, f_{ER} is equipment erection factor, f_{INST} is instrumentation factor, f_{ELEC} is electrical factor, f_{UTIL} is utilities factor, f_{OS} is off-sites factor, f_{BUILD} is buildings factor, f_{SP} is site preparation factor, f_{DEC} is design and engineering factor, f_{CONT} is contingency factor, f_{WC} is working capital factor. All these factors were considered because this part of factory is to be built on ''green field''.

Model results and discussion

In this work, mass flow of air entering the first compressor of 30 t.h^{-1} is considered, with the inlet temperature of 300.15 K and the assumed mass fraction of water vapor of 0.01711. The McCabe-Thiele method helps to determine the number of theoretical stages for each part of the column. For HPC it is 4 stages and for LPC it is 6 stages. The calculated mass flow of condensed water vapor (kg.h^{-1}) in each condenser and adsorber is summarized in Table I. It is assumed that air leaving the adsorber is dry. Material balance is summarized in Table II.

Mass flow of produced oxygen gas, $\dot{O}$, is 5,760 kg.h^{-1} with the purity of 95 %. Stream $\dot{N}$ is almost pure nitrogen, which can also be used as inert gas if ASU is integrated in a refinery, or it can be supplied to other consumers.

The power input of both compressors is approximately the same and reaches 953 kW per item. This leads to specific power consumption for oxygen production of over 325 kWh per ton of oxygen. In a similar study[11], 22.58

MW electric energy are consumed to drive the compressors of a cryogenic air separation unit which produces 68.48 t/h oxygen. This yields specific power consumption of 330 kWh per ton of oxygen. Another study[15], employing a much more integrated plant design, arrived at a value of 229 kWh per ton of oxygen, while pointing out possibilities for further improvement. We can thus conclude that the results of our calculations match well with those published in reference literature but at the same time it is obvious that there is still a substantial potential for oxygen production process efficiency increase.

Table I

Balance of water vapor in the studied process

Mass flow $\dot{m}$ (kg.h^{-1})	*Humidity $\bar{Y}$ (kg.kg^{-1})*
$\dot{m}_3$ = 181.3	$\overline{Y_1}$ = 0.01711
$\dot{m}_6$ = 192.7	$\overline{Y_4^{eq}}$ = 0.01096
$\dot{m}_8$ = 130.7	$\overline{Y_7^{eq}}$ = 4.43 x 10^{-3}

Table II

Material balance of the studied process

Stream Nr.	*Mass flow $\dot{m}$ (kg.h^{-1})*	*Stream Nr.*	*Mass flow $\dot{m}$ (kg.h^{-1})*
10, 13, 14	8,998	22, 23, 24	10,020
11, 12	20,497	25, 26, 27	10,477
15, 16 ($\dot{N}$)	20,690	28 ($\dot{O}$)	105
17, 18, 19 ($\dot{N}$)	2,940	29, 30 ($\dot{O}$)	5,760
20, 21	21,196	31	11,176

Duties of individual heat exchangers and the separation column were also calculated using the enthalpy balance. The duty of the secondary heat exchanger is 159 kW while that of the main heat exchanger is 1,824 kW and that of combined condenser/vaporizer is 994 kW. The amount of work produced in the expander is 45 kW. This work can be used in compressors, and thus net power consumption of compressors will lower to the value 316 KWh per ton of oxygen. The calculated reflux ratio, based on the material and enthalpy balance, is 1.1154.

The total amount of heat recovered for the summer period, 6 months, is 13,548 GJ, which at a heat price of 6 €/GJ, represents a saving of 81.3 thousand €. After deducting the cost of additional electricity consumed, the total savings for the summer period is 64.9 thousand €. The total amount of heat recovered for the winter period, and thus 6 months, is 6,198 GJ, which represents a cost saving of € 37.2 thousand. After deducting the cost of additional electricity consumed, the total savings for the winter period is 22 thousand €. The total expected annual saving is 86.9 thousand €.

Based on the assumed heat exchanger, the overall heat transfer coefficient will be in the range from 60 to 200 W.m^{-2}.K. The price of the heat exchanger was calculated for two limit values of this range. The results of the calculations can be found in Table III.

Table III

Economic analysis

Overall heat transfer coefficient U related to the surface area of the tubes (W.m^{-2}.K)	*Surface area of the tubes A (m$^{2)}$*	*Main equipment cost C_E (€)*	*Total investment cost estimate C_F (€)*	*Simple payback period*
60	460	177 thousand	974 thousand	13.2 year
200	138	78.1 thousand	429 thousand	5.8 year

Conclusion

Based on the literature survey and process material and heat balances, a cryogenic air separation unit was designed, yielding 5,760 kg.h^{-1} of oxygen gas with the purity of 95 % vol. The mass ratio of streams 10 and 11 of 0.439. A literature search found that for operations of approximately the same size, this ratio was 0.14.

It was demonstrated that the mixture of oxygen and nitrogen does not behave as an ideal mixture; therefore, its modeling as a real mixture was necessary. Using the McCabe-Thiele method for both ideal and real mixture, the theoretical number of stages in HPC and LPC was estimated.

Since the amount of supplied air is 30 t.h^{-1}, which has to be compressed from 1 bar to 6 bar, two-stage compression was assumed with the calculated power input of both compressor stages being approximately the same, 953 kW. The power input of compressors is too high compared with the most efficient air separation units operated nowadays, so further optimization is needed. This is one of the long-term goals. Enthalpy balance of the separation column and heat exchangers provided their heat duties as 159; 1,824; 994 and 45 kW for the secondary heat exchanger, the main heat exchanger, the combined condenser/vaporizer and the expander, respectively.

The expected total heat recovery from hot compressed air to hot water is 19,746 GJ per year, which represent savings about 118.5 thousand €. Annual electricity costs will increase by 31.6 thousand €. The achievable net annual savings is therefore 86.9 thousand €. The prize of the additional heat exchanger was calculated for the two limit values of overall heat transfer coefficient. For the lowest value, the total investment is 974 thousand € and for the highest 429 thousand €. The simple playback period for the first one is 13.2 year and for the second one it is 5.8 year. It can be concluded that, under circumstances, heat recovery by hot water production can be a feasible means of operation expenses reduction.

Acknowledgement

This research was supported by the Slovak Research and Development Agency under the contract Nr. APVV-18-0134.

References

1. Baukal, E. C. Oxygen Enhanced Combustion, second edition. CRC Press (2013).
2. Dzurňák R., Jablonský G., Varga A., Kizek J., Pástor, M., Lukáč L.: MATEC Web Conf. *168*, 07016 (2018).
3. Shah I.A., Gou X., Wu J.: Energies *12*, 1949 (2019).
4. Hendershot R.J., Lebrecht T.D., Easterbrook N.C.: Chem. Eng. Prog. *106*, 57 (2010).
5. Dzurňák R., Kizek J., Jablonský G.: AIP Conf. Proc. *1889*, 020007 (2017).
6. Gripenberg H., Johansson A., Torvanger K.: *Six years experience from low-temperature oxyfuel in primary and re-melting aluminium cast houses.* In: Suarez C.E. (eds) Light Metals. Springer, Cham (2012).
7. Yeromin A., Yeromina O., Lukáč L., Kizek J., Dzurňák R.: Acta Montan. Slovaca *23*, 175 (2018).
8. Nemitallah M.A., Abdelhafez A.A., Ali A., Mansir I., Habib M.A.: Int. J. Energy Res. *43*, 7790 (2019).
9. Tan Y., Douglas M.A., Thambimuthu K.V.: Fuel *81*, 1007 (2002).
10. van der Ham L.V., Kjelstrup S.: Energy *35*, 4731 (2010).
11. Ebrahimi A., Meratizaman M., Reyhani H.A., Pourali O., Amidpour M.: Energy *90*, 1298 (2015).
12. Banaszkiewicz T., Chorowski M., Gizicki W.: AIP Conf. Proc. *1573*, 1373 (2013).
13. Perry H.R.: *Perry's chemical engineers´ handbook.* McGraw-Hill, Kansas (1997).
14. Smith A.R., Klosek J.: Fuel Process. Technol. *70*, 115 (2001).
15. Fu, Ch., Gudersen, T.: Energy 44, 60 (2012).

ALTERNATIVE USAGE OF MSCR TEST FOR EVALUATION OF TYPE AND CONTENT OF THE USED POLYMER

Jíša P.[1], Černý R.[1]

[1]*ORLEN UniCRE a.s., Department of Development and Innovation, Areál Chempark, 436 70 Litvínov – Záluží 1, Czech Republic*
petr.jisa@orlenunicre.cz, radek.cerny@orlenunicre.cz

Abstract

MSCR test is frequently used as a part of system SUPERPAVE+ to assess bitumen resistance to rutting. The test is designed for evaluation of temporary and permanent deformation during repeated cycles of stress loading and recovery. From the standard evaluation, recovery and non-recoverable compliance are calculated to obtain the supplemental classification of the evaluated bitumen. However, there are alternative approaches for evaluation of MSCR results that may extend the information which is gained from the standard evaluation. In our work, we deal with evaluation of MSCR results using the Burgers viscoelastic model. For samples of bitumen with different composition the Burgers model is applied on MSCR results. The obtained model parameters are analysed in relation to the type and content of polymers that were used for modification.

Introduction

MSCR test as a part of system SUPERPAVE+ is designed for evaluation of temporary and permanent deformation during repeated cycles of stress loading and recovery. The results of MSCR test indicate the bitumen resistance to permanent deformation, which is significantly influenced by polymer modification[1,2].

The MSCR test is very sensitive to the presence of the polymers in the tested bituminous binder, and it enables effortless and comfortable distinguishing between neat binders (without polymers) and modified binders. However, there is not such a good alternative to distinguish simultaneously between polymer types and polymer contents used for bitumen modification, using only the results of the test. Although, it is possible to obtain this information from gel permeation chromatography[3] it means performing additional analyses. In laboratories for bitumen evaluation the equipment for gel chromatography is not available as widely as the commonly used rheological instruments. Therefore, it would be suitable to obtain the information regarding the polymer type and content directly from the data that are got from the MSCR test.

One of the possibilities can be application of the rheological models on the data from MSCR test. Among the rheological models, Burgers model was considered as suitable in the previous studies[4]. The application of the model equations on the data from MSCR test was described using the constitutive equations for the creep and recovery phase[5].

In this paper we deal with usage of Burgers model for evaluation of MSCR data that were obtained from evaluation of bituminous binders containing linear SBS, radial SBS and reactive terpolymer. For each of the polymers, bituminous binder with low and high content was prepared to evaluate the influence of the polymer content on the parameters of Burgers model if it is used for modelling the data from MSCR. It was found out that especially the elastic and viscous modulus from Maxwell elements of the Burgers model are sensitive to both the type and content of the used polymer and appear to be suitable for the distinguishing purpose.

Materials and methods

For our study, different bituminous binders were used containing various polymers in particular dosage. The overview of the samples is in the Table I. The base bitumen, which has acronym REF, was semi-blown bitumen 50/70 without polymer modification. For each polymer modifier there were 2 concentrations of polymer representing low and high degree of modification. The samples of SBS modified bitumen contained 1 wt % and 5 wt % of linear or radial SBS. The bituminous binders containing 0.5 wt % and 2.5 wt % of reactive terpolymer were included into the study too.

Table I
Materials used

Acronym	Polymer content [wt %]	Characteristics
REF	0	Base bitumen
1% SBSL	1	Linear SBS
5% SBSL	5	Linear SBS
1% SBSR	1	Radial SBS
5% SBSR	5	Radial SBS
0.5 % RET	0.5	Reactive terpolymer
2.5 % RET	2.5	Reactive terpolymer

The work is based on the usage of the Burgers model. This model is a rheological construction in which the deformation behaviour of the tested material is modelled as a series of the two basic rheological elements – Maxwell element and Kelvin-Voigt element. The scheme of the model construction is in the Figure 1. The Maxwell element consists of the elastic and viscous element (E_M and $η_M$) which are connected in series. The whole Maxwell model is in serial connection with the Kelvin-Voigt element that consists of the viscous ($η_K$) and elastic (E_K) sub-elements connected in parallel.

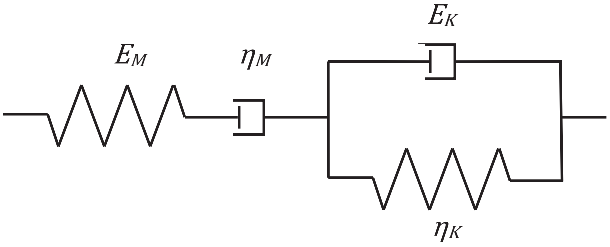

Figure 1. Scheme of the Burgers model η

Mathematical expression of Burgers model is derived from the scheme in the Figure 1 and expressed by the equation (1). The overall material deformation is expressed as a sum of elastic deformation, viscous deformation and viscoelastic (delayed) deformation, which are expressed by equation (1).

$$\varepsilon(t) = \varepsilon_e + \varepsilon_v + \varepsilon_d = \frac{\sigma}{E_M} + \frac{\int \sigma dt + C_1}{\eta_M} + \left(\frac{1}{\eta_K} \int \sigma e^{\frac{E_K}{\eta_K}} dt + C_2 \right) e^{-\frac{E_K}{\eta_K}} \tag{1}$$

where

ε_e	Elastic deformation	[-]
ε_v	Viscous deformation	[-]
ε_d	Viscoelastic (delayed) deformation	[-]
σ	Shear stress	[Pa]
E_M	Elastic modulus of Maxwell element	[Pa]
η_M	Viscous modulus of Maxwell element	[Pa.s]
E_K	Elastic modulus of Kelvin-Voight element	[Pa]
η_K	Viscous modulus of Kelvin-Voight element	[Pa.s]
t	Time	[s]

Then, constitutive equations can be derived for the stages of creep and recovery using the basic equation (1). During the creep phase the sample undergoes to all types of deformations – elastic, viscous, and viscoelastic. The overall deformation is a sum of these particular deformations. During this phase there is a non-zero shear stress applied on the tested material. The creep phase occurs in time which is lower than the time t_1 that represents the time when the creep phase ends, and the recovery phase begins. The constitutive equation (2) expresses the deformation behaviour of the tested material during the creep phase:

$$\varepsilon(t) = \varepsilon_e + \varepsilon_v + \varepsilon_d = \frac{\sigma_0}{E_M} + \frac{\sigma_0 t}{\eta_M} + \frac{\sigma_0}{E_K}\left(1 - e^{-\frac{E_K}{\eta_K}t}\right), t < t_1 \tag{2}$$

During the creep phase the overall deformation from the creep phase lowers due to the absence of the sheer stress. The elastic deformation is completely removed at the beginning of this phase. The viscous deformation is the deformation that remains after reaching the steady state which is approximated by the 9 seconds of recovery in the MSCR test. The elastic deformation decreases continuously during the recovery phase. The constitutive equation (3) describes the deformation behaviour of the tested material during the recovery phase:

$$\varepsilon(t) = \varepsilon_v + \varepsilon_d = \frac{\sigma_0 t_1}{\eta_M} + \frac{\sigma_0}{E_K}\left(1 - e^{-\frac{E_K}{\eta_K}t_1}\right) e^{-\frac{E_K}{\eta_K}(t-t_1)}, t \geq t_1 \tag{3}$$

The particular deformations in the constitutive equations (2) and (3) – and thus also the overall deformation in the equation – are functions of stress and time while the elastic and viscous moduli are parameters of these equations that may be found by regression of the data from creep and recovery tests.

The Burgers model constitutive equations (2) and (3) were applied on the data from MSCR tests that were carried out for the above mentioned bituminous binders at 50 °C. The elastic and viscous elements of the Maxwell and Kelvin-Voigt elements from the model were put into relation with the type and content of the added polymer.

Results and discussion

Figure 2 shows the values of elastic modulus from Kelvin-Voigt element of the Burgers model (E_K) and Figure 3 depicts the values of viscous modulus from Kelvin-Voigt element of the Burgers model (η_K) depending on the type and content of the polymer. In principle, both of the moduli from Kelvin-Voigt element of the model have similar response to the stress level during the creep phase (σ) as well as to the polymer type and content. Both of these parameters are stress sensitive – they reach higher values at σ = 3200 Pa compared to the values at σ = 100 Pa. On the other hand, at higher content of polymers (5 % SBS or 2.5 % RET) the stress sensitivity is partially supressed – while for 5 % SBSL and 5 % SBSR the stress sensitivity persists - but it is significantly lower and at 2.5 % RET it is even negligible. On the other hand, there is not a reliable response to the polymer content – there is only a significant increase in case of high contents of SBS (5 % SBSL and 5 % SBSR). These parameters can indicate only the presence of the high polymer contents, and the indication is according to the loss of their stress sensitivity. The absolute values of E_K and η_K are not useful in this purpose because they react only to high contents of SBS. When RET is used for modification there is even a decrease of these parameters with the increasing content of polymer.

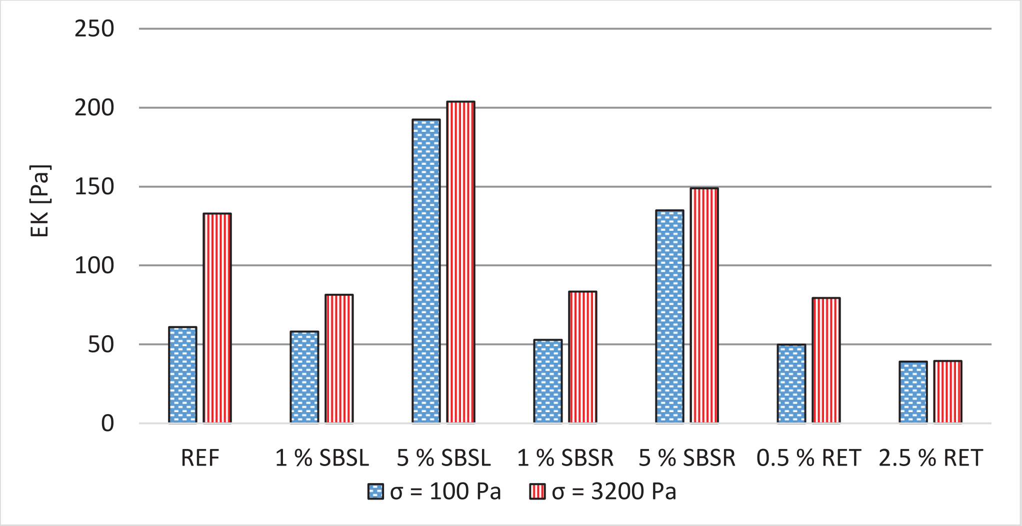

Figure 2. Elastic modulus from Kelvin-Voigt element of the Burgers model

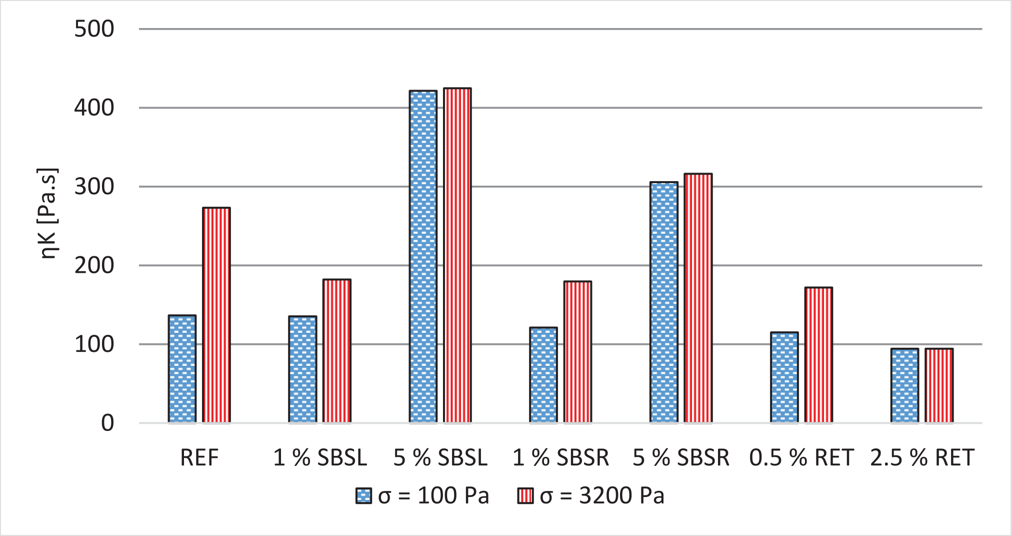

Figure 3. Viscous modulus from Kelvin-Voight element of the Burgers model

The values of elastic modulus from Maxwell element of the Burgers model (E_M) is illustrated in the Figure 4. For this parameter there is no significant stress sensitivity as it was in the case of elastic modulus from the Kelvin-Voigt element. Furthermore, strong impact of the type and content of the used polymers on E_M values was observed. This parameter decreases with increasing polymer content and the dependency is specific according to the polymer type. In case of bitumen containing reactive terpolymer (RET) there is a steepest decrease of E_M with increasing polymer content while for bitumen containing radial type of SBS (SBSR) the decrease of E_M with increasing polymer content gets less steep and for the bitumen with linear type of SBS (SBSR) there is even slower decrease of this parameter with increasing polymer content compared to SBSR and RET.

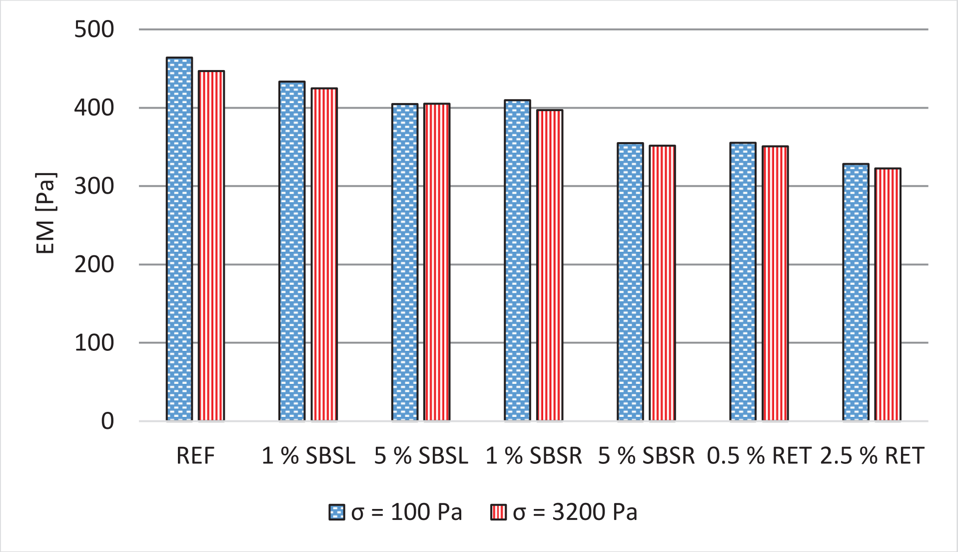

Figure 4. Elastic modulus from Maxwell element of the Burgers model

The values of viscous modulus from Maxwell element of the Burgers model (η_M) are presented in the Figure 5. Similarly to the elastic modulus from Maxwell element of the Burgers model (E_M), η_M is sensitive both to the content and type of the used polymer. With increasing polymer content η_M increases and the steepest increase was found for the linear type of SBS (SBSL) followed by the radial type of SBS (SBSR) and reactive terpolymer (RET).

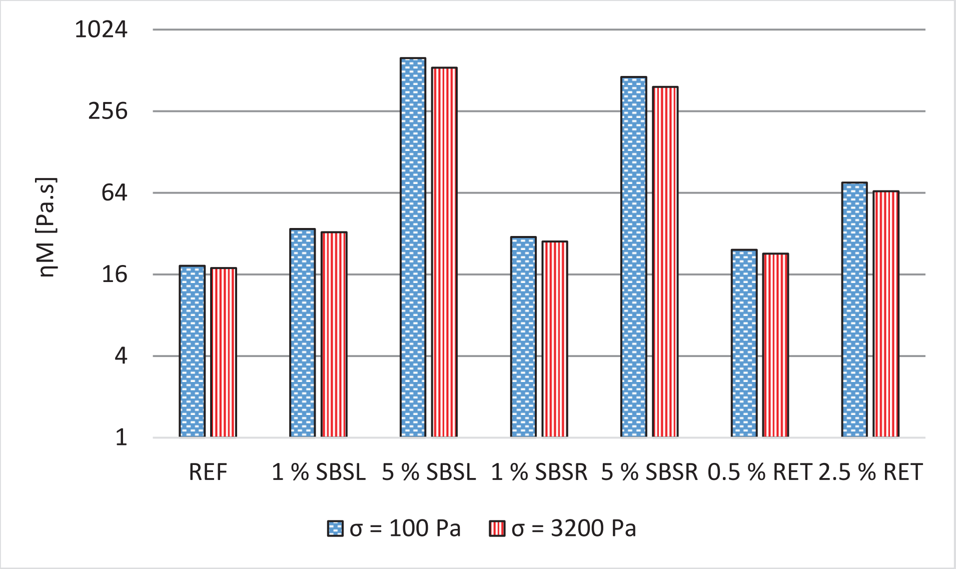

Figure 5. Viscous modulus from Maxwell element of the Burgers model

The dependency of parameters from Maxwell element of the Burgers model on the type and content of the polymer which is present in the given bituminous binder may be modelled by a suitable logarithmic regression. The dependency of elastic modulus from Maxwell element of the Burgers model (E_M) on the polymer type and content for bitumen which was used as base binder for the modification (REF) can be expressed by equation (4) where a, b, c, and d are regression coefficients that can be found by the method of least squares. The values of the regression coefficients for given type of polymer are in Table II.

$$E_M = a \cdot ln(b \cdot x + c) + d \tag{4}$$

Table II
Regression coefficients in equation 4 for the used polymers

Coefficient	SBSL	SBSR	RET
a	-13.7	-31.5	-44.3
b	21.4	22.6	32.0
c	5.3	5.8	3.8
d	469.8	502.2	502.5

Figure 6 shows the results of modelling the dependency of E_M on the polymer content for SBSL, SBSR and RET by equation 4 with coefficients from Table II in a graphical form. It is obvious that there is a different dependency for each type of polymer and therefore this model could enable distinguishing between the types of polymers, as well as prediction of the E_M in dependency on the polymer content.

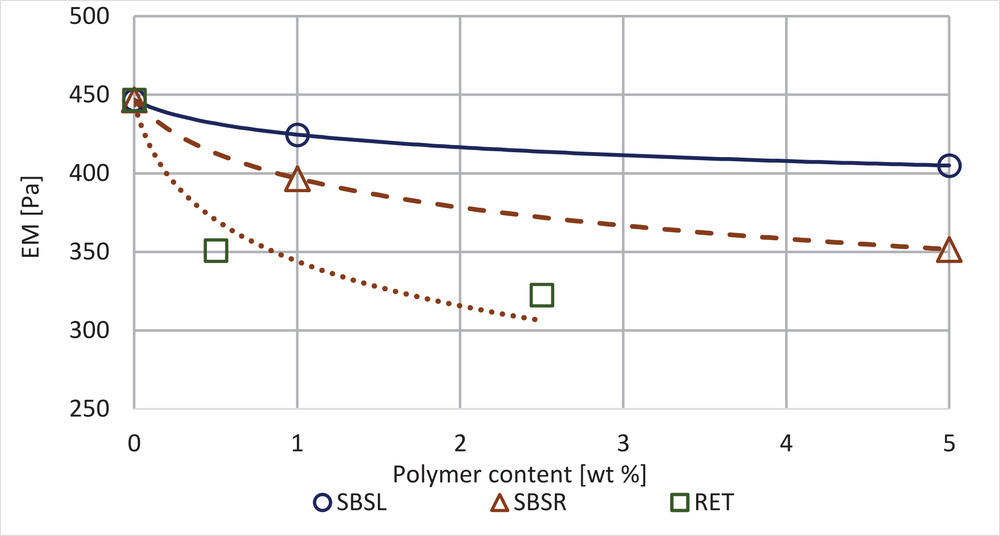

Figure 6. Dependency of elastic modulus of Maxwell element from Burgers model on the polymer type and content in the bituminous binder

Conclusions

Different bituminous binders were prepared containing linear SBS, radial SBS and reactive terpolymer, and all of them in low and high dosage. For the prepared binders MSCR test was carried out at 50 °C and the data from the tests were interpolated by the constitutive equations of the Burgers model for the creep and recovery phase of the test. As a result, the values of the model constants which are viscous and elastic moduli from the Maxwell and Kelvin-Voight element were put into relation to the type and content of the polymers which were used for the bitumen modification.

The viscous and elastic modulus from the Kelvin-Voigt model (E_K, η_K) showed a stress sensitivity (difference between the obtained values at the lower stress level 100 Pa and higher stress level 3200 Pa) which was supressed by higher polymers content. On the other hand, there was not a consistent response of these parameters on the polymers content. Only high contents of linear and radial SBS caused a significant increase of both parameters but they decreased with increasing content of reactive terpolymer. Thus, the parameters E_K and η_K appear to be only suitable for detection of high contents of polymers by the partial loss of the stress sensitivity.

The viscous and elastic modulus from the Maxwell model (E_M, η_M) showed higher potential for distinguishing between polymers type and content in bituminous binders. The stress sensitivity of these parameters was not significant while the influence of polymer content on them was obvious and it was even different according to the polymer type. An empirical logarithmic model was designed to describe the influence of the polymer content on the elastic modulus E_M for the used base binder and for the three different polymers as a demonstration of a possibility to create an apparatus for distinguishing between different polymers in bituminous binders based on application of Burgers model on the results from standard MSCR test.

Acknowledgement

The publication is a result of the project which was carried out within the financial support of the Ministry of Industry and Trade of the Czech Republic with institutional support for long-term conceptual development of research organisation.

References

1. Saboo, N., Kumar, R., Kumar, P., & Gupta, A. (2018). Ranking the rheological response of SBS-and EVA-modified bitumen using MSCR and LAS tests. Journal of Materials in Civil Engineering, 30(8), 04018165.
2. White, G. (2017). Grading highly modified binders by multiple stress creep recovery. *Road Materials and Pavement Design*, *18*(6), 1322-1337.
3. Ma, J., Sun, G., Sun, D., Yu, F., Hu, M., & Lu, T. (2021). Application of gel permeation chromatography technology in asphalt materials: A review. *Construction and Building Materials*, *278*, 122386.

4. Alisov, A., Hagner, T., & Walther, A. (2016). Quantification of polymer content in binder by modified MSCR-test. In Sixth Eurasphalt and Eurobitume Congress, Proceedings, Prague (Vol. 4)
5. Liu, Y., You, Z. (2009). Determining burger's model parameters of asphalt materials using creep-recovery testing data. In Pavements and materials: Modeling, Testing, and performance (pp. 26-36).

COMPATIBILITY OF MARINE FUELS CONTAINING ALTERNATIVE MATERIALS

Schlehöfer D.[1], Vráblík A.[1]

[1]*ORLEN UniCRE a. s., Department of Development and Innovation, Areál Chempark, 436 70 Litvínov – Záluží 1, Czech Republic*
dominik.schlehofer@orlenunicre.cz, ales.vrablik@orlenunicre.cz

Abstract

Following the implementation of IMO 2020, problems with the incompatibility of blended low-sulfur fuels were found. These problems can lead to technological troubles during transport or storage and finally during the combustion of fuel in marine engines. The new implementation of IMO 2020 brought a drastic reduction of sulfur content in marine fuels on the deep seas from 3.5 to 0.5 wt%. The goal of this work was to investigate the compatibility of individual conventional and alternative materials. The first step included verifying the compatibility by spot tests and microscopic analysis before and after long-term storage as well as prediction of suitable mixtures from available conventional and alternative materials. In the second step the preparation of marine fuels from the compatible blends meeting the quality parameters of ISO 8217, was done. The third step was focused on finding suitable ratios of the conventional and alternative materials to produce marine fuels complying ISO 8217 standard and parameters connected with the implementation of IMO 2020.

Introduction

Marine vessel owners and marine fuel producers have had to deal with stricter limits for the maximum sulfur content of marine fuels according to the IMO 2020 implementation from 1.1.2020. The drastic reduction in the sulfur content from 3.5 to 0.5 % by weight[1]. It also created a problem in the compatibility of new low-sulfur marine fuels[2].

Incompatibilities may occur during the blending of high-sulfur and low-sulfur marine fuels or generally when two or more streams of different origin are blended. The considerations ISO / PAS 23263[3] has been issued as supplementary material to the ISO 8217[4] based on new IMO rules. This document provides the guidance for fuel suppliers and users on the quality of new produced low-sulfur marine fuels. The compatibility and subsequent stability of the produced low-sulfur marine fuels can be monitored in addition to ISO 8217 by other complementary methods. These methods include, for example, S-Value, P-value or P-ratio[5]. However, it is necessary to be equipped by very expensive and specific devices to determine these parameters[6]. The big disadvantage of the mentioned methods is their single-purpose use without further alternative applications.

For these reasons, the possibility of using alternative raw materials together with quick and simple methods for assessing the undesirable incompatibilities should be considered. The goal of this study was to use the commonly available laboratory methods in the determination of compatibility for laboratory prepared mixtures of standard and alternative streams. Available alternative raw materials were characterized according to ISO 8217 for residual fractions. Based on the results, limiting parameters were revealed (sulfur content, density at 15 °C). The spot test according to ASTM D 4740 and alternative microscope method[7, 8] were applied as simple and quick screening tests of compatibility before and after storage. Based on the results, suitable mixtures were selected. Appropriate ratios were proposed for these mixtures, and they were subsequently characterized again by the above-mentioned methods. The aim was to prepare the mixtures of starting materials that would meet the quality properties according to the ISO 8217 standard and at the same time meet the new conditions set by the IMO 2020 implementation.

Experimental

The long-term stability of selected blends was assessed as well. Before and after storage (30 days, 25 °C in dark), the spot test and microscope analysis were performed. The obtained results of aged samples were compared with the original ones. Subsequently, the unstable blends were identified and excluded. The compatible blends were analysed according to ISO 8217. The simple prediction model for estimating the suitable marine fuel blends was proposed. Based on this prediction, it was possible to determine a suitable ratio for mixing compatible alternative materials with materials of petroleum origin. The advantage of this solution is the use of common laboratory equipment for determining the density and sulfur content, which are available in both operational and research laboratories. At the same time, to evaluate or predict blends compatibility the spot tests requiring only filter paper and a special drying pad was used. To observe the morphology of the samples and thus reveal possible incompatibilities of the prepared mixtures a microscope evaluation was also done.

Materials and methods

The three types of standard heavy fuel were used for comparison. The marine fuel classified as the high sulfur fuel oil (FO), Steam Cracking Heating Oil (SCHO), and Slurry Oil (SLO) obtained from a fluid catalytic cracking (FCC) were selected for this purpose. The available alternative components were pyrolysis oils from the pyrolysis of waste tires (TPO) and from the depolymerization of plastics (PPO). The second type of alternative materials were materials of plant and animal origin. They were used cooking oil (UCO) which was subjected to basic filtration during its collection only, and animal fat (AF) obtained by processing remains of dead animals.

All used materials were evaluated according to the ISO 8217 standard and new requirements given by the IMO 2020 implementation (0.5 wt% for the deep seas). Density at 15 ° C was determined by the oscillating method on a digital densitometer DA 645 Kyoto Electronics according to the internal procedure PP-LP-322/2 based on ASTM D 4052-18a[9]. Sulfur content was measured on an XOS Sindie + Cl Sulfur and Chlorine instrument according to ASTM D 4294[10]. Images of the morphology of individual samples were taken with a Leica DM2500 LED microscope at 10x magnification (100 µm scale). The drop test was performed according to ASTM D 4740[11].

The most important required parameters, sulfur content and density at 15 °C, were assessed for all the materials (Table I).

The highest sulfur content among the conventional materials was for FO with a value of 2.70 wt%. Among the alternative components, it was, as expected, a TPO with a value of 1.00 wt%. due to the vulcanization process during the production of tires.

Table I

Selected properties of input materials

	FO	SCHO	SLO	TPO	PPO	UCO	AF
Density at 15 °C [kg/m^3]	1004	1110	899	938	1040	920	917
Sulfur [wt%]	2.70	0.06	0.97	1.00	0.04	0.00	0.02

Results and discussion

The following overview (Table II) shows the individual mixtures of conventional materials and alternative components in the mass ratio of 1:1 including the resulting spot tests and microscope images. At the same time there are the results before and after the storage simulation in the columns. The spot tests are further classified into one of five classification classes according to the relevant ASTM D 4740 standard, where class 1 and 2 are marked as compatible, class 3 could cause sludge excretion problems during transport and storage and class 4 and 5 are marked as incompatible mixtures.

Table II

Summary of the result of spot tests in comparison with microscope images before and after the storage simulation

Mixtures in a ratio 1: 1	Before storage		After storage	
	Spot tests	Microscope images	Spot tests	Microscope images
FO+AF	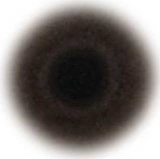 5	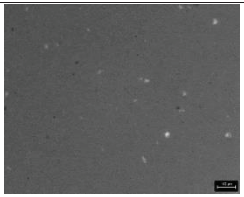	 5	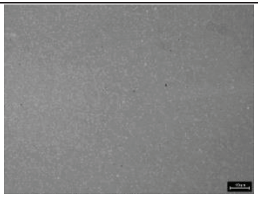
FO+UCO	 5	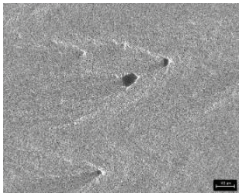	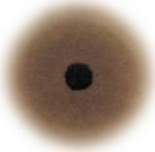 5	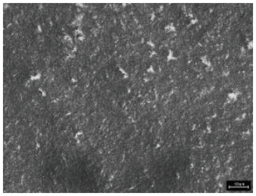
FO+PPO	 5	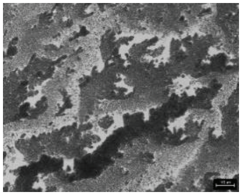	 5	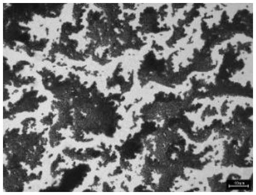
FO+TPO	 1	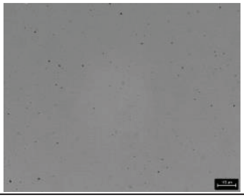	 2	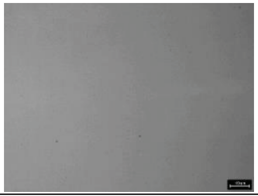
SCHO+AF	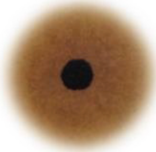 5	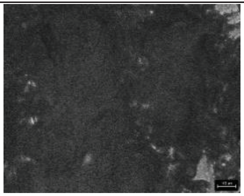	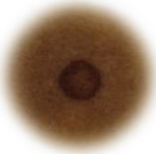 3	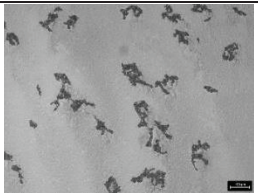
SCHO+UCO	 5	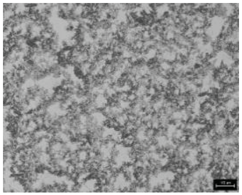	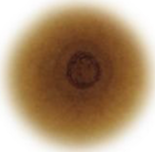 3	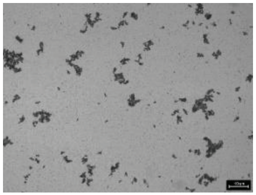
SCHO+PPO	 2	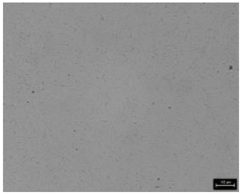	 2	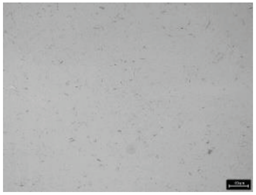
SCHO+TPO	 1	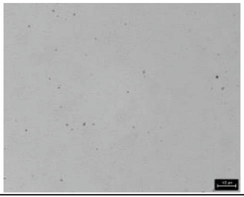	 1	

Mixtures in a ratio 1: 1	Before storage		After storage	
	Spot tests	Microscope images	Spot tests	Microscope images
SLO+AF	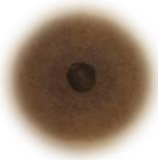 4	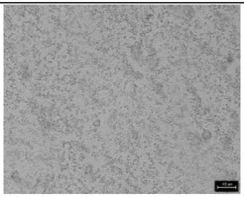	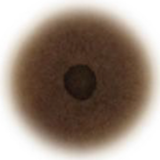 4	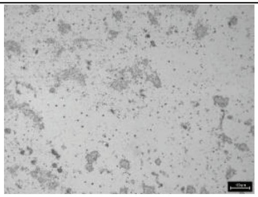
SLO+UCO	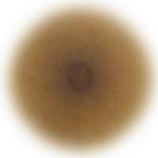 3		 5	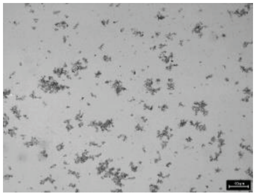
SLO+PPO	 2	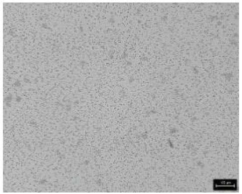	 2	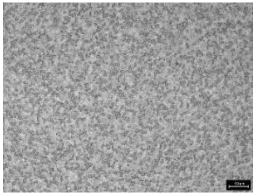
SLO+TPO	 2	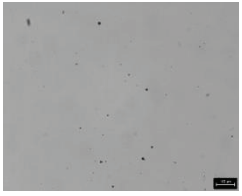	 2	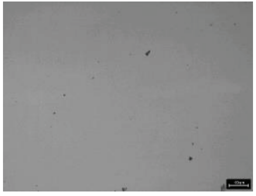

The mixtures prepared by using the alternative components AF and UCO showed considerable incompatibility with all the three conventional materials and the results of spot tests were evaluated as class 5 according to the relevant standard. The images from the microscope supported these results and clusters and signs of the formation of clusters of asphaltenic and mechanical impurities, or a solid layer of one huge sludge were observed. PPO proved to be incompatible as an alternative component in combination with FO, but in a mixture with SCHO and SLO, the tests were evaluated as class 2 and microscopic images were also without signs of incompatibility of these materials. The best results were recorded between all three conventional materials and the alternative component TPO, which in all cases was included into the first and second class of spot test classification before and after storage simulation, and microscope images comprehensively supported these results.

From these results it is clear that the alternative method in the form of visual observation of samples and their morphology is very beneficial. It is very useful in observing the compatibility of prepared mixtures and agrees with the results obtained by the standardized spot test method.

The last phase of the work was focused on the evaluation of the prepared mixtures in suitable weight ratios of conventional materials and alternative components, based on the results of the initial screening. The aim was to comply with all the limiting parameters given by the ISO 8217 standard and thus try to meet all the quality parameters for residual marine fuels. Thanks to the initial screening, it was possible to calculate suitable weight ratios, taking into account especially the density at 15 °C.

The resulting values of the analyses of the individual parameters are then determined by analytical methods, as stated in ISO 8217 standard. The calculation only served to determine the appropriate ratio to avoid unnecessary consumption of a limited amount of starting materials.

Thanks to this calculation, it was also revealed that the mixture SCHO + PPO was not possible to prepare, resp. the mixture would not meet the maximum permitted density value for residual marine fuels, which is 1010 kg/m^3 at 15 °C. The SCHO has a density value 1110 kg/m^3 at 15 °C and PPO 1040 kg/m^3. Therefore, it is clear that for these two samples it is not possible to prepare a mixture in such a proportion that the limits given by ISO 8217 are met. In result, the mixture of these two samples was not prepared.

For FO + TPO samples, it has been shown that they are miscible in any ratio. Nevertheless, the preparation of this mixture did not take place because the sulfur content newly introduced in the IMO 2020 implementation was not met. The other parameters prescribed by the standard were met. The sulfur content could not be reduced below the value of 1.00 wt%, measured in TPO. It could be remarked, the reduction of SOx emissions in the flue gas could be solved directly on board the ship, by installing adequate desulphurisation equipment. Alternatively, by mixing the alternative components themselves with a lower sulfur content than TPO with each other.

In the following table (Tab. III) there are listed the individual mixtures of conventional materials and alternative components, including the prepared ratio.

Table III

Characterization of the resulting ratios

	SCHO+TPO	**SLO+PPO**	**SLO+TPO**
Ratio [wt%]	40:60	30:70	30:70
Density at 15 °C [kg/m^3]	1007	997	926
Sulfur [wt%]	0.62	0.32	0.99

Samples of SCHO + TPO and SLO + PPO mixtures have higher values of total sulfur content than the limit of 0.50 wt%. Other monitored parameters meet the ISO 8217 standard. The SLO + PPO sample comply with all the parameters monitored by the standard and the sulfur content was 0.32 wt%.

In figure 1. the sulfur content increases with increasing amount of the alternative component in the mixture SCHO + TPO.

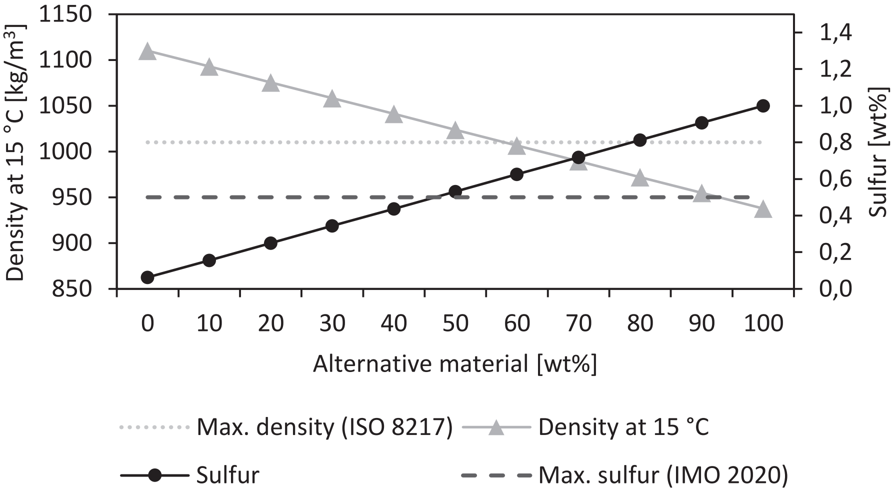

Figure 1. Mixture of SCHO + TPO

The ratio of the SCHO + TPO mixture was chosen in the most suitable area (figure 1), where the maximum permitted value of 1010 kg/m^3 for the density at 15 °C according to the ISO 8217 standard occurs. It was not possible to increase a content of SCHO in the mixture and reduce the sulfur content by 0.62 wt% in the mixture to reach 0.5 % sulfur content. The other qualitative parameters of this mixture proved to be satisfactory and stable.

In figure 2, the higher sulfur values were observed in both original samples of mixture SLO + TPO.

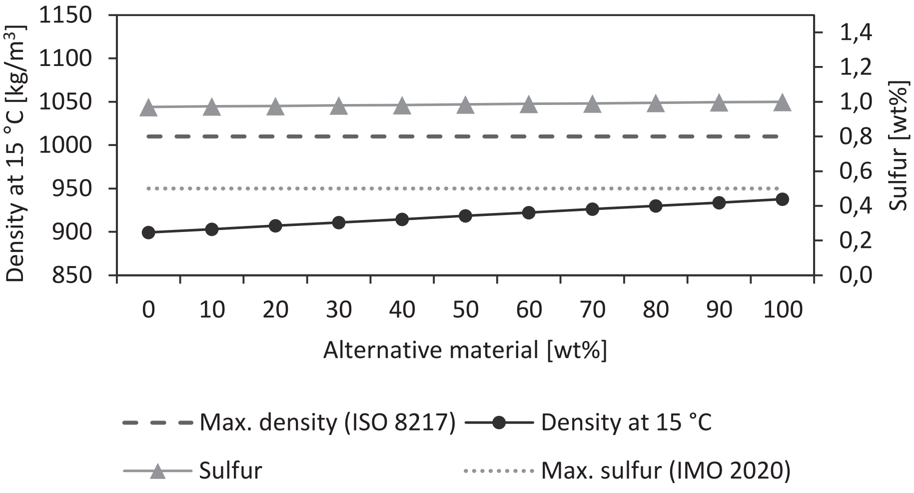

Figure 2. Mixture of SLO + TPO

Due to higher sulfur values in both original samples of mixture (30 wt% SLO and 70 wt% TPO), the sulfur could not be reduced to the newly set maximum value on the deep seas, 0.50 wt%, see figure 2. The resulting value of the sulfur content was thus 0.99 wt%. while a good result was recorded at the density which was the lowest of all prepared mixtures 926.3 kg/m^3. This finding shows that no ratio will reduce the sulfur content below 0.97 wt% of the conventional SLO material.

In figure 3, it is again possible to observe the course of the values of density and sulfur content with respect to the percentage of the alternative component in this case PPO.

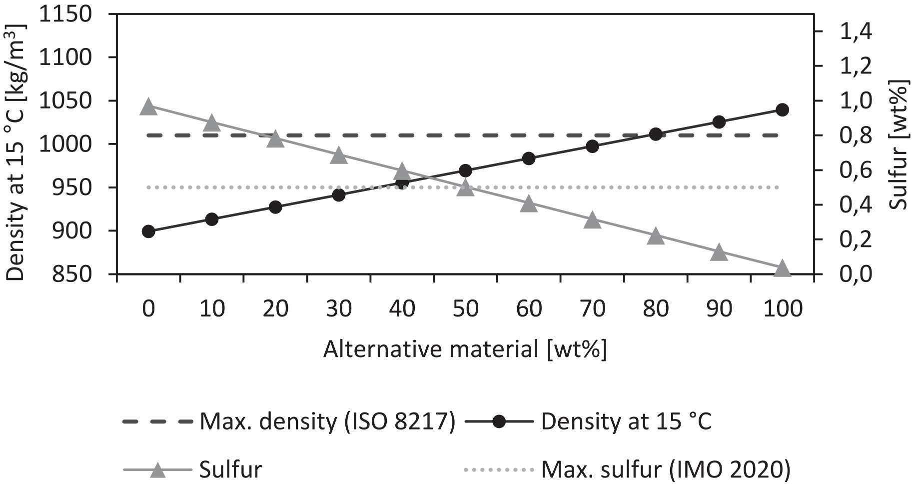

Figure 3. Mixture of SLO + PPO

The proportion of the alternative component PPO was limited by the maximum value for density and was therefore set at maximum 70 wt% (figure 3). As a result, it was possible to reduce the sulfur content of the conventional SLO material by 0.97 wt%. to a final value of 0.32 wt%. Further reduction of the density would increase the sulfur content of the prepared mixture. However, the required limit of sulfur content would still be met at the ratio 50:50. Suitable material can therefore be prepared in the range of SLO 50-30 to PPO 50-70 wt%.

Table IV

Resulting spot tests and microscope images of the prepared mixtures

Sample of mixture	SCHO+TPO	SLO+PPO	SLO+PPO	SLO+TPO
Ratio	40:60	30:70	50:50	30:70
Spot tests		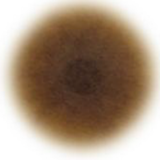		
	1	3	2	1
Microscope images		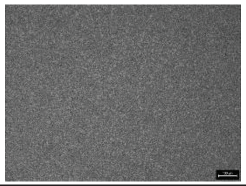	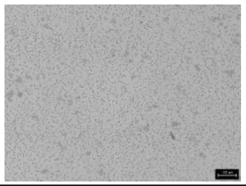	

The spot test of the prepared mixture of SCHO + PO_Pneu in the ratio 40:60 wt% and SLO + TPO in the ratio 30:70 wt% was evaluated by class 1. Sample SLO + PPO in the ratio 30:70 wt% was rated Class 3 for the hint of an inner ring in the centre of the spot. Although a satisfactory standard sulfur content was recorded for this single sample, it appears that the alternative component in the form of PPO causes problems in the resulting stability of the sample, which can have a negative effect during storage. To prevent this problem, it is possible to use a lower content of the alternative material, such the tested ratio 50:50, which shows a higher degree of compatibility (Table II).

Conclusion

Mixtures of conventional and alternative materials in the ratio of 1:1 were subjected to long-term storage. Their compatibility and change in storage were monitored by spot tests and microscope, and the suitable "compatible and stable" mixtures were selected. Based on the blending experiments and the evaluation of qualitative parameters according to standard ISO 8217 the promising materials were identified as perspective for their industrial application. The Steam Cracking Heating Oil + Plastics Pyrolysis Oil blend was predicted to exceed the density limits at 15 °C. The blend Fuel Oil + Tire Pyrolysis Oil could be prepared in any ratio, however, non-compliance with the limits for sulfur content was predicted. The mixtures Steam Cracking Heating Oil + Tire Pyrolysis Oil (40:60) and Slurry Oil + Tire Pyrolysis Oil (30:70) met all the quality parameters given by the ISO 8217 standard, but the sulfur content was exceeded in both cases. The mixture of Slurry Oil + Plastics Pyrolysis Oil (in the range of addition 50-70 wt%) met all the quality requirements of the ISO 8217 standard and at the same time the maximum limit for the sulfur content up to 0.5 wt% according to the new implementation of IMO 2020.

Acknowledgement

The publication is a result of the project which was carried out within the financial support of the Ministry of Industry and Trade of the Czech Republic with institutional support for long-term conceptual development of research organisation.

References

1. Sulphur oxides (SOx) and Particulate Matter (PM) – Regulation 14, 2019. International Maritime Organization. http://www.imo.org/en/OurWork/Environment/PollutionPrevention/AirPollution/Pages/Sulphur-oxides-(SOx)-%E2%80%93-Regulation-14.aspx, staženo 18.9.2020
2. Vráblík, A.; Černý, R. Námořní paliva po roce 2020. Paliva, 9, 83, 2017
3. ISO/PAS 23263:2019 Petroleum products – Fuels (class F) – Consideration for fuel suppliers and users regarding marine fuel quality in view of the imple-mentation of maximum 0.50 % sulfur in 2020, dostupné: https://www.iso.org/news/ref2437.html, staženo 7. 10. 2020.

4. ISO 8217:2017. Petroleum products – Fuels (class F) – Specifications of marine fuels. Geneva: International Organization for Standardization, 2017. 23 p
5. Vermeire, M. B. 5. Chevron Everything You Need To Know About Fuels, 2012.
6. Vermeire, M.; Heyberger, B. Study to evaluate test methods to assess the stability and compatibility of marine fuels in view of the IMO MARPOL Annex VI Regulation 14.1.3 for 2020 Sulphur requirements, 2019. Concawe.eu. https://www.concawe.eu/wp-content/uploads/Rpt_19-11.pdf staženo 11. 10. 2020.
7. Vráblík, A.; Jaklová, K.; Bringlerová, N.; Schlehöfer, D.; Černý, R. Hodnocení stability námořních paliv pomocí mikroskopu. *Paliva* **2020**, *2* (12), 60–65.
8. Schlehöfer, D.; Vráblík, A.; Černý, R. Charakterizace možných alternativních materiálů pro výrobu námořních paliv. *Paliva* **2021**, *1* (13), 16–23.
9. ASTM D 4052-18a. Standard Test Method for Density, Relative Density, and API Gravity of Liquids by Digital Density Meter. West Conshohocken, United States: ASTM International, 2016. 8 p
10. ASTM D 4294. Standard Test Method for Sulfur in Petroleum and Petroleum Products by Energy Dispersive X-ray Fluorescence Spectrometry. West Conshohocken, United States: ASTM International, 2016. 9 p.
11. ASTM D 4740. Standart Test Method for Cleanliness and Compatibility of Residual Fuels by Spot Test. West Conshohocken, United States: ASTM International, 2014. 3 p.

CO-PROCESSING OF PYROLYSIS PRODUCTS

Dlasková Jaklová K., Zbuzková B., Vráblík A.

ORLEN UniCRE a.s., Záluží 1, 436 70, Litvínov
Karolina.DlaskovaJaklova@orlenunicre.cz

Abstract

The current trend of deeper crude oil processing and emphasis on reduction of carbon footprint lead to an increase in the use of secondary and alternative products for diesel production. For example, higher generation of biofuels or other materials produced from waste by pyrolysis and their processing into products with higher added value seem to be very beneficial solution. Because of their low quality (the higher amount of heteroatoms and aromatic hydrocarbons) refineries use catalytic hydrogenation processes during which the heteroatoms of sulfur and nitrogen are removed from feedstock and quality parameters are improved. The addition of alternative pyrolysis products can affect one of the most important properties of a desulfurization catalyst – its activity. Reduced catalyst activity and the presence of pyrolysis products in standard feedstock (SF) affects the quality of products from catalytic hydrogenation. Prior to industrial application, the mentioned aspects are usually tested and verified using experimental pilot units. The aim of work is to evaluate the effect of addition of alternative pyrolysis products on catalyst activity and properties of products from catalytic hydrogenation. The influence of the addition 5% of two alternative pyrolysis products as a component of feedstock was tested. Specifically, it was a product from the steam cracking of petroleum fractions (POPF) and product derived from pyrolysis of sorted waste polystyrene (POPS).

Introduction

Increasing demands of fuel producers in the use of secondary and alternative products for fuels production are based on a bioenergy sustainability policy promoted by the European Union via directive 2009/28/EC. Currently, the first generation of biofuels such as FAME (fatty acids methyl esters) are mostly used. They are produced from land using feedstock which can also be used for food and feed. That is why from the January 2021, their use will be reduced in connection with ILUC (Indirect Land Use Change).[1]

One of the pathways refining industries can utilize is the use of higher generation of biofuels or other materials produced from waste by pyrolysis and their processing into products with higher added value.[2] Landfills represent huge stocks of plastic that can be used as a resource for energy. Unfortunately, plastic materials cannot be recycled endlessly.[3] Nevertheless, this method is meantime the most effective solution to the forthcoming energy and environmental crisis. In a few decades, the population will grow and with that the demand for energy will increase approximately five times. Nowadays, we are getting 80% of required energy from fossil fuels. However, the reserves of these resources are not inexhaustible. Thus, the use of plastics as an energy source has at least two advantages, a reduction in the amount of plastics deposited in landfills and a partial reduction in the use of fossil fuels as an energy source.[4]

One option of waste-to-energy technology for replacing fossil fuel is pyrolysis process. Pyrolysis is a thermal decomposition of raw organic material in the absence of oxygen. This irreversible process involves change of chemical composition and physical phase. Using specific conditions, the waste raw material is processed into pyrolysis gas, pyrolysis oil and solid residue.[4,5] It is easy to prepare plastics for pyrolysis process. The pre-treatment includes their drying, cleaning and sorting. The sorting of plastics is important for easier processing and maintaining stable conditions during pyrolysis. For this reason, plastics are sorted into polystyrene, polypropylene, high and low density polyethylene, polyethylene terephthalate and polyvinyl chloride. The first pyrolysis material used in this work was product derived from pyrolysis of sorted waste polystyrene. The importance of sorting plastics for pyrolysis was demonstrated in an article dealing with co-processing in the journal Hydrocarbon engineering. The article was about co-processing of two alternative pyrolysis products in addition of 5% with the standard feedstock. Two middle distillate fractions from plastic waste were used. The first one was from sorted plastic waste (the mixture of polypropylene and polyethylene only) and was co-processed without any issues. The quality of the product was comparable to the standard production. The second one originated from unsorted plastic waste. During the testing, the reaction temperature had to be increased more to achieve the sulfur level of 10 mg kg^{-1} in the product. Also, the content of aromatic and paraffinic carbon as well as cold-flow properties of the product were higher. [6,7]

The next pyrolysis material, used in this work, was product from the steam cracking of petroleum fractions. Steam cracking is a process used to produce light olefins such as ethylene and propylene. For example, in Western

Europe 95% of ethylene and 70-75% of propylene are produced by the steam cracking. During this process, diesel, ethane or others hydrocarbon feedstocks are converted into light olefins and can be used for the production of plastics or other chemicals.[8]

Diesel fuel is produced by blending of middle distillates. These are obtained from the atmospheric distillation of crude oil or from the processes of thermal and catalytic cracking or hydrocracking of high-boiling petroleum fractions and residues. To improve the properties of these distillates, the refinery uses catalytic hydrotreating. One of the most important properties is the sulfur level of 10 mg kg^{-1}.[9] Pyrolysis products contain inter alia heteroatoms and a large amount of unsaturated hydrocarbons. Removal of heteroatoms and hydrogenation of double bonds in the feedstock, during the catalytic hydrogenation, increases the hydrogen consumption, which can lead to a faster deactivation of the lower part of the catalytic bed. The activity of the catalyst gradually decreases during the process of hydrodesulphurization, which must be compensated by increasing the reaction temperature.[2]

The aim of the experiment described in this work is to evaluate the effect of the addition of alternative middle distillates derived from products of pyrolysis on catalyst activity and properties of products from catalytic hydrogenation. The influence of the addition 5% of two alternative pyrolysis materials as a component of standard feedstock was tested. Specifically, it was a product from the steam cracking of petroleum fractions (POPF) and product derived from pyrolysis of sorted waste polystyrene (POPS).

Experiment

The experiment was performed in the bench-scale unit for testing of HDS catalysts. The testing unit is capable to simulate a single-stage hydrodesulfurization process in the down-flow mode. The reactor is heated by 3-zones electrical heating with independent control according to the selected thermocouple inside the thermo-well. There are six thermocouples inside the reactor. The feedstock is fed from the feedstock container to the top of the reactor, and it is mixed with hydrogen in the reactor head. The commercial catalyst (CoMo/Al_2O_3) was tested in its original form without crushing. Prior the dilution and loading into a reactor the catalyst was sorted to select particles with average dimension of ca. 4 mm. Typically, 100 mL of a catalyst is loaded into the reactor and the catalyst is diluted by an inert material (SiC) to ensure proper liquid and gas flow distribution and efficient heat transfer. The inert material was also placed under and above the catalyst bed. Reactor is equipped with two separators. The products are continuously collected in a high-pressure separator and withdrawn to a low-pressure separator. After the specified time period the sample from the low-pressure separator is withdrawn to the collector where the product is purged with hydrogen to remove dissolved H_2S. After stripping the products are transferred into a sampling flask and analysed. The samples were withdrawn every 3 hours and their density, refractive index and colour were determined to evaluate the stability of the test. Once a day the extended analyses of the selected samples were done and sulfur content was determined.

The testing was divided into five steps (Figure 1). First, the standard feedstock was fed to the reactor. Once the sulfur content of 10 mg kg^{-1} was reached, the feedstock was changed to standard feedstock with the addition of 5% of POPF etc. Average samples were prepared for each of these conditions at the stable testing conditions and when the sulfur content of 10 mg kg^{-1} were achieved.

The analytical methods used are listed in the Table I.

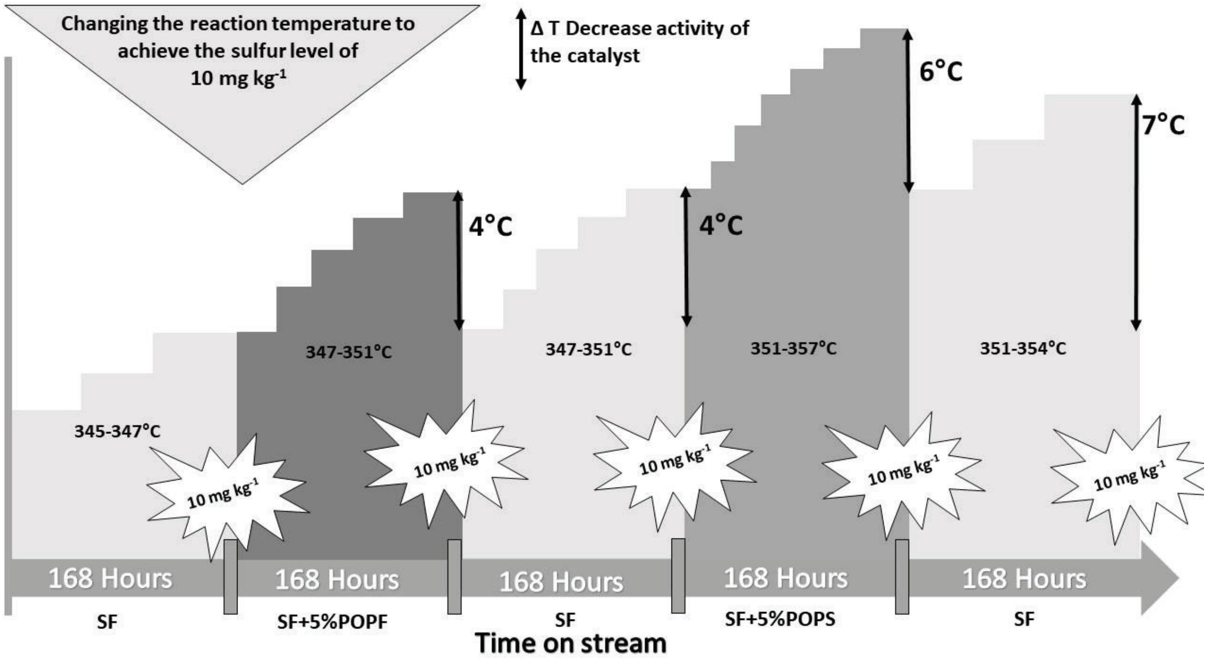

Figure 4. The course of the experiment

Table I

Analytical methods

Method	Standard	Instrument
Density D15	EN ISO 12185	DMA 4500M
Refractive index	ČSN 65 0341	RFM 970
Colour	ASTM D 1500	Lovibond PFX-i
CP	ČSN EN 3015	-
PP	ČSN EN ISO 3016	Manual
CFPP	ČSN EN 116	Orbis BV AirSTAR CFPP
Sulfur content	ASTM D 5453	Trace SN Cube
Nitrogen content	ASTM D 4629	Trace SN Cube
Carbon content	Internal, SOP L3/2	Thermo Scientific FLASH 2000
Hydrogen content	Internal, SOP L3/2	Thermo Scientific FLASH 2000
Aniline point	ČSN 65 6180	Manual
Aromatics (mono-, di-, polyaromatics)	IP 391 / EN 12916	Agilent 1260 Infinity
SimDist	ASTM D 2887	HP 7890 with FID and cool on-column injection

The Table II shows the analytical evaluation of feedstocks used. The feedstock with the addition of 5% of POPS has more than twice the nitrogen content and higher content of polyaromatics hydrocarbons. Also pour point was significantly lower in the case of thus feedstock.

Table II

Feedstocks properties

Properties	SF	SF+5%POPF	SF+5%POPS
Density@15°C, kg m^{-3}	835.8	837.7	838.5
Refractive index 20°C	1.463	1.464	1.466
Colour ASTM D 1500	0.6	0.7	1.2
CP, °C	-8	-7	-7
PP, °C	-22	-22	-30
CFPP, °C	-12	-12	-12
Sulfur content, mg kg^{-1}	7444	7081	7116
Nitrogen content, mg kg^{-1}	109	106	236
Carbon content, wt%	86.3	86.1	86.3
Hydrogen content, wt%	13.6	13.4	13.2
Aniline point, °C	61	62	62
Monoaromatics, wt%	20.5	22.4	22.1
Diaromatics, wt%	7.0	7.3	9.3
Polyaromatics, wt%	0.4	0.6	0.7
Distillation curve			
IBP, °C	115.2	115.6	115.3
5 wt%, °C	168.0	170.6	170.9
95 wt%, °C	371.3	381.1	379.6
FBP, °C	442.6	472.1	453.8

It can be seen from distillation curves (Figure 2), the addition of 5% of alternative pyrolysis product affected the course of the distillation curve only slightly. Therefore, all three distillation curves are almost identical.

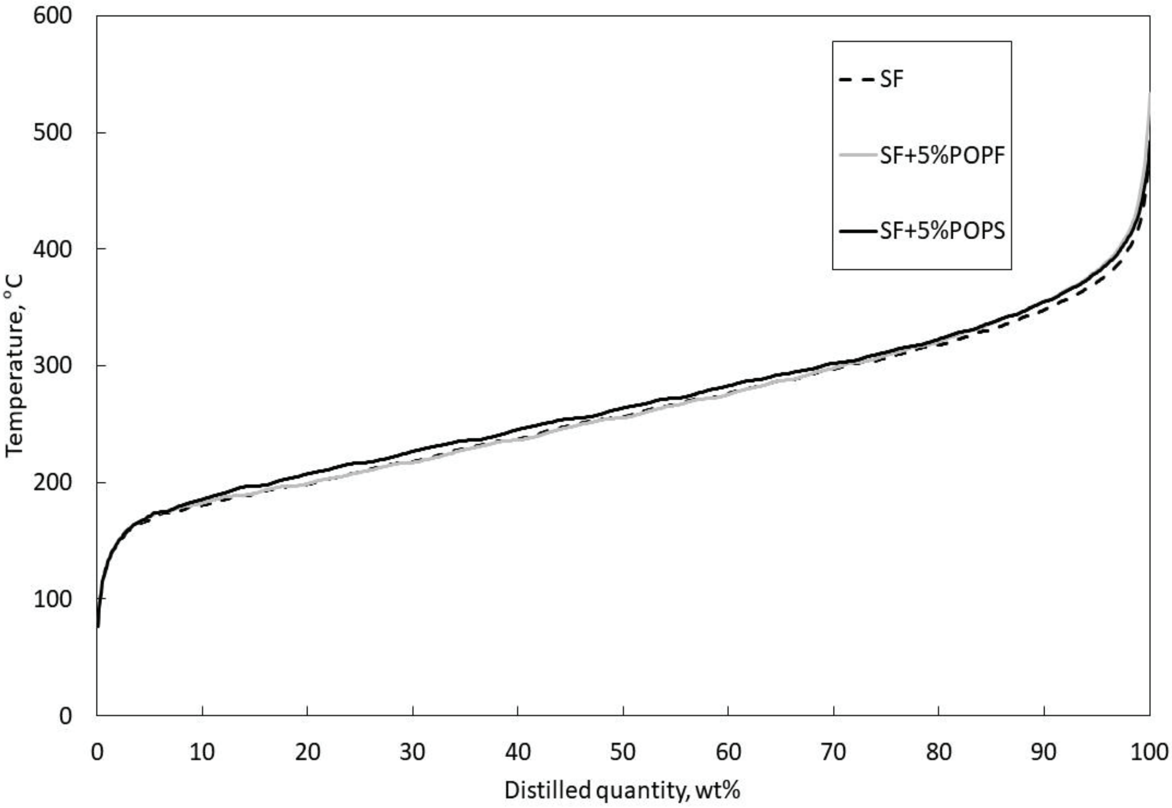

Figure 5. Distillation curves of feedstock

The difference in the content of aromatics is almost negligible (Figure 3).

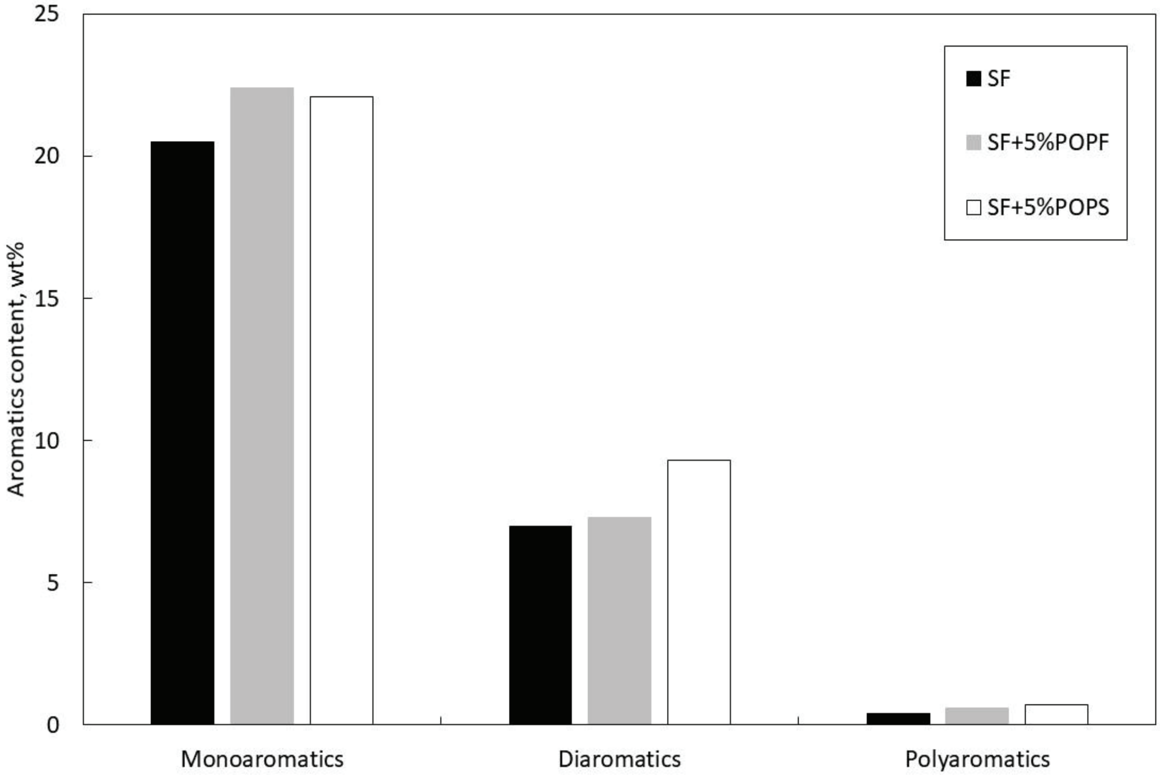

Figure 6. Content of aromatics in feedstock

Discussion and result analysis

During the test temperature inside the catalytic bed was controlled to achieve the sulfur level of 10 mg kg^{-1}. Temperature after first 168 hours of standard feedstock feeding had to be increased by 2 °C to achieve the sulfur level of 10 mg kg^{-1} at 347 °C. During the next phase, when the standard feedstock (SF) with addition of 5% of pyrolysis oil from steam cracking (POPF) was fed, temperature had to be increased by 4 °C to 351°C. Although, the amount of sulfur in the SF+5%POPF is lower than in the SF, the sulfur is sterically hindered and consequently less degradable. That is why the desulfurization was more difficult. In the case of long-term feeding of the feedstock, the temperature difference could be even higher. During the third phase, the standard feedstock was fed again. In the beginning the temperature was decreased to the temperature at which the desired sulfur level was achieved in the first phase. We found that it is necessary to increase the temperature by 4 °C to 351 °C to achieve the sulfur level of 10 mg kg^{-1}. This indicates that the presence of pyrolysis oil POPF affected the activity of the catalyst. In the fourth phase the feedstock was changed to standard feedstock with addition of 5% of pyrolysis oil from polystyrene (POPS). Temperature had to be increased by 6 °C to 357 °C. In this case, the drop in catalyst activity could be caused by less degradable species of sulfur (substituted dibenzothiophenes), aromatics and increased amount of nitrogen in the SF+5%POPS. In the last phase the standard feedstock was fed again.

The presence of pyrolysis oil from polystyrene affected the activity of the catalyst and therefore the temperature had to be increased by 3 °C to 354 °C. The temperature required to achieve 10 mg kg^{-1} sulfur content was 3 °C lower than in the fourth phase of testing. Because of the change of feedstock, which had, among other differences, lower amount of nitrogen and different species of sulfur and aromatics. At the end of the testing, the temperature required to achieve the sulfur level of 10 mg kg^{-1} had to be increased by 7 °C. The products density increased and decreased during the test depending on the used feedstock (Figure 4). The highest density was found for the products from processing of SF+5%POPS.

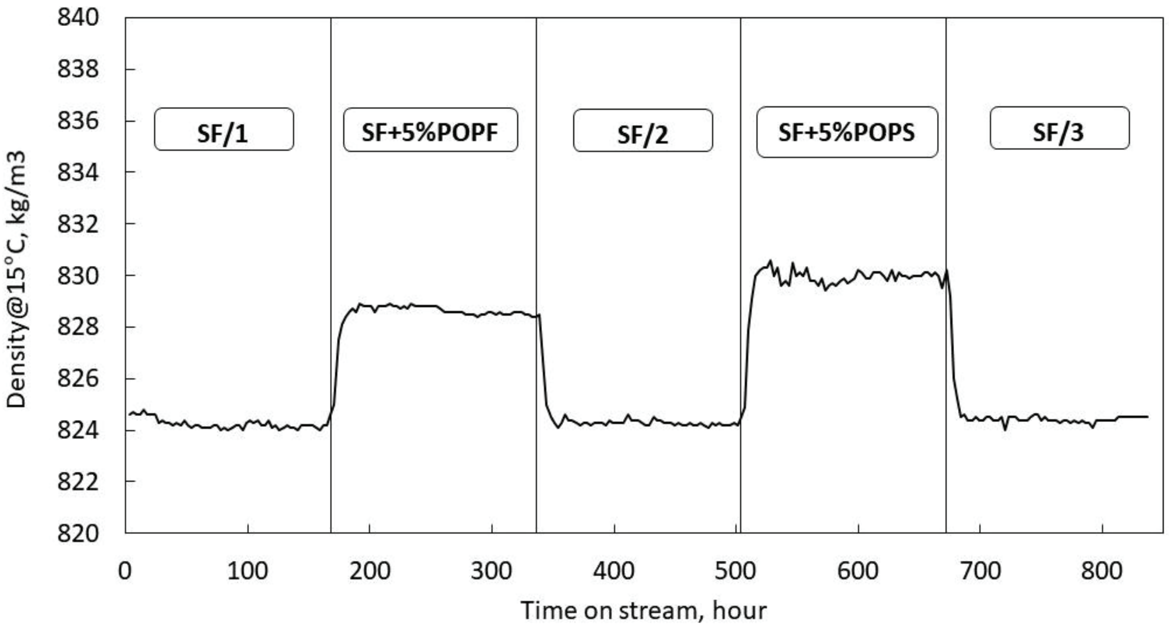

Figure 7. The course of density during the experiment

The parameters of products were affected by feedstocks properties (Table III). Increased amount of nitrogen and polyaromatics hydrocarbons as well as lower values of cold-flow properties, especially pour point in SF+5%POPS also occurs in the average sample from this condition. Increasing amount of nitrogen can be observed during the test in average samples incurred from the processing of standard feedstock. Using the catalytic hydrogenation process the content of aromatic hydrocarbons has been reduced, especially content of polyaromatic compounds.

Table III

Properties of average samples

Properties	SF/1	SF+5%POPF	SF/2	SF+5%POPS	SF/3
Density@15°C, kg m^{-3}	824.2	828.6	824.3	829.6	824.5
Refractive index 20°C	1.457	1.459	1.457	1.461	1.457
CP, °C	-8	-7	-9	-8	-6
PP, °C	-22	-22	-22	-30	-23
CFPP, °C	-11	-12	-11	-12	-11
Sulfur content, mg kg^{-1}	9.5	10.0	10.2	10.3	10.1
Nitrogen content, mg kg^{-1}	7.1	8.4	9.5	15.2	10.9
Monoaromatics, wt%	23.2	24.0	23.8	25.2	22.7
Diaromatics, wt%	2.0	2.0	2.2	4.4	2.2
Polyaromatics, wt%	0.2	0.2	0.1	0.2	0.1
Distillation curve					
IBP, °C	140.3	137.9	139.7	137.8	139.9
5 wt%, °C	174.4	173.8	174.1	174.3	174.0
95 wt%, °C	375.1	373.4	374.4	373.4	374.0
FBP, °C	451.0	450.3	447.7	446.8	445.4

Distillation curves are almost identical (Figure 5) and the addition of 5% of alternative pyrolysis product affected the course of the distillation curve only slightly.

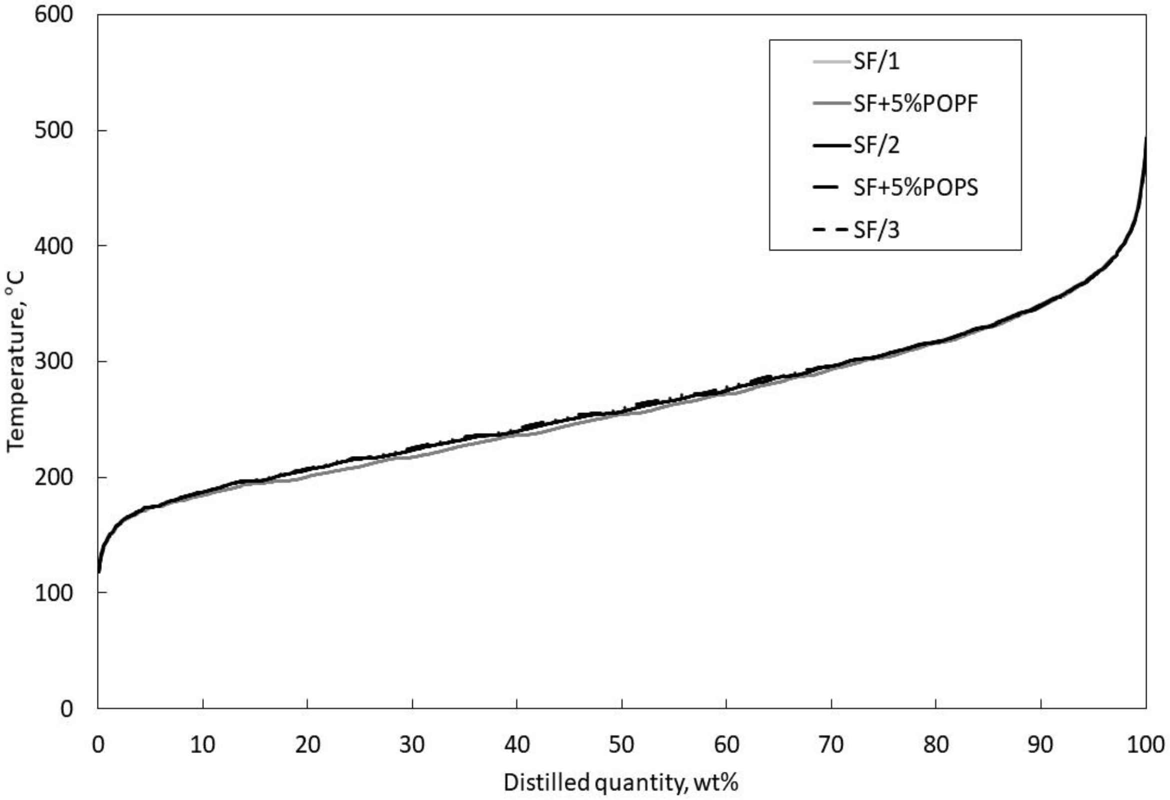

Figure 8. Distillation curves of average samples

The Table IV shows the comparison of properties of average samples with the standard EN 590+A1. All five average samples met the requirements of the standard, except for the requirement to the amount distilled off up to 360 °C. This can be accomplished by pre-distilling the sample or by blending with another hydrogenated middle distillate with a suitable distillation curve. In the case of cold-flow properties (CFPP) average samples meet the requirements for Class D diesel.

Table IV

Comparison of the results with the standard EN 590+A1

Properties	Average samples	Standard EN 590+A1	
		Min.	Max.
Density@15°C, kg m^{-3}	824.2 – 829.6	820.0	840.5
CFPP, °C	-12 – -11	-	-10
Sulfur content, mg kg^{-1}	9.5 – 10.3	-	10
Polyaromatics, wt%	2.2 – 4.6	-	8.0
Distillation curve, 95 wt%, °C	373.4 – 375.1	-	360

Conclusion

This work deals with the effect of addition of alternative pyrolysis products as a component of feedstock processed in the catalytic hydrogenation (HDS) of middle distillates. The alternative feedstocks are product from the steam cracking of petroleum fractions (POPF) and product derived from pyrolysis of sorted waste polystyrene (POPS). Both fractions were co-processed in 5 wt% with the standard feedstock. The effects of the addition of alternative pyrolysis products on the activity of the catalyst and properties of products were studied. The testing was divided into five steps.

The reaction temperature was continuously adjusted to achieve the sulfur level of 10 mg kg^{-1}. In the first step, the standard feedstock used in the hydrogenation unit was processed. When the required sulfur level has been achieved, the feedstock was changed to standard feedstock with addition of 5 wt% of POPF. The addition of POPF was compensated by an increase in reaction temperature by 4 °C to achieve the sulfur level of 10 mg kg^{-1}. Then the feedstock was changed to the standard feedstock. The additions of POPF resulted in higher catalyst deactivation, which had to be compensated by an increase in reaction temperature of 4 °C. In the fourth step, the feedstock was changed to standard feedstock with addition of 5 wt% of POPS. The addition of POPS was compensated by an increase in reaction temperature by 6 °C to achieve the sulfur level of 10 mg kg^{-1}. Then the feedstock was changed last time to the standard feedstock. The additions of POPS resulted in higher catalyst deactivation, which had to be compensated by an increase in reaction temperature of 7 °C.

The used alternative feedstocks showed to be potential material for co-processing with conventional feedstock but the catalyst activity should be compensated by increasing of reaction temperature. The overall effect on activity of catalyst should be verified during long-term testing.

Acknowledgement

The publication is a result of the project which was carried out within the financial support of the Ministry of Industry and Trade of the Czech Republic with institutional support for long-term conceptual development of research organisation. The result was achieved using the infrastructure included in the project Efficient Use of Energy Resources Using Catalytic Processes (LM2018119) which has been financially supported by MEYS within the targeted support of large infrastructures.

References

1. The European Parliament and the Council of The European Union. Directive (EU) 2015/1513 of the European Parliament and of the Council of 9 September 2015 amending Directive 98/70/EC relating to the quality of petrol and diesel fuels and amending Directive 2009/28/EC on the promotion of the use of energy from renewabl. Off J Eur Union 2015:29.
2. Zbuzková B., Jaklová K., Vráblík A., Černý R.: Hydrogenační rafinace středních destilátů s přídavkem pyrolýzního oleje z depolymerizace plastů. Paliva, 3 (12), 107 (2020).
3. Faussone G. C.: Trancportation fuel from plastic: Two cases of study. Waste Management, 73, 416 (2018).
4. Nileshkumar K. D., Patel T. M., Jani R. J., Rathod G. P.: Effect of Blend Ratio of Plastic Pyrolysis Oil and Diesel Fuel on the Performance of Single Cylinder CI Engine. IJSTE – International Journal of Science Technology & Engineering, 1 (11), 195 (2015).
5. Wongkhorsub C., Chindaprasert N.: A Comparison of the Use of Pyrolysis Oils in Diesel Engine. Energy and Power Engineering, 5, 350 (2013).
6. Vráblík A., Černý R.: Finding a new path. Hydrocarbon engineering, November, 32 (2020).
7. Pšenička M., Vráblík A., Černý R.: Comparison of pyrolysis oils from used tires and plastic waste as a component for diesel fuel production. 7th International Conference on Chemical Technology, Mikulov, 15 – 17 Apr. 2019.
8. Ren T., Patel M., Blok K.: Olefins from conventional and heavy feedstocks: Energy use in steam cracking and alternative processes. Energy, 31, 425 (2006).
9. EN 590+A1 – Automotive fuels – Diesel – Requirements and test methods.

HYDROGEN PRODUCTION OPTIMIZATION IN REFINING INDUSTRY

Cibulka T.[1], Variny M.[2]

[1] *SLOVNAFT, a.s., Vlčie hrdlo 1, 824 12 Bratislava, Slovak Republic*
[2] *Department of Chemical and Biochemical Engineering, Faculty of Chemical and Food Technology, Slovak University of Technology in Bratislava, Radlinského 9, 812 37 Bratislava, Slovak Republic*
miroslav.variny@stuba.sk

Abstract

In current economic and environmental situation in refining industry it is very important to increase crude oil conversion to produce more valuable light products. The key factor to deeper conversion is hydrogen, which is mostly produced in refineries by steam reforming technology. These processes belong to most energy consuming, and produce large amount of excess steam, which is not usually utilized on site, but it is exported to refinery steam network. A new hydrogen production plant is to be built in SLOVNAFT refinery. Four investment proposals capable of solving the resulting anticipated steam excess are presented and their impact on steam balance, fuel consumption and electricity production is evaluated.

Introduction

Nowadays, more than 60% of global demand for hydrogen is used in chemical and petrochemical industry, where ammonia production is the largest consumer, followed by methanol production[1]. Demand for both chemicals is expected to increase due to economic and population growth. Refineries represent the second largest consumer of hydrogen with around 30% market share using hydrogen for hydro-processing and hydro-treating of various feedstock which involves removal of impurities (sulphur, nitrogen…), as well as the production of lighter and more valuable fuels and materials[2]. Several ways can be used to produce hydrogen: thermochemical conversion of fossil fuels, water electrolysis, biomass-based or biological production[3]. Natural gas steam reforming constitutes almost half of world´s hydrogen production[3] and is usually the most important hydrogen source for a refinery with gasoline reforming being the second in order. Other sources, such as recovery and purification from syngases[4,5], offgases and process gases[6,7] or steam cracking of gasoline and gases are only minor contributors to the hydrogen pool[8].

Slovnaft refinery is relatively small, but complex refinery processing mostly Russian export blend crude oil. Conversion of crude oil to light products usually exceeds 90%, therefore high amount of hydrogen production is needed to fulfil hydrocracking units' consumption. Two quality grades of hydrogen are produced by steam cracker, catalytic reformer, PSA purification of off-gases and two steam reforming units, but lately, their maximal hydrogen production capacities are reached more often. Hydrogen demand in Slovnaft refinery is expected to grow in future due to:

- Decreasing Russian export blend crude oil quality
- Increasing ratio of heavier and sourer feedstock
- Continual revamp of existing units to increase crude oil conversion to lighter products and to meet tightening fuel quality standards

Therefore, commissioning of a new hydrogen production unit (HPP) based on steam reforming is considered in Slovnaft refinery. As a by-product of steam reforming technology, excess of steam arises[8], therefore, unit connection to refinery steam network is important to reach optimal economical operation of hydrogen production.

Study objectives

Several goals are defined in this work:

- Steam balance after new HPP unit implementation in Slovnaft refinery
- Economical and energy balance of four presented proposals, which solve excess of high-pressure (HP) steam after new HPP implementation
- Comparison of presented proposals and identification of the limits and opportunities for their economic feasibility improvement

Steam balance in Slovnaft refinery

Steam in Slovnaft refinery is produced by two main sources. First one is thermal power plant, TPP, which is currently part of the refinery. Secondary steam sources on different pressure levels utilizing waste heat are found directly on production units.

TPP is not only producing steam but also generates electricity to cover part of refinery's consumption. It is equipped with five boilers, which are producing very high-pressure steam. This steam is in turbines, where electricity is produced, or in reduction station, reduced to three steam pressure levels: high-pressure, HP, medium-pressure, MP and low-pressure, LP[9]. Four turbines, with different configurations of steam extractions are located in TPP. Three of them are condensation turbines and one is back-pressure turbine. Typically, 2 – 3 of them, depending on season, are in operation. It is common, that turbines´ extractions are not able to fully satisfy demand of each pressure level, therefore rest of steam's need is reduced on reduction stations, which are able to produce to all other levels from very high-pressure steam level , but no electricity is produced and therefore energy difference between levels is wasted.

HP steam consumption is highly depended on refinery operation configuration and amount of steam from TPP is often fluctuating. The new hydrogen production plant, HPP3, is estimated to export 43.2 t/h of HP steam to network in average[10], while the old HPP1 plant currently exports just 10 t/h of HP steam in average. As depicted in Figure 1., there will be average surplus of 16.2 t/h of HP steam to refinery steam network after HPP3 commissioning and HPP1 shutdown. Without any intervention, this steam will be reduced to MP steam level and energy difference between HP and MP steam will be lost. Therefore, four alternatives were considered to reduce this economical loss.

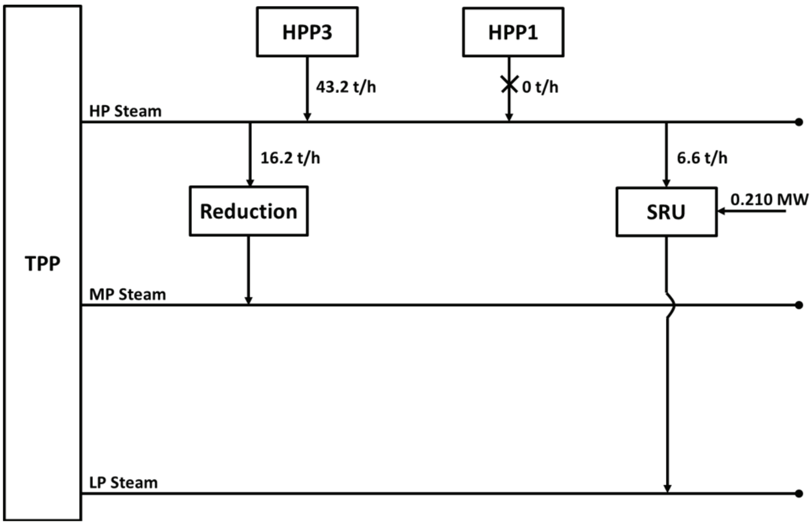

Figure 1. Steam network after new HPP implementation

Replacement of steam drives on Sulphur Recovery Unit

Sulphur Recovery unit, SRU, operates two steam drives, which are reducing HP steam to LP steam, while generating shaft energy to drive pumps directly on unit. Their average steam consumption of those steam drives is 4.7 t/h and 1.9 t/h, respectively. Originally, they should be in operation as frequently as possible to lower low quality HP steam export from unit, but due to decreasing reliability of steam-driven position, their average operation time reaches 66 % and 42 %, respectively at present.

Replacement of those steam drives for new ones, which will be operating between HP and MP steam level, is one of the solutions how to solve HP steam surplus situation. Due to smaller pressure difference between HP and MP steam, compared to HP and LP steam, new steam drives will consume more HP steam than the existing ones[11], lowering the unwanted reduction between HP and MP steam level to minimum, as it is depicted in Figure 2.

Total steam export from TPP maintains at the same level. Also, HP steam supply from TPP maintains at the same level. However, MP steam supply from TPP will decrease, causing loss on electricity production directly on TPP turbines. This loss will be lowered by fact, that 30% of produced MP stream on TPP is reduced without generating any electricity at present. Lack of LP steam, which was originally supplied from SRU unit, will be replaced by TPP production of LP steam, where it will produce additional electricity. Increase of LP steam production from TPP will also help in summer season. Higher operation time of turbine positions, which is expected to reach 79 % in this configuration, will lower average electricity consumption of electromotor positions. In total, installation of new turbines at SRU will cause increase of electricity production by 0.547 MW on average.

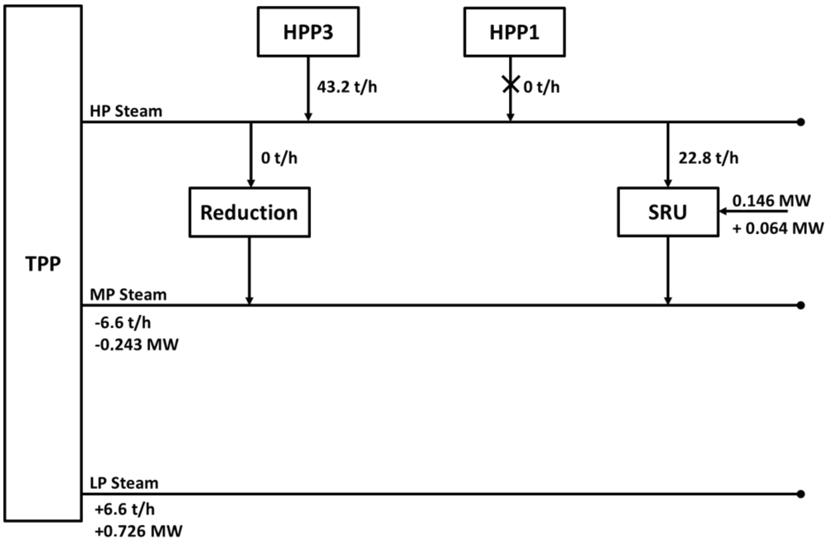

Figure 2. Steam network balance change after replacement of steam drives on SRU

New stand-alone backpressure turbine installation

The basis of this solution is replacement of reduction station by back pressure steam turbine, which will be processing HP steam to MP steam and producing electricity. Enthalpy difference between HP and MP will be much lower than in TPP; therefore, this small turbine will have lower specific electricity production than the large turbines in TPP[11]. Due to fact, that 30 % from total production of MP steam is reduced from HP, this turbine can be used also to avoid this reduction and to produce additional electricity. After data analysis, it was calculated, that in average additional 5 t/h can be processed on this turbine instead of being reduced in TPP. In total, this turbine will be processing 21.2 t/h of HP steam in average and will yield 0.65 MW power output. This situation is depicted in Figure 3.

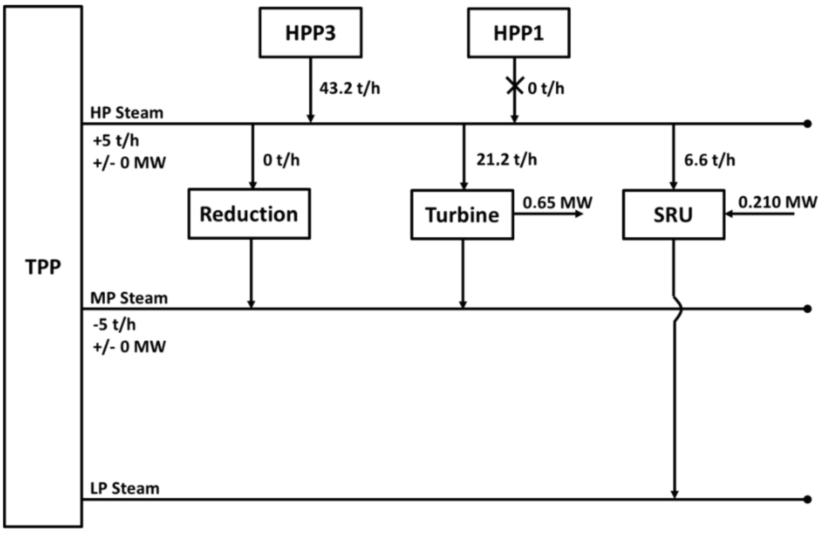

Figure 3. Steam network balance change after new back pressure turbine installation

From the viewpoint of TPP, total steam export will be maintained. More HP steam instead of MP steam, 5 t/h, will be supplied to network to by process on new turbine, but because it is usually reduced on TPP, it will not cause any losses.

Change in design of Hydrogen Production Plant 3

Hydrogen Production Plant 3 is still only in initial commissioning phase, so there is still option to change its design easily. The contractor was asked to propose new design solution, which will decrease HP steam production of unit. Their proposal was to add an external high-temperature reformer, EHTR, which will recover part of heat from steam reformer effluent whereby less heat will be available for HP steam generation.

This configuration will decrease HP steam production by 11.2 t/h on average. Fuel consumption reduction was estimated from enthalpy of HP steam and estimation of 90 % efficiency of steam generation on HPP3. Lower HP delivery to steam network from HPP3 will be covered by TPP and will boost electricity generation on turbines. Altogether, approximately 4 GJ/h more fuel will be consumed but 0.871 MW more electricity will be produced, as results from Figure 4.

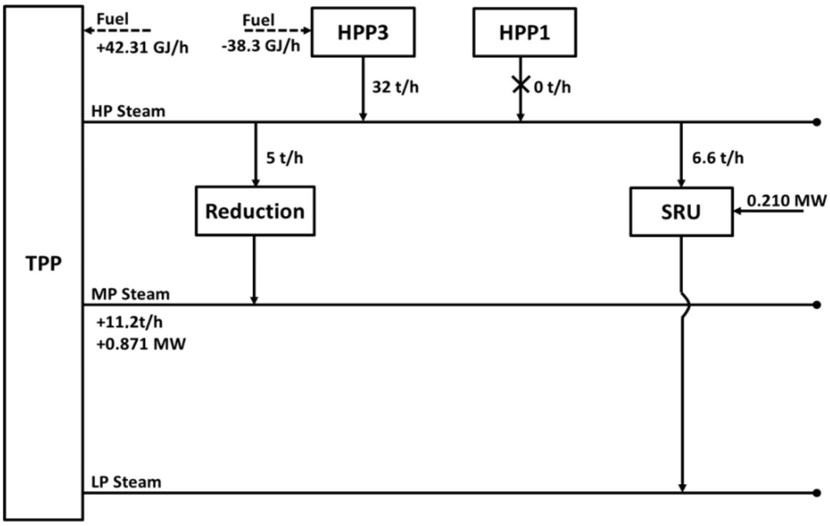

Figure 4. Steam network balance change after EHTR implementation

Usage of HP steam in reboilers in RREF unit

Higher consumption of HP steam directly on units in refinery is also one of the solutions how to handle HP steam surplus in network in future. Reformate splitter unit, RREF, is using reboiler furnaces at present, where refinery fuel gas is burned, to heat process streams in distillation columns. The advanced age of furnaces and their technical condition cause, that they can reach maximal 85 % efficiency. Their replacement by HP steam reboilers, will serve as new HP consumer in refinery, and more electricity will be produced on TPP turbines from this steam. However, this additional steam needs to be produced on TPP, therefore, fuel consumption on TPP will increase, as can be recognized in Figure 5. To sum it up, in average 13.5 GJ/h more fuel will be consumed but power production of TPP increases by around 1 MW.

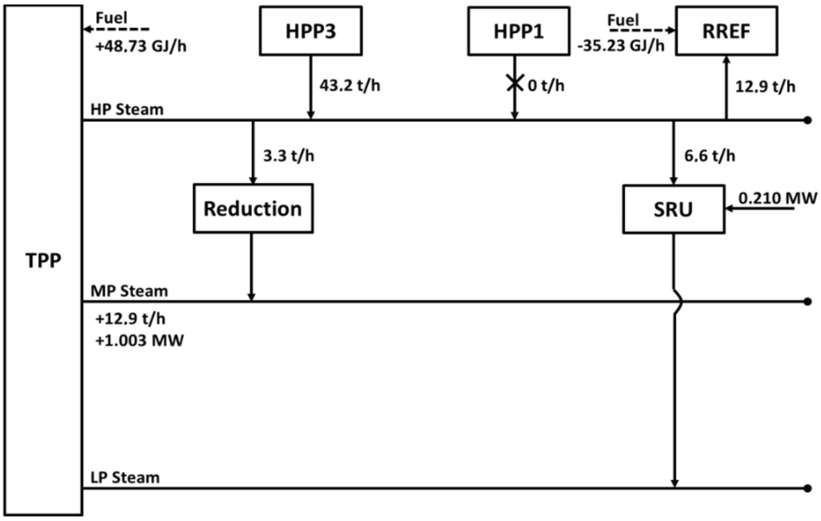

Figure 5. State of steam network after RREF reboiler installation

Discussion

After HPP3 implementation without any intervention, excess of HP steam will be just let down to lower pressure steam network. Therefore, four solutions were presented, which partially, respectively entirely solve this issue.

- Replacement of steam drives on Sulphur Recovery Unit case - all excess steam will be utilized. The still functional old steam drives will be replaced, and 0.547 MW more electricity will be produced.
- New stand-alone backpressure turbine installation case - also all excess steam will be utilized. Approximately 0.65 MW more electricity will be produced and with suitable design of turbine, it can provide flexibility to cover fluctuation of HP steam demand in refinery. On the top of that it can eventually help with processing even more HP steam, if technological changes in refinery caused increase of HP steam excess. On the other hand, technological changes in refinery can cause decrease of HP steam excess and turbine may remain unused.
- Change in design of Hydrogen Production Plant 3 case - excess steam will be utilized just partly. 0.87 MW more electricity will be produced and 4 GJ more fuel will be burnt on TPP. Change of design in this stage of project would be difficult and would slow down the whole project.
- Usage of HP steam in reboilers in RREF unit case - excess steam will be utilized just partly. 1 MW more electricity will be produced and 13.5 GJ more fuel will be burnt on TPP. Old furnaces with low efficiency will be decommissioned, which is desired from environmental point of view.

However, all cases require capital expenses, with the related simple payback period exceeding 7 or even more years. Only coupling Usage of HP steam in reboilers in RREF unit case with condensate recovery project will lower the payback period to an acceptable level. Condensate recovery system usually helps to lower the energy consumption and it is irreplaceable part of every modern refinery. Therefore, usage of HP steam in reboilers in RREF unit case seems to be the best option how to utilize excess HP steam after HPP3 utilization.

Conclusions

In this case study, four proposals, how to solve surplus of HP steam in network after HPP3 implementation were presented. All of them help lowering the operational costs of the energy system of the refinery. However, in cases of new steam drives on SRU, of new stand-alone backpressure turbine and of design change of HPP3 capital expenses are very significant, and payback period exceeds 7 or even more years. This is not acceptable at present. The economic feasibility of HP steam reboilers on RREF project, is closely connected with condensate recovery system project. Without its simultaneous realization only a change in utilities' prices could yield positive benefit from this project. With condensate recovery project in operation, simple payback was calculated to 4 years, which is an acceptable value[12]. However, this project solves the HP to MP steam reduction only partly.

Acknowledgement

This research was supported by the Slovak Research and Development Agency under the contract Nr. APVV-18-0134.

References

1. Yildiz B., Kazimi M. S.: Int. J. Hydrogen Energy *31*, 77 (2005).
2. Song Ch., Liu Q., Ji N., Kansha Y., Tsutsumi A.: Appl. Energy *154*, 392 (2015).
3. Mosca L., Jimenez J. A. M., Wassie S. A., Gallucci F., Palo E., Colozzi M., Taraschi S., Galdieri G.: Int. J. Hydrogen Energy *45*, 7266 (2020).
4. Toth M., Lazar M., Brestovic T.: AIP Conf. Proc. *2118*, 030045 (2019).
5. Brestovic T., Lazar M., Jasminska N., Zivcak J., Toth L., Dobakova R., Duda F., Kmeťova L., Bednarova L.: Processes *9(2)*, 251 (2021).
6. Reddy S., Vyas S.: Energy Procedia *1(1)*, 149 (2009).
7. Aitani A. M.: Int. J. Hydrogen Energy *21(4)*, 267 (1996).
8. Abdin Z., Zafaranloo A., Rafiee A., Mérida W., Lipiński W., Khalilpour K. R.: Renewable Sustainable Energy Rev. *120*, 109620 (2020).
9. Furda P., Variny M., Labovská Z., Cibulka T.: Processes *8(11)*, 1495 (2020).
10. Hanus K., Variny M., Illés P.: Processes *8(5)*, 622 (2020).
11. Ibler Z., Karták J., Mertlová J., Ibler Z.: *Technický průvodce energetika*. Nakladatelství BEN–technická literature, Praha, Czech Republic (2012).
12. Variny M., Blahušiak M., Mierka O., Godó Š., Margetíny T.: Energy Effic. *12(7)*, 1771 (2019).

GAS, COAL, FUEL

INDUSTRIAL COMBINED HEAT AND POWER PLANT REPOWERING PROPOSAL

Kšiňanová M.[1], Variny M.[1]

[1] *Department of Chemical and Biochemical Engineering, Faculty of Chemical and Food Technology, Slovak University of Technology in Bratislava, Radlinského 9, 812 37 Bratislava, Slovak Republic*
miroslav.variny@stuba.sk

Abstract

Industrial combined heat and power plants (CHP) in Middle Europe face the problem of tightening emission limits and decreasing thermal efficiency resulting from their ageing. At the same time, focus and financial support for renovation activities are directed on ageing thermal power plants nowadays, while the need for revamp of industrial CHPs is a less discussed topic generally. To highlight the need for action in this sector a model case study is presented. It showcases an industrial CHP, fueled with heavy fuel oil, producing steam for industrial use and electricity on a condensing-extraction turbine. Several technologies are considered that could augment its actual performance and lead to cleaner heat and power production. Among those, internal combustion engines (ICE) and gas turbines (GT) are the most frequently applied solutions in scientific studies as well in real repowering activities. Both technologies are suitable for industrial use as well. General features and pros and cons of industrial CHP repowering by those technologies are discussed; system balances are set up and resulting improvement of the repowered CHP is obtained.

Introduction

Global climate change highlights our obligation to reduce greenhouse gases emissions. Industrial emissions contribute approximately by 30 to 35 % to total anthropogenic emissions[1], and, amongst them, emissions related to heat and power production play a prominent role[2]. Is it thus of utmost importance to pay attention to this industrial sector.

Several methods can be considered when striving to reduce the carbon footprint of the heat and power production plants[3,4]: fuel switch to cleaner one[5,6] or to biomass or biofuel[7,8], their complete renovation[9] or partial repowering[10]. Apart from this, optimal planning and operational optimization is commonly a low-cost option[11,12]. All those methods should be evaluated from several viewpoints: energetic, economic and environmental[13,14].

For ageing combined heat and power plants (CHP), reconstruction and renovation is necessary. While large thermal and power plants are in the spotlight of researchers and governments[15], industrial CHP receive much less attention[16]. The fundamental method to be considered is partial repowering when a new component is incorporated to the CHP as mentioned above[17]. Even though repowering by internal combustion engines (ICE) is a reasonable option[18], heat in hot water is a by-product with only limited value for heavy industry consumers. Repowering by gas turbines (GT) is more feasible, yielding hot flue gas as the only by-product which can further serve for steam production[19]. All facts considered; GTs are more suitable for this study’s purposes mainly due to the higher overall efficiency potential[20].

Study objectives

The aims of this contribution are in particular:

- analyzing the model operation of an ageing combined heat and power plant, combusting mixed petroleum residue, both in winter and in summer
- introducing the GT and ICE technologies and highlighting their particular features in repowering of the ageing CHP
- deciding the more convenient repowering option and quantifying its impact on CHP operation in terms of change in its efficiency, in overall power production and in fuel consumption and in carbon dioxide emissions

CHP unit description

In this section, more detailed description of the original plant model scheme and calculation assumptions are presented. Main equipment is displayed in Figure 1, where streams in gaseous state are depicted in dashed lines, while solid lines represent liquid streams. The main task of this CHP is to produce at least 60 MW of electric energy and high-, intermediate- and low-pressure (HP, IP, LP) extraction steam in desired amounts for export as well as for own consumption.

The scheme consists of several technological units:

- ECT – extraction-condensing turbine driven by high pressure steam (stream no. 1) produced in steam boiler; besides electricity cogeneration, HP IP and LP extraction steam is produced concurrently for export and for own consumption.
- C – condenser; vapor-liquid mixture (wet steam) from the turbine (stream no. 11), condensates from low temperature water heaters and CHTW (chemically treated water) flow into the condenser. Condenser is operated in broad load range between 20 and 90 t/h of inlet wet steam. Condensate exits after condensation at 30°C and is pumped as feed water to a sequence of three LTWH.
- LTWH – low temperature water heaters (depicted as one in schematics for clarity); each one requires separate extraction steam stream from ECT with the condensation temperature of the inlet steam of 5°C above the temperature of outlet feed water. This way a sufficient heat-exchange driving force is ensured. In each LTWH, the temperature of feed water is increased by 30°C, exiting at 120°C to the degasser.
- CHTW – chemically treated water; while there are a few streams considered as material loss such as blowdown from the boiler, degasser exhaust, even export steam, those need to be replaced.
- DEGASSER – embodies two purposes - feed water degassing and feed water heater; inlet water (stream no. 16) is mixed (into an outlet feed water (stream no. 17) at the temperature of 120°C) with steam from another turbine extraction (stream no. 6a), expander steam, condensates from fuel and air pre-heating and also condensates from HTWH.
- HTWH – high temperature water heater; fulfilling the same role as LTWH with a sequence of two HTWH simplified into one in the scheme.
- BOILER – unit transforming feed water into steam (stream no. 1) at the temperature of 530°C and the pressure of 9 MPa; combustion of pre-heated fuel (stream no. 35, mixed petroleum residue) with air (stream no. 37) takes place resulting in exhaust gas production.

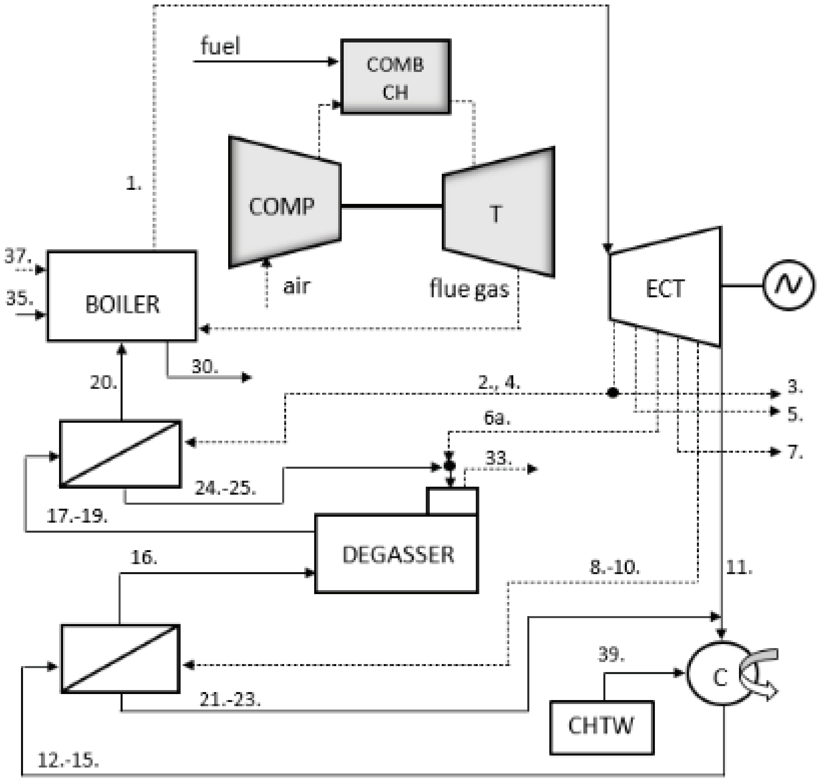

Figure 1. Simplified schematics of CHP unit (with a repowering option in grey). Legend: C = condenser; COMB CH = combustion chamber; COMP = compressor; CHTW = chemically treated water; ECT = extraction-condensing turbine; T = turbine.

Repowering proposals

After we identified the operation conditions of the CHP, the decision-making process concerning altering the CHP unit takes place. The main step of partial repowering is supplementing the original boiler with new heat source fired by natural gas. Choosing a power source in units of up to tens of megawatts, either a combustion gas turbine (GT) or an internal combustion engine (ICE) is used. There are few differences in applications and site performance of both technologies in thermal power plants depending on star-up time, plant repowering cost, power to heat or power to weight ratio etc.

ICE is a machine that produces thermal and electric energy by converting chemical energy contained in fuel into mechanical work of a moving piston[21], all happening in a very fast start-up time with multiple starts in a day[22]. This means incorporating ICE with a system of heat exchangers shows promising results during fluctuating load operation throughout the day, especially in peak hours without the efficiency losses occurring under part load operation. Nevertheless, ICE warms up and some components require cooling. For this purpose, cooling water is usually used, and its amount and temperature are often the limiting factor, which is the reason why such solution is more suitable in cases with significant hot water demand. In the analyzed plant, however, there is little use for hot water, as it is steam, not hot water, that is exported from the CHP unit.

In GT, compressed air from its compressor module and fuel are combusted. Flue gas expands through a turbine leaving it at a high temperature[23]. High rate of used excess air indicates larger amount of oxygen in flue gas. This offers the possibility of using the flue gas as combustion air mixed with the fresh air in the boiler. Comparing both technologies, the total installed masses of GTs are smaller and there is the benefit from lower equipment weight than with ICEs resulting in higher power to weight ratio[22]. Moreover, there is almost no cooling water required. On the other hand, unlike ICEs, gas turbines show poor efficiency at low loadings.

All facts considered, option with GT firing natural gas (NG), using flue gas as a combustion air was chosen and the mathematical model was assembled.

Mathematical model

First step is determination of stream enthalpies. The reference state for water and steam is 0°C, 611 Pa, liquid, thus enthalpies are taken from the water tables and graphs. Steam outlets from turbine and superheated steam enthalpies are determined from the h-s diagram of water vapor and from the properties of boiling water and saturated water vapor[24]. Steam outlets after polytropic expansion and their enthalpy are calculated from equation (1) for isentropic efficiency η_{IS}, where efficiencies of 90 % in superheated and of 80 % in wet steam regions are assumed for the expansion.

$$\eta_{IS} = \frac{h_1 - h_3}{h_1 - h_2} \tag{1}$$

where h_1, h_2 = enthalpies after isentropic expansion, h_3= enthalpy after polytropic expansion.

Condensate enthalpy is obtained from the tables - Properties of boiling water and saturated water vapour[24].

Enthalpy of exhaust gases is calculated using the tables - Molar heat capacity of substances as a function of temperature[24]. The reference state for air is 0°C, 101,3 kPa, gaseous state and the humid air enthalpies are calculated by equation (2)

$$\bar{h}_{\bar{Y}} = \overline{cp}_G \, . \left(T - T_{ref}\right) + \bar{Y} \, . \, (\overline{cp}_W^g \, . \left(T - T_{ref}\right) \tag{2}$$

where $\overline{cp}_G$ = heat capacity of air, T = temperature of humid air, T_{ref} = reference temperature of air (0°C), $\bar{Y}$ = relative mass fraction of water vapor in humid air, $\overline{cp}_W^g$ = heat capacity of water vapor.

Material and enthalpic balances of CHP components, mainly extraction-condensing turbine, low and high temperature water heaters, degasser and boiler were formed. The basic approach is showed in equations (3) and (4)

$$\sum \dot{m}_{in} = \sum \dot{m}_{out} \tag{3}$$

$$\sum h_{in} \dot{m}_{in} = \sum h_{out} \dot{m}_{out} \tag{4}$$

where $\dot{m}$ = mass flow, h = enthalpy, lower index in = inlet output, lower index out = outlet output.

For comparison purposes, specific indicators for the CHP need to be chosen. The most important ones are mass flow of vapor-liquid mixture to condenser $\dot{m}_{11}$, mass flow of produced carbon dioxide $\dot{m}_{CO_2}$ in flue gas, the amount of electricity production $P_{el,total}$, which are calculated from the material and enthalpic balances, cogeneration η_{cog} and electric efficiency η_{el} of the power plant, mass flow of inlet steam to ECT $\dot{m}_1$, heat flow of exported steam Q_{export} and the amount of produced heat by combusting the fuel Q_{fuel} calculated by a set of following equations.

The electrical efficiency of CHP is the ratio of the amount of produced electricity and the total heat obtained by burning fuel as shown in equation (5):

$$\eta_{el} = \frac{P_{el,total}}{Q_{fuel}} \tag{5}$$

Calculation of cogeneration efficiency in equation (6) represents the amount of heat for export, the heat flowing in with chemically treated water and the amount of electricity produced in relation to the total heat obtained by burning fuel.

$$\eta_{cog} = \frac{P_{el,total} + Q_{exp} - Q_{chtw}}{Q_{fuel}} \tag{6}$$

The individual variables from equations (5) and (6) are calculated as follows, equations (7) to (9):

$$Q_{fuel} = LHV_{NG}\dot{m}_{NG} + LHV_{mazut}\dot{m}_{mazut} \tag{7}$$

where LHV_{NG} = lower heating value of natural gas, $\dot{m}_{NG}$ = mass flow of natural gas, LHV_{mazut} = lower heating value of mixed petroleum residue, $\dot{m}_{mazut}$ = mass flow of mixed petroleum residue.

$$Q_{chtw} = h_{39}\dot{m}_{39} \tag{8}$$

where h_{39} = enthalpy of chemically treated water, $\dot{m}_{39}$ = mass flow of chemically treated water.

$$Q_{exp} = h_3\dot{m}_3 + h_5\dot{m}_5 + h_7\dot{m}_7 \tag{9}$$

where h_3, h_5, h_7 = enthalpies of high-, intermediate- and low-pressure export steam, $\dot{m}_3$, $\dot{m}_5$, $\dot{m}_7$ = mass flows of the particular streams for export.

Table I
Steam produced for export

Steam	$\dot{m}_{winter}$ *(t/h)*	$\dot{m}_{summer}$ *(t/h)*
high-pressure	60	60
intermediate-pressure	80	80
low-pressure	130	30

The demand for export steam changes depending on the season. Export stream mass flows are listed in Table I. It is assumed that lowered demand for low-pressure steam during summer results in more waste heat production caused by higher mass flow of wet steam to condenser^{25}. The solution is to cut the extra electricity production in summer to 60 MW both from extraction-condensing turbine and gas turbine. On the contrary, the issue in winter is the exact opposite, when higher amount of produced low-pressure steam reduces the production of wet steam, while ECTs design features allow it to operate within a limited range of wet steam flow. A new restriction is introduced, alongside minimum electricity demand of 60 MW, also minimum production of 20 tons of vapor-liquid mixture per hour is required in winter. Results can be observed in Table II.

Table II
Comparison both for existing (E) and repowered (R) CHP

Indicators	*Winter (E)*	*Summer (E)*	*Winter (R)*	*Summer (R)*
$\dot{m}_1\ (t/h)$	453.7	394.9	453.7	332.6
$Q_{fuel}(MW)$	333.9	289.7	361.0	249.4
$\dot{m}_{11}(t/h)$	20	87.2	20	46.7
$\dot{m}_{CO_2}(t/h)$	92.6	80.6	95.7	71.2
$Q_{export}(MW)$	222.2	143.1	222.2	143.1
$P_{el,total}\ (MW)$	64.3	60	82.1	60
η_{cog} (%)	85.8	70.1	84.3	80.7
η_{el} (%)	19.6	21	23.1	27.8

Model results and discussion

By assembling mathematical model of the CHP in this study, essential understanding of specific technological units functioning was obtained.

Based on the results in Table II, a slight increase in CO_2 production in winter and a small decrease of this indicator in summer can be observed. On the contrary to an ambiguous effect of repowering on carbon dioxide emissions, a substantial decrease in the emissions of other pollutants as a result of partial replacement of mixed petroleum residue by cleaner gaseous fuel combustion, in line with the results of underlying studies[26,27].

Furthermore, an increase in electrical efficiency from 19.6 % to 23.1 % in winter and from 21 % to 27.8 % in summer was obtained by calculations. It can be assumed, that this difference is caused by adding a new, more efficient source of electric energy production, while there is only a slight increase in fuel energy input in winter. The observable increase in electric efficiency is in line with the findings of Rokni who performed a study on repowering an obsolete 250 MWe coal-fired power plant by gas turbines and achieved an increase of electric efficiency from the base value of 33 % to around 50 % in full repowering mode[28]. However, on the contrary to our study, Rokni assumed invasive repowering resulting in an over 100 % increase in total power production of the plant, whereas the repowering in this study yielded only a modest 20 % power production increase. Thus, the impact on electric efficiency of the repowered plant compared to the base design is less pronounced. In summer, the demand for fuel energy input decreases because of lowering the extra electricity production by steam condensation in the condensing turbine, thus lowering the superheated steam production in the boiler.

A decrease of cogeneration efficiency by over 1 % in winter is due to higher fuel energy consumption associated by elevated stack losses, while in summer, the increase of the cogeneration efficiency by almost 10 % occurs. It is worth mentioning that the load of the last expansion stage of the ECT does not fall below the permitted limit of 20 t/h of wet steam.

Conclusion

The aim of this case study was to describe the old thermal power plant functioning with the repowering options evaluation.

In summer, cogeneration and electricity production efficiency appears to be lower. The reason is reduced demand for export steam, which means higher amount of steam expanding in the low-pressure part of the turbine resulting in more waste heat production. This stresses the need to considerate the seasonal impact on CHP operation[29,30]. Repowering yields an increase of cogeneration efficiency, and, as a result, lower fuel consumption and CO_2 emissions.

According to study conducted in Departments of Mechanical Engineering of various universities in Iran, using GT is an essential repowering method used for energy production improvement and operating lifetime of the unit extension[31]. As the results in Table II show, it is obvious that adding GT to the cycle leads to more efficient electricity production.

This study presents one of the many methods how to balance between the increasing energy production demand and the need for a cleaner environment.

Acknowledgement

This research was supported by the Slovak Research and Development Agency under the contract Nr. APVV-18-0134.

References

1. Gerres T., Chaves Ávila J. P., Llamas P. L., San Román T. G.: J. Cleaner Prod. *210*, 585 (2019).
2. Rehfeldt M., Globisch J., Fleiter T.: Energy Strategy Rev. *26*, 100407 (2019).
3. Zroichikov N. A., Prokhorov V. B., Tupov V. B., Arkhipov A. M., Fomenko M. V.: Therm. Eng. *62*, 146 (2015).
4. Rimár M., Abraham M., Fedák M., Kulikov A., Oravec P., Váhovský J.: MM Sci. J. *2019*, 2935 (2019).
5. Cowell R.: Geoforum *112*, 73 (2020).
6. Štofová L., Szaryszová P., Mihalčová B.: Energies *14*, 1720 (2021).
7. Hamels S.: Energies *14*, 2165 (2021).
8. Rimár M., Kulikova O., Kulikov A., Fedák M.: Sustainability *13*, 4405 (2021).
9. Nikbakht Naserabad S., Mobini K., Mehrpanahi A., Aligoodarz M. R.: Front. Energy *9*, 54 (2015).
10. Filippov S. P., Dil'man M. D.: Therm. Eng. *65*, 775 (2018).
11. Havel P., Šimovič T.: Electr. Power Syst. Res. *95*, 47 (2013).
12. Li Z., Zhao L., Du W., Quian F.: Chin. J. Chem. Eng. *21*, 520 (2013).
13. Ameri M., Mokhtari H., Sani M. M.: Energy *156*, 371 (2018).
14. Teplická K., Kováč M., Škvareková E., Seňová A.: TEM J.: Technol. Educ. Manag. Inf. *9*, 1419 (2020).
15. Qvist S., Gładysz P., Bartela Ł., Sowiżdżał A.: Energies *14*, 120 (2021).
16. Harbulakova V. O., Zelenakova M., Purcz P., Olejnik A.: Environments *5*, 19 (2018).
17. Ziółkowski P., Kowalczyk T., Lemański M., Badur J.: Energy Convers. Manage. *192*, 374 (2019).
18. Iliev I. K., Terziev A. K., Beloev H. I., Nikolaev I., Georgiev A. G.: Energy *221*, 119755 (2021).
19. Ahmadi G., Toghraie D., Akbari O. A.: Energy *159*, 937 (2018).
20. Abudu K., Igie U., Roumelitois I., Hamilton R.: Appl. Therm. Eng. *189*, 116703 (2021).
21. Guo Ch., Zuo Z., Feng H., Roskilly T.: Appl. Therm. Eng. *189*, 116679 (2021).
22. Araner: *Turbine Gas Power Plants vs Gas Engine.* https://www.araner.com/blog/turbine-gas-power-plants-vs-gas-engine, [cit. 02.06.2021].
23. Soares C.: *Gas Turbines*. Butterworth-Heinemann, UK (2008).
24. Bafrncová S., Šefčíková M., Vajda, M.: *Chemické inžinierstvo – tabuľky a grafy.* SCHK Bratislava, Slovensko (2018).
25. Ma L., Zhihua G., Zhang F., Wei H.: Energy *201*, 117469 (2020).
26. Křůmal K., Mikuška P., Horák J., Hopan F., Krpec K.: Chemosphere *229*: 51 (2019).
27. Strachan N., Farrell A.: Energy Policy *34*: 2677 (2006).
28. Rokni M.: Energies *9*: 399 (2016).
29. Zymelka P., Szega M.: Energy Convers. Manage. *231*, 113860 (2021).
30. Rimar M., Abraham M., Fedak M., Vahovsky J., Kulikov A.: MATEC Web Conf. *168*, 06003 (2018).
31. Mehrpanahi A., Naserabad N. S., Ahmadi, G.: Energy *179*, 1017 (2019).

MATERIAL ENGINEERING

PHONOLITE. AN AVAILABLE, NATURAL CZECH RESOURCE FOR PRODUCING NOVEL VALUABLE MATERIALS

Hidalgo-Herrador J.M.[1], Tišler, Z.[1], Frątczak J.[1], de Paz Carmona H.[1], Velvarská R.[1], Kocík J.[1]

[1]ORLEN UniCRE a.s., Revoluční 1521/84, 400 01 Ústí nad Labem, Czech Republic
jose.hidalgo@orlenunicre.cz

Abstract

Phonolite is a volcanic rock formed mainly by alkali feldspar and other compounds. It can be used as a dimension stone, aggregate for gravels, ceramics, and glass production. We found that the material can be used as an asphalt binder, an adsorbent or a catalyst support after its modification by using an acid treatment that increases its porosity and changes its structure. Modified phonolite NiW metal supported catalysts were tested for hydrotreatment of triglycerides and mesityl oxide. The experiments were carried out in an autoclave and flow reactor. Satisfactory results were found, indicating that the phonolite could be a low-cost effective valuable material for the industry especially considering that it can be obtained close to the industrial area facilities in the Ústí region located in Czechia.

Introduction

Having near available strategic source materials for industrial production is a key factor obtaining higher economic stability. An example can be the ore resources present in the region. The advantage if the ore is a common mineral present in the region and can be extracted and used for industrial purposes is clear. Concretely, phonolite is an ore present in the Northwest of the Czech Republic and already being extracted mainly as for dimension stone, aggregate for gravels, ceramics and glass production. It can be used for other purposes due to its specific properties. Phonolite is an alkali igneous rock formed composed mainly of feldspar[1]. Many publications were written about phonolite by many researchers, but they were mainly under geology, geochemistry or mineralogy. However, some publications were found about modifying of the phonolite structure at high temperature and pressure[2–5]. For other materials, the acid treatment has been studied for catalysis, agriculture or membranes. It can be an effective way to modify the structure and composition of the raw material (phonolite in this case)[1]. The acid treatment could produce a new and more porous material compared to the initial phonolite. This new solid could be an exciting material to use as a catalyst, adsorbent or asphalt binder for roads[6, 7].

The raw material phonolite can be found in many locations of the Czech Republic near industrial facilities, such as the located one in the Northwest of the Czech Republic in the city of Litvínov. So, this solid is nearly available and could be used as a cost-effective (relatively cheap mineral) raw material in case of using it as asphalt binder or to produce adsorbents or catalysts[6-10].

The acid treatment of the phonolite led to the production of new porous material. It implied a change in its structure and decreased in the total content of Al and an increment in the Si content (including a notable decrease in the Na content)[8, 11]. The raw material and the newly produced solid had a specific surface BET of 4.9 and 167 $m^2\ g^{-1}$. In addition, the acid properties were different for both materials increasing the weak acid sites for the produced solid[8]. The new solid was then tested as an adsorbent for the cleaning of waste cooking oil. The new sample absorbed Ca, Mg, K, P and Na from the waste cooking oil[8].

This new solid was also tested as a catalyst[6-11]. Concretely, the phonolite was tested, in the reaction of deoxygenation-hydrocracking of triglycerides (animal fat) and hydrodesulfurisation of atmospheric gas oil (AGO) and the reduction of mesityl oxide (MES)[6-11]. The new synthesised material applications are useful as probed for the triglycerides hydrodeoxygenation reaction producing second-generation biofuels. By another way, these catalysts can be used directly in the refinery with pure fossil fuels, co-processing or green feedstocks[6-11].

This work aims is to inform about novel possibilities of phonolite as a valuable raw material (Fig. 1). Some novel applications were found in our Research Institute, such as asphalt binder, adsorbent and catalyst[6-10]. Considering that the phonolite is a rich mineral in SiO_2-Al_2O_3, it could be used for similar processes to commercial catalysts based in SiO_2-Al_2O_3, commonly used in the refineries.

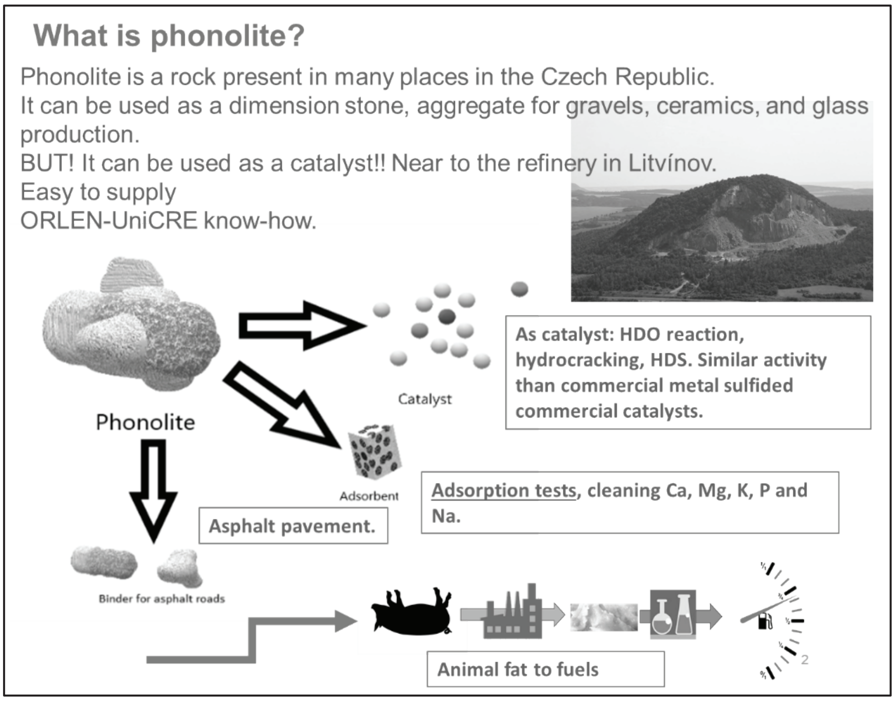

What is phonolite?

Phonolite is a rock present in many places in the Czech Republic.
It can be used as a dimension stone, aggregate for gravels, ceramics, and glass production.
BUT! It can be used as a catalyst!! Near to the refinery in Litvínov.
Easy to supply
ORLEN-UniCRE know-how.

As catalyst: HDO reaction, hydrocracking, HDS. Similar activity than commercial metal sulfided commercial catalysts.

Adsorption tests, cleaning Ca, Mg, K, P and Na.

Asphalt pavement.

Animal fat to fuels

Figure. 1 Modified phonolite uses[7-11].

New experimental results using acid-modified phonolite to reduce MES were included in this work. The MES is a compound that can be obtained from acetone. It can be used as a solvent or as an intermediate to produce methyl isobutyl ketone (MIBK), a commonly used solvent. The steps to produce the MIBK start commercially from the cumene hydroperoxide commercial process to produce acetone (the dehydrogenation of 2-propanol can also prepare the acetone), continuing with the MES or the diacetone alcohol (DAA) production, which can be produced from the aldol condensation of the acetone[12, 13]. The modified phonolite-based catalyst was an active material for producing MIBK, 2,3-dimethyl butane-2, 2-methyl pentane (2MP), and 3-methyl-2-pentene, the main products MIBK and 2MP.

Experiment

MES was produced in ORLEN UNICRE from acetone (Aldol condensation of acetone to form diacetone alcohol (DAA) by using Mg-Al solids (2x Acetone ⇔ 1x DAA / Mg-Al catalyst). The liquid phase acid catalysed dehydration of DAA to form MES and water (DAA ⇔ MES + H_2O) (acid catalyst) was performed.
A NiW/phonolite catalyst was used. The mineral (Ph) was treated by using oxalic acid.
The raw Ph material was treated with oxalic acid (Ph-Ox). Before the catalyst preparation, the phonolite sand was sieved using a Retsch AS300. The solids were dried at 120 °C overnight. Then, it was leached using 1 M of oxalic acid solution (80 °C for 4 h). The Ph/acid solution (g/mL) ratio was 1:10. The product was then filtered, washed (hot demineralized water), and dried overnight at 120 °C. Then the dried samples were calcined at 500 °C for 6 h (1 °C min^{-1}) in air. The resulting solids were impregnated with Ni nitrate and ammonium metatungstate (to 5 and 10 wt% of Ni and W respectively). Finally, the catalyst was calcined for 6 h at 450 °C (1 °C min^{-1}) in air. The catalyst obtained was called NiW/Ph-Ox. The overall summary is represented in Fig. 2.

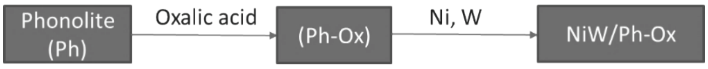

Figure 2. Summary of the NiW/Ph-Ox synthesis.

The composition of the catalysts was obtained by XRF using an S8 Tiger (Bruker AXS, Advanced X-ray Solutions GmbH, Karlsruhe, Germany) with an Rh cathode.
The solids area BET specific surface was determined by N_2 adsorption/desorption using an Autosorb iQ. A Micromeritics AutoPore IV 9510 mercury porosimeter Mercury was used for the porosimetry measurements

(Micromeritics Instrument Corporation, Norcross, GA, USA). All samples were dried before their analysis at 110 °C for 16 h.

An autoclave 4575/76 with a “4848B” controller (Parr Instruments Company, Moline, IL, USA) was used for the tests. The catalyst was activated–sulfided using di-t-butyl polysulfide (Lubrizol Company,Wickli_e, OH, USA). In total, 4.2 g of the catalyst and 20 g of di-t-butyl polysulfide were introduced into the reactor. The reactor was pressurized to 50 bar and heated from room temperature to 340 °C (8.3 °C min^{-1}) while maintaining the temperature for 2 h. The reactor was then cooled to room temperature and depressurized. The catalyst was extracted and conserved under N_2 atmosphere.

For the MES reduction tests, the autoclave was opened, and 25 g of MES, 1 g of previously sulfided catalyst and 0.14 g of di-t-butyl polysulfide were introduced into the reactor. The reactor was then flushed with nitrogen, pressurized to 150 bar (safety pressure test during two hours) and finally depressurized-flushed-prepared-closed at 50 bar (H_2). The autoclave was then heated to 325, 350 and 375 °C (8.3 °C min^{-1}) maintaining this maximum temperature for 0.5, 1 and 1.5 h. The autoclave was then cooled via air flow with an average cooling temperature rate of 4.5 °C min^{-1}. The products were then analysed by GC-FID Agilent 7890 and GC-MS (GCMS – QP2010 Shimadzu) to identify and quantify all the compounds respectively.

Response surface methodology tool (RSM) was used to carry out the tests according to the literature[14]. Least-squares were used to fit the dependent variable, which for the present study was either MIBK or 2MP product content. The used variables and coded factors are shown in Table I.

The response surface methodology (RSM) using only two variables was used as shown in table I.

Table I

Variables used for the RSM. Reactions carried out (MES name).

Level	**Temperature, °C**	**time, min**
-1.00	325	30
0.00	350	60
1.00	375	90

TEST-MES	**X_1**	**X_2**	**Temperature, °C**	**Time, min**
MES-1	-1	-1	325	30
MES-2	1	-1	375	30
MES-3	-1	1	325	90
MES-4	1	1	375	90
MES-5	0	0	350	60
MES-6	0	0	350	60
MES-7	0	0	350	60
MES-8	0	0	350	60
MES-9	0	0	350	60

Discussion and result analysis

The phonolite raw material, the treated phonolite with oxalic acid and the catalyst (non-sulfided and sulfided) presented different compositions. XRF analyses results are shown in the table below. The results were the same as the found ones in a previous publication[11].

Phonolite treatment with oxalic acid indicated a reduction in the Al, Na, Fe, and Ca contents (Table II). The results for nickel and tungsten contents were as expected. The acid treatment resulted in a solid with a higher porosity (Table III). The basic raw material to obtain the catalysts (phonolite) has very poor textural properties, and its treatment with acid led to dramatic changes in the material’s textural properties (an increase in pore volume and specific surface area), with a higher total pore volume compared to the raw material.

Table II.
X-ray fluorescence (XRF) elemental analysis for the supports, original phonolite material (Ph),support (Ph-Ox) and catalyst (NiW/Ph-Ox) and catalyst sulfided (NiWSx/Ph-Ox).

	Ph	**Ph-Ox**	**NiW/Ph-Ox**	**NiWSx/Ph-Ox**
Si, wt%	26.5	34.0	27.5	21.2
Al, wt%	11.8	7.3	6.1	3.0
Ni, wt%	0.0	0.0	4.4	2.2
W, wt%	0.0	0.0	9.5	4.7
Na, wt%	7.9	2.6	2.2	1.0
K, wt%	5.1	6.9	6.3	3.2
Fe, wt%	1.4	0.7	0.7	0.7
Cl, wt%	0.3	0.0	0.0	0.0
S, wt%	0.0	0.0	0.0	22.0
Others, wt%	0.9	0.1	0.5	0.4
O, wt%	46.1	48.3	42.8	41.6

Table III
Textural properties of the original phonolite material and its derived solids.
* Hg porosimetry, ** N_2 physisorption.

	Ph	**Ph-Ox**	**NiW/Ph-Ox**
Total intrusion volume (cm^3 g^{-1}) *	0.008	0.201	0.130
Pore volume 3–50 nm (cm^3 g^{-1}) *	0.003	0.024	0.010
BET surface area, m^2 g^{-1} **	7.6	114.3	49.3

A conversion lower than 2 wt% to C1-C4 gaseous light products was found (mass balance) in all cases. The main products were the MIBK and the 2-methyl-pentane (2MP) in all cases. Other interesting compounds such as the 2-methyl-2-pentene and DMB were obtained as shown in Fig. 3.

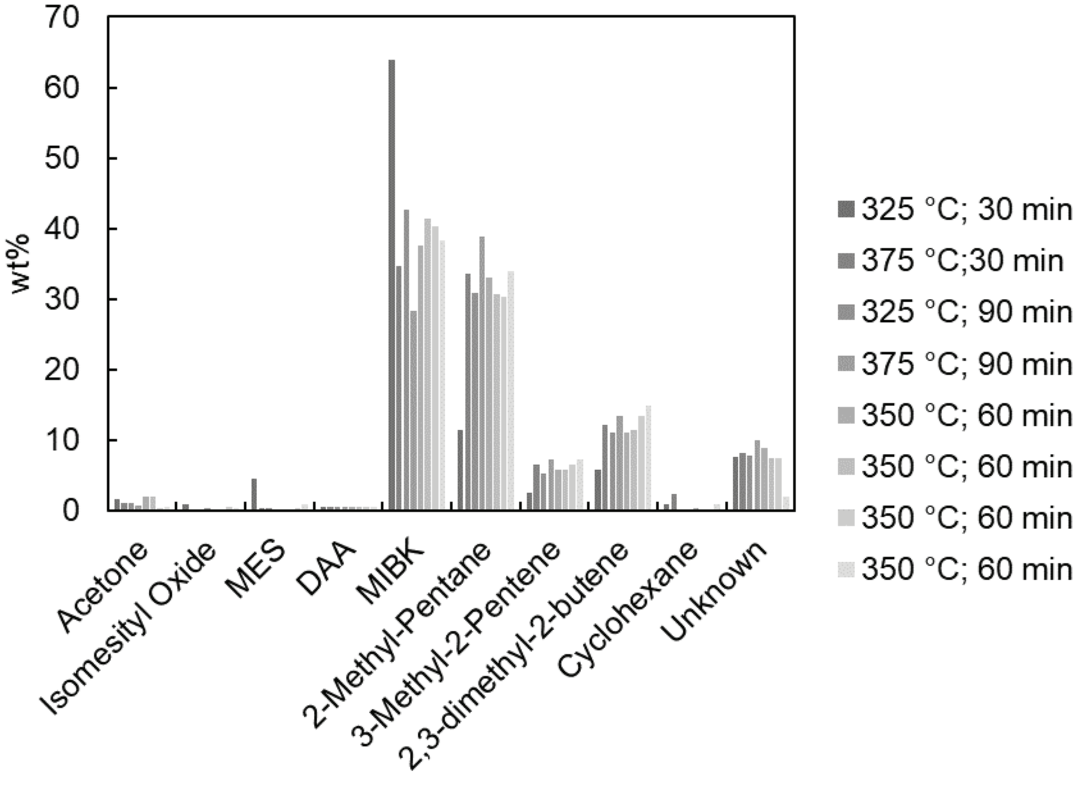

Figure 3. Compounds present in the final product. DAA is diacetyl acetone.

Using the RSM, the theoretical values of the MIBK and 2MP could be obtained at different times of reaction and temperatures. The MIBK content varied from 65 wt% to 35 wt% from 325 to 375 wt%, indicating that the temperature increment led to decreased MIBK and increased the 2MP (Figure 4). The decrease of MIBK in the product implied an increase in the 2MP content, indicating that the MSO is hydrogenated to MIBK and then to 2MP, having unprecedented results (Figure 5). The theoretical and experimental values were similar Figures 4 and 5 were obtained using the theoretical next equations (obtained by using the RSM):

MIBK equation: Y (MIBK content, wt%) = -5.287 + 1.178 T - 2.612 t + 0.005 T t - 0.003 T T + 0.005 t t

2MP equation: Y (2MP content, wt%) = -5.693 - 0.542 T + 2.442 t - 0.005 T t + 0.002 T T -0.005 t t

Being T the temperature of reaction and t the time of reaction (Table I).

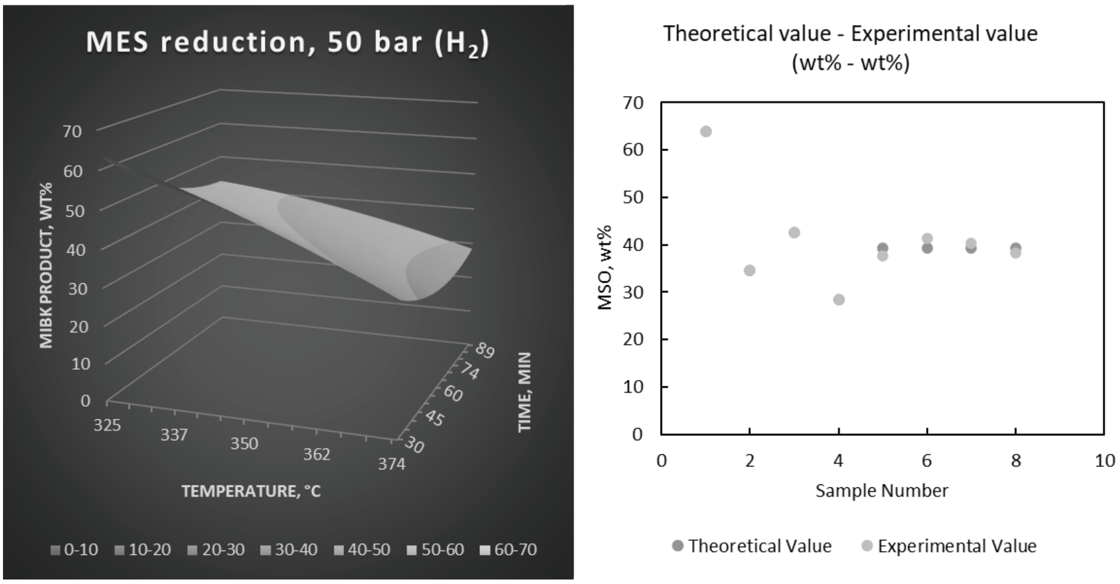

Figure 4. MIBK total amount in the product at different temperatures and times of reaction. The theoretical and experimental values were compared.

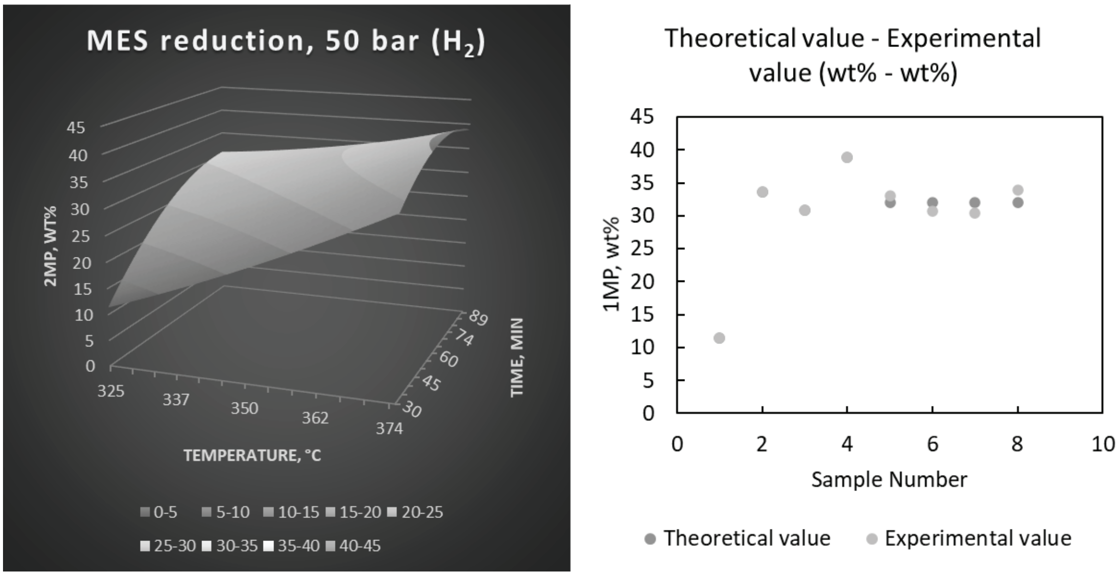

Figure 5. 2MP production at different temperatures and time of reaction. The theoretical and experimental values were compared.

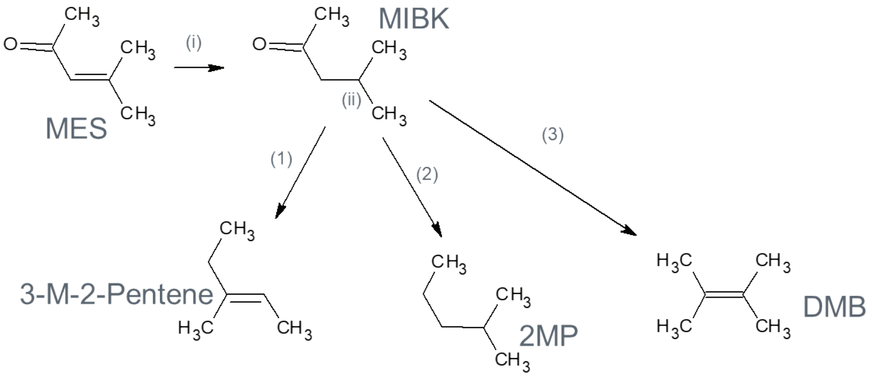

Figure 6. Summary of the reaction pathways: (i) MES to MIBK, (ii) MIBK to (1) 3-methyl-2-pentene, (2) 2MP and (3) DMB.

Conclusion

The phonolite is a potential raw material for adsorbent, asphalt binder and catalyst for hydrotreating reactions. The acid modification of the raw material phonolite led to the production of new catalysts. The produced catalyst containing Ni and W was active for the MES reduction producing mainly MIBK and 2MP. So, a new available near-located to the refinery alternative to traditional commercial catalysts was found.

Acknowledgement

The publication is a result of the project which was carried out within the financial support of the Ministry of Industry and Trade of the Czech Republic with institutional support for long-term conceptual development of research organisation. The result was achieved using the infrastructure included in the project Efficient Use of Energy Resources Using Catalytic Processes (LM2018119) which has been financially supported by MEYS within the targeted support of large infrastructures.

References

1. Britannica, The Editors of Encyclopaedia. "Phonolite". Encyclopedia Britannica, 2 Jun. 2017, https://www.britannica.com/science/phonolite. Accessed 26 May 2021.
2. Moussallam Y., Oppenheimer C., Scaillet P., Kyle R.: J. Petrology *54*, 1285 (2013).
3. Kutolin V. A., Shirokih V. A.: Tailings and mine waste reprocessing for production of the foamed glass, 5th Annual International, Conference on Tailings and Mine Waste, Colorado State Univ., Ft. Collins, Civil Engineering, Geotech Engineering Program, Tailings and mine waste 98, 909 (1998). Edited by J.D. Nelson.
4. Capitaneo J. L., Silva F. T., Vieira C. M. F.: Silic. Ind. *70*, 161 (2005).
5. Teixeira A. M. S., Garrido F. M. S., Medeiros M. E., Sampaio J. A.: Int. J. Miner. Process. *145*, 57 (2015).
6. Morin S., Berreghis A., Ayrault P., Gnep N. S., Guisnet M.: J. Chem. Soc. Faraday Trans. *93*, 3269 (1997).
7. Matoušek L., Jíša P., Černý R.: Proceedings of the 5th International Conference on Chemical Technology, 327 (2017).
8. Hidalgo-Herrador J. M., Tišler Z., Hajková P., Soukupová L., Zárybnická L., Černá K.: Acta Chim. Slov. *64*, 598 (2017).
9. Hidalgo J.M., Tišler Z., Vráblík A., Velvarská R., Lederer J.: React. Kinet. Mech. Cat. *126*, 773 (2019).
10. Hidalgo Herrador J. M., Frątczak J., Tišler Z., Velvarská R.,Kocík J.: Utility Model (Užitný vzor) CZ 35055 U1, Industrial Property Office of the Czech Republic
11 Hidalgo Herrador J. M., Frątczak J., Tišler Z., de Paz Carmona H., Velvarská R.: Molecules, *25*, 3732 (2020).
12. Thotla S., Agarwal V., Mahajani S. M.: Chem. Eng. Sci., *62*, 5567 (2007).
13. Kuśtrowski P., Sułkowska D., Chmielarz L., Rafalska-Łasocha A., Dudek B., Dziembaj R.: Micropor. Mesopor. Mat. *78*, 11 (2005).
14. Pinto F., Paradela F., Gulyurtlu I., Ramos A. M.: Fuel Process. Technol., *116*, 271 (2013).

DECARBONISATION OF THE CHEMICAL INDUSTRY IN LIGHT OF GREEN DEAL

Souček I.[1, 2]

[1] *University of Chemical Technology, Technická 5. Technická 5, 166 28 Prague 6*
[2] *Association of the Chemical Industry of the Czech Republic, Rubeška 393, 190 00 Prague 9*

Abstract

The article comments the development of the EU chemical industry in the last year, esp. in light of effects of the pandemy COVID-19 and options for economic recovery in light of European Green Deal. Green Deal for Europe is commented focusing on the chemical industry. Specifics related to feedback of the Czech Republic are described referring to the strategic document in progress: Decarbonization Study of the Czech industry and Hydrogen Strategy of the Czech Republic. The issue of decarbonization of the chemical industry are elaborated.

Introduction

The development of the chemical industry is significantly dependent on the overall development of the economy, resp. downstream demand and consumer consumption.

In 2020, Czech chemistry recorded a drop in sales, similar to the whole of Europe, due to the COVID-19 pandemic. The expected recovery will undoubtedly be influenced by the promotion of "sustainable development" in relation to new EU legislation: European Green Deal and related Chemical strategy for Sustainability.

Development of the EU chemical industry in 2020

While the overall decline of the EU economy was 6.2%, the development of the EU chemical industry recorded a decline of "only" 1.9%.

The chemical industry expects growth of 3% in 2021, depending on the "dealing with a pandemic", driven by a recovery in demand in the automotive, consumer durables and recovery stocks; monitoring the development of GDP and generating demand for services and investments.

Despite the rapid recovery in China, the chemical industry declined by 0.4% worldwide.

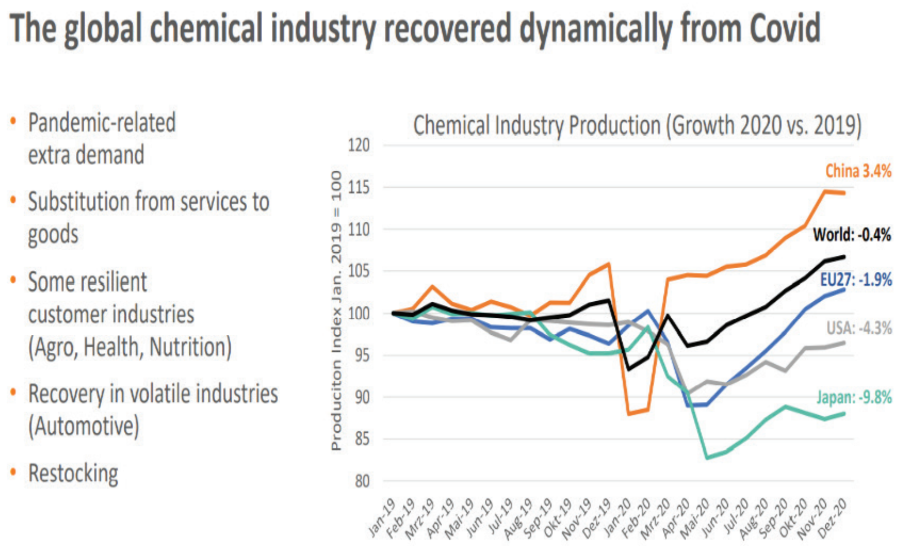

The global chemical industry recovered dynamically from Covid

- Pandemic-related extra demand
- Substitution from services to goods
- Some resilient customer industries (Agro, Health, Nutrition)
- Recovery in volatile industries (Automotive)
- Restocking

Figure 1. Chemical production index development
Source: Cefic

Green Deal for Europe

It renews the EC's commitment to tackling climate change.

Transforming the EU into a fair and prosperous society with a modern, competitive and resource-efficient economy, without net greenhouse gas emissions by 2050 and where economic growth is decoupled from resource use.

Protect, preserve and improve the EU's natural capital and protect the health and well-being of its citizens from environmental risks.

Figure 2. European Green Deal components
Source: European Commission

Main related EU legislative aspects for 2021:

- ETS review (legislative, incl. impact assessment)
- ETS rules for aviation review (legislative)
- ESR review (legislative)
- LULUCF review (legislative)
- Revision of the Energy Taxation Directive (legislative, incl. impact assessment)
- Carbon border adjustment mechanism (legislative, incl. impact assessment); opinion report by the European Parliament's environment committee to be debated on Oct. 28 2020, committee vote expected in Jan. 2021.
- Energy Efficiency Directive review (legislative)
- Renewable Energy Directive review (legislative)
- Proposal for an EU carbon farming initiative (legislative)

Pursuant to Commission Implementing Regulation (EU) 2021/447 of 12.3.2021 setting revised benchmarks for the allocation of free allowances for the period 2021 to 2025 pursuant to Article 10a (2) of Directive 2003/87 of the European Parliament and of the Council / EC there is a drastic reduction in benchmarks for adjusting the free allocation with a significant impact on the need to purchase allowances in the event of a sharp rise in price.

Table I
EU ETS Benchmark definition for industrial sectors (NACE)

	Product benchmarks with exchangeability of fuel and electricity Product benchmark	NACE code	**Benchmark 2021-2025 Commission decision March 2021**	**Benchmark 2021-2025 versus phase 3 2013-2020**
1	Carbon black	20.13	**1,485**	-24,0%
2	Ammonia	20.15	**1,570**	**-3,0%**
3	Steam cracking	20.14	**0,681**	**-3,0%**
4	Aromatics	20.14	**Not applicable**	-24,0%
	Aromatics CWT	20.14	**0,0228**	**-22,6%**
5	Styrene	20.14	**0,401**	-24,0%
6	Hydrogen	20.11	**Not applicable**	-24,0%
	Hydrogen 300 CWT	20.11	**6,840**	**-22,6%**
7	Synthesis gas	20.11	**Not applicable**	-24,0%
	Synthesis gas CWT	20.11	**0,187**	**-22,7%**
8	EO-EG	20.14	**0,389**	-24,0%
	Refinery CWT (CO_2 weighted tonne)		**0,0228**	**-22,6%**

	Product benchmarks without exchangeability of fuel and electricity Product benchmark	NACE code	**Allocation 2021-2025 Benchmark 2023 Commission decision March 2021**	
1	Nitric acid	20.15	**0,230**	-24,0%
2	Adipic acid	20.14	**2,120**	-24,0%
3	VCM, incl. EDC	20.14	**0,155**	-24,0%
4	Phenol/acetone	20.14	**0,230**	**-13,5%**
5	S-PVC	20.16	**0,066**	**-22,7%**
6	E-PVC	20.16	**0,181**	-24,0%
7	Soda ash	20.13	**0,753**	**-10,7%**
	Fall-back benchmarks			
1	Heat benchmark		**47,3**	-24,0%
2	Fuel benchmark		**42,6**	-24,0%

Chemical industry of the Czech Republic response

Expected priorities:

- Decarbonization of energy
- Decarbonisation of energy-intensive industries
- Decarbonisation of other consumers

Conditions:

- Electricity availability (see Sky - Shell scenario)
- Availability of green electricity
- Availability and efficiency of CCSU

At the same time, the estimated electricity consumption in the Czech chemical industry is 3-4 TWh / year. The expected electricity consumption is 8-12 TWh / year, provided that the most energy-intensive operations are shut down. Required measures to achieve the decarbonised 2050 sector - unlike several other sectors, we have not been able to describe specific technological changes for several reasons:
The expected availability of (green) electricity in the Czech Republic is not clear

The perspective of fossil fuel-based industries (coal, natural gas, oil) is not clear
The perspective of the polymer industry is not clear (campaigns against the use of disposable plastics, elimination of microplastics…). The perspective of circular technologies, such as chemical recycling, is not clear
Conditional policies and strategies need to be revised or are still in the process of being processed (Net Mobility vs. Hydrogen Strategy of the Czech Republic).
A 55% reduction in GHG emissions in 2030 is realistic, carbon neutrality is conditional on higher investments as necessary (investment / operating aid.

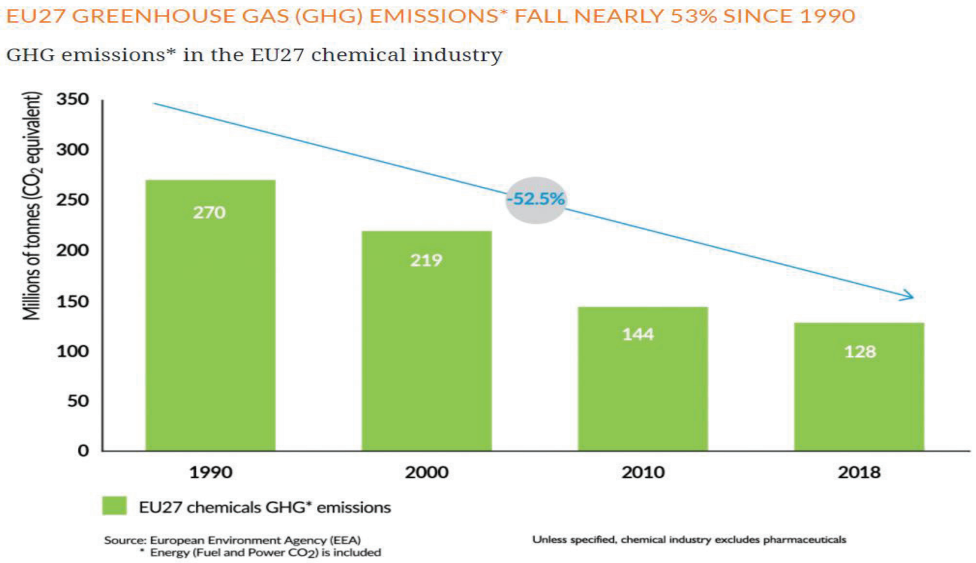

Source: European Environment Agency (EEA)
* Energy (Fuel and Power CO2) is included

Unless specified, chemical industry excludes pharmaceuticals

Figure 3. GHG emission development in EU chemical industry

According Synergy coalition the use of water is becoming the main option for future sustainable and renewable energy sourcing.

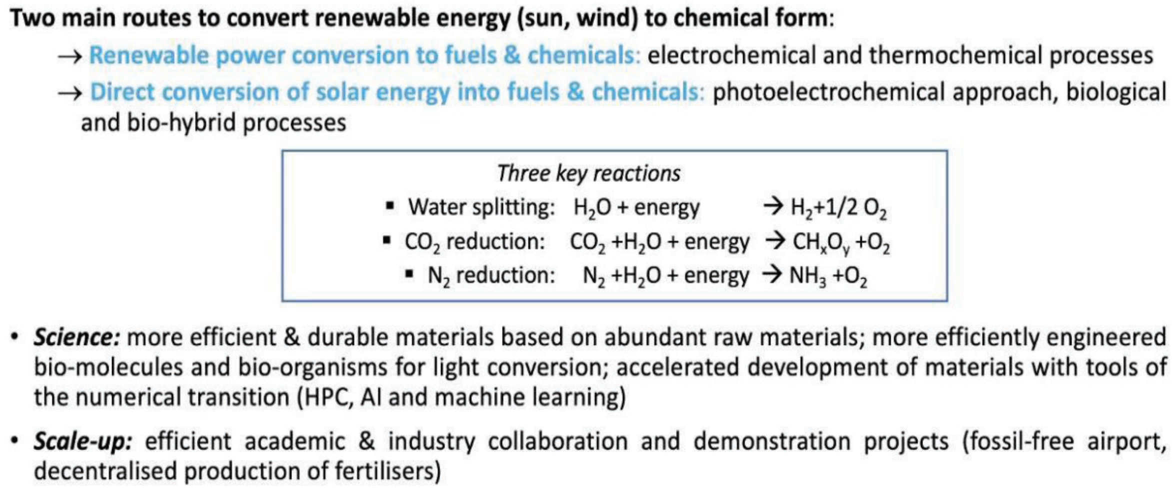

Two main routes to convert renewable energy (sun, wind) to chemical form:

→ Renewable power conversion to fuels & chemicals: electrochemical and thermochemical processes
→ Direct conversion of solar energy into fuels & chemicals: photoelectrochemical approach, biological and bio-hybrid processes

Three key reactions

- Water splitting: $H_2O + \text{energy} \rightarrow H_2 + 1/2\ O_2$
- CO_2 reduction: $CO_2 + H_2O + \text{energy} \rightarrow CH_xO_y + O_2$
- N_2 reduction: $N_2 + H_2O + \text{energy} \rightarrow NH_3 + O_2$

- ***Science:*** more efficient & durable materials based on abundant raw materials; more efficiently engineered bio-molecules and bio-organisms for light conversion; accelerated development of materials with tools of the numerical transition (HPC, AI and machine learning)
- ***Scale-up:*** efficient academic & industry collaboration and demonstration projects (fossil-free airport, decentralised production of fertilisers)

The future of the development of hydrogen consumption in the Czech Republic
Consumption growth for current producers is not yet indicated, but a gradual conversion of production (green hydrogen) for large producers can be expected on the basis of possible massive support from industrial decarbonisation programs while "irreplaceable" existing technologies with regard to their integration into existing technologies (CCU implementation) , for medium - sized sources, it is possible to assume support for the production of hydrogen from biomethane (steam reforming) or with electricity from renewable sources in electrolysers.
The application of new innovative technologies can be expected in the longer term.
An increase in hydrogen production can also be expected due to possible investments in hydrogen mobility. Unfortunately, the wider development of this segment is related to the focus of the automotive industry in Europe on electromobility. In any case, we do not expect an increase in consumption in this segment in the

coming years exceeding a maximum of 1-2,000 t / year (even with the rapid development of, for example, local bus transport).

However, all projects are tied to the economic decision of the owners, again after the political decision on support from the state budget. The aid may be towards the necessary investments or (rather) towards operating costs (gas / electricity).

Current estimated cost for fossil fuel-based hydrogen is around €1.5/kg (US$1.82/kg) for the EU, although this is highly dependent on natural gas prices. Current estimated costs today for fossil fuel-based hydrogen with carbon capture and storage are around €2/kg, and renewable hydrogen €2.5-5.5/kg.

Public presentations by companies such as Hydrogenics and conversations with other electrolyser manufacturers confirm that the assumptions and approaches in the two preceding paragraphs are realistic and valid.

Table II

Hydrogen pricing

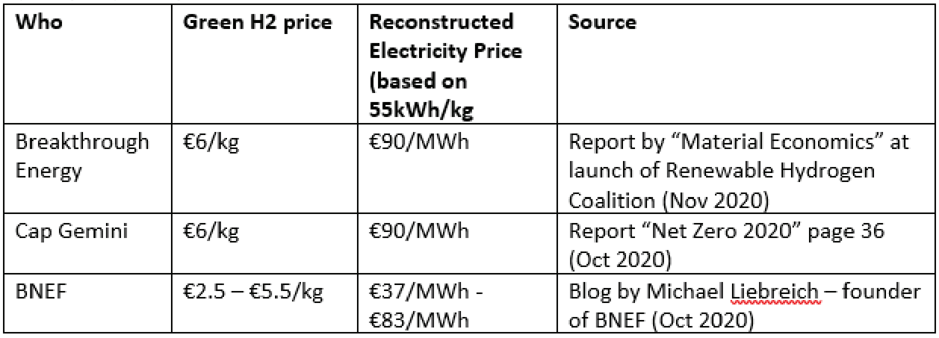

Who	**Green H2 price**	**Reconstructed Electricity Price (based on 55kWh/kg**	**Source**
Breakthrough Energy	€6/kg	€90/MWh	Report by "Material Economics" at launch of Renewable Hydrogen Coalition (Nov 2020)
Cap Gemini	€6/kg	€90/MWh	Report "Net Zero 2020" page 36 (Oct 2020)
BNEF	€2.5 – €5.5/kg	€37/MWh - €83/MWh	Blog by Michael Liebreich – founder of BNEF (Oct 2020)

Source: EIA

Background:

Use of existing (gray hydrogen) and gradual application of promising technologies (blue, green, etc. hydrogen), the possibility of including the possibility of using surpluses for the development of the distribution network.

Estimated share of hydrogen in transport in the EU (Shell 2018) - about 3-6% in 2050 vs. current declarations on the share of hydrogen in total energy consumption in total up to 15%.

Conclusions

The opinion of the Association of the Chemical Industry of the Czech Republic, published last year, appealed several times to separate the recovery of the economy after the Covid crisis from the "green recovery". This is led by the fact that currently most "green investments" are operationally economically "demanding" (meaning: often loss-making if no operating subsidy is provided). Economic recovery needs to be supported in order to create sufficient own resources for further (and green) investment.

However, the EU envisages using the current crisis to carry out a green recovery. It offers huge investment resources for its implementation. These funds should be used mainly for environmental investments, and it would be a shame not to use them in chemical sector as well. However, these resources should be approached with caution with the following priorities:

- Use funds for prepared and already approved ecological investments focused mainly on air protection (reduction of emissions), energy and water savings.
- Consider using funds to decarbonise industry, again by saving energy, switching to less emission fuels (however, it is necessary to take into account the aspect of the future economy of operation), the introduction of renewable energy production (here too the future economy of operation is key).
- Consider the use of funds for technologies aimed at the circular economy: in particular the chemical recycling of waste (specifically plastic waste), the use of CO2 for the synthesis of hydrocarbons (this will often involve the need for investment to ensure hydrogen production).
- Ensure the completion of the development of innovative technologies for the production of hydrogen with the assumption of their economic efficiency,
- And last but not least, it is a range of investments for energy storage. Here it is absolutely necessary to assess the economics of operation at current prices of electricity and support tools, respectively. current support for the development of solar and wind energy, which cannot do without accumulation for the stability of the distribution network. However, the question is whether this is an opportunity for our industry, although "Power-to-X" technologies can be considered as chemical technologies…

Key words

Decarbonisation, Chemical Industry, Green Deal, Hydrogen, Green Recovery

References

1. Association of the Chemical Industry of the Czech Republic: Position to European Green Deal, www.schp.cz (2020)
2. Cape Cod Climate Change*, Net Zero 2020*, conference 23.10.2020 (2020)
3. Cefic, https://cefic.org/a-pillar-of-the-european-economy/facts-and-figures-of-the-european-chemical-industry/ (2021).
4. EIA: *Net Zero by 2050*, https://www.iea.org/reports/net-zero-by-2050 (2021).
5. European Commission: *Directive 2003/87/EC of the European Parliament and of the Council establishing a scheme for greenhouse gas emission allowance trading within the Community*, Article 10a(2) (2003)
6. European Commission: *Chemical Strategy for sustainability towards a Toxic-Free Environment*, COM (2020) 667 (2020).
7. European Commission: *Regulation(EU) 2021/447 of 12 March 2021 determining revised benchmark values for free allocation of emission allowances for the period from 2021 to 2025* (2021).
8. European Green Deal, *COM (2019) 640 of 11.12.2019* (2019).
9. HIS Markit: *Europe emerges as leader in hydrogen economy*, https://ihsmarkit.com/research-analysis/europe-emerges-as-leader-in-hydrogen-economy.html (2020).
10. IEA: *The future of Hydrogen*, Report prepared for G20, Japan (2019)
11. MPO ČR: *Vyhodnocení naplňování Státní energetické koncepce ČR*, https://www.mpo.cz/cz/energetika/strategicke-a-koncepcni-dokumenty/vyhodnoceni-naplnovani-statni-energeticke-koncepce-cr--260428/ (2021).
12. Renewable hydrogen coalition: *Material Economics*, https://renewableh2.eu/ (2020).
13. Shell: *Sky Scenario*, https://www.shell.com/energy-and-innovation/the-energy-future/scenarios/shell-scenario-sky.html (2019)
14. Sunergy: *Research and Investment Opportunities for a fossil-free Europe*, https://www.sunergy-initiative.eu/copy-of-r-d-opportunities-for-a-fossi (2021)

CHITIN-CAFFEINE MODELS IN BIOCIDAL WOOD COATINGS

Kobetičová K.[1], B**öhm** M.[1], Ďurišová K.[2], Nábělková J.[2], Černý R.[1]

[1]*The Department of Materials Engineering and Chemistry, Faculty of Civil Engineering, Czech Technical University in Prague, Prague, Czech Republic*
[2]*The Department of Sanitary and Ecological Engineering, Faculty of Civil Engineering, Czech Technical University in Prague, Prague, Czech Republic*
klara.kobeticova@fsv.cvut.cz

Abstract

Caffeine was confirmed as a suitable bioactive substance in the mixture against wood fungi. On the other hand, chitin is a part of fungal bodies and has been studied in previous research as a potential packing material for caffeine. For this reason, we studied caffeine interactions with chitin (in some biological tests with fungi or chitin-caffeine aquatic mixture). Caffeine concentrations were analyzed spectrometrically. SEM technique was used to visualize for image of some interactions. Chemical experiment with pure chitin and caffeine indicates strong bonds of caffeine to chitin. The results confirmed the negative effects of caffeine on fungal growth from the present and some previous published studies. The SEM analysis observed the ability of chitin to adhere to beech wood.

Introduction

Chitin (*N*-[(2*R*)-2,4,5-trihydroxy-6-(hydroxymethyl)oxan-3-yl]acetamide) is composed of N-acetyl-D glucosamine molecules that are linked by a 1,4-β-glycosidic bonds[1,2]. It is the second most widespread polysaccharide on Earth. Chitin is a part of invertebrate cuticles and it occurs with beta-polyglucans in the cell wall of fungi. From an economic point of view, chitin and its derivative chitosan are of great importance, they are use in medicine (drug coating, gradual release of active substances), in the food industry (diets, drinks) and in an agriculture as scavengers of heavy metals and organic pollutants. In the last years, caffeine and chitin interactions in drugs were also studied[3].

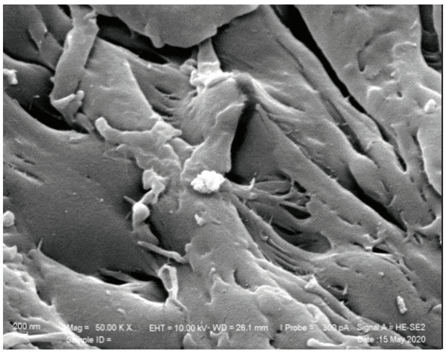

Figure 1. Photos of chitin under SEM - 5,000x magnification (author: M. Böhm)

Caffeine (1,3,7-trimethylxanthin) belongs to the methylxanthines, derivates of xanthine. It is a part of food, energetic drinks, coffee and tea drinks, chocolate. Caffeine is not toxic for humans in normal levels, but Its ecotoxicity was confirmed for water as well terrestrial environment[4,5,6]. It was also confirmed as a suitable active substance against wood pests as are fungi and moulds in the previous studies[7,8,9,10,11]. Caffeine can be up-taken, metabolise and can negatively affect synthesis of chitinase enzymes leading to lower production of chitin and fungal mass. It can leach out of the wood, causing problems with its potential outdoor use. For this reason, it is necessary to try to find a suitable packaging that will allow caffeine to remain on the wood even after exposure to rain, but at the same time to preserve its biocide effects. For this reason we tested caffeine and chitin interactions in the present study.

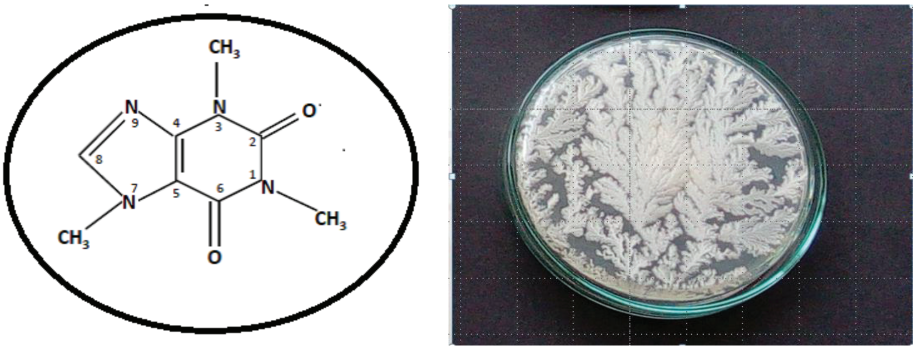

Figure 2. Caffeine chemical structure (left) and crystals (right) – (author: K. Kobetičová)

Experiment

Caffeine ($C_8H_{10}N_4O_2$) and chitin $[C_8H_{15}NO_6]_n$ were purchased from Sigma-Aldrich (Prague, Czech Republic). Deionized water was used as a solvent for the preparation of its solutions. Beech wood (*Fagus sylvatica* L.), which was purchased from company Milan Krátký (České Budějovice, Czech Republic) was a model wood material in the microscopic part of our study.

Serpula lacrymans (Schumacher ex Fries) Karsten (strain BAM Ebw. 315), *Coniophora puteana* (Schumacher ex Fries) Karsten (strain BAM Ebw. 15), *Gleophyllium sepiarium (*Wulfen) Karsten (strain BAM Ebw. 873) and *Trametes versicolor* (Linnaeus ex Freis) Pilat (strain CBS 347.63) were used. They were purchased from Timber Institute, Ltd., Březnice, Czech Republic, except for *T. versicolor* which was donated by the Mycological Department of Technical University of Zvolen, Faculty of Wood Science and Technology, Zvolen, Slovakia.

1 g of caffeine was dissolved in 1 L of boiling distilled water and then mixed with maltose agar (3% w/w). The mix was spilled into sterile glass Petri dishes. Three replicates were used for control (pure agar) and all tested concentrations. The area of agar (~ 1 cm^2) covered by fungi hyphae was transferred on the solidified agars. The agar dishes were packed into aluminum foils and stored in a thermostat in a dark. The appropriate amount of tested substance was dissolved in boiling distilled water and then mixed with maltose agar (3% w/w). The mix was spilled into sterile glass Petri dishes. Three replicates were used for control (pure agar) and all tested concentrations. The area of agar (1 cm^2) covered by fungi hyphae was transferred on the solidified agars. The agar dishes were packed into aluminum foils and stored in a thermostat in a dark.

Water stock solution of caffeine (1 g.L^{-1}) was also prepared for this type of experiment. Chitin as a powder (1 g to a liter of caffeine solution) was added. 3 replicates were used for the chemical analysis. The samples were shaken on a horizontal shaker for 24 hours. After that the samples were pulled out and the solutions were filtered through a paper filter (Machery Nagel No. 6) and analyzed spectrometrically (Spectrophotometer Libra S22) at the optimal caffeine wavelength (287 nm)[12].

Scanning electron microscope (SEM) Phenom XL (Thermo Fisher Scientific Inc.) was used to analyze the microstructure and the interaction between caffeine and the wood. After one-week of drying the solution on the treated wood, the sample was placed in a vacuum desiccator. The vacuum-dried sample was then mounted on aluminum stubs using double-sided conductive carbon tape and sputter coated with gold/palladium using a Quorum SC7620 sputter coater (Quorum Technologies Ltd.). An acceleration voltage of 15 kV, magnification of 150-5,000x, and a working distance of 10-20 mm were used for the microscopic analysis. 1 replicate (caffeine solution containing chitin) was used for the microscopic observation.

Discussion and result analysis

Biological experiments

The results of biological tests indicates gradual growth rate of fungi in the case of 0.5 g.L^{-1}. *Trametes versicolor* was partly less sensitive than the other three species at concentration 1 g.L^{-1}. The concentration 2 g.L^{-1} was 100% effective against all fungal species (see Table 1). The lower sensitivity of *T. versicolor* relates to the way part of the wood degrades fungi – *T. versicolor* represents fungi causing so called white-rot. They degrade all components of wood, including lignin[8]. The lower sensitivity of these fungi was demonstrated in some latest studies[8,12]. The other three model species belong to fungi causing brown-rot and these species are generally less resistant to biocidal substances of natural origin[13].

Table I
Growth inhibition of fungi *Gleophyllium sepiarium*, *Coniophora puteana*, *Serpula lacrymans* and *Trametes versicolor* on agar with caffeine (0.5, 1 and 2 $g.L^{-1}$) after 7, 14, 21 and 28 days of exposure to caffeine. The growth of mycelium on the top side of the samples was visually observed and rated individually using the following 6-degree scale[8] (0 indicating no growth of fungi, 1 indicating < 25% growth of fungi, 2 indicating 25-50% growth of fungi, 3 indicating 50-75% growth of fungi, 4 indicating 75-100% growth of fungi, 5 indicating 100% fungal growth)

Fungal species	7 days	14 days	21 days	28 days
Degree scale				
0.5 $g.L^{-1}$				
G. sepiarium	1	2	3	4
C. puteana	1	3	4	5
S. lacrymans	1	2	2	3
T. versicolor	1	3	3	4
1 $g.L^{-1}$				
G. sepiarium	1	1	1	0
C. puteana	1	1	1	0
S. lacrymans	1	1	1	0
T. versicolor	1	1	1	2
2 $g.L^{-1}$				
G. sepiarium	0	0	0	0
C. puteana	0	0	0	0
S. lacrymans	0	0	0	0
T. versicolor	0	0	0	0

Chemical experiment

The analyzed absorbance values indicate that the pure caffeine solution has the higher mean absorbance value than caffeine solution containing chitin (after substraction of absorbance values for pure chitin suspension) at the same wavelength used (Table II). It means that caffeine and chitin are able to interact with each other.

Table II
The absorbance values for caffeine (3 replicates and their mean values with standard deviations (SDs)) per caffeine (CF), chitin (CH) and mix of caffeine solution with chitin (CF + CH) at the optimal caffeine wavelength - 287 nm

Line	Material	1.replica [A]	2.replica [A]	3.replica [A]	Mean [A]	± SD	Difference: 2b-2a
1	CF	0.391	0.398	0.385	**0.392**	0.007	
2a	CH	0.042	0.038	0.039	0.040	0.002	
2b	CF + CH	0.413	0.409	0.409	0.409	0.004	**0.369**

These results (Table 1, Table 2) confirmed all biological studies with fungi and molds, where caffeine has been indicated as an active biocide substance[7-11,14]. Our results also complement research into caffeine and its effect on chitin production in fungi. Several previous studies have examined the effect of caffeine on the inhibition of chitinase enzyme synthesis. These enzymes are involved in the production of chitin, which is needed for the growth of fungi and molds[1,15,16,17,18]. Our study extends this research to the finding that caffeine is able to interact with already formed chitin. This conclusion is in turn related to studies of the bioaccumulation and the biodegradation of caffeine and the other methylxanthines by fungi[18]. Chitin with caffeine was able to bind to beech wood (Figure 3). This is not surprising, because fungi that commonly grow on dead and living wood in their cell wall contain chitin. The question is whether such bound caffeine can be bioavailable to fungi and cause inhibition of their growth.

The other think is a possibility to include chitin into paintings or some biocidal preparations. The most commercially usable is its derivate chitosan[19]. However, studies with caffeine-chitin have not been yet made.

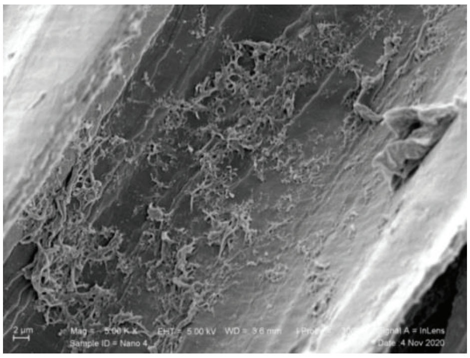

Figure 3. Photo of chitin with caffeine on beech wood (SEM) - 500x magnification (author: M. Böhm)

Conclusion

The affinity of caffeine to chitin was studied in the present preliminary study. The interactions of caffeine and chitin were observed by spectrometric analysis. The SEM analysis confirmed an occurrence of chitin on beech wood. The following research will be focused on effect of chitin-caffeine complex on toxicity to wood pests as fungi and moulds.

Acknowledgement

This research has been supported by the Czech Science Foundation under Project No. 19-02067S and by the Grant Agency of the Czech Technical University in Prague under project No. SGS19/143/OHK1/3T/11 and by Civil Engineering - Scanning Electron Microscopy Laboratory, CTU Prague (CE-SEM Lab).

References

1. Gortari M., Hours R.A.: Mycol. Progress. *7*, 221 (2008).
2. Duo-Chuan L.: Mycopathologia *161*, 345 (2006).
3. Hassan, N.A.F.A., Sahudin, S., Hussain, Z., Hussain, M. Int. J. Appl. Pharm. *10*, 172 (2018).
4. Stolte S., Steudte S., Shebb N.H., Willenberg I.: Environ. Int. *60C*, 123 (2013).
5. Kobetičová K., Mocová K.A., Mrhálková L., Fryčová Z., Kočí, V.: Czech J. Food Sci. *34*, 149 (2016).
6. Zarrelli A., Dellagreca M., Lesce M.R., Lavorgna M., Temussi F., Schiavone L., Criscuolo E., Parrella A., Previtera L., Isidori M.: Sci. Total Environ. *470-471*, 453 (2014).
7. Ratajczak I., Wozniak M., Kwasniewska-Sip P., Szentner K., Cofta G., Mazela B.: Eur. J. Wood Wood Prod. *76*, 775 (2017).
8. Kwasniewska-Sip P., Cofta G., Nowak P.B.: Int. Biodeterior. Biodegrad. *132*, 178 (2018).
9. Broda M., Mazela B., Frankowski M.: Maderas-Cienc. Tecnol. *20*, 455 (2018).
10. Kwasniewska-Sip P., Bartkowiak M., Cofta G., Nowak, P.B.: Bioresources *14*, 1890 (2019).
11. Pánek M., Šimůnková K., Novák D., Dvořák O., Schönfelder O., Šedivka P., Kobetičová K.: Coatings *10*, 1141 (2020).
12. Kobetičová K., Ďurišová K., Nábělková K.: Forests *12*, 533 (2021).
13. Broda M.: *Molecules 25*, 3538 (2020).
14. Kobetičová K., Nábělková J., Ďurišová K., Šimůnková K., Černý R.: Bioresources *15*, 8110 (2020).
15. Oduro-Mensah D. Ocloo A., Lowor S.T., Bonney E.Y., Land B., Okine K.N.A., Ayikailey N.A.: Microbiol. Rest. *206*, 16 (2018).
16. Carrasco-Cabrera C. P., Bell T.L., Kertesz M.A.: Appl. Microbiol. Biot. *103*, 5831 (2019).
17. Kobetičová K., Böhm M., Černý R.: AIP Conference Proceedings *2275*, 020010 (2020).
18. Kobetičová K., Nábělková K., Černý R.: AIP Conference Proceedings *2275*, 020011 (2020).
19. Ramawat G., Merillon K.J.M.: *Polysaccharides Bioactivity and Biotechnology*. Springer International Publishing, Switzerland 2015.

BINDING INTERACTIONS OF METHYLXANTHINES TO BEECH WOOD

Kobetičová K.[1], **Böhm M.**[1], **Černý R.** [1]

[1]*Department of Materials Engineering and Chemistry, Faculty of Civil Engineering, Czech Technical University in Prague, Prague, Czech Republic*
klara.kobeticova@fsv.cvut.cz

Abstract

Methylxanthines are a group of xanthine potentially useful for protecting wood from biological pests. However, their interactions with regard to their properties have not yet been studied. For this reason, we studied the interactions of caffeine (CF), theophylline (TP), and theobromine (TB) with beech wood in the present study. Electron microscopy was used to visualize these interactions. The results confirmed the different binding of the tested methylxanthines to the wood surface. The intensity of binding interactions decreased from caffeine to theobromine. These conclusions are in a good agreement with our previous results of biological and chemical studies.

Introduction

Methylxanthines are a class of drug that are derived from the purine base xanthine. They are produced naturally by plants and occur in tea tree, cocoa tree, coffee tree, or in certain legumes. They can also be produced commercially and are components of food or drinks, cosmetics and drugs. Their toxicity, together with other food additives, has been tested and found to have no effect on the environment at normal concentrations in water or soil samples[1,2,3,4,5]. The most common methylxanthines are caffeine, theophylline and theobromine. The other two substances are by-products of caffeine, but they can also be found in the same plants and their leaves or beans.

Caffeine was confirmed as a suitable active substance against wood pests such as fungi, molds and termites in the previous studies[6,7,8,9,10], however, theophylline and theobromine have not been studied thus far. The pesticide effects of all these three methylxanthines had only been described in one study with an agar medium[11], not wood. Their efficiency against pests increased in the following order: theobromine, theophylline, caffeine. Caffeine interactions with wood were described in two recent studies. The authors confirmed the binding interactions of caffeine with lignin, not with cellulose[12,13]. However, theophylline and theobromine have not been studied yet, but nevertheless they are very similar to caffeine from a chemical point of view. Their structures are shown in Figure 1. It is evident that all of the substances are very structurally similar. Caffeine has 3 methyl-groups, while theobromine and theophylline only 2 groups, but the rest of molecules are the same. Their spatial arrangement in space can affect the physical, chemical, and biological properties of the methylxanthines, as was affirmed for certain other, completely different molecules[14,15].

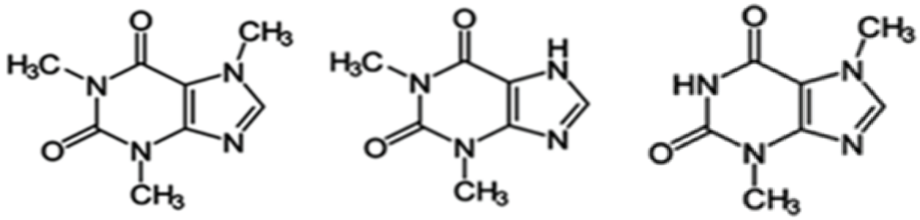

Figure 1. Caffeine (left), theophylline (middle) and theobromine (right).

For this reason, caffeine, theophylline and theobromine were applied to beech wood and their binding interactions were studied under a scanning electron microscope.

Experiment

Caffeine ($C_8H_{10}N_4O_2$), theobromine ($C_7H_8N_4O_2$), and theophylline ($C_7H_8N_4O_2$) were purchased from Sigma-Aldrich (Prague, Czech Republic). Deionized water was used as a solvent for the preparation of methylxanthine solutions. Water stock solutions were prepared up to the solubility limits at 20 °C (caffeine 20 $g.L^{-1}$, theobromine 0.33 g.L^{-1}, and theophylline 5.5 g.L^{-1}). Beech wood (*Fagus sylvatica* L.), which was purchased from company Milan Krátký (České Budějovice, Czech Republic) was a model wood material in this study. A total of four replicates were used for each substance.

The wood samples (110 mm x 7 mm x 2 mm) were immersed in the substance solutions (caffeine, theophylline or theobromine) for 24 hours, then extracted and left at room temperature for one week. They were then subjected to a microscopic analysis (one replicate per substance).

Scanning electron microscope (SEM) Phenom XL (Thermo Fisher Scientific Inc.) was used to analyze the interaction between substances and the wood. After one-week of drying the solutions on the treated wood, the samples were placed in a vacuum desiccator. The vacuum-dried samples were then mounted on aluminum stubs using double-sided conductive carbon tape and sputter coated with gold/palladium using a Quorum SC7620 sputter coater (Quorum Technologies Ltd.). An acceleration voltage of 7-15 kV, magnification up to 5,000x, and a working distance of 10-20 mm were used for the microscopic analysis.

Another three wood replicates for each substance were used for chemical analysis. The wood samples were immersed into new distilled water. Every piece of wood was soused in distilled water and shaken on a horizontal shaker for 24 hours. The samples were then pulled out and the solutions were filtered through a filter and analyzed. The aquatic leachates of wood samples were analyzed spectrometrically (Spectrophotometer Libra S22) at their optimal wavelength (287 nm)[13] or previous unpublished measurements.

Discussion and results

The microscopic images indicate the different interactions of the studied substances (Figure 2,3). Caffeine forms marbles on wood, of which there are many, and the marbles are clearly visible from the magnification 5,000x (Figure 2). Theophylline forms clusters of fibrous formations on the wood (it does not appear that they are specially affixed to the wood. Theobromine does not create any formations and no interactions are visible on the wood surface up to 5,000x magnification (Figure 3).

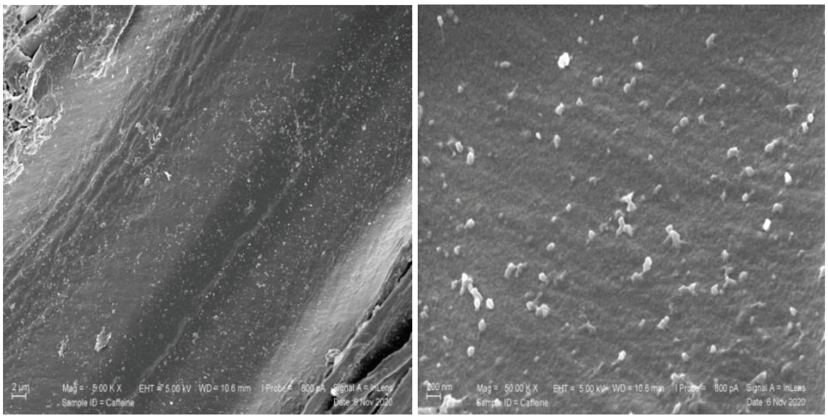

Figure 2. Microscopic images of caffeine (left) – on the surface of beech wood vessels, the magnification 500x (left) and 5,000x (right) (author of the photos: M. Böhm)

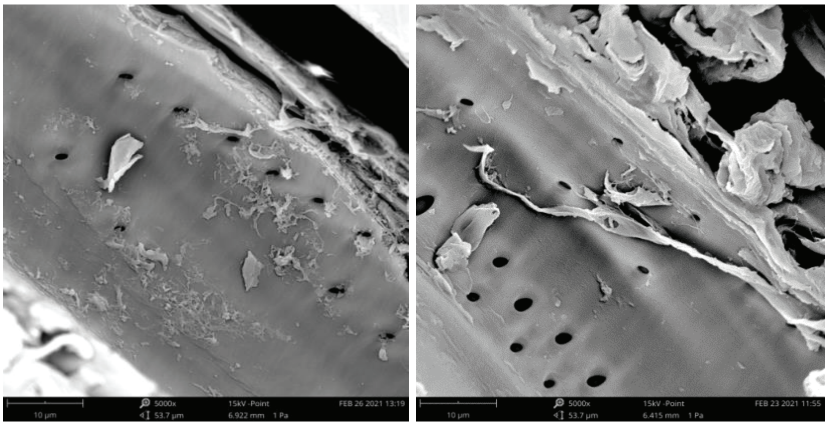

Figure 3. Microscopic images of theophylline (left) – the magnification 5,000x and theobromine (right) – the magnification 5,000x on the surface of beech wood vessels (author of the photos: M. Böhm).

The intensity of binding interactions decreased from caffeine to theobromine (Table 1). We have verified from previous research that the degradation of the studied substances does not play a role in this case, because it is negligible for all three substances over the given period of time[11]. The question is whether the observed variable formations can be caused by different concentrations of substances. However, we selected the used concentrations on the basis of previous toxicological experiments[11]. The toxic potential for fungi and molds was generally different. The Agarose medium can cause higher bioavailability of tested substances than wood, making pests on the agar medium more sensitive to chemicals, meaning that there was a 100% inhibition over the caffeine concentration range of 1-2 $g.L^{-1}$ on the agar. A 100% inhibition of theophylline was confirmed from 0.5 to 1 $g.L^{-1}$, and theobromine was not toxic for pests up to its maximum allowable concentration (0.33 $g.L^{-1}$)[11]. Wood experiments showed the effective concentrations of caffeine from approximately 20 $g.L^{-1}$ on spruce, pine or beech. A study by different authors describes that caffeine may interact with a methylene group derived from the aromatic rings of the guaiacyl group of lignin[12]. The following research confirmed this theory and the other authors verified variable caffeine interaction with lignin alcohol precursors[13]. Unfortunately, similar research focused on theophylline and theobromine has not yet been performed.

Table I
Absorbance values of the tested substances, calculated concentration of the substances ($g.L^{-1}$), and concentration of the substances interacted with wood ($g.kg^{-1}$)

	Tested concentration ($g.L^{-1}$)	Mean A	Substance ($g.L^{-1}$)	Substance in wood ($g.kg^{-1}$)
Control	0	0	0	0
Caffeine	20	1.279	0.037	0.642
Theophylline	5.5	0.172	0.005	0.062
Theobromine	0.3	0.043	0.002	0.029

Chemical experiments with leaching of beech samples and caffeine, theophylline or theobromine indicate their various affinities to wood. The measured values of absorbance and calculated concentrations of tested substance bonded to wood were graded according to the tested concentrations (see Table I). It is evident that the used concentration has an effect on binding of the tested methylxanthines to the wood surface and subsequently the pesticide effects.

Conclusion

The results are affected by the used concentrations of the substances (corresponding to the maximum solubility in water). The binding interactions correspond to the results of experiments performed with wood-destroying fungi, where significant biocidal effects were found for caffeine (20 $g.L^{-1}$), weak effects for theophylline (1-5.5 $g.L^{-1}$) and no effects for theobromine (up to 0.33 $g.L^{-1}$). Our findings prove the potential use of caffeine for wood protection.

Acknowledgement

This research was supported by the Czech Science Foundation under Project No. 19-02067S, by the Grant Agency of the Czech Technical University in Prague under project No. SGS19/143/OHK1/3T/11 and by Civil Engineering - Scanning Electron Microscopy Laboratory, CTU Prague (CE-SEM Lab).

References

1. Stolte S., Steudte S., Shebb N.H., Willenberg I.: Environ. Int. *60C*, 123 (2013).
2 Kobetičová K., Mocová K.A., Mrhálková L., Fryčová Z., Kočí, V.: Czech J. Food Sci. *34*, 149 (2016).
3. Zarrelli A., Dellagreca M., Lesce M.R., Lavorgna M., Temussi F., Schiavone L., Criscuolo E., Parrella A., Previtera L., Isidori M.: Sci. Total Environ. *470-471*, 453 (2014).
4. Bruton T., Alboloushi A., De la Garza B., Kim B.O., Halden R.: *Contaminants of Emerging Concern in the Environment.* American Chemical Society, New York 2010.
5. Lopes de Sousa M., Arves Cursino Dos Salves D.Y., Chow F., Pompeo M.L.M.: Ecotoxicol. *30*, 599 (2021).
6. Ratajczak I., Wozniak M., Kwasniewska-Sip P., Szentner K., Cofta G., Mazela B.: Eur. J. Wood Wood Prod. *76*, 775 (2017).

7. Kwasniewska-Sip P., Cofta G., Nowak P.B.: Int. Biodeterior. Biodegrad. *132*, 178 (2018).
8. Broda M., Mazela B., Frankowski M.: Maderas-Cienc. Tecnol. *20*, 455 (2018).
9. Kwasniewska-Sip P., Bartkowiak M., Cofta G., Nowak, P.B.: Bioresources *14*, 1890 (2019).
10. Pánek M., Šimůnková K., Novák D., Dvořák O., Schönfelder O., Šedivka P., Kobetičová K.: Coatings *10*, 1141 (2020).
11. Kobetičová K., Nábělková J., Ďurišová K., Šimůnková K., Černý R.: Bioresources *15*, 8110 (2020).
12. Kwasniewska-Sip P., Wozniak M., Jankowski W., Ratajczak I., Cofta G.: Materials *14*, 497 (2021).
13. Kobetičová K., Ďurišová K., Nábělková K.: Forests *12*, 533 (2021).
14. Ma B., Chen H., Xu M., Hayat T., He Y., Xu J.: Environ. Pollut. *158*, 2773 (2010).
15. Li N., Qi J., Wang P., Zhang X., Zhang T., Li H.: Anal. Methods *11*, 1816 (2019).

COMBINED EFFECTS OF ADSORPTION AND PHOTOCATALYSIS ON MODEL DYE AO7 REMOVAL FROM AQUEOUS MEDIA USING TiO_2-LDH NANOCOMPOSITES

Starukh H.[1,2,3], Petryk I.[3] , Matějová L.[1], Martaus A.[1]

[1]*Center for Energy and Environmental Technologies,VŠB-Technical University of Ostrava,*
17 Listopadu 15, Ostrava, Czech Republic
[2]*Faculty of Materials Science and Technology VŠB-Technical University of Ostrava*
17 Listopadu 15, Ostrava, Czech Republic
[3]*Chuiko Institute of Surface Chemistry, NAS of Ukraine,17 General Naumov Str., Kyiv 03164, Ukraine*
halyna.starukh@vsb.cz

Abstract

ZnCuAl layered double hydroxides (LDH) with atomic ratio Zn:Cu:Al=3.8:0.2:1 were synthesized and were used for the obtaining of ZnCuAl mixed oxides (MO), Ag NP-contained ZnCuAl LDH. The ZnCuAl MO was combined with TiO_2 and Ag NP to get ZnCuAl/TiO_2/Ag composites. The removal of the anionic dye Acid Orange 7 (AO7) from aqueous solutions with obtained LDH and TiO_2/LDH nanocomposites by adsorption and photodecomposition was studied in neutral and alkaline medium. The adsorption of AO7 on LDH and its composites with TiO_2 can be controllable by pH and by its modification with Ag NP. The highest removal of the dye (99 %) was observed for ZnCuAl MO due to adsorption at pH 7. The photocatalytic degradation of AO7 in the presence of ZnCuAl LDH, its derivatives, and composites with TiO_2 was influenced by pH. The activity of all studied materials to degrade dye under UV light greatly increased at pH 11 due to the more efficient formation of hydroxyl radicals. The highest activity in AO7 degradation under UV light among all materials studied was observed for TiO_2/10ZnCuAl/Ag and TiO_2/20ZnCuAl/Ag composites (92 % of dye was removed).

Introduction

The contamination of surface water and groundwater caused by hazardous organic dyes from industrial wastewater has a growing concern. Recently, many kinds of adsorbents with the photocatalytic function were developed and used for the removal of heavy metals, nitrate, and organic pollutants from water [1,2]. Layered double hydroxides (LDH), a class of ionic lamellar compounds or hydrotalcites, have been known as sorbents, catalysts, anion exchangers, and drug delivery systems. It was reported recently about the application of LDH in photocatalysis as an active component, as a component for hybrid-type photocatalysts, and as support. The chemical, structural, and electronic properties of LDH can be varied for a specific reaction. The abundant interlayer water molecules and hydroxide ions on the heterojunction interface of LDH can produce hydoxyl radicals (•OH)[3]. Thus, the layered structure increases the efficiency of photocatalytic processes by inducing electron transfer, preventing electrons/holes recombination. Titania is the most commonly known photocatalyst. It possesses high oxidation potential, non-toxicity, high photostability, and low cost. But such facts as high band energy of TiO_2 that restricts its application to UV light and electron recombination in TiO_2 challenge researchers to create composites of titania with oxides or nonoxide compounds. The photocatalyst coupled with noble metal nanoparticles demonstrate an outstanding photocatalytic performance for degrading organics[4]. The goal of this study was to design hybrid nanocomposites by combining TiO_2 and Ag nanoparticles with ZnCuAl LDH and to investigate their capability to remove anionic dye MO by adsorption and photocatalytic degradation.

Experimental procedures

LDH synthesis. ZnCuAl LDH with carbonate as the interlayer anion, with [Cu]: [Zn]:[Al]=0.2:3.8:1 were synthesized according to the method described in[5]. The product was isolated by filtration and washed several times with the deionized water until pH 7. Afterward, the solid was dried at 100 °C. The as-synthesized ZnCuAl LDH was calcined in air at 450°C for 2 h. The calcined sample was named as CuZnAl MO. For Ag NPs synthesis 20 mL of 38.8 mM Na_2BH_4 was added dropwise to 100 mL of 10^{-4} M $AgNO_3$ aqueous solution under stirring. It was continued to stir until the solution turned in strong yellow colour. 75 ml Ag NPs solution was added to 0.5 g ZnCuAl mixed oxide under stirring. After 2 hrs of the stirring, the solution was evaporated and the solid was collected. The sample was named as ZnCuAl/Ag. 75 ml Ag NPs solution was added to 0.5 g of ZnCuAl mixed oxide and TiO_2 mixture in which the content of mixed oxide was 10, 20, 50 % wt. After 2 hrs of the stirring, the solution was evaporated and solid was collected. The samples were named TiO_2/10ZnCuAl/Ag, TiO_2/20ZnCuAl/Ag, and TiO_2/50ZnCuAl/Ag.

XRD patterns of the samples were recorded with Rigaku SmartLab diffractometr (Rigaku, USA) with detector D/teX Ultra 250. Co lamp CoKα (λ_1=1,78892 nm, λ_2=1,79278 nm) was used as a source of radiation.

The textural properties of photocatalysts were determined by nitrogen physisorption measurements at 77K performed on an automated volumetric apparatus 3Flex (Micromeritics Instruments, USA). The specific surface area was determined by the multipoint Brunauer–Emmett–Teller (BET) method with relative pressures between 0.05 and 0.25. Diffuse reflectance spectra were obtained with a Shimadzu UV-2600 (IRS2600Plus) spectrophotometer in the range of wavelength 220 - 1400 nm at room temperature.

The photocatalytic activity of studied samples was performed in a cylindrical photocatalytic reactor of 11 cm in diameter and 20 cm in height. A fixed volume of 400 ml of 8.10^{-5} M AO7 solution was taken as an initial concentration for batch studies. The source of light was Pen-Ray 8 W lamp (Analityk Jena US, CA) with a peak intensity at 356 nm. The lamp was inserted into the solution. The dosages of the photocatalyst were 0.25 g L^{-1}. For all batch studies of photocatalytic activities, the dye solution with photocatalyst was magnetically stirred for 16 h in the dark to achieve adsorption-desorption equilibrium, before the light turned on. Each experiment was carried out for 240 min under light irradiation. Samples were collected every 30 min from the suspension using syringes and filter Chromafil GF/RC-20/25 (pore size 1µm) to remove the photocatalyst before further analysis. The optical density of AO7 dye solutions at 470 nm was measured with Compact photometer PF12 Plus.

Results and discussion

The XRD patterns of as-synthesized ZnCuAl LDH, ZnCuAl, ZnCuAl/Ag, TiO_2/10ZnCuAl/Ag, TiO_2/20ZnCuAl/Ag, and TiO_2/50ZnCuAl/Ag are presented in Fig.1. Two kinds of characteristic reflections of LDH was observed for ZnCuAl LDH that were identified as zaccagnaite-3R (PDF-2 card N 00-063-0586) and as copper aluminium carbonate hydroxide hydrate (PDF-2 card N 00-037-0630) (Fig.1, pattern 1). Additionally, crystalline phase of ZnO, wurtzite (PDF-2 card N 01-074-9940) is present in diffractograms of ZnCuAl LDH. It is known that the layered structure for ZnAl LDH is constructed from Zn^{2+} and Al^{3+} cations with ratio Zn/Al not higher than 2[6].

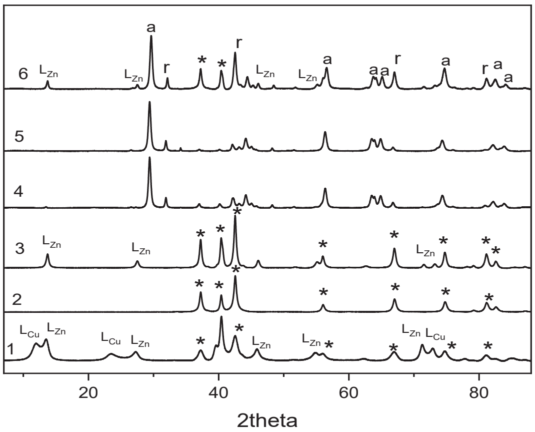

Figure 1. XRD patterns of investigated samples (ZnCuAl LDH - 1; ZnCuAl MO - 2; ZnCuAl/Ag LDH - 3; TiO_2/10ZnCuAl/Ag - 4; TiO_2/20ZnCuAl/Ag - 5; TiO_2/50ZnCuAl/TiO_2/Ag – 6). LZn -ZnAl LDH structure, LCu -ZnAl LDH structure, *- ZnO structure, a - anatase TiO_2, r-rutile TiO_2.

The XRD pattern of ZnCuAl mixed oxide contains exclusively the reflections of ZnO wurtzite phase (Fig.1, pattern 2). The leak of CuO reflections can be explained by the fact that copper oxide content is less than 4% mass. In ZnCuAl MO Cu^{2+} species migrate to the ZnO matrix and occupy positions in its planar defects[7].

The mixture phases of Zn-Al layered hydroxide carbonate hydrate and ZnO can be observed for ZnCuAl/Ag LDH (Fig.1, pattern 3). Evidently, the layered phase was formed under stirring of suspension of ZnCuAl mixed oxide in aqueous solution of silver nanoparticles due to the "memory" effect of LDH. It is known that the mixed oxides resulted from the calcination of LDH at certain temperature can be converted to the original hydrotalcite in an aqueous suspensions [6]. The oxides transfer to the double hydroxides in the form of brucite-like sheets and the positive charges are balanced by anions presented in solutions. In our case, CO_2 dissolved in the solution and CO_2 from air served as a sourse of CO_3^{2-} anions. XRD patterns of TiO_2-ZnCuAl nanocomposites with various content of LDH contain the reflections of anatase and rutile phases (Fig.1, pattern 4-6). The presence of Zn-Al layered double hydroxides structure can be observed only for nanocomposite that contains 50 % of ZnCuAl MO (Fig.1, pattern 6). All XRD patterns were obtained using Co-radiation with wavelength lambda = 1.78 Å. In comparison with Cu-radiation, which is more common, all peaks were shifted to the higher 2 Theta angles (based on the Braggs equation).

The textural properties of ZnCuAl LDH and their composites with TiO_2 were studied with the N_2 physisorption method (Table 1). The nitrogen adsorption/desorption isotherms of all the obtained materials show an uptake that is typical for mesoporous materials (Fig. 2). The isotherms of all samples demonstrate the type IV of the hysteresis loop between the adsorption/desorption branches according to IUPAC classification[8]. The presence of slit-shaped pores or plate-like particles in obtained LDH materials causes the type H3 of the hysteresis loops shape. The values of the BET surface area of studied materials are presented in Table 1.

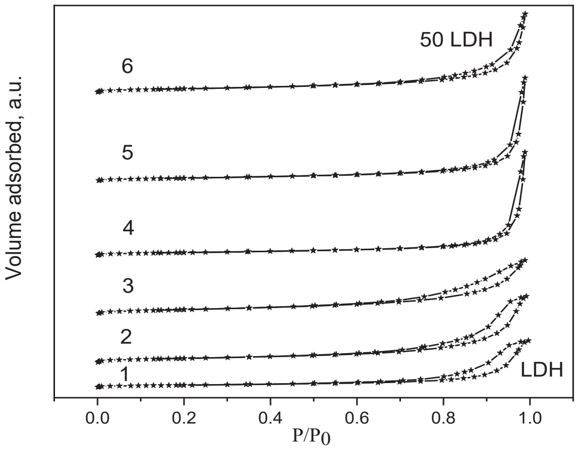

Figure 2. N_2 adsorption–desorption isotherms of investigated samples (ZnCuAl LDH - 1; ZnCuAl MO-2; ZnCuAl/Ag LDH - 3; TiO_2/10ZnCuAl/Ag - 4; TiO_2/20ZnCuAl/Ag - 5; TiO_2/50ZnCuAl/Ag - 6

Table I
Textural properties and the indirect bandgap of ZnCuAl LDH and its composites with TiO_2.

Sample	Surface area, (m^2/g)	BJH (N_2) desorption cumulative pore volume, (cm^3/g)	Average pore width, (nm)	Bandgap, eV
ZnCuAl LDH	31	0.20	24.2	3.21
ZnCuAl MO	57	0.28	24.1	2.60
ZnCuAl/Ag LDH	64	0.23	15.5	3.05
$TiO_2$10ZnCuAl/TiO_2/Ag	43	0.43	50.0	3.06
TiO_2/20ZnCuAl/TiO_2/Ag	48	0.43	53.5	3.05
TiO_2/50ZnCuAl/TiO_2/Ag	53	0.33	54.8	3.05

The optical absorption spectra of ZnCuAl LDH, its derivatives, and composites with TiO_2 are shown in Fig. 3 A. The absorption edge of as-synthesized ZnCuAl LDH was observed at 3.2 eV that can be explained by the presence of the ZnO phase in ZnCuAl LDH. The calcination of ZnCuAl LDH caused the red shift of absorbance on 3,1 eV. The comparison of DRS of ZnAl mixed oxide without Cu evidenced that the red shift was conditioned by the presence of Cu compounds. As ZnCuAl LDH was calcined in the air atmosphere, we suggest that CuO caused the enhancing of the visible light absorption of ZnCuAl MO. The absorbance band with a maximum at 3.0-3.1 eV in DRS of ZnCuAl/Ag can evidence the presence of silver NP surface plasmonic resonance. The optical absorbance of ZnCuAl/Ag composites with TiO_2 corresponded to TiO_2 absorbance. No influence of ZnCuAl/Ag on the absorption edge of composites can be explained the homogeneous distribution mixed oxide in titania. The band gap (Eg) was calculated by fitting with the Tauc/David−Mott model ($(\alpha hv)^{1/n} = A(hv - Eg)$). The Eg value of ZnAl LDH and its composites with TiO_2 are presented in Table I. The band gap energy of ZnCuAl LDH is close to the band gap energy of ZnO (3.32 eV) and is in agreement with reports on ZnO/LDH composites[9]. The presence of CuO in ZnCuAl 450 caused the decrease of band gap energy to 2.6 eV. A similar effect of CuO was observed for its composition with semiconductors [10]. The band gap energy of TiO_2 composites with ZnCuAl/Ag corresponded to the value of TiO_2 band gap.

The removal of AO7 was performed at pH 7 and pH 11. The influence of pH on adsorption capacity of as-synthesized and calcined ZnCuAl LDH was negligible (Table II). ZnCuAl MO adsorbed 99 and 91 % of AO7 at pH7 and pH 11, respectively. The modification of LDH with Ag NP caused the decrease of AO7 adsorption. The significant reduction of the anionic dye adsorption was observed at pH 11. The increase of ZnCuAl content in TiO_2/ZnCuAl/Ag composites caused the rise of AO7 adsorption at pH 7. No adsorption of the dye was observed for TiO_2/ZnCuAl/Ag materials at pH 11. The modification of ZnCuAl LDH and TiO_2/ZnCuAl composites with Ag NP decreases the ability of obtained materials to adsorb anionic dye AO7 in an alkaline medium (Table 2). The highest total removal of the dye (99 %) at pH 7 was observed for ZnAlCu MO due to adsorption. The application of this adsorbent for the removal of dye is suitable if it is desirable to collect the dye for further application.

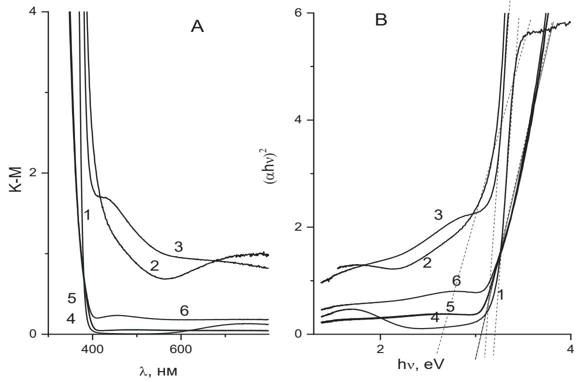

Figure 4. UV-vis/DR spectra (A) and Tauc plots of investigated samples (ZnCuAl LDH - 1; ZnCuAl MO - 2; ZnCuAl/Ag LDH - 3; TiO_2/10ZnCuAl/Ag - 4; TiO_2/20ZnCuAl/Ag - 5; TiO_2/50ZnCuAl/Ag – 6.

The kinetics curves of AO7 photocatalytic degradation via ZnCuAl LDH and their composites with TiO_2 were evaluated with the pseudo-first-order model. The values of reaction rate constants and correlation coefficient are presented in Table II. The activity of ZnCuAl LDH and ZnCuAl/Ag LDH to degrade dye under UV light at pH 7 was low and it greatly increased at pH 11 due to the more efficient formation of hydroxyl radicals. It is obvious that in the case of photocatalysts with high absorption capacity (ZnCuAl MO), the adsorbed dye blocks the penetration of light illumination to the active surface of the photocatalyst and thus reduces photodegradation. Additionally, the more efficient formation of hydroxyl radicals in alkaline pH causes a higher rate of AO7 photocatalytic degradation. The highest activity was observed for TiO_2 composites combined of 10 and 20 % ZnCuAl (Table II) at pH11. The synergy effect of the ZnCuAl, ZnO associated with photoactivity of TiO_2, caused the high photocatalytic capacity of the composite. It is known that the defects that are created under the formation of LDH nanosheets influence on the electronic structure and photocatalytic activity of LDH materials [11]. Among materials studied, TiO_2/10ZnCuAl/Ag and TiO_2/20ZnCuAl/Ag demonstrated the highest total removal of AO7 at pH 11 (92 %) due to the photocatalytic degradation.

Table II

The removal of AO7 by adsorption and by photodegradation

Sample	Adsorption, %		Photodestruction						Total removal, %	
			pH 7			pH 11				
	pH 7	pH11	%	K*10^3, min^{-1}	r_{sq}	%	K*10^3, min^{-1}	r_{sq}	pH7	pH11
blank	—	—	4.2	0.21	0.96	5.2	0.08	0.91	4.2	5.2
ZnCuAl LDH	38.4	35.8	14.6	1.04	0.97	37.6	3.38	0.99	53.0	73.4
ZnCuAl MO	99.2	90.8	—	—	—	—	—	—	99.2	90.8
ZnCuAl/Ag LDH	72.2	23.8	10.6	1.69	0.99	41.6	3.03	0.79	82.8	65.4
TiO_2/10ZnCuAl/Ag	17.2	0.8	39.0	2.71	0.99	89.9	10.93	0.99	56.2	91.7
TiO_2/20ZnCuAl/Ag	25.4	0	37.9	3.18	0.99	91.6	10.92	0.99	63.3	91.6
TiO_2/50ZnCuAl/Ag	45.6	0	43.3	3.62	0.99	72.5	5.85	0.99	77.8	72.5
TiO_2-P25	1.0	3.4	62.9	4.39	0.99	84.6	8.35	0.99	63.9	88.0

Based on the photocatalytic principles, we can propose the following steps that are possible during the AO7 photocatalytic degradation. When the LDH photocatalyst was irradiated by UV light and the photons were absorbed, the electron-hole pairs were generated. As both conduction band (CB) and valence band (VB) of ZnCuAl LDH are higher than those of TiO_2. The electrons from the CB of ZnCuAl LDH can be transferred to the CB of TiO_2 because of the more positive CB of TiO_2 (-0.29 eV) than that of ZnCuAl LDH (−2.03 eV). Simultaneously, the holes from the VB of TiO_2 were transferred to the VB of ZnCuAl LDH. These interfacial transfers of electrons and holes prolonged their lifetime by suppressing the recombination of electron-hole pairs, which were more useful to increase the photocatalytic activity. After that, the separated electrons in the CB of TiO_2 and holes in the VB of ZnCuAl LDH were used for redox reactions of adsorbed molecules. Therefore, the significant increase in photocatalytic degradation of AO7 in the presence of TiO_2/ZnCuAl/Ag photocatalysts is related to the formation of a heterojunction between ZnCuAl LDH and TiO_2, Formation of heterojunction effectively inhibits the process of recombination of photogenerated carriers.

Conclusion

ZnCuAl LDH with atomic ratio Zn:Cu:Al=3.8:0.2:1 was synthesized by co-precipitation method and used for the obtaining of calcined LDH, Ag NP-contained ZnCuAl LDH, and TiO_2/ZnCuAl/Ag nanocomposites. All materials were characterized and applied for the removal of the anionic dye AO7 from aqueous solutions by adsorption and photodecomposition in neutral and alkaline medium. The calcined form of ZnCuAl LDH demonstrated the highest adsorption ability of AO7. The adsorption of AO7 dye on LDH and its composites with TiO_2 can be controllable by pH and by the modification with Ag NP. The highest total removal of the dye (99 %) at pH 7 was observed for ZnCuAl MO due to adsorption. The photocatalytic degradation of AO7 in the presence of ZnCuAl LDH, its derivatives and composites with TiO_2 is influenced by pH. The activity of all studied materials to degrade dye under UV light greatly increased at pH 11 due to the more efficient formation of hydroxyl radicals. The highest activity in AO7 degradation under UV light among all materials studied was observed for TiO_2/10ZnCuAl LDH/Ag and TiO_2/20ZnCuAl/Ag composites. Evidently, the synergy effect of the LDH, ZnO and TiO_2, caused the high photocatalytic capacity of the composite materials. Formation of TiO_2/ZnCuAl LDH heterojunction allowed better separation of generated electrons and holes, which consecutively increased the efficiency of AO7 photodegradation process.

Acknowledgement

The work was supported from ERDF "Institute of Environmental Technology – Excellent Research" (No. CZ.02.1.01/0.0/0.0/16_019/0000853), Large Research Infrastructure ENREGAT (project No. LM2018098)
The authors thank professor K. Koci and prof. L. Capek for the discussion.

References

1. Crini G. Bioresource Technol. 97, 1061 (2006).
2. Belhouchat N., Zaghouane-Boudiaf H., Viseras C. Appl. Clay Sci. 135, 9 (2017).
3. Wang Q., O'Hare D. Chem. Rev. 112, 4124 (2012).
4. Narkbuakaew T., Sujaridworakun P. Opt. Mater. 98, 109407 (2019).
5. Starukh, G. M. Nanoscale Res. Lett. 12, 391 (2017).
6. Kooli F., Depeg C., Ennaqadi A., de Roy A., Besse J.P. Clays Clay Miner. 45, 92 (1997).
7. Fernandes D.M., Silva R., Hechenleitner A., Radovanovic E., Custódio Melo M.A., Gómez Pineda E.A. Mater. Chem. Phys., 115, 110 (2009).
8. Gregg S., Sing K. Adsorption, Surface Area and Porosity. Academic Press, London, 1982.
9. Wu S., Li N., Zhang W. J. Porous Mater. 21, 157 (2014).
10. Janczarek M., Kowalska E. Catalysts 7, 317 (2017).
11. Giri M., Jaggi N. ATTI DELLA "Fondazione Giorgio Ronchi", 2, 255 (2012).

SUBSTITUTION OF HAZARDOUS SUBSTANCES IN PYROTECHNIC COMPOSITIONS

Olšovský M.[1], Krištof M.[1], Kuna P.[2]

[1]ZVS IMPEX, Štúrova 925/27, 018 41 Dubnica nad Váhom
[2]STC, Hlinky 505/18, 603 00 Brno
skusobnictvo@zvsimpex.sk

Abstract

The paper deals with possibilities of substitution of environmentally unsuitable components in the production of pyrotechnic compositions. New compound of pyrotechnic composition must by comply with REACH requirements and be non-toxic. Heavy metal compounds will be removed. The “green” pyrotechnic compositions must retain all required pyrotechnic and ammunition characteristics.

Introduction

Most manufactured pyrotechnic compositions for military applications have been in production since the 1960s - 1970s. Their main disadvantages include toxicological unsuitability and outdated production technology. Hygiene and environmental problems (with increasingly stringent legislation on the use of chemicals) with most of the raw materials used in production lead companies to look for substitutes for raw materials, or to design and develop new environmentally and toxicologically acceptable pyrotechnic compositions. On the other hand, it is extremely important that the “new” components also possess the required pyrotechnic and explosive properties since they are all laboratory-engineered into newly made ammunition and ammunition elements. They occur in lighters, initiators, igniters, stopwatches, initiators and fire extinguishers. Precisely because of the long-term guarantees for the new ammunition (15 years), all new production processes, compositions must be rigorously and properly tested.

Problems with toxicity and the working environment are currently very topical. This is also reflected in EU legislation under the REACH Regulation[1,2]. Under these regulations, all chemicals must meet strict environmental limits. Some substances and compounds have also been banned from use. Therefore, the replacement of heavy metals, especially those containing manufactured pyrotechnic compositions, is a topical problem. These are mainly barium, lead, antimony and mercury compounds and, to a lesser extent, other compounds (ZnO, TiO_2)[3]. The maximum permissible concentrations in the working atmosphere are given in Table I.

Table I
Permitted maximum concentrations of heavy metals in the atmosphere[3]

Compound/element	Allowed limit, $mg.m^{-3}$
Pb	0.1
Ba	0.5
Sb	0.5
ZnO	5.0
TiO_2	6.0

In the future, these limits will be tightened and some of the raw materials currently producing pyrotechnic compositions will be banned soon, ie they will no longer be available on the EU market.

Suitable substitute raw materials for pyrotechnic compositions

The work[4] addresses the problem of the actual replacement of the environmentally hazardous components in pyrotechnic components ($BaCrO_4$ and $KClO_4$). The W/MnO_2 composition is investigated as an environmentally friendly substitute. The basic delay and aging characteristics were investigated in real products and under their actual conditions of use. Accelerated aging was performed over 8 weeks and negligible changes in the burning characteristics were observed. The combustion products were characterized by powder X-ray diffraction and appeared to be harmless based on known available information. The W/MnO_2 system therefore appears to be a suitable substitute with a relatively low combustion rate, low gas evolution and low toxicity with acceptable long-term storage stability.

Metallic manganese has been evaluated as a suitable fuel for delayed combustion compositions[5]. Oxides of antimony, bismuth, copper, manganese and vanadium were used as oxidants. The addition of dried silica to the

Mn/MnO_2 system had little effect on the burning rate, but a small amount of the hollow glass beads added significantly reduced the burning rate. Mixtures with Mn + MnO_2 showed reliable combustion over a wide stoichiometric range. In this system, the fuel and the oxidant share a common metal. They are combined to form a more stable intermediate (MnO), which releases a significant amount of heat in the process. The results confirmed that the stability of various manganese oxides decreases with increasing manganese oxidation number. MnO is the most thermodynamically stable oxide.

Thermochemical calculations have shown that K_2FeO_4 may be an alternative oxidizing agent in compositions[6] for fuses, lighting compositions in tungsten-based compositions. In all cases where K_2FeO_4 was substituted with potassium perchlorate, the burning temperature was higher. K_2FeO_4 is environmentally friendly because it does not contain heavy metals, chlorides or other halogen impurities. Its final by-product is rust (Fe_2O_3). This species is used as the pyrotechnic oxidant itself so that it can provide a secondary reaction or catalytic effect. This could further oxidize combustion products to more environmentally friendly chemicals.

Pyrotechnic compositions composed of boron carbide, sodium periodate and PTFE have been developed for use in the US Army[7]. The new compositions have been developed to replace the currently used compound containing potassium perchlorate and barium chromate - chemicals that are problematic from an environmental and toxicological point of view. $B_4C/NaIO_4$/PTFE compositions can be used as compositions. The most important parameters influencing the resulting properties of the mixture are the stoichiometric ratio of the components and the particle size of the boron carbide.

The pyrotechnic delay components according to paper[8] are manufactured to meet REACH requirements. They comprise an oxidizing agent, a reducing agent and one or more binder additives. Oxidizing agents are selected from iron oxides (FeO, Fe_3O_4 and Fe_2O_3), auxiliary additives include aluminosilicates, silica glass, lithium water glass, ferro-silicone or ferro-zirconium or boron (as reducing agents), iron alloys or tungsten or (as fuels).

Summary of the invention [9] is based on the design of a non-toxic pyrotechnic delay composition which is primarily prepared from the raw materials Si-Al-Fe_3O_4. Such a composition is essentially gas-free, safe to handle, moisture resistant and retains its properties during long-term storage. Specifically, 15 – 35 % Si, 65 – 85 % Fe_3O_4 and at least 1 % aluminum. In addition, it is non-toxic and none of the ingredients present an environmental hazard. This is an excellent candidate for the replacement of conventional compositions.

Modification of pyrotechnic composition

We have modified the high waterproof composition because it contains only 3 components. It is a mechanical mixture of lead-lead oxide and powdered metal zirconium, processed and ginned with an acetone solution of nitrocellulose. It is characterized by simple preparation technology and relatively unambiguous required properties. The component has been manufactured since 1970. The component is intended for the laboratory of fuse delays, amplifiers, transients, hermetizers and other pyro-components of lighters.

External appearance of pyrotechnic composition - in the form of grains of light brown to dark brown color, without foreign admixtures. It must not contain glued clumps of grains that will not break down easily. Partial color change of individual grains to dark grey and black is allowed.

The composition is sensitive to initial pulses, especially to electrostatic charge, chemically and thermally highly stable. They have a high burning rate. Burning produces a long and warm flame. The required physical properties of the are in Table II.

Table II
Physical values of standard pyrotechnic composition

Parameter	Value
Moisture and volatile substances content, %	max. 0.20
Remainder on the sieve with a mesh size of 0.80 mm, %	max. 1.00
Mixture passing through a mesh size of 0.25 mm is weighed, %	max. 3.00
The average combustion time of mixture in the fuse, s	0.09 - 0.24
Gravimetric value of grain, $g.cm^{-3}$	min. 2.30
The explosion temperature of mixture under vacuum 5.33 kPa, °C	min. 250
Intensity of flame height from moulded roller to dust screen	Dust screen for distance min. 400 mm must be fired safely
Sensitivity of flame ray from igniter in the test of tablet from pyrotechnic composition (after 5 days in water)	100 % ignition to distance min. 250 mm

Based on the literature and patent research[10], the substituents were selected to be available under our conditions and at the same time to suit our technology, while maintaining the resulting properties of the pyrotechnic composition. The new samples of the compositions were aimed at substituting the mine with bismuth trioxide, substituting nitrocellulose for fluorocarbon solution, as well as testing several types of zirconium, where the desired composition timing was achieved based on the particle size of the feedstock.

Specification of used materials

- *Viton™ B* is fluor-elastomer - a new generation of terpolymers ideal for sealing applications requiring permeation resistance to fuels; polymer fluorine content: 68 %.
- *Bismuth oxide*, p. a. – content of bismuth: ≥ 89.5 %; purity: min. 99.99 %, molecular weight = 466 $g.mol^{-1}$; particles size (D50): 3.0 – 4.5 µm.
- *Standard Zircon powder* - content of zircon: 93 – 94 %; hydrogen content: max. 0.2 %; Auto Ignition Temperature: 270 – 300 °C.
- *Zircon, type ZM* – content of zircon: 97.3 ± 0.9 %; hydrogen content: max. 0.2 %; Auto Ignition Temperature: 190 ± 30 °C; Average particle Size: 2.5 ± 0.5 µm.
- *Zircon, type GA* - content of zircon: min. 98.8 %; hydrogen content: max. 0.25 %; Auto Ignition Temperature: 240 ± 25 °C; Average particle Size: 5.5 ± 1.0 µm.

Sample preparation and physical properties of samples

Samples were prepared using standard technology for the preparation of standard pyrotechnic composition. We changed only the raw materials used - see Table III. The prepared samples could stand for 14 days, then we measured the physical properties.

Table III
Composition of prepared samples

Sample	Change in composition
standard	standard composition
1	nitrocellulose replaced by Viton
2	Pb_3O_4 replaced by Bi_2O_3
3	used Zircon type ZM
4	used Zircon type GA

Sample preparation was without problems. The color of samples 1, 3, 4 was the same as the standard, sample 2 was green-gray. This was caused by bismuth oxide. The physical properties of the samples of the compositions were carried out according to the technical conditions for the pyrotechnic composition and the NATO military regulation[11]. The measured basic parameters are shown in Table IV. The measured values show that they are comparable with the standard - they meet the prescribed technical conditions for the pyrotechnic composition.

Table IV
Physical properties of samples of pyrotechnic compositions

Parameter	standard	1	2	3	4
Moisture and volatile substances content, %	< 0,20	0,11	0,09	0,08	0,07
Remainder on the sieve with a mesh size of 0.80 mm, %	< 1,00	0,42	0,45	0,45	0,40
Remainder on the sieve with a mesh size of 0.25 mm, %	< 3,00	0,12	0,15	0,17	0,15
The average combustion time of mixture in the fuse, s	0,09 – 0,24	0,17	0,15	0,04	0,13
Gravimetric value of grain, $g.cm^{-3}$	≥ 2,30	2,33	2,34	2,32	2,33
Explosion temperature under vacuum 5.33 kPa, °C	≥ 250	364	368	335	377
Sensitivity to friction, N	50 – 100	248	161	4,5	26

The thermal stability evaluation of pyrotechnic composition samples (according to DTA and DSC) showed excellent stability of all samples. The thermal stability of the samples was evaluated from temperatures corresponding to the origin, onset and peak of the exothermic decomposition. In addition to the characteristics of exothermic decomposition, we evaluated the position of melting and other events that could affect the application properties of the compounds from the DTA and DSC curves.

Conclusion

The measured values of physical properties of samples of pyrotechnic compositions indicate:

- the preparation of the modified samples is identical to the preparation of the standard compound,
- substitution of nitrocellulose with fluorocarbon will increase the safety of work, since fluorocarbon-containing samples have a significantly higher friction sensitivity,
- the physicochemical properties (burning time) of the composition depend substantially on the physicochemical properties of the zirconium powder used (with the same mine and nitrocellulose), namely: grain, grain shape, active metal content and total zirconium content,
- the substitution of mine with bismuth oxide had no effect on physical or ammunition properties.

The results so far prove promising and after testing all the required parameters according to the relevant STANAG and AOP standards as well as after aging tests that will simulate at least 10 years of storage, these compounds can be used as next generation components that also meet environmental requirements in terms of current REACH legislation.

Acknowledgement

This work was supported by the European Union within the project "Environmentally friendly energy materials satisfy the requirements of REACH", no. NFP304010X023.

SK-CZ
14-20
INTERREG V-A
SLOVENSKÁ REPUBLIKA
ČESKÁ REPUBLIKA

EURÓPSKA ÚNIA
EURÓPSKY FOND
REGIONÁLNEHO ROZVOJA
SPOLOČNE BEZ HRANÍC

References

1. Regulation EC No. 1907/2006 of 18th December 2006 *Concerning the Registration Evaluation, Authorization and Restriction of Chemicals (REACH)*.
2. *The Impact of REACH and CLP European Chemical Regulations on the Defense Sector*. European Defense Agency Brussels, 2016. 311 p.
3. The Law of Slovak Republic, No. 137/2010 Z. z.
4. Koenig J. T.: ACS Sustainable Chem. Eng. 5, 9477 (2017).
5. Swanepoel D., Fabbro O. D, Focke W. W.: Propellants Explos. Pyrotech. 35, 105 (2010).
6. Wilharm C. K., Chin A., Pliskin S. K.: Propellants Explos. Pyrotech. 39, 173 (2014).
7. Poret J. C.: ACS Sustainable Chem. Eng. 1, 1333 (2013).
8. Cegiel D., Schulz E., Strenger J.: WO patent 2017084916.
9. Rose J. E., Michay M., Puszynski J.: US patent 7883593.
10. Olšovský M.: *Alternatives to the production of delay pyrotechnic compositions in ZVS holding base on the analysis of world production*. University of Pardubice, 2018.
11. AOP-7, Ed. 2: *Manual of Data Requirements and Tests for the Quantification of Explosive Materials for Military Use*. North Atlantic Treaty Organization, 2003.

ORGANIC TECHNOLOGY

THE EFFECT OF WATER AND SUBSTITUENTS OF AROMATIC RING ON ITS HYDROGENATION OVER A COBALT CATALYST

Valeš R., Dvořák B., Krupka J.

University of Chemistry and Technology in Prague, Department of Organic Technology, Technicka 5, Prague 6, 166 28, Czech Republic
roman.vales@vscht.cz

Abstract

This work focuses on the phenomenon called activation period, the property of Co/$CaCO_3$-Na_2CO_3 cobalt catalyst used for the hydrogenation of aniline to cyclohexylamine. The effect of concentration of water <0.02-2.50 wt. % in the aniline on the activation period and the reactivity of hydrogenation reaction was studied. The water in aniline is leading to origin and progress of activation period. The maximum value of the relative reactivity of the hydrogenation of aniline is achieved with the use of reactant with 1.50-2.00 wt. % of water. However, there is no effect of water on the reactivity of hydrogenation of aniline over the nickel catalysts. The cobalt catalyst is highly active for the hydrogenation of aniline compared to hydrogenation of other aromatic compounds as benzene and toluene. The reactivity of aromatic ring hydrogenation is strongly affected by substituents: benzene 0.54, toluene 1.00 and aniline 1.89.

Introduction

Cyclohexylamine is produced by catalytic hydrogenation of aniline or reductive amination of phenol or cyclohexanol[1,2]. The hydrogenation of aniline is strongly exothermic reaction[3], ΔH = -214 kJ mol^{-1}, which can be carried out in liquid or gaseous phase with application of Ni, Co, Rh, Ru, Pd and Pt catalysts[2]. Cyclohexylamine is not the only product of the catalytic hydrogenation of aniline. During the process are also formed the secondary amines, dicyclohexylamine and *N*-phenylcyclohexylamine. Since the desired product is the primary amine, cyclohexylamine, the selective cobalt catalysts are mainly used for the hydrogenation of aniline[4].

This work dealing with the specific properties of supported cobalt catalyst, with a chemical promoter Na_2CO_3, used for the industrial selective hydrogenation of aniline to cyclohexylamine in gaseous phase. This catalyst has good utility properties: the high catalytic activity and selectivity and lifetime longer than a 15 years. The specific property of the catalyst is a so-called activation period. It is a time period during which, under constant reaction conditions and feed of aniline, the conversion of aniline will increase up two, three times. The activation period was recognized during the kinetics measurements of hydrogenation of aniline over a prepared Co/$CaCO_3$-Na_2CO_3 cobalt catalyst[5]. The activity of the Co-catalyst for the hydrogenation of aniline is low after activation its Co-precursor by hydrogen at temperature 260-350 °C, nevertheless, activity increases with time. Regardless, the reduction (activation) temperature is not related to the incompleteness transformation of cobalt precursor to the Co^0. However, almost no attention has been paid to this phenomenon to present date. The cause of this phenomenon was sought in the context of gradual desorption of hydrogen, but this hypothesis has not been confirmed[6,7]. The new approach to this phenomenon is about the possibility of the effect of water on the activation period of cobalt catalyst. In this study, we focused on the effect of water in the aniline on its hydrogenation, i.e. origin and progress of activation period, conjointly with the effect on the reactivity of hydrogenation of aniline. We also studied the effect of water on the reactivity of hydrogenation of aniline over nickel catalysts. Likewise, we focused on the comparison of reactivates of hydrogenation of aniline, benzene and toluene over the above-described Co-catalyst used in cyclohexylamine process.

Experimental

Chemicals and gases

The reactants aniline (BorsodChem, Czech Republic, 99.9 %), benzene (Unipetrol, Czech Republic, 99.9 %), toluene (Lachner, Czech Republic, 99.9) were used without further purification. For the reduction of catalyst and for the experiments, the hydrogen (Siad, Czech Republic, 99.9 %) and nitrogen (Siad, Czech Republic, 99.99 %) were used. It was used *N*,*N*-dimethylformamide (Penta, Czech Republic, 99.9 %) as solvent.

Experimental apparatus

The experiments were carried out in a glass, tubular, flow through U-shaped reactor, an inner diameter 7 mm. First, the hydrogen (nitrogen) was additionally purified in apparatus filled with copper catalyst, and subsequently dried in apparatus filled by molecular sieve. Liquid reactant was fed into the reactor by a piston pump where it was subsequently vaporized. Reactor was placed in bath of heat transfer medium, low melting metal alloy, the Rose's metal. In order to reliably eliminate premature condensation of the reaction mixture, the outlet section and the side arm of the reactor was still heated by infrared lamp. All condensed components of reaction mixtures (Liebig condenser) were absorbed into *N*,*N*-dimethylformamide in freeze trap placed in a cooling bath filled with a cooling agent ethanol-dry ice mixture, tempered at -10 °C. Waste gases were disposed. The obtained reaction mixtures were analysed by GC method.

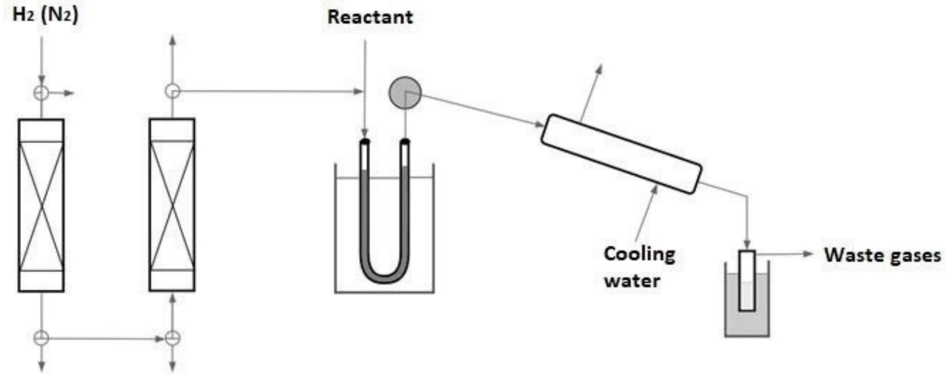

Figure 1. Experimental apparatus for the hydrogenation experiments.

Catalyst reduction and activation

The supported Co/$CaCO_3$-Na_2CO_3 catalyst was reduced at 230 °C for 2 hours with the 50 l h^{-1} of mixture of 70 mol. % N_2 and 30 mol. % H_2, and for 14 hours with the 50 l h^{-1} of H_2. Subsequently, the catalyst was treated at 330 °C in flow of hydrogen (50 l h^{-1}) for 0.5 hour.

There were also used the commercial (reduced and stabilized) nickel catalysts Ni/Cr_2O_3-SiO_2 and Ni/γ-Al_2O_3. The nickel catalysts were activated by hydrogen (50 l h^{-1}) at 185 °C for 1 hour and at 200 °C for 2 hours.

Reactions procedure

The experiments were carried out over a 14.5 g of cobalt catalyst in the form of granulate 0.80-1.25 mm, and 27.5 g of nickel catalysts in the form of granulate 1.25-3.00 mm. All reactions were carried out at the temperature 165 °C, atmospheric pressure and molar ratio of reactant/hydrogen 1:11.

Gas chromatography

The GC-FID analyses were performed on the Rxi®-624Sil MS column (30 m x 0.25 mm x 1.40 μm). Helium was used as carrier gas. The temperature program started at 80 °C for 2 minutes. Then with a rate of 15 °C/min, the temperature was raised to 210 °C.

Water content

The concentration of water was determined by coulometric Karl-Fischer titration on Titrator C 30 (Mettler Toldeo).

Data processing

The obtained GC-data, i.e. area units (Area %), were converted to mass fractions (wt. %) and subsequently to molar fractions (mol. %). The conversion X_R of reactant *R* (aniline, benzene and toluene) was calculated by the equation:

$$X_R = \left(1 - \frac{x_{R(\tau)}}{x_{R(0)}}\right) \cdot 100 \qquad (1)$$

where $x_{R(\tau)}$ is the molar fraction of reactant at time τ and $x_{R(0)}$ initial molar fraction. The activation period of the Co-catalyst for hydrogenation of aniline was characterized by the initial conversion of aniline $X_{AN(1)}$, the conversion of aniline of the steady state $X_{AN(\tau)}$ and the time of the achieving of this steady state τ.

The effect of concentration of water on the reactivity of hydrogenation of aniline was determined by the comparative, simplified kinetic method at the constant conversion of aniline X_{AN}:

$$\mathrm{rel.}\,r_{\mathrm{w}} = \left[\frac{(W/F_{\mathrm{AN}})_{\mathrm{ref}}}{(W/F_{\mathrm{AN}})}\right]_{X_{\mathrm{AN}}} \cdot \mathrm{rel.}\,r_{\mathrm{w,ref}} \qquad (2)$$

where rel.r_w is the relative (weight) reactivity, W is the weight of catalyst layer, F_{AN} mass flow rate of the aniline and the rel.$r_{w,ref}$ reference relative reactivity (equal to one). Comparison of hydrogenation reactivity for different reactants was done by the same method at the constant conversion of reactant R, only with exchange of parameter (W/F_{AN}) for ($W/\dot{n}_R$).

$$\mathrm{rel.}\,r_{\mathrm{m}} = \left[\frac{(W/\dot{n}_R)_{\mathrm{ref}}}{(W/\dot{n}_R)}\right]_{X_R} \cdot \mathrm{rel.}\,r_{\mathrm{m,ref}} \qquad (3)$$

where rel.r_m is the relative (molar) reactivity, $\dot{n}_R$ molar flow rate of the reactant and the rel.$r_{m,ref}$ reference molar reactivity (equal to one).

Results and discussion

The effect of water on the hydrogenation of aniline

First, it was compared the hydrogenation of aniline over a cobalt catalyst at the constant mass flow rate of aniline 15 g h^{-1}, with very low concentration of water, i.e. <0.02 wt. % and aniline with added amount of water, 0.30-2.50 wt. %. It can be seen (Fig. 2) that water has significant effect on the origin and progress of activation period. However, there is insignificant increase in conversion of aniline with application of this amine with very low concentration of water. Even after the 19 hours the conversion of aniline (<0.02 wt. % of water) of steady state conversion was not achieved. In contrast, application of aniline with 0.30 wt. % leading to high value of initial conversion and gradual increase of its conversion to the steady state. The higher concentration of water also shortens the time of achieving the steady state of the conversion of aniline.
It was proved that water has effect on the origin of the activation period of the Co/$CaCO_3$-Na_2CO_3 catalyst for the hydrogenation of aniline.

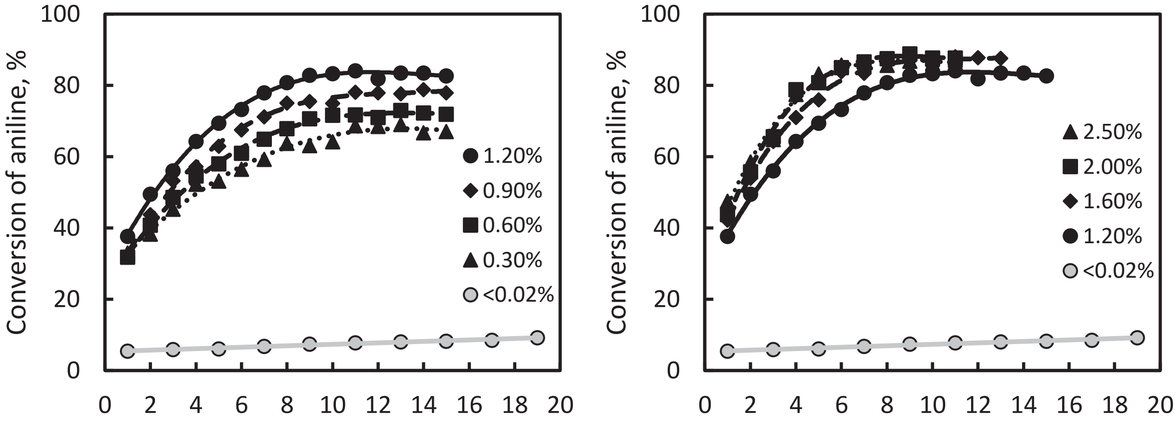

Figure 2. Time dependence of the arise of the conversion of aniline during its hydrogenation at the constant reaction conditions, i.e. constant both reaction temperature and mass flow rate of aniline with water.

Further, the effect of concentration of water in aniline on its hydrogenation reactivity was studied. Promotional effect was quantified by catalytic tests after the achieving of the steady states conversion of aniline. Catalytic tests were performed at the range of mass flow of aniline 6-15 g h^{-1} and the concentration of water in aniline

<0.02-2.50 wt. %. From regression dependences (Fig. 3a) was determined the effect of water on relative (weight) reactivity on aniline when the reference reactant was used the aniline with 0.30 wt. % of water.
It was determined that the highest hydrogenation reactivity is achieved at concentration of water in aniline 1.50-2.00 wt. %.

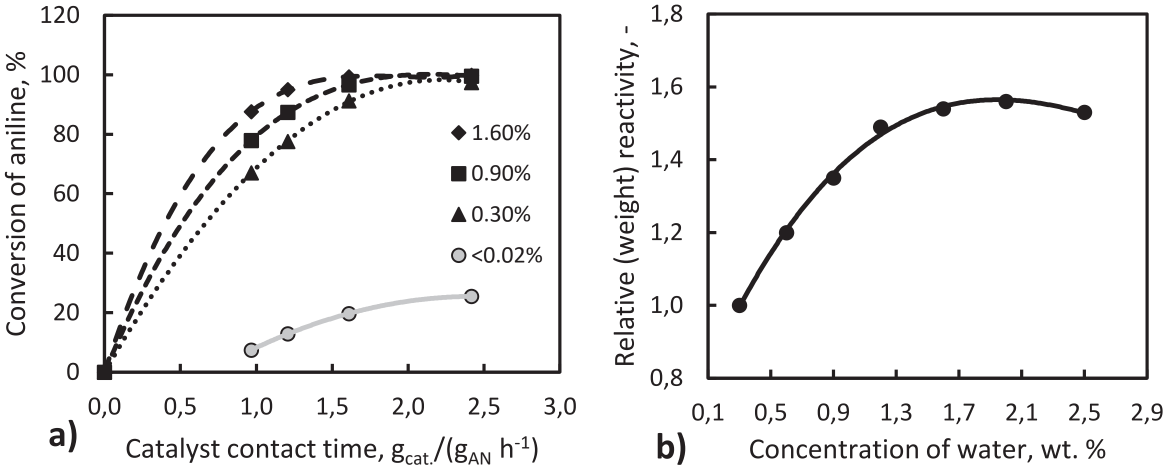

Figure 3. The effect of water on the reactivity of hydrogenation of aniline over a cobalt catalyst is demonstrated by: a) catalytic tests of chosen reactants and b) dependence of the relative (weight) reactivity of hydrogenation of aniline on the concentration of water.

The study of the effect of water on the hydrogenation of aniline was extended. The first results of this study are presented by Figure 4. Three regression dependences which characterize the conversion profiles of the activation period differs by the following conditions pre-treatment of Co-catalyst: a) standard activation and treating at 330 °C/0.5 hour, b) standard activation, c_{H_2O} = 2.0 wt.% in aniline, c) application of procedure b) and after the achieving of the steady state conversion of aniline hydrogenation of aniline with <0.02 wt. % of water. It can be seen significant difference between activation period of Co-catalyst before and after secondary treatment by hydrogenation of aniline with 2.00 wt. % of water. In the case of the hydrogenation of aniline over Co-catalyst (with pre-treatment a)) with very low concentration of water, initial conversion of aniline was $X_{AN} < 6$ % and its steady state conversion was not achieved even after the 19 hours. Compared to that, by the hydrogenation of the same reactant but over Co-catalyst after pre-treatment by aniline with 2.0 wt. % of H_2O was achieved distinctly higher value of the initial conversion of aniline, 52 %, and was observed gradual decrease to conversion of aniline to 46.6 % at 10 hours. Nevertheless, hydrogenation of this reactant on such treated catalyst did not reach the same value of the conversion of the aniline of the steady state as the hydrogenation of aniline with 2.0 wt. % of H_2O.

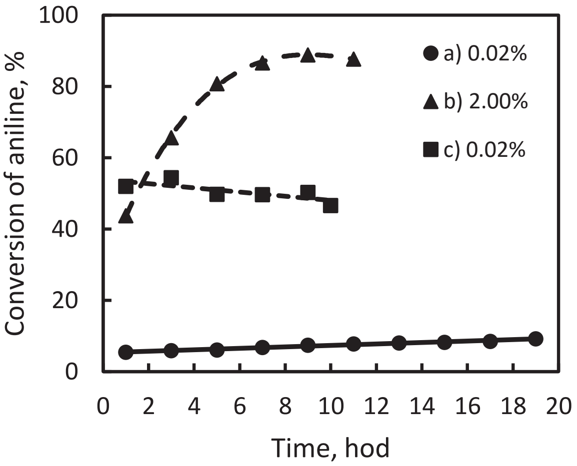

Figure 4. The effect of water in aniline and pre-treatment of Co-catalyst on progress of activation period during aniline hydrogenation at the constant reaction conditions.

From the presented results it's clear that water has dominant effect on the parameters and extent of activation period. It cannot be ruled out the connection of the additional effect of water and the presence of Na_2CO_3 on the secondary activation of the cobalt catalyst for cyclohexylamine process.

The experiments of the effect of water on the reactivity of hydrogenation of aniline were extended by the application of the nickel catalyst for this reaction. Figure 5 presents the dependence between the conversion of aniline and the catalyst contact time. It can be seen that with the use of $Ni/Cr_2O_3\text{-}SiO_2$ and $Ni/\gamma\text{-}Al_2O_3$ there is no effect of water on the reactivity of hydrogenation of aniline. In addition, there is no activation period in the case of nickel catalysts. Only was found that the nickel catalyst $Ni/Cr_2O_3\text{-}SiO_2$ has a 55 % higher activity than $Ni/\gamma\text{-}Al_2O_3$ for hydrogenation of aniline.

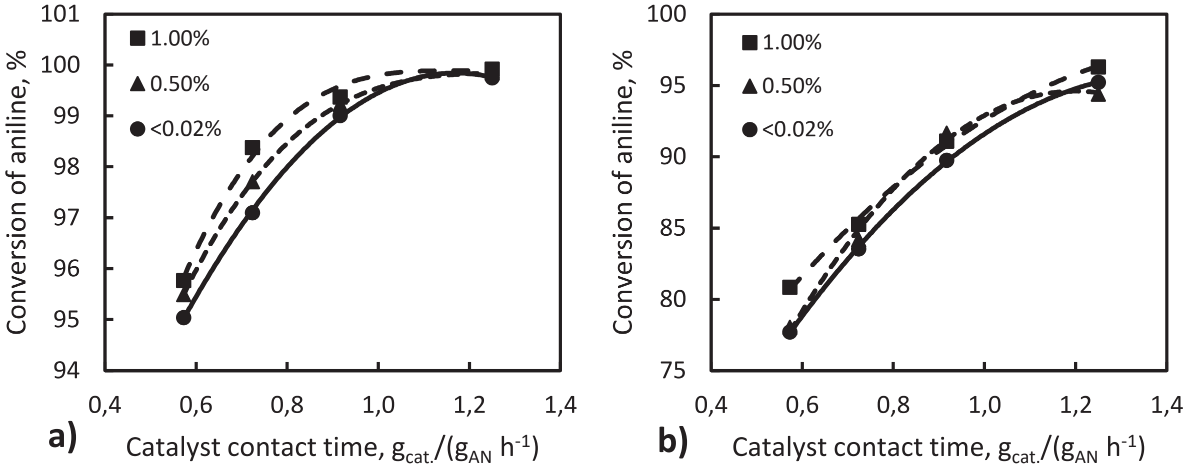

Figure 5. The effect of water on the reactivity of hydrogenation of aniline over nickel catalysts a) $Ni/Cr_2O_3\text{-}SiO_2$ and b) $Ni/\gamma\text{-}Al_2O_3$.

The effect of substituent on the hydrogenation of aromatic ring

It was studied the effect of substituents on the reactivity of hydrogenation of aromatic ring over a cobalt $Co/CaCO_3\text{-}Na_2CO_3$ catalyst. For this study, the aniline, benzene and toluene with low concentration (<0.02 wt. %) were used with the purpose of elimination of the promotional effect of water. In the case of these experiments, catalyst contact time is expressed by the ratio of weight of the catalyst layer to molar flow of the reactant *R*. It can be seen (Fig. 6) that the used cobalt catalyst is highly active for the hydrogenation of aniline. The hydrogenation of toluene was selected as the reference experiment. The values of the relative (molar) reactivity of the aromatic ring: benzene 0.54, toluene 1.00 and aniline 1.89.

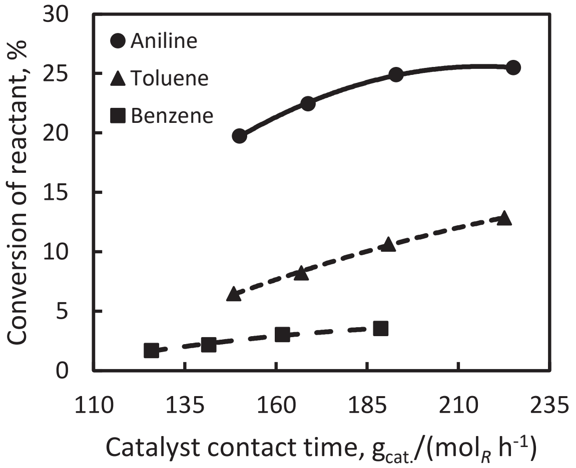

Figure 6. The hydrogenation of aniline, benzene and toluene over a $Co/CaCO_3\text{-}Na_2CO_3$ catalyst.

Conclusion

This work summarizes and expands the interpretation of the phenomenon called the activation period of the cobalt catalyst used for the hydrogenation of aniline to cyclohexylamine. It was proved the hypothesis of the connection of water and the origin and progress of activation period. With the use of aniline with low concentration of water, <0.02 wt. %, led to low value of the initial conversion of aniline, 5.5 %, and very slow increase of the conversion of aniline over a time. In the contrary, application aniline with 0.30 wt. % of water led to significant arise of the initial conversion of aniline, 33.0 %, and the notable increase of the conversion of aniline over a time and after 11 hours achieving of the conversion of aniline of steady state, 68.7 %. Furthermore, it was found that the highest reactivity of the hydrogenation of aniline over a cobalt catalyst is achieved with the application of reactant with 1.50-2.00 wt. % of water. In the contrary water has no effect on the reactivity of hydrogenation of aniline over nickel catalysts. In addition, the Co/$CaCO_3$-Na_2CO_3 catalyst is highly active for the hydrogenation of aniline. The reactivity of the hydrogenation aromatic ring over aforementioned catalyst is following aniline > toluene > benzene.

Acknowledgement

This work was supported from the grant of Specific university research – grant No A1_FCHT_2021_005.

References

1. Araki S., Nakanishi K., Tanaka A., Kominami H.: J. Catal. *389*, 212 (2020).
2. Chatterjee M., Sato M., Kawanami H., Ishizaka T. Appl. Catal., A, *396*, 186 (2011).
3. Cerveny L., Hronec M., Koubek J., Kurc L., Pasek J., Volf J.: University textbook - Zakladni pochody prumyslove organicke syntezy. 1998.
4. Pasek J., Marek J., Grapl J., Rozinek R.: Patent CS 250279 (Apr. 15, 1987).
5. Dvorak B.: Dissertation thesis. UCT Prague, 1966.
6. Dvorak B., Pasek J.: Collect. Czech. Chem. Commun. *32*, 3476 (1967).
7. Vesela D.: Dissertation thesis. UCT Prague, 2016.

HYDROGENATION OF BUTYL SORBATE USING METAL COMPLEXES WITH Ru, Rh AND Ir AS CENTRAL ATOMS

Kotova M., Hrdličková R., Vyskočilová E., Červený L.

Department of Organic Technology, University of Chemistry and Technology Prague, Technicka 5,
Prague 6 166 28, Czech Republic
maria.kotova@vscht.cz

Abstract

In this work, commercially available complexes based on ruthenium, rhodium and iridium were used as catalysts in hydrogenation of butyl ester of sorbic acid. Hydrogenations were carried out in homogeneous arrangement. The reaction conditions were set to 50 °C and 4 MPa. Amount of the catalyst was 5 wt.% to the amount of ester used. The influence of solvent (ethylene glycol, methanol, diethyl ether, methyl *tert*-butyl ether) on the selectivity of the reaction was studied. Butyl sorbate hydrogenation to butyl *cis*-hex-3-enoate, butyl *trans*-hex-2-enoate and butyl hexanoate took place. Reaction rates of hydrogenation was the highest using rhodium complexes, comparing to hydrogenations in the presence of ruthenium and iridium complexes. It was shown that the type of ligand influenced the configuration of the double bond in the final product and that presence of triphenylphosphine ligand in the complex structure accelerates hydrogenation.

Introduction

The syntheses of valuable unsaturated compounds, e.g. alkenes, esters, ketones and acids, are important processes in industry. They can be obtained by selective hydrogenation of the widely available *α,β*–unsaturated compounds such as sorbic acid (hexa-2,4-dienoic acid), sorbic alcohol (hexa-2,4-dien-1-ol), esters of sorbic acid, etc. It is important to use regio- and stereoselective catalytic complex in the hydrogenation step, because the position of the double bond can significantly influence the properties of the product[1].
Selective hydrogenation of sorbic acid and sorbic alcohol[2] can be successfully performed using a half sandwich ruthenium complex containing Cp* (pentamethylcyclopentadienyl) ligand and diene compound coordinated to ruthenium (Fig. 1).

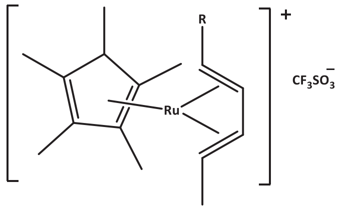

R= $-CH_2OH$, -COOH, -COOMe, -COOBu,-COOBn

Figure 1. Complexes [Cp*Ru(diene)]CF_3SO_3

Sorbic acid[2] was selectively hydrogenated to *cis*-hex-3-enoic acid and the resulting acid could be reduced to the leaf alcohol (*cis*-hex-3-en-1-ol). Selective hydrogenation of sorbic alcohol provides directly *cis*-hex-3-en-1-ol. Significant differences in reaction rates and selectivity were observed. The highest selectivity achieved in the hydrogenation of sorbic acid in a homogeneous arrangement was 96 %, while the selectivity of sorbic alcohol hydrogenation was 82 %. The reaction rate was higher in the case of sorbic acid hydrogenation. Hexenoic acids were detected as the main by-products in the case of sorbic acid hydrogenation. Ethers were the major by-products of sorbic alcohol hydrogenation.
Few years ago, selective hydrogenation of butyl sorbate (butyl ester of sorbic acid) to butyl *cis*-hex-3-enoate was carried out in the presence of a ruthenium complex with the structure [Cp*Ru(butyl sorbate)]CF_3SO_3. The effect of reaction conditions on the reaction rate and selectivity was studied[3]. Optimal conditions for the highest selectivity (up to 98%) were achieved in methyl *tert*-butyl ether (MTBE) as a solvent at a pressure of 4 MPa, a temperature of 50 °C and with 5 wt.% of catalyst. Further research has shown that the [Cp*Ru(butyl sorbate)]CF_3SO_3 complex has catalytic activity even in the hydrogenation of more complex molecules bearing two or more conjugated double bonds[4]. The influence of various diene ligands and anionic part of complexes on hydrogenation has been studied in detail[4, 5]. Ruthenium complexes containing acyclic, cyclic, bicyclic dienes, and *α,β*-unsaturated carboxylic acids and their esters as diene ligands were used in hydrogenation reactions.

The anionic part of the complex was represented by triflate, perchlorate and tetrafluoroborate ions. The desired products with *cis* configuration of the double bond were formed with high selectivity (95-99%).

Based on the above-mentioned results, it can be concluded that the complexes of the type $[Cp^*Ru\ (diene)]^+X^-$ (X= CF_3SO_3, BF_4 or ClO_4) can be used for the hydrogenation of molecules bearing two conjugated double bonds to *cis*-hex-3-ene compounds with high selectivity. The use of metal complexes with other ligands and central metal atoms for the hydrogenation of diene compounds has not been studied yet. The main aim of this work was to study the catalytic activity of metal catalysts based on ruthenium, rhodium and iridium and to analyze the influence of complex structure on the process of hydrogenation.

Experiment

Sorbic acid, *p*-toluene sulfonic acid, triphenylphosphine, pentamethylcyclopentadienylruthenium(III) chloride polymer (**1**), benzeneruthenium(II) chloride dimer (**2**), dichloro(mesitylene)ruthenium(II) dimer (**3**), chloro(indenyl)bis(triphenylphosphine) ruthenium(II) (**4**), chlorocarbonyltriphenylphosphine (1,2,3,4,5-pentaphenylcyclopentadienyl) ruthenium(II) (**5**), tris(triphenylphosphine)ruthenium(II) dichloride (**6**), bis(1,5-cyclooctadiene)diiridium(I) dichloride (**7**), bis(triphenylphosphine)iridium(I) carbonyl chloride (**8**), tris(triphenylphosphine) rhodium(I) chloride (**9**) and tris(triphenylphosphine)rhodium(I) carbonyl hydride (**10**) were purchased from Aldrich and used as obtained. Methanol (Penta), diethyl ether (Penta), ethylene glycol (Penta) and methyl *tert*-butyl ether (Lachner) were used as obtained.

Butyl sorbate preparation

Acid-catalyzed azeotropic esterification was used for the preparation of butyl sorbate from *n*-butanol and sorbic acid. A mixture consisting of sorbic acid (0.36 mol) and *n*-butanol (1.8 mol) was heated under reflux (120°C) in the presence of *p*-toluene sulfonic acid (7 mmol) until the total conversion of sorbic acid was observed. Once the reaction has been completed, the reaction mixture was cooled to room temperature, neutralized with 5% sodium carbonate solution and extracted with water (3 x 20 mL). *n*-Hexane (10 mL) was added to the reaction mixture for better phase separation. The organic phase was dried over magnesium sulfate and filtered. The filtrate was evaporated, and the crude product was distilled under vacuum. Butyl sorbate was obtained as a yellowish liquid with 95% purity (established by GC) in 85% yield.

Hydrogenation

Hydrogenations of butyl sorbate were carried out in a stainless steel autoclave (50 ml) equipped with a Teflon insertion piece. Metal complex, butyl sorbate (100 mg) and solvent (6 ml) were introduced into the autoclave. The autoclave was closed, placed in an oil bath, heated to the required temperature and pressurized by hydrogen. Directly after hydrogen addition the stirring was started. The continuous, uniform stirring was arranged by a magnetic stirrer. The reaction conditions were set to p = 4 MPa, T= 50 °C, the catalyst amount was 10 wt.% of the amount of starting material. Samples were analyzed using GC (DB-5, non-polar column). Hexanoic acid was used as an internal standard. The obtained data were used for the calculation of selectivity and reaction rate.

Selectivity: $S = \frac{c_{desired\ product}}{\sum c_{all\ products}} * 100\ [\%]$

Reaction rate: $rr_{15min} = \frac{\Delta c_{reactant}}{n_{catalyst\ \times t}}\ [mmol_s * ml^{-1} * mmol_{cat}^{-1} * h^{-1}]$

Discussion and result analysis

Ten commercially available compounds **1** - **10** were selected and used as catalysts in the hydrogenation of butyl sorbate (Fig. 2).

The selected complexes differed not only in the central atom and ligands, but also in the number of valence electrons. It is known[6] that their number affects the course of the reaction. The complexes **1** – **10**, used as catalysts in butyl sorbate hydrogenation, were both fully saturated ($18e^-$) and unsaturated ($16e^-$, $17e^-$). The number of valence electrons and the oxidation state of metals in complexes are given in Table I.

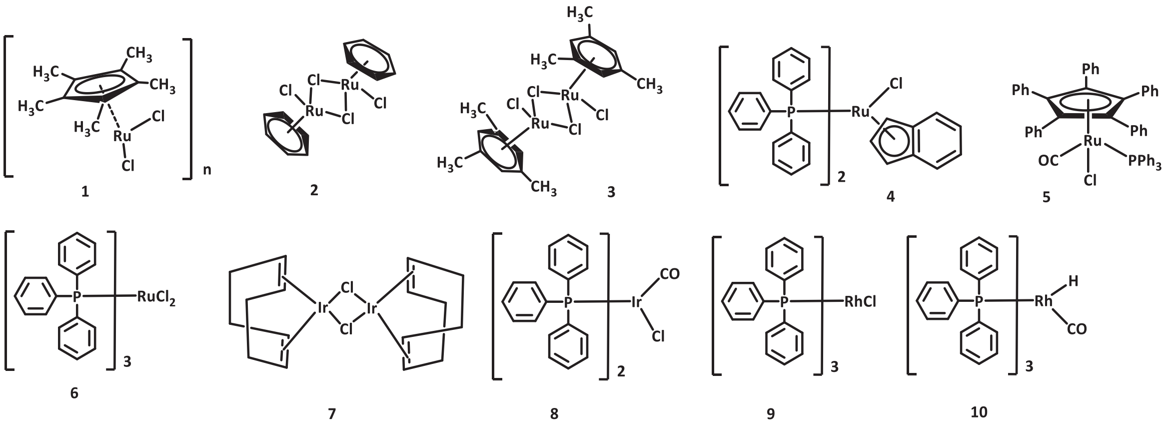

Figure 2. Structures of used metal complexes: pentamethylcyclopentadienylruthenium(III) chloride polymer (**1**), benzeneruthenium(II) chloride dimer (**2**), dichloro(mesitylene)ruthenium(II) dimer (**3**), chloro(indenyl)bis(triphenylphosphine) ruthenium(II) (**4**), chlorocarbonyltriphenylphosphine (1,2,3,4,5-pentaphenylcyclopentadienyl) ruthenium(II) (**5**), tris(triphenylphosphine)ruthenium(II) dichloride (**6**), bis(1,5-cyclooctadiene)diiridium(I) dichloride (**7**), bis(triphenylphosphine)iridium(I) carbonyl chloride (**8**), tris(triphenylphosphine) rhodium(I) chloride (**9**) and tris(triphenylphosphine)rhodium(I) carbonyl hydride (**10**)

Table I
Number of valence electrons and the oxidation state of metals in used complexes

Complex	Metal	The number of valence electrons	The oxidation state of metal
1	Ru	17	III
2		18	II
3		18	II
4		18	II
5		18	II
6		16	II
7	Ir	16	I
8		16	I
9	Rh	16	I
10		18	I

Hydrogenation of butyl sorbate was performed in a homogeneous arrangement at 50 °C and 4 MPa. The amount of catalyst was 10 wt.% of the amount of hydrogenated compound. Influences of central metals and ligands in complexes on the conversion and selectivity were monitored. The solvent effect on the hydrogenation course was also studied.

Influence of the solvent

The solvent influence on the reaction rate and selectivity of butyl sorbate hydrogenation was monitored. Based on the literature[7, 8] and previous investigations[9], ethylene glycol (EG), methanol (MeOH), diethyl ether (DEE) and methyl *tert*-butyl ether (MTBE) were chosen as solvents.

Butyl *trans*-hex-2-enoate (Fig. 3, **I**), butyl *cis*-hex-3-enoate (Fig. 3, **II**), butyl *trans*-hex-3-enoate (Fig.3, **III**) and butyl hexanoate (Fig. 3, **IV**) were detected in the reaction mixture after butyl sorbate hydrogenation. Selectivity was calculated when 90% conversion of the starting substrate was achieved. The results using different solvents are shown in Table II for EG and MeOH and in Table III for DEE and MTBE.

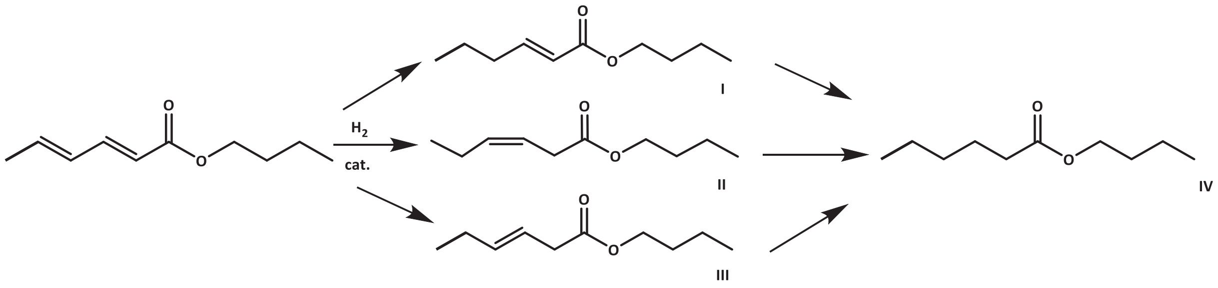

Figure 3. Hydrogenation of butyl sorbate

Table II
Hydrogenation of butyl sorbate in ethylene glycol and methanol (6 mL of solvent, 50 °C, 4 MPa, amount of catalyst - 10 wt.%)

	Ethylene glycol					Methanol				
Complex	Selectivity $_{90\,\%}$ (-)				rr$_{15\ min}$ (mmol*(ml*mmol*h)$^{-1}$)	Selectivity $_{90\,\%}$ (-)				rr$_{15\ min}$ (mmol*(ml*mmol*h)$^{-1}$)
	I	**II**	**III**	**IV**		**I**	**II**	**III**	**IV**	
1	0.06	-	0.07	0.87	2.6	0.11	-	-	0.89	18.0
2	0.18	-	0.02	0.80	6.4	0.21	-	-	0.79	19.8
3	0.39	-	0.08	0.53	16.8	0.22	-	-	0.78	24.9
4	0.25	0.18	-	0.57	21.2	0.18	-	-	0.82	26.8
5	0.23	0.11	-	0.66	22.0	0.15	-	-	0.85	30.5
6	0.14	0.10	-	0.76	23.5	0.20	-	-	0.80	31.6
7	0.23	-	0.03	0.74	12.9	0.14	-	-	0.86	17.4
8	0.20	-	0.07	0.73	19.8	0.18	-	-	0.82	23.8
9	0.11	-	-	0.89	31.5	0.01	-	-	0.99	45.5
10	0.15	-	-	0.85	27.0	0.02	-	-	0.98	37.0

Table III
Hydrogenation of butyl sorbate in diethyl ether and methyl *tert*-butyl ether (6 mL of solvent, 50 °C, 4 MPa, amount of catalyst - 10 wt.%)

	Diethyl ether					Methyl *tert*-butyl ether				
Complex	Selectivity $_{90\,\%}$ (-)				rr$_{15\ min}$ (mmol*(ml*mmol*h)$^{-1}$)	Selectivity $_{90\,\%}$ (-)				rr$_{15\ min}$ (mmol*(ml*mmol*h)$^{-1}$)
	I	**II**	**III**	**IV**		**I**	**II**	**III**	**IV**	
1	Reaction didn't take place					Reaction didn't take place				
2	0.46	-	0.03	0.51	1.7	0.50	-	0.06	0.44	0.9
3	0.54	-	0.15	0.31	3.6	0.60	-	0.19	0.21	1.8
4	0.29	0.23	-	0.48	6.9	0.39	0.27	-	0.35	4.5
5	0.27	0.17	-	0.56	7.7	0.33	0.21	-	0.46	5.6
6	0.35	0.13	0.01	0.51	8.5	0.32	0.14	0.03	0.51	6.2
7	0.36	-	0.08	0.56	5.3	0.46	-	0.10	0.44	2.8
8	0.25	-	0.10	0.65	11.0	0.21	-	0.14	0.65	7.2
9	0.32	-	-	0.68	17.1	0.38	-	-	0.62	12.3
10	0.35	-	-	0.65	14.3	0.40	-	-	0.60	11.7

The highest reaction rate values were obtained in MeOH (Table II). It was found out that the hydrogenation using methanol as a solvent has higher selectivity to the formation of saturated butyl hexanoate (product **IV**) comparing to hydrogenations in other solvents. It can be explained by the low stability of used catalysts in MeOH. During hydrogenation, decomposition of catalysts took place and black powder was observed at the bottom of the autoclave. The resulting powder probably corresponded to the metallic Ru^0, Ir^0 or Rh^0. These metals can successfully catalyze hydrogenation of butyl sorbate to saturated butyl hexanoate[10].

Dimeric (**2**, **3**, **7**) and polymeric (**1**) complexes showed low hydrogenation activity in all solvents. In MTBE and DEE, the hydrogenation catalyzed by complex **1** did not take place at all (Table III). In MTBE and DEE the lowest reaction rates were achieved using complexes **2**, **3** and **7** (Table III). The probable reason is the low rate of dimeric complexes dissociation. The complex **7** has the highest reaction rate values compared to dimeric complexes **2** and **3** (Table III, complex **7** vs. complexes **2**, **3**). The explanation may probably be in the number of valence electrons. In contrast to complexes **2** and **3**, complex **7** is coordinatively unsaturated and therefore this complex can add hydrogen without dissociation. Hydrogen addition accelerates dissociation and further catalytic cycle steps. Quicker transformation of the catalyst to its active form in polar solvents is most probably the reason why the dimeric and polymeric complexes in EG showed higher activity in hydrogenation of butyl sorbate.

Influence of central metals and ligands

Complexes **1**-**10** differed in a central metal ion. The catalytic activity of ruthenium, rhodium and iridium complexes was monitored. The influence of central metal on selectivity was also studied.

Hydrogenations of butyl sorbate using complexes with central rhodium atom (**9** and **10**) had the highest reaction rates comparing to hydrogenations in the presence of other metal complexes. According to the obtained results, it can be concluded that the presence of rhodium atom in the complex's structure accelerates the reaction rate. Conversions of starting material were 80-90% after 30 minutes. Hydrogenation of butyl sorbate to butyl *trans*-hex-2-enoate (product **I**) followed by hydrogenation to butyl hexanoate (product **IV**) was observed. The product **IV** was formed as a major. Rh complexes are not suitable catalyst for the hydrogenation of butyl sorbate to unsaturated products with one double bond.

Formation of butyl *trans*-hex-3-enoate (product **III**) was observed during the hydrogenation of butyl sorbate catalyzed by complexes **1-3, 7, 8** (Table II, III). The formation of butyl *cis*-hex-3-enoate (product **II**) was observed only when complexes **4**-**6** bearing Ru ion in the structure were used as catalysts (Table II, III). Comparing complexes **6** and **8**, which have the same number of valence electrons and may possess by the same hydrogenation mechanism, it can be supposed that the type of metal affects the structure of the product. Comparison of the Ru complexes **1-6** had led to the conclusion, that the type of the ligand also have an impact on the double bond configuration in the obtained products. By analyzing the reaction rates of hydrogenation it can be concluded that the presence of good leaving triphenylphosphine ligand accelerates hydrogenation.

As it was mentioned above, hydrogenation of butyl sorbate using polymeric and dimeric complexes **1**, **2**, **3** and **7** show low reaction rates. So, the attempt to speed up the reaction was performed. An equimolar amount of triphenylphosphine to the selected complex was added to the autoclave prior to hydrogenation. The reason for this addition was to promote cleavage of polymeric catalysts into monomer units, which can then catalyze the reaction[11]. Dissociation occurred due to the ligand exchange. Rapid ligand exchange took place because the electronegativity of phosphorus is considerably less than the electronegativity of chlorine, and the phosphorus ligand is a better electron donor (stronger Lewis base) for the central metal of the complex (Fig. 4). All hydrogenations were performed using MTBE as a solvent and the results are shown in table IV.

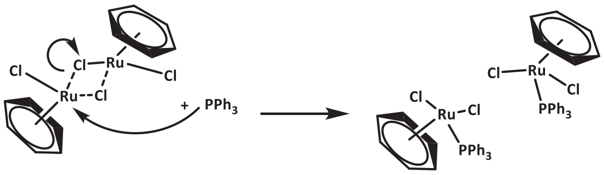

2

Figure 4. Effect of triphenylphosphine addition on complex dissociation

The attempt was successful, and in all cases reaction rates were higher in the presence of triphenylphosphine.

Table IV
Hydrogenation of butyl sorbate with the addition of triphenylphosphine (6 mL MTBE, 50 °C, 4 MPa, amount of catalyst - 10 wt.%, amount of PPh_3 – 1 equiv. to complex amount)

Complex	Selectivity $_{90\,\%}$ (-) with PPh_3 addition				$rr_{15\ min}$ $(mmol^*(ml^*mmol^*h)^{-1})$ with PPh_3 addition	$rr_{15\ min}$ $(mmol^*(ml^*mmol^*h)^{-1})$ without PPh_3 addition
	I	**II**	**III**	**IV**		
1	0.44	-	0.02	0.54	3.9	Reaction didn't take place
2	0.45	-	0.03	0.52	5.5	0.9
3	0.44	-	0.28	0.28	10.2	1.8
7	0.39	-	0.09	0.52	12.4	2.8

Conclusion

The main aim of this work was to test the catalytic activity of different metal complexes with Ru, Rh and Ir as central atoms in hydrogenations of diene compound. Butyl sorbate was chosen as a model diene substrate and pentamethylcyclopentadienylruthenium(III) chloride polymer, benzeneruthenium(II) chloride dimer, dichloro(mesitylene)ruthenium(II) dimer, chloro(indenyl)bis(triphenylphosphine)ruthenium(II), chlorocarbonyl triphenylphosphine(1,2,3,4,5-pentaphenylcyclopentadienyl)ruthenium(II),tris(triphenylphosphine)ruthenium(II) dichloride, bis(1,5-cyclooctadiene)diiridium(I) dichloride, bis(triphenylphosphine)iridium(I) carbonyl chloride, tris(triphenylphosphine) rhodium(I) chloride and tris(triphenylphosphine)rhodium(I) carbonyl hydride were chosen as catalysts for the hydrogenation. Hydrogenation was carried out in homogeneous arrangement at 50 °C under a pressure 4 MPa. Ethylene glycol, methanol, diethyl ether and methyl *tert*-butyl ether were chosen as solvents. The influence of the solvent on the reaction rate and selectivity was monitored. It was shown that reaction rates in methanol achieved the highest values, and the formation of saturated butyl hexanoate proceeds very fast.

Reaction rates of butyl sorbate hydrogenation was the highest using rhodium complexes, but Rh complexes are not suitable catalyst for hydrogenation of butyl sorbate to unsaturated products with one double bond.

By comparison of commercially available complexes in the hydrogenation of butyl sorbate, it has become apparent that the hydrogenation in the presence of complexes, which contained a central ruthenium atom in their structure, were more selective to butyl *cis*-hex-3-enoate formation. Additionally, it was demonstrated that presence of triphenylphosphine ligand in the complex structure accelerated the hydrogenation.

Also, the effect of the triphenylphosphine addition on the course of the reaction was monitored. Hydrogenations in the presence of dimeric and polymeric complexes with triphenylphosphine as an additive proceeded faster. The cleavage of polymeric catalysts into the monomer units was supposed, so the contact between catalyst and substrate was better and the hydrogenation rate was increased.

It can be concluded that metal complexes can be used as catalysts in hydrogenation of diene compounds and products with one double bond can be prepared using suitable reaction conditions.

References

1. Leitmannová E., Červený L.: Perfumer & Flavorist *33,* 50 (2008).
2. Leitmannová E., Malá R., Červený L.: Res. Chem. Intermed. *35*, 63 (2009).
3. Kotova M., Vyskočilová E., Červený L.: Catal. Lett. *147*, 1665 (2017).
4. Kotova M., Karlíčková A., Vyskočilová E., Červený L.: React. Kinet. Mech. Catal. *125*, 619 (2018).
5. Kotova M., Kollárová K., Vyskočilová E., Červený L.: React. Kinet. Mech. Catal. *132*, 729 (2021).
6. Jensen W. B.: J. Chem. Educ. *82*, 28 (2005).
7. Leitmannová E., Storch J., Červený L.: React.Kinet.Catal.Lett. *88*, 11 (2006).
8. Leitmannová E., Malá R., Červený L.: Res.Chem. Intermed *35*, 63 (2009).
9. Leitmannová E. Dissertation, UCT Prague (2006).
10. Kotova M., Karlíčková A., Vyskočilová E., Červený L.: Proc. 5th International Conference on Chemical Technology, Mikulov, Czech Republic (2017).
11. Hirose D., Gazvoda M., Košmrlj J., Taniguchi T.: Chem. Sci. *7*, 5148 (2016).

SELECTIVE MEERWEIN-PONNDORF-VERLEY REDUCTION OF CINNAMALDEHYDE OVER Al-CONTAINING CATALYSTS

Paterová I., Vyskočilová E., Gorlova O. and Červený L.

Department of Organic Technology, UCT Prague, Technicka 5, 166 28 Prague 6, Czech Republic
iva.paterova@vscht.cz

Abstract

Cinnamyl alcohol, the desired compound with large utilization in the perfume industry due to its properties, can be prepared from cinnamaldehyde by the selective hydrogenation of a carbonyl group keeping C=C bond. An alternative way to prepare cinnamyl alcohol is offered by Meerwein-Ponndorf-Verley (MPV) reduction. This reduction can be catalyzed heterogeneously to avoid difficult, costly and time-consuming elimination of homogeneous catalysts. This work focuses on the utilization of solid Al-containing catalysts such as commercial alumina CG-20, acid-activated alumina I 504 C, laboratory pretreated acid-activated alumina, MCM-41 and mixed oxides and their possible recovery and reuse in MPV reduction. Using laboratory prepared acid-activated alumina approx. 70% conversion with 70% selectivity to desired cinnamyl alcohol was achieved after 12 hours of reaction. Acid activated alumina was reused 3 times without significant loss of activity (10 % loss of activity).

Introduction

Cinnamyl alcohol, the desired compound in perfume industry, can be prepared from cinnamaldehyde by the selective hydrogenation of a carbonyl group. Such selective hydrogenation is difficult in the presence of C=C bond, because the hydrogenation of C=C bond is thermodynamically more favoured using especially Ir based catalysts. An alternative way is offered by Meerwein-Ponndorf-Verley (MPV) reduction, which is less demanding to the catalyst and conditions. Industrially, aluminium-2-propoxide[1] is the most often used as catalyst, and propan-2-ol as hydrogen donor for cinnamyl alcohol preparation. Several other homogeneous catalysts, e.g., zirconocene, and hafnocene complexes[2] and macrocyclic nickel complex[3] have also been described for the selective MPV reduction. The use of aluminium 2-propoxide however requires the addition of at least 100-200 % excess of this catalyst in order to obtain acceptable yields. Elimination of the alkoxide excess at the end of the process can be difficult and this process is a costly and time-consuming operation that provides a non-reusable product. On the other side these problems can be eliminated by the use of heterogeneous catalysts.

MPV reduction has been investigated using different heterogeneous catalysts including hydrous zirconia[4-6], hydrotalcites[7-13], magnesium-aluminium mixed oxide[14] previously obtained from a layered double hydroxide or magnesium-gallium, and magnesium-indium hydrotalcite-like compounds[7], zeolites[15-22], TiOx/γ-Al_2O_3[23], metal alkoxides immobilized on mesoporous materials based on silica, aluminosilicates or titanosilicates[24-31] and metal oxides such as MgO[7], ZrO_2, Al_2O_3[32,33], or ZrO_2 modified by boron or alkaline-earth metal (Mg, Ca, Sr, Ba) to enhance their acid and basic properties in MPV reduction[32].

Immobilization of metal alkoxides such as zirconium 1-propoxide or aluminium 2-propoxide[4,22,25] on high surface area supports such as silica and siliceous MCM-41, or Al-MCM-41 offers good dispersion of metal alkoxides and good activity of such catalysts and high selectivity to unsaturated alcohol. Still, comparing aluminium 2-propoxide and zirconium 1-propoxide immobilized on SBA-15 the first one was less active[24]. Moreover, the immobilized zirconium catalysts did not lose their activity in the presence of moisture. On contrary, immobilization of zirconium 1-propoxide on zeolite beta gave less active catalyst in MPV reduction of cinnamaldehyde and the formation of cinnamyl isopropyl ether was more favoured[4].

The aim of this work was to find a suitable heterogeneous catalyst for MPV reduction of cinnamaldehyde to cinnamyl alcohol that should be easily separated from the reaction mixture and reused without loss of activity and selectivity.

Experimental

Kinetic experiments were carried out in a distillation apparatus, for removing the formed acetone, equipped with calcium chloride cover used as air moisture absorber. The oil bath was heated up to 95 °C. Obtained samples of the reaction mixture were analysed on GC Agilent, nonpolar column. Unknown by-products were identified using GC/MS.

MPV reduction

3 g of cinnamaldehyde (Sigma Aldrich) were dissolved in 30 ml of dried propan-2-ol (Penta). To this solution, 3 g of heterogeneous catalyst were added. Alumina CG-20 (Sigma Aldrich), acid activated aluminas – commercial type I 504 C (Sigma Aldrich) and laboratory pretreated, aluminosilicate 80/20, MCM-41 and mixed oxides were used as catalysts. Except for mixed oxides, all catalysts were dried before the reaction at 300 °C. Mixed oxides were obtained by the calcination (6 hrs at 500 °C under air atmosphere) of prepared hydrotalcites prior their use for the reaction. The reaction mixture was inserted into the warm oil bath and kept under reflux. After the reaction the heterogeneous catalyst (acid activated alumina I 504 C) was separated, washed 3 times with propan-2-ol and regenerated under oxygen atmosphere (25-85 % of nitrogen) at 550 °C at least for 8 hours.

Acid activation of alumina (CG-20)

Alumina as obtained from producer was stirred with 10 % HNO_3 for 24 h at room temperature. After this period the solid was filtered, washed three times with distilled water and dried at 300 °C for 6 hours.

MCM-41 preparation

Mesoporous material was prepared adopting the procedure of Kumar et al.[34].

Hydrotalcites preparation

Hydrotalcites with different Mg/Al ratios were prepared by coprecipitation method at constant pH of 9.5 ± 0.1 using 500 ml of nitrates solution ($Al(NO_3)_3{\cdot}9H_2O$ and $Mg(NO_3)_3{\cdot}6H_2O$). The second 500 ml solution contained Na_2CO_3 and NaOH.

Both solutions were filtered before coprecipitation. The reactor was charged with 200 ml of demineralized water and tempered to 75 °C. The salt solutions (pump flow rate 6 ml / min) were gradually dosed while stirring. The flow of a basic solution was regulated to keep the constant pH. After dosing all the volume of solutions, the precipitated mixture was stirred for 1 hour. The resulting mixture was then filtered, the solid phase was suspended in 1 L of warm demineralized water, stirred for 10 minutes and filtered again. This procedure was repeated three times. The prepared hydrotalcite was dried at 105 °C for 12 hours.

Results and discussion

During the experiments some undesired reactions forming the by-products took place. Due to the acidic medium the products of aldol condensation were detectable in the reaction mixture – diacetone alcohol (4-hydroxy-4-methylpentan-2-on) and 4-hydroxy-6-phenylhex-5-en-2-on. Diacetone alcohol was formed from two molecules of acetone and the other by-product from cinnamaldehyde and acetone. The presence of acid solids caused the etherification of cinnamyl alcohol and propan-2-ol (forming 3-(1-methylenethoxy)prop-1-enylbenzene = propylcinnamyl ether), or two molecules of cinnamyl alcohol (forming bis(3-phenylprop-2-en-1-yl)ether = dicinnamylether). This observation is in the agreement with the literature[24]. The last detected by-product was 3-phenyl-1-(1methylenethoxy)prop-2-en-1-ol formed by acetalization of cinnamaldehyde with propan-2-ol (Fig.1). The undesired products are easily separable from the desired alcohol.

As it has been already mentioned MPV reduction can be catalysed by Lewis acids. The selected catalysts were compared on the basis of the aluminium content - from pure alumina to the catalysts without aluminium – siliceous MCM-41. The influence of acid activation of alumina was studied comparing the commercial acid activated alumina (type I 504C) with activated alumina CG-20. The activity of mixed oxides that are also described as quite promising catalysts for such reaction[14] was also studies with the focus on Al content. This parameter was not yet described for MPV reduction of cinnamaldehyde. Due to the elimination of the influence of water, all of the materials were dried prior the reaction.

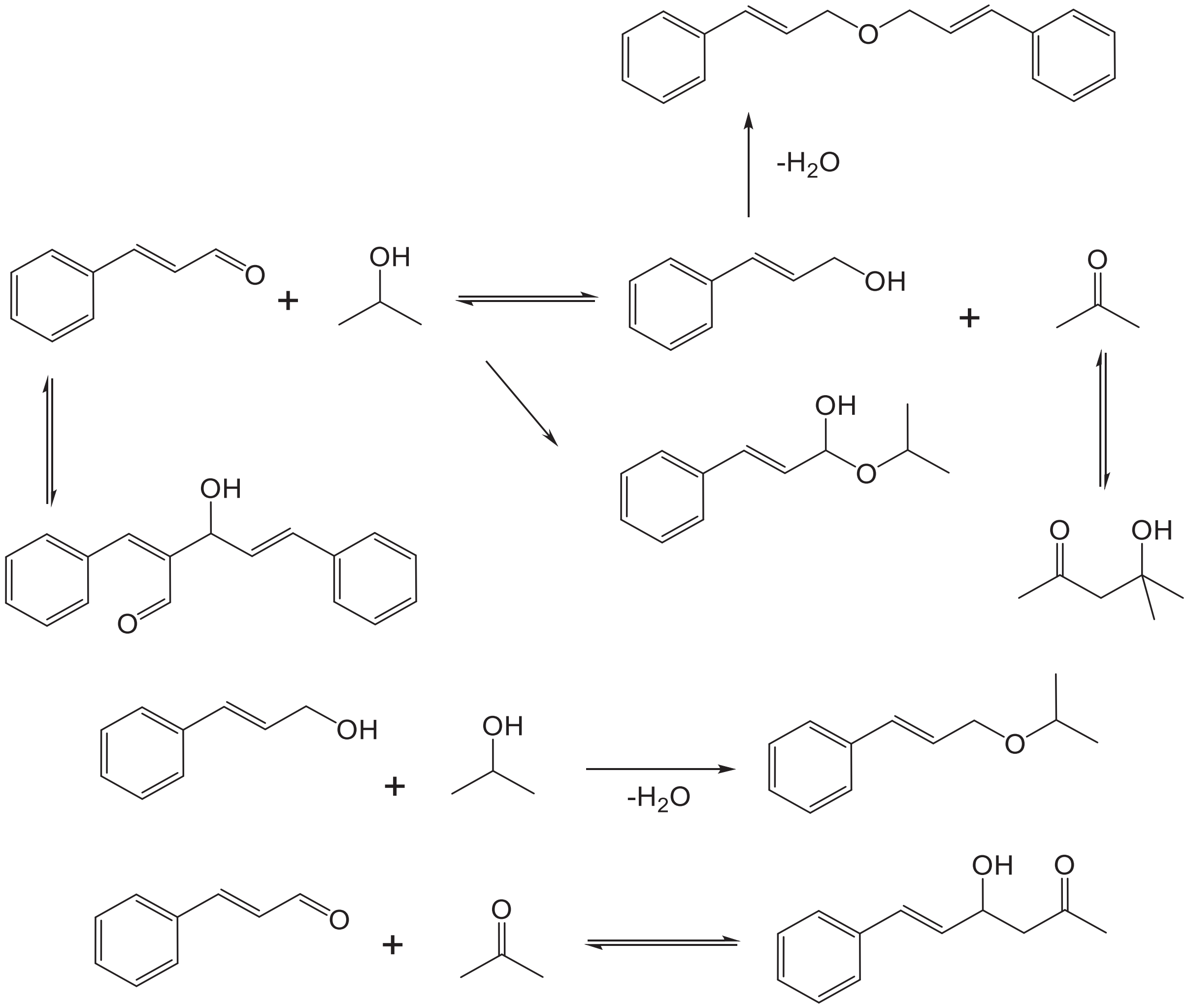

Figure 1. Reaction scheme of MPV reduction of cinnamaldehyde by propal-2-ol

Material comparison

The obtained results are given in the table I and table II. The activity of used materials and the selectivity of cinnamyl alcohol were different. Using alumina and acid activated aluminas the formed by-product in the highest amount was dicinnamyl ether, using aluminosilicate the main by-product was cinnamyl isopropyl ether probably based on the different composition of the catalysts. The formation of cinnamyl isopropyl ether was described in the literature as well using aluminosilicate based zeolite beta[4]. The presence of silicon atoms in the catalyst influenced the formation of different by-product comparing to the aluminous catalyst.

The acid activation of alumina had a positive influence on the reaction rate and also on the selectivity. Within 12 hrs the achieved conversion using acid activated aluminas was higher than 60 % whereas using non activated one only 30 %. Selectivity to cinnamyl alcohol using all of materials after 12 hrs was almost comparable and ranged around 70 %. Little bit higher selectivity of commercial sample may be caused by the slightly different achieved conversion (Table 1). Both acid activated aluminas showed the highest conversion from all of studied materials. However, the use of commercial alumina showed higher selectivity comparing to the pretreated one. Commercial aluminosilicate showed slightly better results comparing commercial non activated alumina, especially from the point of view of conversion. This could be connected with the acidity of used materials. The only fully siliceous material – MCM-41 was totally inactive in the studied reaction.

Table I
Comparison of catalyst used for MPV reduction of cinnamaldehyde to cinnamyl alcohol*

Parameter	Alumina CG-20	Acid activated alumina I 504 C	Acid activated alumina (pretreated)	Aluminosilicate	MCM-41	MO2,5
Time for the 30 % conversion [h]	12	**6**	6	7	-	-
Conversion after 12 h [%]	30	**64**	68	38	4	20
Selectivity after 12 h [%]	71	**77**	71	68	-	62
Conversion after 24 h [%]	42	**70**	72	50	-	24
Time for 100 % conversion [h]	-	**55**	-	-	-	-

*Cinnamaldehyde, 3 g; propan-2-ol, 30 ml; catalyst, 3 g; reflux.

The highest conversion of the starting cinnamaldehyde was achieved with the use of mixed oxides with the higher content of Al (Table II, molar ratio Mg / Al = 2.5) but even using this catalyst, the conversion of cinnamaldehyde after 24 hours did not reach 30%. These results are significantly different from those presented in literature[14] when the cinnamyl alcohol yield of 94% was obtained after 4 hrs of the reaction. Higher conversions were achieved by using higher amount of propan-2-ol (three times higher, gradually dosed for 3 h). In this case, the conversion of cinnamaldehyde reached 34% after 4 hours, but after addition of the whole amount of propan-2-ol, the conversion did not reach 40% after 12 hours.

Table II
Comparison of mixed oxides catalysts used for MPV reduction of cinnamaldehyde to cinnamyl alcohol*

Catalyst	MO2,5	MO3	MO3,5
Conversion after 6 h [%]	17	13	8
Selectivity after 6 h [%]	62	75	70

*Cinnamaldehyde, 3 g; propan-2-ol, 30 ml; catalyst, 3 g; reflux.

From these results, the commercial acid activated alumina was chosen as the most suitable catalyst and the following experiments focused on the possibility of its regeneration and recycling were performed.

From the point of view of the purity of desired cinnamyl alcohol it was necessary to find out whether it would be possible to carry out the reaction up to total conversion. Total conversion was achieved after 55 – 60 hrs, after this time no aldehyde was present in the reaction mixture (monitored by GC). Catalyst reuse was performed due to the optimistic results using this material (Table III).

The material was treated as it is described in the experimental part and reused. After the first cycle, the small loss of the activity and the selectivity was observed. Following experiments showed no additional loss of the activity as same as the selectivity thus in can be concluded that this material may be repeatedly used.

Table III
Recycling of acid activated alumina*

Reuse number	0	1	2	3
Conversion after 3 h [%]	56	45	47	46
Selectivity after 3 h [%]	75	70	68	69

* Cinnamaldehyde, 3 g; propan-2-ol, 30 ml; catalyst, 3 g; reflux.

Conclusions

Solid alumina, silica and magnesium based materials were used for MPV reduction of cinnamaldehyde to cinnamyl alcohol. The use of commercial acid activated alumina showed the optimistic results from the point of view of the possible use in the studied reaction. Despite the fact that the homogeneous catalysts show significantly higher activity the possibility of simple catalyst separation and catalyst reuse are very important in the preparation of desired alcohol. The use of acid activated alumina was the best from all studied catalysts in the achieved conversion as same as the selectivity. Moreover, it was possible to reuse this catalyst without any loss on either activity or selectivity.

Acknowledgement

This work was supported from the grant of Specific university research – grant No A2_FCHT_2020_042.

References

1. Rylander P. N, Steele D. R.: Hydrogenation of unsaturated aldehydes to unsaturated alcohols. BASF Catalysts LLC, Engelhard Minerals and Chemicals Corp. US3655777A.
2. Nakano T., Umano S., Kino Y., Ishii Y., Ogawa M.: J. Org. Chem. *53*, 3753 (1988).
3. Phukan P., Sudalai A.: Synth. Commun. *30*, 2401 (2000).
4. Liu S.h., Jaenicke S., Chuah G.K.: J. Catal. *206*, 321 (2002).
5. Shibagaki M., Takahashi K., Matsushita J.: Bull. Chem. Soc. Jpn. *61*, 3283 (1988).
6. Kuno H., Shibagaki M., Takahashi K., Matsushita H.: Method of producing aldehyde by oxidation of primary alcohol. Japan Tobacco Inc US5210317A.
7. Aramendía M.A., Borau V., Jimenéz C., Marinas J.M., Ruiz J.R., Urbano F.: Appl. Catal. *249*, 1 (2003).
8. Kumbhar P.S., Sanchez-Valente J., Lopez J., Figueras F.: Chem. Commun. 535 (1998).
9. Jyothi T.M., Raja T., Talawar M.B., Sreekumar K., Rajagopal R., Rao B.S.: Bull. Chem. Soc. Jpn. *73*, 1425 (2000).
10. Jyothi T.M., Raja T., Sreekumar K., Talawar M.B., Rao B.S.: J. Mol. Catal. A *157*, 193 (2000).
11. Jyothi T.M., Raja T., Rao B.S.: J. Mol. Catal. A *168*, 187 (2001).
12. Aramendía M.A., Borau V., Jiménez C., Marinas J.M., Ruiz J.R., Urbano F.: Appl. Catal. A *206*, 95 (2001).
13 Xiao Z.: Mol. Catal. *436*, 1 (2017).
14. Ruiz J.R., Jimenéz-Sanchidrián C., Hidalgo J.M., Marinas J.M.: J. Mol. Catal. A: Chem. *246*, 190 (2006).
15. Shabtai J., Lazar R., Biron E.: J. Mol. Catal. *27*, 25 (1984).
16. Creyghton E.J., Ganeshie S.D., Downing R.S., van Bekkum H.: Chem. Commun. 1859 (1995).
17. Creyghton E.J., Ganeshie S.D., Downing R.S., van Bekkum H.: J. Mol. Catal. *115*, 457 (1997).
18. van der Waal J.C., Tan K., van Bekkum H.: Catal. Lett. *41*, 63 (1996).
19. van der Waal J.C., Kunkeler P.J., Tan K., van Bekkum H.: J. Catal. *173*, 74 (1998).
20. Corma A., Domine M.E., Nemeth L., Valencia S.: J. Am. Chem. Soc. *124*, 3194 (2002).
21. Corma A., Domine M.E., Valencia S.: J. Catal. *215*, 294 (2003).
22. Zhu Y.Z., Chuah G.K., Jaenicke S.: Chem. Commun. 2734 (2003).
23 Cai W.; Yang J., Sun H., Wang Y., Ling T., Guo X., Peng L., Ding W.: Cuihua Xuebao, *38*, 1330 (2017).
24. Zhu Y., Jaenicke S., Chuah G.H.: J. Catal. *218*, 396 (2003).
25. Zhu Y., Chuah G.-K., Jaenicke S.: J. Catal. *241*, 25 (2006).
26. Ramanthan A., Klomp D., Peters J.A., Hanefeld U.: J. Mol. Catal. A: Chem. *260*, 62 (2006).
27. Anwander R., Palm C., Gerstberger G., Goeger O., Engelhardt G.: Chem. Commun. 1811 (1998).
28. Leyrit P., McGill C., Quignard F., Choplin A.: J. Mol. Catal. A *112*, 395 (1996).
29. Inada K., Shibagaki M., Nakanishi Y., Matsushita H.: Chem. Lett. 1795 (1993).
30. Quignard F., Graziani O., Choplin A.: Appl. Catal. A *182*, 29 (1999).
31. Bruyn M.D., Limbourg M., Denayer J., Baron G.V., Parvulescu V., Grobet P.J., De Vos D.E., Jacobs P.A. : Appl. Catal. A *254*, 189 (2003).
32. Urbano F.J., Aramendía M.A., Marinas A., Marinas J.M.: J. Catal. *268*, 79 (2009).
33. Ivanov V.A., Bachelier J., Audry F., Lavalley J.C.: J. Mol. Catal. *91*, 45 (1994).
34. Kumar D., Schumacher K., du Fresne von Hohensche C., Gruen M., Unger K.K.: Colloids. Surf. A *187-188*, 109 (2001).

THE EFFECT OF TEMPERATURE AND CONCENTRATION OF WATER ON OXIDATION OF DICYCLOHEXYLAMINE WITH AIR

Valeš R., Kukučková A., Dvořák B., Krupka J.

University of Chemistry and Technology in Prague, Department of Organic Technology, Technicka 5, Prague 6, 166 28, Czech Republic
roman.vales@vscht.cz

Abstract

This work focuses on the kinetics of non-catalysed low-temperature oxidative dehydrogenation of dicyclohexylamine to its imine, *N*-cyclohexylidenecyclohexanamine, with air in liquid phase. The influence of reaction temperature 50-100 °C and concentration of water 0.04-0.60 wt. % on the reaction rate was studied. The activation energy of this reaction was calculated, E_a = 52.7 kJ mol^{-1}. Likewise, the consecutive reactions of this system were studied, especially the hydrolysis of abovementioned imine to cyclohexanone and cyclohexylamine. It was found that consecutive hydrolysis of imine with application of reactant with low concentration of water, 0.04 wt. %, is relatively slow reaction. The activation energy of imine hydrolysis was calculated, E_a = 356 kJ mol^{-1}. Furthermore, the content of water in the reactant accelerates up five times the rate of oxidative dehydrogenation of dicyclohexylamine and almost ten times the rate of imine hydrolysis.

Introduction

Dicyclohexylamine (DCHA) is mostly produced by gas-phase hydrogenation of aniline or disproportionation of cyclohexylamine over nickel catalysts. DCHA, alongside with it salts have good anticorrosion properties[1]. For the example, as a corrosion inhibitor is used dicyclohexylamine nitrite[2]. Furthermore, DCHA is used for production of cure accelerators, pharmaceutical agents, lubricants and cutting fluids[3]. In all application, the quality (purity) of DCHA is very important. During the storage of DCHA in stainless steel barrels, its quality probably decreases due to the contact with the air atmosphere, leading to increase in the concentrations of contaminants, especially *N*-cyclohexylidenecyclohexanamine (NCCHA). The content of NCCHA in DCHA is undesirable due to the difficulty of its separation.

The published data about the oxidative dehydrogenation (ODH) of DCHA to NCCHA are very limited. Literature dealing with this reaction are mostly about the catalytic oxidation of DCHA with complex-cobalt catalysts[4] and organic peroxides[5]. Nevertheless, there is no useful data to describe the kinetics of this reaction. Therefore, this contribution is focused on the study of kinetics of non-catalysed low-temperature oxidative dehydrogenation of DCHA to NCCHA with air in liquid phase. In this study, we focused on the effect of temperature and concentration of water in DCHA (**I**) on rate of its ODH to NCCHA (**II**), conjointly with the effect of temperature and water on the rate of hydrolysis of NCCHA (**II**) to cyclohexanone (CHON) (**III**) and cyclohexylamine (CHA) (**IV**) and consecutive oxidation of cyclohexylamine (**IV**) to cyclohexanone oxime (CHOX) (**V**).

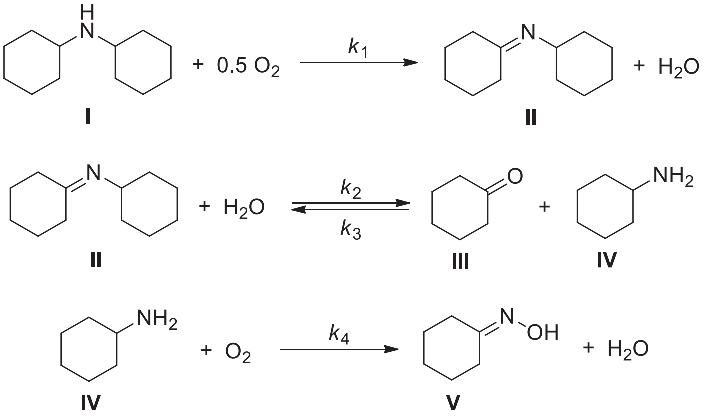

Figure 1. Reaction scheme of oxidative dehydrogenation of DCHA (I) to NCCHA (II), consecutive hydrolysis to cyclohexanone (III) and cyclohexylamine (IV) followed by oxidation to cyclohexanone oxime (V).

Experimental

Chemicals and gases

Dicyclohexylamine (BorsodChem, Czech Republic, 99.9 %) was used without further purification. For the experiments of oxidations was used technical air (SIAD, Czech Republic).

Experimental apparatus

The experiments were carried out in a reactor (three-neck round-bottom flask, 250 ml) located in glycerine bath. Temperature of bath was regulated by thermostat. The air from gas cylinder was distribute into 106-109 g of liquid reactant by sparger. The Dimroth condenser was connected to side neck of the reactor. The samples of reaction mixtures were collected by syringe hereupon analysed.

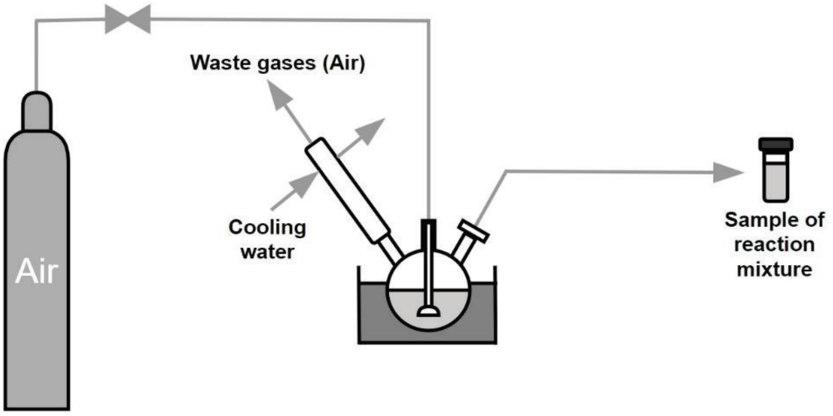

Figure 2. Experimental apparatus for the experiments of oxidative dehydrogenation of DCHA.

Reaction procedure

The oxidative dehydrogenation experiments of 106-109 g of DCHA were carried out at temperature 50-100 °C, atmospheric pressure and flow of air 1 l h^{-1}. The experiments were carried out for 7 hours with collection of samples of reaction mixture per hour.

Gas chromatography

The GC-FID analyses were performed on the Rxi®-624Sil MS column (30 m x 0.25 mm x 1.40 μm). Helium was used as carrier gas. The temperature program started at 80 °C for 2 minutes. Then with a rate of 15 °C/min, the temperature was raised to 210 °C.

Water content

The concentration of water was determined by coulometric Karl-Fischer titration on Titrator C 30 (Mettler Toldeo).

Data processing

The regression analysis of experimental data was performed using the ERA (Easy Regression Analysis) software[6]. The dependence of the rate constant k_i on temperature for the reaction i was expressed by the Arrhenius relation:

$$k_i = k_{i0}\exp\left[\frac{E_{ai}(T-T_0)}{RTT_0}\right] \qquad (1)$$

where k_{i0} is a rate constant at reference temperature T_0, T is the temperature, E_{ai} is the activation energy of reaction i, R is the universal gas constant. The reference temperature was used in order to eliminate the strong correlation between the activation energy E_{ai} and the pre-exponential factor A in the Arrhenius relation[7]. The studied reaction system presented by Figure 1 was described by power-law kinetics. The model is simplified by assumption that dicyclohexylamine is saturated by oxygen, thus concentration of O_2 is constant, hence not taken into account in the model. The regression model consists of following equations:

$$r_1 = k_1 c_{\mathrm{DCHA}} \tag{2}$$

$$r_2 = k_2 c_{\mathrm{NCCHA}} c_{\mathrm{H2O}} \tag{3}$$

$$r_3 = k_3 c_{\mathrm{CHON}} c_{\mathrm{CHA}} \tag{4}$$

$$r_4 = k_4 c_{\mathrm{CHA}} \tag{5}$$

$$\frac{\mathrm{d}C_{\mathrm{DCHA}}}{\mathrm{d}t} = -\, r_1 \tag{6}$$

$$\frac{\mathrm{d}C_{\mathrm{NCCHA}}}{\mathrm{d}t} = r_1 - r_2 + r_3 \tag{7}$$

$$\frac{\mathrm{d}C_{\mathrm{CHON}}}{\mathrm{d}t} = r_2 - r_3 \tag{8}$$

$$\frac{\mathrm{d}C_{\mathrm{CHA}}}{\mathrm{d}t} = r_2 - r_3 - r_4 \tag{9}$$

$$\frac{\mathrm{d}C_{\mathrm{CHOX}}}{\mathrm{d}t} = r_4 \tag{10}$$

$$\frac{\mathrm{d}C_{\mathrm{H2O}}}{\mathrm{d}t} = r_1 - r_2 + r_3 + r_4 \tag{11}$$

Results and discussion

The effect of temperature on the reaction rate

The experiments of ODH of DCHA were carried out at the temperature range of 50-100 °C. There was not recognized the arise of concentration of NCCHA at 50-60 °C at the time range of 7 hours. Already at the temperature 70 °C there was concentration changes of NCCHA and DCHA. At 80-100 °C there was the stagnation in concentration of NCCHA (Fig. 3).

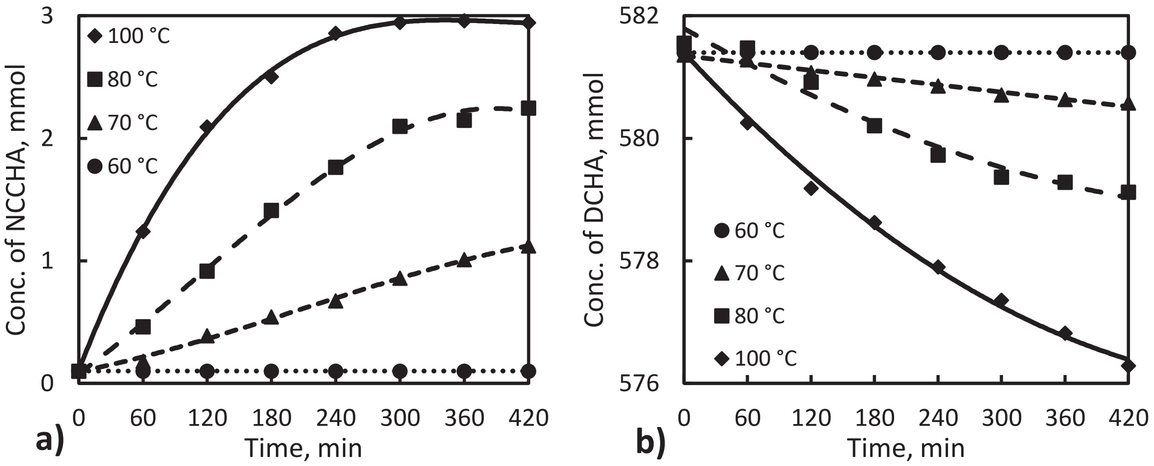

Figure 3. The concentration profile of a) NCCHA at 60-100 °C and b) DCHA at 60-100 °C.

The stagnation of concentration of NCCHA was due to the consecutive reactions (Fig. 1) of this imine. The Figure 4 presents the concentration profiles of products of oxidative dehydrogenation of DCHA at 80-100 °C. There was observed far greater extent of NCCHA hydrolysis to CHON and CHA at the reaction temperature 100 °C compared to reaction temperature of 80 °C.

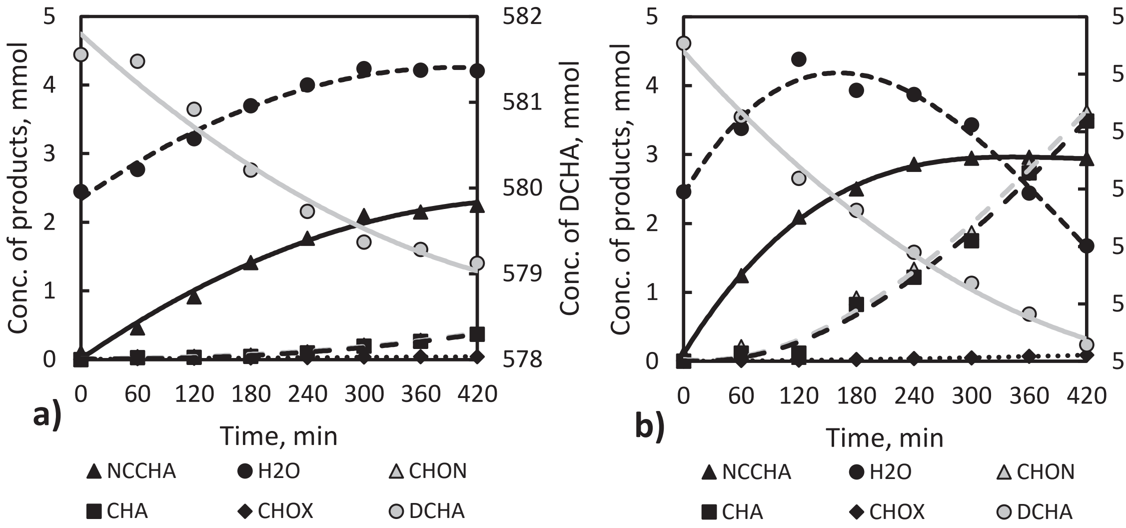

Figure 4. Time dependence of concentration profiles of products and DCHA at a) 80 °C and b) 1000 °C.

From the experimental data was calculated the value of activation energy, E_a = 52.7 kJ mol^{-1}, for the ODH of DCHA to NCCHA. It was used dicyclohexylamine with low concentration of water, 0.04 wt. %. The DCHA is strong base, with pKa = 10.4[8]. For this reasons, low initial concentration of water and lack of acid catalyst[9], the hydrolysis of NCCHA was accelerated primarily by the reaction temperature. The value of the activation energy of this reaction is E_a = 356.0 kJ mol^{-1}. The reaction (3), i.e. condensation of CHON and CHA to NCCHA, is probably supressed by the excess of NCCHA continuously produced by ODH of DCHA. The consecutive oxidation of CHA to CHOX is insignificant due to the preferential reaction of DCHA with oxygen.

Table I
Results of the regression analysis of the kinetic model including reactions 1-4.

Reaction (No.)	$k_{i(80\,°C)}$ x 10^8	E_{ai}
	[mol l^{-1} min^{-1}]	[kJ mol^{-1}]
DCHA + 0.5 $O_2 \rightarrow$ NCCHA + H_2O (1)	0.88	52.7
NCCHA + $H_2O \rightarrow$ CHON + CHA (2)	0.22	356.0
CHON + CHA $\rightarrow$ NCCHA + H_2O (3)	0.15	44.7
CHA + $O_2 \rightarrow$ CHOX + H_2O (4)	0.13	53.6

The effect of water on the reaction rate

The experiments were carried out at the reaction temperature 100 °C and concentration of water 0.04-0.60 wt. % in DCHA. For simplicity, the effect of water on the reaction rate of oxidative dehydrogenation of DCHA was expressed by the ratio of reaction rate constants, $k_{H2O}/k_{(0.04\,\%)}$, where the k_{H2O} is for ODH of DCHA with explicit concentration of water and $k_{(0.04\,\%)}$ for the reference experiment of ODH of DCHA with 0.04 wt. % of water. The maximum of reaction rate (fivefold increase) of the ODH of DCHA with air was achieved at the concentration of 0.40 wt. % of water in DCHA. It is possible that at 100 °C the 0.40 wt. % is the upper limit for solubility of water in DCHA. At higher concentrations forms water in DCHA micro-emulsion. So, the oxygen solutes in aqueous phase and therefore there is no further effect of water on the reaction rate. However, there are no published data about the solubility of water or oxygen in DCHA.

The hydrolysis of NCCHA to CHON and CHA was significantly affected by the increasing concentration of water in DCHA. The increase of concentration of water in DCHA from 0.04 to 0.60 wt. % leading to almost ten times increase in the reaction rate of hydrolysis of NCCHA. Compared to that, there is almost no effect on the reaction rate of the oxidation of CHA to CHOX.

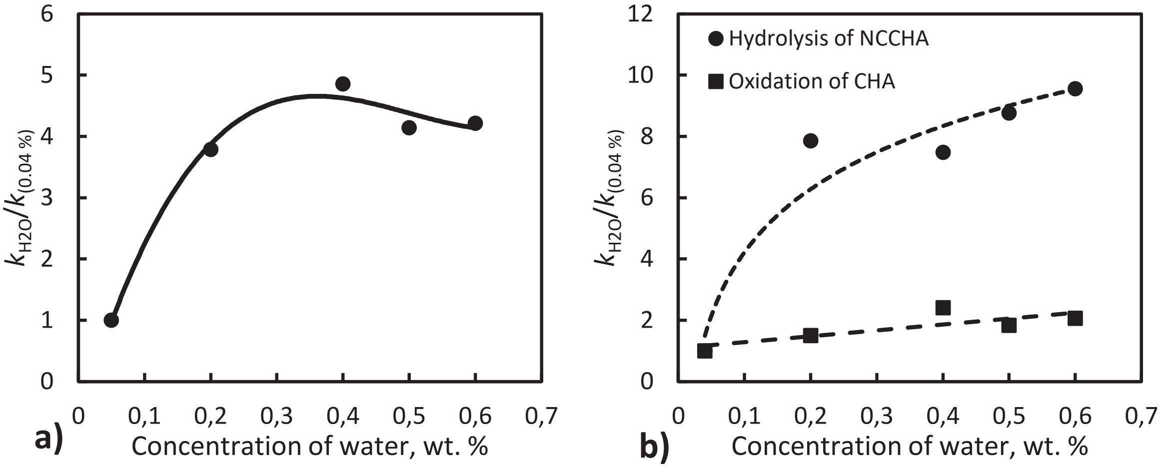

Figure 5. The effect of water on the reaction rate of a) oxidative dehydrogenation of DCHA to NCCHA and b) hydrolysis of NCCHA to CHON and CHA, and oxidation of CHA to CHOX.

Conclusion

In this study, it was investigated the effect of temperature 50-100 °C and the concentration of water 0.04-0.60 wt. % in dicyclohexylamine on the reaction rate of its oxidative dehydrogenation with air in liquid phase. It was proved that the impurity, *N*-cyclohexylidenecyclohexanamine, in commercial produced and stored dicyclohexylamine is truly formed by its oxidative dehydrogenation with air. For the oxidative dehydrogenation of DCHA to NCCHA and its consecutive reactions, the kinetic parameters as the activation energy were calculated. Furthermore, it was found that the water significantly accelerates the reaction rate of the oxidative dehydrogenation of DCHA and the consecutive hydrolysis of NCCHA.

In conclusion, this paper particularly contributes to the production practise of dicyclohexylamine. Its fundamental to store this amine under dry and inert atmosphere to eliminate the formation of impurities.

Acknowledgement

This work was supported from the grant of Specific university research – grant No A1_FCHT_2021_005.

References

1. Roose P., Eller K., Henkes E., Rossbacher R., Hartmut H.: Amines, Aliphatic in Ullmann's Encyclopedia of Industrial Chemistry (2015).
2. Pan M., Wang W., Zhou Q., Zhang J., Zhang Q.: Adv. Anal. Chem. *8*, 124 (2018).
3. Technical data sheet (TDS), Dicyclohexylamine, BorsodChem. [Cited: Apr. 27, 2021.] https://www.borsodchem-cz.com/getdoc/93499a7a-56ba-4f29-a961-5305c93f61f6/default.aspx
4. Khatri P., Jain S. L., Sivakumar L. N. K., Sain B.: Org. Biomol. Chem. *9*, 3370 (2011).
5. Hawkins E. G. E.: J. Chem. Soc., Perkins Trans. *1*, 13 (1972).
6. Zamostny P., Belohlav Z.: Comput. Chem. *23*, 479 (1999).
7. Krupka J.: Reac. Kinet. Mech. Cat. *116*, 315 (2015).
8. Monograph, Dicyclohexylamine, Merck Index Online. [Cited: May 6, 2021.] https://www.rsc.org/Merck-Index/monograph/m4376/dicyclohexylamine?q=authorize
9. Cordes B. H., Jencks W. P.: J. Am. Chem. Soc. *84*, 832 (1962).

POLYMERS, COMPOSITES

DEACIDIFICATION AND PRESERVATION OF CELLULOSIC OBJECTS OF CULTURAL HERITAGE

Králik M.[1], Horváth B.[1], Vizárová K.[2], Vajová I.[2], Gašparovičová D.[1], Danielik V.[3], Jurišová J.[3]

[1]*Institute of Organic Chemistry, Catalysis and Petrochemistry*
[2]*Institute of Natural and Synthetic Polymers*
[3]*Institute of Inorganic Chemistry, Technology and Materials*
Faculty of Chemical and Food Technology, STU, Radlinského 9, SK-81237, Bratislava, Slovak Republic
milan.kralik@stuba.sk

Abstract

This contribution presents a brief overview of the deacidification and preservation of aged cellulosic objects. Aqueous, organic liquid and air - solid/liquid systems are discussed. The global aim of all these techniques is to deliver alkaline species to acidic sites in the volume of the paper, to neutralize them and to create the so-called alkaline reserve, which ensures a significant decrease in further degradation. The success of this process strongly depends on mass transport phenomena. The simplest example of such a process uses aqueous liquid-based systems (e.g., hydrogen carbonate as a base); however, damage of the paper sheets can occur due to the effects of water. Organic liquid processes with dissolved organometallic compounds are much more compatible with paper, however, they are more sensitive to process parameters, e.g., wetness in the pre-dried material, contact time and post-treatment parameters (humidity, concentration of CO_2, temperature, time). When solid particles are used (most frequently MgO), the situation is even more complicated, because of the dissolution of the solid particles, diffusion into the body of the paper sheet and the reactions with acidic sites. Several approaches to modelling and optimization of deacidification procedures are outlined in this paper.

Introduction

From the beginning of the papermaking history, lignocellulosic materials represent the main resources to produce paper[1,2]. The principle of the technology remains virtually the same for hundreds of years, i.e., to minimize the presence of soluble and less stable species, such as inorganics, pectins, lignins and hemicelluloses, and to improve the quality of the pulp by bleaching (if necessary), adding sizing agents, fillers and colorants (if desired)[2]. The industrial progress in papermaking in the early 19th century led to the technologies using a pulp (from wood) processed with alum ($KAl(SO_4)_2$), then later with a cheaper $Al_2(SO_4)_3$ and rosin (abietic acid being the main component of it) [2]. Therefore, papers became more acidic, and the degradation processes have proceeded more rapidly. The effect of the degradation of the paper is demonstrated by an experiment simulating 200 years of ageing. (Fig. 1).

Figure 1. Changes in the colour and overall appearance of the newspaper sheet after artificial aging simulating 200 years, prepared by INSP STU in Bratislava.

Fig. 2 depicts the structure of a paper sheet with the indication of cellulose fibres, macrofibrils, microfibrils and bounds of cellulosic chains. It´s worth to mention that the amorphous parts of the chain give the flexibility to the paper sheet. However, these sections are less stable during ageing and undergo degradation sooner than the well-crystallized regions (i.e well-ordered cellulose). Acid-catalysed cleavage, oxidation, reactions with nitrous or sulphuric oxides, microbiological (mainly filamentous fungi) attack (all the reactions being accelerated by higher humidity) represent the main types of reactions yielding the degradation of cellulosic cultural objects [3,4,5].

Consequently, the paper loses mechanical strength, color changes, turns to be more fragile and falls apart at the end (Fig.1).

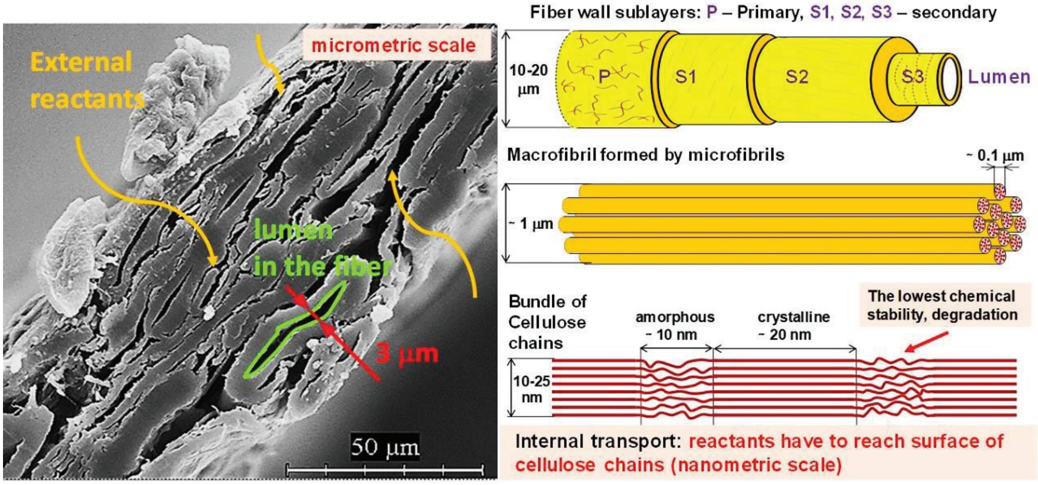

Figure 2. The cross-section of the newspaper sheet with the indication of cellulose fibres, their constitution by layers, macrofibrils formed by microfibrils and a bundle of cellulose chains. (Rests of lignin and hemicellulose materials are not depicted).

Deacidification methods

Intentions to improve the quality and to stabilize aged (acidic) papers using stabilisation systems with soluble basic inorganics, e.g. hydrogen carbonates, were applied in the past [6]. Due to the elaborateness (the books were disassembled to individual pages, and recomposed after the end of the deacidification procedure) and due to the danger of damaging/curling of paper sheets, organometallics (e.g. $Mg(OCH_2CH_3)_2$) dissolved in organic solvents or solid basic substances (e.g. MgO) in organic carriers have commenced being applied [7,8]. A comprehensive description of the rationality of various deacidification systems can be found in papers of Baty [9], Zervos [10], Hubbe [11] and refrs. therein. Figure 3 and Table I illustrates the main deacidification systems applied so far, their compositions and the year of implementation of their commercial application.

Reliable-non-biased characterization of acidic and basic sites in the body/volume of paper sheets is important both for the evaluation of the state of aged objects as well as for the quantification of the effects of the deacidification/preservation procedures. A wide set of pH measurements, chromatographic analysis of extracts, colorimetric measurements and microscopic characterizations of the surface and cross-sections of paper sheets is reported [12]. The most successful and reliable methods are based on EDX (Energy-dispersive X-ray spectroscopy) and WDS (Wavelength-Dispersive X-Ray Spectroscopy) [13].

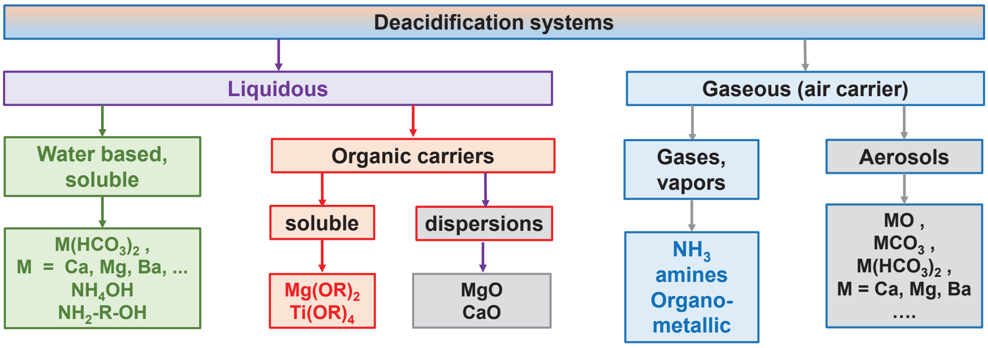

Figure 3. Classification of deacidification systems.

Mass transport effects

There are two aims for the utilization of deacidification systems:

- to neutralize the acidic species already formed
- to generate an alkaline reserve, which serves as a buffer for the neutralization of the acidic species.

The application of the so-called sizing agents (as alum – rosin) amplifies the hydrophobic/hydrophilic differences between the properties of the paper surface and the bulk of the paper sheet. These facts necessitate the utilization of either polar (water-based) or non-polar (alkanes, perfluoroalkanes, hexamethyldisiloxane and similar) deacidification systems.

Table I

Most widespread deacidification systems and the year of their commercialization.

Act. elem.	Environment/ solvent/ carries	Process	Fy (start of utilization / advanced application)	Deacidifying agent	Resulting deacid. subst.
Aqueous systems					
Mg	water	Neschen	Neschen AG, Buckeburg und Hoppegarten Berlin, Germany (1988/1998)	$Mg(HCO_3)_2$	$Mg(HCO_3)_2$, $MgCO_3$
Mg Ca	water	Vienna	National Library, Vienna, Vienna, Austria (1986)	$Ca(OH)_2$ $MgCO_3$	$Ca(OH)_2$, $CaCO_3$, $MgCO_3$
Liquid non-aqueous systems					
Mg	methanol+ dichlordifluoro methane (freon 12)	Wei ´To	National Library of Canada,Ottawa, Canada, (1972/1981)	Methoxy magnesium methyl carbonate (MMMC)	$MgCO_3$, $Mg(OH)_2$
Mg	methanol+ tetrafluoroethane (freon 134a)	Sablé	National Library of France (1987)		
Mg	hexamethyl disiloxane (HMDO)	Papersave	Battelle Ingenieurtechnik, Eschborn, Germany (1989)	Magnesium titanium ethoxide (METE)	$Mg(OH)_2$, $MgCO_3$
			Zentrum für Bucherhaltung, Leipzig, Germany, (1994)		
			ZFB, Papersave, San Diego, USA, (2003)		
		Papersave Swiss	Nitrochemie Wimmis AG, Wimmis, Switzerland, (2000)		
Mg	n-propanol + heptafluoropropane (HFC 227)	CSC BookSaver	Conservación de Sustratos Cellulosicos, Barcelona, Spain (1990/1999)	Carbonated di-n-propylate magnesium	$MgCO_3$
		CSC BookSaver	Preservation Academy Leipzig, Leipzig, Germany (2003)		
Mg	freon 113, substitution of heptane	FMC	Lithium Corporation of America (lithco), North Carolina, USA (1988/1990)	Carbonate magnesium dibutoxytriethyl ene glycolate	$MgCO_3$
G / S (L) systems					
Mg	submicroparticles/ perfluorheptane+ polyoxyperfluoro-alkane acid	Book Keeper	Bookkeeper Preservation Technologies, L.P., Cranberry Township, PA, USA (1994)	MgO	$MgCO_3$
Mg Ca	submicroparticles/ air	Libertec	Libertec Bibliothekensdienst, Nurnberg, Germany, (1996)	MgO CaO	$CaCO_3$, $MgCO_3$
Mg Ca	submicroparticles/ air	SoBu	SOBU Sonder-maschinenbau und Buchentsäurung, Fürth, Germany, (2001)	MgO + dolomite	$CaCO_3$, $MgCO_3$, $Mg(OH)_2$
Zn	G / diethyl zinc	DEZ	Library of Congress, Washingthon, USA (1985-1994)	Diethyl zinc	ZnO

Fig. 4 illustrates the mechanism of action for the polar (aqueous based) system. The hydrophobic resistance of the paper is overcome by the excess of water here. Hydrophilic -OH groups of the cellulose are solvated, the fibres of cellulose swell, thus allowing the solution of $Mg(HCO_3)_2$ to penetrate to the body (volume) of the paper sheet. Acidic species are neutralized according to the formula:

$$Mg(HCO_3)_2(aq.) + 2\ H_3O^+ \leftrightarrows Mg^{2+}(aq.) + 4\ H_2O + 2\ CO_2\ (g) \tag{1}$$

After the drying of the paper sheet, the alkaline reserve is present either in the form of $Mg(HCO_3)_2$ or as a carbonate, accordingly:

$$Mg(HCO_3)_2 \leftrightarrows MgCO_3\ (s) + H_2O + CO_2\ (g) \tag{2}$$

Procedures with water-based systems allow the formation of a huge alkaline reserve, but disadvantages (necessity to disassemble the books to individual pages, pages can be corrugated after being wetted by water) strongly overwhelm the exploitation of this kind of methods.

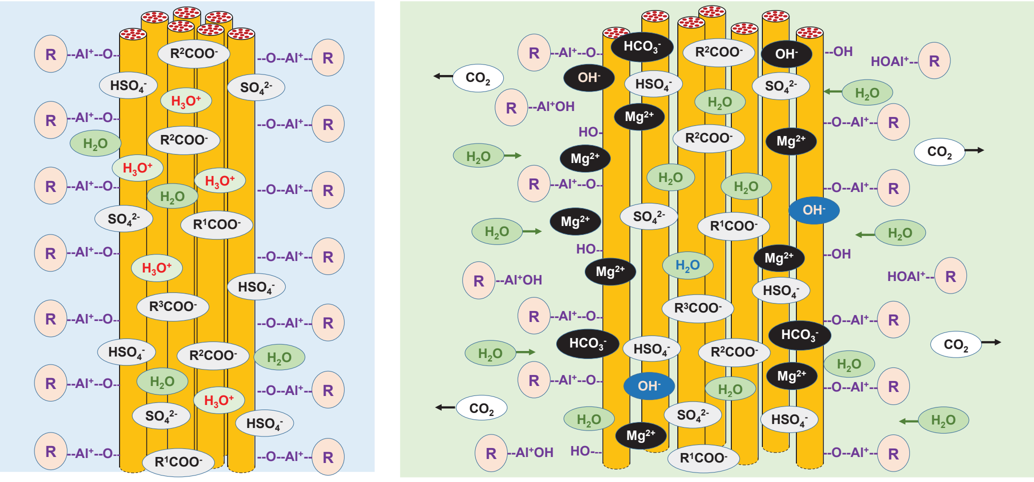

Figure 4. ***Left:*** visualisation of microfibrils in a paper sheet prepared from pulp using Alum ($(KAl)(SO_4)_2$), or $Al_2(SO_4)_3$ and a hydrocarbon segment of abietic acid (denoted as R) with the rest of sulphonic groups and the generated acidic species ($RCOO^-$, H_3O^+); ***Right***: swelling, penetration of $Mg(HCO_3)_2$ to the volume of the paper sheet, after contacting with an aqueous solution of neutralization agents.

Deacidification procedures using organic solvents and carriers are much more "paper-friendly" in comparison with aqueous systems. Fig. 5 illustrates the situation with magnesium ethoxide ($Mg(OEt)_2$) as a neutralisation agent dissolved in hexamethyldisiloxane (HMDO).

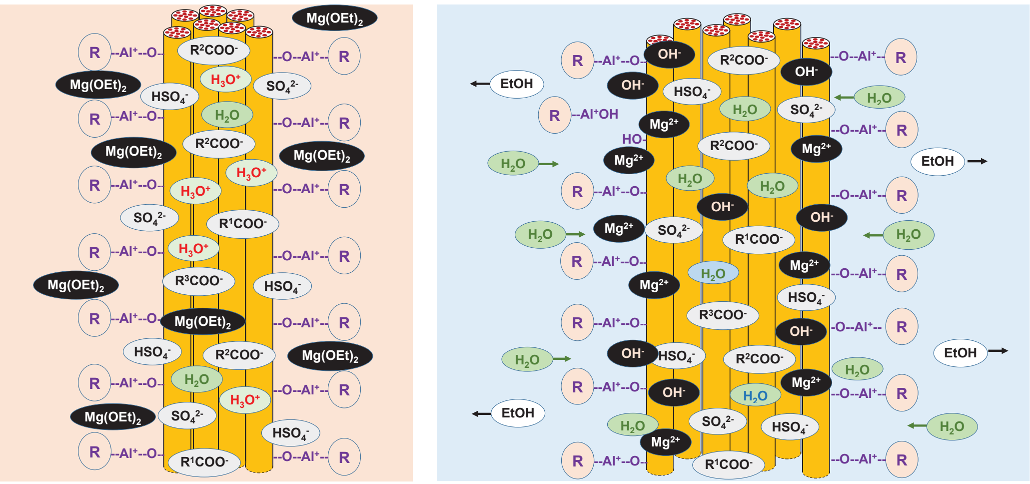

Figure 5. ***Left***: visualisation of microfibrils in a paper sheet prepared from pulp using Alum ($(KAl)(SO_4)_2$), or $Al_2(SO_4)_3$ and a hydrocarbon segment of abietic acid (denoted as R) with a rest of sulphonic groups and the generated acidic species ($RCOO^-$, H_3O^+) in contact with magnesium ethoxide ($Mg(OEt)_2$); ***Right***: swelling after contact with water vapours, penetration of Mg^{2+} and OH^- ions, neutralization of H_3O^+ and evolution of ethanol vapours (EtOH).

Due to the hydrophobic (non-polar) feature of this mixture, this does not penetrate inside the microfibrils. After the removal of the excess solution, drying and contacting with air containing water vapour and CO_2, the following reactions proceed:

$$Mg(OEt)_2 + 2\,H_2O \leftrightarrows Mg^{2+} + 2\,OH^- + 2\,EtOH\,(g) \qquad (3)$$

$$OH^- + H_3O^+ \leftrightarrows 2\,H_2O \qquad (4)$$

The crucial factors influencing the mass transport in praxis are:

- impregnation of the books with organic solution (transport to cellulose fibres)
- transport of water and CO_2 to macrofibrils and microfibrils, as well as swelling

- transport of Mg^{2+} and OH^- ions to the bulk of microfibrils.

The alkaline reserve, as mentioned above, is present in the form of magnesium hydroxide, magnesium hydrogen carbonate, or magnesium carbonate, respectively. In spite of the outlined problems and expenses, these procedures are the most successful for the deacidification of the paper and the formation of the alkaline reserve [14].

Fig. 6 depicts the case with the most frequently used deacidification system, the so-called Bookkeeper process, where the particles of alkaline oxides are used in the form of spray using organic a hydrophobic carrier and a subsequent exposition to water vapours. The deacidification process typically involves these reactions:

$$MgO + H_2O \leftrightarrows Mg^{2+} + 2\ OH^- \qquad (5)$$

$$OH- + H_3O^+ \leftrightarrows 2\ H_2O \qquad (4)$$

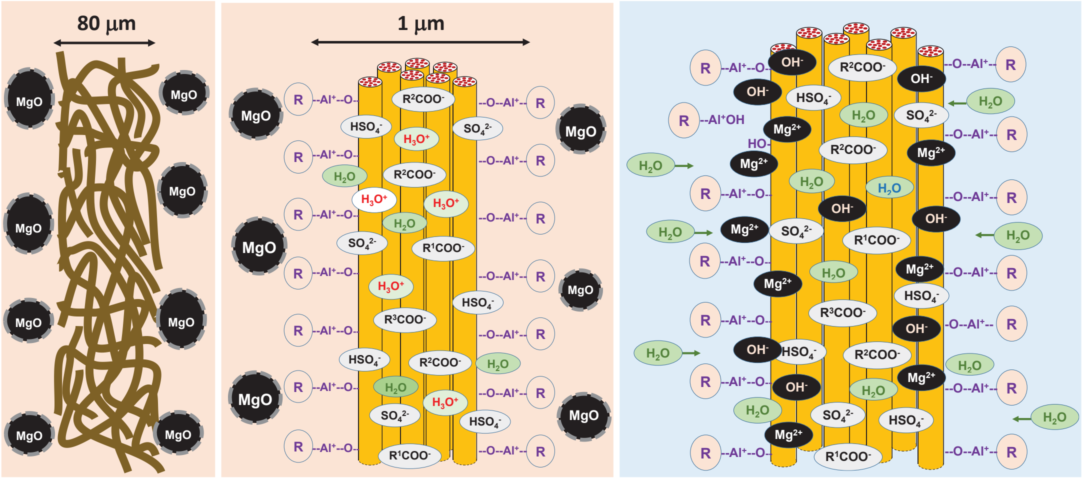

Figure 6. ***Left***: slightly dried paper sheet covered with MgO submicroparticles deposited by spraying of perfluoroalkane dispersion (particles, fibres, fibrils and atoms are not in a proportional scale); ***Middle***: MgO particles penetrated to the cellulose macrofibrils; ***Right***: slight swelling, generation of Mg^{2+} and OH^- ions, penetration to microfibrils, neutralization of acidic species and a formation of an alkaline reserve.

The alkaline reserve is represented by magnesium hydroxide, magnesium hydrogen carbonate or magnesium carbonate. However, the effects of mass transport play a more significant role here in comparison with the processes using homogeneous solutions. There are at least five steps of mass transport and neutralization processes of acidic species which are necessary to distinguish:

- Covering the surface of the paper sheet with MgO particles.
- Transport (convective) of solid MgO particles to the bulk of the sheet (close to cellulose microfibres).
- Transport of water (conductive - diffusion) to MgO particles and a formation of Mg^{2+} and OH^- ions close to the microfibrils, swelling of microfibrils.
- Transport (conductive - diffusion) of Mg^{2+} and OH^- ions to the microfibrils.
- Transport (conductive - diffusion) of CO_2 and a formation of the alkaline reserve.

Fig. 7 shows a typical distribution of the pH in the cross-section of a paper sheet treated with MgO particles in a nano-suspension, in a climate box. It is supposed that Mg^{2+} and OH^- moieties will migrate to the volume of the paper sheet and do neutralize further acidic sites; a formation of an alkaline reserve appears as well.

Hube et al. distinguish 4 types of "nano-transport" of the active deacidification species toward the acidic sites[11]:

- Gas phase diffusion
- Surface diffusion
- Hydrogel-like diffusion
- Diffusion in the capillary condensate

The identification of a particular system and estimation of relevant parameters requires more detailed data.

Conclusions

Despite the mass application of deacidifying systems for the preservation of cellulosic cultural heritage, a quantitative description of process phenomena has not yet been published. This gives a great challenge for further investigations in terms of:

- Liquid flow (wetness, swellability), dissolution depending on pH in the case of solid particles - as well as diffusion of solvated ions in a (micro) porous material accompanied with chemical reactions with acidic species - are necessary to consider.
- A formation of an alkaline reserve is important.
- A design and testing of possible reliable methods for the validation of deacidification processes and alkaline reserves are inevitable.

The outlined problems are the subject of the SK project APVV 18-0155, (MUFUSCEM, 2019-2022), which is solved in connection with the previous project KnihaSK, http://www.knihask.eu/). The two main goals of this project are:

- Preparation, description, and testing of new deacidification/stabilization systems.
- Analysis of the processes of ageing/deacidification and the development of mathematical models to describe the transport of the reaction components and to identify the most relevant chemical reactions.

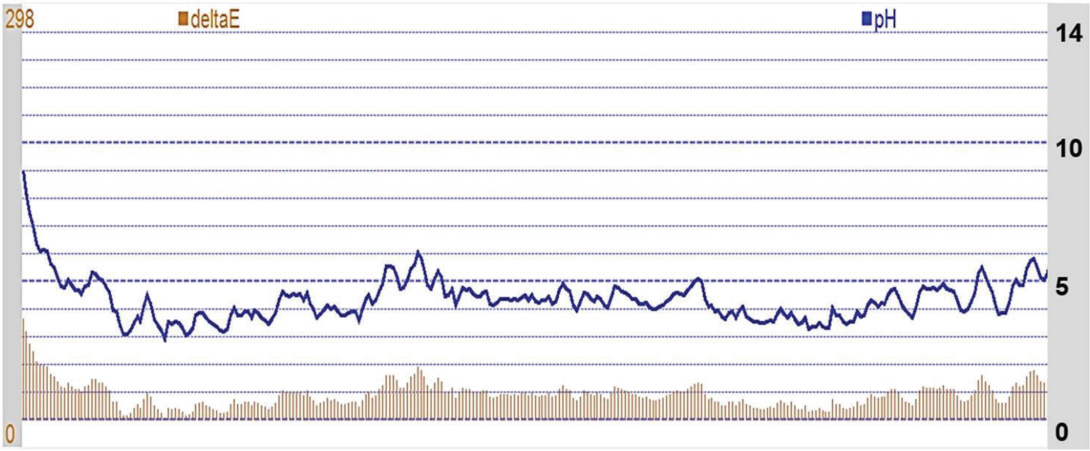

Figure 7. The distribution of the deacidification components and pH, throughout the cross-section of a paper sheet. The value of the pH of the parent “NOVO” acidic paper was 4.5. This sample was treated with a suspension of 4.3 g/L MgO particles in perfluoroheptane and stabilized in a climate box. (50% RH, T: 25°C, for 48 hours) (source: INSP STU and CERTEX, 2020, measurements and data.)

Acknowledgement

This work was supported by the Slovak Research and Development Agency in the framework of the project APVV 18-0155: Synthesis, compatibilization and transport of components of multifunctional systems suitable for the stabilization of cellulosic materials (MUFUSCEM). The authors also thank Prof. Katuščák, Prof. Tiňo and Prof. Jablonský from STU in Bratislava for providing data and counselling.

References

1. Munsell, J.: *Chronology of the Origin and Progress of Paper and Paper-making*. 5th Ed., Albany, 1876.
2. Biermann, C.J.: *Handbook of pulping and papermaking*. Elsevier, 1996.
3. Smith, R.D.: The Library Quarterly, 39(2), 1969, 153.
4. Williams, J.C.: Bulletin of the American Group. International Institute for Conservation of Historic and Artistic Works, 12(1), (1971) 16.
5. Fellers, C., Iversen, T., Lindström, T., Nilsson, T. and Rigdahl, M.: *Ageing degradation of paper*, Report No. 1E, ISSN 0284-5636, Stockholm 1989.
6. Schierholtz, O.J.: Process for the chemical stabilization of paper and product. U.S. Pat. 2,033,452 (1936).
7. Smith, R.D.: Treatment of cellulosic materials. U.S. Pat. 3,676,182 (1972).
8. Kundrot, R.A.: Deacidification of library materials. U.S. Pat. 4,522,843 (1985).
9. Baty, J.W., Maitland, C.L., Minter, W., Hubbe, M.A. and Jordan-Mowery, S.K.: BioResources, 5(3), 2010, 1955.
10. Zervos, S. , Alexopoulou, I.: Cellulose, 22(5), 2015, 2859.
11. Hubbe, M.A., Smith, R.D., Zou, X., Katuščák, S., Potthast, A., Ahn, K.: BioResources, 12(2), 2017, 4410.
12. Area, M.C., Cheradame, H.: Bioresources 6(4), 2011) 5307.
13. Katuščák, S., Vodný, Š., Vizárová, K.: pH Distribution measurement in a porous material microstructure. Method and apparatus. PCT/IB2018/053927, WO/2019/229504 (2019).

14. Katuščák S., Jablonský M., Holubková S.: Comparative evaluation of deacidification processes. Zeitschrift für Bibliothekswesen und Bibliographie Sonderbände, 106, 2012, 149.

AMINE-FUNCTIONALIZED POROUS POLYMERS FOR SELECTIVE CO_2 ADSORPTION

Setnickova K. [1,2], Jerabek K. [1], Strasak T. [1,2], Soukup K. [1]

[1]*Institute of Chemical Process Fundamentals of the Czech Academy of Science, v.v.i., Rozvojova 135, 165 02, Prague 6, Czech Republic*
[2]*University of Jan Evandelista Purkyně in Usti nad Labem, Pasteurova 3544/1, 400 96, Usti nad Labem, Czech Republic*
setnickova@icpf.cas.cz

Abstract

Porous materials have always attracted high scientific interest because of their outstanding performance and potential applications in various fields, including adsorption and gas separation. Hyper-crosslinked polymers (HCLPs) have several advantages over other porous materials, they show extremely high surface areas and porosity, low density, outstanding adsorption properties, high chemical, and thermal stability.

Herein, we reported a synthesis, characterization, and the CO_2 (and other gases) adsorption performance of series of novel styrene-divinylbenzene based HCPs. The material was prepared in two steps. The first step involved the radical copolymerization of divinylbenzene (DVB) and 4-vinylbenzyl chloride (VBC), under solvothermal condition to generate porous polymers with high surface area above 700 $m^2\,g^{-1}$. In the second step, various polyamine species were applied to react with the alkyl chloride groups and functionalize the pore surface to improve the CO_2/N_2, CO_2/CH_4 and CO_2/H_2 selectivity.

Introduction

The increasing release of CO_2 to the atmosphere due to human activities has initiated considerable interest in the development of new materials and technologies for CO_2 capture. A cheap alternative solution represents a design and synthesis of microporous organic polymers, porous materials generally possess low skeletal density, in which the precise control over the material's chemical composition and textural properties can lead to a significant enhancement in gas storage[1]. This work is focused on the synthesis of hypercrosslinked vinylbenzyl chloride (VBC) - divinylbenzene (DVB) microporous material and its application for CO_2 capture and gas separation[2].

Experiment

Material

All chemicals needed to synthesis of the hypercrosslinked vinylbenzyl chloride (VBC) - divinylbenzene (DVB) microporous material were purchased from Sigma Aldrich. Pure gases used for the solubility and permeation experiments were purchased from Linde Gas with a stated purity of at least 99.995%.

Synthesis of porous polymer

The hypercrosslinked vinylbenzyl chloride (VBC) - divinylbenzene (DVB) microporous polymer was prepared and functionalized in two steps as shown in Scheme 1. The first step involved the suspension polymerization of divinylbenzene (DVB) and 4-vivylbenzyl chloride (VBC). Then, the resulting polymer was hypercrosslinked under conditions given in Scheme 1a. In the second step, various polyamine species were applied to react with the alkyl chloride groups and functionalize the pore surface to improve selectivity of material to CO_2 (see Scheme 1b).

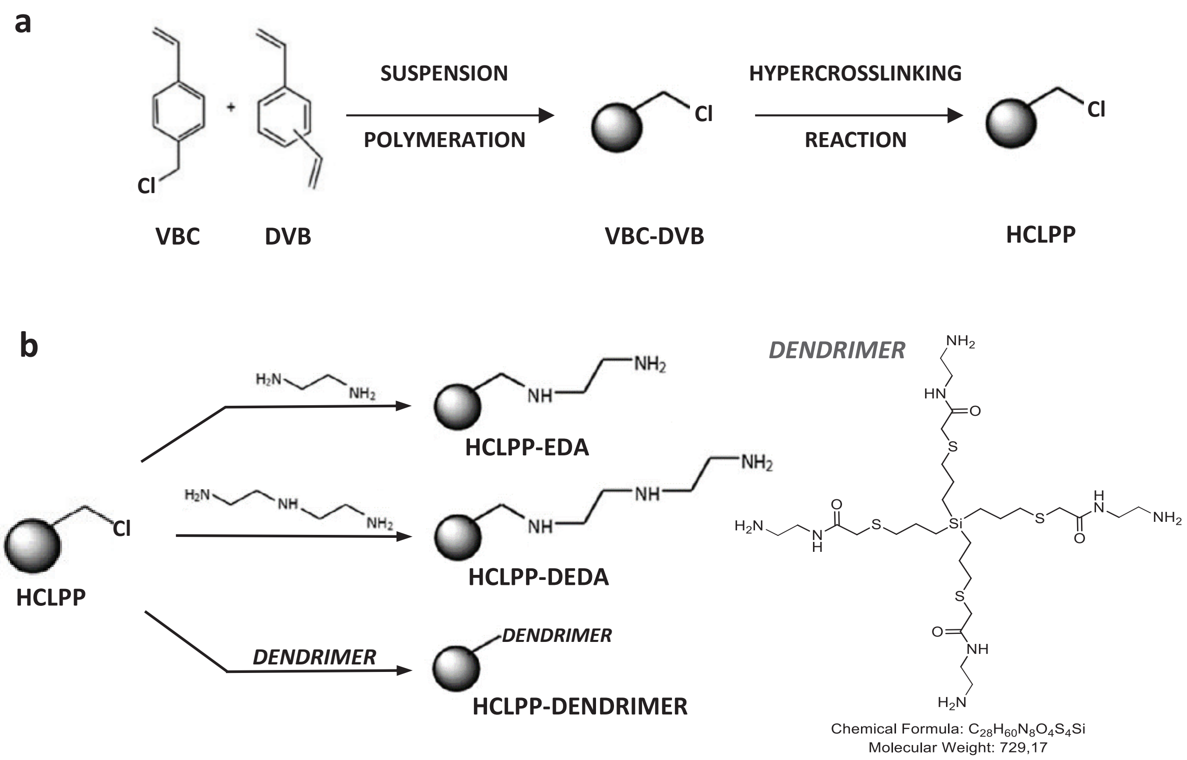

Scheme 1 (a) Synthesis of hyper-crosslinked porous polymer (HCLPP) and (b) the post-polyamine functionalization by ethylenediamine, diethylenetriamine and dendrimer[4].

Gas adsorption measurement

The measurement of the absorption isotherms was based on the volumetric method[3]. The adsorption of pure gas in prepared materials was measured using an apparatus shown in Figure 1.

The thermostated apparatus consists of two chambers with calibrated volumes V_1 and V_2 separated by a valve. Pressure in the apparatus is measured by pressure transducer. In the case of liquid measurement, the apparatus is placed on a magnetic plate that mixes the sample to accelerate the achievement of the absorption equilibrium. The constant temperature of the whole system during the absorption experiment was provided by a heated box.

Before the experiment the weighted amount of sample was placed in the adsorption chamber, V_2. The system was thermostated at experimental temperature 25 °C. The apparatus was evacuated in order to remove dissolved gases and impurities at least 5 h at temperature 80 °C. Then the chamber V_2 is closed, while the volume V_1 is filled with a studied gas at a certain pressure p_1. At the start of measurement, the volumes V_1 and V_2 are connected and the pressure value inside apparatus was monitored by computer. The pressure first dropped immediately to a certain value due to the interconnection of the chambers. Subsequently, the pressure value decreased already more slowly, it corresponds to the adsorption of gas in the sample material. After reaching the equilibrium the pressure p_{eq} is subtracted and use to determination of adsorbed amount of gas in sample. The time needed to achieve equilibrium is about 3 hours.

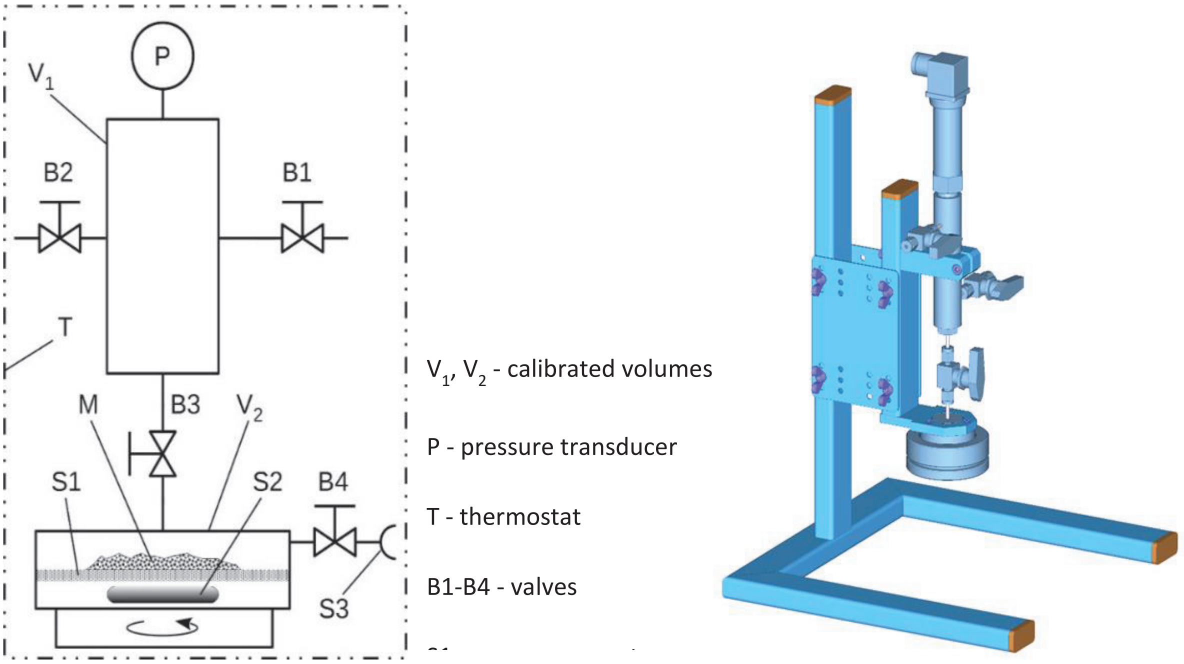

Figure 1. Design and schema of the experimental apparatus for gas adsorption capacity measurement.

The gas amount adsorbed in the material is calculated from the balance as the difference of the initial and the equilibrium amounts:

$$N_{(adsorbed)} = N_{(gas\ initially)} - N_{(rest\ gas\ in\ equilibrium)} \tag{1}$$

$$N_{(adsorbed)} = \frac{p_1V_1 - p_{eq}(V_1 + V_2 - V_x)}{RT} \tag{2}$$

The ideal gas state eq. (3) is used to the moles in gas phase calculation (*N* gas moles number):

$$N = \frac{pV}{RT} \tag{3}$$

The adsorbed amount is related to the material weight *m* to determine the adsorbed phase concentration, *q*:

$$q = \frac{N_{(adsorbed)}}{m} \tag{4}$$

Discussion and result analysis

Characterization

The surface properties of the produced materials were characterized by gas adsorption analysis, see Table I. The results revealed that pristine hyper-crosslinked porous polymer showed the highest Brunauer-Emmett-Teller surface area (S_{BET} = 757 m^2 g^{-1}). It was found that reaction of prepared porous material with polyamine species (amines and amine groups containing dendrimer) decreased the specific surface area and the total volume of pores as well, wherein in the case of modification by dendrimer the decrease was smaller than for amines.

Table I

Texture properties of pure and functionalized porous polymers HCLPP based on VBC

Sample	S_{BET}[a] [m^2g^{-1}]	S_{meso}[b] [$m^2\ g^{-1}$]	V_{tot}[c] [$mm^3_{liq}\ g^{-1}$]	V_{micro}[d] [$mm^3_{liq}\ g^{-1}$]	ρ_{He}[e] [$g^1\ cm^{-3}$]
HCLPP	757	310	408	226	1.15
HCLPP-EDA	283	93	157	97	1.18
HCLPP-DETA	277	132	159	76	1.16
HCLPP-DENDRIMER	616	194	341	218	1.69

[a]S_{BET} specific surface area calculated by the BET method; [b]S_{meso} specific surface area of mesopores (*t*-plot method); [c]V_{tot} specific total volume of pores; [d]V_{micro} specific volume of micropores (*t*-plot method); [e]ρ_{He} skeletal density (Helium pycnometry)

Elemental analysis of prepared polymers was investigated by EDX method and obtained data are given in Table II. It can be seen that after functionalization of porous polymer the nitrogen content in material considerably increased, after modification by amines on value higher than 8 % and in case of dendrimer on lower value about 5 %. At the same time, the chlorine content is lower, indicating a reaction with the chloride units.

These data can indicate that the reaction of the pristine polymer with dendrimer was not so effective as the reaction with amines.

Table II

EDX analysis of pure and functionalized porous polymers HCLPP based on VBC

Sample	*C* [%]	*Cl* [%]	*N* [%]	*S* [%]	*Si* [%]
HCLPP	93.49	0.40	1.66	-	0.05
HCLPP-EDA	82.96	0.07	8.43	-	0.09
HCLPP-DETA	85.09	0.05	8.76	-	0.07
HCLPP-DENDRIMER	90.62	0.29	5.18	0.19	0.20

Gas adsorption

The experimental results for the gas adsorption in the synthesized porous polymer and functionalized variants at temperatures of 25 °C evaluated from adsorption isotherm for pressure 1 bar are presented in Table III.

Table III

Gas adsorption performance of pure and functionalized porous polymers HCLPP based on VBC*

Sample	CO_2 [$mmol\ g^{-1}$]	CH_4 [$mmol\ g^{-1}$]	N_2 [$mmol\ g^{-1}$]	H_2 [$mmol\ g^{-1}$]	O_2 [$mmol\ g^{-1}$]
HCLPP	1.01	0.31	0.090	0.021	0.012
HCLPP-EDA	0.91	0.13	0.033	0.015	0.047
HCLPP-DETA	0.82	0.13	0.029	0.012	0.042
HCLPP-DENDRIMER	1.10	0.24	0.063	0.017	0.089

* Amount of captured gases in porous material at 1 bar.

The polymer modification led in most of cases to the decrease of gas adsorption, except for oxygen. This could be due to a reduced surface area of amine-functionalized forms of polymer. However, the selectivity of the material to the gas separation after animation increased in all cases, only CH_4/H_2 selectivity was lower, see Table IV.

Table IV

Selectivity performance of pure and functionalized porous polymers HCLPP based on VBC*

Sample	CO_2/CH_4 [-]	CO_2/N_2 [-]	CO_2/H_2 [-]	O_2/N_2 [-]	CH_4/H_2 [-]
HCLPP	3.3	11.2	48.1	0.1	14.8
HCLPP-EDA	7.0	27.5	60.6	1.6	8.7
HCLPP-DETA	6.3	28.3	68.3	1.3	10.8
HCLPP-DENDRIMER	4.6	17.5	64.7	1.4	14.1

The adsorption (and desorption) isotherms of CO_2 in all studied materials up to 10 bars are shown in graphs in Figure 2. The original polymer and its dendrimer modified form showed a higher CO_2 capacity compared to the amine variants. However, when the CO_2 capacity is related to the material surface area, the amine modified polymer appears to be the most effective CO_2 adsorbent, see Figure 3.

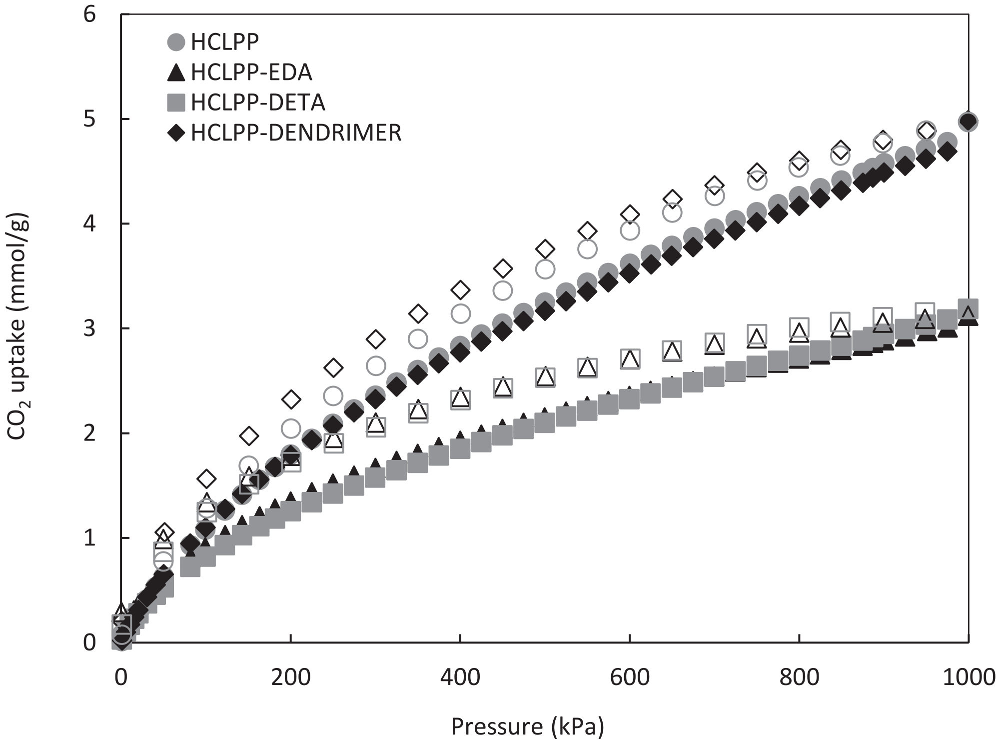

Figure 2. The CO_2 adsorption isotherms in the porous polymer materials at temperature 25 °C, adsorption (full points) and desorption (empty points).

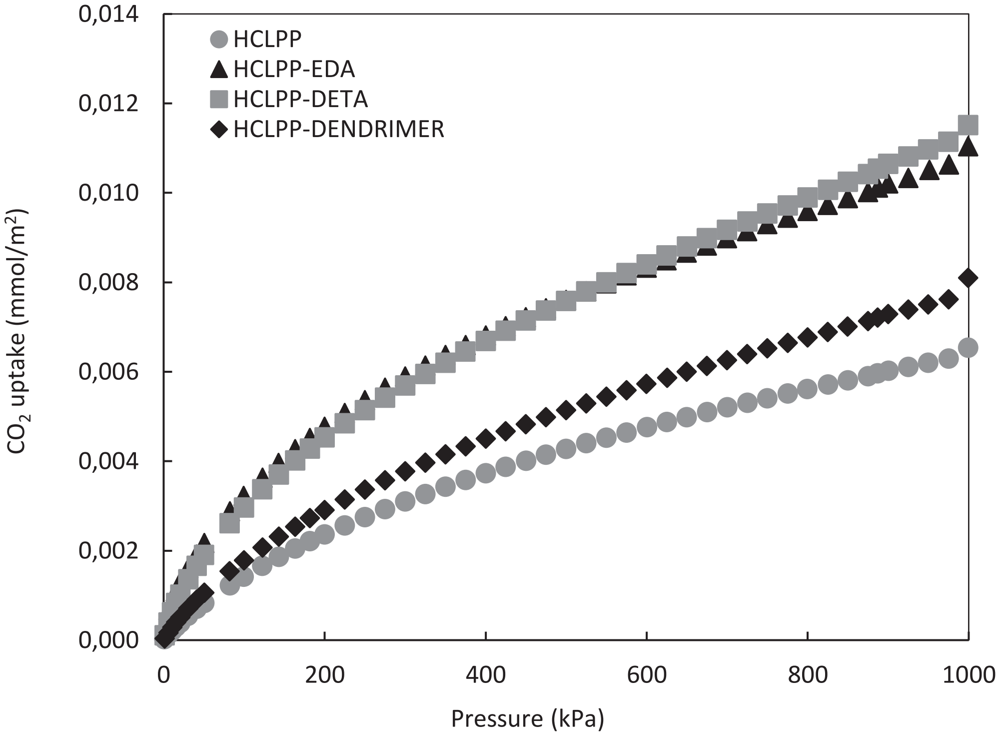

Figure 3. The CO_2 adsorption in the porous polymers at temperature 25 °C related to the specific surface area of material.

Conclusion

New porous polymeric adsorbent with a high apparent surface area showing selective CO_2 adsorption over CH_4 and N_2 and H_2 was prepared by suspension polymerization of vinylbenzyl chloride and divinylbenzene, followed by modification with polyamines and dendrimer containing amino groups resulting in an enhanced CO_2/CH_4, CO_2/N_2 and CO_2/H_2 selectivity. Produced polymer represents a promising organic porous material for CO_2 capture from gas mixtures. We plan to use the developed porous polymer and its amine-functionalized forms as fillers for preparation of mixed matrix membranes with improved CO_2/CH_4 and CO_2/N_2 separation performance[5].

Acknowledgement

This work was supported from the Czech Science Foundation project no. 19-23760J and the ERDF/ESF project "UniQSurf-Centre of Biointerfaces and Hybrid Functional Materials" (no. CZ.02.1.01/0.0/0.0/17_048/0007411).

References

1. Luo YL., Tan BE.: *Porous Materials for Carbon Dioxide Capture Book Series: Green Chemistry and Sustainable Technology.* Springer, New York 2014.
2. Veverka P., Jeřábek K.: React. Funct. Polym. *41*, 21 (1999).
3. Uchytil P., Petrickovic R., Thomas S., Seidel-Morgenstern A: Separ. Pur. Technol. *33*, 273 (2003).
4. Stastna L.C., Krupkova A, Petrickovic R., Mullerova M., Matousek J., Kostejn M., Curinova P, Jandova V., Sabata S., Strasak T.: ACS Sustain. Chem. Eng. *8*, 11692 (2020).
5. Setnickova K., Sima V., Petrychkovych R., Reznickova J., Uchytil P.: Separ. Pur. Technol. *160*, 132 (2016).

ECONOMICS OF CHEMICAL INDUSTRY

THE CURRENT TRENDS IN THE CHEMICAL INDUSTRY OF THE CZECH REPUBLIC – COVID 19 IMPACT

Souček I.[1, 2]

[1] *University of Chemical Technology, Technická 5, 166 28 Prague 6*
[2] *Association of the Chemical Industry of the Czech Republic, Rubeška 393, 190 00 Prague 9*

Abstract

The article comments the main aspects of the development of the chemical industry in the EU and the Czech Republic in 2020 identifying potential directions of development of the chemical industry for mid-term future, recognizing the outcomes from actions related to European Green Deal: Decarbonization od industry and Hydrogen strategy.

Impacts of the COVID-19 pandemics is commented in light of industrial development in EU.

Introduction

The development of the chemical industry is significantly dependent on the overall development of the economy, resp. downstream demand and consumer consumption. Europe is the second largest chemical region in the world (total sales: 543 bn EUR) followed by USA, Japan, South Korea and India. Europe has the largest chemical trade surplus in the world (most European countries, incl. the Czech Republic are export oriented). The European chemical industry is of major importance for economic development and wealth and is a key pillar for sustainable society providing employment to 1,1 million people. The key sectors in EU are speciality chemicals, rubber and plastic production and petrochemicals. The biggest users of European chemicals are rubber and plastics processors, construction, consumer goods industries and automotive.

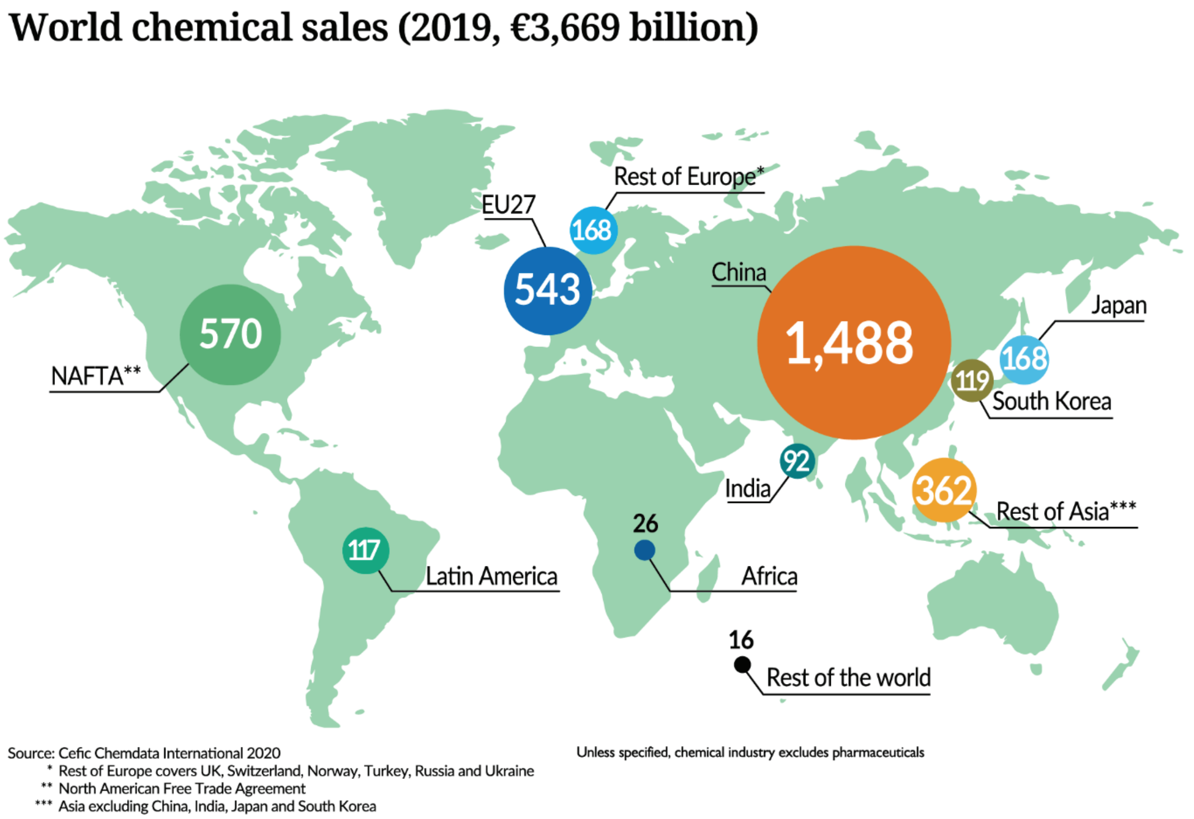

World chemical sales (2019, €3,669 billion)

Source: Cefic Chemdata International 2020

* Rest of Europe covers UK, Switzerland, Norway, Turkey, Russia and Ukraine

** North American Free Trade Agreement

*** Asia excluding China, India, Japan and South Korea

Unless specified, chemical industry excludes pharmaceuticals

Figure 1. Overview of World Chemical Industry (*Source: Cefic – Facts and Figures 2021)*

Whole industry, incl. chemical industry as one of the key industrial pillar, have been impacted by pandemy COVID-19.

In 2020, Czech chemistry recorded a drop in sales, larger than in the whole of Europe, due to the COVID-19 pandemics. The overall pandemic impact is associated with the following effects coming from a new aim for greening the Planet:

- The expected recovery will undoubtedly be influenced by the promotion of "sustainable development" in relation to European Green Deal (further EGD) and following Chemical Strategy for Sustainability.
- Ongoing pandemics had impacts on demand developments and at the same time bringing by governments compensatory effects.
- EGD and further regulatory tightening, while considering the protection of the European market with a "fair" restriction on imports
- EGD and impacts of energy decarbonization on industry, support of alternative energies incl. hydrogen
- Sustainability strategies of chemical substances with an impact on further reduction of disposable plastics, reduction of energy intensity, replacement of SVHC, etc.…

While the overall decline of the EU chemical industry recorded a decline of "only" 1.9%, the Czech chemical industry finally declined by cca 10 %.

Current trends for mid-term development and its conditions

Current trends of industry development and its recovery after pandemics of COVID-19 is connected with directions defined by European Green Deal package. It brings new requirements to the industry either deriving directly from EU legislation or its transposition to the national legislation.

The main new Czech legislative acts impacting chemical industry:

- EU ETS - new programming period: tightening of benchmarks, reduction of free allowances, compensation of indirect costs for 2020 (Government decision has been published in May 2021), but reduction of the sector for compensation of indirect costs in the following years.
- Waste legislation with effect from 1 January 2021. Before all implementing decrees are approved, companies will be able to follow the methodological instructions of the Ministry of the Environment. Higher pressure on circularity: an opportunity for material recycling, resp. chemical recycling.
- Reduction of TA CR resources (in anticipation of massive use of EU funds)
- Employment support, compensatory instruments due to the pandemic
- Subsidy programs (Recovery Fund, Fair Transformation Fund, Modernization Fund) in the context of economic recovery after the pandemic and EGD
- Civil Construction law
- Water law

The industry should react on that requirements and re-direct its development. Assumption of strategic technological direction of the chemical industry:

- Technology for CO_2 processing into chemical products, incl. hydrocarbons
- Hydrogen technologies
- Technology for the production of materials and equipment for energy storage
- Recycling technology for recovering material from waste, not (only) energy
- Technology for the production of materials effectively replacing SVHC
- Technology of production of more efficient pharmaceuticals

However, all projects identified as strategic technological direction are linked to the economic decision of the owners, further development of legislative requirements for the availability of know-how for application on an industrial scale and in some cases to incentive tools / public support for investment in these directions by the EU and the Czech Republic.

One of the prioritised directions is to build Hydrogen economy in EU. The future of the development of hydrogen consumption in the Czech Republic. But consumption growth for current Czech producers is not yet indicated, but a gradual conversion of production (green hydrogen) for large producers can be expected on the basis of possible massive support from industrial decarbonisation programs while "irreplaceable" existing technologies with regard to their integration into existing technologies (CCU implementation) should remain on place. For medium - sized sources, it is possible to assume support for the production of hydrogen from biomethane (steam reforming) or with electricity from renewable sources in electrolysers.

Another prioritised direction is decarbonisation, e.g. reduction or elimination of emission of CO_2. The main driver for this goal is the growing price of CO_2 allowances. The CO_2 allowances price development during the last 12 months is shown on the figure 2.

Figure 2. Development of the CO2 Allowances price (*Source: Energy Hub)*

When speaking about decarbonisation the following order of steps could be considered:

1. Decarbonisation of energy
2. Decarbonisation of energy-intensive industries
3. Decarbonisation of other consumers
4. Electrification (see Sky – Shell scenario)

The conditions of implementation of the 4th step are especially:
- Electricity availability (see Sky - Shell scenario)
- Green electricity availability
- Availability and efficiency of CCSU technologies

Required actions to achieve in the Czech Republic a decarbonised 2050 sector - unlike several other sectors, for the chemical industry are challenging but future decisions will be influenced by several aspects requiring further clarification and definition:
- The projected availability of (green) electricity in the country is not clear.
- The prospects for fossil-based sectors (coal, natural gas, oil) are not clear
- The perspective of the polymer industry is not clear (campaigns against the use of single-use plastics, elimination of microplastics...)
- No clear perspective on circular technologies, e.g. chemical recycling

On the other hand the legislative development will significantly influence the sustainability and feasibility of any investment and operational solution. The key legislation upon which CO_2 emission will be "controlled" during the current decade are EU ETS and CBAM. EU ETS and CBAM can be considered as two completely different instruments that can be used in parallel. The EU ETS is an established CO_2 charging system in EU countries for large industrial and energy emitters. This system has clearly defined rules and gives participants a degree of certainty in terms of future emissions expenditure and a predetermined allocation of free allowances. The last phase of the EU ETS was planned for the period 2020 - 2030 and this continuity, including free allowances, should be maintained. The CBAM proposal, on the other hand, is entirely new and is based de facto on taxing products imported from countries without a rigorous system in place to reduce greenhouse gas emissions. However, it is unclear at this point in time how the WTO and the countries targeted by the mechanism will approach this mechanism. There is a risk of retaliatory trade measures. The CBAM mechanism should apply to the energy sector, but also to the production of cement, steel, aluminium, oil refineries, fertilisers, paper, glass and, of course, chemicals. The another aspect of the current legislative development is the chemicals regulation (REACH and CLP) and the waste legislation which will undoubtedly have an impact on future development of the chemical industry. Chemical recycling has also received significant impetus from others and has now become the standard agenda of the European Parliament and the European Commission. In addition to chemical and waste legislation, there is /in the Czech Republic) also the new construction and water law in place. In the case of emission allowances, indirect costs can be compensated, even if the effects of the period have affected costs. In waste legislation, chemical industry sees significant scope to assert ourselves in chemical recycling beyond other opportunities.

The European Green Deal will offer subsidy programmes, whether the Recovery Fund, the Just Transition Fund or the Modernisation Fund. The last issue is also the issue of the decline of coal. The Union considers that it is prepared to offer the State the possibility of adverting negative impacts by wanting to come up with the possibility of chemical processing of coal,

Impact of Pandemics COVID-19

The development of the European and Czech chemical industries last year was influenced by the coronavirus pandemic. It is worth noting that in end of March 2020, thanks to the cooperation of the Ministry of Industry and Trade, the Ministry of Health, the Union of Chemical Industry of the Czech Republic and its subsidiary Regartis, the society managed to secure a legislative framework that allowed 33 manufacturers to ensure the production of disinfection.

But disinfection production and supportive pharmaceuticals was the only positive trend during the first wave of pandemic (see the Figure 3 – development of the chemical industry in the world regions). It is well documented in the development of the pharmaceutical sector during 2020 compared to the other industrial sectors. (see Figure 4). But the picture in the Czech Republic was significantly different. True is that the Automotive industry was impact most of all but the Czech chemical industry sales declined more than 10 % compared to “only” 1,9 % decline in EU chemical industry.

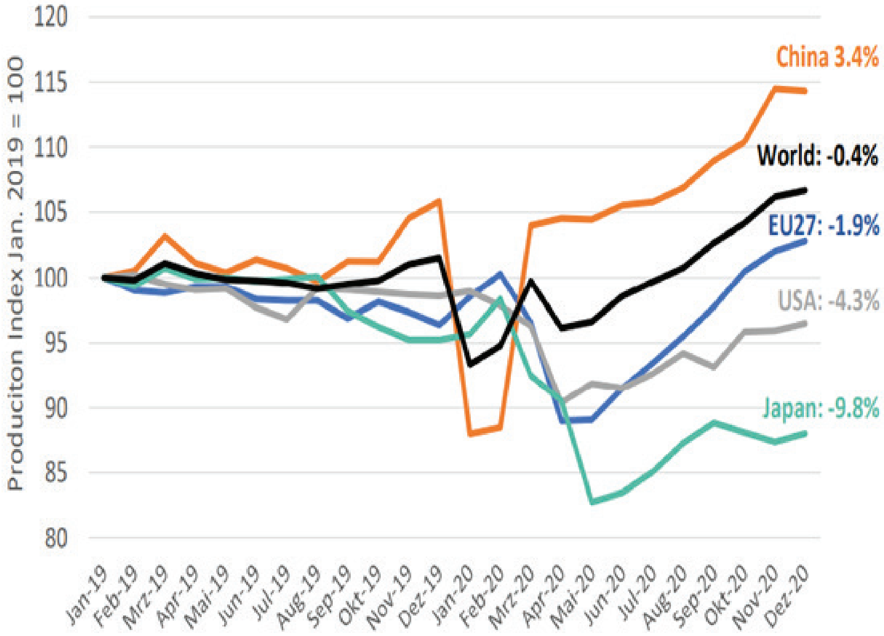

Figure 3. Chemical Industry Production (Growth Index 2020 vs. 2019) (*Source: Eurostat and Cefic Analysis-24th February 2021)*

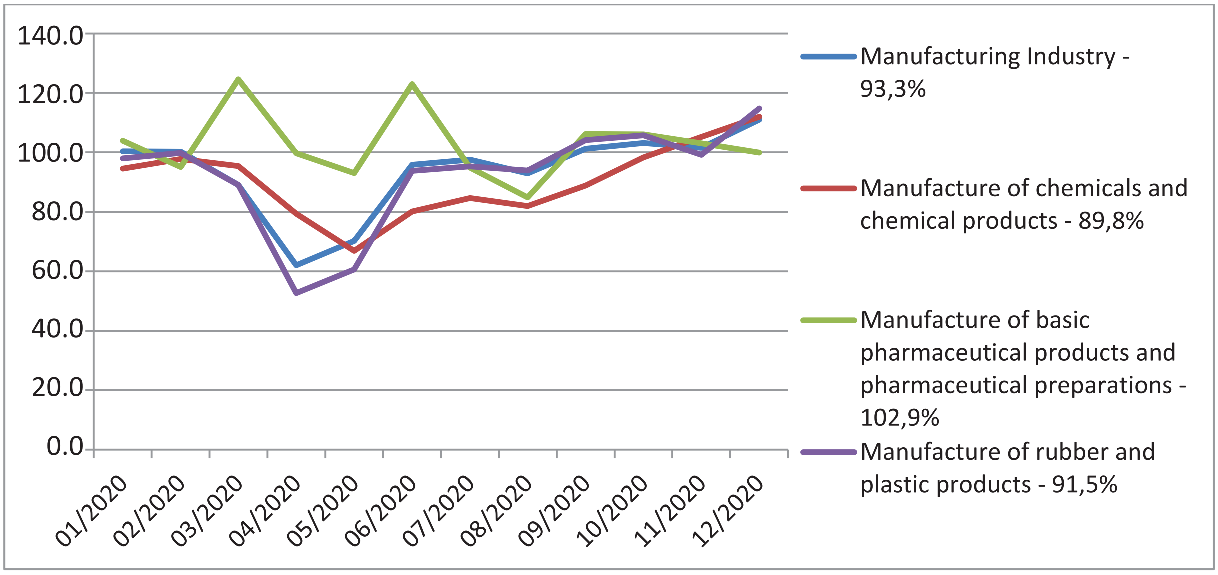

Figure 4. Czech Chemical Industry Production vs. Manufacturing industry - Growth Index 2020 vs. 2019 (*Source: Czech Statistics Office*)

The restart of the chemical industry after the first wave of the pandemics COVID-19 was probably to early and did not count with the second wave. On the Figure 5, there is well documented the August became a critical for the chemical industry due to the very high stocks and the industry had to be again slowing-down. The capacity use compared to the previous years is shown on the figure 6.

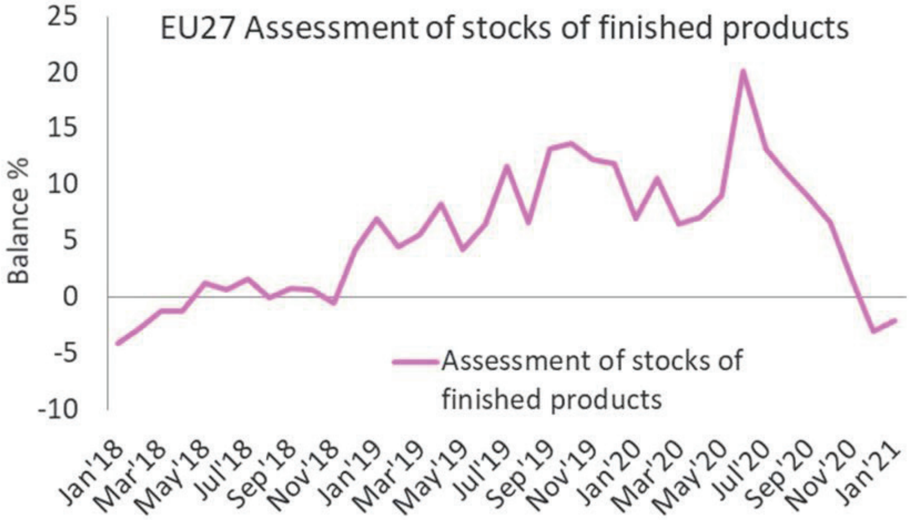

Figure 5. Chemical feedstock development in 2018-2020 (Source: Eurostat and Cefic Analysis-24th *February 2021)*

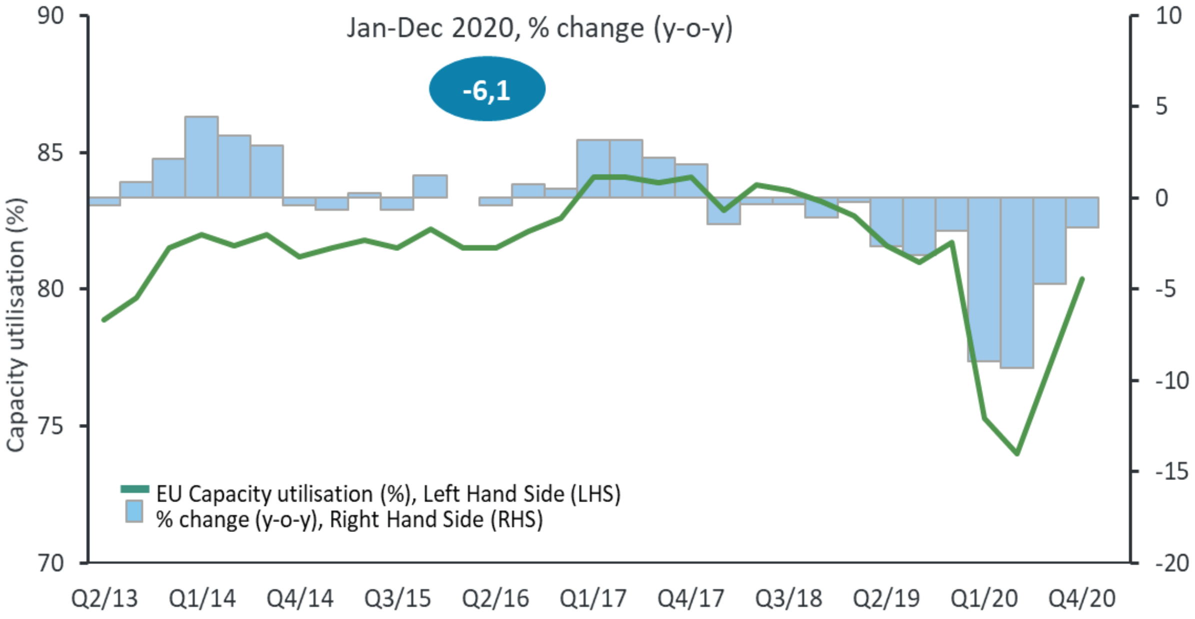

Figure 6. EU Chemical Industry Capacity Utilisation 2013 – 2020 (*Source: Eurostat and Cefic Analysis-24th February 2021)*

Overall impact of the pandemics COVID-19 on the different sectors is demonstrated on the Figure 7. Apart of the positive grow of the Pharmaceutical industry, also the overall impact on the EU chemical industry was minor compared to, for example, to Automotive industry.

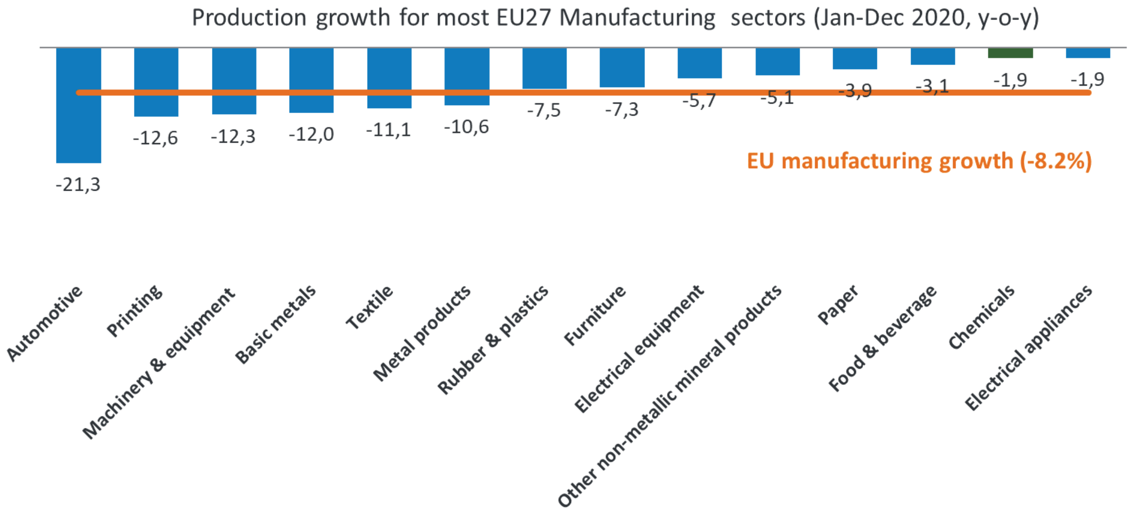

Figure 7. EU Selected Industries Growth Index in 2020 (*Source: Eurostat and Cefic Analysis-24th February 2021)*

Conclusions

The opinion of the Association of the Chemical Industry of the Czech Republic, published last year, appealed several times to separate the recovery of the economy after the COVID-19 crisis from the "green recovery". This is led to us by the fact that currently most "green investments" are operationally economically "demanding" (meaning: often loss-making if no operating subsidy is provided). Economic recovery needs to be supported in order to create sufficient own resources for further (and green) investment. The positive expectation of the industry recovery is demonstrated on the Figure 8.

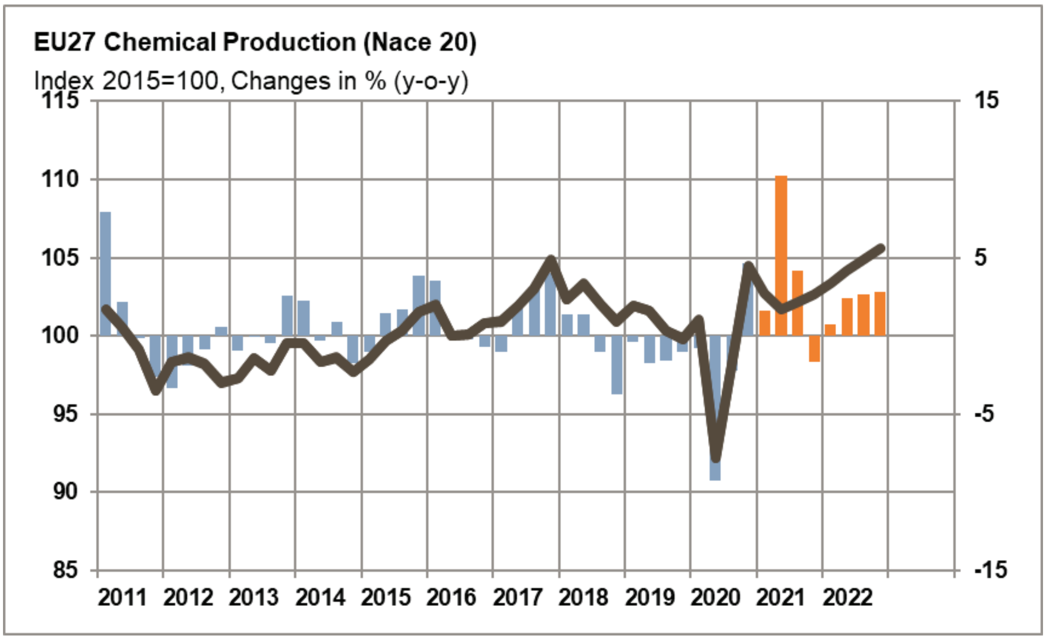

Figure 8. Forecast of EU Chemical Industry Growth in 2021-2022 (*Source: Eurostat and Cefic Analysis-24th February 2021)*

However, the EU envisages using the current crisis to carry out a green recovery. It offers huge investment resources for this. These funds should be used mainly for environmental investments, and I admit that it would be a shame not to use them in our sector as well. However, I think we should approach these resources with caution with the following priorities:

- Use funds for prepared and already approved ecological investments focused mainly on air protection (reduction of emissions), energy and water savings.
- Consider using funds to decarbonise industry, again by saving energy, switching to less emission fuels (however, it is necessary to take into account the aspect of the future economy of operation), the introduction of renewable energy production (here too the future economy of operation is key).
- Consider the use of funds for technologies aimed at the circular economy: in particular the chemical recycling of waste (specifically plastic waste), the use of CO2 for the synthesis of hydrocarbons (this will often involve the need for investment to ensure hydrogen production).
- Ensure the completion of the development of innovative technologies for the production of hydrogen with the assumption of their economic efficiency,
- And last but not least, it is a range of investments for energy storage. Here it is absolutely necessary to assess the economics of operation at current prices of electricity and support tools, respectively. current support for the development of solar and wind energy, which cannot do without accumulation for the stability of the distribution network. However, the question is whether this is an opportunity for our industry, although "Power-to-X" technologies can be considered as chemical technologies…

Key words

Chemical Industry, Green Deal, Pandemics COVID-19

References

1. Association of the Chemical Industry of the Czech Republic: *Position to European Green Deal*, www.schp.cz (2020).
2. Cefic: https://cefic.org/a-pillar-of-the-european-economy/facts-and-figures-of-the-european-chemical-industry/ (2021).
3. Cefic Analysis, February 24, 2021 (2021).
4. Czech Statistics Office: *Sales index 2020 of Industrial Production,* www.czso.cz/csu/czso/pru_cr (2021)
5. Energy Hub: *Vývoj cen povolenek EU ETS 3.6.2020-3.6.2021*, www.schp.cz/Trendy/Emise, 3.6.2021 (2021).

6. European Commission: *Chemical Strategy for sustainability towards a Toxic-Free Environment*, COM (2020) 667 (2020).
7. European Green Deal, *COM (2019) 640 of 11.12.2019* (2019).
8. Eurostat*, Industry Statistics 2020* (2021).
9. IEA: *The future of Hydrogen*, Report prepared for G20, Japan (2019)
10. Jandusova M.: *Dopad pandemie na chemický průmysl není tak katastrofální, jako na jiná odvětví*, Průmyslová ekologie, 11.2.2021 – on-line (2021)
11. SCHP ČR: *210311 Stanovisko EU ETS_CBAM*, www.schp.cz/Trendy/Stanoviska, 11.3.2021 (2021).
12. Souček I.: *Výhled českého chemického průmyslu v roce 2021*, conference "Chemical legislation 2021", on-line, Regartis (2021)

TECHNO-ECONOMIC OPTIMIZATION OF STEAM CRACKER'S STEAM NETWORK

Hanus K.[1], Variny M.[2]

[1]*SLOVNAFT, a.s., Vlčie hrdlo 1, 824 12 Bratislava, Slovak Republic*
[2]*Department of Chemical and Biochemical Engineering, Faculty of Chemical and Food Technology, Slovak University of Technology in Bratislava, Radlinského 9, 812 37 Bratislava, Slovak Republic*
miroslav.variny@stuba.sk

Abstract

Challenging market environment, tightening customers' requirements as well as commitment to reduce the environmental impact make the energy efficiency a very actual topic. In the petrochemical industry, energy costs are the second largest expenditure right after the feedstock. Examined Steam Cracker´s (SC) steam network in SLOVNAFT refinery operates on six steam pressure levels and allows operating as a standalone network or import, alternatively export, steam from/to outer network. Outer steam network is fed by steam from Combined Heat and Power Unit (CHP) as well as from secondary steam sources located in the refinery. This layout complexity and operation flexibility offers the possibility for overall techno-economic optimization reflecting both technical limitations and actual economic situation. This study provides a brief comparison of its operation before and after debottlenecking (implementation of regulation valve) and shows the importance of proper regulation possibility. Annual savings resulting from debottlenecking reach up to 1 million € and the simple payback period is less than 1 year. Propriate key performance indicators (KPI) were also determined to assess the overall steam network performance as to maximize energy efficiency and savings.

Introduction

Efficient, safe, and economic operation of industrial steam and power systems belongs to key issues when speaking about industrial energy efficiency[1,2]. Especially in refineries[3], petrochemical plants[4,5], and fertilizer production units[6] such systems are deeply process-integrated, as the substantial amounts of steam produced on-site are usually consumed in general purpose steam turbines driving key process equipment. Steam on three to five main pressure levels is commonly produced and utilized in such plants[7,8], where individual levels are fed from extractions from steam drives or from their backpressure, being complemented by let-down stations serving as regulation buffer. Such deeply intertwined plants can be viewed, modeled, and optimized as polygeneration units[9], where only a coupled energetic, economic, and environmental approach to their operation optimization ensures a sustainable development[10,11].

More specifically, steam crackers (or ethylene plants) usually produce very high pressure (over 10 MPa) steam both in convection sections of cracking furnaces and in a separate steam boiler[12]. Produced steam is used in extraction-condensing turbines driving key process compressors, while the extracted steam is used in process and in smaller steam drives, resulting in a system of up to five main pressure levels[13]. As such plants are often integrated in a larger industrial cluster, steam export to and import from adjacent production units is possible, offering significant space for cost optimization and for utilization of possible synergies[14,15]. Moreover, such interconnections increase the system flexibility, offering extra space to cope with variable seasonal heat demand. Their exploitation is often the key point of various optimization studies that are published nowadays, stressing the need for unified and efficient steam network management within the whole industrial cluster[16-18]. Bearing this in mind a study on operational costs reduction of steam system in a steam cracker integrated in a refinery-petrochemical cluster SLOVNAFT was conducted with the aim of simultaneous cost and carbon footprint reduction and of energy efficiency increase. This study follows our previous activities related to optimization of steam networks and cutting down operational expenses of refinery units[19-21]. At the same time, it intends to highlight the contribution of industrial innovation and optimization to industrial energy efficiency increase and greenhouse gases emissions reduction in the Middle European area[22,23].

Study objectives

The aims of this contribution are in particular:

- To analyze existing SC's steam network with focus on technical limitations of selected KPI.
- To assemble benefit calculation methodology after implementation of new let-down valve.
- To utilize obtained data and methodology as a basis for a new real-time optimizer in order to secure optimal regulation and economic results.

Description of steam crackers´ steam system

The Steam Cracker (SC) in SLOVNAFT refinery has a complex steam system, that can act as a standalone system or, if needed, is able to import or export steam from/to outer steam network. The steam network operates on six different pressure levels with typical parameters:

- SS steam: 11.0 MPa (g), 520 °C
- HS steam: 3.5 MPa (g), 350 °C
- MS steam: 1.2 MPa (g), 250 °C
- LS steam: 0.4 MPa (g), 170 °C
- PS steam: 0.25 MPa (g), 138 °C
- DS steam: 0.7 MPa, 190 °C

SS steam is produced internally in cracking furnaces and in an auxiliary steam boiler. The shares used to be almost equal in the past, as shown in Fig. 1. However, the share of process steam increased in the recent years, both due to increased SC feedstock processing (2017 – 2019) and due to energy saving measures described in this contribution (2020).

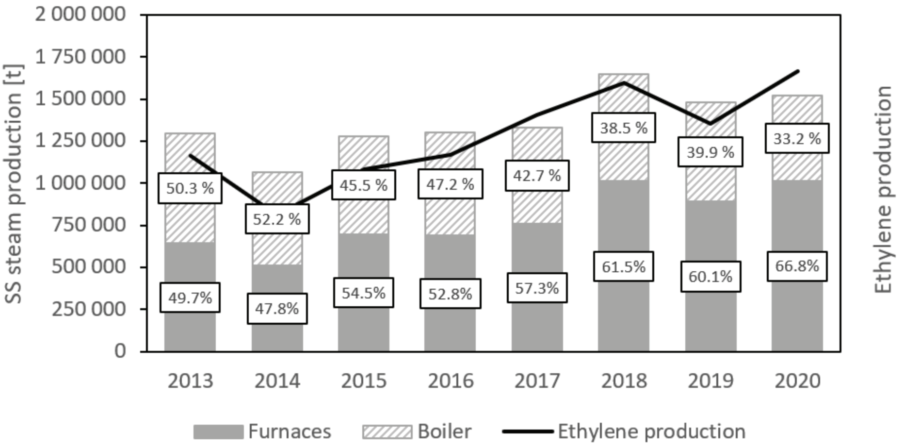

Figure 1. Annual SS steam production and ethylene production from 2013 to 2020 (Ethylene production is intentionally omitted since it belongs to business sensitive data).

The SS steam is consumed in combined extraction-condensing steam drives driving process gas compressors. Excess steam is reduced on let-down station to HS steam. Similarly, HS and MS steam is used to drive various steam drives and the rest is reduced to lower pressure level steam. The LS steam is used mostly as a heating medium in fractionators, boiler feed water (BFW) preparation or steam tracing. Moreover, HS, MS and LS steam export or import are possible; however, only HS and LS steam import is usually utilized. PS steam is produced by LS steam reduction and is utilized as heating medium in few heat exchangers and vessels. The DS steam is used directly in the process as a dilution steam added directly into the feedstock.

Fig. 2 shows the consumption of SS steam. Steam-drives consumption varies according to SC feed rate, naturally. On the other hand, there was almost constant SS steam reduction share in the past years.

Constant share of steam reduction is the first indication of non-functional regulation element. And really, the let-down valve “A” lost its regulation ability due erosion under extreme conditions of SS steam. The valve opening was rather constant at 14 % before turnaround in 2019 and yet the steam inlet flow varied a lot, as shown in Fig. 3.

External energy audit performed in 2013 recommended installation of parallel let-down valve with smaller capacity and independent regulation to ensure smooth and functional regulation of SS steam network. This was in line with best practice, recommending reducing the amount of steam flowing through let-down stations to minimum. Preliminary analysis found two possible benefits:

- Direct fuel (natural gas) saving due more efficient HS steam production by extraction instead of steam reduction. Thus, improved energy efficiency of SC and whole SLOVNAFT is expected. Moreover, less CO_2 emissions will be produced.
- Enabled HS and LS steam import due less steam being reduced internally. Imported steam is usually produced from cheaper fuel (mixed petroleum residue, MPR, that is usually in excess). Additional extraction electricity generation would be possible thanks to increased steam supply from CHP unit. These effects contribute to better economic results. On the other hand, there is negative CO_2 effect

accompanied with MPR fuel utilization since the CO_2 specific production factor of MPR is higher than of natural gas. Increased steam supply from CHP unit is thus in contrary with the shift towards cleaner fuels[24,25] proposed to lower the industrial carbon footprint but is justified from economic point of view.

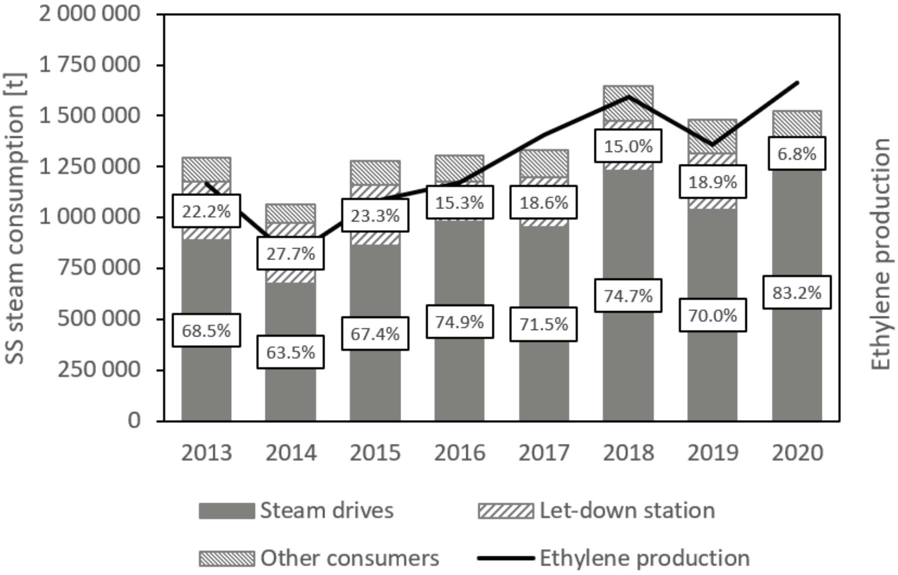

Figure 2. Annual SS steam consumption and ethylene production from 2013 to 2020 (Ethylene production is intentionally omitted, since it was evaluated as business sensitive information).

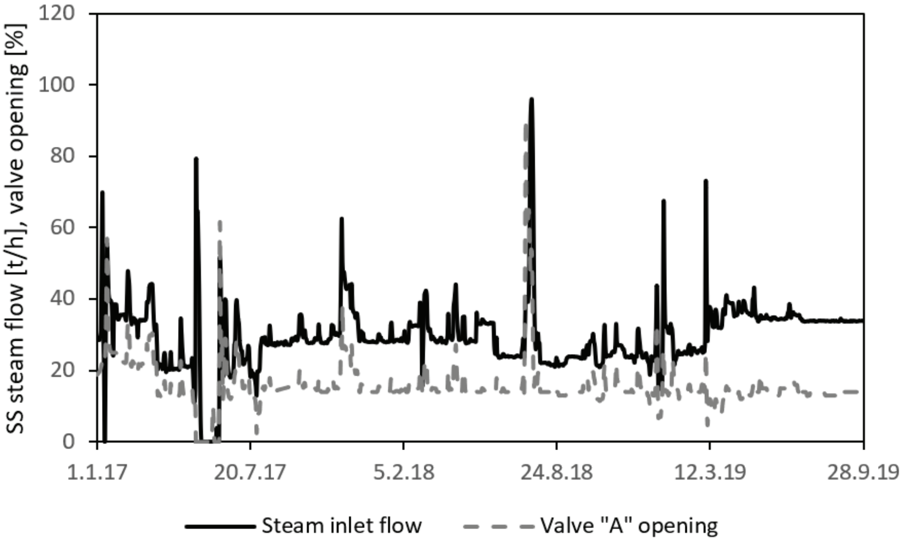

Figure 3. Let-down valve “A” opening and steam inlet flow before turnaround 2019.

New parallel let-down valve “B” was installed in turnaround 2019. Lower steam throughput allows two-zone regulation. Valve “B” is utilized at lower steam inlet flows, usually below 30 t/h. Above this threshold, “A” valve takes over the control.

The impact of new “B” valve installation can be observed in Fig. 2 showing significant SS steam reduction decrease in 2020 as well as in Fig. 4, showing the opening of valves “A” and “B” after turnaround 2019. “B” valve is used as a replacement of “A” valve, except non-standard operational states (unit shut-down/start-up, etc.).

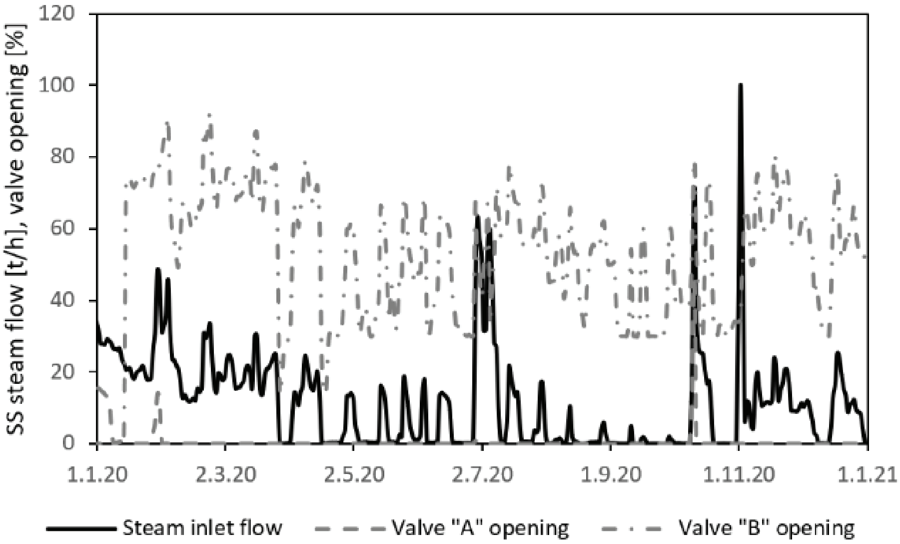

Figure 4. Let-down valves' opening and SS steam reduction after turnaround 2019.

Real-time optimizer development

Functional regulation element suddenly offers higher flexibility in steam operation. Steam import due decreased steam reduction and the resulting benefits were possible; however, there was no decision support tool to say what to do in order to get optimal economic performance.

The methodology is based on savings calculation compared to baseline. The baseline determined based on filtered field data from 2017 to 2019 represents typical operation before turnaround 2019. The aim was to select valid data corresponding to a steady operational state without ongoing furnace decoking, when the SS steam reduction is higher. Few issues had to be solved in order to get a proper data set, e.g. steam inlet flow calculation based on valve opening (at low steam flows), missing data refill, etc. Benefit calculation methodology compilation required the knowledge of used hardware, therefore steam drives' performance curves and lots of technical documentation was needed. Internal and external energy pricing list was inevitable element as well.

Subsequently, an in-house built real-time optimizing tool was developed using the benefit calculation methodology. Limits were added to KPI occurring in the calculation to evaluate gaps. The tool compares the actual benefit with the highest possible benefit in every single moment and calculates the optimal steam balance with respect to set limits of KPI.

Fig. 5 shows the model decision tree. There are two directions that the model can decide for. Either the steam import or steam extraction are preferred. The decision depends on the benefit belonging to increased steam import or extraction. If the decision is to maximize steam extraction, four different operational states (State 1 to 4) can occur, depending on the actual conditions. Gap on steam let-down station (the actual steam flow vs. the maximal steam flow) is compared to gaps on steam extraction, import and export. Four states are defined also for steam import maximization (State 5 to 8). In that case, gap on steam let-down station is the key parameter.

The objective is to achieve optimal steam balance with the highest benefit. Each state defines targets for SS steam reduction and extraction as well as HS and LS steam import. The output of the real-time optimizer is the definition of KPI values. The rest is up to the energy controllers and operators.

Results

Implementation and fine-tuning phase were finished in April 2020. Since the very first year of evaluation, the 12-month cumulative benefit exceeded 1 million Euro. Exact numbers are not shown here, since they are subject to company data protection. The average natural gas savings since May 2020 reached 8.04 GJ/h and additional 25.02 GJ/h of natural gas is replaced by MPR utilization at TPP on average. Moreover, 0.92 MW of additional electricity was generated on average. The resulting payback period is approx. 3 months. Fig. 6 shows variable monthly benefit distribution, that demonstrates the continuing active steam network management. Moreover, involvement of operators results in the overall potential utilization close to 100 % in most time periods whereby the importance of human assets in overcoming barriers to industrial energy efficiency is documented[26,27].

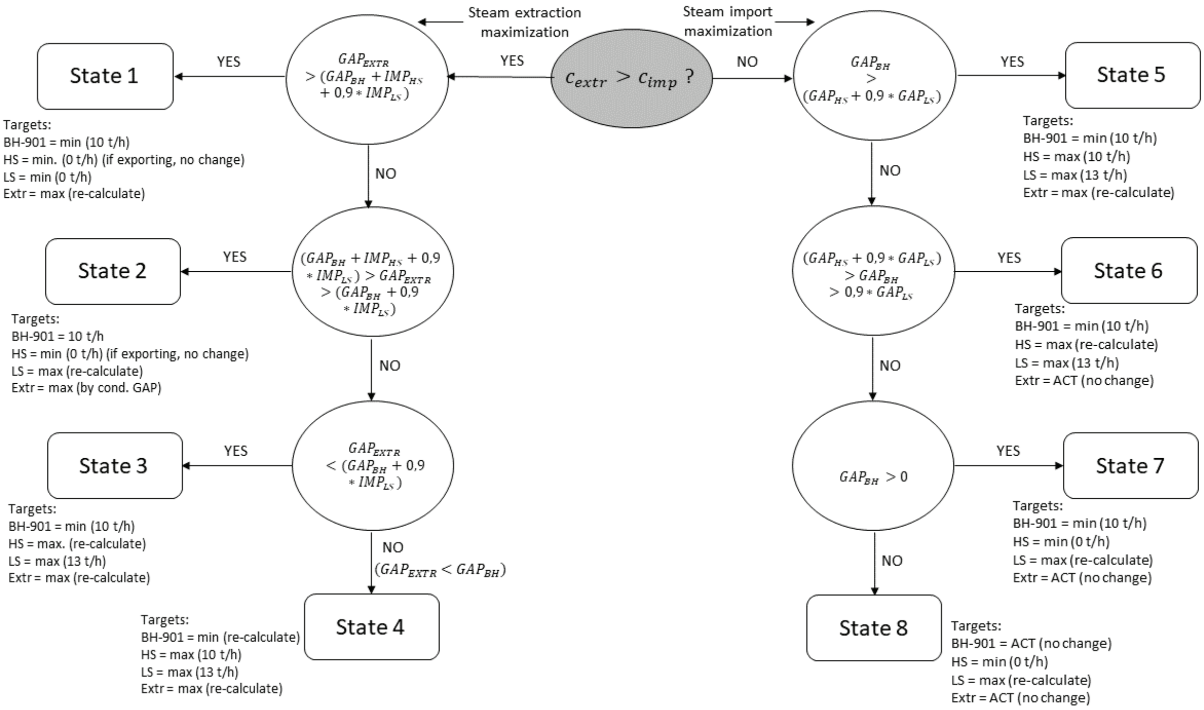

Figure 5. Real-time optimizer model decision tree.

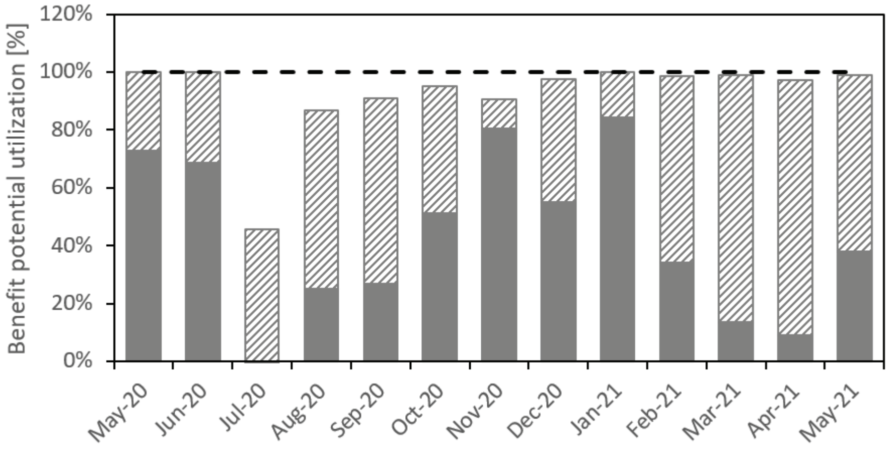

Figure 6. Monthly benefit utilization and composition.

The presented real time optimizing tool found its application in everyday practice. Its decisions help the operators to react on changing operational conditions and market environment.

The benefit calculation benefit includes CO_2 effect, whose importance is rapidly increasing in the recent period. The interesting fact is, that steam network optimization and increased steam import to SC are accompanied with CO_2 emissions production increase. Monthly balance depends on the ratio of steam import and steam extraction, but a net increase by 0.26 % of SC CO_2 emission production is observed on average. There is a positive economic result related to optimization, but on the other hand, the negative environmental impact in contrary to SLOVNAFT's long-term strategy of CO_2 emissions reduction. Sharply increasing carbon price and therefore increasing charges might outweigh the benefits from MPR utilization. It is likely that the model decisions will change under the influence of carbon prices.

Conclusions

The main goal of this contribution was to perform detailed analysis of existing SC's steam network to develop benefit calculation methodology and to set targets for subsequent optimization using in-house built real-time optimizer. The analysis confirmed lost regulation ability of SS steam let-down station and therefore of the whole steam network. Recovered regulation ability after implementation of 2013's energy audit proposal, installation of parallel let-down valve, has created a need for optimizing tool to maximize economic related to this project.

The analysis was also helpful to set targets necessary for correct setting of the optimizer. Let-down valve installation and subsequent steam network optimization have yielded interesting economic benefits resulting in a simple payback period in the magnitude of months. The KPI are monitored on a daily basis to ensure optimal performance.

During the project evaluation, an interesting fact was revealed. There is a benefit related to substitution of natural gas by MPR; however, it is coupled with increased overall CO_2 emission production. That is the opposite to SLOVNAFT's long-term strategy of carbon footprint reduction. Since the business driving force is the economy, changes in steam network regulation due to environmental issues are not expected; however, sharply increasing carbon prices may have significant impact soon.

Acknowledgement

This research was supported by the Slovak Research and Development Agency under the contract Nr. APVV-18-0134.

References

1. Seiler D., Donovan D., O'Donnell D. E.: J. Cleaner Prod. *231*, 1307 (2019).
2. Therkelsen P., McKane A.: Energy Policy *57*, 318 (2013).
3. Svensson E., Morandin A., Harvey S., Papadokonstantakis S.: Energies *13*, 958 (2020).
4. Ahmadi G., Toghraie D., Akbari O. A.: Energy *159*, 937 (2018).
5. Morandin M., Hackl R., Harvey S.: Energy *65*, 209 (2014).
6. Wenzel S., Misz Y.-N., Rahimi-Adli K., Beisheim B., Gesthuisen R., Engell S.: Optim. Eng. *20*, 969 (2019).
7. Bungener S. L., Van Eetvelde G., Maréchal F.: Front. Energy Res. *4*, 1 (2016).
8. Douglas T., Big-Alabo A.: Energy *164*, 881 (2018).
9. Ng K. S., Hernandez E. M.: Chem. Eng. Res. Des. *106*, 1 (2016).
10. Rong A., Lahdelma R.: Renewable Sustainable Energy Rev. *53*, 363 (2016).
11. Ifaei P., Safder U., Yoo Ch. K.: Energy Convers. Manage. *197*, 111851 (2019).
12. Li Z., Zhao L., Du W., Quian F.: Chin. J. Chem. Eng. *21*, 520 (2013).
13. Zhao L., Zhong W., Du W.: Processes *7*, 744 (2019).
14. Li J., Xiao X., Boukouvala F., Floudas Ch. A., Zhao B., Du G., Su X., Liu H.: AIChE J. *62*, 3020 (2016).
15. Ahmadi G., Toghraie D., Akbari O.: Renewable Sustainable Energy Rev. *99*, 234 (2019).
16. Bungener S., Hackl R., Van Eetvelde G., Harvey S., Marechal F.: Energy *93*, 220 (2015).
17. Hassiba R. J., Linke P.: Appl. Therm. Eng. *127*, 81 (2017).
18. Ramanaiah V., Khanam S.: Chem. Eng. Res. Des. *133*, 142 (2018).
19. Furda P., Variny M., Labovská Z., Cibulka T.: Processes *8*, 1495 (2020).
20. Variny M., Blahušiak M., Mierka O., Godó Š., Margetíny T.: Energy Effic. *12*, 1771 (2019).
21. Hanus K., Variny M., Illés P.: Processes *8*, 622 (2020).
22. Baláž V., Nežinský E., Jeck T., Filčák R.: Sustainability *12*, 2611 (2020).
23. Martins F., Felgueiras C., Smitkova M., Caetano N.: Energies *12*, 964 (2019).
24. Rehfeldt M., Fleiter T., Worrell E.: J. Cleaner Prod. *187*, 98 (2018).
25. Štofová L., Szaryszová P., Mihalčová B.: Energies *14*, 1720 (2021).
26. Mahapatra K., Alm R., Hallgren R., Bischoff L., Tuglu N., Kuai L., Yang Y., Umoru I.: Energy Effic. *11*, 1103 (2018).
27. Cagno E., Neri A., Trianni A.: Energy Effic. *11*, 1193 (2018).

DIGITAL WELLBEING FOR HIGHLY SKILLED STAFF

Dvorakova Z. [1]

[1]*University of Chemistry and Technology, Prague, Technická 5, 166 28, Prague 6*
Zuzana3.Dvorakova@vscht.cz

Abstract

Today devices' unconstrained use causes substantial negative consequences. Multitasking and constant notifications lead to lower levels of creativity and concentration; the difficulty of effective interpersonal communication causes higher stress, while heavy screen use links to eyesight problems and headaches. These issues deteriorate productivity and health. Corporations already address digital overload via wellbeing policies within their human resource management. Some high-profile universities have also developed policies. Research showed that no university had developed structured support for teaching staff on the topic. The paper aims to practices enhancing the digital wellbeing of highly skilled staff. Employers can master these challenges by increased compliance efforts, an old-new emphasis on the problem of stress and maintaining mental health, overall accent on health, employee-assisted programs, telehealth services, intelligent personal protective equipment., and secure against loss of knowledge the retirement of employees through the sharing of knowledge between employees 50+ and new less experienced employees.

Introduction

Growing scientific evidence from workers in digital environments has shown that devices' unconstrained use can have substantial negative consequences. Multitasking and constant notifications are associated with lower levels of creativity and concentration; the difficulty of effective interpersonal communication causes higher stress, while heavy screen use links to eyesight problems and headaches. These issues are caused by technology and organizational expectations, leading to deterioration in productivity/performance and employees' mental and physical health.

Many large corporations are already addressing digital overload via well-being policies within their human resource/corporate social responsibility work. Some high-profile higher education institutions (HEI) have also developed policies. However, research showed that no providers had developed structured support for teaching staff on the topic.

The paper aims to identify how employers can improve the digital well-being of highly skilled staff, focusing on higher education lecturers as distance teaching and international team cooperation become a standard part of their working life. Achieving this intention requires the following:

- to identify the state-of-the-art of digital well-being,
- to get an overview about digital well-being at higher education institutions,
- to find the best personnel/human resource practices addressing digital overload via well-being policies as perspectives towards improving digital well-being.

The methodology insists on analyzing secondary sources in the Web of Science and Scopus databases, leading three semi-structured interviews with human resource managers, and using a focus group with six higher education lecturers. The primary research provides data for writing two narrative cases – one about lecturers' labor conditions when they work online, and the second one – about human resource management (HRM) used for improving the quality of digital work.

Literature overview

The state-of-the-art digital well-being sources suggest 82 692 bibliographic records that matched the query in database search in 2000-2021: records from the Web of Science databases count for 3 916 and Scopus 78 776. The enormous amount of literature on various sciences does not allow conducting a complete analysis of all of them in the paper. Data allows getting a gross imagination about an emerging trend. Well-being belongs to a primarily analyzed theme since 2000; however, digital well-being has become a hot topic approximately in the last three years, as shown in Table I. The studies in the databases outline the development of promising directions in several areas, e.g., computer science (preciously in theory methods, interdisciplinary applications, cybernetics, information systems, artificial intelligence), hospitality, leisure, sport, and tourism, philosophy, and ethics. The existing literature on the ethics of digital well-being identifies significant issues related to social domains:

healthcare, education, governance, and social development, and media and entertainment, and questions for the future research dedicated to three broader themes: positive computing, personalized human-computer interaction, and autonomy and self-determination[1].

Table I
Bibliographic records by the query in the Web of Science and Scopus databases 2000-2021[a]

Query	Web of Science 2000-2021	Web of Science 2018-2021	Scopus 2000-2021	Scopus 2018-2021
Digital wellbeing	19	0	123	113
Digital well-being	31	30	123	120
Digital well-being and health	6	5	83	81
Digital well-being and mental health	2	2	45	45
Well-being and employment	3 839	1 481	77 382	27 812
Well-being and academic career	19	12	1 020	499
Total	3 916	1 530	78 776	28 670

[a] Calculated by the author. Accessed 2021/06/12.

Digitalization and robotization lead to a working environment characterized by conditions that work is increasingly overseen and coordinated by algorithms and artificial intelligence (AI) based on big data, tracking data on workers' productivity, location, vital signs, stress indicators, micro-facial expressions, and even tone and sentiment analysis. Machines can learn the same emotion recognition ability and do better than humans if they can continue learning new data. Heraz and Clynes[2] believe that force-sensitive screens may recognize users' emotions and share emotional insights with users, increasing users' emotional awareness and allowing researchers to design better technologies for well-being.

The situation can progress as about 40 % of human resources (HR) departments in international companies estimate that they use AI applications, and 70 % consider that this trend will develop a high priority for their organization. Furthermore, according to a survey of senior executives in several sectors and industries worldwide, more than 7 out of 10 think it will be common to use AI to evaluate workers' performance and set rewards in the next ten years[3].

HR managers from corporations monitored in the EU-OSHA document predict negative impacts of digitalization on workers' mental health as the following[3]:

- employees will lose control over work content, pace and scheduling and the way they do their work,
- they are unable to interact socially or take breaks when they want to,
- their privacy is invaded,
- they will sense growing insecurity and stress.

Some researchers identify the consequences of digitalization on education, arguing that it is negatively associated with users' perceived digital overuse and positively with digital communication use and digital social pressure[4]. The concept of teacher well-being and concerns for developing digital well-being and other related concerns for using digital technologies in education have been previously studied. The idea that digital technologies can support teacher well-being (or not) and ways that users might do this have not been studied to the same extent[5].

Higher education belongs to a turbulent sector, eroded academic well-being, and challenged the traditional silence about stress in academia[6]. Distance education creates the best possible pre-conditions for effecting flexible work – for both HE lecturers and students. The COVID-19 and the Czech government administration measures have fundamentally affected daily pedagogical life and researching HEIs. Public expectations and moral attitudes to education in society have generated pressure on university management to ensure a smooth pedagogical process. Using the 24/7 economy, HEIs observe an increase in the demand for permanent availability, irregular working hours, blurred boundaries between work and private lives, and even precarious forms of work. So, flexibility brings its pros and cons. Potential safety and health risks can report similarities that are known from other sectors:

- workers are likely to experience an increased workload, excessive working hours, and an unhealthy work-life balance.
- lone working and the feeling of isolation, the lack of collective support, and problems related to reduced support from the organization,

- musculoskeletal disorders[7],
- environments at the home office are not often ergonomically suitable, but employers have little control over them,
- health problems such as obesity, type-2 diabetes, and cancer increasingly occur as digitalization increases sedentary working.

The personal attitude to distance employment has its gender dimension. Teleworking continues to spread and becomes one of the most effective forms of labor relations, improving the women's quality of life in socio-cultural, family, parental, and reproductive terms, mainly in the upbringing and education of children, household care, and health care lifestyle[8]. For illustration, the analysis in Turkish state universities where academic women who managed to achieve academic status and esteem seemed to have paid the price in their private lives and given in a lot concerning their well-being, so findings appeal to a re-design of work conditions the academia[9].

HRM believes that the digital well-being of highly skilled staff can achieve by designing and implementing practices that reflect trends that appeared in 2021 and amplified due to COVID-19. Therefore, it puts high demands on any employer regardless of a sector as consisting of:

- increased compliance efforts, i.e., to utilize the compliance program effectively,
- an old-new emphasis on the problem of stress and maintaining mental health[10],
- overall emphasis on overall health and well-being[11],
- employee-assisted programs,
- telehealth services,
- intelligent personal protective equipment., and
- secure against loss of knowledge, incl. knowledge in occupational safety and health, the retirement of employees through the sharing of knowledge between employees 50+ and new less experienced employees to ensure knowledge continuity[12].

Results

Case 1. HE lecturers and digital well-being

The focus group was held online in May 2021 and covered six HE lecturers, from whom two women aged 25-30, two ones aged 31- 40, and two men aged 45-55. All of them agreed that since March 2020, their HEIs ensured a smooth pedagogical process and work on team projects.

Distance education and e-teachers develop a mass worldwide affair. The radical change across borders occurs due to the COVID-19 measures. HE lecturers mastered the change equipped only with a laptop having minimum knowledge of an ergonomically correct workstation. They lecture distance courses using online platforms, e.g., the e-learning system/Moodle, the MS Teams, ZOOM, Google Meet, or Webex. The distance work from home under occupational health and safety regulations was contractually concluded with the employer. However, nobody takes care of working conditions at the home office. In this perspective, they need to understand the ramifications of the poor workstation. Some accept students' demand to provide office hours on an open university's principle and consult in the regime 24/7. Less experienced lecturers are feeling the fear of missing out (FoMO) on social media, i.e., the fear that online content and interactions from others are unseen and reacted to in a timely fashion leading to anxiety, interrupted sleep, lack of concentration, and dependence on social media to generate gratification[13]. The emphasis is given on self-management and the will to avoid procrastination on social networking sites. This phenomenon analyses a study arguing that procrastination on social media can reduce academic performance and undermine well-being[14]. Lecturers with lower self-discipline incline to be constantly connected and updated whenever they receive a notification as they believe they are expected to interact immediately and seek relatedness and popularity.

Specific pressure on well-being creates a blurred perspective of an academic career. Senior lecturers feel employment uncertainty caused by several reasons. Being employed full-time indefinitely seems to be an unattainable goal. Requirements for climbing the academic ladder and achieving an associate professor position are increasing, tapping the weight of publishing in high-quality journals and research projects financed by renowned institutions. However, in the post-covid times, HEIs can expect strict austerity measures. This budget problem will gradually worsen thanks to the demographic development: Czech youth in cohorts aged 18 will substantially increase in four-five years. Job insecurity, together with the salary level, which younger academic staff consider to be inadequate compared to salaries on the Prague labor market, motivates them to rethink their expectations and change employers.

Case 2. HRM and digital well-being.

The semi-structured interviews were conducted with three HR managers from Czech local subsidiaries of multinational enterprises and two HR freelance consultants. Interviews were online in May 2021. The questions included four areas: mental health and well-being of highly skilled staff, changes in HR/personnel services caused by the COVID-19, training and development, and performance management/performance appraisal.

Respondents agree that employers put greater emphasis on employees' mental health and well-being and focus on digital communication, which means to be accessible to employees (the ideal regime 24/7), have empathy, and provide long-term support. They predict an open opportunity to increase the importance of the HR department within the organization and put stress on internal communication, mainly to train and integrate new employees. Digital tools are massively used for distance recruitment and onboarding. Selection happens virtually and includes a criterion of whether a candidate is suitable for distance work. During the virtual staffing and training, HR activities must transfer corporate culture and infiltrate employees. They hold the opinion that in uncertain times employees are looking for a reliable and supportive environment. HR departments should design programs to ensure well-being and benefits to cope with new life situations, such as paid leave, health insurance, and health prevention, employee assistance programs, mental health support services, delivery of goods and meals at home. The challenge for managing people creates moving from offline working to online working and finding effective practices for team building and employee engagement. Hybrid workplaces represent teleworking for wholly or partly throughout working hours, shared workplaces, e.g., desk reservation in advance, and the increase of human resource diversity. Flexible working hours search for new schemes, like self-rostering, daily or hourly flexible working hours. Occupational safety and health (OSH) require contactless work or limited contact at the workplace and the provision of personal protective equipment (respirators, disinfection). Performance management leads to more frequent employee control by direct superiors and monitoring their performance using data collected daily as a long-term trend seems to emerge fluid labor relation that can cause the growing amount of precariat.

Strategies regarding OSH usually get on the edge of the HRM agenda as this agenda is a part of work in another department. Czech HR managers assume that problems related to digitization and its effects on human resources need to be solved. However, they suffer from a lack of funding for the latest protective equipment and risk prevention.

Conclusion

The digital economy will transform the labor market and bring new forms of labor relations between employers and employees, impacting health and safety protection or the reconciliation of work-life balance. Distance teaching will be a substantial part of the pedagogic job due to pandemic measures, and secondly, Education 4.0. Czech, public universities resolved the responsibility for safe performance management by a contractual arrangement between the employer and the employees. The agreements respect the labor law provisions dealing with health and safety at work in the case of a home office.

Digitalization means challenges for HRM and OSH regardless of the sector. Benefits for HE lecturers pose the use of sensors for monitoring risk exposure, relieving workers of repetitive or routine tasks, higher levels of autonomy and flexibility, and facilitating the access of a more diverse workforce to the labor market, e.g., disabled people, aging workers, those with care duties at home, and living abroad. Risks of digitalization mean ergonomic and safety risks, including risks associated with cybersecurity, an increase in work-related stress and poor mental health, increasing performance pressure and work complexity, irregular working hours, less social interaction and support at work, blurred boundaries between work and private life, and new forms of work with unclear employment status. The digital wellbeing for HE lecturers can achieve by practices that reflex trends emerged in 2021 and are emphasized by the COVID-19, i.e., increased compliance efforts, an old-new emphasis on the problem of stress and maintaining mental (osha, prevention-psychosocial-risks), the overall emphasis on overall health and wellbeing (kff, mental-health-and-substance-use), employee-assisted programs, telehealth services, intelligent personal protective equipment., and secure against loss of knowledge, incl. knowledge in occupational safety and health, the retirement of employees through the sharing of knowledge between employees 50+ and new less experienced employees.

Acknowledgement

This work was supported by Russian Foundation for Basic Research (RFBR) under Grant № 19-010-00705 'Development of tools for assessing the impact of social pollution of labor relations on the employees' wellbeing in a digital economy'.

References

1. Burr, C., Taddeo, M., Floridi, L.: The ethics of digital well-being: a thematic review. Science and Engineering Ethics*, 26*, 2313 (2020).
2. Heraz, A., Clynes, M.: Recognition of emotions conveyed by touch through force-sensitive screens: observational study of humans and machine learning techniques. JMIR Mental Health*, 5,* e10104. (2018).
3. Digitalisation and occupational safety and health (2019). An EU-OSHA research program. [cit. 2021-04-27]. European Agency for Safety and Health at Work. Retrieved from <https://osha.europa.eu/en/publications/digitalisation-and-occupational-safety-and-health-osh-eu-osha-research-programme/view>.
4. Gui, M.R., Buchi, M.: From use to overuse: digital inequality in the age of communication abundance. Social Science Computer Review, 20, 3 (2021).
5. Passey, D.: Digital technologies – and teacher wellbeing? Education Sciences*, 11,* 117 (2021).
6. Hurd, F., Singh, S.: 'Something has to change': A collaborative journey towards academic well-being through critical reflexive practice. Management Learning. 1350507620970723 (2020).
7. Crawford, J.O. and Davis, A.: Work-related musculoskeletal disorders: why are they still so prevalent? Evidence from a literature review. EU-OSHA. (2020).
8. Tonkikh, N., Fedorova, A., Koropets, O.: Female distance employment: opportunities and challenges. In Paoloni, P., Paoloni, M., Arduini, S. (eds): Proceedings of the 2nd International Conference on Gender Research (ICGR 2019). Roma Tre Univ, Ipazia Sci Observ Gender Issues, Rome, ITALY. APR 11-12, 2019, 622-629 (2019).
9. Gokturk, S., Tulubas, T.: Survival of the fittest: women's academic experiences of navigating neoliberal expectations in Turkish universities. Gender and Education*, 33,* 267 (2020).
10. Working on stress. Prevention of psychosocial risk and stress at work at practice. [cit. 2021-05-30]. Retrieved from <https://osha.europa.eu/en/publications/report-prevention-psychosocial-risks-and-stress-work-practice>.
11. Panchal, N., Kamal, R., Cox, C., Garfield, R.: The implications of COVID-19 for mental health and substance use. [cit. 2021-04-20]. KFF. Retrieved from <https://www.kff.org/coronavirus-covid-19/issue-brief/the-implications-of-covid-19-for-mental-health-and-substance-use/>.
12. Botek M.: Knowledge continuity in business continuity context. In Jedlička P. (ed.): Hradecke ekonomicke dny 2015, Univerzita Hradec Kralove, Feb 03-04, 2015. 5(1). 89 (2015).
13. Alutaybi, A., Al-Thani, D., McAlaney, J., Ali, R.: Combating fear of missing out (FoMO) on social media: the FoMO-R method. International Journal of Environmental Research and Public Health*, 17,* 6128 (2020).
14. Alblwi, A., McAlaney, J., Altuwairiqi, M. Stefanidis, A., Phalp, K., Ali, R.: Procrastination on social networks: triggers and countermeasures. Psihologija*, 53,* 393 (2020).

PERSONAL AND TRANSVERSAL COMPETENCIES IN BIO-BASED ECONOMY

Botek M.[1], Diaz M.[1]

[1]*School of Business, University of Chemistry and Technology, Prague, Technická 5, 166 28 Prague 6, Czech Republic*
botekm@vscht.cz

Abstract

The new trends in the 21st century economy require new competencies for successful implemenatation within the modern workplace. This article focuses on three of these competencies, namely Personal, Transversal, and Technical. It briefy describes each and gives ideas for improvement within these areas via relevant education of bio-based workers.

Such economic trends are present within the bio-based economy as well. As part of the BioComp project, an analysis of competencies experts consider the most important for workers in the bio-based economy was carried out. Interviews were conducted with experts in these fields in the spring of 2020. 139 respondents from eight European Union countries took part.

The results show that the chosen competencies are considered very important by the addressed experts. The average rating in the category of Personal competencies was 8.41 while the category of Transversal competencies rated 8.31, with 10 indicating an extremely important competence.

Introduction

Professional competencies are associated with the knowledge and skills important for successful job performance[1]. It is possible to teach them and train them, but this is not enough. At the same time, personal competencies, associated with individual motives, traits, and self-concepts, are very important for successful job performance[1]. These competencies are similar to soft skills in that they have the ability to affect others and help one to get what he/she wants[2]. This means that such competencies are based on emotional intelligence. Unfortunately, students in universities are usually only taught (mostly) in a manner suitable for the acquisistion of professional competencies. Lack of personal competencies has been observed in many professions (eg. nursing[3], industrial employees[4]) and employees often need to develop these skills and behaviours at their place of work because such comprentencies are primarily outside the scope of university study activities[4]. The competencies which new graduates often lack the most are teamwork and social skills[4].

It is worth noting that while similar in meaning, there is a distinct difference between skills, which can be defined as specific learned physical tasks or activities, and competencies, which are behaviours that arrive as a result of one's values, attitudes, skills, and knowledge/critical understanding[5]. While a competence can be acquired via specialized training, personal competencies are often acquired via a combination of extracurricular activities[3,6] such as self-government, recreation, sports, and social activities. While these activities are generally voluntary[7], attention can also be given to them during lecturing. Goleman[8] belives that personal competencies can be developed through both formal and informal life experiences. Conventional training methods reinforcing memorization of information are not effective. Instead, it is necessary to focus on critical thinking and self-regulation, as many authors have found[9].

It is also possible to work on emotional management for use in the workplace as well. However, according to Cherniss and Goleman, this requires writing down all the emotions one can think of and then isolating one or two which he/she can expect to experience during the day, concluding with an analysis of the reason(s) why these emotions stand out[10]. Video can also be used to present a relevant emotion for analysis[10]. However, it is generally perceived as easier to work on communication and teamwork development instead, although knowledge of emotions remains very useful.

At no time in history has there been such a radical change in working habits as during the COVID-19 Crisis. As a result of the pandemic, virtual teams have been supported, work from home has increased, and the demand for different employee skill levels has been created[11]. The Covid crisis has shown us that to succeed in the modern workplace, it is neccesary to be digitally competent and able to adapt to sudden work-related changes. Therefore, not only professional and personal but also transversal competencies should be devoloped. Transversal competencies are essential skills and attitudes that contribute to a learners' holistic development by making them capable of adapting according to the needs and changing demands encountered in different situations and conditions[12]. Reserachers often claim that the most frequently used transversal competencies are communication skills, teamwork, creativity, and innovation[13]. We distinguish personal competencies as being more oriented towards soft skills and transversal competencies as consisting of digital and entrepreneurial competences, following the framework documents of the European Union. These frameworks include *LifeComp* – European Framework for the Personal, Social and Learning to Learn Key Competence[14] for personal competencies; *DigComp 2.1* - The Digital Competence Framework for Citizens[15] for digital competencies; and *EntreComp* - The European Entrepreneurship Competence Framework[16] for entrepreneurial competencies.

Questionnaire survey

In our project, we started from the idea that the necessary competencies of workers in the bioeconomy can be divided into three areas. These are personal, transversal and technical competencies. While technical (professional) competencies are closely linked to the relevant area of bioeconomy, these will not be addressed further in this article. However, personal and transversal competencies will be addressed comprehensively. In identifying them, we relied on the framework documents of the European Union.

The research was conducted via questionnaire, the respondents had the task of assigning a score of one to ten points to determine the importance of individual competencies within bio-based industries. The questionnaire was created based on previous interviews conducted with experts from the bio-based economy and the three previously mentioned European frameworks. Questionnaire research was conducted with experts in bio-based fields in the spring of 2020. 139 respondents from eight European Union countries took part. The results show that the chosen competencies are considered very important by the addressed experts. The average rating in the category of Personal Competencies was 8.41 while the category of Transversal Competencies scored an average rating of 8.31, with 10 indicating an extremely important competence. The detailed results are shown in Tables I-III.

Table I

Personal Competencies

Abbr.	Competencies Ranked According to Importance	AM	SD
P1	Collaboration - Being part of a relational system in which stakeholders pool together resources, ideas, and actions to meet common goals that neither could meet individually – with shared commitment and ownership.	8.78	1.27
P2	Communication - Using words, sounds, signs, or behaviours to express or exchange information, thoughts, or feelings to someone else. It may be vocally, written (using printed or digital media such as books, magazines, websites, or emails), visually (using logos, maps, charts, or graphs) or non-verbally (using body language, gestures, and/or the tone and pitch of voice).	8.76	1.39
P3	Adaptability - The ability to be flexible and respond positively to a rapidly evolving environment, coming out the better for it (bouncing forward).	8.6	1.30
P4	Growth Mindset - Being motivated to reach higher levels of achievement by continuously learning new skills in order to move with a changing market. Essentially, it is being adaptable and willing to go above and beyond the soft and hard skills you already have.	8.5	1.46
P5	Critical Thinking - Skilful analysis and assessment of information, beliefs or knowledge, with ongoing reconstruction and improvement of one's thinking. It can bridge convergent and divergent (creative) thinking.	8.48	1.70
P6	Wellbeing - Achieving a state of contentment, with low levels of distress, overall good physical and mental health, and good quality of life.	8.34	1.68
P7	Self regulation - The ability to understand, activate, monitor, control, and adapt emotions, thoughts, attention, behaviour, and cognitive strategies.	8.30	1.46
P8	Empathy - The ability to understand, vicariously experience, and respond to another person's feelings, emotions, and thoughts (emotional, cognitive, and perspective taking).	8.00	2.09
P9	Managing Learning - Knowledge of oneself (as learner, of strategies, tasks, and context) and as regulation (applying it to plan, monitor, and evaluate learning).	7.80	1.97

Table II
Transversal Competencies - Digital

Abbr.	Competencies Ranked According to Importance	AM	SD
D1	Communication - Interacting through Digital Technologies - To interact through a variety of digital technologies and to understand appropriate digital communication.	8.50	1.46
D2	Collaboration - Collaborating through Digital Technologies - To use digital tools and technologies for collaborative process, and for co-construction and co-creation of data.	8.32	1.62
D3	Safety - Protecting the Environment -To be aware of the environmental impact of digital technologies and their use.	8.27	1.80
D4	Safety - Protecting Personal Data and Privacy - To protect personal data and privacy in digital environments. To understand how to use and share personally identifiable information while being able to protect oneself and others from damages. To understand that digital services use a “Privacy Policy” to inform how personal data is used.	8.21	2.13
D5	Information and Data Literacy - Managing data, information and digital content: To organise, store, and retrieve data, information, and content in digital environments. To organise and process them.	8.05	1.99
D6	Problem Solving - Identifying Needs and Technological Responses - To assess needs and to identify, evaluate, select, and use digital tools and possible technological responses and to solve them. To adjust and customise digital environments to personal needs (e.g. accessibility).	7.91	1.99
D7	Problem Solving - Creatively Using Digital Technology - To use digital tools and technologies to create knowledge and to innovate processes and products. To engage individually and collectively in cognitive processing to understand and resolve conceptual problems and problem situations in digital environments.	7.89	1.86
D8	Problem Solving - Solving Technical Problems - To identify technical problems when operating devices and using digital environments, and to solve them (from trouble-shooting to solving more complex problems).	7.89	2.01
D9	Problem Solving - Identifying Digital Competence Gaps - To understand where one’s own digital competence needs to be improved or updated. To be able to support others with their digital competence development. To seek opportunities for self-development and to keep up-to-date with the digital evolution.	7.68	1.99
D10	Use of Augmented Reality (AR) - To identify the benefit of AR technology and possibilities of use in training and creatively using AR technology in training situations.	6.52	2.76

Table III
Transversal Competencies - Entrepreneurial

Abbr.	Competencies Ranked According to Importance	AM	SD
E1	Into Action - Working with Others - To work together and cooperate with others to develop ideas and turn them into action. Network. Solve conflicts and face up to competition positively when necessary.	8.59	1.25
E2	Into Action - Learning through Experience - To use any initiative for value creation as a learning opportunity. Learn with others, including peers and mentors. Reflect and learn from both success and failure (your own and other people's).	8.48	1.30
E3	Into Action - Taking the Initiative: To initiate processes that create value. Take up challenges. Act and work independently to achieve goals, stick to intentions and carry out planned tasks.	8.44	1.30
E4	Ideas and Opportunities - Creativity - Develop several ideas and opportunities to create value, including better solutions to existing and new challenges. Explore and experiment with innovative approaches. Combine knowledge and resources to achieve valuable effects.	8.38	1.43
E5	Ideas and Opportunities - Ethical and Sustainable Thinking - Assess the consequences of ideas that bring value and the effect of entrepreneurial action on the target community, the market, society, and the environment. Reflect on how sustainable long-term social, cultural, and economic goals are, and the course of action chosen. Act responsibly.	8.24	1.31
E6	Ideas and Opportunities - Valuing Ideas - Judge what value is in social, cultural, and economic terms. Recognise the potential an idea has for creating value and identify suitable ways of making the most out of it.	8.18	1.47
E7	Resources - Mobilising Resources - To get and manage the material, non-material and digital resources needed to turn ideas into action. Make the most of limited resources. Get and manage the competences needed at any stage, including technical, legal, tax and digital competences (for example, through suitable partnerships, networking, outsourcing, and crowdsourcing).	8.08	1.66
E8	Ideas and Opportunities - Spotting Opportunities - Identify and seize opportunities to create value by exploring the social, cultural and economic landscape. Identify needs and challenges that need to be met. Establish new connections and bring together scattered elements of the landscape to create opportunities to create value.	8.05	1.49

Discussion

Current labor markets are characterized by a shortage of talent, rising demands of technical skills, aging of the population, and disappearance of repetitive jobs. Competitiveness in the industrial sectors and the implementation of modern technologies is made up of specialists with the science, math, and engineering background of the critical labor force, and dealing with personal competencies has become crucial for perspective organizational development[17].

The results from our questionnaire showed that the two most important Personal Competencies were Collaboration (C1) and Communication (C2). Collaboration (D1) and Communication (D2) (through digital technologies) were also the two most important Transversal (Digital) Competencies. The most important Entrepreneurial Competence was "Working with others" (E1), which again means Collaboration. The third position in this field was Taking the Initiative (E3), which is also connected with Collaboration. Others which were deemed important were Adaptability (C3) and Learning through Experience (E2). These can be initialised by collaboration but also via individual activity.

These results are consistent with the idea that teamwork and social skills are the skills and behaviours most often missed among employees in the modern workplace. A consistent theme highlighted by our questionnaire results is the necessity for good communication, which we think is the most important social skill needed by members of the workforce today. It is needed not only to be able to explain what we want, but also to understand others and negotiate successfully. It has been suggested that managers spend at least 80 percent of every day in direct communication with others[18] and, as evidenced by the emphasis on the key competences of Communication and Collaboration in our questionnaire, it can be inferred that this is not a skill necessary only for management.

In an attempt to adequately prepare students for these relevant personal competencies, it is possible to include communication activities during university lectures. Students may, for example, receive control questions concerning specific professional topics and/or themes and then be asked to ascertain respective answers in groups and then report the results. It is also possible to give students large documents with excess information or ask them to find important information on the internet and then prepare either individual or group presentations to the class. One good approach is to record some of these activities so students can see and study any potential mistakes made via teamwork activities as well as any potential problems pertaining to nonverbal communication. An experienced teacher should be able to do this well enough, even if he/she is not specialized in soft skills. Regardless, our questionnaire results show how essential it is for educational institutions aiming to prepare students for the modern workplace to place a premium on communication competencies in addition to the regularly taught professional competencies as well.

Outside the realm of communication and collaboration, the questionnaire respondents emphasized the importance of safety, both environmentally and digitally. Safety - Protecting the Environment (D3) and Safety - Protecting Personal Data and Privacy (D4) were the third and fourth ranked Transversal Digital Competencies, respectively. The latter features prominently in the EU framework *Digicomp 2.1.* However, it is worth noting that digital competencies often fall under the umbrella of communication and collaoboration as well. Whittemore describes such a link, arguing that a digital skillset involves the effective and integrated use of a wide range of soft skills, which provide the ability to deploy the technical skills and the digital tools in the service of organisational strategy and business objectives[19]. Furthermore, *Digicomp 2.1* identifies Collaboration as one of the key soft skills involved in digital competencies in addition to Protecting Personal Data and Privacy. As for skills related to safely protecting the environment, this is a concern that currently affects all major industries, primarily within a European context.

Conclusion

The bio-based economy finds itself on par with other 21st century industries regarding the trend towards communicative and collaborative personal competencies combined with digitization and its inherent safety concerns. The European Union recognizes the importance of these competencies in the 21st century economy and has called on educational institutions and industry partners to help with the formulation of policies aiding the ability of graduates and workers to acquire them. As the results of our questionnaire showed, bioeconomy workers will need to master these competencies as well, with special focus on all communicative aspects. Further research regarding bio-economy specific competence training and implementation among Vocational Education and Training (VET) employees should seek to follow the framework set out in the questionnaire while highlighting the communicative and collaborative nature of 21st century bio-based economy.

Acknowledgement

This work was supported by Biocomp, Erasmus+ Project No 2019-1-CZ01-KA202-061409.

References

1. Spencer L.M., Spencer S.M.: *Competence at Work: Models for Superior Performance*. John Wiley & Sons, New York 1993.
2. Nye J.S.: *Soft Power: The Means to Success in World*. Politics Public Affairs, New York 2005.
3. Hsing-Yuan Liu; Chun-Yen Chao; Victoria J. Kain; Su-Ching Sung: The relationship of personal competencies, social adaptation, and job adaptation on job satisfaction. Nurse Edu. Today, 83, 104199. (2019).
4. Pyrhönen, V.P., Niiranen S., Pajarre E.: Newly graduate engineers' development of expertise and personal competencies. Információs Társadalom 20(2), 70 (2020).
5. Blankestijn H., Halm E.: BBE Competences Navigator – Introduction: Skills and Competences. www.biocompetences.eu (2020).
6. Yeh P.L.: Exploring the development of soft power from the development of student club activities counseling. J. Taiwan Edu. Rev. 6, 167 (2014).
7. Fares J., Saadeddin Z., Al Tabosh H., Aridi H., El Mouhayyar C., Kolellat M.K., Chaaya M., El Asmar K.: Extracurricular activities associated with stress and burnout in preclinical medical students. J. Epidemiology and Global Health, 6 (3), 177 (2016).
8. Goleman D.: *Emotional intelligence*. Bantam Books, New York 1995.
9. Punia N., Dutta J., Sharma Y.: Emotional Intelligence: A Theoretical framework. International. J. Sci. & Engineering Res. 6(5), 988 (2015).
10. Cherniss C., Goleman D. *Bringing emotional intelligence to the workplace*. Rutgers University, Consortium for Research on Emotional Intelligence in Organizations, New Brunswick 1998.

11. Jílková P.: Sustainable Corporate Strategy: The Role of Human Capital in the Time of COVID-19 Crisis. TEM J. 10(2), 699 (2021).
12. Raj D. P., Venugopal A., Thiede B., Herrmann Ch., Sangwan K. S. Development of the Transversal Competencies in Learning Factories. Procedia Manufacturing 45, 349 (2020).
13. Cruz M. L., Saunders-Smits G. N., Groen P.: Evaluation of competency methods in engineering education: a systematic review, EJEE, 1 (2019).
14. Caena F.: *Developing a European Framework for the Personal, Social and Learning to Learn Key Competence (LifEComp)*. Publications Office of the European Union, Luxembourg 2019.
15. Carretero G. S., Vuorikari R., Punie Y.: *DigComp 2.1: The Digital Competence Framework for Citizens with eight proficiency levels and examples of use*. Publications Office of the European Union: Luxembourg 2017.
16. Mccallum E., Weicht R., Mcmullan L., Price A.: *EntreComp into Action - Get inspired, make it happen: A user guide to the European Entrepreneurship Competence Framework*. Publications Office of the European Union, Luxembourg 2018.
17. Dvorakova Z.: Labor Economics and Career Development in the Context of Globalized World. In Kliestik, T. (Ed.). The 20th International Scientific Conference Globalization and its Socio-economic Consequences 2020. Zilina, Slovak Republic, October 21-22, 2020. SHS Web of Conferences, 92 Article Nr. 07019 (2021).
18. Daft R. D.: *Management*. Thomson South-Western, 2008.
19. Whittemore S. T.: *Transversal Competencies Essential for Future Proofing the Workforce*. White Paper, Skilla Library, 2018.

CONSUMER ATTITUDES TOWARDS HOUSEHOLD WASTE SORTING

Frohlich A.[1], Branska L.[2], Patak M.[3], Pecinova Z.[4]

[1,2,3,4] *University of Pardubice, Faculty of Chemical Technology, Studentská 95, 530 09, Pardubice*
lenka.branska@upce.cz

Abstract

Manufacturers of consumer chemicals have been endeavouring in recent years to increase the sustainability of their product packaging. They apply various strategies, in particular reduce, reuse and recycle. The recycle strategy presupposes the cooperation of final consumers. The role of final consumers in relation to the recycling process and household waste sorting has not yet been addressed in the literature. Therefore, a primary quantitative research was conducted among 350 users of consumer chemicals aimed at finding out their attitudes to individual activities in the sorting of household waste. It was found that consumers' willingness to engage in these activities varies, also depending on the classification characteristics of the respondents (gender, age, education, income level and form of housing). A critical group in terms of willingness to sort the waste are university-educated young high-income men living in flats.

Introduction

Packaging is often considered to be one of the main culprits in the pollution of our planet, because its time of use is relatively short. The packaging becomes waste essentially immediately after it has been used[1]. Packaging waste significantly increases the volume of solid waste in cities and municipalities. In the dominant industrial economies, packaging waste accounts for about 20% of municipal solid waste[2]. Therefore, companies in various industries are looking for a way to minimize the negative impact of packaging on the environment, without giving up the opportunity to benefit from its positive properties[1]. According to Mehereshi (2019), these sectors are mainly the food industry, however, companies in the chemical and pharmaceutical industries have started to implement sustainable packaging as well[3]. Companies such as Henkel, Colgate-Palmolive or Dow are working hard on the sustainable packaging of their own end-use products[1,4,5]. Their efforts are mainly focused on limiting the single use of primary plastic packaging.

Packaging waste can be reduced through three important and effective strategies, namely reduce, reuse and recycle[3,6]. The focus is on all three strategies. However, as many consumers are reluctant to cooperate in return systems[7], the reduce and/or recycle strategies could be more interesting for businesses. Dow Chemicals is focusing on reducing the amount of plastic per package[3], and Colgate Palmolive is introducing fully recyclable packaging for all products in three (out of four) product lines in order to enhance the recycle strategy.

The increased recycling rate of plastic packaging leads to a significant reduction in environmental impact[8]. In the field of plastic recycling, the greatest interest is in recycling PET bottles, as the recycled material is used the most[9]. Recycled PET can be used to produce new PET bottles or silicone fibre, which is then used for the production of car interiors, fillings for sleeping bags and home bedding, roofing, etc. In the case of processing mixed plastics, a lower-quality recycled material is produced (used for the production of garden and park furniture, crates and pallets, playgrounds, etc.)[10].

There are a number of barriers to a higher recycling rate. These include the use of a large number of different types of plastics[11], the combination of different materials in the production of one package[11,12], insufficient collection of used packaging[13], dirt in collected plastics[10], insufficient recycling infrastructure and high sorting costs[10,13]. In particular, this causes incorrectly sorted materials to enter recycling systems, which can cause a number of other environmental and economic problems[14].

Sběr a třídění odpadů (a v rámci nich obalů z výrobků) probíhá na třech základních úrovních, a to na úrovni domácností, na úrovni měst a obcí a konečně ve specializovaných firmách, které provádějí recyklaci nebo vytříděné obaly k recyklaci dodávají. These companies eliminate the shortcomings in the classification at previous levels. They use not only mechanical but often also automatic systems for sorting, including increasingly reliable detectors and sophisticated software[15]. However, investment in and use of these technologies increases recycling costs and causes packaging manufacturers to give preference to raw materials over recycled use for economic reasons[10].

Insufficient sorting of waste (including packaging waste) in households is caused by a number of existing barriers. According to the literature[10,14,16,17,18,19] the barriers include in particular:

- necessity to sacrifice the time associated with sorting (time for washing, disassembling packaging by different types of materials, removing labels, etc.),
- reduction of convenience - the consumer must make an effort to sort waste,
- financial costs - arise in connection with, for example, washing and removing labels (e.g. water consumption, energy consumption for heating used water),
- lack of space for storage of sorted waste,
- limited possibility for households to place sorted waste in special containers due to insufficient infrastructure in the place of residence,
- distrust of the need for sorting - the consumer does not appreciate the role of sorting from the point of view of environmental protection and/or his/her own role in environmental protection.

However, despite the existence of these barriers, the sorting of household and packaging waste takes place. This may be related to both the motivation caused by public pressure[20], and the satisfaction evoked by the perceived value of sorting and the level of recycling infrastructure. According to the literature,[21] the level of satisfaction resulting from sorting depends on education, income and age and affects three dimensions of involvement: enthusiasm (trying to learn more about sorting), social interaction (sharing sorting-related experiences with friends and other community) and active participation in sorting.

Overcoming the above-mentioned barriers, resistance to various external pressures and the size of the perceived value of sorting are fundamentally related to the willingness of households to sort waste and the packaging of products used within it. However, this willingness has not yet been theoretically examined, although the issue is already being highlighted. For example,[18,19] state that the reluctance of consumers to participate in the recycling scheme is a major problem that needs to be thoroughly examined. Therefore, primary quantitative research was focused on this area. Its purpose was to reveal the willingness of consumers to carry out individual activities related to waste sorting (including packaging waste) in their own households.

Research methodology

The aim of the primary research was to specify the willingness of consumers to carry out activities that facilitate recycling. The objectives were to find out:

- what activities consumers are willing to do in preparing packaging for recycling,
- what is the willingness of consumers to sort waste, and
- how long consumers are willing to keep sorted waste in the household and to what distance they are willing to take it.

The research was organized as a quantitative one, an electronic questionnaire was used to collect data. It contained 14 statements, in which the respondents expressed the degree of agreement. A five-point Likert scale was used to express the degree of agreement (where 1 indicated the position "strongly disagree" and 5 the position "strongly agree"). The questionnaire also included questions examining the characteristics of the respondents such as gender, age, education, monthly income and type of household.

Data collection took place from 9 March to 9 April 2021 in the economically active population of the Czech Republic aged 15–64. 350 respondents took part in the research. Their structure by age and gender is shown in Table I.

Table I
Structure of respondents by gender and age

Gender	Age (Frequencies)					
	15–24	25–34	35–34	45–44	55–54	Total
Male	25	32	16	14	5	92
Female	76	69	39	40	34	258
Total	101	101	55	54	39	350

The sample of 350 respondents included 182 (52%) respondents without a university degree and 168 (48%) respondents with a university degree, 179 (51%) respondents living in housing units and 171 (49%) respondents living in family houses. The structure of respondents by income is shown in Table II.

Table II
Structure of respondents by income

Income	Frequencies	Percentages
Up to CZK 20,000	98	28 %
CZK 20,001 – 30,000	66	19 %
CZK 30,001 – 40,000	72	21 %
CZK 40,001 and more	54	15 %
I do not want to answer	60	17 %
Total	350	100 %

After the data collection was completed, they were checked and adjusted. The data obtained were checked for representativeness in terms of gender and age. The detected deviations were removed by weighing the data according to the available information on the structure of the examined population[22]. Subsequently, the categories of respondents by education were merged (so that only two evenly represented segments of respondents were created).

The research results were processed by descriptive statistical analysis using IBM SPSS Statistics software. First, the entire sample of individual research areas was processed in accordance with the objectives. Subsequently, a comparison of groups of respondents according to their characteristics (gender, age, education, income and type of household) was performed. In both cases, the mean and median were calculated. Missing answers were not included in the analysis ("I can't judge" category).

Discussion and result analysis

The research made it possible to find out a number of facts concerning the willingness of households to prepare waste for recycling, to sort it and to store it at home and take it out.

Regarding the willingness of consumers to prepare packaging for recycling, it was found that consumers are most willing to use common equipment (common composter and common plastic press) and to wash packaging from product residues (see Table III).

Table III
Consumer willingness to prepare waste for recycling

Consumer willingness to prepare waste for recycling	Mean	Median
I am willing to wash the packaging from product residues	3.8	4
I am willing to remove stickers and top foils from the packaging	3.5	4
I am willing to buy a biodegradable waste composter for my own household	3.2	3
I am willing to use a composter shared several households	4.0	4
I am willing to buy a press for plastics for my own household, thus reducing the volume of packaging waste	2.4	2
I am willing to use a press for plastics shared by several households	3.7	4

Analysis of the difference of opinion according to the individual classification features showed that:

- Women are more willing to prepare waste for recycling than men. In particular, they are more willing than men to wash packaging from product residues and remove stickers.
- Young respondents (under 34) are less willing to prepare waste for recycling than older respondents. The oldest consumers (aged 55-64) are most willing to prepare waste for recycling.
- Respondents without a university degree are more willing to wash the packaging from product residues, remove stickers and top foils from the packaging than respondents with a university degree. Less educated people are more willing to buy a composter for biodegradable waste, while college graduates are more willing to use a common composter purchased for multiple households.
- Higher income groups are less willing to prepare waste for recycling. In principle, the higher the income, the less willingness to prepare waste for recycling.
- Respondents living in family houses are more willing to do all activities in the preparation of waste for recycling than respondents living in housing units. They are significantly more willing to buy a composter and a plastic press for their own household.

In terms of consumers' willingness to sort waste, there is a greater willingness to actually sort than to keep different containers or bags for sorted waste. There is a greater willingness to sort waste by different types of materials (paper, plastics, glass…) than by the type or colour of the material. There is also a greater willingness to keep fewer containers (bags) for sorted waste than to keep a larger number of containers (bags), see Table IV.

Table IV
Consumer willingness to sort waste

Consumer Willingness to Sort Waste	Mean	Median
I am willing to sort packaging waste consisting of several types of materials (especially plastics, paper, glass, …)	4.3	4
I am willing to sort packaging waste according to other criteria (eg. type or color of material)	3.5	4
I am willing to keep a maximum of 10 containers (bags) for sorted waste in my household	3.4	4
I am willing to keep more than 10 containers (bags) for sorted waste in my household	2.2	2

However, the willingness to sort waste varies depending on the characteristics of the respondents.

- Women are more willing to sort waste than men. Unlike men, they are more willing to sort packaging waste by the type or colour of the material and to keep more than 10 containers for sorted waste at home.
- With age, the willingness to sort waste by the type or colour of materials increases. Younger respondents (up to 34 years) are more willing to keep a smaller number of containers (bags) for sorted waste in the household, while older respondents (from 45 years) are more willing to keep a larger number of containers (bags).
- In principle, the willingness of consumers to sort waste does not depend on education. Only one minor difference was revealed, namely the willingness to keep more than 10 containers (bags) for sorted waste in the household. More willing to do so are respondents without a university degree.
- With the income, the willingness to sort packaging waste by basic materials (plastic, metal, glass...) and also the willingness to keep containers (bags) for sorted waste decreases.
- Respondents living in family homes are more willing to keep containers for sorted waste, either in smaller or larger quantities.

An analysis of the results of research in the field of storage and disposal of sorted waste showed that respondents are more willing to take sorted waste to a collection point within 300 m of the household and to store sorted waste in households for one week (see Table V). Significantly less willingness was identified to carry the sorted waste over a longer distance and to keep the sorted waste in the household for more than one week (see Table V).

Table V
Consumer willingness to store and take out sorted waste

Consumer willingness to store and take out sorted waste	Mean	Median
I am willing to take out sorted waste to a collection point within 300 m of my household	4.3	4
I am willing to take out sorted waste to a collection point more than 300 m from my household	3.5	4
I am willing to store sorted waste in my household (within 1 week) and prepare it for periodic local collection from households	4.1	4
I am willing to store sorted waste in my household (for more than 1 week) and prepare it for periodic local collection from households	3.4	4

Regarding the differences of opinion according to the different groups of respondents, it was found that:

- Women are more willing to store and take out sorted waste than men. They are more willing to store sorted waste in the household for more than one week and to take the sorted waste to a collection point more than 300 meters away. Men are more willing than women to just take sorted waste to a collection point within 300 m of the household.
- Middle-aged respondents (35-44 years), followed by the oldest respondents aged 55-64, are most willing to do any sorting and disposal activities.
- The willingness of consumers to store and take out sorted waste does not depend on education.
- Respondents with the highest income are the least willing to take household waste more than 300 m away and keep sorted waste for more than one week.

- Respondents living in family houses are significantly more willing to take sorted waste to more distant collection points and at the same time keep sorted waste in the household for more than one week.

Conclusion

Based on the results of the research, it can be stated that consumers are willing to prepare household waste for recycling. However, their willingness varies depending on the specific activities. This fact must be respected and the system of sorting (and collection) of waste at the municipal level and in specialized companies reselling or processing sorted waste must be adapted accordingly. If we consider the possibilities of improving the classification on the part of households, financial motivation as well as consumer education and training are important[21]. To actually raise awareness about environmental protection, it should start as early as in kindergarten[21]. Based on the results of research, it can be estimated that education will be a more effective tool. This should be primarily aimed at college educated young men (under 34) with high incomes living in flats. They represent a critical group, currently the least willing to sort waste.

References

1. Henkel: https://www.henkel.cz/udrzitelnost/udrzitelne-obaly.
2. Casarejos F., Bastos C. R., Rufin C., Frota M. N.: J Clean Prod, *201*, 1019 (2018).
3. Meherishi L., Narayana S. A., Ranjani K. S.: J Clean Prod, *237*, 117582 (2019).
4. Colgate-Palmolive: https://www.colgatepalmolive.com/en-us/core-values/sustainability/sustainability-2025-our-strategy-for-the-future.
5. Dow: https://corporate.dow.com/en-us/science-and-sustainability/plastic-waste/economy.html.
6. Geueke B., Groh K., Muncke J.: J Clean Prod, *193*, 491 (2018).
7. van Weelden E., Mugge R., Bakker C.: J Clean Prod, *113*, 743 (2016).
8. Burek J., Kim D., Nutter D., Selke S., Auras, R., Cashman S., Sauer B., Thoma G.: J Ind Ecol, *22*, 180 (2018).
9. Kizlink J.: *Odpady: sběr, zpracování, zužitkování, zneškodnění, legislativa*. Akademické nakladatelství CERM, Brno 2014.
10. Niaounakis M.: *Recycling of Flexible Plastic Packaging*. William Andrew, Oxford/Cambridge 2020.
11. Kuczenski B., Geyer R.: (2010). Material flow analysis of polyethylene terephthalate in the US, 1996–2007. Resour Conserv Recy, *54*, 1161 (2010).
12. Davis G., Song J. H.: (2006). Ind Crop Prod, *23*, 147 (2006).
13. Szaki T.: https://www.packagingdigest.com/sustainability/consumers-are-confused-about-recycling-and-heres-why.
14. Ledsham N.: https://www.sustainability.com/thinking/engaging-consumers-to-reduce-and-recycle/.
15. Hopewell J., Dvorak R., Kosior E.: Philos Trans R Soc Lond B Biol Sci., *364*, 2115 (2009).
16. McDonald S., Oates C.: Resour Conserv Recy, *39*, 369 (2003).
17. Klaiman K., Ortega D. L., Garnache C.: Food Control, *73*, Part B, 291 (2017).
18. Schumaker E.: https://www.huffpost.com/entry/psychology-of-why-people-dont-recycle_n_57697a7be4b087b70be605b3.
19. Sinai M.: https://recyclenation.com/2017/06/most-common-excuses-people-use-to-avoid-recycling/.
20. Lam M. M. L., Wong C. W. Y., Chan W. T. Y., Leung, C., Mei-chun C.: Resour Conserv Recy, *150*, 104402 (2019).
21. Wang Q, Long X., Li L., Kong L., Zhu X., Liang H.: J Clean Prod, *267*, 122046 (2020).
22. Czech Statistical Office: https://vdb.czso.cz/vdbvo2/faces/cs/index.jsf?page=vystup-objekt&pvo=DEMD001&z=T&f=TABULKA&katalog=33156&str=v4&c=v3~2__RP2020MP12DP31.

SYSTEM MODEL OF MAITENANCE DYNAMICS

Vytlačil D.

University of Chemistry and Technology, Department of Economics and Management, Technická 5, 16628, Prague 6
vytlacid@vscht.cz

Abstract

Facility maintenance became one of the most important factor which influences the profitability of companies with continuous production processes. Therefore, the facility management is the important task for the production department. The paper describes the sources of dynamics in this complex problem. The tool for the description is causal loop approach that identifies the back-loops. These loops include the planned maintenance and solving ad-hoc problems, it means repairs of defects in the production line. The management system has the features of operations management and project management. For both issues it is necessary to solve the problem of resources and costs. The dynamic model is designed as a system dynamics model where the main parameters are calculated. The key flows are the defect creation and the defect elimination by means of planned maintenance and through repairs. The model can help to find the strategy for both kind of maintenance and it can be used as education aid for understanding the dynamic of the described problem.

Introduction

The sources of dynamics it is possible to find in the external and internal system environment[1]. There are changes in the external environment as the change of technology, the change of machines, the changes in the supply chain (nowadays e.g. component shortage). This paper deals with internal environment such as the change of maintenance management system and particularly with resources setting.

The appearance of loops is another important feature of the problem. The example of the loops in the investigated problem is depicted in Figure 1. The existence of the loops creates the feedbacks in the system. Using this approach needs the change from event-oriented thinking to feedback system thinking[1]. By means of feedbacks it is possible to control the system[2]. The management system would ensure to reach the desired output.

The elements in Figure 1 create two basic loops – the first one describes the planned maintenance and includes the takedown rate and the second one describes the reactive maintenance with breakdown rate.

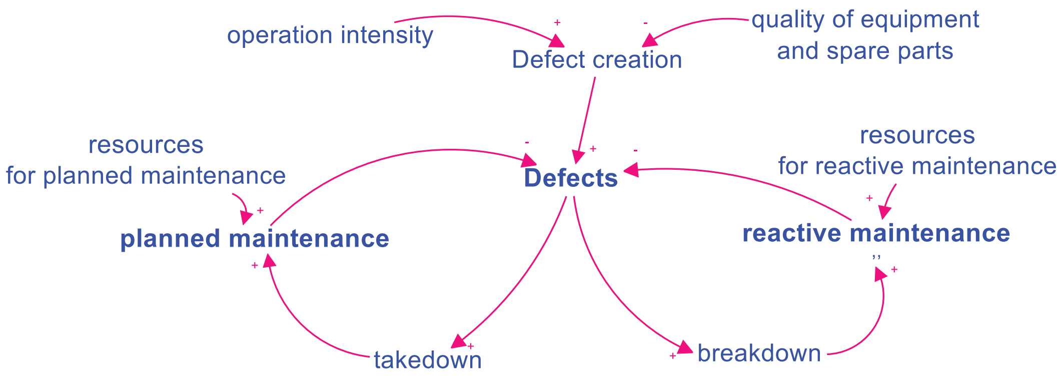

Figure 1. Loops in the investigated problem.

Methodology

The goal is to design the dynamic model that will be the basis for the proposal of the policy in the field of maintenance. The identification of the feedbacks is the first step for solving described problem. The next step is to design the adequate model for the calculation of the parameter values.

The model is based on system dynamics methodology that makes possible to connect the technical view with management issues of the problem. It includes stock elements for description of the key parameters and flow elements which will evoke the changes of the parameter values. Another elements are convertors that provide the auxiliary calculations or they can include the decision making process[3].

System model

The system dynamics model for above described problem is in Figure 2. Two main stocks are number of defects and number of workers available for the maintenance. The first subsystem describes the defect creation and defect elimination in the production plant[3]. It depends on the plant size and exploitation of the technology. The elimination of the defects depends on the planned maintenance and the reactive maintenance (repairs of broken machines). The maintenance effort is strongly connected with the second subsystem – number of available resources, in this case workers. The resources can include also components or overhead materials (e.g. cleaning liquids). Initially, only workers for planned maintenance are considered, but as number of defects is increased, breakdowns will occur and the part of the workers are moved for the repairs. After repairs they are moved back to basic stock.

Important feature in this system is the delay. The repairs will take time and also it is useful to consider the time for new workers training. All these parameters will influence the dynamics of the system and will cause low predictability of the system behavior.

In Figure 2 is the model for continuous maintenance. It means that every day same part of the production line is under maintenance. Another possibility is to do the maintenance according the schedule in certain days or weeks. In this case, the structure for defect elimination through planned maintenance is depicted in the left bottom corner of the Figure 2.

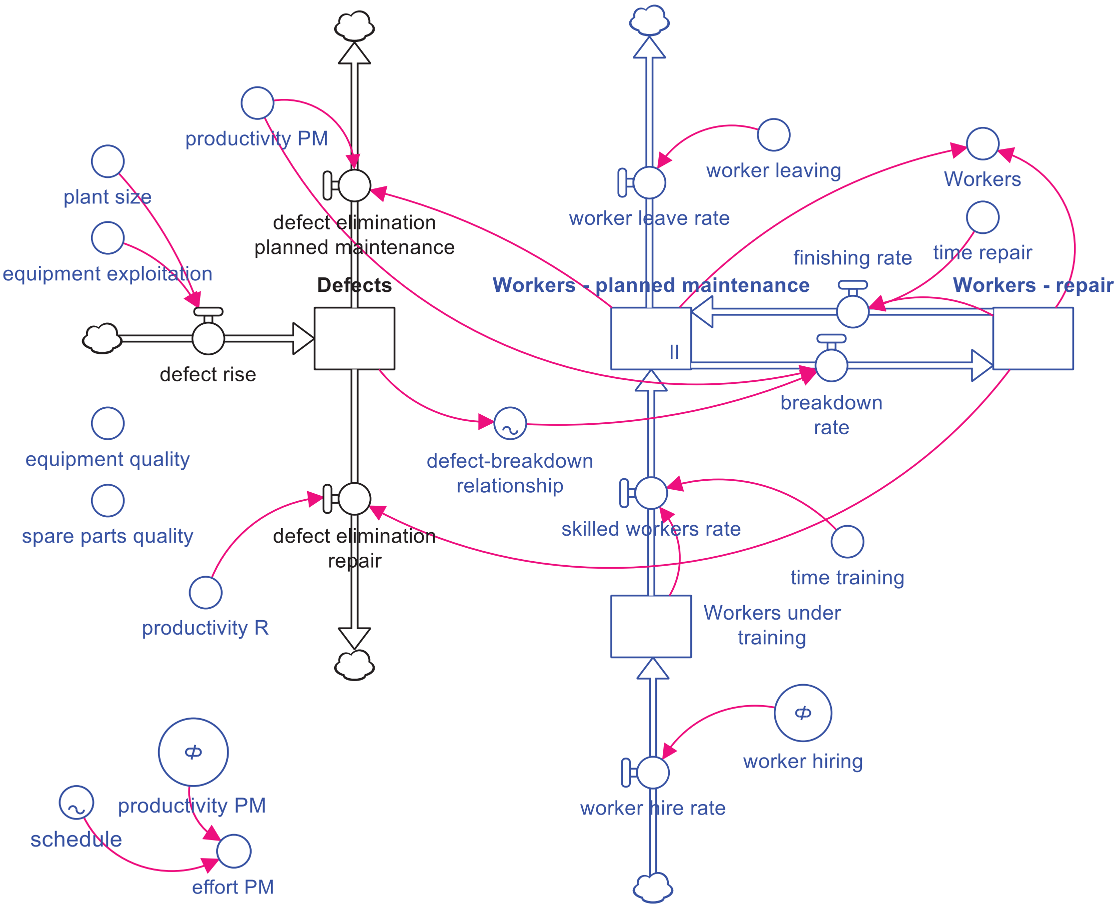

Figure 2. Dynamic model.

Results and discussion

Two models were used for the simulations with the goal to find relationship between manpower and defect elimination for continuous and intermittent supply of maintenance. The graphs in Figure 3 and in Figure 4 present results for continuous supply of maintenance. Two extreme cases were chosen – the initial condition with estimated number of workers and with number of workers which ensures zero defect during one year. Input and output values for both cases are in Table I.

Table I
Input and output parameters values

Parameter	Case 1		Case 2	
	Initial value [-]	Final value [-]	Initial value [-]	Final value [-]
Workers	10	15	10	92
Workers - planned maintenance	10	13.2	10	92
Workers - repairs	0	1.8	0	0
Workers under training	10	12	10	12
Worker hiring	5	5	5	12
Worker leaving	5	5	5	5
Defects	100	801	100	0

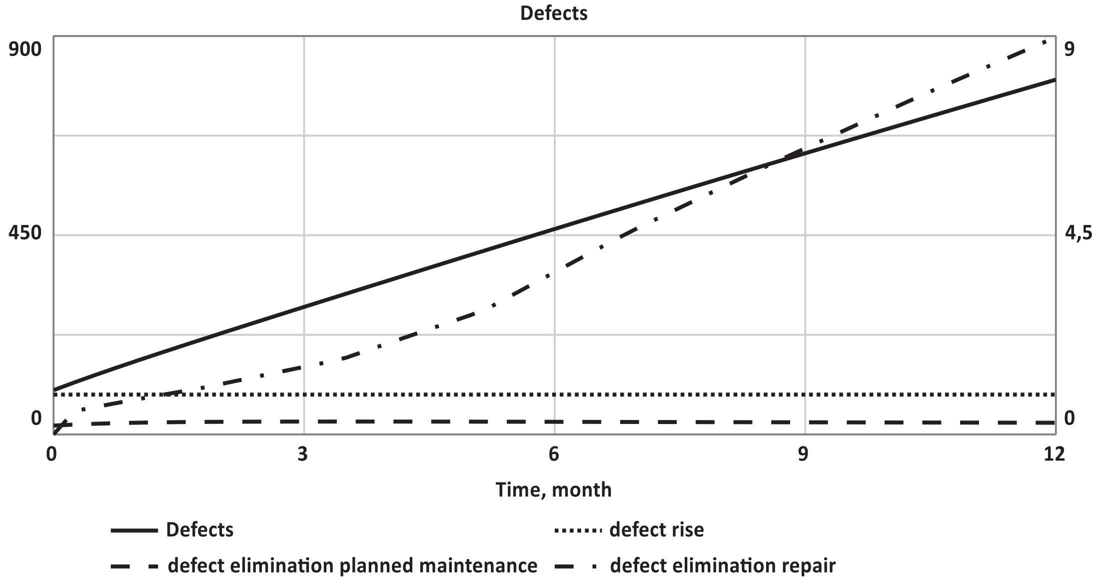

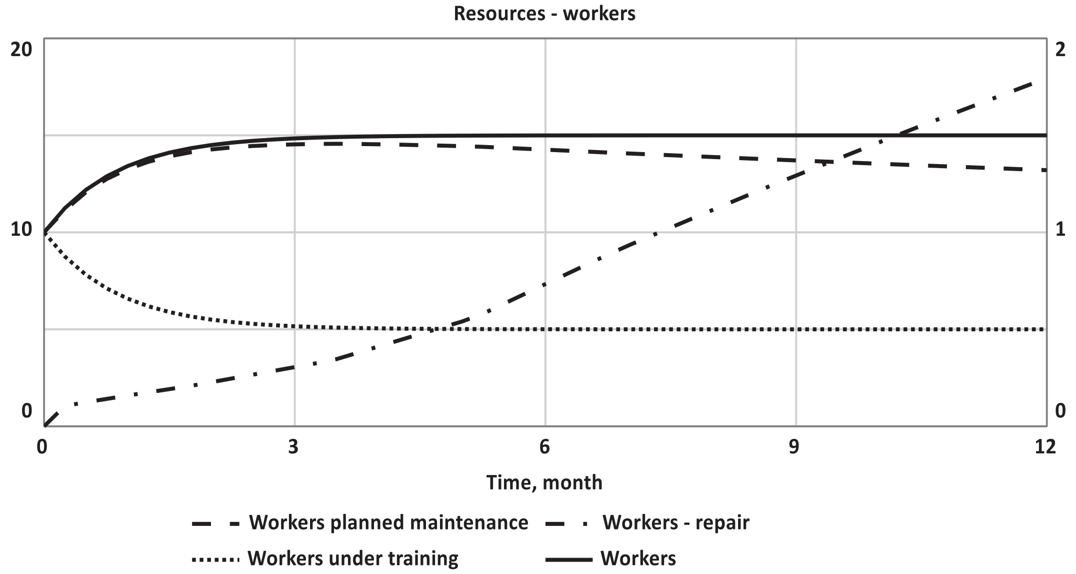

Figure 3. Number of defects and resource using for the case 1, initial conditions (right axis – defects eliminated by repairs and workers used for repairs).

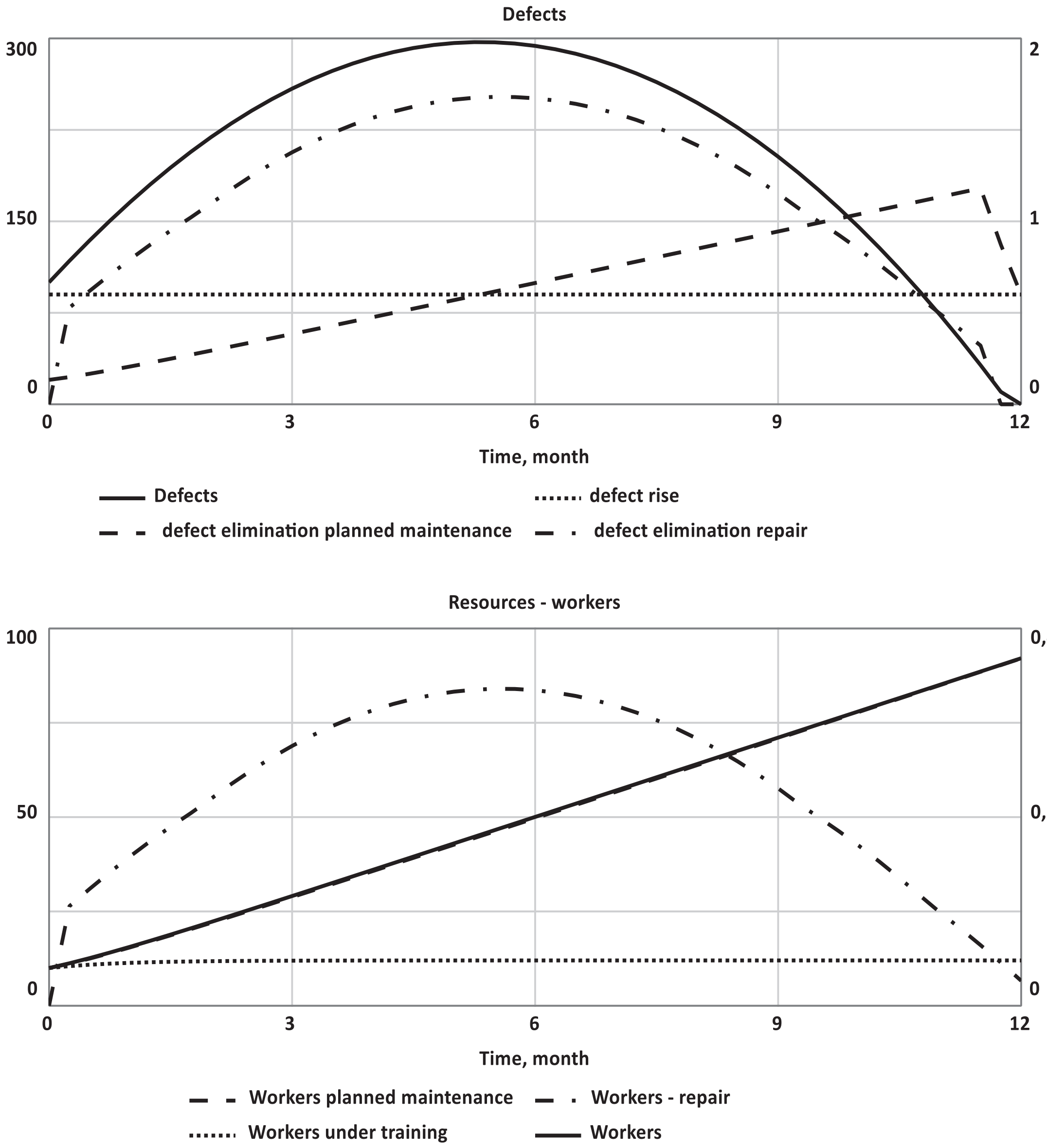

Figure 4. Number of defects and resource using for the case 1, changed conditions (right axis – defects eliminated by repairs and workers used for repairs).

The results in Figure 3 describe the situation when the capacity for the maintenance is estimated at 10 workers and 5 new workers is hired per month. The same number of works leave the company. The result is higher number of defects (8 times more than in the beginning). The second case is calculated with the aim to achieve zero number of defects by means of higher hire rate of maintenance workers. The value is 12 workers per month. The total number of workers is 92 compare to 15 in the first case, see Figure 4.

The simulation was performed also for discontinuous maintenance as it was described in the past paragraph. In this case the maintenance is done only one week every month and the hire rate is 18 workers per month for zero defect demand.

Conclusion

The presented results are only examples of all possible simulations. The dynamic model can be used for testing strategies for the management system, the capacity of resources, the allocation resource strategies etc.

The important question is what is it the long time goal in this problem. The result - zero defects – can be difficult to reach in practice. It is also evident that the model needs to consider costs because users require to compare the output (e.g. number of defects or breakdown time) to the expenditures. To find the balance between equipment reliability and maintenance costs is very important. Another significant factor for decision making is the amount of the investment costs which is associated with the equipment quality[4].

The developed model is good tool for understanding the basic principles of maintenance dynamics and can be used for the education as management simulator when managers or students of management learn the consequences of their decisions. The relative simplicity is the advantage for the system behavior investigation but the presented model can be considered as the basis for the next development. In this problem it is the introduction of another elements that are connected with the costs and profit items or with the logistic issues. The system modeling together with optimization methods can also provide new findings.

References

1. Morecroft J.: *Strategic Modelling and Business Dynamics – A Feedback Systems Approach*. Wiley, Chichester 2008. on 2000.
2. Pidd M.: *Tools for Thinking – Modelling in Management Science*. Wiley, Chichester 2000.
3. Sterman J.D.: *Business Dynamics – System Thinking and Modeling for a Complex World*. McGraw-Hill, Boston.
4. Plat H.: *The Economics of Property Management*. Butterworth Heinemann, Oxford 2001.

LIMITS AND BARRIERS TO PRODUCT LIFE CYCLE MONITORING FOR CHEMICALS – A CASE STUDY

Vavra J., Hemelikova M.

University of Pardubice, Studentská 95, 532 10, Pardubice
Jan.vavra@upce.cz

Abstract

Monitoring the product life cycle and the introduction of the eco-design principle is a prerequisite for the effective implementation and enforcement of the circular economy concept. The presented paper focuses on the issue of the possibility of monitoring the life cycle of chemicals with emphasis on the ability to monitor chemicals in the value chain. Finding out the possibilities of life cycle monitoring of a selected chemical substance – basic inorganic acids – are presented and the limitations and limits of life cycle monitoring of chemical substances for the needs of the circular economy are discussed.

Introduction

Today, society is increasingly aware of the need to better protect the environment and strive for its sustainability. One of the priorities on the path to sustainability is a higher rate of cyclical use of materials and products, which is promoted within the concept of Circular Economy[1]. It is an effort to better monitor the life cycles of products and, in the end, to minimize irreversible forms of its termination in the form of storage, discharge or incineration[2]. During its existence, each product enters several important phases with different impacts on the environment[3]. The product life cycle includes the following phases: raw materials extraction and treatment for the production, design & production, packaging & distribution, use of the product and final disposal of the product[4]. Understanding the potential environmental impacts at each stage of the product life cycle helps to make decisions about the technologies and products that have the least environmental impact and facilitates circular material management[5].

The Life Cycle Assessment - LCA method has been used for many decades to understand life cycle impacts, which makes it possible to identify and quantify environmental impacts[6]. LCA is a standardized method of evaluating impacts based on, defining the objectives and scope of the study, inventory analysis, the impact assessment itself and the final interpretation[7]. However, the ability to track the product throughout its life cycle is crucial to performing the analysis. The post-production phases of the life cycle are especially important for the needs of the circular economy, but especially in these phases it is often difficult to monitor the product and data collection is demanding and expensive[8].

Monitoring the product life cycle in the post-production phases involves packaging & distribution, use & maintenance, and finally product disposal[7]. It is the decision on the form of disposal, or the ability to reuse or recycle, that is crucial for defining the benefits for the circular economy. Efforts to achieve recycling, where the product is processed into materials or products or substances for new uses, which may be for original or new purposes, are highly desirable[9]. Recycling is not always financially advantageous, and therefore the possibility of reusing the product without the need to change its properties is often explored in the design process (stage) of product[10], which is important for circular use, but often unattainable due to product consumption[11].

It is highly desirable to support the concept of circular economy in the chemical industry - the production of many chemicals is very expensive, energy-consuming, using non-renewable resources with a high Carbon Footprint values[12]. However, the monitoring of chemicals in the post-production phases is very specific. Chemicals are often very dangerous and are subject to strict legislation on the part of their mandatory registration[13], evaluation and authorization - especially REACH measures, etc., which seemingly helps to monitor the product. However, they have many multipurpose uses in industry and in households, and an important aspect of chemicals is that they are often the basic input for further production, changing their composition, state and properties and therefore very difficult to monitor. Even during the use (without further chemical transformation), they often dissolve, evaporate, or they become part of other products (solvents, coatings, additives, pesticides, fertilizers, cleaning products, etc.)[14]. For these reasons, monitoring chemical products is significantly more difficult than most other products, which do not change their composition during use. The degree of ability to monitor chemicals has been the goal of several previous studies, however, these are marginal and partial outputs in the field of metal elements and materials, plastic or paper products, not basic chemicals [15, 16, 17].

On the basis of prior researches [18, 19, 20], we expected, that chemical companies within EU space are not able to follow life cycle of chemicals for several reasons: (1) unclear use of the product by the final consumer (2) transformation of the product into another substance (3) association of the product with another product with uncertain life cycle post-production phases and (4) difficulty and low motivation to monitor the product in the post-production phases.

As a result of our theoretical study and assumptions we formulate three business case goals to confirm:

BC Goal 1: The contribution of basic chemical substances to the circular economy is limited by the ability to monitor the product life cycle.

BC Goal 2: Businesses do not have an overview of end consumers or end uses of basic chemical substances.

BC Goal 3: Businesses do not feel the needs / motivation to monitor the life cycles of chemicals.

Method and design of the case study

Academic researches and studies from relevant fields of research, LCA theories and product life cycle guidelines are used to address the validity of theoretical problems and assumptions concerning expected reasons to follow and assess life cycle of chemicals[21]. Previously realized analysis suggests that the chemical industry (unlike other sectors) has not been significantly affected by the effects of the COVID19 + epidemic[22] and companies can devote their efforts, sources and time to developing environmental activities and understanding their consumers[23].

Based on theoretical basis were realized structured one-to-one interviews with managers of chemical company producing basic inorganic acids. To achieve business case goals, qualitative research was carried out at the manufacturer of basic inorganic acids. Selected chemicals - nitric acid and sulfuric acid are considered to be basic inorganic compounds with a wide range of uses for both direct consumption and further processing. Primary sources at the manufacturer (interview, business information, trade statistics, etc.) were selected as a source of information, and customers of this chemical were also interviewed through peer-to-peer interviews to find out and confirm additional information.

The respondents were business managers and marketing managers of the company. The research was carried out in the period September 2020 - November 2020. Information obtained was processed using content analysis. The first set of questions inquired into the structure of customers, knowledge of the end use of the products sold and the volumes of products sold on average per year. The second set of questions investigated company's effort to follow and assess life cycle of chemicals. The third set of questions focused on motivation and abilities to monitor and assess the life cycles of chemicals.

The company's key customers include mainly manufacturers of paints and inks, dyes for the textile, paper and leather industries. Furthermore, the company is one of the major manufacturers of products for pharmaceutical companies, manufacturers of agrochemicals, cosmetics, ammunition and explosives and more. The company's production is focused on three quarters for export to developed European markets or overseas. The main export territories include the USA, Germany, Italy, France and Poland.

The field of inorganic compounds was chosen for qualitative research because they have a wide and different applicability in the subsequent production stages or other chemical transformations. Based on a preliminary survey, two basic inorganic acids with a wide range of customers and different uses - nitric acid and sulfuric acid - were selected for more detailed life cycle research and potential monitoring.

Research findings

For both acids, the ratio is 1: 1 to foreign and domestic customers, of which there are approximately forty. Customers are usually regular, there is constant communication with customers about possible changes in the range or modifications, but the company does not produce any special modifications according to customer requirements. Production is stable for a long time, which is mainly due to the quality of raw materials and the production technology used. Nitric acid is produced in the company concentrated and diluted (concentration 53%). Up to 80,000 tons are produced annually, of which about 20,000 tons remain for internal use. Sulfuric acid is produced in the company mainly as a technical acid in a concentration of 94-98%. Up to 55,000 tons are produced annually, of which about 15,000 tons for internal use.

The first set of questions was directed to determine the ability to monitor the product life cycle. The responses agree that despite their simplicity in terms of use and application, selected chemicals can be monitored with high difficulty, which does not balance the benefits of the information thus obtained. By forming various salts, oxides, mixtures or complexes from acids, it is almost impossible to say when the monitored product ceases to be an acid - its own product, and thus when its life cycle ends. A simplistic view is acceptable to the company that the acid will terminate its existence at the moment of entering the customer's plant, although in reality it may continue to be in its chemical nature and be subsequently resold.

The second set of questions investigated the level of knowledge of consumers or end uses of both inorganic acids. Although the company does not monitor the life cycles of chemicals, dealing with customers identifies their needs and product requirements. In addition, safety data sheets are issued for both acids in the sales process, where the expected scope of use of these substances is defined. For many customers, information on the end use of the product (or about the final consumer) is obtained during negotiations. The responses estimate that for up to 80% of the production volume, the company can monitor where the product is used and can derive from about 60% what is probably created from the product. It was confirmed that the company knows this information for its key customers, who consume most of the production, as shown in Figure 1 for nitric acid and Figure 2 for sulfuric acid.

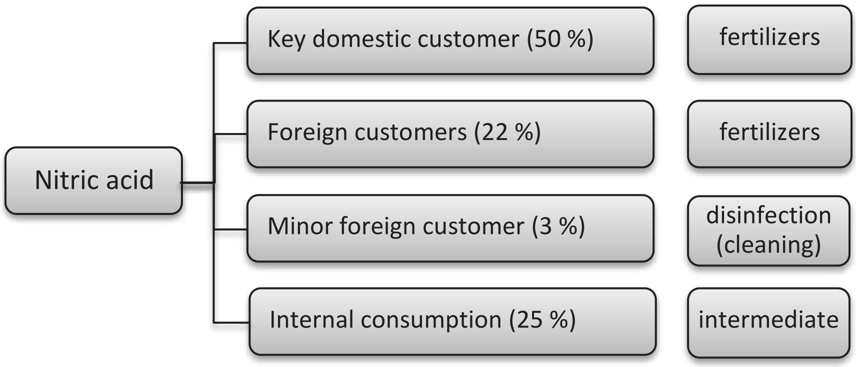

Figure 1. Estimated customer structure (shares and utilization) – Nitric acid

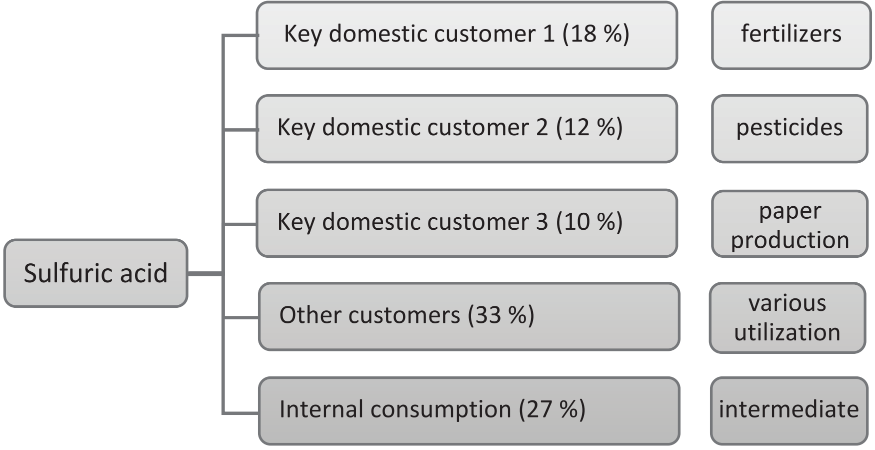

Figure 2. Estimated customer structure (shares and utilization) – Sulfuric acid

The stated percentage distributions show a significant proportion of key customers, for whom the purpose of use and usually also the end user is always known. It is also clear from the end use that most of the production is irretrievably consumed. It is also clear from the end use that most of the production is irretrievably consumed. From the mentioned uses of both substances, it is clear that they are mostly used for further production and thus end the life cycle in their original composition. Only for the use of nitric acid for cleaning (3% of production) does this compound remain in its original structure, although heavily contaminated.

The third set of questions focus on motivation or needs to follow and assess product life cycles by company's management. Respondents stated that they do not need to monitor the life cycle of their products and do not consider it as a common practice in the industry. This information is not important to them, not even from the marketing point of view, when they could get feedback from customers or end consumers, or from an environmental point of view. They consider the monitoring of chemicals to be very difficult, costly and inefficient compared to the usability of this information and/or other benefits. In general, monitoring is considered impossible for most chemicals; respondents are of the opinion that chemicals do not go through real cycles in which it would be possible to recycle or otherwise use part of the product. For these reasons too, they consider life cycle monitoring of these substances to be ineffective.

Discussion and result analysis

When monitoring the life cycle of chemicals, there are a number of objective (but also subjective) limits and barriers. One of the most important barriers is the multipurpose widespread use of these substances for subsequent production. In subsequent productions, the chemical composition of substances usually changes - only a very small proportion of production is directly consumed by the customer as a final utilization. Manufacturing companies also do not have a complete overview of the end use of chemicals, which can be directly utilized, used as materials or resold. However, the assumption formulated for the second objective of the Business Case was not confirmed; businesses know to a large extent the final consumers and the intended use of the products. The reason is the increased intensity of negotiations and the long-term relationship with key customers, who purchase most of the production. The use is clarified with these partners, which, however, means the end of the life cycle of the original product. Last but not least, the prevailing opinion among management representatives is that it is possible to identify only low benefits from life cycle monitoring compared to the cost of obtaining this information. Thus, the assumption was made that life cycle monitoring is not important for the manufacturers, the motivating or economic relevant factors are not known, although tracking product along the life cycle could be used to increase the company's image, e.g. due to increased environmental performance.

Conclusion

During the qualitative research, the complexity and even impossibility of monitoring chemicals along the life cycle was confirmed. Unlike mechanically produced products, chemical products change their composition and structure and it is difficult to define the life cycle on its own. Although the management of chemical companies knows its customers and the intended use of its products, it cannot follow the life cycle beyond the gate of the customer's plant.

Despite their simplicity in terms of use and application, selected chemicals can be monitored with high difficulty, which does not balance the benefits of the information thus obtained. A simplistic view is acceptable to the company's management that the acid ends its life cycle when it enters the customer's plant, although in reality it may continue to occur in its chemical nature and be subsequently resold.

The acids sold are most often used for the production of other compounds. By forming various salts, oxides, mixtures or more complex complexes from acids, it is almost impossible to say when the monitored product ceases to be the acid - its own product - and thus when its life cycle ends. The life cycle of the original substance thus ends in terms of its original chemical structure. It can be stated that at present there are not enough motivating factors to monitor product life cycles and it is also not considered as a common practice in this industrial sector.

Acknowledgement

This work was supported project "Research in Significant Areas of Environmental Engineering and Sustainable Innovation Management" No. SGS_2021_003.

References

1. Webster K.: Circ. Econ. Sustain., In press (2021).
2. Kloepffer W.: Int. J. Life Cycle Ass. *13(2)*, 89 (2008).
3. Kočí V.: *Posuzování životního cyklu Life Cycle Assessment - LCA*. Ekomonitor, Chrudim 2009.
4. Jacquemin L., Pontalier P.-Y., Sablayrolles C.: Int. J. Life Cycle Ass. *17*, 1028 (2012).
5. WBCSD: *Life Cycle Metrics for Chemical Products* [available online: https://www.wbcsd.org/cU5j] - [cit. 2020-12-19] 2014.
6. Remtová K.: *Posuzování životního cyklu - Metoda LCA*. Ministerstvo životního prostředí, Praha 2003.
7. Int. Org. Stand.: *Environmental management—life cycle assessment—principles and framework*. Stand. 14040, Int. Org. Stand., Geneva 2006.
8. Archodoulaki V. -M., Jones M. P.: Resour. Conserv. Recy. *168,* 105333 (2021).
9. Nußholz J.L., Whalen K.: IOP Conference Series: Earth and Environmental Science, 225, 0120422019 (2019).
10. Kleinekorte J., Fleitmann L., Bachmann M., Kätelhön A., Barbosa-Póvoa A., Von Der Assen N., Bardow A.: Annu. Rev. Chem. Biomol. Eng. *11(1)*, 203 (2020).
11. Zyma O., Stefanski R., Golub M.: Econ. Dev. *19,* 13 (2020).
12. Wada Y.: J. Life Cycle Ass. Jpn. *6,* 201 (2010).
13. Carson P., Mumford C.: *Hazardous chemicals handbook*. Butterworth-Heinemann, Boston, 2002
14. Voigt K., Benz J., Matthies M., Mücke W.: Inf. Serv. *Use. 10*, 215 (1990).
15. Tabone M. D., Cregg J. J., Beckman E. J., Landis A. E.: Environ. Sci. Technol. *44,* 8264 (2010).
16. Grossmann I. E., Drabbant R., Jain R. K.: *Chem. Eng. Commun. 17,* 151 (1982).

17. Yamada E.: J. Life Cycle Ass. Jpn. *2,* 363 (2006).
18. von der Assen N, Voll P., Peters M., Bardow A.: *Chem. Soc. 43,* 7982 (2014).
19. Parvatker A.G., Eckelman M.J.: *ACS Sustain. Chem. Eng. 7,* 350, (2018).
20. Simon B., Bachtin K., Kiliç A., Amor B., Weil M.: Integr. Environ. Assess. Manag. *12*, 465 (2016).
21. Zamagni A.: Int. J. Life Cycle Ass., *17*, 373 (2012).
22. Vlcek D., Kostalova J.: Economic analysis of the chemical industry of the Czech Republic in the period of economic growth. Hradec Economic Days, 2.-3.4.2020, Hradec Králové, Czech Republic, 848 (2020).
23. D’ Astous A., Legendre, A.: Understanding Consumers’ Ethical Justifications: A Scale for Appraising Consumers’ Reasons for Not Behaving Ethically. J. Bus. *Ethics. 87,* 255 (2008).

GREEN HUMAN RESOURCE MANAGEMENT IN COMPANIES OF CZECH CHEMICAL INDUSTRY

Bednarikova, M.[1], Kostalova, J.[2]

[1,2] *Univerzity of Pardubice, Faculty of Chemical Technology, Pardubice, Czech Republic*
Jana.Kostalova@upce.cz

Abstract

Green human resource management (GHRM) includes specific human resource (HR) policies, procedures and measures in compliance with the sustainability pillars – environmental, social, and economic. Success of these measures depends, to a considerable extent, on the employees and their so-called green behaviour. Most employees feel co-responsible for the environment and show stronger determination, and loyalty to employers going a “green way” and taking an active part in support of the environment. As a result, GHRM can help companies implement measures decreasing the environmental impacts. This paper focusses on chemical companies and emphasises the irreplaceable role of their HR in implementation of Green HRM procedures and principles. The research was aimed at the environmental pillar of GHRM and examined its fulfilment in the practice of chemical companies in the Czech Republic (CZ). The paper aims to identify the rate of incorporation of GHRM-oriented activities into the main corporate HR activities.

Introduction

Human resource management can be defined as a strategic approach to management of the most valuable item companies have – their employees. These people contribute, both on an individual and on a team basis, to achievement of corporate targets. Each company has the same priority: to hire, to retain, and to utilize capable and active employees. Work with human resources (HRs) is not only a job of the HR department, but it is also an everyday integral part of the job of each manager in the company. Companies do not focus on their own business activities only, but they are more and more involved in some other activities beyond their own business. They more and more often face problems threatening not only them, but also the mankind as such (climatic changes, migration, economic crises, pandemics, etc.). This results in the necessity of behaving socially responsibly. Leading companies are now finding a modern and key strategy in Green Human Resource Management (GHRM). In the current globalized world, the environmental awareness affects both dimensions of our lives, working and living. Our lifestyle has such adverse effects on the environment that it is necessary to change our approach. It is definitely less painful than facing the consequences of our behaviour. GHRM includes specific HR policies and procedures in compliance with the three sustainability pillars – environmental, social, and economic.

Literature review

Environmental problems are becoming hotter and hotter issues, which induces big worries about sustainable development of the environment (Priyankara, Luo, Saeed et al., 2018). The environment is degrading fast as a result of natural resource depletion and other human impacts. To slow down fast degradation of the environment, it is necessary that governments and companies take effective countermeasures. Due to the harmful effects of industrial pollution, the whole world is trying to slow down, and to a certain extent to turn, destruction of the natural resources, the environment, and thus to reduce the negative impacts on the mankind (Shrivastava & Berger, 2010). Successful implementation of sustainable corporate strategies in the social, economic, and environmental areas requires clear definition of the means and processes that might help to achieve it (Glavas, Senge & Cooperrider, 2010). Success of such measures depends, to a certain extent, on the employees and their green behaviour. The practice shows that most employees feel responsible for the environment and show stronger determination, job satisfaction, and loyalty to their employers going the ‘green way’ and taking an active part in the support of the environment.

Changes in corporate perspectives relating to environmental initiatives can be found in different written declarations and principles, names of jobs in the area of the environment, marketing strategies, auditing procedures, design and development of new products, and manufacturing processes (Sharfman & Fernando, 2008). The efforts of GHRM lead, among other tangible advantages, to increased effectiveness, lower costs, employee retention, and improved work efficiency. To achieve the desired performance with respect to the environment, it is not enough to rely on implementation of GHRM only, but what is also necessary is pro-environmental behaviour of the employees of the company (Rubel, Kee & Rimi, 2021). Green behaviour of the staff in the workplace and their personal moral norms can also be called pro-social behaviour. GHRM joins performance of an employee and procedures of environmental management, and Green Talent Management becomes an important prerequisite for the company's survival and success. GHRM plays a dynamic role in policy formulation, law implementation, and support of awareness campaigns for the purpose of training the staff in the essential importance of environmental protection. As a result, it can help companies to decrease devastation of the environment and make it possible for them to be both physically and financially healthier. HR plays an irreplaceable role in implementation of GHRM procedures and principles. It plays the main role in recruitment of new employees that are more responsible towards green business practices, and employees are stimulated to accept environmental procedures for greener business. GHRM is the most important element of sustainability (Ahmad, 2015). Although implementation of a responsible approach into corporate strategies and their fulfilment is important, it does not arise by itself. What is the principal element is the staff – be they corporate executives, managers, or ordinary employees – and unless they are cultivated and directed at a responsible approach, the company can hardly be responsible as such. A businessman that is not environment-oriented will not implement GHRM, and employees that are not educated in this area and do not espouse it will hardly be able to put it in practice.

Nowadays, GHRM does not only include awareness of environmental issues, but it also means social and economic balance of the company and the employees from the point of view of a wider perspective. It is directly responsible for creation of the "green labour force", which understands, appreciates, and practises the green initiative, and maintains its green targets within the entire process HR management (HRM) recruitment, acceptance, education, and development of the company's human capital. Important policies in the areas of recruitment, performance and management of assessment, staff training and development, staff stimulation, employee relations, and remuneration systems are considered as strong tools of harmonization of the employees with the corporate environmental strategy. It is important to maintain environmental HR procedures and the knowledge capital. It is necessary to direct the employees' behaviour at the environmental issues, inform them about the complexity of environmental protection management. They are then able to understand and appreciate the green culture in the company, and they play an important role in creation of the sustainability culture in the company. GHRM stimulates the company's staff, and then they create and strengthen the corporate environmental culture. It stimulates the employees' responsible behaviour and their approach and commitment to the environment (Ansari, Farrukh & Raza, (2021).

One of the bottlenecks of HRM is the staff turnover. The corporate social responsibility (CSR) ideas recommend that the staff recruitment process is not considered as a mere formality, and so it is possible to make use of **green recruitment**. If a company has taken the green way, it is logical that such a company will mainly be looking for applicants with pro-environmental feelings, who will be able to identify with the company's way. Environmental activities and CSR help companies to achieve a competitive advantage and sustainable performance. Environmental activities help to attract talented, hardworking, and qualified workforce, while CSR creates a good corporate image in the eyes of the stakeholders, it improves the brand image and solves the company's problems. Effective implementation and strengthening of environmental measures significantly depend on the employees' approach to the organizational citizenship behaviour towards the environment (OCBE) (Priyankara, Luo, Saeed et al., 2018).

Acquisition of the reputation of a green employer is an effective way how to attract new talents (Phillips, 2007). The recruitment documentation includes green descriptions of jobs with environmental aspects. It is a process of acquiring employees with the knowledge, skills, approaches, and behaviour that enables them to identify with the company's environmental management systems. This can ensure that new employees will easily become acquainted with the company's environmental culture and will be able to maintain its environmental values. The company will acquire new employees who are aware of sustainable processes, such as reuse, recycle, reduce, and repair.

Performance management is a process enabling employees to improve their professional skills that help to achieve the corporate targets better. **Green performance management** also focusses on utilization of the responsibility for the environment. Apart from fulfilment of the reliability and performance criteria, it also provides a useful feedback and supports continuous improvements of the company's environmental results.

Employee assessment should include an assessment dialogue, where both parties can clarify a lot of things. When making assessment, the attention should be paid not only to the employee's performance as such, but also to their work behaviour and personality traits. When assessing performance, it would also be suitable to focus on environmental accidents, responsibility for the environment, communication of the environmental policy, and the green information system and audits. A job description should follow green tasks and targets to be reached. HR department staff should modify the performance assessment system in the way to include evaluation dimensions in the following behavioural and technical competences: teamwork, cooperation, diversity, innovation, and environmental protection (Liebowitz, 2010).

The current market environment is developing very dynamically. Employees thus often face a situation where it is necessary to innovate their knowledge and skills partly or completely. Staff education and development is not cheap at all. However, if a company can afford it, it is the best investment they can make for themselves. For one thing they maintain the current staff abilities and skills at the desired level, and for another they also, by doing so, achieve the stimulation target of the assessment, where it is possible to use the employee potential optimally and, at the same time, to fulfil their own longing for self-perfection and personal development. A company going the green way naturally also includes education in the area of environment in this process.

Green education and development improve the employee awareness of the value of environmental management, train them in work methods saving energy, reducing waste, spread environmental knowledge within the company, and they provide the employees with the opportunity to get involved in solving environmental issues. They help them to become acquainted with various environmental protection methods, including waste management in the company. In addition to that, these employees will then be able to educate the customers as for the advantages of environment friendlier shopping and purchase of green products.

Incentives and bonuses can greatly affect the employee attention in the workplace and instigate them to exert maximum efforts to achieve the corporate targets. They join the interest of the individual and the interest of the company. This is why they can also be considered as potential tools supporting environmental activities in the company. The company can link the remuneration system to the support of environmental initiatives commenced by their employees, or it can be presented as compensation for the acceptance of obligations relating to the responsibility for the environment (Ahmad, 2015). If the **green bonuses** are harmonized with the process of HRM, they will then support the green culture in the company. Similarly, the company could remunerate their employees for prosocial activities.

In fact, positive relationships with employees are intangible and permanents assets and a source of a competitive advantage of each company. The level of employee relationships depends on the fact whether there is mutual confidence between the employees and the employer or not, whether the employer acts equitably and openly or not, whether the employer cares about harmonic relationships in the workplace or not, whether the employer can solve potential conflicts to satisfaction of all involved parties or not, whether the employees are loyal to the company's interests or not, and whether the company's management acts with the employees as with the stakeholders whose interests should be protected as much as possible or not (Armstrong & Taylor, 2015). The basis of good relationships in the workplace is clear, open, honest, and partner communication in the workplace, in the entire company, and towards the external environment (Munzarova et al., 2016). Communication must be conducted in all directions and in the atmosphere that the employees are not afraid to express their opinions openly. Involvement of the employees in the company's green activities increases the chance of better green management (GM), it harmonizes the employees' targets, abilities, motivations, and perceptions with the GM procedures and systems. It can lead to more effective utilization of machinery, reduction of waste, or to pollution reduction. Involvement of the employees has positive effects on their performance, and it facilitates their self-control, individual thinking, and skills when solving problems (Wee & Quazi, 2005).

Employers must create a participative work environment, where their employees can freely assert their opinions on environmental issues, but also on social problems, i.e. to enable **green employee relations**. Achievement of green results depends, to a significant extent, on the employees' willingness to cooperate (Collier & Esteban, 2007). Each employee, from the top to the bottom levels, must get a chance to contribute to the GM system somehow. This is the only way how to obtain new ideas from different sources. Another advantage of employee involvement is improvement in their health, an increase in safety at work, and development of eco-staff. Confidence between the company management and its employees must be built up on a long-term basis.

If a company intends to implement any initiatives, it is first necessary to consider thoroughly what its target in the given area is. The second step that must be made is to enthuse their employees with this initiative. The thing is that it is them who decide how the given initiative is put into practice. And a similar situation is in the environmental area. Companies are now implementing environmental initiatives in their administration through their HR. Technical and managerial skills of all company employees must lead to a more effective corporate GM system (Daily, Bishop & Govindarajulu, 2009). However, this means a change in the approach to the existing HR procedures both on the part of the management, and on the part of the employees. HR department must train the staff to be supporters of the environmental approach and create networks of problem solvers willing to discuss a change of the status quo.

The main **green initiatives of the HR department** are a green building – an alternative to traditional offices reducing natural resources in construction and use; a paperless office – reducing or eliminating the use of paper; energy saving – including a reduction in energy consumption or utilization of energy from renewable resources; waste recycling and disposal – utilizing used materials or working on the principles of the three R's: reduce, reuse, and recycle (Ahmad, 2015).

Methodology

This paper focusses on chemical companies and emphasises the irreplaceable role of their HR in implementation of GHRM procedures and principles, focussing on the environmental pillar of GHRM. The paper draws on literature reviews of secondary sources. Based on the definition of the term of GHRM and its partial forms of fulfilment, its fulfilment in practice was evaluated. The authors focussed on chemical companies in the CZ, where the situation is, according to the available sources, stabilized from the economic point of view (Kraus and Spicka, 2013; Vlcek and Kostalova, 2020), and activities leading to social responsibility, responsible behaviour in the area of environmental protection, and to active HR have already been confirmed by a lot of practice analyses (Tetrevova et al. 2017, Bednarikova and Kostalova, 2019). Within the research, the authors examined GHRM fulfilment in the practice of chemical companies in the CZ. The paper aims to identify the rate of incorporation of GHRM-oriented activities into the main corporate HR activities - recruitment and selection of new employees who are more responsible towards green business practices, stimulation of employees to accept environmental procedures for greener business, education for a responsible approach, bonus allocation, and implementation of some initiatives for human resources. The research was conducted through a questionnaire, where the respondents were HR managers of the selected chemical companies in the CZ.

Results

Our research was focussed on the problems of GHRM and its implementation in corporate practice. Chemical companies had the possibility of responding to our questionnaire online and sharing their experience and opinions about the viability of GHRM in their companies with us. The possibility was used by 10 large companies (i.e. companies with more than 250 employees).

All the respondents confirmed that they comply with all the statutory procedures in the area of environmental protection. At the same time, they declared that they also perform, in addition to the statutory ones, other activities for the public beyond their business activities: the most frequent one is support of sports activities – three companies support sports events in their regions, two respondents support sustainable projects, two run charities, and one of them always supports activities such as science education and cultural events, support of the adjacent town and villages, and cooperation with secondary schools and universities. Although all the companies are environment-oriented, the phase of staff recruitment and selection does not, with two exceptions only, include any questions concerning the job applicants' knowledge of the area of the environment. Although GHRM primarily focusses on the environmental protection, it also places emphasis on the economic prosperity of the company, and last but not least on the prosocial environment, where healthy, motivated, properly evaluated and remunerated employees can achieve the desired level of performance. Four respondents stated that their recruitment proceedings touch upon the social and economic pillars of sustainability.

The following part of the research dealt with the question whether and what green targets the companies set for their employees. The offered possibilities were chosen by the respondents as follows: waste separation in the workplace (supported by 9 respondents), use of a bicycle in the company and/or for travelling to and from work (8), reducing paper consumption in the workplace (8), reducing document printing and copying (8), reducing water waste (6), utilization of reusable packaging (4), defining procedures for electric energy saving in regular operations (4), using recycled paper (3), utilization of a shared car when travelling to and from work (2), another form of shared transport (2), and waste separation in the employees' households (2).

The respondents could also mention any other forms of green targets if they have any – no respondents used this possibility. The overview mentioned above shows that most respondents focus on waste separation in the workplace, reducing paper consumption in the workplace, reducing document printing and copying, and utilization of bicycles in the company and/or for travelling to and from work. As for bicycles, it is also utilization of bicycles when moving around the company at work, as they are large companies and bicycles significantly save time when moving between buildings inside the company. Utilization of recycled paper and support of shared transport are not very frequent in the given companies. The same low number of respondents (2) mentioned utilization of waste separation in the employees' households. However, this does not necessarily have to be caused by the fact that the employees do not separate waste in their homes, but by the fact that the company does not try to find out this information.

With one exception, all the companies provide their employees with education for a responsible approach aiming to develop knowledge and skills the employees are required to have. Six respondents declare that they touch upon this area within employee assessment. In view of the fact that employers consider observance of the environmental protection as an integral part of employee work performance, none of them reflects green behaviour of their employees in their remuneration.

The respondents answered the question whether their companies implement green initiatives in HR or not as follows: a green building has been implemented by none of them, a paperless office, utilization of green energy, and minimization of transport always by one of them only, water saving was declared by 5 respondents, energy saving by 7 respondents, and recycling and separated waste disposal by 8 respondents. None of the companies used the possibility of mentioning another initiative.

Sharing of environment-friendly knowledge was identified in a half of the companies involved in the research. As for this area, we can expect that employees of all the companies share information relating to performance of their work, and as a result of that they have an impact on the maintenance or improvement of the environment. Apparently, the companies giving an affirmative answer pay more attention to the fact whether their employees share the information or not. These companies state that such sharing takes place e.g. at meetings and workshops, during regular training (e.g. of new employees), within regular evaluation of environmental and CSR activities, or through an in-house magazine. With the exception of one company, the employees can make proposals or recommendations concerning improvements in this area. This happens through improvement proposals or comments, or they can put their proposals into a special box or hand them over to their superiors, or to the head of their environmental protection department. They can also propose a motion to a committee (Safety, Health, Environment and Quality), at departmental meetings, or at team or whole-company meetings. One respondent has a special programme of cost saving through good ideas, and one company has a permanent improvements department, where their employees can submit a proposal of saving, or improvement project. In such a case, successfully evaluated proposals are connected with financial remuneration. However, one respondent declared that their employees do not use this possibility, and five respondents wrote that it is used minimally. On the other hand, three respondents declared that their employees get involved quite often, and one of them that even regularly. Employees of six companies take the initiative to act in an environment-friendly way in the workplace by themselves, and all the respondents state that their employees accomplish the assigned duties specified in the job description adequately, in an environment-friendly way. As for the question about their employees' attitude to implementation of similar procedures, four respondents replied that it is positive, and six respondents indicated a neutral approach. A half of the respondents also declare that their employees use the opportunity to take an active part in the environmental protection beyond their job obligations. A half of the respondents declare that their employees are also involved in such activities outside the company.

A half of the respondents declare that they communicate the activities relating to the environmental protection through an in-house magazine, mass email, intranet, CSR reports, through mass media, or within training. Four respondents specify that they also communicate this information externally through an in-house magazine and company web pages, mass media, a magazine, or within the programme of The Green Company. The research showed that companies have, and use, a lot of ways how to inform their employees and external stakeholders about their activities.

Discusion

The research showed that chemical companies comply with the legislative requirements concerning environmental protection. Within the social responsibility and aiming to achieve sustainability, they also pay attention to activities beyond their obligations. They direct these activities towards the company, towards their employees, and towards their closest surroundings. In compliance with their green orientation, they also set green targets for their staff. The research showed that the green targets of most respondents include waste separation in the workplace, enabling the employees to use bicycles, trying to reduce consumption of paper in the workplace. The researched companies do not include green activities into the process of staff recruitment and selection, but they pay great attention to education of their employees for the responsible approach, and they try to develop their knowledge and skills they can use in their jobs.

As for implementation of green initiatives for HRs, the research showed that the companies mainly focus on recycling and disposal of separate wastes and on energy and water saving. On the other hand, none of the respondents has implemented a green building, and only one of them declares that they have introduced a paperless office, utilization of green energy, or minimization of transport, so there is a large space for extension. In view of the fact that 8 respondents state that they are trying to reduce consumption of paper in the workplace and to cut down on copying and printing documents, but only one has introduced a paperless office, it seems that the companies still have a large reserve in this initiative.

As they are chemical companies, compliance with the legislation in the area of the environment is a must for their employees. For this reason, the companies declare that this behaviour does not reflect in the employee remuneration system of the company. The companies have a lot of possibilities how to share green information (meetings, workshops, training, an in-house magazine, etc.). The employees can also (except for one respondent) make their own proposals and recommendations (e.g. in the form of improvement proposals or remarks). However, the research implies that the employees do not make use of these possibilities very often. Employees of some companies also take an active part in environmental protection beyond their job responsibilities and in activities outside the company (a half of the respondents stated this fact). However, the question is how active the companies are in finding out about these facts. The same number of respondents communicates their activities. This results in the fact that the information gets not only to their employees, but also to the stakeholders, and generally to the company's surroundings.

The research shows that the assessed companies set the basic GHRM conditions, but the activity of a large part of their employees is not very extensive in this area. Therefore, there is a space for more extensive incorporation of the GHRM procedures into the corporate activities, for consideration of the possibility of reflecting them in the employee remuneration system, for implementation of a larger number of communication tools, and for setting further green targets. We can conclude that there is a sufficient space for greater motivation towards green behaviour in the researched companies.

Conclusions

GHRM is becoming a modern and key corporate strategy. GHRM includes specific HR policies, procedures, and measures in compliance with all the sustainability pillars. This paper focusses on chemical companies and emphasises the irreplaceable role of their HR in implementation of GHRM procedures and principles. The research was aimed at the environmental pillar of GHRM and examined its fulfilment in the practice of chemical companies in the CZ. The paper aims to identify the rate of incorporation of GHRM-oriented activities into the main corporate HR activities. GHRM is being applied to the extent of mandatory activities, and some GHRM procedures, e.g. education in environmental protection or communication of such activities, have been implemented. However, the research discovered large reserves in implementation of green activities in the corporate practice. It would certainly be suitable to focus further research on the other two sustainability pillars – economic and social – and to look into the interconnection of all the three pillars (including the environmental one) in chemical companies, or also in some other areas for comparison.

Acknowledgement

This study was supported by a grant from the Fund for Bilateral Relations within the framework of the EEA and Norway Grants 2014-2021 (EHP-BFNU-OVNKM-3-134-01-2020).

References

1. Priyankara, H., Luo, F., Saeed, A.: Sustainab. 10/1, 271 (2018).
2. Shrivastava, P., Berger, S.: Org. Manag. J. 7, 246 (2010).
3. Glavas, A., Senge, P., Cooperrider, D. L.: Peop. & Strat. 33, 26 (2010).
4. Sharfman, M. P., Fernando, C. S.: Strat. Manag. J. 29, 569 (2008).
5. Rubel, M.R.B., Kee, D.M.H., Rimi, N.N.: Empl. Relat.: The Int. J. (2021)
6. Ahmad, S.: Cog. Bus. & Manag. 2/1 (2015).
7. Ansari, N.Y., Farrukh, M., Raza, A.: Corp. Soc. Resp. and Env. Manag. 28/1, 229 (2021).
8. Phillips, L.: Peop. Manag. 13, 9 (2007).
9. Liebowitz, J.: J. of sust. Dev. 3, 50 (2010).
10. Armstrong, M., Taylor, S.: *Řízení lidských zdrojů. Moderní pojetí a postupy*. Grada Publishing, Prague 2015.
11. Munzarova, S., Lostakova, H., Vavra, J., Bednarikova, M., Kurtulikova, N. Code of Ethics in the reporting corporate social responsibility activities, the evidence from the Czech chemical companies. SGEM2016, 24.-30.8.2016, Albena, Bulgaria, 761-768, (2016).
12. Wee, Y. S., Quazi, H. A.: Ind. Manag. & Dat. Syst. 105, 96 (2005).
13. Collier, J., Esteban, R.: Bus. Eth.: A Europ. Rev. 16, 19 (2007).
14. Daily, B. F., Bishop, J. W., Govindarajulu, N.: Bus. & Soc. 48, 243 (2009).
15. Kraus, J., Spicka, J.: Chem. Listy 107, 563–600 (2013)
16. Vlcek, D., Kostalova, J.: Economic analysis of the chemical industry of the Czech Republic in the period of economic growth. Hradec Economic Days, 2.-3.4.2020, Hradec Králové, Czech Republic, 848-860 (2020).
17. Tetrevova, L., Vavra, J., Bednarikova, M., Munzarova, S., Kostalova, J.: *Společenská odpovědnost firem společensky citlivých odvětví*. Grada Publishing, Prague 2017.
18. Bednarikova, M., Kostalova, J.: Chem. Listy, 113/11, 691 (2019).

SUSTAINABLE PACKAGING INNOVATIONS FOR COSMETIC PRODUCTS

Škraňková P., Paták M., Branská, L., Pecinová, Z.

University of Pardubice, Faculty of Chemical Technology, Studentská 95, 53210 Pardubice, Czech Republic
michal.patak@upce.cz

Abstract

Most packaging for consumer chemicals is made from raw materials for single use and ends up in a landfill or incinerator at the end of life cycle, which has significant impacts on the environment, society, and the economy. To increase the sustainability of packaging, researchers are currently focusing on the concept of circular economy, in which material flows are closed into functional and endless cycles. The aim of the paper is to identify sustainable packaging innovations that are based on the principles of circular economy. Qualitative research was carried out at two manufacturers of cosmetic products using the method of semi-structured interviews. The content analysis of interviews from both companies and their subsequent synthesis identified opportunities and barriers for sustainable innovations of primary packaging for cosmetic products, namely in the areas of reducing, reusing, and recycling of packaging materials.

Introduction

At present, the issue of sustainable packaging is appearing more and more frequently in the literature, because the excessive use of packaging and the associated generation of large amounts of waste has a major impact on sustainability[1]. The definition of sustainable packaging is difficult due to the large number of criteria that should be taken into account. In principle, however, it is packaging that meets higher environmental, economic and social standards compared to conventional packaging, has better quality properties and at the same time brings new possibilities in the field of waste recovery and waste management[2].

The traditional linear flow of packaging combined with unsustainable sourcing and consumption results in dramatic impacts on the environment, society and the economy. Therefore, one of the possible ways to sustainable packaging is the implementation of the principles of circular economy in packaging management, i.e. the looping of material flows and maintaining their value in the cycle for as long as possible[3]. The most common and most frequently mentioned principles of circular economy in the literature are reduce, reuse, and recycle[4].

The reduce principle includes the innovation of a product, process or business model aiming to replace the consumption of non-renewable raw materials with biodegradable, renewable or recyclable resources[5]. At the same time, it seeks to minimize the consumption of energy, raw materials and materials by introducing better technologies, producing more compact and lighter products or simplifying product design[6]. Therefore, the redesign of the packaging most often focuses on the thinning, lightening or overall reduction of the packaging[7]. In the case of consumer chemical products, it is possible to reduce environmental impacts, for example by producing more concentrated detergents[8].

The reuse principle is synonymous with any operation in which products or their components are reused for the same purpose for which they were created[9]. In packaging management, the principles of reuse are most often applied in the introduction of refillable packaging in households or through returnable packaging[10]. A specific reuse strategy is zero waste business where customers buy products into their own, reusable packaging[11].

Recycling involves the active reduction of waste by converting waste products into new resources, thus creating a balance between production and consumption of resources[5]. While metallic materials can be recycled indefinitely[6], most packaging materials deteriorate significantly after being recycled or cannot be recycled at all[12]. For this reason, packaging manufacturers are trying to replace traditional packaging materials with renewable and biodegradable materials, including compostable materials, biopolymers and synthetic biodegradable polymers.

Packaging made of compostable material can be recycled by industrial or domestic composting to produce carbon dioxide, water, heat and biomass and humus[13]. The main difference between industrial and domestic composting is that the temperatures in industrial composting plants are much higher and kept constant. Home composting is therefore a much slower process with lower efficiency than can be achieved in industrial conditions[14].

Biopolymers are any plastics made from plant-based materials[15], while synthetic biodegradable polymers are materials of synthetic origin that contain a hydrolytically labile bond. They can therefore be decomposed in an aqueous medium[16]. The literature[17] states that the use of biopolymer-based materials can minimize the generation of packaging waste due to its biodegradability. The problem, however, is their poor mechanical and barrier properties, which limits their wide use in practice.

Sustainable packaging innovations and their barriers largely depend on the type of product and the industry. Since these innovations for chemical products are not sufficiently reflected in the literature, the aim of the paper is to identify opportunities and barriers to sustainable packaging innovations in selected chemical products (cosmetic products).

Research methodology

To achieve the research goal, qualitative research was carried out in two chemical companies using the method of semi-structured interview with a selected company manager. The basic characteristics of selected companies are given in Table I.

Table I
Characteristics of the surveyed companies

Characteristics	Company A	Company B
Company size by number of employees	50-99 employees	250-499 employees
Subject of production	Body, hair and skin cosmetics	Body, hair, skin and bath cosmetics
Type of primary packaging used	PET, PE and PP plastic packaging; PBL laminate tubes; glass containers	PET or PE plastic packaging; PBL laminate tubes; glass containers
Certificates and awards in the field of environmental protection	ISO 140001, FSC®, PEFC, RSPO	-

The respondent from Company A was the sales manager, who is also responsible for quality management in the company. The respondent from Company B was the development manager. Both interviews took place in March 2021 in the form of an online video call lasting a total of 6 hours. The interviews involved a semi-structured questionnaire, which was divided into three areas:

- packaging innovation in the field of resource saving and waste minimization,
- packaging innovation in the field of packaging reuse, and
- packaging innovation in the field of packaging recyclability.

The information obtained was processed by content analysis of the audio-visual recording of the interview. The synthesis of research results from both companies made it possible to identify the main opportunities and barriers to the innovation of consumer packaging for cosmetic products, namely in the areas of resource saving, reuse and recycling of packaging materials.

Results and Discussion

Innovation of packaging for cosmetic products in the field of resource saving and waste minimization

Both companies put the accent on the reduction of waste of both product and packaging material. However, the introduction of innovations associated with changing the size and type of packaging is not easy, because such innovations usually affect the appearance and functionality of the packaging in a significant way. In particular, resizing packaging often encounters obstacles stemming from the demands of retailers and consumers.

The reduction of product waste is technically possible by reducing the viscosity of creams which adhere to the walls of the tubes. With a lower viscosity, the product would be more fluid, but it would be perceived by the consumer as less effective. Tubes for creams can also be replaced by the so-called airless packaging, which contain a movable plate. When used, it pushes all the product out of the packaging, thus preventing its waste. Airless packaging better protects creams from microbial contamination than conventional tubes and is easier to recycle thanks to the use of a single type of material.

A possible way to reduce the environmental impact of packaging is to introduce concentrated products. Such an innovation would not only reduce the overall share of packaging in the weight of the product, but the lower water content of the product significantly contributes to reducing transport costs and the associated environmental impacts. According to the respondents, however, a higher concentration of the product will not guarantee optimal dosing by the consumer; on the contrary, it may cause an increase in waste of the product (habitual behaviour of consumers). A change in concentration also leads to an undesirable change in the character of some products (e.g. body lotion, cream, butter). The introduction of anhydrous products (e.g. solid soap as an alternative to liquid soap) will usually avoid product waste, however both respondents agreed that the biggest barrier to anhydrous products is low consumer demand.

Packaging materials can be saved mainly by reducing the number of consumer packaging levels and maximizing the filling of the packaging. According to both respondents, the number of packaging levels is already optimized for all products. The main barrier to further innovations in this area is the tradition of the brand, the disruption of the protective function (boxes for glass packaging) and the information function of the packaging (enough space to provide all the necessary information or insert a package leaflet).

The degree of filling of the packaging with the product is an important criterion in the design of packaging for all cosmetic products, because it significantly affects not only the consumption of packaging material, but also the risk of product degradation due to air humidity in the empty space in the packaging. It is because it is not protected by preservatives and mould could grow in it. Although companies try to fill the packaging space as much as possible, in the case of tubes this is not possible for technological reasons (welding more filled tubes would degrade the product).

Opportunities and barriers to resource-saving packaging innovations are summarized in Table II.

Table II
Reduce Innovations and Their Barriers

Innovation	Barrier
Change of the size and type of packaging	Requirements of customers and consumers
Reduction of product viscosity	Psychological barrier in consumers
Introduction of concentrated products	Optimal dosing by the consumer Significant change in the nature of the product (in the case of creams)
Introduction of anhydrous (water-free) products	Significant change in production technology Consumer behaviour
Reduced number of levels of consumer packaging	Preservation of brand tradition Protection of the primary packaging and product from damage Lack of space on the primary packaging for all information Keeping the package leaflet included in the package
Maximised amount of the product in the packaging	Packaging technology (welded packaging in the case of tubes)

Innovation of packaging for cosmetic products in the field of packaging reuse

The research confirmed the possibility of reusing packaging for cosmetic products, namely by introducing refillable dispensers, returnable packaging or through zero waste sales.

In the case of refillable packaging, both respondents agreed on the need to purchase a specialized line for packaging refills, which is currently the main barrier for them. In addition, one respondent stated that the packaging available for refills on the market is not recyclable.

A major barrier to introducing waste free products is related to the hygienic requirements resulting from high quality standards for cosmetic products. While one respondent cited cross-contamination on the consumer side as another possible barrier, according to the other respondent, the introduction of non-packaging sales represents a significant change in the way cosmetics are distributed and sold. The recycling of packaging in which products are transported to filling stations (multi-type materials) is also problematic. However, it is the reluctance of consumers to change their shopping behaviour (buying into his/her own packaging the customer brings to the store) that can be considered the biggest barrier.

Respondents were most sceptical about the introduction of returnable packaging. In their view, the return logistics of consumer packaging for cosmetic products is highly expensive and has much greater environmental impacts than recyclable packaging, which can be reused as a secondary material in packaging production. In addition, a respondent from a company, most of whose sales are done through the company's own stores, cited as a barrier the need to introduce waste management in stores (a legislatively demanding process) and the disruption of the current system of waste sorting in consumer households.

Opportunities and barriers to packaging innovation in the field of reuse are summarized in Table III.

Table III

Reuse Innovations and Their Barriers

Innovation	Barrier
Introduction of refillable packaging	Significant change in packaging technology Available packaging materials are not recyclable
Introduction of zero waste (package free) sales	Possibility of cross-contamination at the consumer Meeting high hygiene requirements Significant change in the method of distribution and sales Handling packaging for zero waste (package free) sales is not reusable and recyclable Consumer behaviour
Introduction of returnable packaging	Legislation (introduction of waste management in stores) Demanding logistics of returnable packaging Low return rate of packaging Disruption of the waste sorting system in consumers' households Consumer shopping behaviour

Innovation of packaging for cosmetic products in the field of recycling

The respondents differed in perceiving the issue of recycling packaging from cosmetic products. According to the first of the respondents, from the point of view of economic and environmental costs of recycling, the most problematic are aluminium containers, which are widely used in the cosmetics industry. Their replacement with plastic containers is usually hindered by requirements for the aesthetic side of the packaging. In the case of their replacement with glass containers, he sees a problem in the breakage and greater weight of the glass. According to the second respondent, on the other hand, it is laminate tubes that are the biggest problem. Laminate tubes could be replaced with multilayer paper-coated tubes, which would have lower environmental impacts but at the same time provide lower product protection. Another option is PE tubes, which can be easily recycled. Even with this option, there is a risk of their deformation during transport, and in addition, they cannot be sufficiently filled due to the welding of the containers.

More room for sustainable innovation lies in the use of secondary plastic materials (recycled) in the production of packaging. Both respondents have a positive experience with the introduction of rPET containers for some products. They consider the lack of rPET material on the market and the associated higher price to be the main barriers to their greater expansion. This currently allows the use of a maximum of 50% recycled material in the production of a plastic bottle, although in theory it is possible to produce a functional bottle with a 100% recycled content. The use of rPET also affects the appearance of white plastic bottles (unwanted grey discoloration). For this reason, even less recycled material is used for white bottles, at the limit of the expected EU standard for the mandatory proportion of recycled material in packaging (25%).

In the area of recycling, the respondents also discussed the possibilities of using renewable and biodegradable materials. However, in the case of the packaging of cosmetic products, they associate them with a number of barriers. The first of the respondents is discouraged mainly by the high price of packaging material. At the same time, he expressed doubts about the full degradability of materials outside industrial composters and also considered their production from agricultural crops to be inappropriate (occupying arable land with a crop that would not be primarily processed as food). The other respondent is rather discouraged by the negative experience with these containers on filling lines, but also by the high risk that waste from these containers may be poorly sorted in consumer households and recycling organizations (biopolymers can be easily mistaken for petroleum-derived plastics), compromising the quality of the whole batch of recycled material.

The last area of innovation is adapting the design of packaging to easier recycling. When recycling, there may be a problem with labels that are made of a different material and cannot be easily separated from the packaging during household sorting (in accordance with legislation according to which the label must not be easily removable from the packaging). Such labels can be replaced with engraving the packaging. However, it is a technology for marking goods that has higher investment and operating costs.

Opportunities and barriers to packaging innovation in the field of recycling are summarized in Table IV.

Table IV
Recycle Innovations and Their Barriers

Innovation	Barrier
Introduction of biodegradable packaging materials	Higher price of biodegradable materials Problems with packaging (when filling packages) Sorting-related problems (easy interchangeability with other types of materials) Doubts about environmental benefits (waste degradability) Production of biodegradable packaging from agricultural crops Negative perception of product quality by consumers
Introduction of plastic packaging with a high percentage of recycled material (rPET)	Higher price of packaging material Lack of quality recycled material on the market Aesthetic aspect of the packaging (in the case of white bottles)
Replacement of laminate tubes with multilayer tubes with a layer of paper or PE tubes	Lower product protection (in both cases) Smaller amount of product in the packaging (in the case of PE tubes)
Replacement of aluminium packaging with glass or plastic packaging	Fragmentation and heavier weight of the packaging (in the case of glass) Aesthetic aspect of the packaging (in the case of plastic)
Introduction of engraving instead of labelling	Higher costs Significant change in packaging technology

Conclusion

The results of the primary research revealed the possibilities of sustainable innovations associated with cosmetic products and their packaging. However, putting them into practice requires overcoming many barriers throughout the supply chain. Packaging redesign is often associated with significant technological innovations and overcoming customer attitudes and habits. These can be barriers that are difficult to overcome. The reuse of packaging is associated with a number of logistical problems, but also it is also met with consumers' reluctance to change their shopping behaviour. The introduction of plastic packaging with a high proportion of recycled material can be considered the most promising strategy in the area of sustainable packaging of cosmetic products. However, their wider application in practice is hindered mainly by the unavailability of high-quality recycled material, resulting from an insufficient system of sorting and recycling of plastic waste.

References

1. Salkova D., Regnerova O.: Methods of eliminating waste from food packaging as a globalization tool. In: SHS Web of Conferences, *74*, 04025 (2020).
2. Kozik N.: Sustainable packaging as a tool for global sustainable development. In: SHS Web Conferences, *74*, 04012 (2020).
3. Korhonen J., Nuur C., Feldmann A., Birkie S. E.: J. Clean. Prod., *175*, 544 (2018).
4. Prieto-Sandoval V., Jaca C., Ormazabal M.: J. Clean. Prod., *179*, 605 (2018).
5. Goyal S., Esposito M., Kapoor A.: Thunderbird Int. Bus. Rev., *60*, 729 (2018).
6. Ghisellini P., Cialani C., Ulgiati S.: J. Clean. Prod., *114*, 11 (2016).
7. Reichert C. L., Bugnicourt E., Coltelli M-B., Cinelli P., Lazzeri A., Canesi I., Braca F., Martínez B. M., Alonso R., Agostinis L., Verstichel S., Six L., De Mets S., Gómez E. C., Ißbrücker C., Geerinck R., Nettleton D. F., Campos I., Sauter E., Pieczyk P., Schmid M.: Polymers, *12*, 1558 (2020).
8. Verghese K., Lewis H., Fitzpatrick L. (eds.): *Packaging for Sustainability*. Springer-Verlag, London 2012.
9. Castellani V., Sala S., Mirabella N.: Integr. Environ. Assess. Manag., *11*, 373 (2015).
10. Coelho P. M., Corona B., ten Klooster R., Worrell E.: Resour. Conserv. Recycl. *6*, 100037 (2020).
11. Fuentes C., Enarsson P., Kristoffersson L.: J Retail. Consum. Serv., *50*, 258 (2019).
12. Escursell S., Llorach-Massana P., Roncero M. B.: J Clean Prod, *280*, 124314 (2021).
13. Krzan A.: http://www.plastice.org/fileadmin/files/EN_Biorazgradljiva_plastika_in_polimeri_Krzan.pdf, (2012).
14. Havstad M. R.: In: *Plastic Waste and Recycling.* https://doi.org/10.1016/b978-0-12-817880-5.00005-0, (2020).

15. Iacovidou E., Gerassimidou S.: In: *Reference Module in Food Science*. https://doi.org/10.1016/b978-0-08-100596-5.22488-8, (2018).
16. Kumar S., Singh P., Gupta S. K., Ali J., Baboota S.: In: *Reference Module in Materials Science and Materials Engineering.* https://doi.org/10.1016/b978-0-12-803581-8.10934-8, (2019).
17. Abdul Khalil H. P. S., Davoudpour Y., Saurabh C. K., Hossain Md. S., Adnan A. S., Dungani R., Paridah M. T., Islam Sarker Md. Z., Nurul Fazita M. R., Syakir M. I., Haafiz M. K. M.: Renew. Sustain. Energy Rev., *64*, 823 (2016).

IDENTIFICATION OF FACTORS INFLUENCING OIL AND GAS PRICES AND THEIR MUTUAL CORRELATIONS

Košťálek J.[1], Koťátková Stránská P.[2]

UCT Prague – Department of Economics and Management, Technicka 5, 166 28, Prague 6
[1]josef.kostalek@vscht.cz, [2]pavla.kotatkova.stranska@vscht.cz

Abstract

The oil and gas market is under the control of price volatility and uncertainty. Significant influences that suppress or increase uncertainty and volatility include production cuts for major miners, an increasing number of active wells in the United States, etc.

The aim of the contribution is to identify relevant factors influencing commodity prices, oil and natural gas. For this purpose, the mathematical and statistical apparatus will be used in the form of a tool of multiple regression and correlation analysis. The selected instruments will allow us to quantify the strengths of individual dependencies and it will be possible to verify relevant factors describing the behaviour of the prices of both commodities at a specified level of significance. Input factors will be selected based on economic relevance. We will also consider the impact of the current COVID-19 pandemic. The output of the presented article will be that the input factors are evaluated (positive influence or negative influence), what effect they have on the price of oil or the price of natural gas. The next outcome of this paper will be a comparison of the sensitivity analysis of the model describing oil price development with a sensitivity analysis of the model describing the price development of natural gas using the elasticity indicator.

Introduction

Oil and natural gas are undoubtedly among the most important commodities in the world. The mutual influence of the price of oil and gas flows in terms of their economic irreplaceability in the developed world. In consumption, they are substitutes, and in production they are complements.

The price of oil and natural gas is characterized by high volatility in times of surplus and scarcity. The sensitivity of volatility is determined by the demand and supply of the commodities in question. If oil prices rise, the demand effect will take effect. The rising price of oil will cause economic operators to substitute relatively cheaper gas. There will be an increase in demand for natural gas and the price of gas will slowly rise.

In the field of oil, direct sales are possible or oil can be sold as a commodity on the stock exchange. The most important oil trading exchanges are New York (WTI oil designation) and London oil (Brent oil designation). World trade is globalized and therefore prices tend to level out on both exchanges. Price is generally the result of supply and demand on the market. An important factor is consumption and mining. The situation is complicated because consumption is not constant and is affected by seasonality. In the summer months, more travel is made. This leads to an increase in consumption. On the other hand, large producers regulate mining. In doing so, it creates its favourable prices. A new phenomenon is emerging, and that is shale oil production in the US. This method of extraction is associated with higher costs. Its implementation occurs in a situation where there is a shortage on the oil market and its price is high enough.

Calculations and experiment

Many scientific studies deal with the identification of the most important factors influencing the price of oil and natural gas. It also strives for mathematical modelling of price prediction. These are studies of predominantly private companies. Commodity consumption, volume of production (mining), amount of stocks, exchange rate of the US dollar, geopolitical situation. These and others are important factories. For example, the exchange rate of the US dollar - if the dollar is strong, the price of oil falls and vice versa. The poor geopolitical situation can negatively affect the level of oil production and the possibilities of its transport. Bad weather, such as hurricanes, will also lead to rising oil and gas prices.

The aim of the article is to compile a mathematical model that includes selected relevant factors affecting the price of oil or natural gas. The entry into the model will be selected factories: the exchange rate of the US dollar against other currency, stocks, consumption, health (number of infected with viral or bacterial infections), decision-making by paper oil/natural gas traders, decision-making of mining companies, political situation (promotion of political goals). The output is the price of oil or natural gas for the period 2000-2020. The data thus reflects the influence of all the above factors.

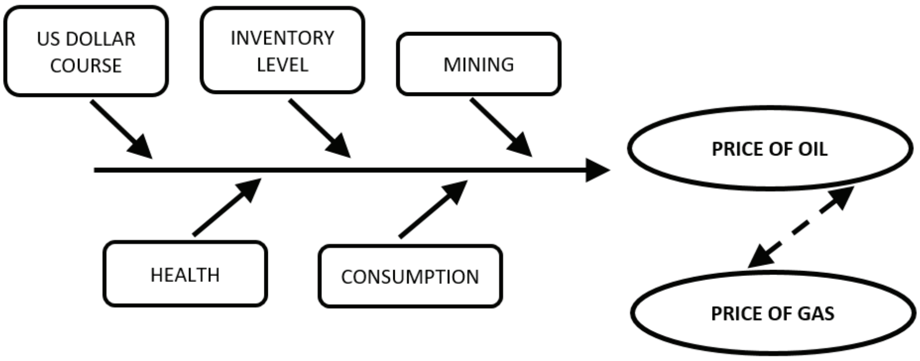

Figure 1. Key factors affecting the price of oil

Mathematical deterministic model has this form:

Deterministic model I.
Allows to examine the effect of the dependent variable (Brent Oil in USD) on independent variables (Mining, Consumption, Health, USD/SDR) according following relation (1):

$$\text{Brent Oil\_USD} = \beta 0 + \beta 1(\text{Mining}) + \beta 2(\text{Consumption}) + \beta 3(\text{Health}) + \beta 4(\text{USD/SDR}) + \varepsilon(\text{other non-quantifiable factors}) \tag{1}$$

Deterministic model II.
Allows to examine the effect of the dependent variable (Brent Oil in USD) on independent variables (Mining, Consumption, Health, USD/SDR) according following relation (2):

$$\text{Natural Gas\_USD} = \beta 0 + \beta 1(\text{Mining}) + \beta 2(\text{Consumption}) + \beta 3(\text{Health}) + \beta 4(\text{USD/SDR}) + \varepsilon(\text{other non-quantifiable factors}) \tag{2}$$

Selected factors enter the model (I. and II.) as uncorrelated (multicollinearity verified) and decomposed, i.e. without trend. The trend was detected only in consumption. This variable has been removed. We are working here with time series where it is necessary to find out if there is a time delay. A time delay was detected only for consumption, where the time delay is 6 months.
The verification of both mathematical models will be assessed by the p-value for the regression coefficients and the p-value of the entire regression model.

Table I
Result of MODEL I.

Variable	BETA	SIG.
Mining	0.8475	0.2756 *
Consumption	6.3207	0.0201 *
Health	0.3056	0.4857 *
USD/SDR	-4,258	0.4678*
DW		1.2584
Modifi. coefficient of determination		0.6452
P-value (model)		0.0328*

Dependent variable “Brent Oil_USD volume” is positively influenced Mining, Consumption, Heat, on the contrary dependent variable is negatively USD/SDR.

Table II
Result of MODEL II.

Variable	BETA	SIG.
Mining	0.0398	0.3096 *
Consumption	2.8417	0.4581 *
Health	0.3056	0.6357
USD/SDR	-1.5698	0.4697*
DW		1.2356
Modifi. coefficient of determination		0.5897
P-value (model)		0.4507

Dependent variable “Natural Gas_USD volume” is positively influenced Mining, Consumption, Heat (but statistically insignificant), on the contrary dependent variable is negatively USD/SDR.
Furthermore, the relationship between the oil and gas price will be analysed using the elasticity indicator. The figure (Figure 2) below shows the influence of the price of natural gas on oil.

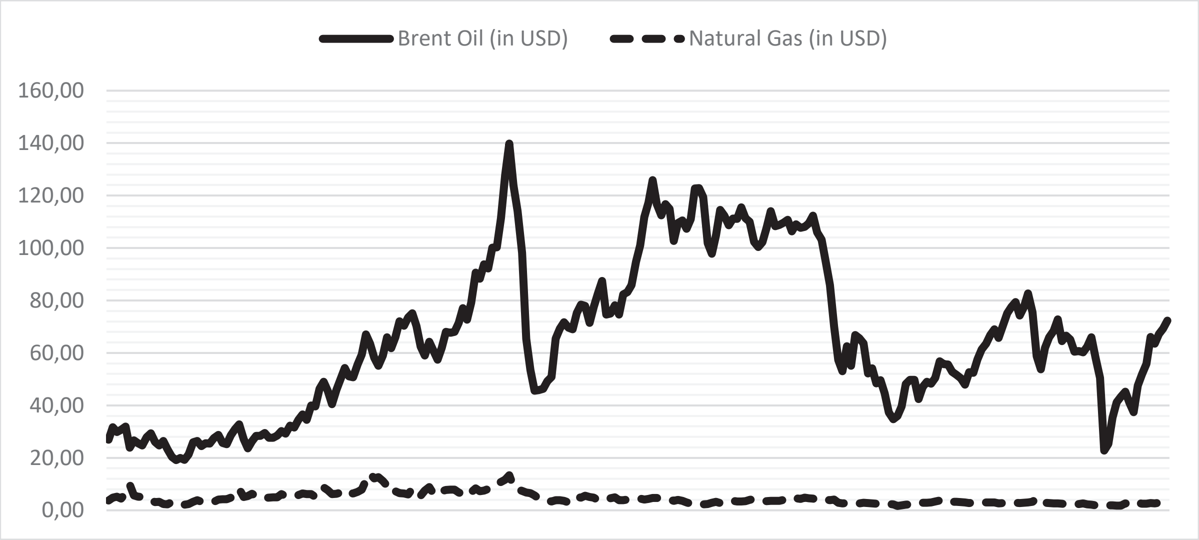

Figure 2. Price of oil (USD/barrel) and price of gas (USD/MMBTU) in period 2000-2020
Source: own according to https://www.investing.com/commodities/brent-oil
https://www.kurzy.cz/komodity/zemni-plyn-graf-vyvoje-ceny

Quantification of the effect from the above figure will be expressed using an elasticity indicator. The indicator measures the percentage change in the price of oil to the percentage change in the gas price. This is due to the fact that the price of oil is determined on the world market and the price of natural gas shapes them into regional segmentation of the gas markets.
The elasticity of the oil price (*EBG*$_t$) is calculated according to the following formula (3)

$$EBG_t = \frac{\frac{B_t - B_{t-1}}{B_{t-1}}}{\frac{G_t - G_{t-1}}{G_{t-1}}} \qquad (3)$$

Elasticity values *EGB*$_t$ for period 2000 – 2020 are shown in the following chart (Figure 3)

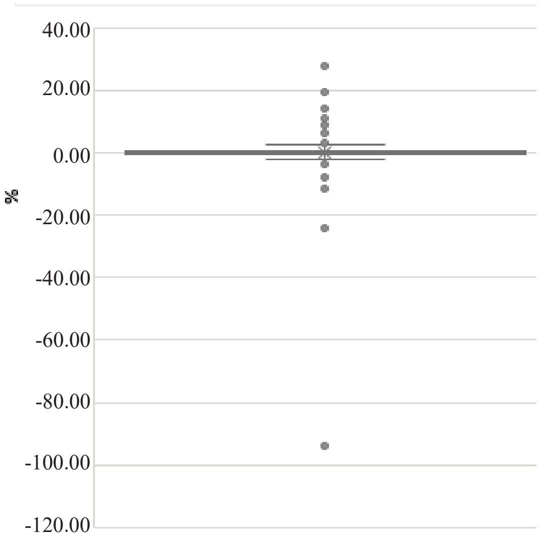

Figure 3. Elasticity values EGB_t for period 2000 – 2020
Source: own according to https://www.investing.com/commodities/brent-oil
https://www.kurzy.cz/komodity/zemni-plyn-graf-vyvoje-ceny

Discussion and result analysis

The mathematical model of the oil and gas price has shown positively influenced Mining, Consumption, Health (but statistically insignificant), on the contrary dependent variable (oil price and natural gas price) is negatively USD/SDR.

The elasticity indicator shows that the price of gas shows lower volatility.

The chart in Figure 2 illustrates the sharp fall in the price of oil at a time when the Covid-19 pandemic was beginning to spread. It can also be seen that, after the improvement in the situation in the world, the price of oil began to rise again to pre-pandemic levels. This is due to the economic downturn, which is linked to a decline in industrial production, a decrease in mobility and, in particular, a very strong decrease in air transport. These factors caused a big drop in oil consumption and this lowered its price. Although the price of oil collapsed in 2018 (a barrel of Brent crude fell from $85 to $63 in six weeks), the price of gas soared from $3 per unit of volume to $4.5.

Global oil consumption is on an ever-increasing trend.

While efforts are growing around the world to reduce fossil fuel consumption to reduce CO_2 emissions, oil consumption continues to grow. This is due to many factors, such as the increase in the volume of freight transport (road, boat and air). Increase in passenger car and air transport. Industrial growth in China and India. Replacement of traditional material with plastics, which are also produced from oil, etc.

Conclusion

The price of both oil and natural gas is interesting for any economic entity. The price of both commodities is affected both on the supply side and on the demand side. The price of oil reacts the most due to high volatility compared to the price of natural gas. The significant fall in the price of oil in period 2000-2020 is evident in 2015, when the US began extracting shale oil. The effect of demand was reflected in 2014, when there is a worldwide effort to make transport and production environmentally friendly.

The oil price also reacted to the COVID-19 pandemic in 2019/2020. There is a significant drop, mainly due to restrictions on air transport and transport as a whole. The reaction of natural gas was moderate, i.e. there was a slight increase in the price of natural gas.

References

1. Artl, J., Artlová, M.: Ekonomické časové řady. Professional Publising, Praha 2009.
2. BP Global. Statistical Review of World Energy June 2016.
3. Brent oil. Investing.com. [online]. https://www.investing.com/commodities/brent-oil
4. Hošek, J., Komárek, L., Motl, M.: Měnová politika a cena ropy. Politická ekonomie, 1 (2011).

5. Independent Statistics & Analysis. U.S. Energy Information Adminisration. [online]. https://www.eia.gov/outlooks/steo/data/browser
6. Natural Gas. Investing.com. [online]. https://www.investing.com/commodities/natural-gas
7. Price of Natural Gas. Kurzy.cz. [online]. https://www.kurzy.cz/komodity/zemni-plyn-graf-vyvoje-ceny

SYNTHESIS AND PRODUCTION OF DRUGS

RHEOLOGICAL PROPERTIES OF POWDER MIXTURES AS A FACTOR OF HARD-GELATIN CAPSULE FILLING PERFORMANCE

Komínová P.[1], Havelková P.[1], Zámostný P.[1]

[1]University of Chemistry and Technology Prague, Faculty of Chemical Technology, Department of Organic Technology, Technická 5, Prague 6, 166 28, Czech Republic
pavlina.kominova@vscht.cz

Abstract

One of the key factors affecting production of hard gelatine capsules are bulk properties of filled powders. The bulk properties are reflected not only in the required quality attributes of a final product, such as the filled weight or weight uniformity, but also in the efficiency and trouble-free running of this unit operation. Therefore, it is necessary to pay a considerable attention to the evaluation of bulk properties. They are given both by the nature of used materials and included particles, but also by external conditions (such as temperature, humidity, bed voidage and stage of compaction). Because of that, the requirements for filled formulations can be relatively complex and both of these aspects must be taken into account when optimizing them. Moreover, the necessary knowledge of synergy between the properties of particulate system (powder, granulate) and the set machine parameters can become a major challenge of hard gelatine capsule topic.

The aim of this work is to bring a case study dealing with optimization of a three-component mixture (corn starch, active pharmaceutical ingredient (API) and dimethicone), which is used by an industrial partner for filling hard gelatine capsules. Based on the performed measurements, the effects of the chosen formulation strategy - mixture composition and mixing time on rheological properties were evaluated.

Introduction

Hard gelatine capsules are a commonly used dosage form in the pharmaceutical industry. Together with tablets, they belong to the most often used solid dosage forms for peroral administration[1].

The main used devices for capsule filling include high-speed automatic filling devices. This group includes a dosing disc and a dosing tube (also known as a dosator) machines. Devices with a dosing disc generally consist of a rotating dosing disc containing dies and a series of tamping pins. It is possible to see a certain analogy with a tablet press. During filling, the powder gravitationally flows into the hole and is compressed by the first tamping pin. While compressing with the pin, additional filling of the hole is occurred. This filling/compressing phase is repeated until the last pin position. The created compact (slug) is then ejected into a capsule body and the body is closed with a cap. In case of devices using a dosator, the main part is a dosing tube with a movable piston inside. During immersion (penetration) into the mixture layer, the dosing tube is filled with powder. Then, the powder inside the tube is consolidated by movement of the dosing tube deeper into the layer of the powder. This again leads to the formation of the slug that is then transferred inside the dosing tube above the capsule body and ejected into the body by moving the piston downwards[2].

Thus, suitable flow properties are required to successfully fill the holes of the disk and the dosing tube of the dosator. On the other hand, the powders must also have a certain degree of cohesivity. This is in order to create a stable slug that can be ejected into the capsule body without any possible premature disintegration[3]. In case of dosator operation principle, a certain degree of cohesivity is also needed to keep the slug inside the tube during its transport[1].

Researches up to now have also shown that the range of powders that can be filled with a dosing disk is wider than with a dosing tube[4]. This is especially valid for powders with very good flowability that cannot be filled via dosator due to the formation of a weak slug. However, a dosator is also inconvenient for very cohesive powders with poor flow properties because of their tendency to surface friction and adhesion to the filling device. As a result, the desired filling weight and its uniformity do not meet the required criteria.

From this brief description about operation principle of a dosing disk and a dosator, it is clear the flow requirements of powders to be suitable for filling into hard gelatine capsules can be quite complex, and thus flowability of powders must be adjusted, according to the chosen filling device. With respect to this, some surveys exist that define the range of optimal values for flowability parameters such as Carr compressibility index[5] determining suitability of powders for capsule filling.

Materials and Methods

Materials

The below list summarizes materials that were used for the preparation of studied mixtures in this study:

- native corn starch Merizet 141 (Azelis Czech Republic s.r.o.)
- liquid dimethicone (supplied by industrial partner)
- active pharmaceutical ingredient (supplied by industrial partner)

Preparation of Binary Mixtures

The preparation of the studied mixture is a three-step process graphically expressed in Figure 1. First step included the preparation of so-called *premix CS/D* which consists of dimethicone and a defined proportion of corn starch. After that, a mixture containing API with another proportion of corn starch, *active mixture*, is created. In the last step, the remaining amount of corn starch is added to form the final mixture.

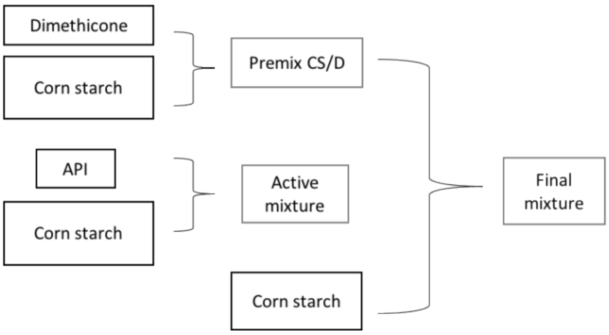

Figure 1. Preparation procedure of mixture.

Premix CS/D

In this work, 4 premixes CS/D were created in total, differing in the ratio of corn starch and dimethicone. Table I shows the composition of individual premixes CS/D. The premix CS/D marked No. 1 corresponds to premix in the original final mixture used by the industrial partner, other premixes CS/D correspond to modified final mixtures. All premixes CS/D were prepared in the same way. After adding given amount of dimethicone to the weighed corn starch, a mixture was stirred by hand for 8 minutes at about 80 rpm/min. The prepared premix was then lightly ground in a mortar for better homogeneity and to destroy larger agglomerates presented in the mixture.

Table I
Composition of prepared premixes CS/D.

Premix CS/D number	Dimethicone (w/w %)	Corn starch (w/w %)
1	6	94
2	3	97
3	2	98
4	1	99

Active mixture

After weighing, corn starch and API were placed together in a plastic sealable container and mixed using a 3D laboratory mixer Turbula T2F for 11 minutes at 67 rpm/min.

Final mixture

To prepare the final mixture, the active mixture, premix CS/D and finally the remaining corn starch were sieved through a 1 mm sieve into a plastic sealable container. The prepared mixture was mixed using again the 3D laboratory mixer Turbula T2F at 67 rpm/min. All studied mixtures had identical final composition. Thus, in the case of modified mixtures, the amount of corn starch added in the last step was adequately adjusted with regard to the proportion of corn starch in the premix CS/D to meet this condition. To evaluate time dependence of flow properties, final binary mixtures were mixed for different amount of time.

All investigated final mixtures with their composition and mixing times are listed in Table II.

Table II
Composition and mixing time of prepared final mixtures.

Mixture	Number	Premix CS/D (w/w %)		Active mixture (w/w %)		Corn starch (w/w %)	Mixing time (min)
		Dimethicone	Starch	API	Starch		
original mixture	1	0.11	1.76	5.06	32.92	60.15	35, 55, 75, 400
modified mixture	2	0.11	3.66	5.06	32.92	58.25	15, 35
	3	0.11	5.56	5.06	32.92	56.35	35, 55, 75, 400
	4	0.11	9.35	5.06	32.92	52.56	35

Measurement of Flow Properties

<u>*Carr compressibility index*</u>

Two methods were used to measure flow properties. The first one was widely used pharmacopoeial *Carr compressibility index* (*CI*). For this measurement, an adequate instrumentation was not available to obtain tapped and bulk densities. Therefore, the corresponding values of *CI* were marked as modified. A procedure of density measurements was simulated using a laboratory stand and a clamp holder with a clamp as pictured in Figure 2. Space for movement of a test tube containing sample of defined volume was created between the bottom of laboratory stand and the clamp. The test tube was moved up and down for 1 minute in this space. Tap density was determined from volume read and known weight of the sample. Bulk density was determined from the full filled tube prior to testing.

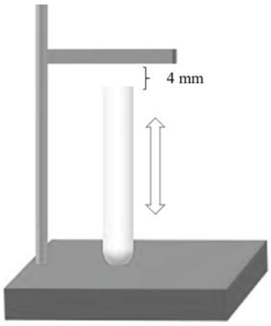

Figure 2. Apparatus for tap density measurement.

<u>*FT4 powder rheometer*</u>

Further, the assessment of flow properties of mixtures was performed using a FT4 powder rheometer. Compressibility and shear methodology were applied to determine flow properties. Before the measurement itself, the samples were dried overnight in an oven at 35 °C to avoid the effects of moisture.

In the case of *compressibility methodology*, the obtained parameter is so-called *compressibility* (*CPS*). It is defined as a percentage change in powder volume after the application of defined normal load, usually 15 kPa. It is an important parameter of particulate systems and can describe their behaviour during operation where volume change takes place, such as slug creation. High *CPS* corresponds with the resistance of particles to take the tightest arrangement and indicates worse flow characteristics. It means that cohesive powders show higher value of *CPS* than less cohesive ones.

Next used methodology, *shear methodology*, gives information about powder behaviour from no-flow to flow. The principle of a shear test is to apply predetermined normal force using a shear cell. It rotates slowly, creating shear force on the top powder layer, while the bottom layer is prevented from moving. It reflects shear strength of powder and friction between particles. Because of that, it is suitable for the description of a dosator or a dosing disc hole filling. Several parameters are obtained via shear methodology. One of them is the *effective angle of internal friction* (φ_E) or the *cohesion (C)*. Generally, their higher values reflect more significant interparticle friction and powder tendency to sticking.

Scanning Electron Microscopy

SEM images of representative premixes CS/D or mixtures were taken during this study using a scanning electron microscope TESCAN Lyra3 GMU (Tescan Orsay Holding a.s., CZE) at acceleration voltage of 10 kV. Each mixture was coated with a thin layer of gold (Q150R ES, Quorum Technologies Ltd., UK) before imagining to neutralise the charging effects and increase an SE yield at final micrographs.

Results and Discussion

Visual Observation

SEM images were taken to evaluate internal composition and character of prepared premixes CS/D and final mixtures. From the images of premix CS/D included in the original final mixture and containing 6 % dimethicone by weight and the corresponding final mixture (Figure 3a) and images of the premix CS/D with 2 % dimethicone included in the final modified mixture and the final mixture (Figure 3b), it can be seen that both premixes CS/D contain a structure of agglomerates and the original premix shows higher degree of agglomeration. Moreover, the liquid bridges are also visible. They are the result of the dimethicone presence on the particle surface of the remaining components of the mixture and their amount proportionately corresponds to the amount of dimethicone in the premix CS/D. Therefore, they are more pronounced in the original premix CS/D. Similar outcomes were observed for final mixtures reflecting the effect of premix CS/D structure on their character.

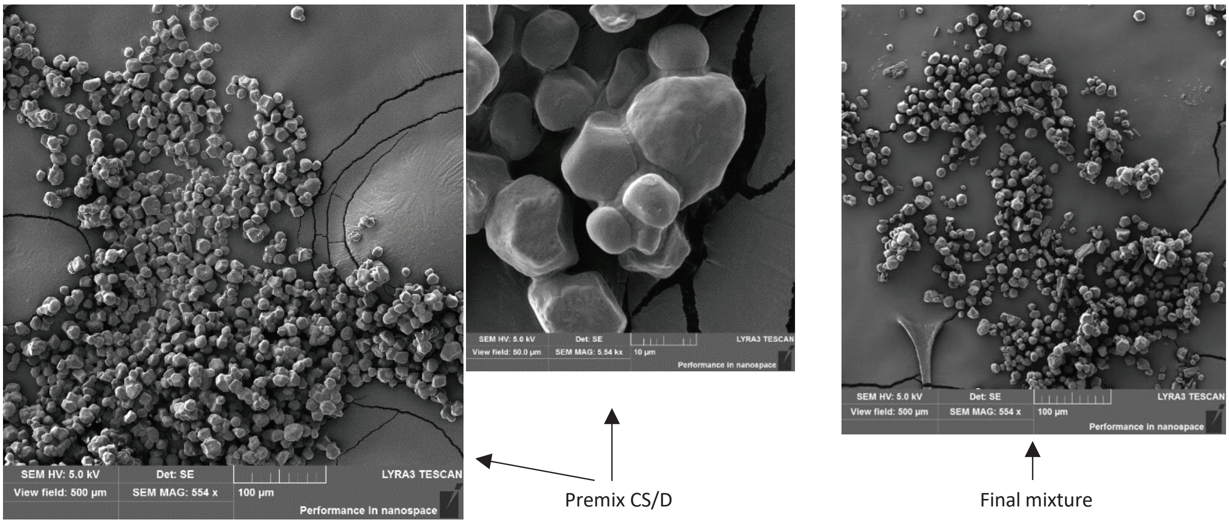

Figure 3a. SEM images of premix CS/D included in the original mixture and SEM image of the original final mixture.

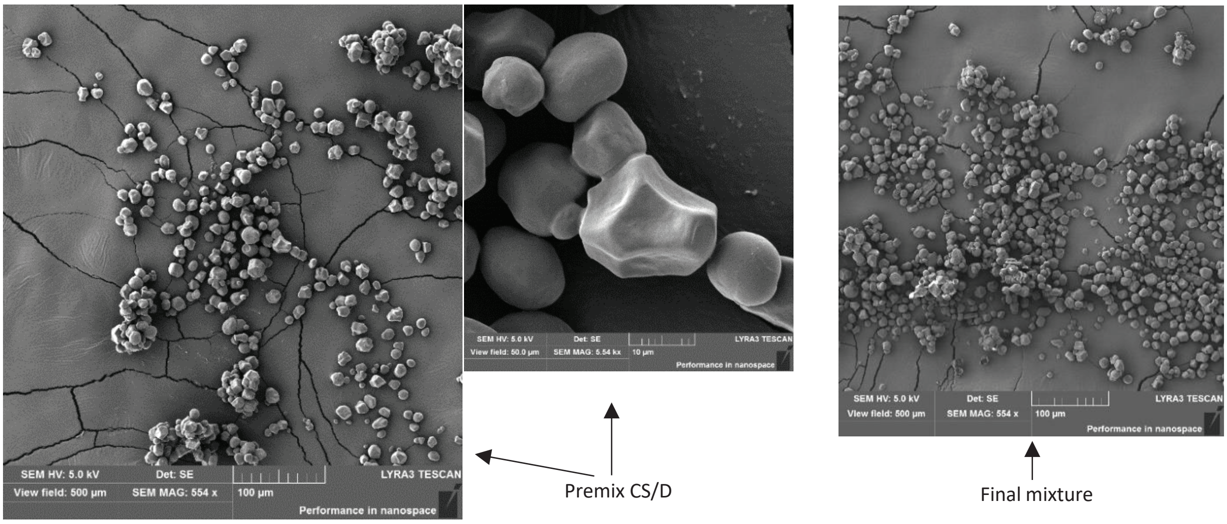

Figure 3b. SEM images of premix CS/D included in the modified mixture No.3 and SEM image of the modified final mixture.

FT4 Powder Rheometer

a) Compressibility methodology

The results for the studied final mixtures are expressed as a dependence of *CPS* on the mixing time (Figure 4). It shows that with increasing mixing time, the *CPS* first increases and then stabilizes at a certain value. This trend is probably due to the destruction of the present premix agglomerates, which occurs at shorter mixing times. As the newly formed and smaller agglomerates have poorer flow properties, this phenomenon is reflected in the increase of *CPS*. However, with prolonged mixing times, the size of agglomerates does not change appreciably, and the resulting *CPS* becomes stable. We can say from this foundation that longer mixing times are not suitable with regard to flow properties and rather have negative impact on the studied systems. From comparison of studied mixtures, better flow behaviour of the modified mixture compared to the original one is observed.

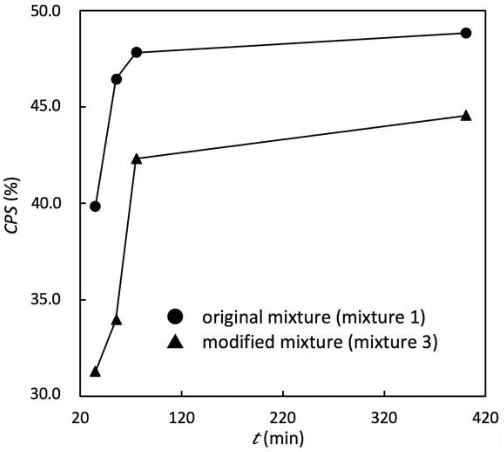

Figure 4. Dependence of *CPS* of final mixtures on mixing time.

b) Shear methodology

Values of φ_E and *C* for all studied mixtures are plotted in Figure 5. It can be seen the obtained outcomes correlate with the *CPS* and those with modified premixes CS/D show better surface properties. However, the improvement is not proportional to the amount of dimethicone in the premix CS/D. All modified final mixtures exhibit similar values. This indicates the existence of a certain optimum range of the ratio of corn starch and dimethicone in the premix CS/D necessary to achieve the best possible surface properties.

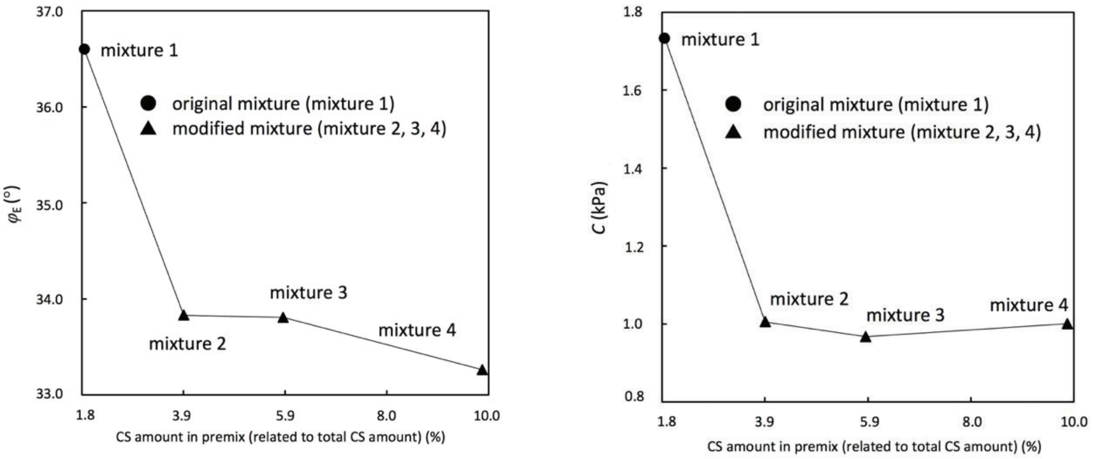

Figure 5. Dependence of φ_E and *C* of final mixtures on the amount of corn starch in premix CS/D.

If we graphically express the dependence of φ_E on the mixing time (Figure 6), the initial increase followed by a slight decrease is visible from this correlation. There are probably two phenomena that occur during mixing - namely the mentioned disintegration of the premix agglomerates and the distribution of dimethicone on the surface of the particles. The destruction of agglomerates is responsible for the formation of new interfaces and the friction intensification that reflects in the increase of value of φ_E. The subsequent value decrease indicates a positive effect of the dimethicone distribution on the surface of the particles. However, this effect is time limited, as the φ_E values increase again for long mixing times. This may be due to the unevenness of surface of the starch and the API particles, where the dimethicone is concentrated mainly in their cavities and not on the surface. Thus, dimethicone loses its effectiveness to modify the surface properties (Figure 7).

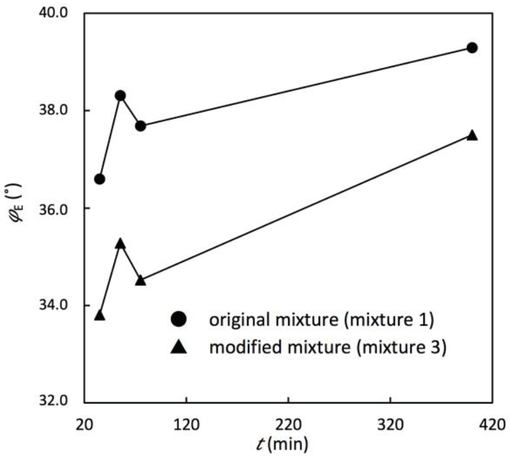

Figure 6. Dependence of φ_E of final mixtures on mixing time.

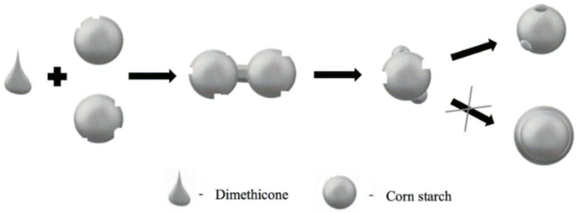

Figure 7. Possible mechanism of dimethicone distribution in a final mixture.

Carr Compressibility Index

For possible comparison of the final mixtures with the published *CI* values defined as optimal for successful powder filling using a dosator or a dosing disc, and thus determination of the mixture suitability for filling into capsules, modified *CI* was measured (Table III). From the given *CI* values for each mixture, it was found that the modified mixtures show better attributes than the original one. Based on the comparison with the published range of optimum *CI* values, only mixtures prepared with short mixing times fell into this range. However, this statement is only valid for values set for a dosator. None of the studied mixtures met the criteria for a dosing disc. Thus, it would be necessary to carry out an extension study or an adequate reformulation of the mixture.

Table III
Modified *CI* values for studied mixtures and literature optimal *CI* values.

Mixing time (min)	Modified *CI* (%)			
	mixture 1	mixture 2	mixture 3	mixture 4
35	35.0	30.1	31.9	31.2
55	47.7	-	37.3	-
75	44.6	-	38.9	-

Literature optimal value of *CI*	
18 - 30 %	dosing disc[5]
25 - 35 %	dosator[5]

Conclusion

We found out the rheological properties of model CS/D mixtures were dependent on the parameters of the mode of preparation and parameters of the premix CS/D preparation/final mixing sequence. Regarding the recommended *CI* values, only a part of mixtures evinces suitable behaviour for capsule filling using a dosator technique. No mixture was appropriate for filling via a dosing disc. Using FT4 powder rheometer, it was found out that the rheological properties of studied mixtures are affected by the mixing time and the composition of premix CS/D. The results point to the complex kinetic behaviour where corn starch - dimethicone aggregates are formed and disintegrated, followed by redistribution of dimethicone.

Acknowledgement

This research was financially supported by grant of specific university research, grant No A2_FCHT_2021_025.

References

1. Loidolt P., Madlmeir S., Khinast J. G.: Int. J. Pharm. *532*, 47 (2017).
2. Armstrong N. A., in book: Tablet and Capsule Machine Instrumentation (Ridgway Watt P., Armstrong N. A., ed.), cap. 10, p. 208-9. Pharmaceutical Press, London 2007.
3. Jones B. E.: Int. J. Pharm. *227*, 5 (2001).
4. Podczeck F., Newton J. M.: Int. J. Pharm. *185*, 237 (1999).
5. Carr P. K.: Dissertation. University of Maryland, Baltimore, Maryland 1998.

TABLET MICROSTRUCTURE EVOLUTION DURING THE COMPACTION PROCESS

Römerová S.[1], Dammer O.[2], Zámostný P.[1]

[1]University of Chemistry and Technology Prague, Department of Organic Technology, Technická 5, 166 28, Prague 6 - Dejvice, Czech Republic
[2]Zentiva, k.s., U Kabelovny 130, 102 37, Prague 10 – Dolní Měcholupy, Czech Republic
Simona.Romerova@vscht.cz

Abstract

Direct compression of bulk powder mixtures is a complex process with a significant influence on the final tablet structure and subsequently also the tablet performance during disintegration and drug release. Understanding and description of the final product properties and their dependency on individual material selection and compaction settings can therefore be very useful in the drug formulation or compaction process development and this study was aimed at improvement of one aspect of this understanding.

In the presented work, the combination of a hard, brittle excipient and a plastically deformable drug was used as a model system to introduce a methodology for the description of tablet microstructure evolution during compaction. Series of tablets containing different ratio between plastic drug (ibuprofen) and brittle excipient (EmCompress) were manufactured. The parameter describing tablet microstructure obtained by examination of SEM image was correlated with drug dissolution rate studied by a flow-through dissolution cell.

Introduction

Amongst various drug formulations, tablets remain the most common dosage form used perorally[1]. Formulation of the drug (API, active pharmaceutical ingredient) into the tablets is however usually complicated due to the significant dependence of the final tablet properties on different characteristics of used materials and also the material composition of the final product[2] and compaction process parameters. Material characteristics with high significance in the formulation process can be particle size, shape, viscoelastic and surface propeties[1]. The compaction process parameters can influence the particle deformation and fragmentation and subsequently the amount and strength of the interparticulate forces in the final tablet[3], which can further impact tablet deformation and disintegration. Considering fragmentation, apart from the compaction process settings (compaction force), viscoelasticity (propensity to deformation or fragmentation) of the material and particle shape are also very important. For example, needle-like particles are typically prone to fragmentation and size reduction is significant even when low compaction loads are used[4].

All of the reasons mentioned above implicate, that it is very beneficial to monitor the particulate microstructure of the resulting tablet, to make specific adjustments thereof, and to correlate it with the bulk properties of the resulting product such as hardness, disintegration, content uniformity, and also, the process of the active substance release from the tablet[1].

Adjustments of the dissolution process and dissolution rate are particularly important for poorly water-soluble APIs, which currently represent most of the newly registered drugs[5]. Faster dissolution can be achieved by reducing the active substance particle size and thus increasing the specific surface area thereof. It can be done for example by milling, micronisation or spray drying[6]. A decrease in the particle size however usually leads to increased hardness of the final tablets and therefore to slow dissolution[7-8]. In these cases, it is usually advantageous to combine a micronized active substance with suitable excipients with a larger particle size.

In addition to the initial particle size distribution, dissolution may also be affected by the ratio of the materials used in the formulation. If the API is well soluble and the excipients solubility is limited, then with the higher amounts of excipients in the tablet, the active substance may remain enclosed in the middle of a poorly soluble excipient aggregate. The API will not be dissolved and released until this aggregate disintegrates[2]. On the contrary, if soluble excipients are used with poorly soluble API, their fast dissolution exposes the surface of the API particles or aggregates and its release thus can be significantly enhanced[9].

Currently, the main used indicator of a tablet microstructure is the tablet porosity[1, 10]. The influence of the microstructure of the tablet, created during the compaction process, on its resulting properties and behaviour is often studied for single-component tablets[3, 8, 11-12]. However, the correlation between the compaction process and the resulting microstructure (and thus the dissolution properties) for mixtures of substances with different viscoelastic properties is nowadays not studied thoroughly.

Materials and methods

Materials for model mixtures were chosen based on values of their Young modules during compaction. The combination of a hard, brittle excipient and a plastically deformable drug was in the centre of attention. The choice was made based on the premise of the brittle material being protected from fragmentation by the plastic one, when present in a sufficient amount.

Materials

As a model API, plastically deformable Ibuprofen (Young modulus, E = 2.12 GPa, kindly provided from Zentiva, k.s., CZ) was used. The excipient in the model binary formulations was hard and brittle $CaHPO_4 \cdot 2H_2O$ (EmCompress®; Young modulus, E = 2.89 GPa, JRS Pharma GmbH & Co., DE).

Model tablets preparation

Model binary mixtures of Ibuprofen and EmCompress in three different weight ratios (85, 50 and 15 wt.% of Ibuprofen) were prepared and homogenized at 55 rpm for 5 minutes using Turbula T2F mixer (Glen Mills Inc., USA). Compaction of the tablets was performed using the compaction analyzer Gamlen GTP-1 (Gamlen Instruments, UK) equipped with the 5 mm die. Compaction load was set to 250 MPa and the amount of mixture used was adjusted, so all of the model tablets have height of around 2.3 mm.

Tablet microstructure evaluation

Model tablets inner microstructure was evaluated on their horizontal cross-section areas using scanning electron microscopy (SEM) and image analysis. To obtain tablet cross-section area samples, the tablets were incorporated into a paraffin wax matrix and sectionally cut on rotary microtome Leica RM2255 (Leica Mikro spol. s.r.o., CZ) with the step width of 10 µm. After the cross-section areas were obtained the samples were coated with 1.5 nm of platinum in sputter coater Q150R ES (Quorum Technologies Ltd, UK). The SEM analysis was performed on FE MIRA II LMU (Tescan, CZ) using the back-scattered electron detector (BSE). The model materials can be easily distinguished on the BSE detector since the used EmCompress excipient contains phosphorus atoms in its molecule and therefore appears in lighter shades of grey (brighter) on the resulting pictures.

This aspect of the pictures was further utilized in the image analysis of the SEM pictures. It was performed with a simple original programme created in the Matlab environment. Generally, the analysis consisted of the following steps: contrast adjustment, lowpass filtering and region segmentation (Figure 1).

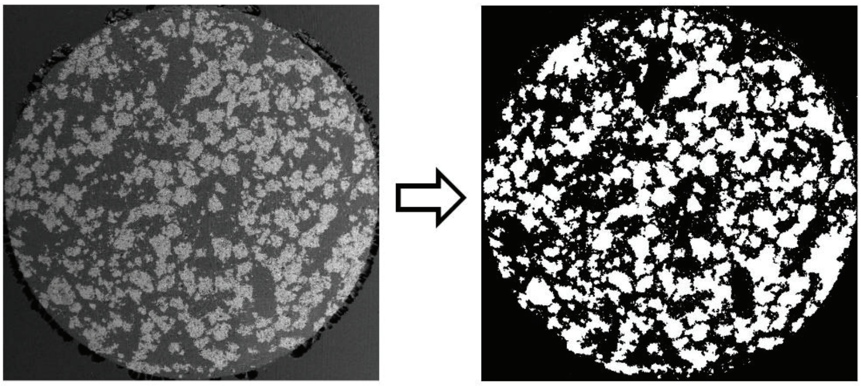

Figure 1. Illustration of the image analysis programme workflow. Left – an original SEM picture of tablet containing 50 wt. % of Ibuprofen after contrast adjustment, right – black and white map of the segmented regions of interest (particles/aggregates of the excipient, EmCompress). 50× mag.

For the segmented regions (particles/aggregates of EmCompress) size distributions were constructed and quadratic means of equivalent diameter ($d_{eq,QAvg}$) were determined for each of the tested formulations.

Flow-through dissolution

To describe model tablets drug release flow-through dissolution tests using Sotax CE-7smart (Sotax AG, CH) were performed. The used method was consistent with American pharmacopoeia. The machine was equipped with small tablet cells (12 mm diameter), tablets were placed in a holder located in the middle of their height. The tests were performed with an open-loop configuration, therefore, the dissolution medium (phosphate buffer) passed through the cells only once at a flow rate of 6 $ml \cdot min^{-1}$ and the samples were taken continuously throughout the entire duration of the dissolution test (1 h). Measurements took place at a temperature of 37 °C. The samples were subsequently analysed on a UV/VIS spectrophotometer SPECORD 200 PLUS (Analytik Jena AG, DE) using wavelengths equal to 234 and 264 nm. After the dissolution profiles were constructed for each sample their limit release rates (r_{lim}) of Ibuprofen were also determined.

Discussion and result analysis

As particle size distribution of excipient in the tablets (subsequently $d_{\mathrm{eq,QAvg}}$) and drug release (subsequently r_{lim}) were determined for each sample, the correlation analysis between them was performed to establish their relationship and possible dependency.

Tablet microstructure – EmCompress size distribution and $d_{\mathrm{eq,QAvg}}$

Firstly, the equivalent diameter area distribution for each tested formulation was obtained through the image analysis of SEM pictures of tablet crosssection areas, as shown in Figure 2. For further correlation with the dissolution characteristics, a quadratic mean of equivalent diameter ($d_{\mathrm{eq,QAvg}}$) was used as a one-parameter description and its values are presented in Table I. For better comparison, the same value for raw excipient material is also included.

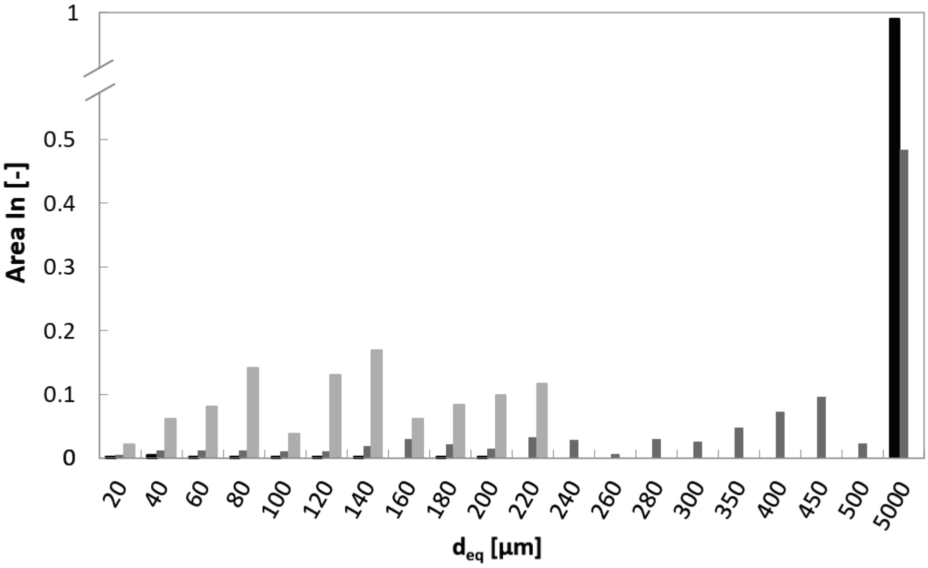

Figure 2. EmCompress particle/aggregate size distribution in the model tablets. ● - formulation with 15 wt. % of Ibuprofen, ● - 50 wt. % and ● - 85 wt. %, respectively.

Table I

Quadratic means of the equivalent diameter of EmCompress in prepared tablets (and as a raw material).

w_{API} [%]	0 (raw EmCompress)	15	50	85
$d_{\mathrm{eq,QAvg}}$ [µm]	127.6	226.2	127.9	61.3

Dissolution – Ibuprofen release and r_{lim}

The second major part of the presented work was the tablets dissolution process description. As shown in tablets dissolution profiles in Figure 3, the dissolution of Ibuprofen from model tablets was slow and insufficient. It is caused by the compactness and hardness of the model tablets, which were practically non-disintegrating. For illustration, Figure 4 show the tablet containing 50 wt. % of Ibuprofen after the 1 hour of flow-through dissolution. It is nicely visible that the dissolution apparently takes place predominantly on the tablet surface where Ibuprofen plastic areas were formed during the compaction process. And subsequently on the free surface of these Ibuprofen plastic areas deeper in the tablets. However, the goal of this study was not to obtain a well disintegrating formulation, but rather to compare the Ibuprofen release with the earlier described tablet microstructure parameter.

The limit release rate (r_{lim}) of Ibuprofen was chosen for the description of the dissolution behaviour since the previously described poor disintegration led to slow dissolution, therefore the maximum release rate or amount of released drug would not be as descriptive. Firstly, specific release rates obtained from dissolution profiles for each formulation were plotted against the already released amount of Ibuprofen. The intercept of its linear regression corresponded to the value of limit release rate (evaluated for the ibuprofen release higher than 1 %). Limit release rate values are summarized in Table II.

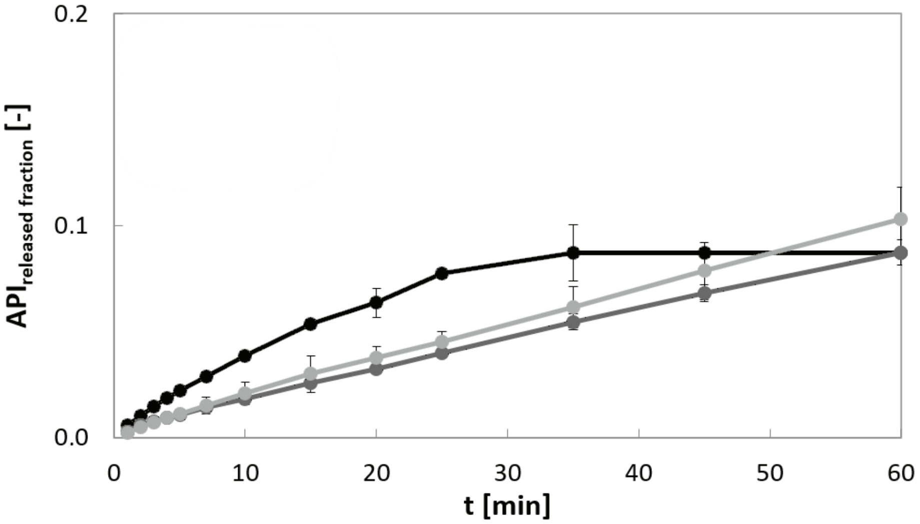

Figure 3. Ibuprofen dissolution from the model tablets. ● - formulation with 15 wt. % of Ibuprofen, ● - 50 wt. % and ● - 85 wt. %, respectively.

Figure 4. Tablet with 50 wt. % of Ibuprofen after the 1-hour flow-through dissolution. Optical microscopy, 1.5× obj. mag.

Table II

Ibuprofen limit release rates of tested formulations.

w_{API} [%]	15	50	85
r_{lim} [min^{-1}]	$16 \cdot 10^{-4}$	$4 \cdot 10^{-4}$	$5 \cdot 10^{-4}$

Mean excipient particle size and drug limit release rate

Finally, the obtained characteristics – excipient quadratic mean of the equivalent diameter, $d_{eq,QAvg,}$ and drug limit release rate, r_{lim}, were correlated, see Figure 5. From that, it is clearly observable, that the release rate of the drug increases with the quadratic mean diameter of the excipient in the formulation. The observed dependence can be explained by the formation of compact Ibuprofen areas thanks to its plastic deformability. Large compact Ibuprofen areas are formed in tablets with a smaller size of excipient (same or lower in comparison with the input material), which corresponds with higher Ibuprofen content (50, 85 wt. %). In these formulations the dissolution rate is low. For low Ibuprofen content (related to higher excipient size values than the input material), the dissolution rate is higher, since the API is only allowed to form smaller clusters/compact areas in size, in comparison with the previous formulations. Smaller compact areas lead to a bigger surface available for dissolution relatively to the loading. Considering all of the above-stated findings, the use of the excipient particle size proved to be reasonable and sufficiently descriptive for such binary system, possibly even more suitable than conventionally used drug particle size. Moreover, the positions of the points in the plot indicate, that the studied model system exhibits percolation behaviour (illustrated by a dotted line in Figure 5). During the performed measurements it was observed, that Ibuprofen, thanks to its plastic deformability, can create compact masses of non-distinguishable deformed particles under the compression. Therefore, it can be presumed, that in a certain amount it would create a uniform continuous mass in the tablet, which can dramatically change its properties. Further investigation in this area is, however, necessary to assess the percolation threshold presence in this system and its exact value of composition.

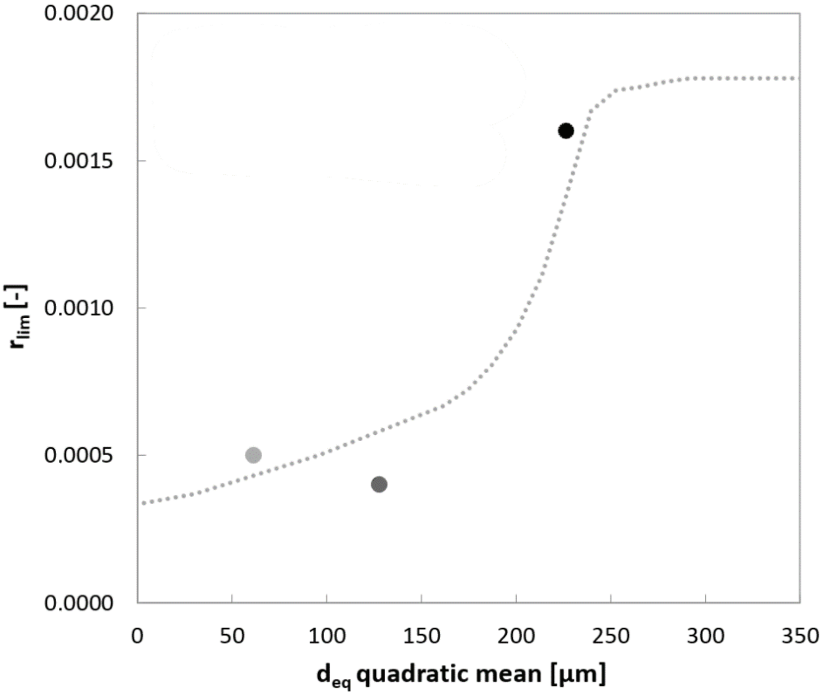

Figure 5. Correlation between the EmCompress mean particle/aggregate size and the Ibuprofen limit release rate for tested model tablets. ● - formulation with 15 wt. % of Ibuprofen, ● - 50 wt. % and ● - 85 wt. %, respectively. The dotted line illustrates the possible percolation behaviour of the model system.

Conclusion

During the presented work, a methodology for the correlation of the dissolution rate with the tablet microstructure parameter for the model system was developed. It was found that the API release can be influenced by the ibuprofen content in the formulation and the trend shows the features of percolation behaviour. Presented model binary mixtures proved the premise about the protective function of plastic material, Ibuprofen, when present as a major mixture component. The excipient, EmCompress, used in this formulation did not undergo extensive fragmentation when surrounded by Ibuprofen mass. It led to its presence in the final tablet usually in a form of original primary particles, which did not interrupt the uniform mass of deformed Ibuprofen particles effectively, causing the decrease in API limit release rate with the increasing amount of it in the formulation. Further work is already planned to study the percolation threshold phenomena in the presented model binary mixture. With the more precise information about the excipient size-drug release relationship, the release rate can be adjusted by setting the excipient amount or particle size used in the final tablet. Furthermore, the goal for the next work is also to complete the methodology with different material combinations and to ultimately use it for practical tablet formulation development.

Acknowledgement

This work was supported from the grant of Specific university research – grant No A2_FCHT_2021_043. Technical and scientific support was also provided from The Parc.

References

1. Sun, C. C.: Pharm. Res., *34*, 918 (2017).
2. Kimber, J. A.; Kazarian, S. G.; Štěpánek, F.: Comput Chem Eng, *35*, 1328 (2011).
3. Eriksson, M.; Alderborn, G.: Pharm. Res., *12*, 1031 (1995).
4. Šimek, M.; Grünwaldová, V.; Kratochvíl, B.: Pharm Dev Technol, *21*, 583 (2016).
5. Kawabata, Y.; Wada, K.; Nakatani, M.; Yamada, S.; Onoue, S.: Int. J. Pharm., *420*, 1 (2011).
6. Khadka, P.; Ro, J.; Kim, H.; Kim, I.; Kim, J. T.; Kim, H.; Cho, J. M.; Yun, G.; Lee, J.: Asian J. Pharm. Sci., *9*, 304 (2014).
7. McKenna, A.; McCafferty, D. F.: J. Pharm. Pharmacol., *34*, 347 (1982).
8. Sun, C.; Grant, D. J. W.: Int. J. Pharm., *215*, 221 (2001).
9. Štěpánek, F.: Comput. Mater. Sci., *44*, 145 (2008).
10. Krupa, A.; Tabor, Z.; Tarasiuk, J.; Strach, B.; Pociecha, K.; Wyska, E.; Wronski, S.; Lyszczarz, E.; Jachowicz, R.: Eur. J. Pharm. Sci., *119*, 234 (2018).
11. Yohannes, B.; Gonzalez, M.; Abebe, A.; Sprockel, O.; Nikfar, F.; Kiang, S.; Cuitiño, A. M.: Int. J. Pharm., *503*, 68 (2016).
12. Adolfsson, Å.; Olsson, H.; Nyström, C.: Eur J Pharm Biopharm, *44*, 243 (1997).

APPLICATION OF HANSEN SOLUBILITY PARAMETERS IN THE PHARMACEUTICAL INDUSTRY

Petříková E.[1], Hriňová E.[2], Čerňová M.[3], Dammer O.[3], Krejčík L.[3], Patera J.[1]

[1]*University of Chemistry and Technology Prague, Faculty of Chemical Technology, Department of Organic Technology, Technická 5, Prague 6, 166 28, Czech Republic*
[2]*University of Chemistry and Technology Prague, Faculty of Chemical Engineering, Department of Chemical Engineering, Technická 5, Prague 6, 166 28, Czech Republic*
[3]*Zentiva, k.s., Prague, U Kabelovny 130, 102 37 Prague 10, Czech Republic*
eva.petrikova@vscht.cz

Abstract

The solubility of APIs in water is very crucial for the pharmaceutical industry. Poor water solubility leads to poor bioavailability. The bioavailability of API must be enhanced by a suitable drug formulation, for instance, the amorphous solid dispersions or amorphous solid solutions, to provide safe, quality and effective drugs to patients. In the preformulation process, the proper excipients for formulation with API must be selected. A suitable formulation could prevent, for example, API recrystallization or the inappropriate interactions between API and some excipients. The Hansen solubility parameters can be used to simplify the problem by choosing a proper excipient for the API. This work aimed to verify predictions of compatibility based on the Hansen theory between selected API and chosen polymers to enhance the APIs' bioavailability. The goal was to formulate API with compatible polymers into amorphous solid solutions or amorphous solid dispersions.

Introduction

In the pharmaceutical industry, preformulation is the key step to select the proper final drug formulation. During this process, it is crucial to select proper excipients for certain API for further formulation. However, there may occur several problems beginning with the inappropriate API-excipient interaction and ending with API degradation. Nowadays, many software for predicting compatibility of API with excipients are available on the market, which can solve this problem. [1, 2] Nevertheless, each software has its limitation, including its computing capacity, the variable reliability of computed predictions or software complexity, and high hardware requirements. For that reason, there is an effort to simplify this process without any special complex software or additional special equipment.

Hansen solubility parameters (HSPs) are based on the general well-known fact: like dissolves like. It means if the measured API has similar HSPs with certain excipients, they will be compatible. The HSPs are composed of three individual elements: atomic dispersion forces δ_D, molecular non-binding dipole interactions δ_P and molecular hydrogen bonds δ_H.[3] Each of these partial HSPs can also form one of the three elemental axes in the 3D Hansen space (Figure 1).

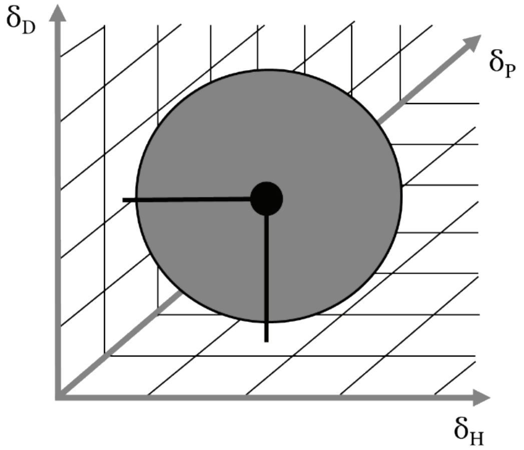

Figure 1. Hansen 3D space

In this 3D space, if the sample forms the centre of the sphere and the other measured excipients are close to the sample and thus creates the space of the sphere, it is assumed, that they will be compatible. Excipients which are placed out of the sphere will not be compatible with the measured sample.[4] The *Ra* parameter serves to determine the distance between two substances in the Hansen 3D space. The smaller will be the value of the *Ra* parameter, the more will two substances be compatible. The *Ra* parameter can be calculated from Equation 1:

$$(Ra)^2 = 4 \cdot (\delta_{D2} - \delta_{D1})^2 + (\delta_{P2} - \delta_{P1})^2 + (\delta_{H2} - \delta_{H1})^2 \tag{1}$$

where δ_D represents the dispersion element of HSPs, δ_P stands for the polar element of HSPs and δ_H is the element for hydrogen bonding of HSPs, indexes 1 and 2 are for excipient and measured substance, respectively.[4] HSPs can be determined both experimentally and theoretically. The experimental determination of HSPs can be held by the solvent experiments[5, 6] and for theoretical HSPs determination, the van Krevelen additive method[7, 8] can be used.

The theoretical additive method according to van Krevelen can be used only for the APIs which are in form of the free base, not in form of salts, solvates, cocrystals, etc.

Van Krevelen requires only knowledge of the chemical structure of the API. By a combination of the van Krevelen, Hoftyzer[7] and Fedors[9] approaches, the individual elements of HSPs can be calculated using Equations 2 - 4:

$$\delta_D = \frac{\sum_i F_{D_i}}{\sum_i V_i} \tag{2}$$

$$\delta_P = \frac{\left(\sum_i F_{P_i}^2\right)^{0,5}}{\sum_i V_i} \tag{3}$$

$$\delta_H = \left(\frac{\sum_i F_{H_i}}{\sum_i V_i}\right)^{0,5} \tag{4}$$

where *i* is a structural group in the molecule, F_{Di} represents the group contribution to a dispersion component, F_{Pi} stands for the group contribution to a polar component, F_{Hi} is attributed to the group contributed to a hydrogen bonding component and V_i is the molar volume of the calculated substance. These constants can be obtained from the literature[3, 7, 9].

One of the crucial problems for the pharmaceutical industry is the solubility of API in water. A significant number of APIs are poorly soluble or insoluble in water. The formulation to solid dispersions can be used to enhance the poor water API solubility. However, the term solid dispersion could contain several dispersion systems with different physicochemical properties. The carrier could be in a crystalline or amorphous state and equally the API. The amorphous solid solution can be obtained if the API is dispersed molecularly in the carrier. The API is actually dissolved in the carrier. Solid dispersion can be obtained if the API is in solid-state dispersed in the carrier. The API can be in amorphous form (amorphous solid dispersion) or crystalline form (solid dispersion).[10] The pure amorphous solid solutions are the preferred candidates for further formulation because there is an expectation that they should improve the API release from the polymer matrix more significantly than the amorphous solid dispersions[11,12].

This work was focused on the applicability of Hansen's theory as a novel and reliable prediction model for the compatibility of API with excipients for the pharmaceutical industry. API with poor water solubility was chosen to be a model API. The goal was to prepare the chosen API in the form of the amorphous solid solution or amorphous solid dispersion with selected polymers.

Materials and methods

In this study, several binary mixtures were prepared for hot-melt extrusion (HME) experiments as one of the most common methods for obtaining amorphous solid solutions or amorphous solid dispersions. Several measured polymers were used for the formulation.

Materials

Materials for HME experiments: HPMCP HP-55, Methocel™ Premium K100 LV, Methocel™ K15, Methocel™ K100, Methocel™ K4M, Methocel™ E5, Kollidon® 12 PF, Kollidon® VA 64, Eudragit® L100-55, Soluplus®, and API were kindly provided by Zentiva k.s.

Solvents for solvent experiments: hexane, heptane, octane, nonane, cyclohexane, methanol, ethanol, 2-butanol, 2-propanol, 1,4-dioxane, ethyl acetate, butyl acetate, tetrahydrofuran, ethylene glycol, diethylene glycol, acetic acid, diethylamine, diethyl ether, benzene, toluene, ethanolamine, 2-pentanone, 2-butanone, acetone, 1-nitropropane, dichloromethane, chloroform, acetaldehyde, acetonitrile, acetic anhydride, dimethyl sulfoxide, anisole were kindly provided by Zentiva k.s.

Solvent method

The solvent method was used to determine the HSPs of each used polymer. The solvent method was held according to the literature[5, 6]. The conditions of these experiments were the following: 0.5 g of polymer was weigh to the preweighed 25 mL Erlenmeyer flask, 5 mL of solvent was added to the flask and then samples were stirred for 24 h. After stirring, the samples were filtered and dried for another 24 h. After the drying, samples were weighed. From the knowledge of HSPs of used solvents (at least 20 solvents were used for the determination), the HSPs of the sample was determined as the weighted average of used solvents and the amount of solubilized polymer.

HME experiments

HSPs of API were calculated using van Krevelen additive method[7, 8] using Equations 2 - 4. A criterion for the selection of proper polymers to the API was the parameter *Ra*. After the determination of HSPs of polymers, the *Ra* parameter was calculated using Equation 1. According to the *Ra* parameter, Table 1 of preferable candidates for the binary mixtures (polymer-API) for HME experiments was created. The unpreferable candidates were excluded based on the higher value of their *Ra* parameter: Methocel™ Premium K100 LV (24.99), Methocel™ K15 (25.72), Methocel™ K100 (25.95), Methocel™ K4M (26.10) and Methocel™ E5 (26.16).

Table I

Polymers prioritized by the *Ra* parameter

Polymer	*Ra*
HPMCP HP-55	23.10
Kollidon® 12 PF	23.57
Soluplus®	23.68
Eudragit® L 100-55	24.12
Kollidon® VA 64	24.24

Binary mixtures polymer-API were prepared to verify the usability of the Hansen theory in terms of formulation to amorphous solid solutions or amorphous solid dispersions, which can increase the API bioavailability. Selected ratios API:polymer (w:w) were 1:1, 1:2 and 1:3. These mixtures were blended using a Turbula T2F (10 minutes, 49 rpm) in order to achieve a sufficiently homogeneous blend. The mixtures were further processed by a twin screw-type extrusion (Three Tec Twin-Screw Extruder ZE 5, Three-Tec Ltd., Switzerland) using different temperature settings. The extrudates were subjected to milling using a ball mill (35 Hz, 2 minutes). After milling, samples were analysed by X-ray powder diffraction (XRPD) and differential scanning calorimetry (DSC) to discover whether the amorphous solid solution or amorphous solid dispersion were obtained.

Results and discussion

Each sample prepared by HME was firstly subjected to XRPD analysis. Samples that contained API in amorphous form were further subjected to DSC analysis to discover if the binary mixture forms an amorphous solid solution or amorphous solid dispersion. The only exception was for HPMC HP-55, where one sample containing the crystalline API was also measured on DSC to quantify the crystalline API form.

The ratio of API:polymer (Ratio), the temperature used for HME experiments (T), results from XRPD and DSC analyses, including the temperature of glass transition (T_g), melting point (T_{mp}) and temperature of recrystallization (T_{rec}) are summarized in Table 2. Unfortunately, samples containing Eudragit® L 100-55, which T_g value is 111 °C[13] and was extruded at 150 °C, 170 °C and 190 °C, exhibit the presence of API only in the crystalline form for all studied Ratios.

Table II
Results from XRPD and DSC analyses

		XRPD	DSC	
HPMCP HP-55				
Ratio	T [°C]	Form		
1:1	170	crystalline	T_g = 104 °C, T_{mp} = 175.7 °C (31.3 J/g)	crystalline dispersion
	180	amorphous	T_g = 96 °C, T_{rec} = 147 °C (17.4 J/g) T_{mp} = 177.5 °C (20.8 J/g)	amorphous solid solution with unknown impurity
	190	amorphous	T_g = 85 °C, T_{mp} = 138.6 °C (2.8 J/g)	amorphous solid solution with unknown impurity
1:2	170	crystalline	–	–
	180	amorphous	T_g = 97 °C	amorphous solid solution
	190	amorphous	T_g = 94 °C, T_{mp} = 139.5 °C (9.8 J/g)	amorphous solid solution with impurity
1:3	170	crystalline	–	–
	180	amorphous	T_g = 103 °C	amorphous solid solution
	190	amorphous	T_g = 95 °C, T_{mp} = 133.2 °C (13.6 J/g)	amorphous solid solution with unknown impurity
Kollidon® 12 PF				
Ratio	T [°C]	Form		
1:1	160	crystalline	–	–
	190	amorphous	T_g = 109 °C	amorphous solid solution
1:2	160	amorphous	T_g = 108 °C	amorphous solid solution
	190	amorphous	T_g = 108 °C	amorphous solid solution
1:3	160	crystalline	–	–
	170	amorphous	T_{g1} = 62 °C, T_{g2} = 109 °C	amorphous solid dispersion
	190	amorphous	T_{g1} = 62 °C, T_{g2} = 109 °C	amorphous solid dispersion
Soluplus®				
Ratio	T [°C]	Form		
1:1	150	crystalline	–	–
	170	crystalline	–	–
	190	amorphous	T_{g1} = 64 °C, T_{g2} = 91 °C	amorphous solid dispersion
1:2	150	crystalline	–	–
	170	crystalline	–	–
	190	amorphous	T_{g1} = 62 °C, T_{g2} = 90 °C	amorphous solid dispersion
1:3	150	crystalline	–	–
	170	crystalline	–	–
	190	amorphous	T_{g1} = 63 °C, T_{g2} = 89 °C	amorphous solid dispersion
Kollidon® VA 64				
Ratio	T [°C]	Form		
1:1	150	crystalline	–	–
	170	crystalline	–	–
	190	amorphous	T_g = 109 °C	amorphous solid solution
1:2	150	crystalline	–	–
	170	crystalline	–	–
	190	amorphous	T_g = 110 °C	amorphous solid solution
1:3	150	crystalline	–	–
	170	crystalline	–	–
	190	amorphous	T_g = 110 °C, T_{mp} = 175.7 °C (0.2 J/g)	crystalline dispersion

Based on the XRPD results, it was discovered that amorphous API in a binary mixture with HPMCP HP-55 can be obtained using higher temperatures for HME experiments. The T_g value of HPMCP HP-55 was found to be 139 °C; however, the selected temperature of 170 °C for HME experiments was not sufficient to obtain the API in amorphous form. The inability to form the amorphous solid dispersion at 170 °C could be caused by the higher viscosity of the melt of the polymer. The higher viscosity of the melt could prevent the API to entirely dissolve in the melt.[14] The interesting phenomenon was observed at the binary mixture of API with Kollidon® 12 PF. The value of T_g for Kollidon® 12 PF is 90 °C[15]. For that reason, the chosen temperature for HME experiments was 160 °C. In Ratio 1:1 and 1:3, the temperature of 160 °C was not sufficient to achieve the API in amorphous form. From these results, it can be considered that the temperature used in HME experiments is not the only crucial parameter for obtaining the pure amorphous solid solution, but the used ratio also has an influence. For the binary mixtures with Kollidon® VA 64, which T_g value is 101 °C[15], the API in amorphous form was achieved only using the temperature 190 °C at all three Ratios. The same phenomenon was also observed for the binary mixtures with Soluplus®, which has a value of T_g around 70 °C[15].

Based on the DSC results, it was found that the T_g of pure amorphous API is 101°C and the T_{mp} of crystalline API is 190.9 °C (67.6 J/g). For HPMCP HP-55 at Ratio 1:1 extruded at 170 °C, it was observed that this sample contains a large amount of crystalline API when comparing the enthalpies of this sample (31.3 J/g) and the crystalline API (67.6 J/g). For HPMCP HP-55 at Ratio 1:1 (180 °C), the amorphous solid solution was obtained. However, at the temperature of 140 °C, the amorphous API recrystallizes into crystalline form, which melts at 177.5 °C, or there could be some ingredient of the crystalline form of API. On the contrary, the amount of HPMCP HP-55 used in the Ratios 1:2 and 1:3 extruded at 180 °C was sufficient to dissolve the API entirely. When comparing the enthalpy values for all mixtures with HPMCP HP-55 extruded at 190 °C, it can be observed that with an increasing amount of polymer in the mixture, the amount of the crystalline impurity increases. According to the DSC data, this crystalline impurity does not belong to crystalline API, so it is presumed that it belongs to some degradation product of the used polymer or API. The interesting results were observed for Kollidon® 12 PF. Based on the DSC analysis, the amorphous solid solutions were obtained for the Ratio 1:1 extruded at 190 °C and Ratio 1:2 extruded at 160 °C and 190 °C. However, for Ratio 1:3 extruded at 170 °C and 190 °C, the amorphous solid dispersion was observed. The value of T_{g1} (62 °C) does not fit the T_g of polymer (90 °C). In this case, the origin of the T_{g1} value was not clarified. The value of T_{g2} (109 °C) can be attributed to the amorphous solid solution. The other explanation of these results could be that two amorphous solid solutions were obtained, which one of them could contain an excess of water. This possibility was excluded after drying these samples for three days at 40 °C in the vacuum drier.

In the case of Soluplus®, solid dispersions were observed. It was found that the lower value of polymer T_g also lowered the value of T_{g2} of the amorphous solid solution. In this case, the T_{g1} values can be attributed to polymer, and the T_{g2} values belong to the amorphous solid solution.

For Kollidon® VA 64, we were able to obtain an amorphous solid solution in two cases. The sample with Ratio 1:3 extruded at 190 °C was on the limit of detection of the instrument; however, a very small amount of the crystalline API was observed.

From 43 sample we were able to obtain 17 amorphous solid solutions of which 7 samples created the amorphous solid solutions. From above, it can be presumed, that predictions based on Hansen's theory have the potential to be very useful to select a suitable polymer into the formulation. The predictions were established on the *Ra* parameter, which was selected as a compatibility criterion for measured polymers and calculated API according to their values of HSPs. The *Ra* parameter values of selected polymers were in the range from 23.10 to 24.50. Certainly, the HME experiments should be performed for the larger number of polymers to verify the theory and the reliability of chosen criterion, the *Ra* parameter. For polymers with higher *Ra* values, amorphous solid dispersions cannot be formed. However, from these results, it can be concluded that HSPs have significant potential for the prediction of compatibility of APIs with excipients.

Conclusion

A prediction compatibility model based on the Hansen theory was introduced. The *Ra* parameter was chosen as the compatibility criterion for the binary mixtures of API-polymer. Binary mixtures of API:polymer were subjected to HME experiments using different temperatures and ratios. All samples were subjected to XRPD to investigate if the amorphous API was obtained. Samples that contained API in amorphous form were further subjected to DSC analysis to discover, whether the amorphous solid solution or amorphous solid dispersion was obtained. Despite the low number of binary mixtures, we were able to successfully reach several amorphous solid solutions and amorphous solid dispersions which can enhance the API bioavailability. Further investigation of the reliability of the prediction model based on the Hansen theory is necessary to verify its full implication for the pharmaceutical industry.

Acknowledgement

This work was supported by the grant of Specific university research – grant No. A2_FCHT_2021_026 and from the Zentiva k.s.. The authors would like to thank to The Parc for all the support during the research.

References

1. Gaikwad, V. L.; Bhatia, N. M.; Desai, S. A.; Bhatia, M. S., Carbohydr Polym, *151*, 593 (2016).
2. Niederquell, A.; Wyttenbach, N.; Kuentz, M., *546*, 137 (2018).
3. Hansen, C. M., Hansen Solubility Parameters: *A User's Handbook*. CRC Press: 2007.
4. Adamska, K.; Bellinghausen, R.; Voelkel, A. *1195*, 146 (2008).
5. Nielsen, T. B.; Hansen, C. M., Polymer Testing, *24*, 1054 (2005).
6. Navarro-Lupion, F. J.; Bustamante, P.; Escalera, B., J. Pharm. Sci., *94*, 1608 (2005).
7. Krevelen, D. W. v.; Hoftyzer, P. J., Properties of polymers, their estimation and correlation with chemical structure. Elsevier Scientific Pub. Co.: Amsterdam; New York, 1976.
8. Pearce, E. M., Krevelen, D. W. v., J. Polym. Sci., Polym. Lett. Ed., *15*, 56 (1977).
9. Fedors, R. F., Polym. Eng. Sci.**,** *14*, 147 (1974).
10. Gruberová, L.; Kratochvíl, B.,. *Chem. Listy, 113*, 383-390 (2019).
11. Helbling, M.; Luna, J.A.; Cabrera, M.I.. J. Control. Release 149, 258–263 (2011).
12. Siepmann J.; Siepmann F., J Control Release, *161*, 351 (2012).
13. Thakkar, R.; Thakkar, R.; Pillai, A.; Ashour, E. A.; Repka, M. A., Int. J. Pharm., *576* (2020).
14. Repka, M. A., Bandari, S., Kallakunta, V. R., Vo, A. Q., McFall, H., Pimparade, M. B., & Bhagurkar, A. M., Int J Pharm, *535*(1-2), 68–85 (2018).
15. Kolter, K.; Karl, M.; Nalawade, S.; Rottmann, S.; Hot-Melt Extrusion with BASF Pharma Polymers. Extrusion Compendium. BASF. (2011).

CERAMIDE LIPOSOMES: FORMULATION OF STRATUM CORNEUM LIPIDS FOR SKIN BARRIER RECOVERY

Vovesná A.[1], Zbytovská J.[1]

[1]*University of Chemistry and Technology Prague, Technická 5, 166 28, Prague 6*
vovesnaa@vscht.cz

Abstract

Atopic dermatitis and psoriasis are skin diseases caused by lowered levels of skin lipids, namely ceramides, in the stratum corneum lipid matrix. Viable alternative to the conventional corticosteroids is topical delivery of appropriately formulated skin lipids. For this purpose, we developed unique ceramide liposomes (cerosomes) with excellent efficiency in disrupted skin barrier repair. Thin lipid film hydration and high pressure homogenization were used to prepare various types of liposomal systems. To determine the stability, the particle size and polydispersity index were measured. The optimal systems were found to include ceramide 3 and 6, cholesterol and stearic acid, with 10% urea in phosphate-buffered saline as the aqueous phase. Next, the ability of the system to repair chemically-damaged porcine skin was tested. While treatment by a standard lipid suspension reduced the passage of a model permeant only to a limited extent, drug flux through the liposomally-treated skin was much closer to permeation through intact skin. The non-homogenized liposomes were more effective than their homogenized version. This suggests that our approach to liposomal development has considerable potential for the repair of a disrupted skin barrier.

Introduction

Ceramides are one of the main lipids of the skin and play a crucial role in its barrier function[1, 2]. Their correct arrangement and content amongst other lipids in SC lipid matrix is necessary to maintain the barrier function of the skin[3]. Otherwise, the barrier can become so disrupted that the skin cannot fully protect the body, potentially leading to skin conditions, the most prevalent of which is atopic dermatitis (AD). The reason for skin barrier disruption is not yet fully understood, but owing to variety of AD triggers necessitate a complex treatment methodology that is able to protect the skin, lower trans-epidermal water loss and, ultimately, heal the disrupted skin barrier.

The most frequently prescribed treatment for AD are topical corticosteroids; however, their use is associated with a variety of side-effects. One viable alternative to conventional skin disease treatments involves supplying the skin with ceramides, cholesterol or other native lipids[4, 5]. Research is especially focused on ceramide 3 (Cer 3) and ceramide 6 (Cer 6) because they play an important role in the correct arrangement of lamellar SC lipids. It has been shown that the best way to achieve the highest efficacy of ceramide treatment is to administer the lipids in a form similar to that of the composition of lipid bilayers in the SC lipid matrix[6-9]. One or more such bilayers can be found in liposomes, which structure is well suited for ceramide nanoformulation. Ceramides and ceramide nanoparticles have already been tested several times as (trans-)dermal vehicles for other active substances or even as excipients in skin repair formulations[10-13]. Although a number of liposomal ceramide formulations have been investigated, there has not yet been an attempt to explore the potential of ceramide liposomes themselves as the active ingredient responsible for skin barrier repair.

For this purpose, we developed several liposomal formulations containing ceramides and other skin lipids in various ratios, and tested their feasibility and stability. We established the efficacy of this treatment by administering the liposomes on chemically damaged porcine skin which served as model of AD impaired barrier. We show that our proposed liposomal systems are able to restore damaged skin to a state close to that of healthy skin.

Experiment

Preparation of liposomes

The compositions of prepared liposomal systems are stated in Table I. Ceramides, cholesterol (chol), stearic acid (SA) and phospholipon (PL) were all in equimolar ratio. Liposomes were prepared by a modified thin lipid film hydration method[14]. Briefly, the lipids were weighted into a round-bottom flask and dissolved in a mixture of chloroform : methanol 2:1 (v/v) in order to obtain a 10% lipid solution. The mixtures were sonicated at 37 kHz power and 40 °C for 5 minutes until all lipids dissolved. The solvent was then evaporated on a rotary evaporator at 50 °C and 100 rpm, until a thin lipid film formed on the walls of the flask. The dried lipid film was hydrated by

10% urea solution in phosphate buffered saline (PBS+U). The amount of added aqueous phase resulted in the final concentration of lipids of 1 %. The hydrated lipid film was then repeatedly heated to 90 °C and vigorously mixed on a vortex until all lipids dispersed in the aqueous medium and a smooth white liposome mixture was formed. So prepared multilamellar nonhomogenized (NH) liposomes were processed by high pressure homogenization (HPH) by 10 homogenization steps (H10 version of liposomes).

Table I
Composition of tested liposomal systems.

Type	C3+PL	C6+PL	C3+C6+PL	C3	C6	C3+C6
CER3	✓	-	✓	✓	-	✓
CER6	-	✓	✓	-	✓	✓
PL	✓	✓	✓	-	-	-
SA	✓	✓	✓	✓	✓	✓
CHOL	✓	✓	✓	✓	✓	✓

Characterization of liposomes

Liposomes were characterized by dynamic light scattering (DLS) in order to obtain particle size distribution and polydispersity index of the system. To exclude the influence of undissolved lipids or aggregated nanoparticles on DLS measurement, liposomes were observed under optical microscopy. To determine the shape and morphology of liposomes the systems were observed by transmission electron microscopy (TEM).

In vitro skin disruption, repair and permeation test

Squares sized 1.5 × 1.5 cm were cut out from a porcine external ear skin and mounted on Franz diffusion cells (FCs). The acceptor phase was filled with PBS (pH = 7.4). A mixture of chloroform : methanol 2:1 (v/v) was added into the donor space and the FCs were left on a shaker for 5 minutes. The solvent was withdrawn from the donor part after the elapsed time. Next, the donor compartments were filled with 300 µl of various "repairing" formulations. The first were the NH and H10 cerosomes, the second were lipids mixed in the same ratio as in actual liposomes, but solely suspended in PBS+U. The last applied substance on disrupted skin samples was sole PBS+U as a control 'renewing' agent. The PBS+U was also applied on the control non-disrupted skins. The repair process took place for 24 hours. After this time, the donor compartments were thoroughly washed and 300 µl of indomethacin (IND) suspension in 60% propylene glycol in water (v/v) was placed in the donor compartment. This permeation experiment ran for 48 hours with samples of acceptor phase being taken out in predetermined time intervals. All acquired samples were analysed by HPLC.

Discussion and result analysis

Liposomal systems were prepared in 6 different variations (Table I). They contained cholesterol and stearic acid accompanied by various combinations of ceramide 3, ceramide 6 and phospholipid. The types of liposomes were divided into two groups: with and without PL and named CER3+PL, CER6+PL, CER3+CER6+PL, CER3, CER6, CER3+CER6. Liposomes created by thin lipid hydration method were multilamellar, sized between 500-2000 nm and the size varied in each individual sample. Next step was the HPH process, which enabled creation of smaller liposomes of more uniform size. The liposomal types responded differently to the HPH step some being more malleable than others. The group of liposomes containing PL was less open to the size change and homogenization was less effective compared to the group without PL. Initial size of multilamellar PL liposomes was around 500 nm and maintained this value during observed 21 days. PdI of NH PL liposomes remained at value 0.5, except the sample containing CER3, PdI of which reached high values at preparation and rose more during time. Liposomes of the size about 100 nm and of similar PdI value were achieved by HPH in every PL type. CER3+CER6+PL sample expressed peculiar attributes. H10 version started to gelatinize around 5th day after preparation, the size and PdI values rose and moreover, this phenomenon hindered DLS measurements because of low solubility of gelatinized sample.

Liposomes without PL showed remarkable difference between NH and H10 variations. NH liposomes without PL started with larger particles than their PL versions. NH liposomes of all types without PL contained particles sized from 800 to 1500 nm. PdI of these samples was around 0.5. Liposomes sized in tenths of nm and of PdI 0.4 were achieved by homogenization. One exception was the sample containing only CER3, where H10 liposomes expressed higher PdI values. Overall work with CER3 was accompanied by number of burdening attributes and required special treatment during preparation. CER3 also brought negative effects to sample stability.

Optical microscopy was conducted in order to explain certain unusual attributes observed in some types of formulations. The problematical properties of the CER3 liposomes were the first issue of concern. The measurement revealed the tendency of CER3 to crystallize therefore forming incomparably larger particles in the system, which was in accordance with the DLS and stability data. This occurred in both NH and H10 version; however, the crystals were scarcer in the H10 liposomes. In the case of the CER3+CER6+PL sample, its NH version did not contain any disturbing objects or imperfections; however, aggregates of particles were clearly visible in the H10 version. This may be related to the observed gel-like nature of H10 liposomes. In the case of the CER6 system, its non-problematic nature was confirmed.

Liposomes were tested for their capability to act as renewing agents in impaired skin. The CER3+CER6 liposomes simulating the composition of SC were chosen as the most suitable representative of prepared systems. It was compared to suspension of liposomal lipids dispersed in aqueous phase and with sole aqueous phase (10% urea solution in PBS). The lowest amount of IND permeated through intact skin (Figure 1). This is the basic permeation rate of IND through native skin not influenced by any chemicals or other disrupting methods. Disrupted skin not treated by any formulation expressed notably higher permeation rate of IND. The passed amount is almost three times higher than through intact skin. The treatment by lipid suspension and H10 cerosomes was able to lower the drug uptake only to a limited extend. However, NH liposomal treatment was the most efficient in the repair and the permeation of IND through such treated skins was the closest one to that of the control sample. This shows that liposomes were the most efficient in repairing the disrupted skin and were the most successful in returning the damaged skin closest to its initial state. On top of that, values for other treatment types were marked as significantly different by statistical evaluation showing, that neither the lipid suspension, nor the H10 cerosomes was able to offer good results in returning impaired skin to its initial state.

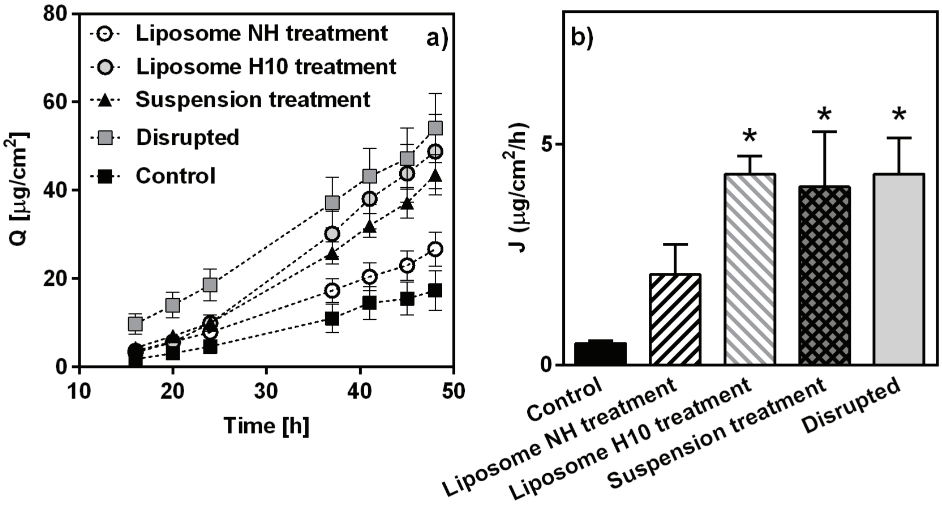

Figure 1. Permeation characteristics explaining the efficiency of different renewing substances on the disrupted skin. a) Permeation profiles of IND permeating through differently treated skins. b) Intensities of IND mass flow (flux, J) through the skins. * marks significantly different values from the control.

Conclusion

We successfully prepared SC lipid matrix-like liposomes containing two ceramide analogues in combination with other native skin lipids. Employed methods of lipid film hydration and high pressure homogenization were feasible and effective in preparation of larger multilamellar or smaller uniform liposomes. The novelty of our methodology lies within the use of urea as a main component of the liposomal aqueous phase. Renewing experiments on chemically disrupted porcine skin showed that the liposomal treatment was able to return the damaged skin to its initial properties possessed prior to the disruption. Based on presented results, it could be concluded that suitably prepared ceramide liposomes might be used as a promising formulation for the treatment of psoriatic or dermatitic skin conditions.

Acknowledgement

The work was supported by the Czech Science Foundation (GACR19-09600S)

References

1. Harding, C. R.: Dermatol. Ther. *17 Suppl 1*, 6 (2004).
2. Lai-cheong, J. E.; McGrath, J. A.: Medicine. *41 (6)*, 317 (2013).
3. Norlén, P. W.: Skin, Hair, and Nails, CRC Press 91 (2003).
4. Shao, M.; Hussain, Z.; Thu, H. E.; Khan, S.; Katas, H.; Ahmed, T. A.; Tripathy, M.; Leng, J.; Qin, H. L.; Bukhari, S. N. A.: Coll. Surf. B. *147*, 475 (2016).
5. Wolf, R.; Wolf, D.: Clin. Dermatol. *30 (3)*, 329 (2012).
6. Goyal, R.; Macri, L. K.; Kaplan, H. M.; Kohn, J.: J. control. rel. *240*, 77 (2016).
7. Huth, S.; Schmitt, L.; Marquardt, Y.; Heise, R.; Luscher, B.; Amann, P. M.; Baron, J. M.: Exp. Dermatol. *27 (9)*, 1009 (2018).
8. Mota, A. H.; Rijo, P.; Molpeceres, J.; Reis, C. P.: Int. J. Pharm. *532 (2)*, 710 (2017).
9. Roekevisch, E.; Leeflang, M. M. G.; Schram, M. E.; Campbell, L. E.; Irwin McLean, W. H.; Kezic, S.; Bos, J. D.; Spuls, P. I.; Middelkamp-Hup, M. A.: Br. J. Dermatol. *177 (6)*, 1745 (2017).
10. Fathi-Azarbayjani, A.; Ng, K. X.; Chan, Y. W.; Chan, S. Y.: Adv. Pharm. Bull. *5 (1)*, 25 (2015).
11. Jung, S. H.; Cho, Y. S.; Jun, S. S.; Koo, J. S.; Cheon, H. G.; Shin, B. C.: Die Pharmazie. *66 (6)*, 430 (2011).
12. Noh, G. Y.; Suh, J. Y.; Park, S. N.: Korean J. Chem. Eng. *34 (2)*, 400 (2017).
13. Raza, K.; Singh, B.; Lohan, S.; Sharma, G.; Negi, P.; Yachha, Y.; Katare, O. P.: Int. J. Pharm. *456 (1)*, 65 (2013).
14. Bangham, A. D.; Standish, M. M.; Watkins, J. C.: J. Mol. Biol. *13* (1965).

MORPHOLINE DERIVATIVES: NOVEL SUBSTANCES FOR MODULATING THE PERMEABILITY OF THE SKIN BARRIER

Dvořáková K.[1], Štěpánek, P.[1], Zbytovská J.[1]

[1]*University of Chemistry and Technology Prague; Technická 5, 166 28 Prague 6*
dvorakof@vscht.cz

Abstract

Transdermal drug delivery is an attractive non-invasive method offering numerous advantages to conventional routes of administration, mainly due to elimination of side effects. However, the main obstacle for drugs entering the skin is its uppermost layer, the stratum corneum (SC). To facilitate drug transport through this barrier, the passage can be modulated by transdermal penetration enhancers that are able to influence the skin barrier resistance. In this study, we investigated the enhancing activity of a series of morpholine derivatives. We tested these compounds with two model drugs differing in their physicochemical properties. Theophylline represented small molecules with balanced hydrophilicity; indomethacin was selected as larger lipophilic representative. All the examined enhancers were efficient; however, it was evaluated that the most effective enhancers were the ones with 10, 12 and 14 carbons in their side chain. The results also showed a bell-like relationship between the enhancing activity and the hydrocarbon chain length of the morpholine derivatives. Therefore, in this study we present a summary of the properties of morpholine derivatives identifying them as candidates for effective transdermal application.

Introduction

Transdermal application is an important method of drug administration because the targeted delivery of pharmaceuticals through the skin has many advantages. These benefits include avoidance of the first-pass metabolism, stable plasma concentration, increased patient compliance, and controlled delivery over long time period[1,2]. Moreover, topical delivery through the skin is used in a large number of skin care and dermatological applications[3]. However, the uppermost skin layer, the *stratum corneum*, which is responsible for the skin's exceptional barrier properties, limits transdermal penetration and the delivery of compounds into the blood system. This limitation represents a complication that cannot be overlooked[4,5,6].

A common way of overcoming this unique barrier is the use of permeation enhancers[5,7]. Typically, permeation enhancers are small hydrophilic/hydrophobic compounds, surfactants, lipids or solvents. For use with the skin, such compounds are required to be non-irritating, non-toxic and non-allergenic. Moreover, they must have no pharmacological activity in the body, their effect must be reproducible and predictable, and any changes they induce in the skin's properties must be reversible[5,7,8]. In recent years, many different structures that interact with *stratum corneum* lipids and reversibly change their physicochemical properties, have been evaluated for their efficiency and ability to enhance permeation via the skin. Although several established compounds are known as permeation enhancers, including fatty acids, urea and Azone®, no such enhancer possesses the complete set of ideal properties that would suit it for general use[9,10].

Penetration enhancer activity is commonly studied *in vitro* in Franz diffusion cells (figure 1). These cells, which, in skin research, are primarily used to evaluate membrane permeability, consist of two compartments, donor and acceptor. The compartments are separated by the evaluated membrane, typically human skin, animal skin or a synthetic membrane[11,12]. To determine the effect of potential enhancers on the barrier features of the skin, electrical impedance measurements is also utilized. Collectively, these measurements are a useful tool for monitoring skin integrity because they demonstrate the state of the skin both before and after the application of an enhancer[13].

The potential enhancing activity of morpholine derivatives has not yet been tested. Indeed these compounds are not commercially available. However they share a structural similarity with previously evaluated enhancers (e.g. Azone®). This, together with the constant effort to find compatible and safe transdermal enhancers that facilitate drug transport, suggests that these structures are worth testing for any enhancing activity.

Here, we test morpholine derivatives for their ability to enhance the permeation of two model drugs through porcine ear skin. We show that all tested compounds can act as permeation enhancers. In addition, we find correlations between the enhancing activity measured by the permeation experiment and electrical impedance measurements. The results enable us to identify a clear relationship between the morpholine derivatives structure (length of side chain) and enhancing activity.

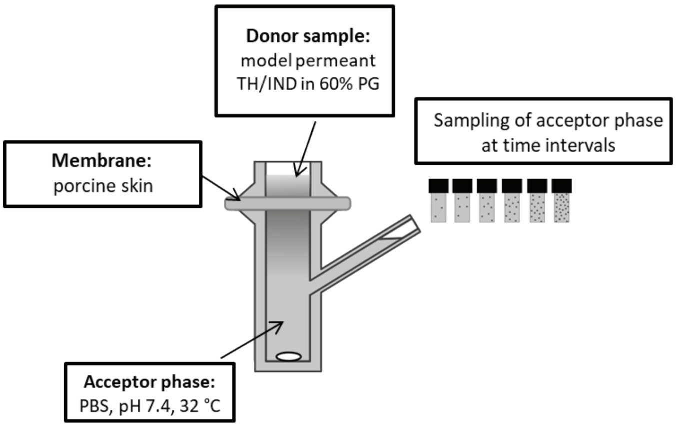

Figure 1. Franz diffusion cell

Experiment

Skin

Because of similar properties to human skin and good availability, porcine skin was used. In the first step, hairs were removed by a trimmer. After that skin was isolated with dissector. Skin fragments were washed in PBS and stored at -20 °C.

Donor and acceptor phase for permeation studies

Donor samples were prepared as a 5% (w/v) suspension of theophylline or 2.5% (w/v) suspension of indomethacin in 60% propylene glycol in distilled water. Some donor samples were used as blind samples. To others 1% (w/v) of enhancers was added. Phosphate buffered saline (PBS) containing 50 mg/l of gentamicin as preservative served as an acceptor phase (pH=7.4). PBS was used because it is capable to maintain physiological pH and isotonicity; therefore it is suitable as a model of inner body environment.

Permeation experiment

The permeation studies were performed using Franz diffusion cells with diffusion areas of 1 cm^2. The squares sized fragments of skin were mounted into the diffusion cells dermal side down and donor and acceptor compartments were then clamped together. The acceptor phase (PBS buffer, pH 7.4) was stirred by a magnetic bar in a water bath at 32 °C throughout the experiment. In the next step, skin integrity was verified by measurement of electrical impedance. Afterwards, 300 µl of donor suspensions were applied onto the skin. The donor chamber and sampling arm of each cell were covered by paraffin foil to minimize evaporation. The experiment ran for 48 hours. For the following HPLC analysis, 300 µl of the acceptor phase was taken periodically and replaced with the same volume of fresh acceptor buffer solution. The concentrations of model drug in acceptor samples were established by HPLC based on calibration curve from a line of standards. The concentration of model drugs was then converted to the mass in the acceptor phase. Then, the cumulative amount (Q) versus time (permeation profile) was plotted. The mass flow intensity of IND or TH (flux) was calculated as the slope of the linear part of this dependence.

Electrical impedance

To monitor skin integrity and characterize the effect of the permeation enhancers, the electrical impedance was measured by Voltcraft LCR 4080 MULTIMETER (Hirschau, Germany). After the hydration period, the donor compartments were filled with 500 µl of PBS. One wire of the multimeter was placed in PBS in the acceptor phase and the second one was immersed in the donor phase to determine the electrical impedance. The values of electrical impedance were remeasured after the permeation experiments. Then, electrical impedance ratio was calculated for each cell as $\mathrm{EIR} = \frac{\mathrm{EI1}}{\mathrm{EI2}}$, where EI1 is electrical impedance before the permeation study and EI2 is electrical impedance after the effect of donor formulations.

Results and discussion

In this study, we tested seven new morpholine derivatives as potential permeation enhancers that have not yet been studied. The structures of all compounds are based on morpholine. They only differ in the length or saturation of the side chain connected to the nitrogen atom (figure 1). We monitored the effects of the enhancers´ structure have on their activity. The effect of enhancers was investigated on porcine skin using two model drugs – theophylline (TH) and indomethacin (IND). The potencies of the individual enhancers are reported as the enhancing ratio - $\text{ER}=\frac{\text{flux with enhancer}}{\text{flux without enhancer}}$.

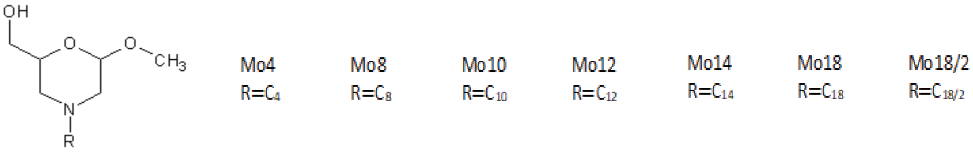

Figure 1. Structure of morpholine derivatives

We found that all of the morpholine derivatives are efficient as permeation enhancers and all of the studied compounds were able to increase flux of all model drugs – TH, IND. Generally, our compounds showed expected trend concerning their side chain length because derivatives with 10+ carbon atoms showed higher effectivity than their shorter analogues. Comparing the structures of the molecules of the individual compounds, it is clear that the derivatives with 10, 12 and 14 carbon atoms in side chain showed the most enhancing potency which corresponds to the highest fluxes (figure 2) and to the highest enhancing ratio (table 1). Contrary, the activity of our molecules with a short chain (Mo4, Mo8) caused lower enhancing activity for all permeants. The lower efficiency of our derivatives with short alkyl chain is probably due to the lack of lipophilicity that is important for the enhancers to interact with the lipids in the *stratum corneum*.

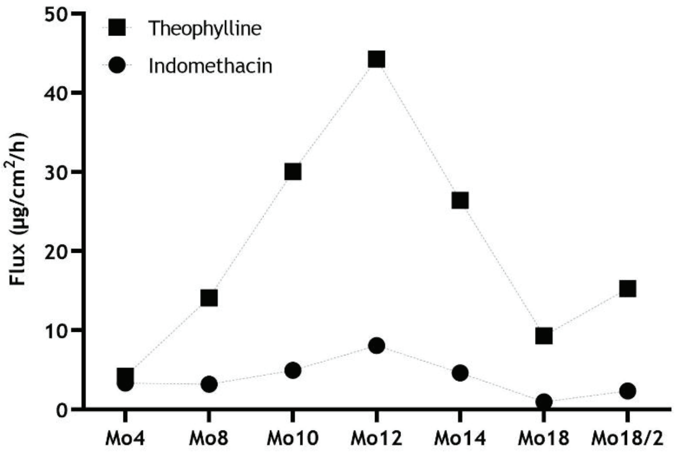

Figure 2. Dependency of fluxes on alkyl side chain length

Even tough lone oleic acid acts as an efficient transdermal enhancer, our morpholine derivative with the corresponding side chain (Mo18/2) surprisingly did not show the highest enhancing effect. The data, however, show that introduction of oleyl into the molecule still leads to increased enhancing activity compared to Mo18 which has saturated side chain. These results confirm the hypothesis that the introduction of *cis* double bond into the centre of the hydrophobic chain disrupts the lamellar organization in the skin more than saturated chains[15].

Collectively, we found an interesting bell - like relationship between the enhancing activity and enhancers' side chain length for both used model drugs. These results demonstrate the most effective enhancers containing 10-14 carbons in the side chain, which are the chain lengths leading to the strongest enhancing effects and which corresponds to previously reported data[5,16]. The highest permeation-enhancing effect for TH and IND was found for Mo12 ($\text{ER}_{\text{Mo12, TH}} = 14.5$ and $\text{ER}_{\text{Mo12, IND}} = 10.0$).

Table I
Enhancing ratio of all studied enhancers

	ER	
	TH	**IND**
Mo4	1.4	6.6
Mo8	4.6	6.3
Mo10	9.9	7.8
Mo12	14.5	10.0
Mo14	8.7	9.1
Mo18	3.1	1.9
Mo18/2	5.0	4.6

The electrical impedance helps us understanding barrier properties of the skin because it is characterized as the resistance of the membrane to the passage of small charged molecules[17]. We therefore used this method for testing the effectivity of our enhancers. The skin impedance was measured before and after exposure to the permeants. The degree of influence the enhancers was evaluated as the electrical impedance ratio –

$$\text{EIR} = \frac{\text{Impedance } \textbf{after} \text{ the exposure}}{\text{Impedance } \textbf{before} \text{ the exposure}}.$$

The smallest EIR corresponds to the highest enhancing ratio. That means that the more the substance disrupts the *stratum corneum* barrier the greatest difference between the electrical impedance after and before the experiment can be found. From our results it is clear that the smallest values of EIRs were determined for Mo10, Mo12 and Mo14 (figure 3). This correlates with the findings from the enhancing activity measurements.

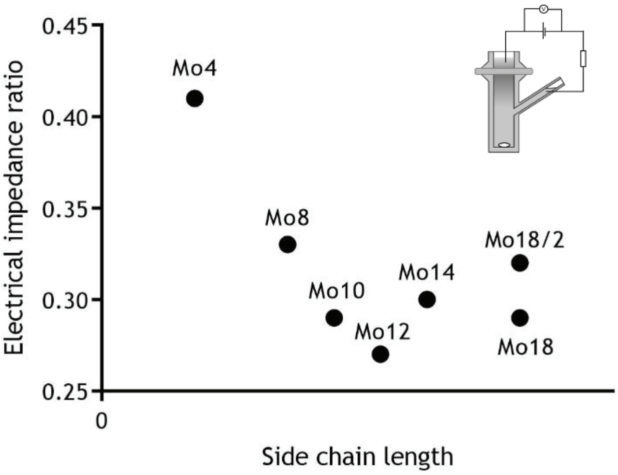

Figure 3. Dependency of electrical impedance ration on side chain length

Conclusion

To our best knowledge, morpholine derivatives have not yet been studied as permeation enhancers. Therefore, we conducted several permeation experiments with two model drugs with different physicochemical properties -theophylline and indomethacin - in which an enhancing activity of all tested compounds was discovered. Moreover, the activity shows a bell-like dependence on morpholine derivatives' hydrocarbon chain length and saturation. Furthermore, the electrical impedance measurements showed a clear correlation between the enhancing activity and the impedance values. Thus, our research shows that electrical impedance could serve as a good indicator for monitoring skin integrity. While the most effective enhancers were Mo12, the permeation-enhancing capabilities of all of the studied morpholine derivatives suggest that collectively they can broaden the spectrum of enhancers used in topical drug application.

Acknowledgement

This study was financially supported by Czech Science Foundation (GACR19-09600S).

References

1. Ashok, K.; Nikhila, P.; Lakshmana, P.; Gopal, V.: *Int. J. Pharm. Sci. Rev. Res. 3*, 49 (2010)
2. Sharadha, M.; Gowda, D. V.; Vishal Gupta, N.; Akhila, A. R., *Int. J. Res. Pharm. Sci.*, *11*, 368–385 (2020)
3. Akomeah, K. F.: *Curr. Drug Deliv.7*, 283 (2010)
4. Fox, L. T.; Gerber, M.; Plessis, J. Du; Hamman, J. H.: *Molecules*, 10507 (2011)
5. Vavrova, K.; Zbytovska, J.; Hrabalek, A.: *Curr. Med. Chem. 12*, 2273 (2005)
6. Prausnitz, M. R.; Langer, R.: *Nat. Biotechnol.*, *26*, 1261 (2008)
7. Lane, M. E.: *Int. J. Pharm.*, *447*, 12 (2013)
8. Williams, A. C.; Barry, B. W.: *Adv. Drug Deliv. Rev.56*, 603 (2004)
9. Kopečná, M.; Macháček, M.; Nováčková, A.; Paraskevopoulos, G.; Roh, J.; Vávrová, K.: *Sci. Rep.*, *9*, 1 (2019)
10. Dragicevic, N.; Maibach, H. I.: *Percutaneous Penetration Enhancers Chemical Methods in Penetration Enhancement 1* (2015)
11. Čuříková, B. A.; Procházková, K.; Filková, B.; Diblíková, P.; Svoboda, J.; Kováčik, A.; Vávrová, K.; Zbytovská, J., *Int. J. Pharm.*, *534*, 287 (2017)
12. Sekkat, N.; Kalia, Y. N.; Guy, R. H., *J. Pharm. Sci.*, *91*, 2376 (2002)
13. Karande, P.; Jain, A.; Mitragotri, S., *J. Control. Release*, *110*, 307 (2006)
14. Nair, M. K. M.; Joy, J.; Vasudevan, P.; Hinckley, L.; Hoagland, T. A.; Venkitanarayanan, K. S.: *J. Dairy Sci.*, *88*, 3488 (2005)
15. Green, P. G.; Guy, R. H.; Hadgraft, J.: *Int. J. Pharm.*, *48*, 103 (1988)
16. Kanikkannan, N.; Kandimalla, K.; Lamba, S.; Singh, M.: *Curr. Med. Chem.*, *7*, 593 (2012)
17. Fasano, W. J.; Hinderliter, P. M.: *Toxicol. Vitr.*, *18*, 725 (2004)

IMPROVING DISSOLUTION RATE OF POORLY SOLUBLE DRUGS BY MILLING AND CO-MILLING TECHNIQUE

Slámová M.[1], Beránek J.[2], Patera J.[1], Zámostný P.[1]

[1]*Department of organic technology, UCT Prague, Technická 5, 166 28, Prague 6 Dejvice*
[2]*Zentiva k.s., U Kabelovny 130, 102 37 Prague 10, Czech Republic*
slamovam@vscht.cz

Abstract

Milling of APIs alone or co-milling of APIs with an excipient are used as one of the efficient techniques that improve physicochemical properties such as solubility and dissolution rate. The enhancement of solubility may be caused by the drug amorphization. Each drug has a different ability to form an amorphous phase (glass forming ability). The influence of excipients is also crucial because the proper choice thereof increases the dissolution rates of API. The aim of this work was to compare the dissolution behavior of drugs having different glass forming ability. Furthermore, the effect of the mixture preparation method was compared in terms of dissolution properties. Our results indicate that co-milling is a valuable approach in enhancing the dissolution rates of poorly water-soluble APIs. Co-milling results in a much faster release of the API, than its milling itself and subsequent mixing with the excipient.

Introduction

Many newly developed drugs have poor or almost no solubility in aqueous media. Therefore, improving solubility is one of the major challenges in the pharmaceutical industry. One of the most effective strategies for improving the solubility and thus the bioavailability of hydrophobic APIs is milling, which affects both the particle size and their specific surface area and shape.[1-3] Decrease in particle size can theoretically increase the dissolution rate by increasing the specific surface area of the particles, but in practice, the micronization effect is often negatively affected by agglomeration of fine hydrophobic API particles (via van der Waals or other interaction), which in turn leads to decrease in effective surface area available for solvent interaction.[4-6]

In order to avoid such undesirable agglomeration, which occurs during the milling of the APIs themselves, the drugs are co-milled together with the co-formers. These co-formers are inert, non-toxic pharmaceutical excipients that stabilize drug in the milled product (often hydrophilic excipients such as polyvinylpyrrolidone or cellulose derivates). Co-milling is an intensive mixing technique capable of producing mixtures comprising amorphous drug forms intimately mixed with suitable co-former at the molecular level (particles of API are in close contact with the co-former particles). This interaction between API and co-former increases the wetting and dissolution of API. Hence, choosing appropriate drug-co-former pair is strongly related to the product quality and performance.[7-8]

During milling and co-milling, changes may occur at the level of the crystal structure of the API. Various disorders of the crystal structure may occur, the accumulation of defects, and ultimately to the disappearance of the crystal structure. This leads to complete amorphization of the API or to form amorphous regions on the surface of the API.[9] Each drug has a different tendency to form an amorphous phase. For better insight, the APIs were divided into three groups based on their glass forming ability: stable glass formers (sGF), unstable glass formers (uGF), and non-glass formers (nGF).[10-12]

The aim of this work was to compare the dissolution behavior of two model drugs with different glass forming ability (GFA). Mefenamic acid was chosen as a model drug with poor GFA, while indomethacin was a model drug with a high tendency to form a glass phase. Furthermore, the effect of the mixture preparation method was compared. Our previous study[13] revealed co-milling of sGF and nGF drug leads to different effects based on their glass forming ability. Surface modifications due to milling were reported as the key factor contributing to altered dissolution properties. In this study, we aim at comparing the results of the previous study as a base case with altered preparation methods involving separate milling to elucidate the mechanism of surface activation.

Methods

Materials

Mefenamic acid (MA) and Indomethacin (IND) were obtained from Sigma-Aldrich (Prague, Czech Republic). Ac-Di-Sol® (ACD), meglumine (MG), and povidone 25 (PVP) were purchased from Zentiva, k.s. (Prague, Czech Republic). Methanol (LC/MS grade) and Acetonitrile (LC/MS grade) were obtained from Fisher Chemical (Prague, Czech Republic). Acetic acid p.a., Sodium hydroxide, and Potassium dihydrogen phosphate p.a. were purchased from Penta (Prague, Czech Republic).

Preparation of mixtures

Firstly, physical mixtures (PMs), as reference material, were prepared by mixing IND or MA with selected co-formers in 1:1 drug to carrier ratio (w/w) using 3D blender Turbula TF2 (W.A. Bachofen, Basel, Switzerland) at 50 rpm and 15 min. Subsequently, the mixtures were mechanically processed in a Planetary ball mill Retsch PM 100 CM (Haan, Germany) using 5 stainless steel balls (diameter 10 mm) for 20 min at 250 rpm to create co-milled mixtures (COM). Finally, the APIs were milled alone and then mixed with one of the appropriate excipient (M1).

Dissolution tests

Dissolution tests were carried out in the flow-through cell apparatus (USP4) using an open-loop system Sotax Dissotest CE1 (Sotax Basel, Switzerland) and a piston pump Sotax CY 1 (Sotax Basel, Switzerland). Approximately 20 mg of powder was weighted into the cell (12 mm diameter and 32 mm height), and the cell was tempered in a water bath at 37 °C. The dissolution medium (phosphate buffer pH 6.8) was pumped through the cell with a flow rate of 16 ml·min^{-1}. Solution samples were collected at short time intervals and analysed using HPLC. The relative release rate of the drug was calculated as the ratio of mass flow and initial mass of drug in a mixture, and the released fraction of drug w was calculated using the trapezoid integration rule.

HPLC analysis

The concentration of API was determined by HPLC Dionex Ultimate 3 000 (Sunnyvale, California, USA) with a C18 Kinetex® column 5 µm 100 Å (Phenomenex® Torrance, CA, USA). The injected volume of the sample was 10 µl, the flow rate 1 ml·min^{-1}, and the oven temperature 30 °C. Indomethacin was monitored at 267 nm and mefenamic acid at 285 nm. A mobile phase for indomethacin consisted of acetonitrile/water/acetic acid 90/60/5 (v/v), for mefenamic acid acetonitrile/0.1M acetic acid 70/30 (v/v).

SEM

All samples were taken with FE MIRA II LMU scanning electron microscope (Tescan, Brno, Czech Republic). First, the powder was fixed to a graphite double-sided adhesive tape and then covered with 5 nm gold combined sprayer Quorum Q150R ES (Quorum Technologies Ltd., Laughton, UK). The images were performed at magnifications 1 000 and 2 000.

Results and discussion

Dissolution of pure APIs

The dissolution properties of pure APIs and prepared mixtures were studied using flow-through cell apparatus for powders. Results of measurements of pure and milled APIs are depicted in Figure 1. These figures show the percentage of the released drug over time.

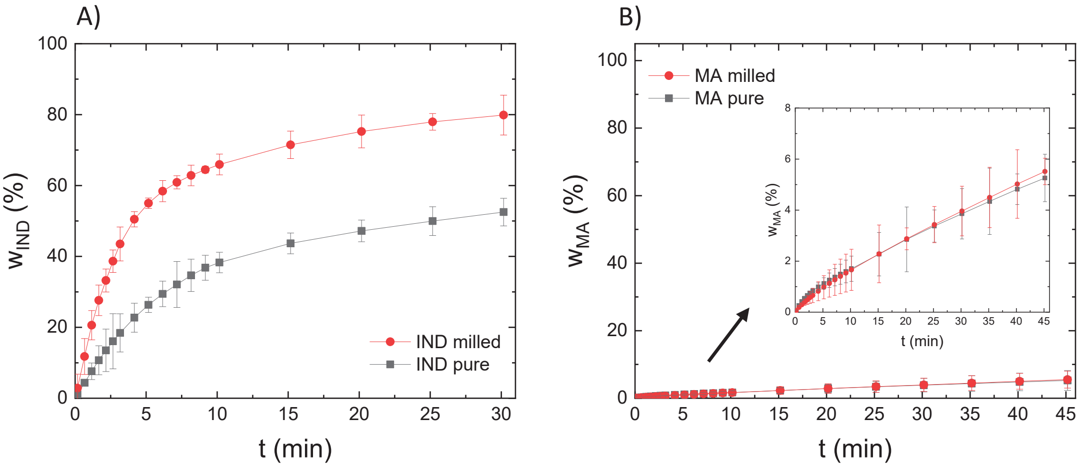

Figure 1. Dissolution profiles of pure and milled drugs – indomethacin (A) and mefenamic acid (B)

Milling is a process of applying mechanical energy that affects particle size and thus specific surface area. Moreover, prolonged transfer of mechanical energy to drug particles provides mechanochemical activation leading to the disordering of the crystal structure and thus drug amorphization.[7] IND is a representative drug of glass former (a drug with a high tendency to form an amorphous phase). Figure 1A shows that the released amount of milled IND is higher than the corresponding pure un-milled IND. Probably some surface amorphization may occur and the amorphous regions were spread out after the sample surface. However, only a very small amount of amorphous phase was found in the volume of the sample as was shown in our previous study.[13] MA is a model drug of non-glass formers and Figure 1B shows that the released amounts of pure and milled MA are almost the same. Despite a longer period of time (than in the case of IND), only 8% of MA was released from the measured sample. This system was lacking the propensity to create amorphous regions upon milling (mechanical treatment). The results of dissolution tests of pure APIs reported in this study confirmed the results already published in our previous study.[13]

Effect of preparation method

Subsequently, the effect of the preparation method has been studied. The morphology of prepared mixtures and the effect of particle size reduction after milling and co-milling has been investigated using electron microscopy (SEM) for a mixture containing co-former MG. SEM images show that in the case of PM (Figure 2A, D), the drug and MG particles are in close contact. In the case of M1 mixtures, the needle-like MG particles were partially covered by milled IND (Figure 2B) or MA (Figure 2E). Respectively, the drug was uniformly dispersed over the surface of the co-former. SEM analysis of co-milled IND (Figure 2C) and MA (Figure 2F) with MG confirmed the formation of agglomerates. Such morphology of prepared mixtures has significant implications in the dissolution rates of both drugs (see below).

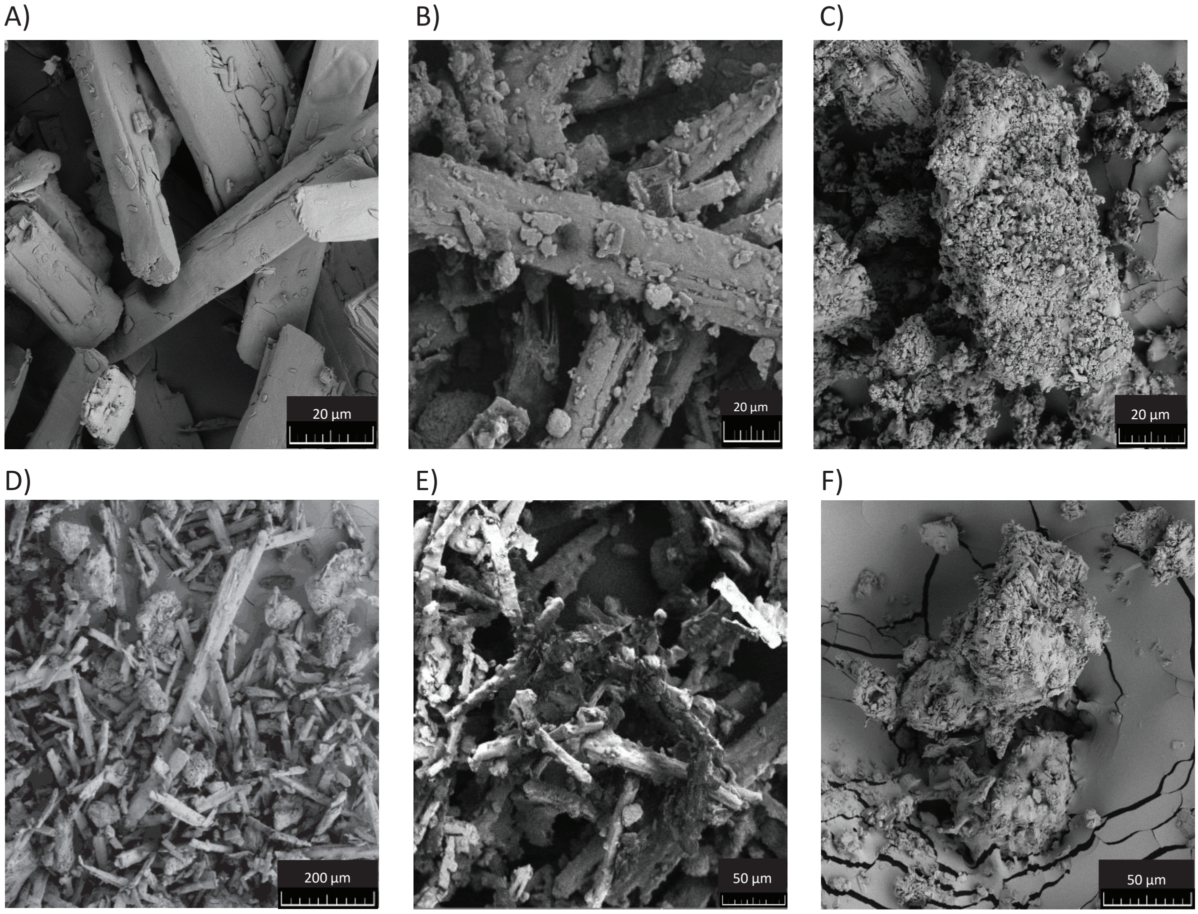

Figure 2. SEM images for binary mixtures containing meglumine (MG) and indomethacin (IND) or mefenamic acid (MA) prepared by physical mixing (PM), milling of API and subsequent mixing with meglumine (M1) or co-milling (COM): IND PM (A), IND M1 (B), IND COM (C), MA PM (D), MA M1 (E), MA COM (F)

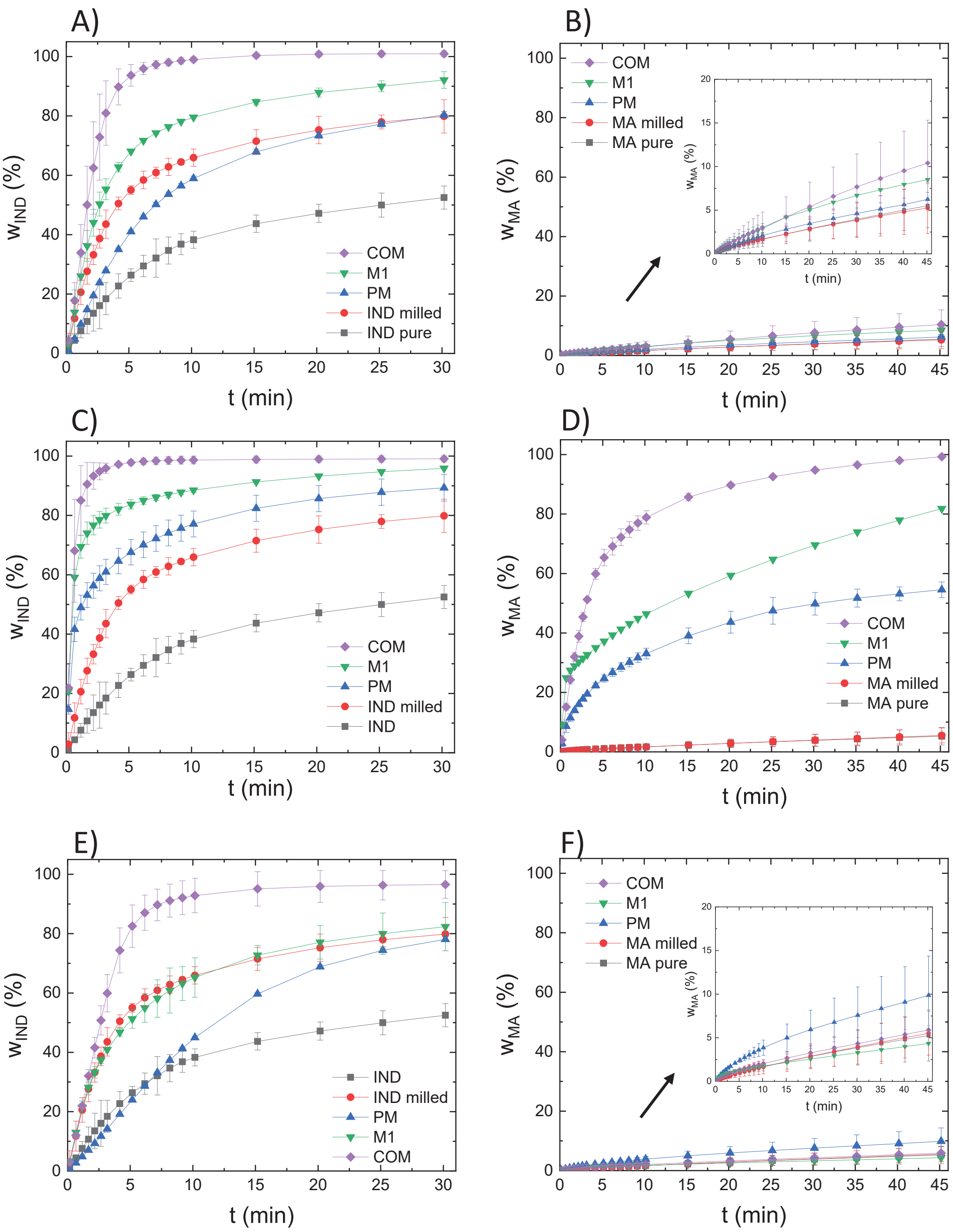

Figure 3. Dissolution profiles of physical mixtures (PMs), mixtures of milled API and non-milled excipient (M1) and co-milled mixtures (COM) containing indomethacin (IND) or mefenamic acid (MA) and one of the appropriate excipient – Ac-Di-Sol® (ACD), meglumine (MG) or povidone (PVP) – IND-ACD (A), MA-ACD (B), IND-MG (C), MA-MG (D), IND-PVP (E), MA-PVP (F) (data for COM and PM mixtures in Figures C, D, E, F were already published in our previous study[13])

The dissolution profiles of prepared mixtures show significant improvement of dissolution of the drug compared to pure untreated or milled drug (Figure 3). For all mixtures, the slowest release was observed in the case of PM. In contrast, drug release was increased for M1 and the fastest release was found in COM. In the case of the M1 mixtures, the particle size of the drug was observed to shift to a smaller particle size, and also the drug surface was hydrophilized due to the mixing with the appropriate co-former (Figure 2B, E). During co-milling, some agglomerates were formed (no such milled particles were visible – Figure 2C, F), which can affect the dissolution rate of both drugs. Furthermore, more defects were generated, and more –OH groups of co-former adhere to the drug surface, turning it into hydrophilic (especially in the case of MA with MG). Moreover, the enhanced dissolution profiles of IND and MA might be due to the amorphous phase after co-milling, as was demonstrated in our previous study.[13] The results showed that co-milling is a far more effective technique than just milling API alone and subsequent mixing with the excipient.

Significant differences were also evident between drugs. It was confirmed that IND amorphized even when milled separately, while MA needs co-milling with an appropriate excipient to enhance the dissolution rate. The influence of the excipient type also plays an important role.[4-5] Meglumine had a significant influence on improving the dissolution behavior of both APIs. Very rapid wetting of the sample occurred, followed by a very rapid release of MA. ACD increased the relative release rate of indomethacin. The slightest enhancement was observed in the mixtures with PVP. Probably, ACD and PVP as large molecules which have polymeric structure were likely to cover the drug surface partially, swelled, and therefore slowed the drug dissolution rate.

Conclusion

This study compared the effect of the preparation method on the dissolution rate of model drugs with different glass forming ability. Our results indicate that co-milling is a valuable approach in enhancing the dissolution rates of poorly water-soluble APIs. Co-milling results in a much faster release of the API than milling the API alone and mixing it with the excipient only after the milling is finished. Therefore, in addition to surface activation and particle size reduction, the mechano-chemistry of the API and co-former pair are of great importance. The effect of excipient type on the dissolution rate was observed. The basic excipient meglumine appeared to be the best dissolution enhancing additive. Also, it was confirmed that the tendency to form an amorphous phase affects the efficiency of milling and co-milling.

Acknowledgement

This work was supported from the grant of Specific university research A1_FCHT_2021_002.

References

1. Lim, R.; Ng, W.; Tan, R. Powder Technol. 2013, 240, 79–87.
2. Chieng, N.; Aaltonen, J.; Saville, D.; Rades, T. Eur. J. Pharm. Sci. 2009, 71 (1), 47–54.
3. Lim, R.; Ng, W. K.; Widjaja, E.; Tan, R. J. Supercrit. Fluids 2013, 79, 186–201
4. Varghese, S.; Ghoroi, Ch. Int. J. Pharm. 2017, 533 (1), 145–155.
5. Li, J.; Yang, Y.; Zhao, M.; Xu, H.; Ma, J.; Wang, S. Mater. Sci. Eng., C 2017, 78, 780.
6. Khadka, P.; Ro, J.; Kim, I.; Kim, J.; Kim, H.; Cho, J.; Yun, G.; Lee, J. Asian J. Pharm. Sci. 2014, 9 (6), 304–316.
7. Szafraniec, J.; Antosik, A.; Knapik-Kowalczuk, J.; Kurek, M.; Syrek, K.; Chmiel, K.; Paluch, M.; Jachowicz, R. Int. J. Pharm. 2017, 533, 470.
8. Loh, Z.; Samanta, A.; Heng, P. Asian J. Pharm. Sci. 2015, 10 (4), 255–274.
9. Boldyrev, V. Russ. Chem. Rev. 2006, 75 (3), 177–189.
10. Baird, J.; Van Eerdenbrugh, B.; Taylor, L. J. Pharm. Sci. 2010, 99 (9), 3787–3806.
11. Wyttenbach, N.; Kirchmeyer, W.; Alsenz, J.; Kuentz, M. Mol. Pharm. 2016, 13 (1), 241–250.
12. Alhalaweh, A.; Alzghoul, A.; Kaialy, W.; Mahlin, D.; Bergström, C. Mol. Pharm. 2014, 11 (9), 3123–3132
13. Slámová, M.; Prausová, K.; Epikaridisová, J.; Brokešová, J.; Kuentz, M.; Patera, J.; Zámostný, P. Int. J. Pharm. 2021, 597

DISSOLUTION KINETICS OF COMMERCIALLY AVAILABLE TABLETS USING AN OPTICAL MICROSCOPY TECHNIQUE

Bittner R.[1], Zámostný P.[1]

[1]*University of Chemistry and Technology Prague, Faculty of Chemical Technology, Department of Organic Technology, Technická 5, Prague 6, 166 28, Czech Republic*

radim.bittner@vscht.cz

Abstract

Many commercially available products show poor water solubility nowadays, which affects subsequent drug concentration in patient's body. One of the limiting factors is disintegration speed. Slow disintegration process will hinder subsequent dissolution process necessary to reach and maintain the desired therapeutical concentration. Several methods offer different options to closely monitor specific parts of the disintegration process. One of the possible methods is optical microscopy. This allows quite precise monitoring of an initial fragmentation during the disintegration process, since the released fragments are not subjected to any outer force and can be analysed in their true size, unlike using methods where a stirrer is used to keep the fragments from sedimentation during the measuring process (e.g. static light scattering).

This paper describes the use of optical microscope as a method for monitoring fragment populations released from tablets of a commercially available analgetic containing 400 mg of API. The tablet was placed into a small volume of tested medium, and after a certain amount of time placed under optical microscope to obtain PSD using image analysis. The key parameters of disintegration kinetics were estimated using erosion-fragmentation regression model. Deeper and more precise knowledge of the disintegration process associated with poorly soluble drugs can help to identify the rate-controlling step of their release and to find proper measures to improve their dissolution rate.

Introduction

Poor water solubility is a major problem for many pharmaceutical products. It hinders the onset of therapeutical effects and lowers the bioavailability of solid dosage forms[1]. There are many ways to deal with this issue, from changing used excipients to changing the size of particles[2]. In order to better control the onset of therapeutical effects, it is necessary to know more information about how each solid dosage form disintegrates in human body[3].

Disintegration in itself is a very complex process that involves the penetration of liquid medium into the structure of tablet and its subsequent destruction into smaller particles. The limiting step in this process is very often the speed of liquid medium penetrating into the tablet structure[4]. This speed is determined by the structure of tablet, especially the size and distribution of pores, the strength of bonds between particles, as well as the process parameters used during creation of the tablet, like compression pressure[5,6].

All these factors determine how the tablet is going to disintegrate in human body, and thus they present the need to know more about these factors to be able to improve the disintegration rate of poorly soluble drugs. The pharmacopeia disintegration test that is used during the development of drugs is too simple and does not provide any information about the size of released particles or the mechanism of their release. It only states whether the tablet disintegrated within the given amount of time or not[7]. To obtain more information about the disintegration process other methods were developed, based on image analysis, for example[5,8]. These methods include nuclear magnetic resonance imaging[9] or high-frequency imaging camera as part of optical microscopy[10]. Both of these methods were used to successfully describe the disintegration process of many different tablets. There are other methods not based on image analysis that are available for describing the process of disintegration, e.g. laser diffraction[11]. This method provides particle size distribution over time, which allows to monitor how the released particles change in size during the experiment. It allows to measure a large number of particles in a short amount of time, but it is impossible to prevent the contact of particles with the stirrer that is present at the bottom of measuring beaker to keep all the present particles in constant movement. This contact of particles with stirrer can easily break large particles into smaller ones before they get into the measuring cell leading to possibly inaccurate results. It also does not provide any information about the shape of particles.

Thus, it would be beneficial to have an image analysis method, like optical microscopy, that would compliment laser diffraction and provide all the missing information that cannot be obtained this way.

Materials and Methods

Materials

The list below summarizes materials that were used in this study:

- APO-Ibuprofen 400 mg (Aurovitas Ltd.)
- Hydrochloric acid (p.a., Penta a.s.)
- Monopotassium phosphate (p.a., Penta a.s.)
- Sodium hydroxide (p.a., Penta a.s.)

Disintegration measurement

The tablet was placed in a Petri dish and submerged in chosen liquid medium (distilled water, HCl, phosphate buffer). The amount of liquid medium was always small (75 ml) to prevent any possible dissolution of released fragments. After 10 minutes, the initial fragmentation was completed, and the tablet was placed under an optical microscope (SMZ 18, Nikon Japan) to obtain three images from different areas of the Petri dish. The tablet together with its fragments was then placed in a beaker with a stirrer to stir for a predefined time interval (5, 10, 15 minutes) and subsequently transferred into a Petri dish under optical microscope to obtain another three images. This process was repeated until the final time of 60 min was achieved. Combined together, there were 21 images taken during one measurement, three for each specified time (0, 5, 10, 20, 30, 45, 60 min).

Image analysis

Each image was analysed in software NIS Elements provided by the manufacturer of the optical microscope, Nikon. Particles on each image were highlighted manually. The first step was to create a region of interest (ROI) in the image, as can be seen in Figure 1. Inside such region, every particle was highlighted if it was possible to determine it is not an aggregation of several particles. Combining all three images that were taken during each time interval, the number of analysed particles was always more than 100. This made sure there was always enough data for each specified time for further analysis and the obtained data had some statistical value.

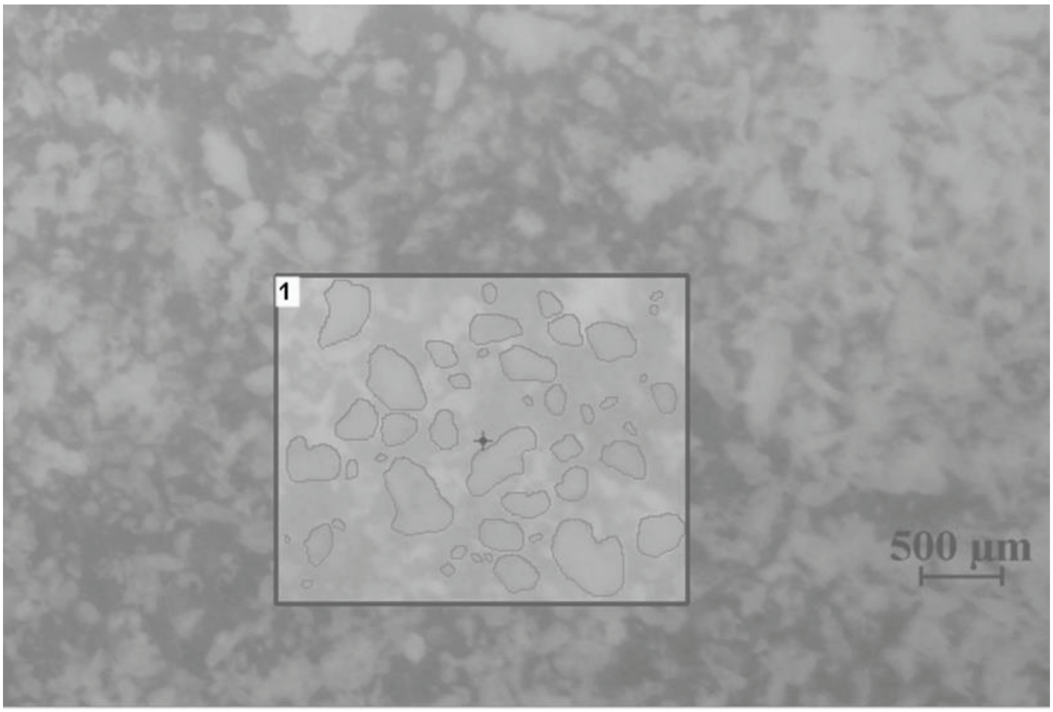

Figure 1. Example of image analysis in NIS Elements.

Each particle was then evaluated through several parameters, such as projection area, circularity, and an equivalent diameter of a circle with the same projection area as the specific particle (Figure 2). Given the high circularity of particles, it was possible to use such diameter in further evaluations to be able to describe each particle with some characteristic size.

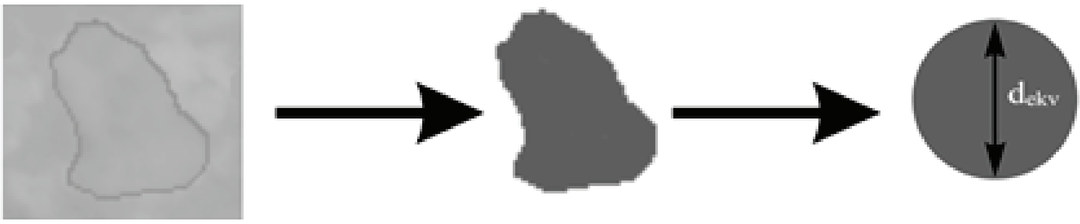

Figure 2. Approximation of a circle diameter equivalent to the particle's projection area.

Disintegration kinetics – population balance

Given that only the knowledge of particle size does not describe the dynamic of disintegration process very well, a population balance model was created. This mathematical model describes the disintegration process as a fragmentation of the tablet into four different particle size categories, where the particles of bigger size categories continue to disintegrate into smaller particle size categories over time (Figure III).

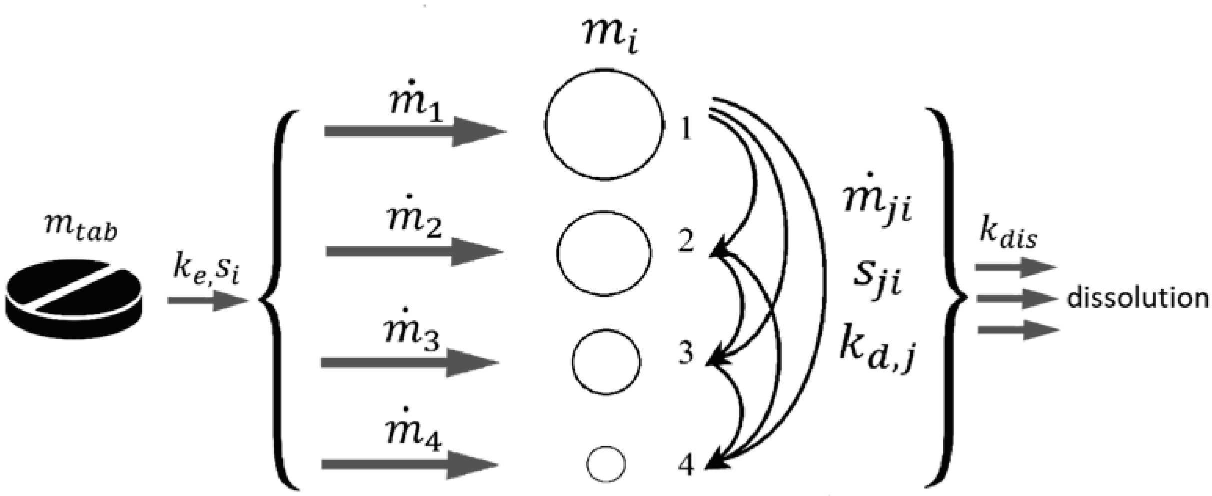

Figure 3. Disintegration model of tablet fragmentation into four size classes.

This model assumes that the initial fragmentation was performed fully and instantly, and thus the mass of the studied system does not change over time. This also means no dissolution is assumed, since the amount of liquid media used during the experiment is very small (75 ml). This means the model can be mathematically described as:

$$\frac{dm_i}{dt} = \sum_j^{i-1} s_{ji} m_j k_{d,j} - k_{d,i} m_i \tag{1}$$

where m_j is the mass of *j* class of particles, s_{ji} is the selectivity of *j* class of particles to disintegrate into *i* class of particles and $k_{d,j}$ is the disintegration constant of *j* class of particles
Thanks to this model it is possible to further evaluate particles in terms of disintegration kinetics to obtain the corresponding constants of selectivity and disintegration. This task was performed in a statistical software ERA 3.0 using a regression analysis.

Results and Discussion

Mean equivalent diameter

The obtained results confirmed the possibility of using this optical microscopy method as a way to observe the disintegration process of tablets. As can be seen in Figure IV, the mean equivalent diameter of particles in water started at 753 µm and gradually fell to 162 µm over the interval of 60 minutes. The same thing can be observed in case of phosphate buffer (Figure V), where the mean equivalent diameter started at 388 µm and during the interval of measurement fell down to 137 µm. This corresponds with the fact that the tablet dissolves faster in higher pH, like in case of phosphate buffer. It is noticeable how the first points of the measurement are significantly higher than all other points on the graph in case of both media. This suggests the tablet's initial fragmentation results in particles of significant size that could probably be missed using methods where the stirrer is present during this phase. Having more accurate knowledge about initial fragmentation can be useful in case of any disintegration optimalisations, where the size of initial fragments plays a major role in further steps of this process. The potential manufacturer can then adjust his manufacturing process to produce tablets with smaller particle size to improve the subsequent disintegration if the current one would not be suitable.

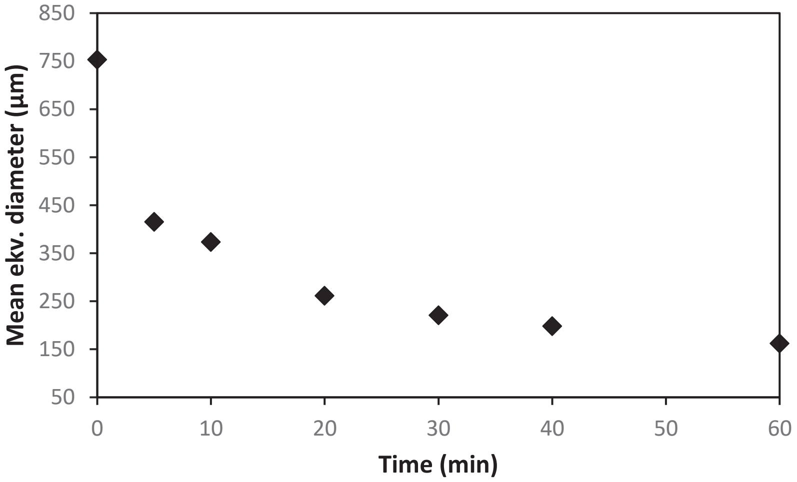

Figure 4. Change of mean equivalent diameter for tablet particles in water.

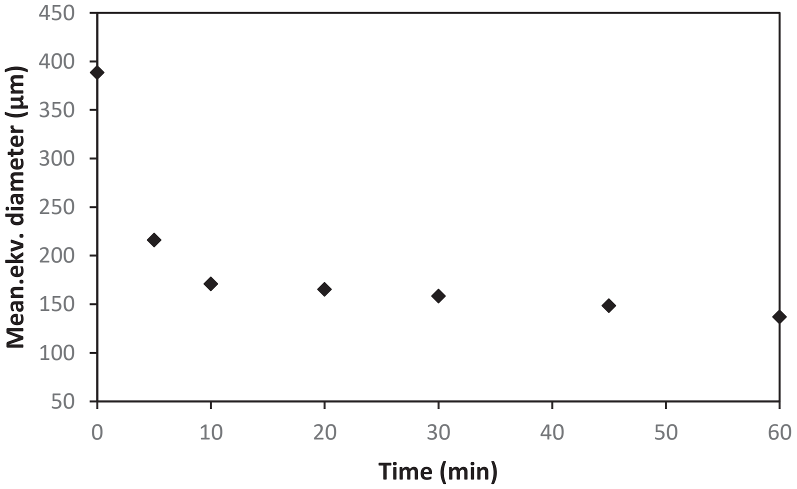

Figure 5. Change of mean equivalent diameter for tablet particles in phosphate buffer.

Disintegration kinetics

Using the mentioned regression model, the following disintegration constants were obtained for this commercial tablet in water (Table I). It is noticeable how the value of disintegration constant $k_{d,1}$ is significantly higher than all the other values. This supports the fact that the tablet disintegrates into fragments of higher size and over time those fragments become smaller. The selectivity constant $S_{1,2}$ is also higher than other selectivity constants of the first class, which indicates the fragments gradually reduce their size. This behaviour can be seen in Figures 4 and 5 as well, where the value of mean equivalent diameter does not instantly decreases to 150 µm, but it gradually lowers over the course of twenty minutes.

Table I
Disintegration constants and selectivities in water.

	API 400 mg
$k_{d,1}$ [min^{-1}]	138.7 x 10^{-3}
$k_{d,2}$ [min^{-1}]	2.3 x 10^{-3}
$k_{d,3}$ [min^{-1}]	0.1 x 10^{-3}
$S_{1,2}$ [-]	7.9 x 10^{-1}
$S_{1,3}$ [-]	1.5 x 10^{-1}
$S_{1,4}$ [-]	0.6 x 10^{-1}
$S_{2,3}$ [-]	3.9 x 10^{-1}
$S_{2,4}$ [-]	6.1 x 10^{-1}

Using this model to compare several commercial products in terms of their disintegration kinetics can lead to finding the optimal particle size and possibly mixture composition for any future drug manufacturer. Having the knowledge about which particle size classes are preferred during disintegration can also help optimise the disintegration speed. Thus, this method can help predict which pharmaceutical formulation will disintegrate faster and into smaller particles than others, leading to a faster dissolution and possibly also a faster onset of therapeutical effects, which can be a very desired characteristic, especially in terms of analgesics.

Conclusion

A new method for observing the disintegration process of tablets using optical microscopy has been developed. This method has been tested on the disintegration of a commercially available analgetic containing 400 mg of API in different media. It was discovered that the tablet initially disintegrates into fragments of noticeable size, which was subsequently confirmed by a mathematical model for population balance to describe the disintegration kinetics of this system, where the class of particles with the biggest size had the highest values of disintegration constants. It is therefore possible to use this method to describe the kinetics and the size of particles released during disintegration process of studied tablets. Possible improvements could be made in the area of analysing particles to reduce the need for manual highlighting. In general, this method offers potential for further application in disintegration studies of any solid dosage forms.

Acknowledgement

This work was supported from the grant of specific university research – grant No A2_FCHT_2021_038.

References

1. Okárová, L.; Vetchý, D.; Franc, A.; Rabišková, M.; Kratochvíl, B.: Chem. List., *104*, 21 (2010).
2. Markl, D.; Zeitler, J. A.: Pharm. Res., *34*, 890 (2017).
3. Desai, P. M.; Liew, C. V.; Heng, P. W. S.: Journal of Pharmaceutical Sciences, 2545 (2016).
4. Dufková, K.: Master thesis, VŠCHT Praha (2019).
5. Mesnier, X.; Althaus, T. O.; Forny, L.; Niederreiter, G.; Palzer, S.; Hounslow, M. J.; Salman, A. D.: Powder Technol., *238*, 27 (2013**).**
6. Riippi, M.; Antikainen, O.; Niskanen, T.; Yliruusi, J.: Eur. J. Pharm. Biopharm., *46*, 339 (1998).
7. The United States Pharmacopeia and National Formulary USP 40 - NF 35; The United States Pharmacopeial Convention, Inc.:Rockville, MD (2017)
8. Rajkumar, A. D.; Reynolds, G. K.; Wilson, D.; Wren, S.; Hounslow, M. J.; Salman, A. D.: Eur. J. Pharm. Biopharm*., 106*, 88 (2016).
9. Tritt-Goc, J.; Kowalczuk, J.: Eur. J. Pharm. Sci., *15*, 341 (2002).
10. Desai, P. M.; Liew, C. V.; Heng, P. W. S.: J. Pharm. Sci., *101*, 2155 (2012).
11. Quodbach, J.; Kleinebudde, P.: J. Pharm. Sci., *103*, 3657 (2014)

MONITORING THE ROLL COMPACTION PROCESS VIA RIBBON STIFFNESS MEASUREMENT

Petr J.[1], Stasiak P.[2], Zámostný P.[1]

[1]*University of Chemistry and Technology Prague, Faculty of Chemical Technology, Department of Organic Technology, Technická 5, Prague 6, 166 28, Czech Republic*
jan.petr@vscht.cz
[2]*Pharma Development, Zentiva, k.s., Prague, the Czech Republic*

Abstract

Typical industrial development of a roller compaction process includes changes in scale from laboratory to pilot, and then further to production scale and also transfer to different equipment designs due to equipment availability in different manufacturing facilities. Different equipment designs, such as feeding system, side seals, roll width or surface, and ribbon milling systems, as well as the process control regime can lead to changes in downstream quality attributes, including granules and tablets. The objective of this work was to monitor the process performance by measurement of compacted ribbon properties using the texture analysis.

The compactors [Alexanderwerk AG, Germany] and [Gerteis Maschinen and Processengineering AG, Switzerland] were used for this study. They have the roll force control using a hydraulic pressure system, but they differ in raw material loading, roll width, and roll diameter. The formulation comprising the atorvastatin API and calcium carbonate, as major excipient was used as the model mixture.

The production was carried out following a common design of experiments in which three levels of pressure or compaction force were measured on each compactor. The gap width, roll/screw/sieve speed were also investigated. The ribbons taken out from the compaction process were collected and characterized by compression test method using CTX Texture Analyzer [AMETEK Brookfield, USA]. While the ribbon compression testing with blade probe did not provide results reflecting the state of compaction, the compression testing with needle probe allowed to measure relative ribbon stiffness, which correlated with the compaction pressure and reflected the local ribbon properties.

The measured relative ribbon stiffness was used to evaluate ribbon uniformity and compare the performance of different compaction equipment. It was found the Alexanderwerk facility exhibit lower lateral ribbon uniformity leaving a large amount of uncompacted material compared to Gerteis. The uneven filling of the gap in the lateral direction of for the Alexanderwerk compactor is the likely cause. The instrumented method of monitoring the product quality can be further used for optimizing the process parameters and technology transfer between the different manufacturing facilities.

Introduction

Dry granulation by roll compaction is a particle size-enlargement technique. A primary/feed powder with low flowability and homogeneity is densified into a ribbon. The ribbon is crushed to form granules, afterwards. The granules with improved flow properties, content uniformity and adequate material compactability should undergo further forming processes as tableting or capsule filling.

One of the most important characteristics of the ribbons coming out of a roller compactor is their solid fraction. Solid fraction is defined as the ratio of apparent or envelope density of a ribbon sample to true density of the material. It is being increased as the primary powder gets compacted and depends on several processing factors including hydraulic roll pressure, screw speed to roll speed ratio and gap width. Mechanical properties such as tensile strength, hardness and elasticity of compacted powders depend on the solid fraction. By maintaining comparable ribbon solid fractions across different scales from pilot to production, it is expected to achieve similar tensile strengths and subsequently similar particle size distribution when milled under same conditions[1-4]. Since the ribbon apparent density is difficult to measure, the objective of this work is using texture analysis as an alternative measurement technique to investigate if the ribbon stiffness parameter and other properties of granulate can be used to monitor the compaction process performance.

Materials and methods

The design of experiments had been furnished using two different compactor types; large scale Alexanderwerk AG WP 200 PHARMA (AW) and small scale MINI-PACTOR Gerteis Maschinen and Processengineering AG (GER). The formulation comprising the atorvastatin drug and calcium carbonate, as major excipient was used as the model mixture. The primary/feed powder was compacted inside fully automated mode with three specific settings on each device. As the devices differ in their design and operation details they use different process parameter as the main measure of the compaction load; specific compaction force (*SCF*, kN/cm) is used by GER the hydraulic pressure (*p*, bar) is used by AW. AW compactor has no gap control, while the GER has a gap control system.

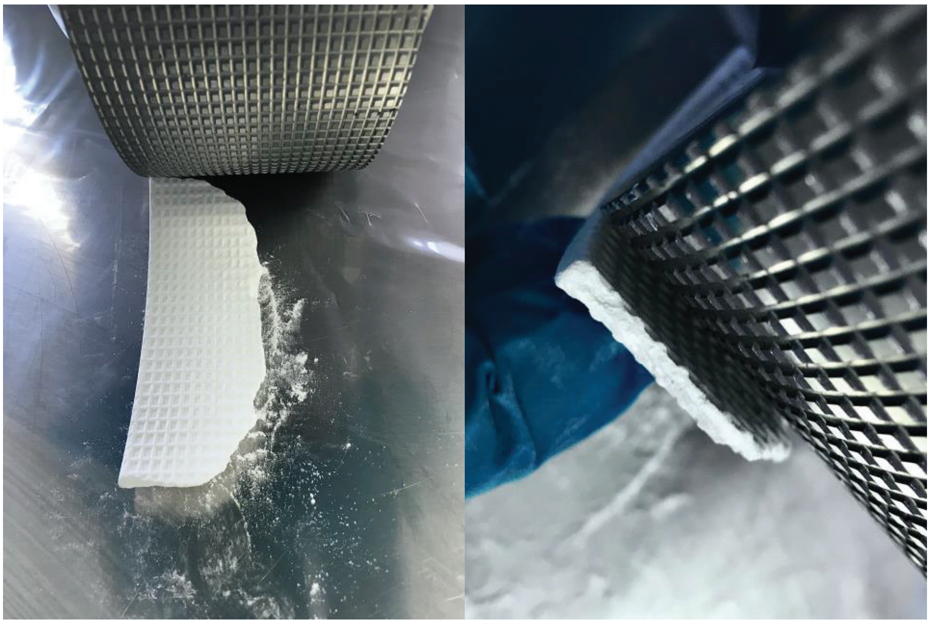

Figure 1. Schematic illustration of compaction rolls with the fragment of an extracted ribbon

The primary powder was compacted with operation regime of three settings of *SCF* = 9.6; 11.2; 12.5 kN/cm on GER and *p* = 120; 140; 160 bar on AW. The roll compactors were used without changing the gap setting. Fig. 1 shows an illustration of a roll and compacted ribbon, illustrating also that the ribbons were of non-uniform strength, with weak zone in the middle. Because of this, complete ribbon width could not be obtained and only ribbon fragments from the one or the other side were available for further analysis. The ribbons were considered symmetrical, and the edges were not distinguished.

The ribbon samples had been analyzed on their texture inside the ribbon by the CTX Texture Analyzer (AMETEK Brookfield, USA) using the blade and the needle instrumentation. The blade arrangement was not able to produces reliable results and this technique was abandoned. All the relevant results were thus measured using the needle arrangement, where the needle was pressed to a specific point on the ribbon, while the force required to reach certain penetration depth was recorded (Fig. 2). The calculations determined the ribbon stiffness (k, N/mm) as the slope of the recorded curve at the maximum gradient thereof (Fig. 3). The ribbon stiffness was obtained for different lateral co-ordinate for each compaction process. All measurements were done in triplicate and the lateral co-ordinate was determined by the distance from the edge *DE* (mm).

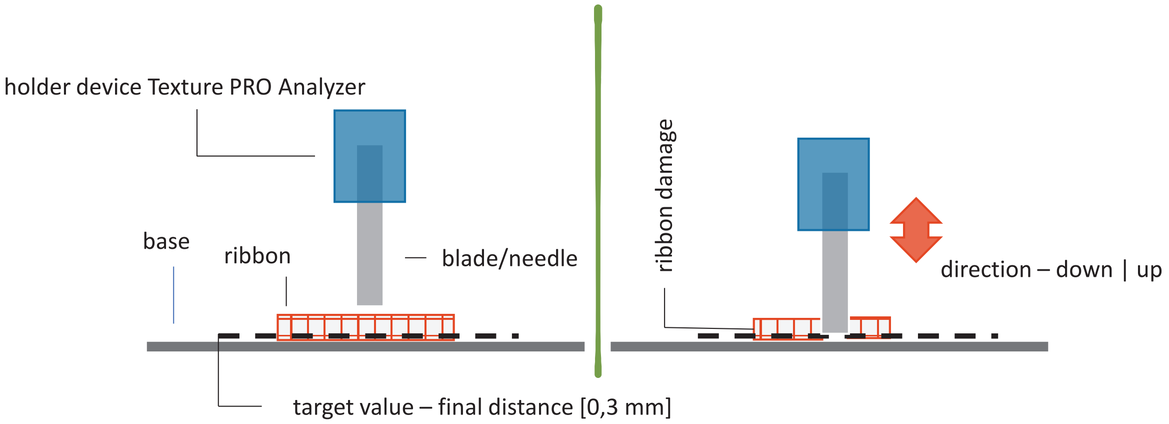

Figure 2. Schematic illustration of the texture analysis measurement setup

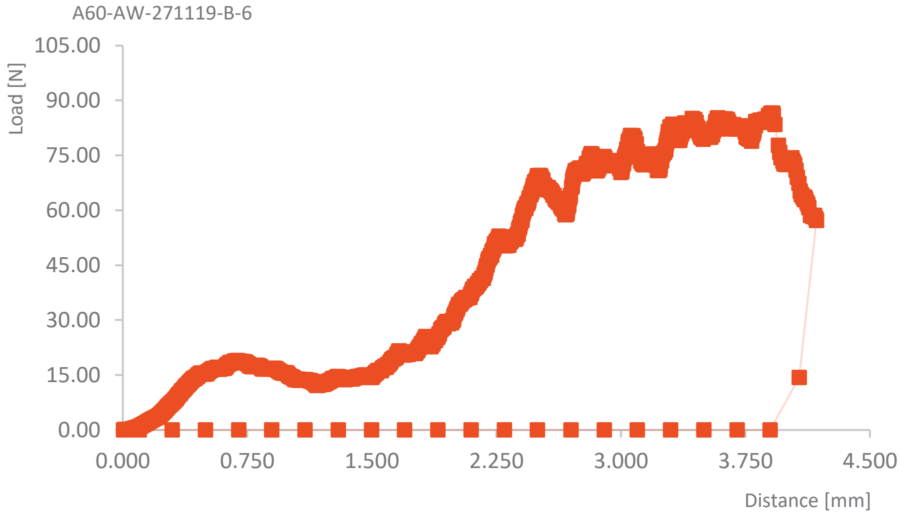

Figure 3. Schematic illustration of the measurement record (bottom)

Results and discussion

Fig. 4 and 5 show ribbon stiffness profiles for both compactors. The scale on the horizontal axis corresponds to the maximum ribbon width given by the roll width for each compactor.

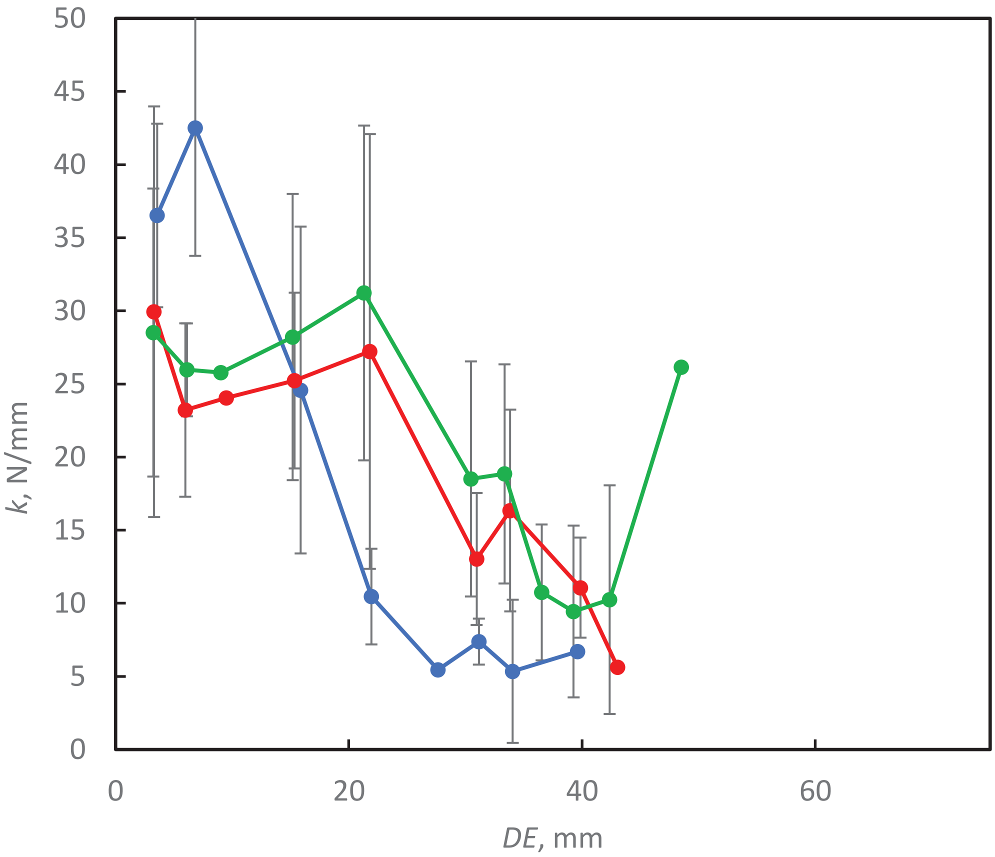

Figure 4. Ribbon stiffness *k* at different distance from outer edge *DE* for AW ribbons compacted at *p* = **120**, **140**, **160** bar.

Complete ribbons were impossible to obtain on AW (see Fig. 4), because the ribbon stiffness decreases substantially towards the middle of the ribbon for all pressure settings. In overall, the ribbon stiffness increased with increased compaction pressure.

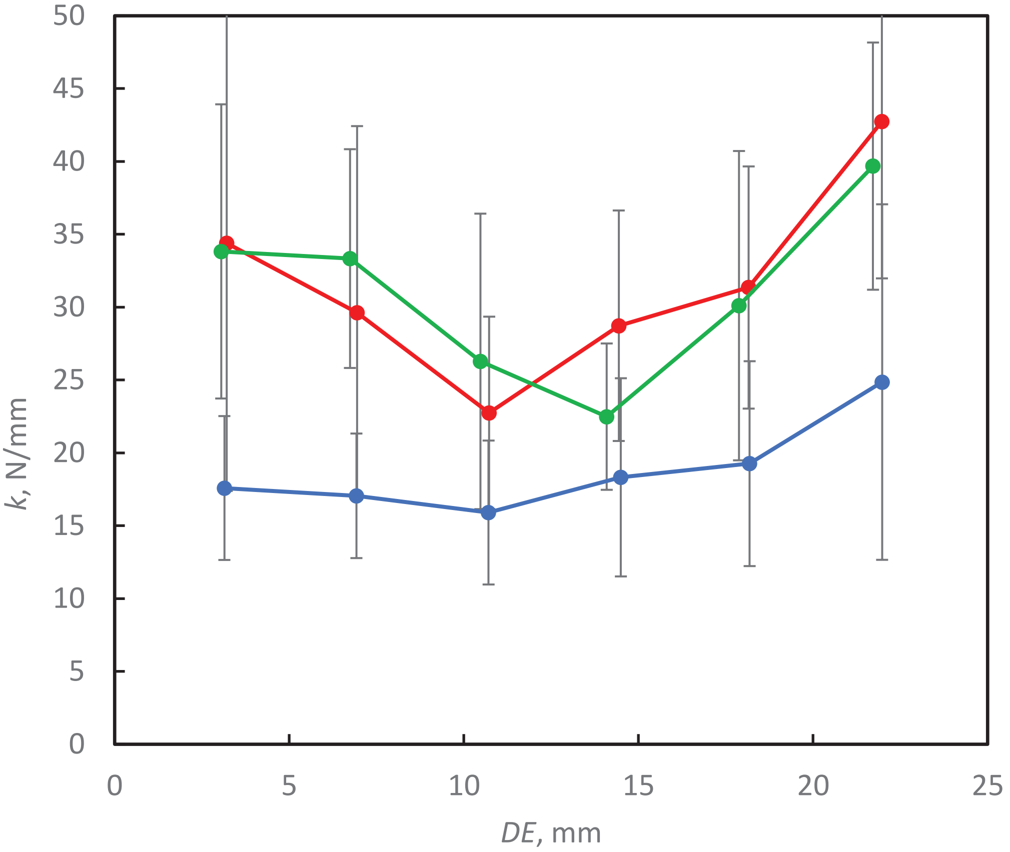

Figure 5. Ribbon stiffness *k* at different distance from outer edge *DE* for GER ribbons compacted at *SCF* = **9.6**, **11.2**, **12.5** kN/cm.

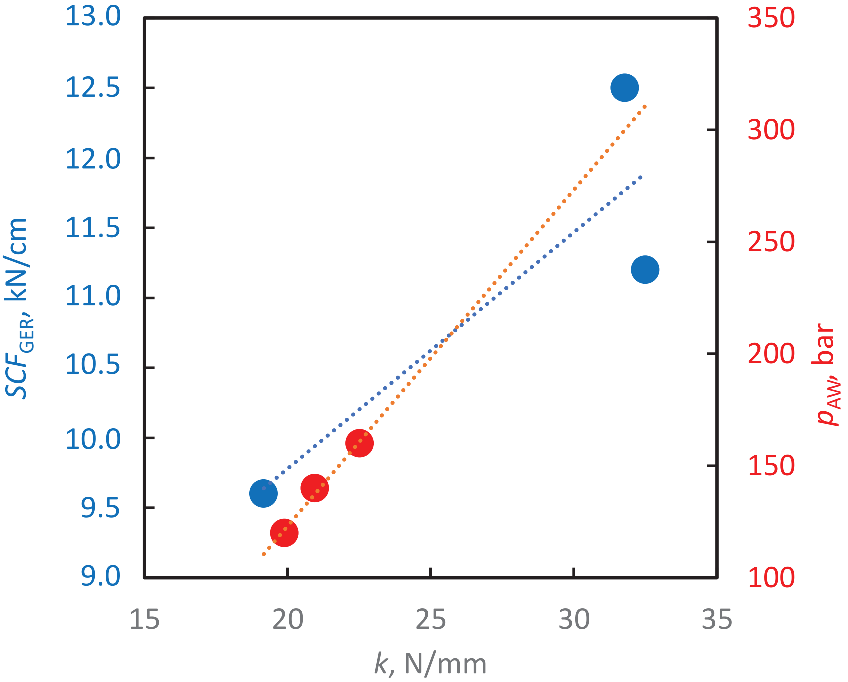

Figure 6. Force/pressure parameters for GER and AW compactor required to obtain ribbons of certain stiffness. Dotted lines present linear fits of the trend.

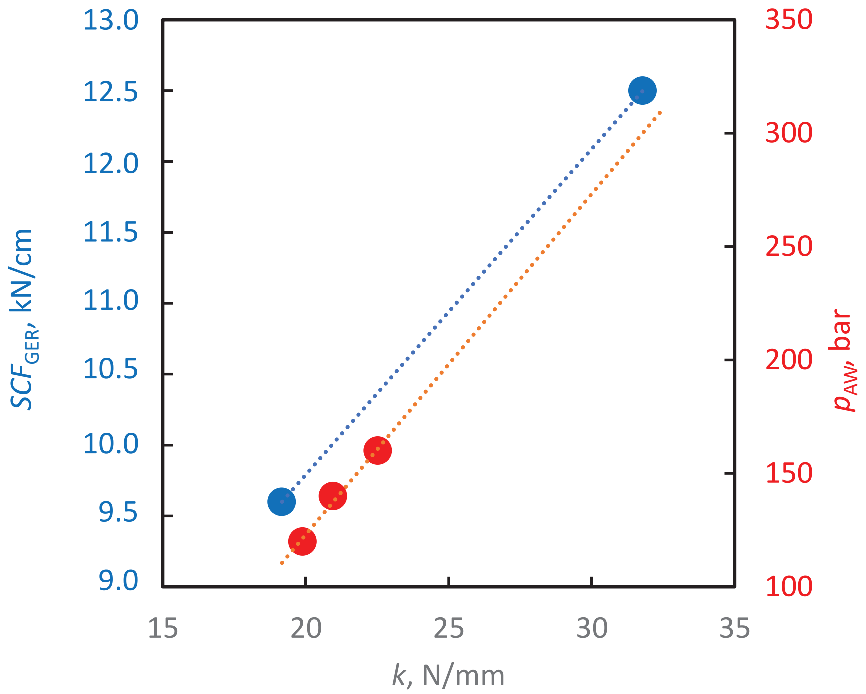

Figure 7. Force/pressure parameters for GER and AW compactor required to obtain ribbons of certain stiffness using the over-compaction correction. Dotted lines present linear fits of the trend.

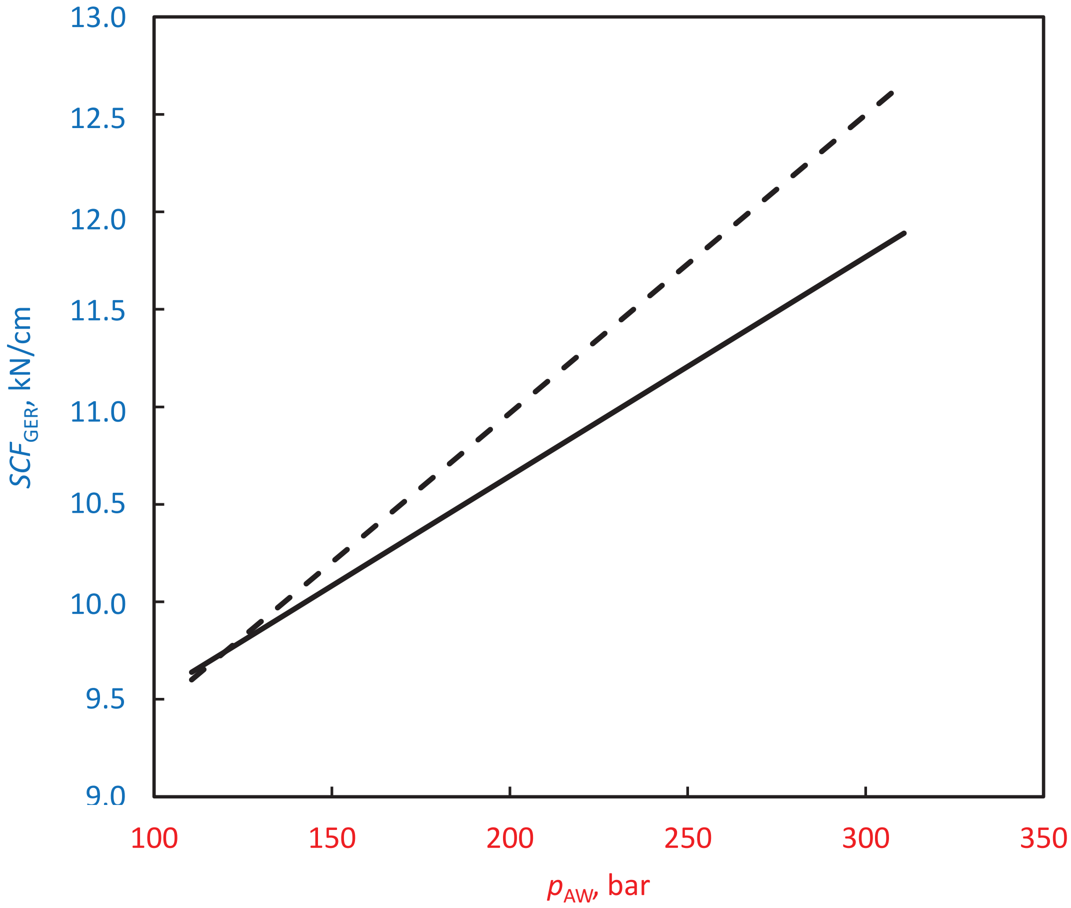

Figure 8. Compaction force transfer chart using the uncorrected (solid) and corrected (dashed) stiffness profile. The lines indicate compatible settings of both compactors to produce ribbons of equal stiffness.

GER produced whole ribbons owing to the smaller width of the rolls and more uniform stiffness profile (Fig. 5). The overall stiffness increased between 9.6 and 11.2 *SCF*, but it decreased afterwards. It is assumed this stiffness drop is caused by over-compaction of the material due too high deformation reaching significantly out of the plastic region. Mean stiffness values were calculated from the profiles as the mean integral values. The (mean) stiffness – force/pressure diagrams are shown in Fig. 6 and 7, the first being displayed using all the measured data while the second assumes the validity of the over-compaction explanation and discards the data measured at 12.5 kN/cm on GER.

The linear approximation of the stiffness – force/pressure profiles were used to define the compaction force transfer chart (Fig. 8). The lines displayed on this chart correspond to the p_{AW} and SCF_{GER} value pairs which should produce ribbons of equal stiffness according to the linear models shown in Fig. 6 a 7. A line is defined for both the corrected and uncorrected data sets. In the region, which is well covered by the experimental data, i.e. up to p_{AW} = 180 bar, both predictions are quite similar and the parameter transfer should likely produce similar ribbons. The difference between both predictions for higher p_{AW} is large and the parameter transfer in this region is likely to be invalid. The main cause of this deviation is the much greater ribbon non-uniformity for AW device. Using the mean stiffness characteristics for this device is a rough approximation as the edge and central parts of the produced ribbon have substantially different properties. Therefore, further improvement of this procedure should involve detailed utilization of the stiffness profile data.

Conclusions

The ribbon stiffness parameter was tested as the main parameter to characterize compacted powders in the roll compaction process. It provided a good correlation with process parameters in the effective range of compaction, but the correlation did not extent to very high compaction force region due to over-compaction of the material. In overall, if used within machine operability limits, it can be utilized to produce ribbons with the same properties at two different scales of compactors AW and GER. Broader utilization of this finding for the scale-up of the compaction process would require a more rigorous accommodation for the ribbon nonuniformity, which is a substantial difference factor between both devices. Nevertheless, using the stiffness parameter is a promising alternative to monitoring the ribbon parameters as it is much easier to get as compared to the envelope density of the ribbon.

Acknowledgement

This work was realized and financially supported from the grant of Specific university research – grant No A1_FCHT_2021_002. The research data have been released with the Zentiva authorization – Pharmaceutical Applied Research Center, The Parc.

Literature

1. Perez-Gandarillas L., Perez-Gago A., Mazor A., Kleinebudde P., et al.. Effect of roll-compaction and milling conditions on granules and tablet properties. European Journal of Pharmaceutics and Biopharmaceutics, Elsevier, 2016, 106 (SI), pp.38-49. 10.1016/j.ejpb.2016.05.020. hal-01609014
2. Wu C.-Y., Hung W.-L., Miguélez-Morán A.M., Gururajan B., et al.. Roller compaction of moist pharmaceutical powders. International Journal of Pharmaceutics, Elsevier, 2010, 391, pp.90-97.
3. Csordas K., Kleinebudde P.. Evaluation of the performance of different types of roll compactors. Powder Technology, Elsevier, 2018, 337, pp.84-91.
4. Nesarikar V.V., Vatsaraj N., Patel Ch., Early W., et al.. Instrumented roll technology for the design space development of roller compaction process. International Journal of Pharmaceutics, Elsevier, 2012, 426, pp.116-131.

TECHNIQUE OF PHARMACEUTICAL POWDER COMPRESSIBILITY MEASUREMENT FOR UTILIZATION IN PREDICTIVE MATHEMATICAL MODELLING OF COMPACTION PROCESSES

Marinko N., Krpelan T., Zamostný P.

University of Chemistry and Technology, Prague, Department of Organic Technology, Technická 5, Prague 6, 166 28, Czech Republic

marinkon@vscht.cz

Abstract

Mathematical modelling of pharmaceutical operations requires fundamental data that covers many aspects of the process and roller compaction of pharmaceutical mixtures is not an exception to this practice. Rheological and mechanical properties of the pharmaceutical powders must be accurately determined for practical application in the modelling of this process. A key mechanical property of a powder is compressibility, which describes the volume reduction of a bulk powder when subjected to compaction pressure. It is used in mathematical modelling to predict the extent of compaction, which governs the final envelope density of the compact. In this work we adapt a method to determine compressibility for application in mathematical modelling of roller compaction. The method presented is based on practical implementation of Johanson's compressibility model (1965) and was executed using a uniaxial compression machine that records applied load on the powder and displacement of the punch to determine compressibility. The applicability of this approach was demonstrated on real pharmaceutical mixtures and the measured values of compressibility for these mixtures were used in mathematical modelling to predict the final envelope densities for their compacts.

Introduction

Roller compaction is generally the preferred pharmaceutical unit operation for the granulation of solid fine powders. This is because the operation itself is low-cost, easy to control and it allows for high material throughput. Additionally, the pharmaceutical ingredients in the process are not exposed to moisture or heat, which is a benefit over its counterparts, wet granulation and spray drying. The objective of roller compaction is to transform inferior fine powders into granulates with better flowability and fixed homogeneity[1].

The tactic that is currently favoured to understand this process involves maintaining identical quality of the first intermediate in the unit operation, the ribbon (roller compacted compact). Prior to milling in to the granulate, ribbons can be sampled in-process to obtain data about their properties. Most important quality of the intermediate to maintain process reproducibility is the ribbon envelope density. Therefore, preliminary experiments have to be performed to identify the optimal ribbon. Mathematical modelling of this process is helpful to speed up this process and simplify potential scale-up operations. It is based on equipment geometry, applied process parameters and the knowledge of rheological and mechanical properties of the studied powders[2-4]. A key mechanical property of a powder is compressibility, which describes the volume reduction of a bulk powder when subjected to compaction pressure. It is used in mathematical modelling to predict the extent of compaction, which governs the final envelope density of the ribbon. Johanson et. al.[5] introduced a compressibility relation (Eq. 1) between applied pressure (σ_i) and powder bulk density (ρ_i) and Reynolds et. al.[6] expanded on this work and introduced a practical implementation (Eq. 2) that allows to predict ribbon envelope density from initial bulk density, process parameters and known compressibility.

Eq. (1) $\dfrac{\sigma_1}{\sigma_2} = \left(\dfrac{\rho_1}{\rho_2}\right)^K$

Eq. (2) $\rho_{bulk} \cdot P_{max}^{\frac{1}{K}} = \rho_{max}$

Although compressibility can be determined from experimental data of ribbon envelope density, it requires a number of preliminary roller compaction experiments which results in material loss during development. An alternative to this approach is the utilization of uniaxial compression using a tablet press. The pressure-density relation for powders can be obtained from prepared compacts, by measuring their density at different compaction settings[7]. However, limited work has been done with instrumented tablet presses that record force-displacement data that can be readily interpreted as pressure-density relationship for powders[6].

In this work we adapt the method to determine compressibility with the instrumented tablet press for two real pharmaceutical mixtures. The compressibility values obtained are used in predictive mathematical modelling of ribbon envelope density. The effectiveness of prediction capability is compared to experimental ribbon envelope density data obtained from roller compaction of these mixtures.

Materials and methods

Materials

Two pharmaceutical mixtures Z1 and Z2 (with different active ingredients) that are currently in development were provided by Zentiva k.s. (Czech Republic). The excipient and API components for these mixtures are known to the author but cannot be disclosed. In some experiments, a slight amount of sodium stearyl fumarate (bn 622724, Zentiva k.s.) was used to lubricate the die in the uniaxial compression test to counter low reproducibility of the experiments due to sticking of the powder to the surfaces of the die and punches. Surface lubrication is sometimes used in roller compaction for poorly flowing or sticky powders as well.

Simulated compaction

Preparation of compacts was simulated using a uniaxial compression in Gamlen GTP-1 instrumented tablet press (Gamlen tableting Ltd., United Kingdom). The instrumentation of the tablet press records the load applied to the powder and the displacement of the tabletting punch. Approximately 85 mg of each mixture was weighed out for every experiment and transferred to a round 5 mm die with a flat base plate. The compacts were pressed by applying a load of 500 kg (max. pressure of approx. 250 MPa) with a flat face punch travelling at 60 mm/min. The hold time of the material in the die was set to zero in order for the punch to retract immediately when the target load was reached; this was done to better mimic roller compaction.

Compressibility solution K_{sim}

The solution for compressibility was accommodated to the setting of uniaxial compression and it is based on the Johanson's relation as shown in Equation 3. Since the one-dimensional punch displacement allows to substitute bulk density (ρ_i) for relative height (h_i) of the compact at any given pressure range (σ_i), it is then possible to transform this equation to a linear format and find compressibility K_{sim} as the slope of this relation.

Eq. (3) $$\frac{\sigma_1}{\sigma_2} = \left(\frac{\rho_1}{\rho_2}\right)^K \rightarrow \frac{\sigma_1}{\sigma_2} = \left(\frac{V_2}{V_1}\right)^K \rightarrow \frac{\sigma_1}{\sigma_2} = \left(\frac{h_2}{h_1}\right)^K \gg \boldsymbol{ln\frac{1}{h} = \frac{1}{K_{sim}} \cdot ln\,\sigma + C}$$

The necessary data were obtained from the compaction experiments and used to plot charts displaying the relation between applied load and punch displacement. This data can also be interpreted as relationship between applied pressure and punch displacement; therefore, the data points of both axes can then be transformed logarithmically and the slope for the largest linear relationship of the data is used to find material compressibility value K_{sim} of the selected pressure range (example of solution on Figure 1). Compressibility for both mixtures was evaluated in a range of 30-250 MPa.

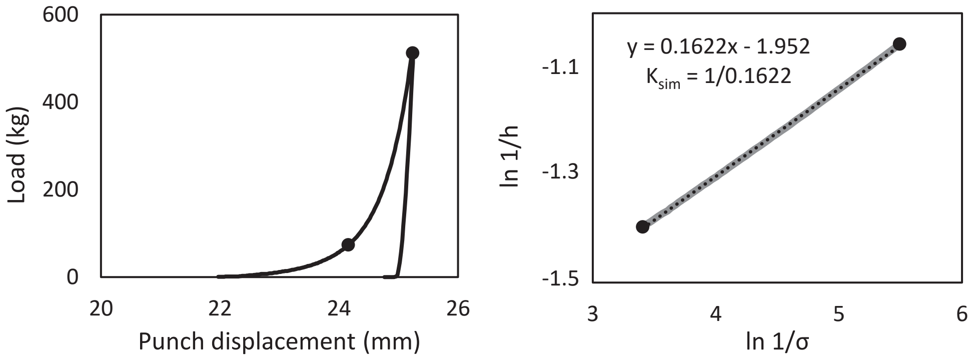

Figure 1. Illustration of the data processing to obtain compressibility (example from one sample of Z1 mixture)

Roller compaction of ribbons

Roller compaction experiments with mixtures Z1 and Z2 were conducted on Mini-Pactor® (Gerteis Maschinen, Switzerland) to provide ribbons. The process parameters of these experiments are summarized in Table I.

Table I
Process parameters for roller compaction experiments

Z1 Batch	RPM	Gap (mm)	Force (kN/cm)	Z2 Batch	RPM	Gap (mm)	Force (kN/cm)
A1	5	4	3	**B1**	2.4	2.5	8
A2	5	2	3	**B2**	2.4	3.5	8
A3	1	4	3	**B3**	2.4	2.5	12
A4	1	2	3	**B4**	2.4	3.5	12
A5	5	4	7	**B5**	2.4	3	10
A6	5	2	7	**B6**	2.4	3	10
A7	1	4	7				

Experimental envelope density of ribbons

Experimental ribbon envelope densities from roller compacted ribbons of each mixture were acquired to compare simulated and experimental compaction. Different approaches were applied to determine experimental envelope density. A direct method of liquid volume displacement was used to determine envelope density for Z1 mixture (ρ_{liq}); while the envelope density of Z2 mixture (ρ_{gap}) was determined with an indirect method at-gap from mass throughput and volume flow. Mass throughput was collected for one minute at two separate occasions for each batch and volume flow was determined from roll geometry and process parameters (Figure 2).

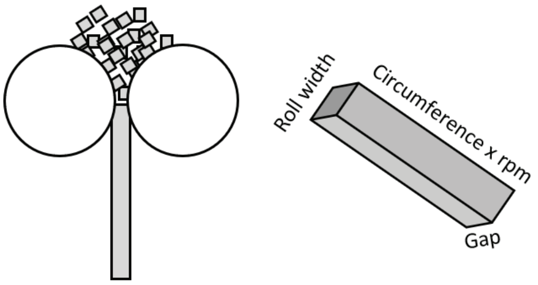

Figure 2. At-gap density concept

Mathematical modelling

A roller compaction model that is based on the practical implementation proposed by Reynolds et. al. (2010) deployed in gPROMS FormulatedProducts® software was used to simulate the processes on the Mini-Pactor® unit in-silico. Initial state for the modelling environment had to be specified for each mixture from powder flow properties and bulk density. These properties were measured on FT4 Powder Rheometer (Freeman technologies, United Kingdom). The model was used to predict envelope densities ρ_{sim} corresponding to the designed process parameters by utilizing the obtained compressibility values K_{sim} from uniaxial compression. Additionally, it was used to obtain model validated compressibility values K_{exp} from experimental envelope densities (ρ_{liq} for Z1 mixture; ρ_{gap} for Z2 mixture) of the roller compacted ribbons.

Results and discussion

The uniaxial compression test was performed with 30 samples of each mixture. The Z1 mixture was measured in 10 sets of 3 experiments and the die had to be lubricated to achieve this reproducibility. The Z2 mixture was measured in 3 sets of 10 experiments without reproducibility issues. Compressibility for each experiment was obtained as described in Figure 1 from measured force-displacement data. Material compressibility K_{sim} for both mixtures was obtained as an average from 30 experiments. The compressibility values K_{sim} of each mixture were then used in mathematical modelling to predict ribbon densities ρ_{sim} according to the planned process parameters for each batch experiment (Table 1). Experimental ribbon densities for all batches were determined with different techniques and the obtained density data were used to model validate the compressibility value K_{exp} for both mixtures. The compressibility values that were obtained this way had very narrow confidence intervals. These results are summarized in Tables 2 and 3 for discussion.

The model validated compressibility of the Z1 mixture from experimental ribbon densities ρ_{liq} is similar to the one obtained from uniaxial compression experiments and if we compare the experimental ribbon densities of Z1 mixture to the predicted ones, we can see that the model prediction was rather successful (Table II). Therefore, the compressibility value obtained from uniaxial compression experiments for Z1 mixture is plausible for predictive mathematical modelling of ribbon density in the roller compaction design space for the selected process parameters.

Table II

Comparison of predicted ρ_{sim} to experimental ρ_{liq} for Z1 mixture; Initial bulk density: 686 kg/m^3

Z1 Batch	Z1 K_{sim}	ρ_{sim} of Z1 (kg/m^3)	ρ_{liq} of Z1 (kg/m^3)	Model validated Z1 K_{exp}
A1	6.15 ± 0.05	1203	1248	5.71 ± 0.08
A2		1249	1281	
A3		1203	1306	
A4		1249	1273	
A5		1381	1391	
A6		1434	1422	
A7		1381	1377	

The extension of design space for ribbon density prediction was simulated with gProms global analysis and the results are shown in Figure 3. It is visible that the prediction capability of the model with K_{sim} is quite acceptable compared to the model validated K_{exp} analysis over four gap sizes and wide range of roll force.

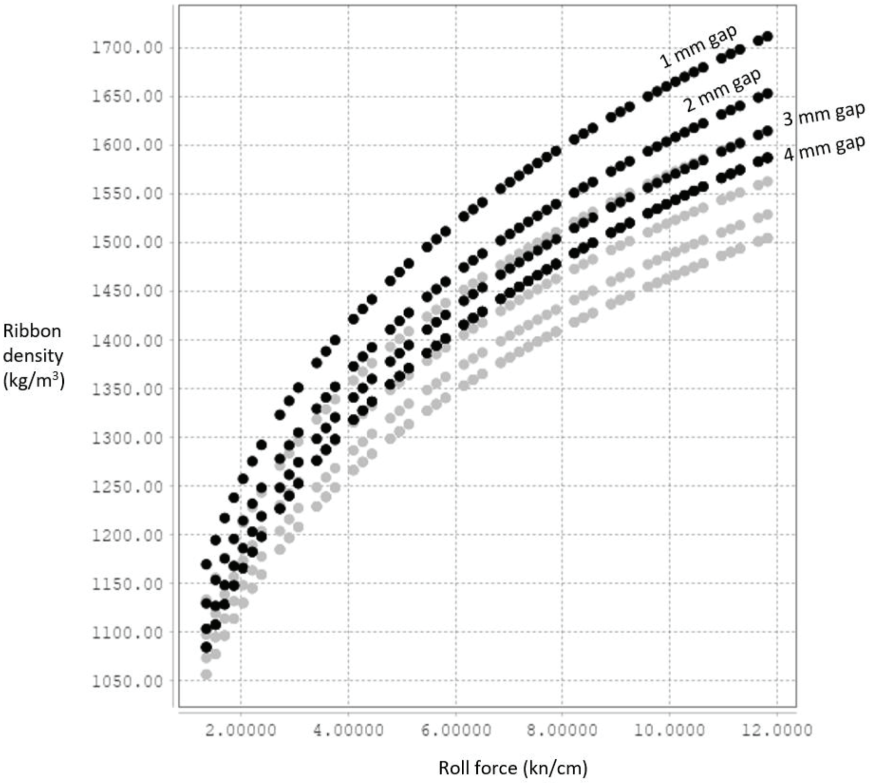

Figure 3. Global analysis of design space for Z1 mixture; black dots represent Z1 mixture with K_{sim} = 6.15, gray dots represent Z2 mixture with K_{exp} = 5.71; each mixture shown in four gap sizes (top to bottom - 1 to 4 mm)

On the other hand, the difference between the measured K_{sim} and model validated K_{exp} compressibility and consequently ρ_{sim} and ρ_{gap} density values for Z2 mixture is very apparent. This is most likely caused by the different method utilized to measure the experimental ribbon density $\boldsymbol{\rho_{gap}}$ and that is because the at-gap density technique is an indirect method for obtaining envelope density. Although the experimental ribbon densities of Z2 mixtures correspond to the process parameters, they are much larger than the densities ρ_{sim} predicted with K_{sim} that was established from uniaxial compression. This large difference may be caused by the fact that the at-gap density is based on idealized volume flow of a regular non-porous compact without spring-back elasticity; therefore, its density would be naturally higher and model validated compressibility better (smaller value). Because of this, it was not possible to confirm that uniaxial compression test of Z2 mixture provided a compressibility value that reflects reality. Which means that at-gap density technique was not suitable to verify our approach and a direct method to measure actual ribbon density of Z2 mixture, such as liquid displacement for Z1 mixture, would provide better results. However, at the time of writing this conference paper, the direct method of envelope density measurement for Z2 mixture is still in development.

Table III

Comparison of predicted ρ_{sim} to experimental ρ_{gap} for Z2 mixture; Initial bulk density: 436 kg/m^3

Z2 Batch	Z2 K_{sim}	ρ_{sim} of Z2 (kg/m^3)	ρ_{gap} of Z2 (kg/m^3)	Model validated Z2 K_{exp}
B1	6.05 ± 0.01	931	1648	3.29 ± 0.05
B2		996	1488	
B3		911	1749	
B4		975	1606	
B5		955	1683	
B6		955	1674	

Conclusion

It was shown that a uniaxial compression test can be used to estimate material compressibility for use in predictive mathematical modelling of ribbon envelope density. This estimated compressibility can be used as a starting point in the design of experiments for roller compaction processes and can be further validated for higher precision with experimental data of ribbon densities, as demonstrated with Z1 mixture. It was found that the experimental ribbon density data must be obtained with a direct physical measurement, such as liquid displacement. As opposed to the indirect measurement with at-gap density technique that was used with Z2 mixture. The at-gap density measurement essentially determines a different type of density that is more idealized but still proportionate to the material in question and corresponding with the process controls. Furthermore, because the at-gap technique is simple to perform it can be utilized to check the ribbon quality in-process on the same machine or in transfer of the process to a different scale.

Nomenclature

K_{sim}	Compressibility constant evaluated with uniaxial compression experiments
K_{exp}	Compressibility constant determined from experimental ribbon envelope density data
ρ_{sim}	Ribbon envelope density predicted with K_{sim}
ρ_{liq}	Experimental data of ribbon envelope density acquired with liquid volume displacement
ρ_{gap}	Experimental data of ribbon envelope density acquired with at-gap density measurement
σ_i	Applied pressure in Pa

Acknowledgement

This work was supported from the grant of Specific university research – grant No. A2_FCHT_2021_080.

We would also like to acknowledge Zentiva for providing the materials and The Parc for supporting the project.

References

1. Yu, S. Roll compaction of pharmaceutical excipients. University of Birmingham, **2013**.

2. Toson, P.; Lopes, D. G.; Paus, R.; Kumar, A.; Geens, J.; Stibale, S.; Quodbach, J.; Kleinebudde, P.; Hsiao, W.-K.; Khinast, J., Model-based approach to the design of pharmaceutical roller-compaction processes. *Int J Pharm X* **2019,** *1*, 100005-100005.
3. Sousa, R.; Valente, P. C.; Nakach, M.; Bardet, L.; Wacquet, M.; Midoux, N.; Authelin, J.-R., Roller Compaction Scale-Up Made Simple: An Approximate Analytical Solution to Johanson's Rolling Theory. *Journal of Pharmaceutical Sciences* **2020,** *109* (8), 2536-2543.
4. Mansa, R. F. In *Roller compaction of pharmaceutical excipients and prediction using intelligent software*, **2007**.
5. Johanson, J. R., A Rolling Theory for Granular Solids. *Journal of Applied Mechanics* **1965,** *32* (4), 842-848.
6. Reynolds, G.; Ingale, R.; Roberts, R.; Kothari, S.; Gururajan, B., Practical application of roller compaction process modeling. *Computers & Chemical Engineering* **2010,** *34* (7), 1049-1057.
7. Rowe, J.; Crison, J.; Carragher, T.; Vatsaraj, N.; McCann, R.; Nikfar, F., Mechanistic Insights into the Scale-Up of the Roller Compaction Process: A Practical and Dimensionless Approach. *Journal of pharmaceutical sciences* **2013,** *102*.

WASTE TREATMENT, WATER PROTECTION

POZOLAN ACTIVITY OF CALCINED CLAYS AND OTHER POZZOLANS USING THE FRATTINI TEST

Rak P.[1], Šídlová M.[1], Doležal T.[1], Šulc R.2, Formáček P.[2]

[1]*Univesity of Chemistry and Technology, Prague, Faculty of Chemical Technology, Czech Republic*
[2]*Czech Technical University in Prague, Faculty of Civil Engineering, Czech Republic*

The presented work deals with the determination of pozzolanic activity according to the Frattini test (ČSN EN 196-5) of selected high-temperature fly ash (FA), biomass ash (BMA), calcined clays (CC) fired at a temperature of 600 - 1000°C and SiO_2. The results showed that the reactivity of individual substances differs significantly. All FA showed pozzolanic activity, while biomass ash showed significantly worse pozzolanic properties, which, however, is directly related to the high proportion of calcium ions in these ashes. Stachema silica fume with a very high specific surface had excellent pozzolanic properties, while the waste silica did not show pozzolanic properties. By monitoring the effect of calcination temperature on the subsequent reactivity of the selected clay, it was found that the temperature has no significant effect on the reactivity of the clay according to the performed Frattini test. The reduction of reactivity was achieved only at a temperature of 1000 ° C, when mullite was formed in the sample.

Introduction

Pozzolans have been used for many decades as an important raw material in construction industry. These are siliceous and aluminum materials that, in the presence of water and calcium hydroxide, are able to form a C-S-H binder phase. C-S-H phase is responsible for the strength of hardened cement. Cement replacement, whether total or partial, has a significant influence on reducing CO_2 emissions and can improve concrete properties[1]. The pozzolans commonly used in concrete include fly ash, natural pozzolans or silica fume. In addition, with the closure of coal-fired power plants, the demand for the possibility of using stockpile and ponded ash is growing. The issue of preserving the pozzolanic properties of this material over time is related to this[2]. In addition, there has been an increase in other alternative additives, such as calcined clays in recent years[3]. In addition, Snelling mentions a potential utilization in his work biomass ash[4].

For optimal use of pozzolans, it is necessary to know their reactivity, resp. pozzolanic activity. There are a number of methods for determining pozzolanic activity, the main division is into direct methods and indirect methods. Direct methods include the Frattini test, which is described by the ČSN EN 196-5 standard[5]. Other direct methods include the Chapelle test and its various modifications[6]. Indirect methods include the measurement of the strength activity index (SAI), which is based on the measurement of the compressive strength of prepared mortars with pozzolan against a reference cement mortar[7]. Another indirect method of measuring pozzolaic activity is the electrical conductivity test[8,9].

The aim of this work was to compare the pozzolanic activity for selected pozzolans from Czech Republic with a focus on fly ash, biomass ash, calcined clays and SiO_2 using the Frattini test, resp. according to ČSN EN 196-5.

Materials and methods

The input materials for the pozzolanic activity tests were Czech fly ash from coal-fired power plants (FA), biomass ash (BMA), calcined clays (CC) to different temperatures and silica. Specifically, it was two FA from the Počerady power plant (labeled 2 C, 3 C), one FA from the Tušimice power plant (labeled 8 C) and one FA from the heating plant from Dvůr Králové (labeled 14 C). Biomass ash BM 1 comes from the Energy Center in Jindřichův Hradec and is burning hay and straw bales in a grate boiler. Biomass ash BM 2 was delivered from the Hodonín power plant and is produced by fluid co-combustion coal and biomass (80 % coal + 20 % biomass). Silica was represented by one commercially available silica fume Stachesil S from Stachema (labeled MS). Waste SiO_2, which arises as waste from grinding kitchen worktops, was supplied by Technistone, s.r.o. (labeled TC). This TC was calcined to a temperature of 500°C before measuring the pozzolanic properties in order to remove residues of organic substances and cellulose. Furthermore, WS clay from Keraclay was used, which was fired at a temperature of 600 - 1000°C and marked WS 600 - WS 1000. The WS 750 sample was additionally refined by grinding and marked

WS 750m. Furthermore, it was used cement CEM I 42.5 R, Mokrá, Českomoravský cement, a. s. (labeled CEM) in this work. The elemental composition of the input raw materials is given in Table I

Table I
The elemental composition of the input raw materials by XRF

	SiO_2	Al_2O_3	Fe_2O_3	CaO	MgO	Na_2O	K_2O	TiO_2	SO_3	P_2O_5	Cl^-	MnO	Others
CEM	18.6	35	6.7	1.9	0.9	0.5	1.3	3.6	0.5	-	-	-	0.7
2 C	53.8	33.9	4.8	1.6	1.1	0.4	2.4	1.6	0.5	0.2	0.0	0.0	0.4
3 C	54.9	33.2	4.2	1.6	1.5	0.4	2.3	1.6	0.21	0.2	0.0	0.0	0.4
8 C	49.8	33.9	8.9	1.8	1.2	0.6	1.7	1.2	0.6	0.2	0.0	0.0	0.5
14 C	32.8	27.3	10.8	11.4	2.5	1.6	1.2	1.8	9.5	0.3	0.0	0.0	1.1
BM 1	39.1	0.8	0.6	13.5	2.9	0.3	25.7	0.1	5.5	2.2	9.3	0.1	0.2
BM 2	43.1	5.9	2.6	28.2	4.9	0.8	7.4	0.4	0.9	5.5	0.0	2.0	0.7
MS 1	89.5	1.2	4.2	0.3	0.8	0.3	1.9	0.0	1.4	0.1	0.0	0.0	0.7
MS 2	97.2	0.4	0.1	0.28	0.4	0.3	0.9	0.0	0.2	0.1	0.1	0.0	0.1
TC	87.9	3.6	0.2	2.7	0.8	3.4	1.6	0.1	0.6	0.0	0.1	0.0	0.1
WS	50.0	46.1	0.8	0.2	0.1	0.0	0.7	1.6	0.2	0.1	0.0	0.0	0.2

The phase composition of the raw materials 2 C, 3 C, 8 C, 14 C, BM 1, BM 2 and WS is given in Table II. Samples 2 C, 3 C, 8 C additionally contained 1% magnetite and hematite, sample 8 C contained 1% hercinyte. Sample BM 1 additionally contained 1% calcite, 2% anorthoclase and 1% albite, sample BM 2 additionally contained 6% orthoclase and 3% leucite. The silica fume MS sample was predominantly amorphous, containing minor crystalline SiO_2 and SiC. TC sample, on the other hand, contained a predominantly crystalline quartz phase. In addition, Figure 1 shows the Diffraction patterns of calcined clays at temperatures of 600 - 1000°C. Other important parameters in terms of characterization of the supplied materials are given in Table III, which is the particle size characterized by the quantiles d10, d50, d90, specific density (ρ) and specific surface (S).

Table II
The phase composition of the raw materials 2 C, 3 C, 8 C, 14 C, BM 1, BM 2 and WS by XRD

	Amorphous phase	Quartz	Mullite	Kaolinite	Anhydrite	Akermanite	Arkanite	Sylvite	Muscovite
2 C	53	15	31	0	0	0	0	0	0
3 C	50	14	35	0	0	0	0	0	0
8 C	54	9	35	0	0	0	0	0	0
14 C	74	10	6	0	6	3	0	0	0
BM 1	74	2	0	0	0	0	6	13	0
BM 2	48	38	0	0	0	1	0	0	0
WS	37	4	0	57	0	0	0	0	2

The elemental composition of all raw materials was calculated as oxides and determined by X-ray fluorescence (XRF) analysis by ARL 9400 XP sequential WD-XRF spectrometer. The obtained data were evaluated by standardless software Uniquant 4. The diffraction patterns were collected at room temperature with an X'Pert^3 Powder θ-θ powder diffractometer with parafocusing Bragg-Brentano geometry using Cu Kα radiation (λ = 1.5418 Å, Ni filter, generator setting: 40 kV, 30 mA). An ultrafast PIXCEL detector was employed to collect XRD data over the angular range from 15 to 75° (2θ) with a step size of 0.013° 2θ and a counting time of 180 s/step. The fixed divergence slit was used for the measurement. The Rietveld method was used to calculate mass content for present crystalline phases and amorphous phase using ZnO as an internal standard.

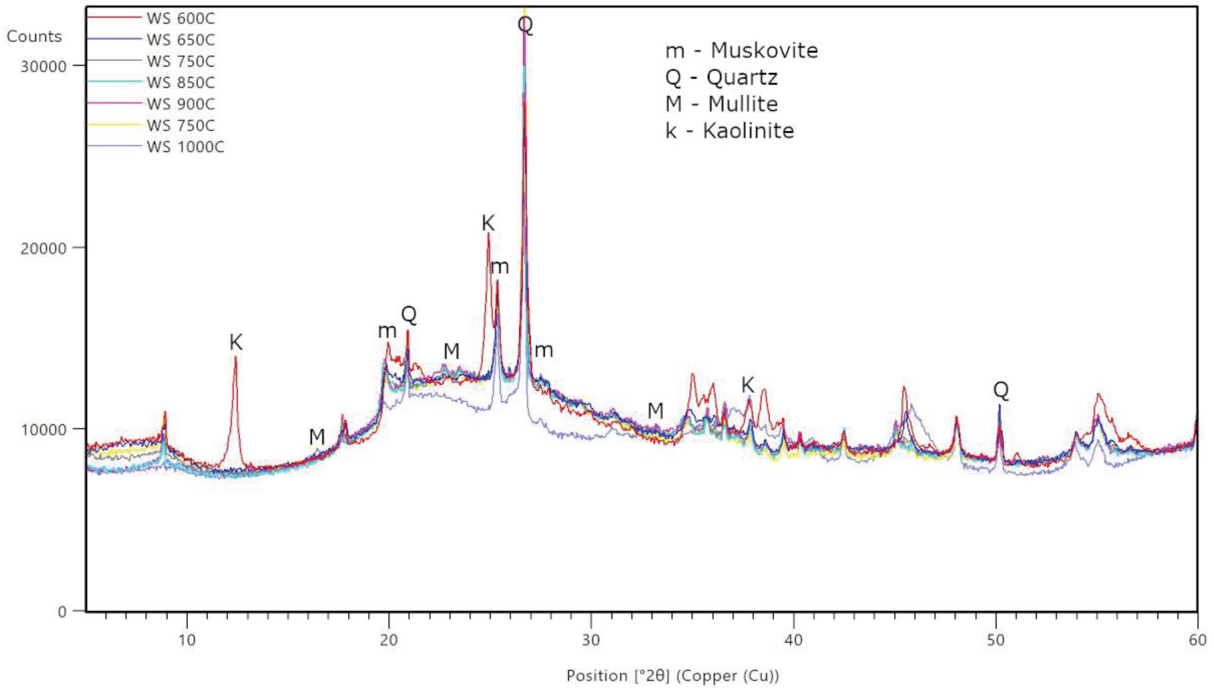

Figure 1. Diffraction patterns of calcined clay WS at different temperatures 600 - 1000°C.

Physical properties included analyzes particle size distribution (PSD), specific density (ρ) and specific surface (S). A laser-light scattering analyser Bettersizer (Dandong Bettersize Instruments Ltd., China) was used to determine the particle size distribution. Specific density (ρ) was performed by the pycnometric method and the specific surface (S) of the samples was measured by air permeability Blain method (ČSN EN 196-6). The WS 750 sample was grounded in a planetary mill Pulverisette from company FRITSCH at 300 rpm for 10 minutes.

Table III

Raw materials characterized by quantiles d10, d50, d90, specific density (ρ) and specific surface (S)

	d10 [µm]	d50 [µm]	d90 [µm]	Specific density [kg.cm^{-3}]	Specific surface [m^2.kg^{-1}]
2 C	4.3	41.5	138.9	1829	3058
3 C	3.8	36.3	142.7	2119	4796
8 C	1.7	12.2	66.5	2059	4608
14 C	6.0	37.2	106.5	1978	5631
BM 1	8.4	64.3	268.5	2036	5997
BM 2	124.7	231.9	424.3	2649	1014
MS 1	1.4	7.5	20.5	2149	62 132
MS 2	5.8	49.3	147.7	2258	2312
TC	1.9	11.7	49.3	2566	2856
WS	1.4	7.5	20.5	2643	10894

Pozzolanic activity was determined by Frattini test according to ČSN EN 196-5. It was added 100 ml of boiled and distilled water to a polyethylene bottle. The bottle was closed and placed in a thermostat set at 40 °C. After approximately 1 hour, the bottle was removed and 20 ± 0,01 g of the tested cement with pozzolan in the required ratio was poured into the bottle using a funnel. After mixing, the bottle was stored in a thermostat at 40 °C for 8 days. After the required time, the contents of the bottle was filtered through a Büchner funnel with a double filter into a suction flask. The solution was cooled to ambient temperature and then 50 ml was pipetted into a 250 ml flask. A few drops of methyl orange indicator was added to the solution and the solution was titrated with dilute hydrochloric acid until the color changes from yellow to orange. The solution was thus titrated adjusted to pH 12.5 ± 0.2 with sodium hydroxide solution and a pH meter. Calcon was added to the solution as an indicator and titration was performed with EDTA solution to change the color from purple to blue.

Results and discussion

The graph in Figure 2 shows the pozzolanic activity of FA, BMA, silica fume MS and TC. All FA show pozzolanic activity. The results for biomass ash show significantly worse pozzolanic properties according to the Frattini test. However, it should be noted that this direct method is not suitable for substances containing a high proportion of calcium ions (as well as Na^+, K^+, Mg^+ ions), which may adversely affect the results of this method. The results obtained in this way are therefore very debatable. Similarly, it is necessary to take into account the high content of calcium ions (11.41 wt.%) for FA from the heating plant from Dvůr Králové (14 C) when assessing its pozzolanic activity. While very low pozzolanic activity can be determined for BM 2, BM 1 is completely nonreactive. The graph on Figure 2 also shows the pozzolanic activity of silica fume MS and TC. It can be seen that while MS has excellent pozzolanic activity, TC does not exhibit pozzolanic activity and can therefore be classified as a common silica microfiller. The high pozzolanic activity of MS is in agreement with the very high value of the specific surface area. The results show that the specific surface area has a significant effect on the pozzolanic activity of the material.

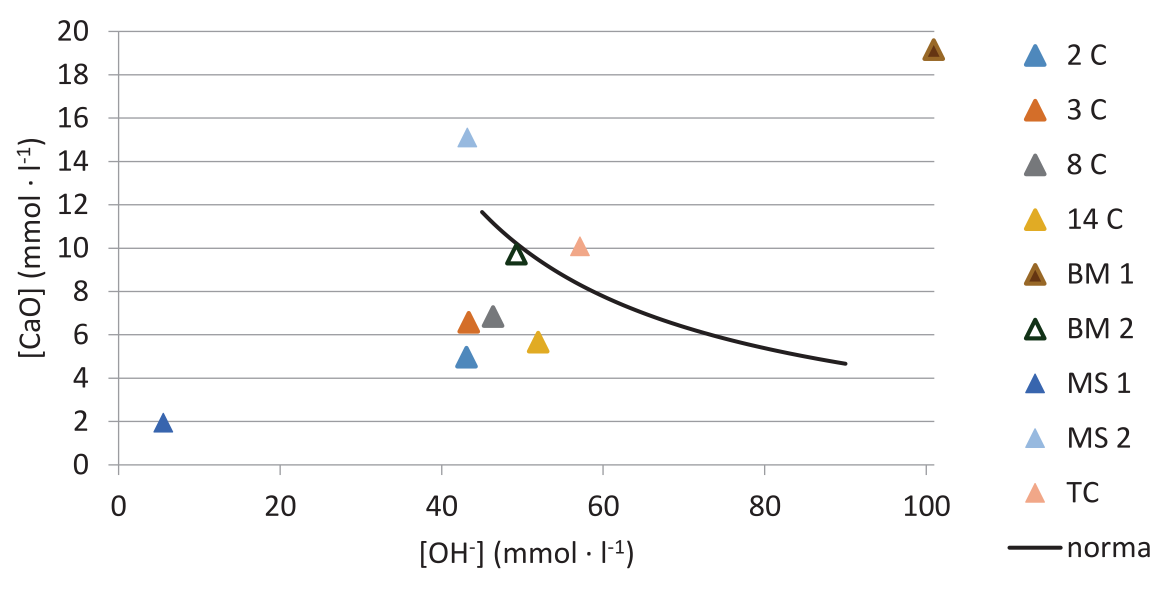

Figure 2. The results of the pozzolanic activity of FA, BMA, silica fume MS and TC

The following graph in Figure 3 shows the pozzolanic activity of WS clay as a function of firing temperature. In addition, the graph presents a WS 750m sample that has been mechanically treated and it's specific surface area increased from 10.738 $cm^2 \cdot g^{-1}$ (WS 750) to 18.738 $cm^2 \cdot g^{-1}$. The pozzolanic activity of WS clay according to the Frattini test practically does not change up to a firing temperature of 900°C. The change occured in the sample fired at a temperature of 1000 °C, when a mullite phase was formed from metakaolinite, as confirmed by phase XRD analysis, as shown in Figure 1. In contrast, a sample calcined to the lowest temperature of 600 °C, which still contained some unreacted kaolinite, has comparable pozzolanic properties to samples with complete kaolinite to metakaolinite transition (detected from XRD analysis). If we focus on the sample WS 750°C m, it was found that the grinding of the sample did not have a significant effect on its pozzolanic activity determined according to the Frattini test. Here, it would be interesting to observe the reactivity of these two samples during the first hours of hydration, after 8 days both samples reached the same equilibrium state. The excellent pozzolanic activity of WS clay calcined in the range of 600 – 900 °C agrees with the strength activity index (SAI) performed by Wang et al.[10]. However, their reported dependence of pozzolanicity on firing temperature was not confirmed. According to Wang et al., the best properties showed clay fired at 750°C, Frattini test in this work did not confirm any significant differences between individual clays fired in the temperature range 600 - 900 °C.

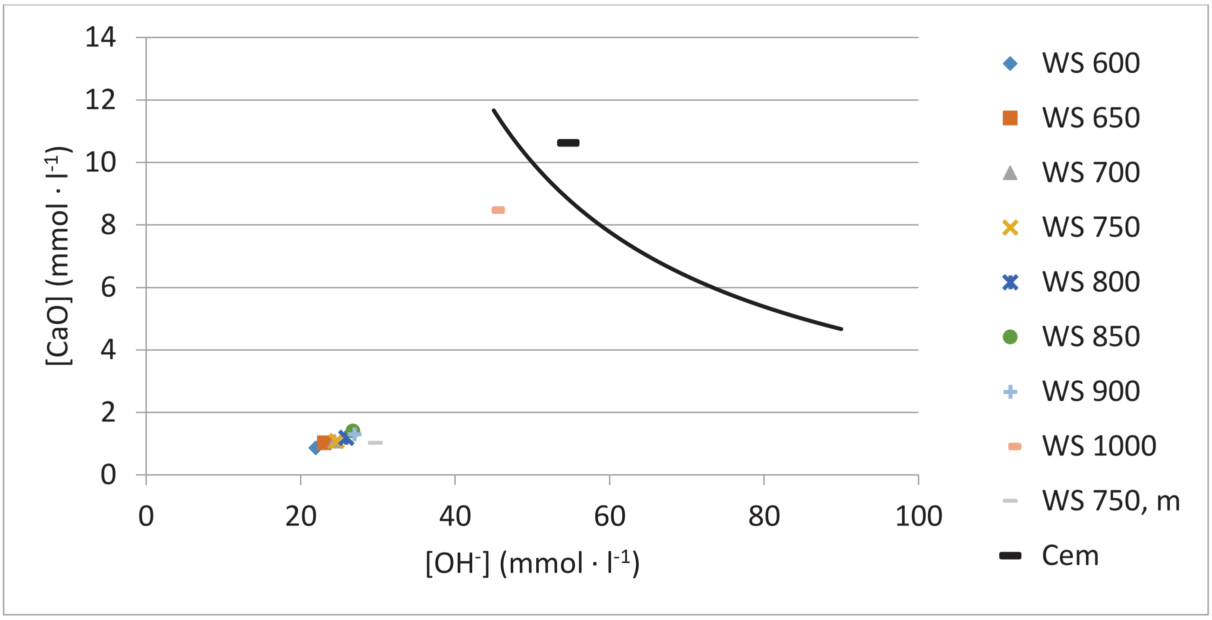

Figure 3. Frattini test results for variously calcined clay WS 600 - 1000 and WS 750m.

Conclusion

The results of the 8-day Frattini test according to ČSN EN 196-5 showed that:

- All fly ash showed pozzolanic activity. The results for biomass ash show significantly worse pozzolanic properties according to the Frattini test. However, it should be noted that this direct method is not suitable for substances containing a high proportion of calcium ions (as well as Na^+, K^+, Mg^+ ions), which may adversely[11] affect the results of this method.
- Silica fume from Stachema with a very high specific surface area is an excellent pozzolan, while waste silica from Technistone does not have pozzolanic properties.
- For a selected WS clay fired at a different temperature of 600 - 900°C, it was found that the temperature does not have a significant effect on the pozzolanic activity of the clay. By firing WS clay at a temperature of 1000 °C, the pozzolanic activity of this clay decreases, which was related to the formation of mullite. Influence of grinding, resp. a slight increase in specific surface area does not affect the pozzolanic activity of this clay calcined at 750 °C.

Aknowledgement

This project was co-financed by the Technology Agency of the Czech Republic as a part of programme TREND FW01010195.

Reference

1. M.H. Zhang, V.M. Malhotra, N. Bouzoubaa, Mechanical properties and durability of concrete made with high-volume fly ash blended cements using a coarse fly ash, Cem. Concr. Res. 31 (2001) 1393–1402.
2. T. Robl, A. Oberlink, R. Jones, Coal Combustion Products (CCPs): Characteristics, Utilization and Beneficiation, 1st ed., Woodhead publishing, 2017.
3. K. Scrivener, F. Martirena, S. Bishnoi, S. Maity, Calcined clay limestone cements (LC3), Cem. Concr. Res. 114 (2018) 49–56. https://doi.org/10.1016/j.cemconres.2017.08.017.
4. R. Snellings, Assessing, Understanding and Unlocking Supplementary Cementitious Materials, RILEM Tech. Lett. 1 (2016) 50. https://doi.org/10.21809/rilemtechlett.2016.12.
5. ČSN EN 196-5, Methods of testing cement – Part 5: Pozzolanicity test for pozzolanic cement, (2011).
6. E. Ferraz, S. Andrejkovičová, W. Hajjaji, A.L. Velosa, A.S. Silva, F. Rocha, Pozzolanic activity of metakaolins by the French standard of the modified Chapelle test: A direct methodology, Acta Geodyn. Geomater. 12 (2015) 289–298. https://doi.org/10.13168/AGG.2015.0026.
7. S. Donatello, M. Tyrer, C.R. Cheeseman, Comparison of test methods to assess pozzolanic activity, Cem. Concr. Compos. 32 (2010) 121–127. https://doi.org/10.1016/j.cemconcomp.2009.10.008.
8. M.M. Tashima, L. Soriano, J. Monzó, M. V. Borrachero, J.L. Akasaki, J. Payá, New method to assess the

pozzolanic reactivity of mineral admixtures by means of pH and electrical conductivity measurements in lime: Pozzolan suspensions, Mater. Constr. 64 (2014). https://doi.org/10.3989/mc.2014.00914.

9. S. Sinthaworn, P. Nimityongskul, Quick monitoring of pozzolanic reactivity of waste ashes, Waste Manag. 29 (2009) 1526–1531. https://doi.org/10.1016/j.wasman.2008.11.010.
10. B. Wang, Y. Zhang, M. Li, The preparation and pozzolanic activity of metakaolin admixtures, Key Eng. Mater. 539 (2013) 230–234. https://doi.org/10.4028/www.scientific.net/KEM.539.230.
11. S.Y. Lee, S.J. Park, A review on solid adsorbents for carbon dioxide capture, J. Ind. Eng. Chem. 23 (2015) 1–11. https://doi.org/10.1016/j.jiec.2014.09.001.

RESISTANCE OF MIXTURES PREPARED FROM DIFFERENT CZECH FLY ASHES TO FREEZING AND THAWING

Pulcová K.[1], Šídlová M.[1], Rak P.[1], Šulc R.[2], Formáček P.[2]

[1]University of Chemistry and Technology Prague, Department of Glass and Ceramics, Technická 5, 166 28, Prague 6, Czech Republic
[2]Czech Technical University in Prague, Faculty of Civil Engineering, Thákurova 7, 166 29, Prague 6, Czech Republic

pulcovak@vscht.cz

Abstract

Fly ashes (FAs) from Czech power plants and heating plants belong among the valuable secondary raw materials used in the construction industry. Their use as an admixture in cements reduces the consumption of primary raw materials and the amount of CO_2 emissions arising from the production of new clinker. The aim of the work was to verify the utilization of various FAs from the Czech Republic as admixtures into cement pastes by means of freezing and thawing cycling (F-T) in the environment of H_2O and 3 % NaCl solution. Furthermore, the effect of aeration and the effect of the amount of ash substitutes on F-T were investigated. It was found out that individual FAs have different resistance to F-T, as the resistance generally decreases with increasing number of F-T cycles. It was also confirmed that the paste containing FA resists F-T better in the environment of H_2O than NaCl. Higher aeration of the pastes caused their higher resistance to F-T. In the NaCl environment, the paste with the highest degree of aeration exhibited the lowest corrosion. With the increasing replacement of FA by cement, the resistance of the mixture decreases in both environments.

Introduction

In the Czech Republic, about 7 million tons of FA are produced annually. These FAs are formed at temperatures around 1100–1600 ° C in powder fireplaces, which are commonly used in most power plants. They are products of combustion of a finely ground powdered form of coal. This type of combustion is fast due to the large specific surface area of coal particles[1]. The mechanism of FA formation begins with the melting of mineral components contained in coal. With gradual firing the agglomeration of the ash particles follows to form FA grains. Due to this mechanism and high temperature, the morphology of FA consists mainly of spherical particles. From a mineralogical point of view, FA usually contains about 50 % of amorphous phase, silicates and aluminosilicates (quartz, mullite, cristobalite), carbonates (calcite and siderite), Fe-containing minerals (magnetite, hematite, maghemite) and Ti-containing minerals (rutile, anatase). From the oxide point of view, these are SiO_2, Al_2O_3, Fe_2O_3, CaO, SO_3, TiO_2 and other minor phases[1, 2, 3].

FA is used mainly in construction as an admixture in concrete and plaster mixtures, sealants, autoclaved aerated concrete, for lightweight aggregates, bricks and ceramics. In road and railway construction it is used in the form of stabilizers and solidifications for road and railway substrates or, for example, for backfilling of bridge supports[1]. From the point of view of the use of FA as a part of building materials, the pozzolanic activity they show is used. As pozzolans, they can react with $Ca(OH)_2$ in the binder and water to form hydration products. FA must meet the quality parameters controlled by the standard ČSN EN 450-1, Fly ash for concrete, definitions, requirements and quality control[4].

Resistance to F-T is a very important criterion for the use of FA in construction. During F-T, various mechanisms of concrete damage occur, such as peeling, D-line cracking, pop outs or scaling[5]. Water entering the cavities and pores in concrete has a major influence on the mechanisms of F-T. When water changes to ice, it expands by about 9 % of its volume, which creates hydraulic pressure. If the concrete is additionally exposed to deicing salts, the resistance of the concrete to F-T is further reduced[6]. When deicing salts are used, salts crystallize in the pores and the degree of saturation of the concrete increases, both of which lead to increased damage caused by frost[7]. It has been found that the combined effect of hydraulic, osmotic and crystallization pressure under the concrete surface causes aforementioned damages to concrete[8].

Even though it has been found that the resistance to deicing salt deposition can be reduced by increasing the amount of supplementary cementitious materials (SCMs)[9], the preparation and composition of concrete are important factors. Concretes that are properly designed, placed and cured may exhibit good F-T resistance, despite the high doses of some of these SCMs. The resistance of concrete to deicing salt is significantly increased using a low water/cement ratio (w), suitable aeration and enough curing time before F-T. The effect of the amount of air-entraining agent on F-T is very significant, with a recommended total entrapped air in concrete being about 4–7 %[10].

Materials and methods

The input raw materials used in this work were FAs from Czech power plants, specifically from the Počerady (FA-2C, FA-3C), Tušimice (FA-ETU), Prunéřov (FA-10C) power plants and from the Dvůr Králové (FA-14C) heating plant. The basic characteristics of these FAs, including XRD, XRF and particle size distribution (PSD), are given in the following sub-chapter, specifically in Tables I-III. Furthermore, Portland cement CEM I 42.5 R from the Mokrá cement plant, Českomoravský cement a.s., was used.

VP characterization

Table I

Quantitative phase composition of FAs (%), XRD analysis. Rietveld method (error Rw <5%)

FA	amorphous phase	quartz	mullite	magnetite	hematite	anhydrite	acermanite	others
FA-2C	53.0	15.0	30.5	0.5	0.5	0.0	0.0	0.5
FA-3C	50.5	14.0	34.5	0.5	0.5	0.0	0.0	0.0
FA-10C	64.5	5.5	26.0	0.5	0.5	0.0	0.0	3.0
FA-14C	73.5	9.5	6.0	1.0	1.5	5.5	2.5	0.5
FA-ETU	53.5	9.0	34.5	1.0	1.0	0.0	0.0	1.0

The main share in the analyzed FA is occupied by the amorphous phase, the value of which ranged from 50.5 to 73.5 %. The main crystalline phases were mullite and quartz. In addition, there were detected traces of crystalline phases as gypsum, hercynite, anatase, calcite and free lime in the analyzed FAs.

Table II

Oxide composition of FAs (%), XRF analysis

FA	SiO_2	Al_2O_3	CaO	K_2O	SO_3	Fe_2O_3	TiO_2	MgO	others
FA-2C	53.8	33.9	1.6	2.0	0.5	4.8	1.6	1.0	0.9
FA-3C	54.9	33.2	1.6	2.3	0.2	4.2	1.6	1.1	0.9
FA-10C	48.6	32.2	3.4	1.7	1.7	8.4	1.4	1.4	1.3
FA-14C	32.8	27.0	11.4	1.2	9.5	10.8	1.8	2.5	3.0
FA-ETU	49.8	33.9	1.8	1.7	0.6	8.9	1.2	1.0	1.2

Using the XRF analysis, oxides listed in Table II were found; Na_2O and P_2O_5 were further identified as minority oxides. From the measurement of the particle size distribution, it was found that the finest FA was from the Tušimice power plant with a mean particle size of 12.2 µm. The other FAs were coarser, and their mean particle size ranged from 36.3 µm to 52.7 µm.

Table III

Particle size distribution analysis, PSD (µm)

FA	D10	D50	D90
FA-2C	4.3	41.5	138.9
FA-3C	3.8	36.3	142.7
FA-10C	6.6	52.7	171.9
FA-14C	6.0	37.2	106.5
FA-ETU	1.7	12.2	66.5

Paste preparation

Several pastes containing 75 % of cement and 25 % of FA were prepared (2C, 3C, 10C, 14C, ETU5). After that, FA pastes from the Tušimice power plant with a content of 15 % (ETU15%) and 35 % (ETU35%) were prepared. All these mixtures were made with respect to the optimal amount of entrapped air 4-7 % using the pressure measuring method ČSN EN 12350-7[11]. Afterwards another two mixtures were prepared from the Tušimice power plant FA with aeration of 2 % (ETU2) and 9 % (ETU9). The composition of all pastes is presented in Table IV.

Table IV

Composition of pastes

paste	cement [g]	FA [g]	w	entrapped air [%]
2C	1500	500	0.32	4.8
3C	1500	500	0.29	4.1
10C	1500	500	0.30	6.1
14C	1500	500	0.35	4.6
ETU2	1500	500	0.28	1.9
ETU5	1500	500	0.28	4.7
ETU9	1500	500	0.28	9.3
ETU15%	1700	300	0.28	6.0
ETU35%	1300	700	0.28	6.5

After 28 days of curing, the mixtures were subjected to a freezing and thawing cycling in the environment of H_2O and 3 % NaCl solution. The resistance of their surface was examined in the sense of the standard ČSN 73 1326, Z1, method C[12].

Methods

Freeze-Thaw

For the F-T, 100 mm diameter cylindrical specimens were prepared and cured in a moisture cabinet for 28 days in order to ensure enough strength before F-T cycling. Tap water or 3 % NaCl solution was then poured on the surface of the samples to a height of about 20 mm and the samples were placed in an F-T chamber Memmert CTC256. Automatic F-T cycling according to ČSN 73 1326, Z1, method C, took place in the test chamber for the environment[12]. The temperature alternated from -18 ± 2 ° C to 5 ± 2 ° C with residence time of 3 hours at each extreme. The waste was scraped, filtered, washed with distilled water, dried and weighed after every 25 cycles. F-T cycling was performed for up to 100 cycles. The evaluation, carried out according to the standard ČSN 73 1326, Z1, method C, is shown in the following Table V.

Table V

F-T corrosion evaluation according to standard ČSN EN 73 162, Z1, method C[12]

corrosion evaluation	[g.m^{-2}]	waste type
1. undisturbed	up to 50	Very fine dusty particles up to 1 mm
2. slightly disturbed	50–500	As in stage 1, a larger number of particles up to 1 mm, a proportion of particles up to 2 mm less than 50 % by weight of the waste
3. disturbed	500–1000	As in stage 2, the proportion of particles above 2 mm over 500 g.m^{-2}
4. severely disturbed	1000–3000	As in stage 2, the proportion of particles above 2 mm over 500 g.m^{-2}
5. crumbled	over 3000	As in stage 4, the proportion of particles above 4 mm is more than 20 % by weight of the waste

XRD

XRD (X-ray diffraction analysis) was performed at room temperature on a θ-θ X'Pert3 Powder diffractometer from PANanalytical in a Bragg-Brentan parafocusing geometry using CuKα radiation wavelength (λ = 1.5418 Å, U = 40 kV, I = 30 mA). Samples were scanned with an ultrafast linear detector PIXCEL in the angular range 15–78 ° (2θ) with a measurement step of 0.013 ° (2θ) and with the counting time of 180 s step^{-1}. A fixed aperture was used for the measurement. Qualitative and quantitative analysis was then performed by evaluation in HighScore Plus 4.0 software (PANalytical, The Netherlands) using a Rietveld method. The amorphous content was determined indirectly by the internal standard method. As internal standard 7.5 % ZnO was added to the samples.

XRF

A sequential wave-dispersive X-ray spectrometer ARL 9400 XP equipped with an X-ray lamp with a Rh anode type 4GN with a 50 µm thick Be window was used to measure the X-ray fluorescence analysis (XRF). The intensities of the spectral lines of the elements were measured in vacuum using the WinXRF software. Combinations of 52 generator-collimator-crystal-detector settings were optimized for 82 measured elements with a time of 6 s per each of the elements. The obtained intensities were processed using the Uniquant 4 software without the need to measure standards. The analyzed powder samples were compressed into 5 mm thick tablets with 40 mm in diameter without the use of a binder or with the use of Dentacryl as a binder (for important elements B–F). They were pressed with or without a 4 µm thick polypropylene cover film. The measurement time of each sample was about 15 min.

PSD

The Bettersizer ST Laser Particle Size Analyzer (Dandong Bettersize Instruments Ltd., China) was used to determine the particle size distribution in the pastes. The measurement was performed in the laboratory of Korund Benátky, s.r.o. Czech Republic.

Results and Discussion

The following graphs (Figure I–III) show the resulting values of cumulative waste after F-T in the environment of H_2O or 3 % NaCl for all prepared pastes. Figure I for optimally aerated pastes shows both a decrease in resistance with a gradually increasing number of F-T cycles and a generally lower resistance in the NaCl environment. Furthermore, it can be seen from Figure 1 that the lowest resistance is attested by pastes 2C and 3C formed from the Počerady power plants FA. All the pastes, except for one 2C, have slightly disturbed surface in H_2O environment according to standard ČSN EN 73 162, Z1.

In Figure 2, which compares differently aerated pastes made from the finest ETU FA, the high resistance of the most aerated paste ETU9 in both environments may be observed. There is no explanation for better F-T resistance of ETU9 in NaCl environment yet. Further research on the connection between aeration ant F-T is needed because results do not correspond with previous research[10].

In the last Figure 3 for differing amounts of ETU FA used, it is possible to observe the dependence of decreasing resistance on the increasing amount of FA in the NaCl environment. These results are consistent with the literature, which reports lower resistance to F-T with an increasing proportion of cement replacement[9]. In the H_2O environment it was found that the resistance of all pastes is high and corresponds to slightly disturbed surface according to standard ČSN EN 73 162, Z1.

F-T optimal aeration

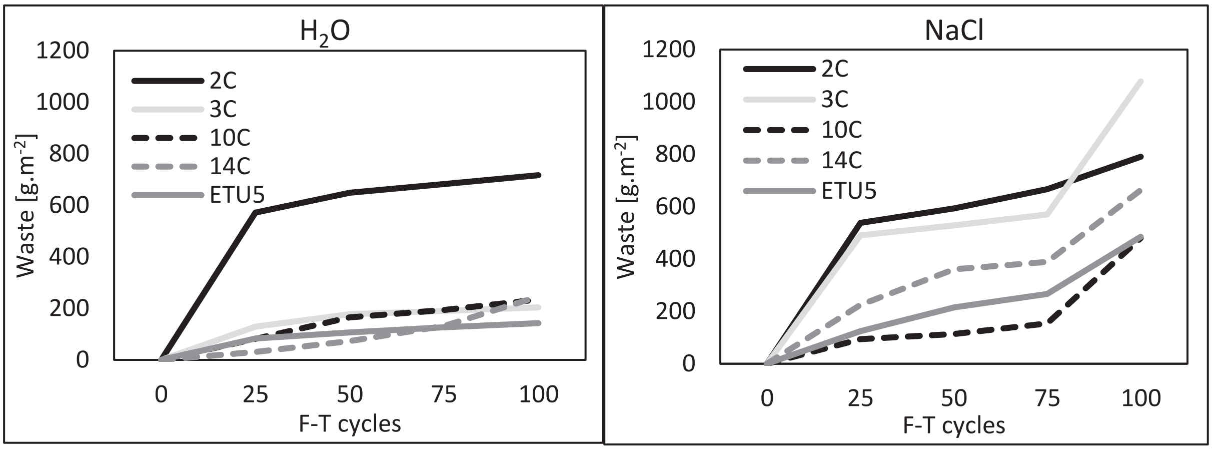

Figure 1. F-T resistance of optimal aerated pastes in H_2O (left) and NaCl (right)

F-T various aeration

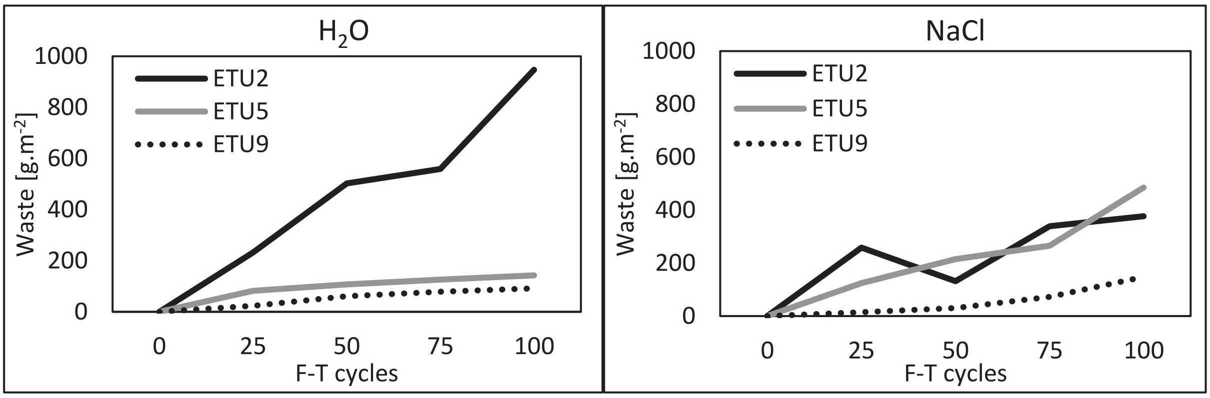

Figure 2. F-T resistance of variously aerated pastes in H_2O (left) and NaCl (right)

F-T various amount of FA

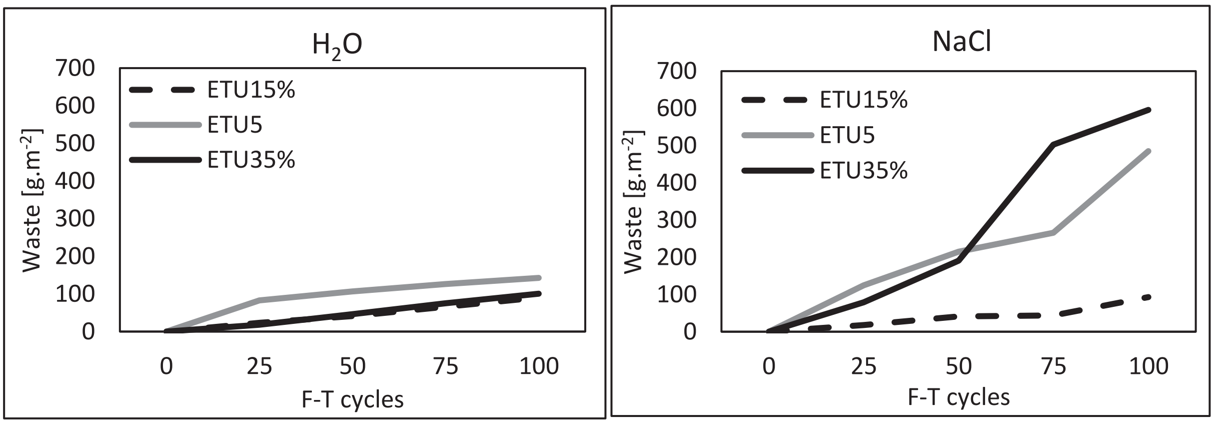

Figure 3. F-T resistance of pastes with various amount of FA in H_2O (left) and NaCl (right)

Conclusion

It seems apparent that the individual fly ashes exhibit different resistance to F-T. It may be concluded that with the increasing number of F-T cycles, the amount of waste generally increases and the resistance decreases. Furthermore, it was confirmed, according to Litvan[7], that pastes containing FA generally resist F-T better in H_2O environment than in NaCl. In terms of the amount of aeration, it was found that higher aeration of pastes resulted in their higher resistance to F-T in both environments, which does not correspond with the literature[10]. It may be caused by enough space created to balance hydraulic, osmotic or crystallization pressures; however, further research is needed. Even in the NaCl environment, it was the most aerated paste that exhibited the best resistance. With the increasing substitution of FA with cement, the resistance of the mixtures decreased both in the H_2O environment and in the NaCl environment, as assumed based on the results reported in the literature[9].

Acknowledgement

This work was financially supported by the Czech Technology Agency in the program TREND FW01010195 - " Advanced and innovative processing technologies for strategic utilization and storing of coal combustion products (CCPs) " and the company ČEZ Energetické Produkty, s r.o.

References

1. Fečko, P. *Fly ash*, 1st ed.; VŠB-TU Ostrava: Ostrava, 2005.
2. Šídlová, M.; Maixner, J.; Škvára, F.; Kohoutková, M.; Cibulková, J.; Polonská, A. Characterization of Czech coal combustion ashes and their hydrated products. *Waste Forum* 2019, *3*, 276–286.
3. Škvára, F.; Šulc, R.; Snop, R.; Peterová, A.; Šídlová, M. Hydraulic clinkerless binder on the fluid sulfocalcic fly ash basis. *Cement and Concrete Composites* 2018, *93*, 118–126.
4. ČSN EN 450-1 (722064). *Fly ash for concrete - Part 1: Definition, specifications and conformity criteria,* Praha: Czech office for standards, metrology and testing, 2013. 28 p.
5. Page, C. L.; Page, M. M. *Durability of concrete and cement composites*, 1st ed.; Woodhead Publishing Limited: Cambridge England, 2007.
6. Harnick, A. B.; Meier, V.; Rosli, A. Combined influence of freezing and deicing salt on concrete: physical aspects, *Durability of building materials and components, Eds. P J Sereda and G G Litvan* 1980, 474–484.
7. Litvan, G. G. Frost action in cement in the presence of deicers. *Cement and Concrete Research* 1976, 6 (3), 351-356.
8. Wang, K.; Nelsen, D. E.; Nixon, W. A. Damaging effects of deicing chemicals on concrete materials. *Cement and Concrete Composites* 2006, *28*, 173–188.
9. Kosmatka, S. H.; Kerkhoff, B.; Panarese, W. C.; Design and Control of Concrete Mixtures. 14th edition *Portland Cement Association*, PCA R&D Serial Number SN 2561, 2002.
10. Bilodeau, A.; Malhotra, V. High-Volume Fly Ash System: Concrete Solution for Sustainable Development. *ACI Materials Journal* 2000, *97* (1), 41-48.
11. ČSN EN 12350-7. *Testing fresh concrete - Part 7: Air content - Pressure methods,* Praha: Czech office for standards, metrology and testing, 2009. 20 p.
12. ČSN 73 1326, Z1. *Resistance of cement concrete surface to water and defrosting chemicals,* Praha: Czech Standards Institute, 2003. 24 p.

AIR PROTECTION, TECHNOLOGIES FOR SOIL DECONTAMINATION

INNOVATIVE TECHNOLOGY PLASMICAT FOR HAZARDOUS AIR TREATMENT

Kroužek J.[1,2], Mašín P.[1], Rippelová V.[2], Škarohlíd R.[2]

[1]*Dekonta, a.s., Dřetovice 109, 273 42, Stehelčeves*
[2]*University of Chemistry and Technology, Technická 5, 166 28, Prague 6*
krouzekj@vscht.cz

Abstract

In the case of sudden massive hazardous chemical release due to improper handling, air should be treated to minimize the damaging consequences, as prevention measures cannot be absolutely safe. Currently, the most commonly used air decontamination technologies do not meet all required features such as reliability, stability, or autonomy in addition to efficiency, versatility and deployment speed. We developed an innovative technology PLASMICAT based on microwave generated atmospheric plasma combined with microwave-assisted catalytic oxidation. Microwave irradiation in chemistry enables many specific effects that lead to process intensification, particularly in heterogeneous catalysis. Moreover, a new mixed cobalt-manganese oxide catalyst was applied as a lower cost available material with a high activity. Using a new-build dedicated pilot demonstration unit, the technology performance and parameters were tested and verified under simulated conditions close to its real industrial implementation. First, we examined its performance characteristic in the destruction of several VOCs representing various chemical structures under different temperatures and air flow rates. Then, PLASMICAT was implemented in the simulation of indoor chemical release of phosgene. This contribution briefly presents the progress of technology development and results from both experimental series.

Introduction

Air pollutants are hazardous from the perspective of environmental protection or occupational hygiene due to expected industrial emissions monitored, but they can also directly threaten people's health and security through a sudden massive release and spread in the case of industrial incidents or intentional criminal uses. Common emissions of inorganic or organic hazardous compounds are controlled by effective industrial decontamination systems which mostly use traditional separation technologies, such as filters, cyclones, absorbers, adsorbers or condensers; or destructive technologies based on thermal or catalytic oxidation. However, technical air protection against acutely dangerous chemical accidents or even terroristic attacks is much less common in industry, critical infrastructure or overcrowded objects, although everybody can remember several events in the past, e.g. in Bhopal. The measures for such situations can be applied to the prevention or at least to the reduction of potential incident consequences. For such technologies, high reliability, independence and versatility are required in addition to efficiency and other practical requirements. To meet these conditions, we proposed and developed a new unique technology based on microwave plasmochemical oxidation combined with microwave-assisted catalytic oxidation as a safe, high-performance and energy- or material-saving instrument useful for both safety and environmental engineering applications.

Plasma or catalytic oxidation technologies have been considered the promising processes in the treatment of air contaminated by VOCs for decades[1]. Non-thermal plasma technology is characterised by the production of highly reactive species at uncharacteristic low temperatures which allow rapid and non-selective decomposition of VOCs[2]. Plasma can be generated using various techniques which determine other parameters of the plasma. Microwave generated plasma presents a volumetric plasma stream with high electron density, high efficiency, lower temperature and pressure independence and is contactless[3]. In recent research, much effort has been devoted to the development of combined plasma-catalytic processes, either post-plasma catalysis or in-plasma catalysis[4]. Catalytic oxidation is a traditional method of decomposition of VOCs by their reaction with oxygen, which enables decrease of effective combustion temperature on the surface of the catalyst in comparison to a common thermal oxidation process. As catalysts, transition metal oxides and precious metals are the most frequently used material in VOC decomposition. Recently, especially mixed metal oxides variously structured[1] appear to be able to fully replace very expensive Pt, Pd, Ru etc. catalysts which have great activities but are strongly sensitive to poisoning effects. Many studies have described the exceptional properties of materials based on cobalt and manganese oxides, for example, in the oxidation of acetone and acetaldehyde[5]. Microwave heterogeneous catalysis has become an emerging scientific area due to the specific effects of microwave interaction with solid materials often resulting in various process improvements, intensification, higher reaction yields or energy savings[6]. Such effects were also confirmed in the cases of microwave implementation in catalytic oxidation of VOCs[6]. With respect to the previous research, the functional combination of microwave generated

plasma with microwave catalytic oxidation together with the application of innovative dedicated catalyst seems to be of great perspective in the reliable solutions of random hazardous chemical incidents.
The aim of this contribution is to present our research progress during a four-year project focused on the development of an innovative air treatment technology called PLASMICAT.

Experiment

PLASMICAT technology

The uniqueness of the concept lies in the functional junction of plasmochemical and catalytic oxidation accompanied by microwave irradiation. The technology is described in Figure 1 using a patented scheme. As the first air decontamination step, a six kW assembly of the source of microwave generated atmospheric plasma with an industrial microwave generator from MUEGGE is applied for polluted air which runs through the source and simultaneously serves as plasma carrier media. A microwave tuner must be used too for each start of plasma generation in this assembly. In this setup, all volume is in direct contact with plasma which is generated directly in situ in the air, leading to very efficient oxidation of organic pollutants. However, the device is limited in air volume capacity only to 300-500 l.min^{-1}. To increase the capacity, a dedicated plasmo-oxidation chamber was developed and built up. In the chamber, the plasma stream is contacted with the additional portion of the polluted air, which has not been treated yet; therefore, the chamber is somewhat analogous to a combustion chamber. It is possible to measure the air temperature at the output from the chamber. For an additional increase in the decomposition effect, the air can be moisturised at the technological input, or a photocatalyst can be inserted in the chamber around the inner plasma torch. However, the crucial second step in air decontamination is a microwave catalytic chamber which is closely connected to the plasmochemical chamber and equipped by second microwave 6 kW generator. This reactor is filled with pellets of a special catalyst based on mixed cobalt and manganese oxides on alumina support.

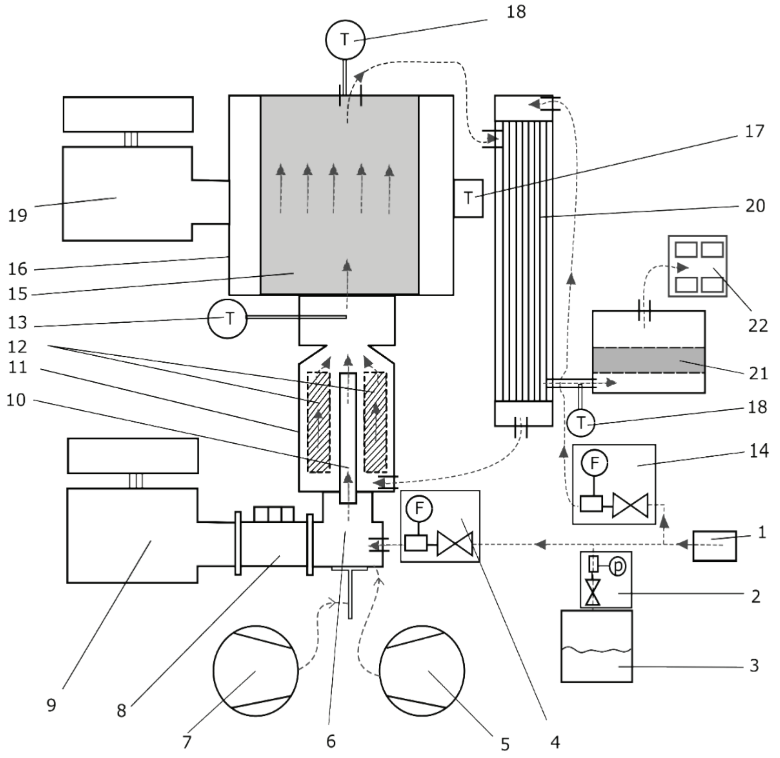

1 – air input
2 – steam pressure valve
3 – evaporator
4 – plas. source airflow control
5 – working air pump
6 – plasma source
7 – compressor for ignitor
8 – microwave tuner
9 – microwave generator
10 – quartz tube
11 – plasmo-oxidation chamber
12 – photocatalyst
13 – gas thermometer
14 – chamber airflow control
15 – catalytic bed
16 – reactor vessel
17 – infrared pyrometers
18 – output temperature
19 – microwave generator
20 – heat exchanger
21 – adsorber
22 – air monitoring
23 – PLC control

Figure 1. PLASMICAT technological scheme[7]

During technology operation, the catalyst is heated by microwaves up to a predefined efficient temperature for the specific contaminant, measured at the output of the air stream. During our verification tests, we measured the temperature of the catalyst bed in detail using optical fibre sensors inserted directly at various points in the bed or using infrared pyrometers targeted on the surface of the inner glass tube, in which the catalyst has been loaded. After all decomposition steps, the air is conducted through a heat exchanger to recover energy from the input air. At the end, small adsorber is applied for the partial removal of process by-products such as ozone or

NOx. The efficiency of technology by variable settings of main process parameters: microwave generator power, total air flow rate or the ratio of stream into plasma source to that of the plasmo-chemical chamber, and temperatures of input air, air in plasmo-oxidation chamber and output air, all of them are controlled remotely by developed software.

Technology development

For this one of the main results of our project, research and development were performed in couple follow-up and interlinked phases and steps. At the earlier phase of the project, we developed the technology in two divided directions: microwave plasma system and microwave catalytic oxidation. Later, the linkage of these two steps was studied and developed in detail, and finally, the completed technological unit was tested in two phases in which this innovative process was verified under simulated conditions.

As a reliable plasma source for the first microwave step, the commercially available and mass-manufactured system from the MUEGGE company was chosen and acquired. We had to get acquainted with the device, learn how to start using a specific ignitor and accurate microwave tuning, and how to operate it, optimize the operation and adapt the monitoring system. Thereafter, we designed and constructed a dedicated plasmochemical chamber, which had several modifications. Simultaneously, the system for air flow rate control was assembled and optimized together with a special system of generating defined contaminated air stream. Only then can the experiments with contaminated air be started and provided. These tests were focused on the investigation of decontamination effect of both plasma source alone and that air mixed with an additional air stream conducted directly into the plasmo-oxidation chamber.

The microwave catalytic oxidation process, as the second technological step, was examined first on a laboratory scale using model experiments with various catalytic materials which are commercially available. The characterization of their interaction with microwaves, especially the temperature dependence, was the first crucial aim in narrowing the material selection. For laboratory model simulation of catalytic oxidation, the new apparatus based on Milestone MicroSynth system equipped with fibre optic temperature measurement was prepared. The optimization of defined contaminated air generation together with process control was quite a demanding task, but necessary for well reproducibility of achieved results. We tested the oxidation of couple VOCs representing various chemical structures: aromatic, chlorinated, aliphatic, oxygenated etc., and the effect of some oxides of Mn, Co, Ce, Cu, Cr, V, Ti or Fe; and platinum over alumina were investigated under various process conditions such as temperature up to 250 °C, GHSV and humidity. The final selection of catalyst for scale-up was also dependent on the market offer of these materials, while a couple of kilograms was required, but this amount is not easy to obtain from suppliers. The development of new material was not among the original scope of our project; however, the market approach also led to material development. The scale-up of microwave technologies is also a specific issue as the microwave interactions with materials is a very complex phenomenon. There are many aspects involved in reactor design which are often contradictory. In the microwave industry, mathematical models for these purposes are indispensable. Following the previous laboratory research, we posed a complex predictive model in COMSOL environment to find the optimal parameters of a scaled microwave reactor. According to the results of these numerous numerical simulations, the reactor was prepared on the basis of the steel cylindrical vessel with an inner glass holder of the catalyst bed. Similar to the experiments of plasma technology, we studied the decontamination effect of our new reactor using various VOCs at variable process parameters. In the first experimental series, a smaller bed of palladium over alumina was applied as the catalyst. Nevertheless, the results were not satisfactory; therefore, a larger bed of catalyst must have been provided. Due to the very high price of the Pd catalyst, for the final solution of the reactor, a new mixed Co and Mn oxide over alumina support was developed, prepared in the amount of 21 kg and filled into the reactor for the last tests.

Technology verification experiments

For all pilot tests, both of the technological steps alone and of the completed unit, the system of artificially contaminated air stream generation was applied. It was based on the defined dosing of the contaminant mixture into a heated glass vessel under nitrogen atmosphere to generate a saturated vapor stream, which was then fed into the air stream produced by a vacuum pump from ambient air. As model contaminants, toluene, hexane, ethyl acetate, chloroform and perchloroethylene were used in most of the experiments; moreover, butanol, xylene, cyclohexane or pentyl acetate were tested in some cases. The VOC concentrations up to 2000 ppm were applied in this way. For decontamination evaluation, the generated air stream was analysed by collecting the sorption tube samples (Anasorb SKC) at air input into the technological unit, as well as in the output from the plasmochemical chamber and from the catalytic reactor. Each sampling was performed after stabilisation of the process parameters and conditions which were continuously monitored and controlled. In addition, the output air stream was continuously analysed using the system of electrochemical or infrared detectors for the measurement of inorganic gases: NO, NO_2, O_3, O_2, HCl or CO_2.

In the last experimental series, we applied new technology in the model simulation of accidental release of phosgene in a closed indoor space. In compliance with all necessary security measures, the simulations were performed in the Large-Scale Testing Facility at the National Institute of Nuclear, Chemical and Biological Protection (NINCBP). There are several airtight large steel cylinders which can be artificially contaminated even by very hazardous toxics, for example chemical warfare agents, in a controlled manner, being equipped with an additional air treatment system. The technology was installed in an 80 m^3 cylinder, while contaminated air was prepared in the other 60 m^3 cylindrical laboratory. Both cylinders were connected by tubes together with monitoring and control PC located outside, secured technology hall as well. The cylinder was contaminated using a phosgene pressure bottle up to 500 ppm, the concentration was continuously measured using a photoionization detector ppbRAE during experiments. The concentration of phosgene was also monitored at the output of the technology or in the space of the second cylinder, where the technology was placed, using detection tubes.

Results and discussion

At a beginning, the brief summary of the results achieved in the early phase of research and technology development is provided to understand the input assumptions for the final technology solution. Thereafter, the data from the technology verification tests are discussed.

Technology development

The testing of the microwave plasma source in the early phase without contamination brought rather valuable practical experience with the operation of the process. In particular, we focused on the behaviour of plasma torch, plasma ignition and measurement of reflected power as functions of applied power and air flow rate. During these tests, moreover, usual temperature measurement based on thermocouples showed to be inappropriate system at the plasma output, as the gas is highly electrically conductive, resulting in uncertainties of temperature determination. For this reason, the gas thermometer is a better solution. The temperature at plasma torch output was 450 – 550 °C if air was conducted only through the generator. If the additional stream was fed into the plasma chamber where it was mixed with the air from the torch, the temperature decreased according to the actual ratio of both flow rates to 150 °C. Simultaneously, this increase in the total flow rate in the chamber, i.e. in the technology capacity, shortened the retention time in the contact of pollutants with plasma torch.

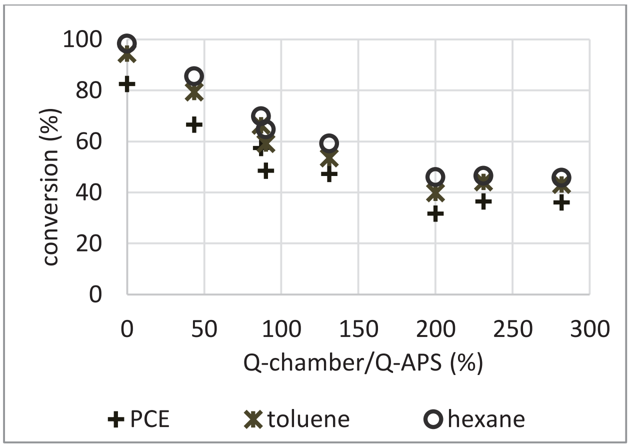

Figure 2. Conversion of VOCs as function of air flow rate ratio through chamber to plasma source.

Table I
Limiting parameters of efficient plasma oxidation of selected VOCs

Contaminant (% conversion)	Min. MW power [kW] (for 90 $l.min^{-1}$)	Max. flow rate [$l.min^{-1}$] (for 6 kW)
Hexane (100%)	1.9	300
Butanol (100%)	1.4	410
Toluene (100%)	2.5	250
PCE (90%)	2.5	200

The model simulations of microwave plasma decontamination of artificially polluted air confirmed the expected effects of the process parameters. In Table I, the limits of the operation of plasma source alone, without an additional air stream in the chamber, are presented. We observed the influence of applied microwave power and air flow rate simultaneously as these two parameters are interlinked during the operation of the plasma source. For each flow rate, there are limits in the applied power and vice versa. The minimal values for operation were 90 $l.min^{-1}$ at approximately 1.4 kW, while the conditions for plasma ignition are around 1 kW at 60 $l.min^{-1}$. Butanol, representing oxygenated pollutants, was completely decomposed independently of the set parameters;

on the other hand, this required goal for perchloroethylene (PCE) was not reached under any conditions during tests, only 90 % conversion at maximum. Figure 2 presents the dependence of contaminant conversion on the mixing ratio of air that additionally feeds into the chamber to air that flows through the plasma source. The significant decrease in oxidation efficiency is clear, which can be a result of the reduction of contaminant time retention in the chamber, of temperature reduction mentioned above and probably also of worse contact of plasma with the added air. In these tests, a maximum total air flow of 900 $l.min^{-1}$ was achieved. These findings confirmed that the application of plasma technology is quite strictly limited in the capacity, which is one of the reasons for the application of catalytic oxidation as a second technological step. During the experiments, the concentrations of NOx produced by plasma were measured at levels of hundreds ppm and ozone levels of tens ppm in the air.

In laboratory microwave catalytic experiments focused on the microwave interaction with various catalytic materials, these were somewhat classified into three groups with respect to the intensity of microwave absorption. Low absorption is typical for catalyst supports such as SiO_2 or Al_2O_3, and also for catalytic TiO_2 or CeO_2. On the contrary, the oxides of Mn, Cu, Co or V, and obviously powdered metals too are materials that interact very intensively with microwaves. For upscaled microwave technology, a strong microwave interaction is not required due to the too short penetration of microwaves into the catalyst bed, leading to process inhomogeneities in the bed or technology capacity reduction. That is why the needed solution is based on a transparent support with a thin surface layer of strongly absorbing material. We applied precious metal over alumina at the beginning; then, we developed a new material with mixed Co and Mn oxide supported by alumina for technology scaleup. These three catalytically active phases were confirmed in following laboratory simulations of the decontamination process as efficient materials. Precious metals, i.e. Pt or Pd, over alumina exhibited the best properties; for complete toluene oxidation, the temperature under 200 °C was sufficient. In the case of various types of Co and Mn oxides over alumina, we had to apply slightly higher temperatures of 220 – 240 °C to efficient contamination removal. Nevertheless, the use of the oxides is a more cost-effective way in the technology.

Table II
Results from pilot tests of MW catalytic oxidation at 6 kW microwave power

Flowrate [$l.min^{-1}$]	T_{OUT} [°C]	Conversion [%] hexane	ethyl acetate	toluene
1350	255	43.5	99.9	75.4
1150	278	49.6	99.8	73,5
900	310	64.8	99.7	83.8
800	335	86.3	99.9	91.3
750	278	79.3	98.4	94.6
900	317	78.4	98.3	80.1
1150	315	74.5	99.7	79.2
1350	272	46.6	99.7	50.5
1600	243	43.8	99.5	49.8
1900	214	29.4	99.7	36.5

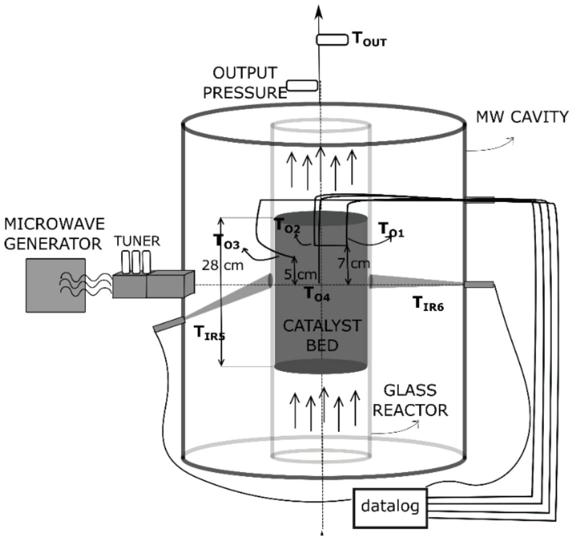

Figure 3. Scheme of temperature measurement during pilot MW catalytic oxidation experiments

The pilot experiments of microwave catalytic oxidation were carried out in two series, first with 8 kg of Pt/Al_2O_3 and then, with 21 kg of $Mn\text{-}Co/Al_2O_3$. These amounts of catalysts were results of a thorough evaluation of the requirements of microwave technology and air capacity, which had to be compromise. For this evaluation, our team posed a complex mathematical model in a COMSOL environment, which helped simulate various solutions and searched for as big as possible volume of catalyst bed in which microwaves penetrate sufficiently and homogeneously and in which high temperature can be achieved. These calculations are very demanding on computer performance and time, as they must be performed in 3D and involve multi-physical phenomena as microwave interaction, heat transfer, convection a porous environment, each of them completely interlinked. The tests were focused on monitoring the temperature distribution in the catalytic bed (Figure 3), when we were able to observe the gradient in both directions of vertical air flow and its perpendicular directions. On our numerous sensors, the variability was ranged from 130 °C up to 350 °C. This means that the catalytic oxidation has different yield and progress in all parts of the catalyst bed. The most important representative temperature in the system is that of the air output from the reactor. All measured temperatures were strongly dependent on the flow rate and the microwave power as expected. At 6 kW, the output temperature reached from 210 °C in the air of 1900 $l.min^{-1}$ to 330 °C in 800 $l.min^{-1}$. Therefore, all these parameters significantly influenced the conversion of contaminants, as shown in Table II for the Mn-Co/Al2O3 pilot experiments at 6 kW of microwave power. For hexane and toluene, which needs more energy for their decomposition, a significant decrease in their conversion was observed at flow rates greater than 1 m3.min-1, resulting from a reduction in temperature and retention time too at too high air velocity.

Technology verification

When each technological step was incorporated into one functional unit PLASMICAT, the final version of type MCA 2.0, we performed pilot tests in two series again. At the beginning, similar tests as in the case of experiments were carried out for each technological part, meaning the application for artificially generated contaminated air stream. The achieved results confirmed our expectations that this junction of microwave plasma and catalytic oxidation can significantly increase the decontamination power and capacity of the technology in comparison with their application alone. Our large dataset allowed us to define technological limits and basic performance parameters in the decontamination of VOCs. Based on our knowledge and experiences obtained, we can estimate these parameters for different groups of contaminants, as the level of decontamination is more influenced by the main aspects and bonds in the structure of the molecule than by the individual structure. As we estimate, the contaminants on the basis of oxygenated hydrocarbon derivatives such as alcohols, esters, aldehydes, etc., and probably nitrogen derivatives too, Plasmicat MCA 2.0 unit is able to treat efficiently more than 2 $m^3.min^{-1}$ of air at temperatures 100 – 150 °C. In the case of aromatic VOCs (BTEX), and probably alkenes or alkynes too, the efficiency is limited by the air flow rate of 1.5 $m^3.min^{-1}$ requiring 250 – 300 °C. Alkanes, including halogenated alkanes, are also decomposed in max. 1 $m^3.min^{-1}$ and min. 300 °C, and halogenated ethylenes are the most energy demanding as the conditions of a temperature of 350 °C at less than 1 $m^3.min^{-1}$ are required.

Conclusion

At the end of the project, we applied our new developed technology at NINCBP for phosgene removal from a closed indoor space, simulating accidental chemical release. During all tests, phosgene was not detected in the technology output, even at 20% applied power of the technology under even less than 150 °C, also for each individual technological part. The curve of decrease of phosgene concentration in the contaminated cylinder was monitored and fell below the quantification limit of 500 ppm in approximately 2 hours. Phosgene was shown to be not an appropriate representative of a hazardous compounds because of its simplicity in decontamination and the large relative content of chlorine atoms in the molecule. Unfortunately, in the output cylinder with our technology, we detected a hazardous concentration of chlorine molecules in the air. However, these tests served as a practical verification of the implementation of technology in industry and confirmed a high level of technological readiness.

Acknowledgement

This work was financially supported by the Ministry of the Interior of the Czech Republic (grant no. VI20172020091)

References

1. Kamal M.S., Razzak S.A, Hossain M.M: Atm. Env., *140*, 117 (2016)
2. Van Den Broucke, A.M., Morent R., De Geyter N., Leys C.: J. Adv. Ox. Tech., *15*, 232 (2012)
3. Leonelli C., Mason T.J.: Chem. Eng. Process. Proc. In., *46*, 885 (2010)
4. Trinh Q.H., Mok Y.S.: Kor. J. Chem. Eng., *33*, 735 (2016)
5. Sun Y., Li N., Xing X., Zhang X., Zhang Z., Wang G., Cheng J., Hao Z.: Cat. Tod., *327*, 389 (2019)
6. Hirano T.: *Microwaves in Catalysis: Methodology and Applications*, Wiley, Weinheim 2015
7. Krouzek J, Masin p, Rippelova V., Skarohlid R., Hendrych J., Durdak V.: utility model no. CZ U1 34405

PHOTOCATALYTIC DECOMPOSITION OF N_2O OVER S MODIFIED GRAPHITIC CARBON NITRIDE

Kočí K.[1], Šihor M.[1], Reli M.[1] and Praus P. [1,2]

[1] *Institute of Environmental Technology, CEET, VŠB-Technical University of Ostrava, 17. listopadu 2172/15, 708 00 Ostrava-Poruba, Czech Republic*
[2]*Department of Chemistry, VŠB-Technical University of Ostrava, 17. listopadu 2172/15, 708 00 Ostrava-Poruba, Czech Republic*
petr.praus@vsb.cz

Abstract

Graphitic carbon nitride (CN) belongs among a very promising photocatalysts, however, due to several well-known disadvantages, various modifications were tested. One such possibility is the change of precursor in CN preparation or modification by non-metal elements. In this study, the modification was based on the direct synthesis from thiourea (S-CN) and the second one was the modification of prepared CN from common melamine with mesyl chloride (Mes-CN). The synthesized photocatalysts were used for the photocatalytic decomposition of nitrous oxide. It was found out that the way of sulfur modification influences the degree of CN condensation and consequently its photocatalytic activity. The S-CN photocatalyst with the highest condensation degree proved to have the highest photocatalytic activity. Another important finding is connected with the type of nitrogen groups on the surface of the photocatalyst analyzed by X-ray photoelectron spectrometer (XPS). The NC2 group has a positive effect on the photocatalytic decomposition of N_2O.

Keywords: sulfur modified graphitic carbon nitride; photocatalysis; decomposition of N_2O.

Introduction

Nitrous oxide is one of the greenhouse gasses. Although N_2O is nontoxic, its global warming potential is approximately 310 times higher than carbon dioxide's. Furthermore, N_2O is a significant contributor of the ozone layer destruction. Development of effectual technologies to eliminate N2O is becoming a challenging mission for environmental scientists. A direct decomposition of nitrous oxide into nitrogen and oxygen is recognized to be the most effective and economical method to reduce the emissions of N_2O. The photocatalytic decomposition of N_2O is one of the possible and promising methods of its direct decomposition. N_2O can be decomposed by electrons and holes generated by irradiated photocatalysts evolving N_2 and O_2 (Eq. 1)[1-3] as follows

$$N_2O \xrightarrow{hv,photocatalyt} N_2 + \frac{1}{2}O_2 \tag{1}$$

The N_2O photocatalytic decomposition was investigated in the presence of various semiconductor materials mostly based on, e.g., ZnS, TiO_2 or CN in the past years[4-9]. A remarkable attention was mainly focused on metal free polymeric semiconductor graphitic carbon nitride. CN attracted significant attention in the photocatalytic field and is considered a promising photocatalyst with the narrow band gap of 2.7 eV, which is suited to visible light absorption. Moreover, CN is amenable to a large-scale synthesis. In comparison with many other semiconductors, graphitic carbon nitride also shows high thermal and chemical stability to oxidation[10-13]. In spite of being such a promising photocatalyst, CN is also related to some disadvantages, such as very low specific surface area and fast recombination rate of photo induced charge carriers, which lowers the quantum efficiency. These limitations of CN can be overcome by various strategies, for example, by the preparation of mesoporous structure (texture modification), heterojunction with other semiconductors, or by elemental and molecular doping[10]. Modification by non-metals, such as sulfur, phosphorus, oxygen, nitrogen, boron, and carbon, can lead furthermore to a red shift of absorption edge[14,15].

This work follows the previous work of Praus et al.[16] who prepared sulfur-modified CN. The article was focused mainly on the preparation and thorough characterization of the sulfur-modified CN materials and the photocatalytic activity was investigated only indicatively on the decomposition of the dye Acid Orange 7 (AO7) under UVA irradiation. The goal of this short work was to investigate the influence of S modification on the photocatalytic activity of CN in the decomposition of N_2O under UVA irradiation. The obtained results were compared with the commercial TiO_2 photocatalyst (Evonik P25), which is often used as a comparative one.

Materials and methods

Sample preparation

CN was synthesized by melamine heating at 550°C for 4 hours in a muffle furnace. Sulfur modified CN photocatalysts were synthesized by two different ways (i) under the same conditions as CN but using thiourea as a precursor and (ii) by the derivatization of already prepared CN with mesyl chloride[16]. S-CN was prepared under the same conditions like bulk CN but using thiourea as a precursor. Mes-CN was prepared by suspending CN in 1,4-dioxane triethylamine. Mesyl chloride was added and the mixture was further diluted by 1,4-dioxane.

Photocatalytic degradation of N_2O

The N_2O photocatalytic decomposition was conducted in a stainless-steel batch photoreactor (the diameter and volume of photoreactor was 78 mm and 184 ml, respectively) with an 8 W Hg lamp (λ = 365 nm, 0.665 mWcm^{-2}) as a source of irradiation. The photocatalyst was tested in powder form where 0.1 g was placed and uniformly spread over the bottom of the reactor. The photoreactor was sealed and the UVA lamp was placed in a horizontal position over a quartz glass visor in the reactor cover. The photoreactor with the photocatalyst inside was purged with a N_2O/He mixture (the N_2O concentration was 1050 ppm) and the pressure in the photoreactor was 150 kPa. The gas samples were discontinuously taken in the interval 0-12 hours and immediately analyzed on a gas chromatograph (GC) equipped with a barrier discharge ionization detector (BID). The reproducibility of N_2O photocatalytic decomposition was checked by repeated tests and photolysis (reaction without the photocatalyst) was conducted as well. The photocatalytic experiments were repeated minimally twice.

Results and Discussion

Characterization of investigated photocatalysts

Pristine CN and S doped CN structures (S-CN, Mes-CN) were characterized by common techniques, such as X-ray diffraction, UV-Vis diffuse reflectance spectroscopy, Fourier transform infrared spectroscopy, X-ray fluorescence spectroscopy (XRFS), elemental analysis (EA), N_2 physisorption evaluated according to the BET isotherm (S_{BET}), transmission electron microscopy and XPS[16]. Commercial TiO_2 photocatalyst (Evonik P25) was chosen for the comparison of photocatalytic efficiency toward the photocatalytic decomposition of nitrous oxide.

The band gap energies decreased in the order: CN (2.69 eV) > Mes-CN (2.66 eV) > S-CN (2.63 eV) and the specific surface area decreased in the order: S-CN (20 m^{2}g^{-1}) > CN (11 m^{2}g^{-1}) > Mes-CN (8 m^{2}g^{-1}). It means that the presence of sulfur significantly increased the S_{BET} of S-CN. On the other hand, the derivatization of CN with mesyl chloride decreased its S_{BET}. The XPS analysis identified the presence and bonds of C, N, O and S[16]. The surface elemental composition determined by XPS is summarized in Table I. The NC2 (pyridinic) nitrogen atoms are the dominant nitrogen ones in the CN structure and are located at the edges of melem units.

Comparing XRFS and XPS results, one can see the differences in the C and N content on the surface (XPS) and in the bulk (XRFS) and in C/N atomic ratios as well. Unlike XRF, the XPS method collects information only from surface layers with thickens of about 5 nm. The XPS results indicate the lower content of nitrogen likely due to surface defects in terms of nitrogen vacancies.

Table I
Surface elemental composition and overall NC2 portion of CN photocatalysts[16]

Sample	C [at.%]	N [at.%]	O [at.%]	S [at.%]	H* [at.%]	C/N	NC2 [%]	S** [wt. %]
CN	53.37	38.43	7.81	---	0.33	1.39	77	---
S-CN	46.93	47.77	5.13	0.08	0.09	0.98	81	0.22
Mes-CN	57.20	28.96	11.73	0.89	1.22	1.98	66	0.26

Note: *Amount of surface hydrogen was calculated to 100%. ** S determined by XRFS.

Photocatalytic decomposition of N_2O in the presence of S modified CN

The effect of irradiation time on the N_2O photocatalytic decomposition was evaluated in the presence of the investigated photocatalysts for the period of 0-12 h. The N_2O concentration was determined before switching on the UVA lamp and then every two hours during the irradiation. Apart from nitrogen and oxygen, no other N_2O decomposition products were found.

The time dependence of the N_2O conversion for the photocatalysis and photolysis is shown in Figure 1. It is evident that the conversion of nitrous oxide was increasing at a steady rate over time. The photolysis led only to the 2.5% conversion after 12 h of irradiation and each prepared material was found to be more effective. The activity of the investigated photocatalysts after 12 hours of irradiation decreased in the order: S-CN > CN > P25 > Mes-CN. The activities of the first three photocatalysts were significantly higher than photolysis. It might seem that the photocatalytic activity of the CN materials corresponds with their specific surface area. However, the SBET did not determine the photoactivity of other investigated materials even though it can have some influence on their photoactivity[17].

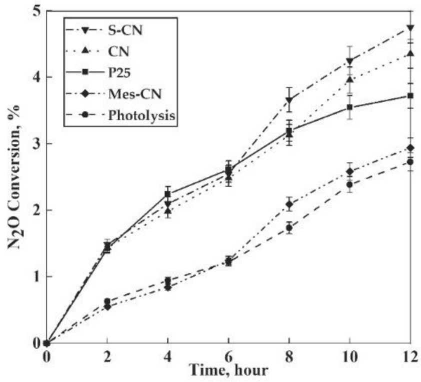

Figure 1. Time dependence of N_2O conversion in the presence of prepared photocatalysts under UVA irradiation (λ = 365 nm).

As mentioned above, the modification of CN with mesyl chloride significantly decreased its S_{BET} and photocatalytic efficiency. The Mes-CN photocatalyst contained beside of sulfur but also chlorine atoms (1.43 %). The effect of inorganic ions on the photoactivity of systems containing TiO_2 was discussed in literature[18,19]. The conclusion from the literature survey is that the presence of inorganic ions (chloride) can inhibit the effectiveness of the photocatalytic degradation. There are two possible inhibition mechanisms. The first one is the adsorption of inorganic ions on the active surface because the ions block the adsorption sites for goal molecules. The second one is represented by consuming the photogenerated holes by these ions, which consequently leads to a reduced efficiency of the photocatalytic process.

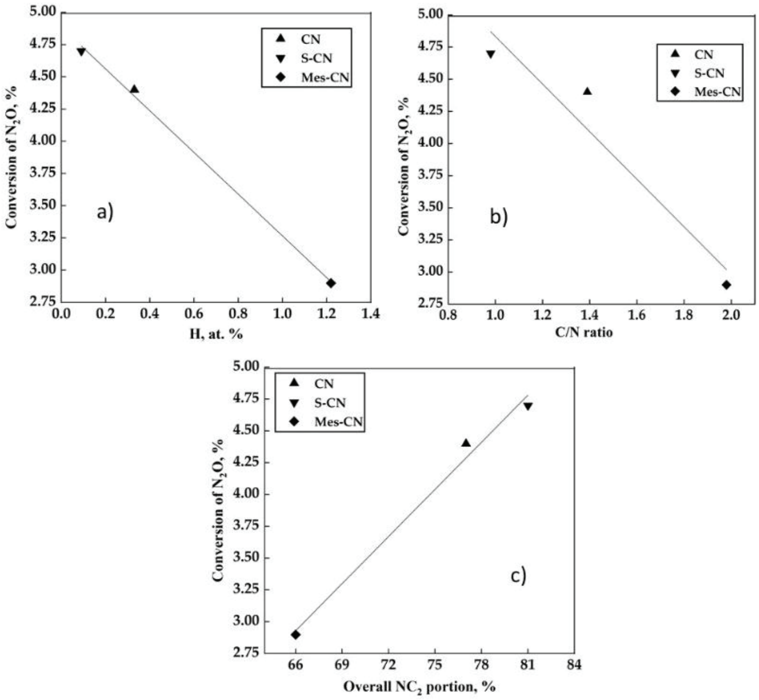

Figure 2. Correlation between the N_2O conversion in the photocatalytic decomposition of nitrous oxide and hydrogen content (a), and C/N atomic ratio (b), and overall NC2 portion (c) determined by XPS.

The XPS analysis (Tab. 1) shows that preparation and modification of graphitic carbon nitride can influence the degree of condensation and ordering of the carbon nitride structure. For that reason, we payed attention to the correlation between these factors and photocatalytic activity. First, an increase of the condensation degree leads to a decrease in the amount of hydrogen bound in $-NH_2$ and -NH- groups. Figure 2a depicts the dependence of N_2O conversion on the content of hydrogen in the investigated photocatalysts. The linear decrease of the N_2O conversion with increasing structure protonation was found. This result was also obtained by Martin et al.[17] and Alwin et al.[20] who dealt with the preparation of CN from different precursors. The different hydrogen content was likely caused by the substitution of nitrogen with sulfur in the case of S-CN[21,22] and the addition of $-SO_2CH_3$ groups in the case of CN-Mes.

Second, the parameter, which can describe the increase of carbon nitride condensation, is the C/N atomic ratio. The smaller C/N ratio accords to the higher content of nitrogen in the photocatalysts. Figure 2b clearly demonstrates the decreasing dependence of the N_2O conversion on the C/N atomic ratio. The different C/N rations can be explained by the same reasons as the content of hydrogen.

Third, the important parameter is the type of nitrogen in the materials. In Figure 2c, we observed a significant increase in the photoactivity of the photocatalysts as the overall NC2 portion increases. This trend was also observed by Martin et al.[17]. The content of NC2 in S-CN was the highest, likely due to the substitution of nitrogen in >NH and $-NH_2$. The lowest content of NC2 in Mes-CN was likely a result of the attack of mesyl chloride on these most nucleophilic triazine nitrogens[16] and their removal. It also explains the lowest specific surface area of Mes-CN.

To summarize, the acquired activity of the photocatalysts (toward the N_2O conversion) is a result of several effects, such as (i) hydrogen contents (proton concentration), (ii) C/N atomic ratio and (iii) type of nitrogen atoms. All these parameters are connected with the preparation and modification of graphitic carbon nitride and influence the condensation degree of its structure. It is possible to say, the higher condensation degree, the higher the activity of the photocatalyst.

Mechanism of N_2O photocatalytic decomposition

The N_2O decomposition was performed under UVA irradiation (λ = 365 nm). In literature[5,23], a mechanism of the N_2O photocatalytic decomposition is suggested. The first step is the illumination of photocatalyst by light with sufficient photonic energy (hν) followed by the generation of electrons (e^-) and holes (h^+) on the surface of photocatalysts (Eq. 2). At first, the generated electrons react with N_2O molecules adsorbed on the photocatalyst surface creating molecules of N_2 and radicals $\bullet O^-$ (Eq. 3). According to the literature, the desorption of adsorbed oxygen species is generally assumed as the slowest step of the proposed mechanism[23]. The created $\bullet O^-$ radicals can react with the generated holes (Eq. 4) or also with another molecule of N_2O to form $_{O2}$ molecule (Eq. 5). Whether the reaction (Eq.4) and/or reaction (Eq. 5) occurs, it depends on the type of photocatalysts and conditions of reaction[23,24]:

$$\text{Photocatalyst} \rightarrow e^- + h^+ \quad (2)$$

$$N_2O + e^- \rightarrow N_2 + \bullet O^- \quad (3)$$

$$2\,\bullet O^- + 2\,h^+ \rightarrow O_2 \quad (4)$$

$$\bullet O^- + N_2O \rightarrow N_2 + O2 + e^- \quad (5)$$

The generation rate of electrons and holes is increased with increasing energy of irradiation due to the higher density of electron states at higher energies in photocatalysts. The higher efficiency of electron-hole generation with a shorter wavelength of irradiation allows the higher efficiency of the photocatalyst[25,26].

Conclusions

The N_2O photocatalytic decomposition was performed in the presence of photocatalysts based on graphitic carbon nitride and compared with commercial TiO_2 photocatalyst (Evonik P25) and with photolysis. The choice of the preparation of the CN photocatalysts (it means the precursor type and the sulfur modification) were found to have impact on their physico-chemical properties and photocatalytic activity.

The N_2O conversion in the presence or without the photocatalyst (photolysis) decreased in order to S-CN > CN > TiO_2 (P25) > Mes-CN > photolysis. It was proved that the preparation process influences the degree of carbon nitride condensation. The S-CN photocatalyst with the highest photoactivity had the highest degree of condensation. As the polymerization degree increases and the proton content decreases, the activity of photocatalysts based on graphitic carbon nitride was significantly enhanced. The photoactivity of the CN materials was also influenced by the content of NC2 nitrogen.

Acknowledgement

This research was funded by Scientific Science Foundation of the Czech Republic (No. 19-15199S), by ERDF "Institute of Environmental Technology–Excellent Research", (No. CZ.02.1.01/0.0/0.0/16_019/0000853) and by Large Infrastructure ENREGAT supported by the Ministry of Education, Youth and Sports of the Czech Republic (No. LM2018098).

References

1. Wang L., Liu J., Song W., Wang H., Li Y., Liu J., Zhao Z. Tan J., Duan Z. Deng J.: Chem. Eng. J. *366*, 504 (2019).
2. Tan J., Cheng H., Liu J., Sun J., Li Y., Wang H., Liu J., Zhao Z.: ChemistrySelect *4*, 5338 (2019)
3. Song W., Wang L., Gao Y., Deng J., Jing M., Zheng H., Liu J., Zhao Z., Gao M., Wei Y.: J. Mater. Chem. A *6*, 19241 (2018).
4. Obalová L., Šihor M., Praus P., Reli M., Kočí K.: Catal. Today *230*, 61 (2014).
5. Kočí K., Krejčíková S., Šolcová O., Obalová L.: Catal. Today *191*, 134 (2012).
6. Kočí K., Matějová L., Ambrožová N., Šihor M., Troppová I., Čapek L., Kotarba A., Kustrowski P., Hospodková A., Obalová L.: J. Sol-Gel Sci. Technol. *78*, 550 (2016).
7. Kočí K., Reli M., Troppová I., Šihor M., Kupková J., Kustrowski P., Praus P.: Appl. Surf. Sci. *396*, 1685 (2017).
8. Troppová I., Šihor M., Reli M., Ritz M., Praus P., Kočí K.: Appl. Surf. Sci. *430*, 335 (2018).
9. Praus P., Svoboda L., Ritz M., Troppová I., Šihor M., Kočí K.: Mater. Chem. Phys. *193*, 438 (2017).
10. Hasija V., Raizada P., Sudhaik A., Sharma K., Kumar A., Singh P., Jonnalagadda S.B., Thakur V.K.: Appl. Mater. Today *15*, 494 (2019).
11. Kumar S., Karthikeyan S., Lee A.: Catalysts *8*, 74 (2018).
12. Nikokavoura A., Trapalis C.: Appl. Surf. Sci. *430*, 18 (2018).
13. Wen J., Xie J., Chen X., Li X.: Appl. Surf. Sci. *391*, 72 (2017).
14. Jiang L., Yuan X., Pan Y., Liang J., Zeng G., Wu Z., Wang H.: Appl. Catal. B: Environmental *217*, 388 (2017).
15. Starukh H., Praus P.: Catalysts *10*, 38 (2020).
16. Praus P., Smýkalová A., Foniok K., Velíšek P., Cvejn D., Žádný J., Storch J.: Nanomaterials *10*, 20 (2020).
17. Martin D.J., Qiu K.P., Shevlin S.A., Handoko A.D., Chen X.W., Guo Z.X., Tang J.W.: Angew. Chem. Int. Ed. *54*, 9240 (2014).
18. Guillard C., Puzenat E., Lachheb H., Houas A., Herrmann J.-M.: Int. J. Photoenergy *7*, 1 (2005).
19. Krivec M., Dillert R., Bahnemann D.W., Mehle A., Strancar J., Drazic G.: Phys. Chem. Chem. Phys. *16*, 14867 (2014).
20. Alwin E., Kočí, Wojcieszak R., Zieliński M., Edelmannová M., Pietrowski M.: Materials *13*, 2756 (2020).
21. Wang K., Li Q., Liu B., Cheng B., Ho W., Yu J.: Appl. Catal. B: Environmental *176-177*, 44 (2015).
22. Lin S., Ye X., Gao X., Huang J.: J. Mol. Catal. A-Chem. *406*, 137 (2015).
23. Kapteijn F., Rodriguez-Mirasol J., Moulijn J.A.: Appl. Catal. B *9*, 25 (1996).
24. Kondratenko E.V., Pérez-Ramírez J.: J. Phys. Chem. B *110,* 22586 (2006).
25. Kočí K., Zatloukalová K., Obalová L., Krejčíková S., Lacný Z., Čapek L., Hospodková A., Šolcová O.: Chin. J. Catal. *32*, 812 (2011).
26. Tan S.S., Zou L., Hu E.: Catal. Today *115*, 269 (2006).

BIOTECHNOLOGY AND BIOREFINERY

BIOSYNTHESIS OF METAL NANOPARTICLES USING VITIS VINIFERA EXTRACT AND THEIR ANTIMICROBIAL ACTIVITY

Miškovská A.[1], Michailidu J.[1], Čejková A.[1]

[1]*University of Chemistry and Technology Prague, Technická 5, 166 28, Prague 6*
miskovsa@vscht.cz

Abstract

Nowadays, the world faces challenges related to the spread of antibiotic resistance. One of the possible solutions to this problem could be the use of metal nanoparticles, objects with dimensions below 100 nm. Due to the high surface to volume ratio, nanoparticles have exceptional properties, including antimicrobial activity. In general, metal nanoparticles can be prepared in three ways: chemically, physically, and biologically. The biological route is the most eco-friendly and cost-effective of the mentioned methods. This study aims to biosynthesize gold nanoparticles using *Vitis vinifera* extract and to determinate their antimicrobial activity. The extract was prepared using viticultural waste, specifically the dried canes of *V. vinifera*. The obtained nanoparticles were characterized using UV-vis spectroscopy and transmission electron microscopy (TEM). TEM analysis showed that the nanoparticles had heterogenous shape and size mostly in the range 8–22 nm. Subsequently, the effect of nanoparticles on planktonic cells of two strains of *Pseudomonas aeruginosa* was studied. The antimicrobial activity of the nanoparticles varied depending on the tested strain of the microorganism.

Introduction

Nanotechnologies using metallic nanoparticles have become an integral part of human activity in recent years. The expansion of this sector is related to the current possibilities of industrial production of nanoparticles. There are many approaches to how to prepare nanoparticles. However, it is necessary to consider the sustainability of these methods, and therefore environmentally friendly, fast, and economically undemanding methods are sought. Biological (also called "green") methods, which use biological agents such as plants, plant extracts, microorganisms, or lysates for the synthesis of metal nanoparticles, are very promising approaches[1].

The attractiveness of nanoparticles lies in its unique properties, such as antibacterial effects. In terms of antibacterial activity, nanoparticles of metals such as silver (Ag), gold (Au), copper (Cu), and platinum (Pt) are the most often studied. In particular, gold nanoparticles (AuNPs) attract the attention of scientists and physicians due to their low toxicity to animal cells[2]. Although gold as a metal is found to be safe and chemically inert[3], nanoparticles can exhibit antibacterial effects[4]. It has been found that the degree of antibacterial effect of gold nanoparticles depends on the mode of surface functionalization[5]. Gold nanoparticles prepared using plant extracts deserve special attention, because they are surrounded by biomolecules, which are naturally present in plant extracts and thanks to them these nanoparticles tend to be more stable and biocompatible than abiotically prepared ones[6]. Other benefits of using plant extracts include speed, simple scale-up, low energy consumption, environmental friendliness, and economic simplicity[7].

The aim of this work was to prepare gold nanoparticles using an extract from the waste parts of an agriculturally important plant – grapevine (*Vitis vinifera*) and investigation of their antibacterial potential against the opportunistic pathogenic bacterium *Pseudomonas aeruginosa*. Gold nanoparticles were prepared using an extract from the canes of this plant. It was found that these parts of the plant are still full of biologically active compounds such as polyphenols and could be an excellent source for the preparation of high stable and biocompatible particles[8]. The antibacterial effect was monitored on planktonic cells of two *P. aeruginosa* strains - ATCC 10145, ATCC 15442.

Experiment

Preparation of the extract from *Vitis vinifera*

For the extract preparation, we used dried woody canes of grapevine. First, the canes were crushed and homogenized with a laboratory mixer. Then 150 g of homogenized canes were mixed with 600 ml of 40 % ethanol and let react for 24 hours in a dark at room temperature. Subsequently, the prepared extract was filtered through a microfilter with porosity 0.22 µm. The prepared extract was stored in the dark at 4 °C until further use.

Biosynthesis of gold nanoparticles

For the biosynthesis of gold nanoparticles, we used the ethanolic extract of *V. vinifera* canes prepared in the previous step. Nanoparticles were prepared by mixing 6 % v/v of this extract with aqueous solution of chloroauric acid ($HAuCl_4$) to the final concertation 1 mM. The mixture was then let to react for 24 hours in the dark at room temperature. The formation of gold nanoparticles was preliminary detected by the change in a colour from light yellow to dark purple. The final biosynthesized nanoparticles were stored in the dark at 4 °C for antimicrobial experiments.

Characterization of prepared nanoparticles

To detect the presence of nanoparticles UV-vis spectra were recorded in a microtiter plate using the Reader TECAN device in the range of 300-700 nm and 10 nm resolution.

To determine the morphology and particle size of biosynthesized nanoparticles, transmission electron microscopy was performed.

Antibacterial activity of the prepared nanoparticles

The cryopreserved bacterium was first and aseptically inoculated into 100 ml of fresh, sterile LB medium. The cells were cultured on an orbital shaker (37 ° C, 150 rpm) for 24 hours. The next day, the culture was centrifuged, and the optical density (OD_{600}) of the fresh inoculum was adjusted to 0.100 ± 0.020.

Antibacterial activity of biosynthesized nanoparticles was performed using 100 microtiter plates for the BioscreenC device. Gold nanoparticles were first pipetted into the microtiter plate in the concentration range of 3.1–40.6 % (v/v) of the well (excluding controls). The wells were then made up to 130 µl with sterile phosphate buffer (PBS) with pH 7.4. Finally, 160 µl of sterile LB medium and 30 µl of prepared fresh inoculum were added to each well. All operations described above were performed in a laminar box and the effect of individual concentrations of AuNPs was monitored in 10 replicates. Additionally, the activity of the plant extract was tested. The prepared microtiter plate was then placed in a BioscreenC, where the optical density (OD_{600}) of the suspension in each well was scanned every 30 minutes for 24 hours. The effect of gold nanoparticles on the growth of bacterial suspension cells was subtracted from the change in OD versus control (wells without AuNPs).

Results and discussion

Characterization of prepared nanoparticles

As the metal precursor ($HAuCl_4$) was added into the extract, the colour of the solution started to change from light yellow to dark purple after an hour because of the reduction of Au ions and the formation of gold nanoparticles (Figure 1).

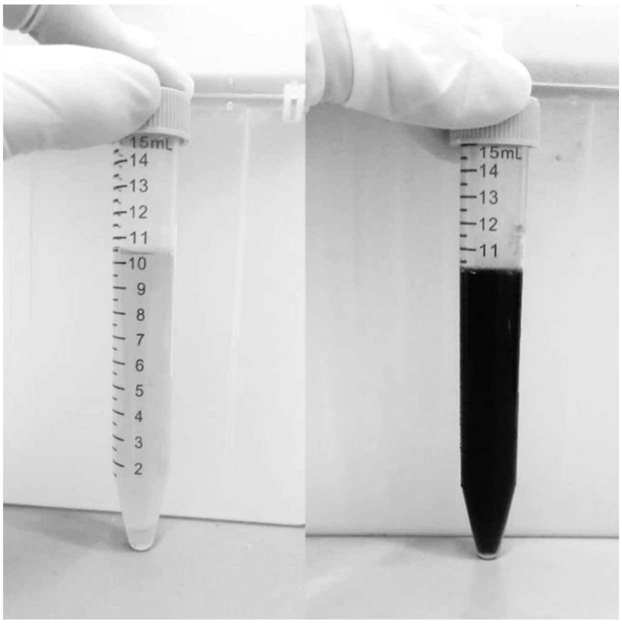

Figure 1. Detection of the formation of gold nanoparticles; *left* – solution immediately after addition of the metal precursor into the extract, *right* – colloidal gold after 24 hours

Presence of nanoparticles was also observed by measuring the UV-vis spectra of the final solution (Figure 2). The presence of the absorbance band at 540 nm indicates the formation of gold nanoparticles. For the further characterization of the particles (determination of the size and shape), TEM analysis was done (Figure. 3).

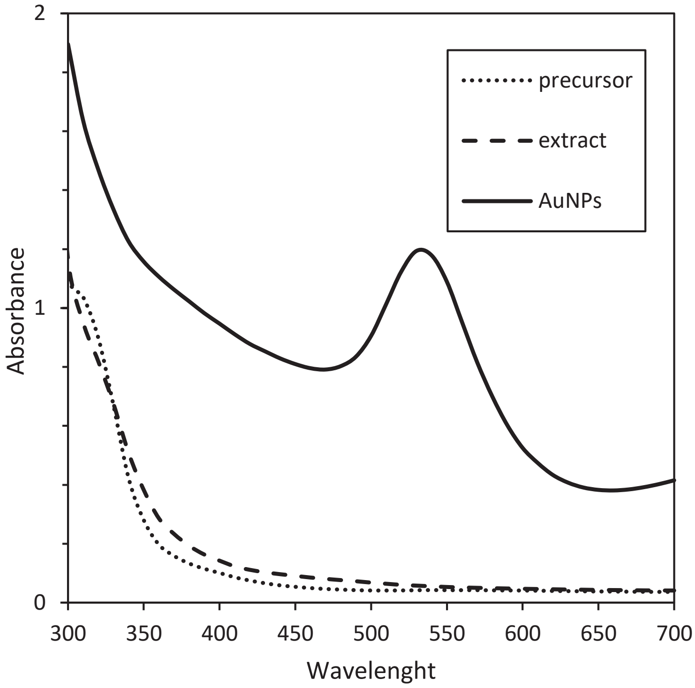

Figure 2. UV-vis spectra of the control – metal precursor ($HAuCl_4$), extract of *V. vinifera* canes and biosynthesized gold nanoparticles

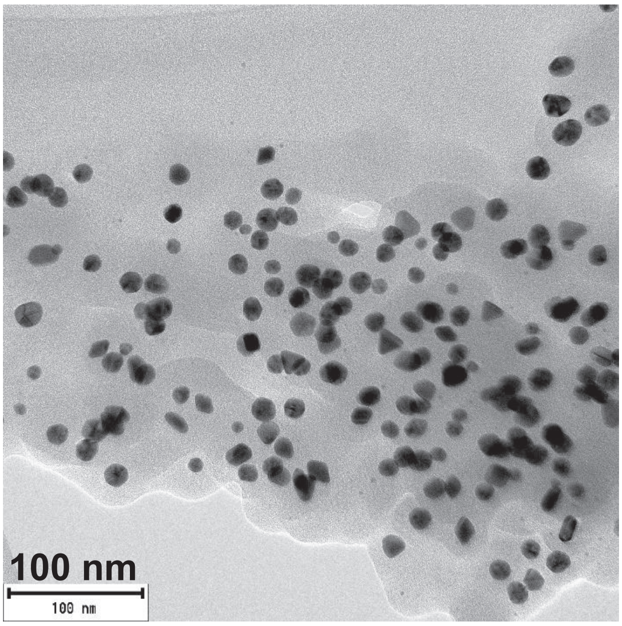

Figure 3. Gold nanoparticles visualised by transmission electron microscopy

TEM analysis shows that the biosynthesized gold nanoparticles are heterogenous in shape (mostly spherical, triangular, and oval). The size of the particles lies mostly in the range 8–22 nm.

Antibacterial activity of biosynthesized nanoparticles

The results of the antibacterial experiment expressed as a growth of bacterial planktonic cells of both strains of the bacteria in relative % related to the control (without addition of gold nanoparticles) are shown in Figure 4. The activity of nanoparticles varied depending on the bacterial strain used. While *P. aeruginosa* ATCC 10145 growth was inhibited by 60 rel. % at a concentration of 21.9 % v/v, the second strain of the bacteria was not demonstrably inhibited by any of the tested concentrations of nanoparticles. This result could be explained as a consequence of variability in response to antimicrobials due to the phenotypic characteristics of the individual strains[9]. The *Vitis vinifera* extract did not inhibit the growth of the bacteria by more than 20 rel. % (2.4 % v/v; experimental background for the highest concentration of Au nanoparticles).

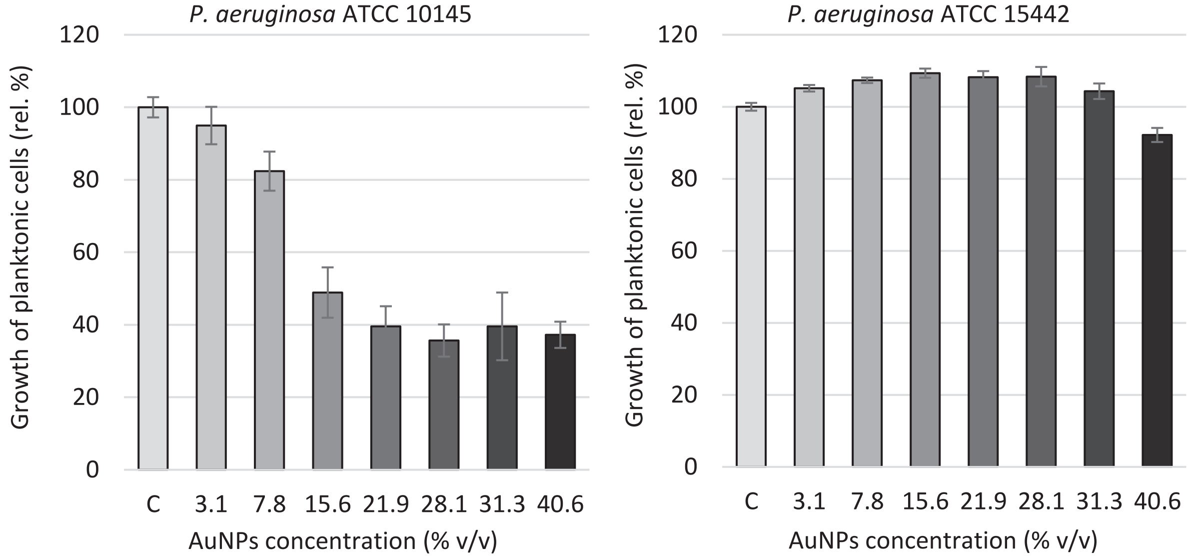

Figure 4. Antibacterial effects of biosynthesized gold nanoparticles. Growth of planktonic cells of the tested strain of *P. aeruginosa* at the tested concentrations (% v/v) of gold nanoparticles expressed in relative % related to the control ("C", 100 %, without nanoparticles).

Conclusion

The present work describes the biosynthesis of gold nanoparticles using the extract from waste parts of the *Vitis vinifera* plant. The canes of *Vitis vinifera* contain many bioactive compounds which are responsible for the reduction of $HAuCl_4$. They are also responsible for the formation and further stabilization of nanoparticles. It was found that this extract could be used for simple, fast, cheap, and eco-friendly preparation of small (< 25 nm) and stable gold nanoparticles. Moreover, the prepared nanoparticles showed antibacterial activity (growth inhibition by 60 rel. %) against *P. aeruginosa* ATCC 10145.

Acknowledgement

This project was supported from the grant of Specific university research – grant No. A2_FPBT_2021_011

References

1. Thakkar K. N., Mhatre S. S., Parikh R. Y.: Nanomed. Nanotechnol. Biol. Med. *6*, 257 (2010).
2. Lara Y., Nguyen T., Marilena L., Alexander M.: Nano Today *6*, 585 (2011).
3. Alkilany A. M., Murphy C. J.: J. Nanopart. Res. *12*, 2313 (2010).
4. MubarakAli D., Thajuddin N., Jeganathan K., Gunasekaran M.: Colloids Surf. B. Biointerfaces *85*, 360 (2011).
5. Zhang Y., Shareena Dasari T. P., Deng H., Yu H.: J. Environ. Sci. Health C *33*, 286 (2015).
6. Schröfel A., Kratošová G., Šafařík I., Šafaříková M., Raška I., Shor L. M.: Acta Biomater. *10*, 4023 (2014).
7. Geethalakshmi R., Sarada D.: Int. J. Nanomedicine *7*, 5375 (2012).
8. Cviner P., Pádrová K., Kolouchová I.: Chem. Listy *111*, 103 (2017).
9. Chandler C. E., Horspool A. M., Hill P. J., Wozniak D. J., Schertzer J. W., Rasko D. A., Ernst R. K.: J. Bacteriol. *201*, e00595 (2019).

GENUS *MONASCUS* AND ITS SECONDARY METABOLITES

Husakova M.[1], Patakova P.[1]

[1]*University of Chemistry and Technology, Prague, Czech Republic*
husakovm@vscht.cz

Abstract

Genus *Monascus* belongs to the kingdom Fungi. These ascomycetes are known and used in Asia for centuries. They are used for food dyeing and conservation or as a part of traditional Chinese medicine. In the western world, *Monascus* fungus is nowadays used to produce food supplements that prevent hypercholesterolemia and cardiovascular diseases. The representatives of the genus *Monascus* produce a wide range of primary and secondary metabolites, some of them having significant biological effects. The most important metabolites are pigments, monacolins, and mycotoxin citrinin. Other metabolites are, for example, γ-aminobutyric acid, dimerumic acid, or ethanol. *Monascus* pigments are polyketides with antiproliferative, anti-inflammatory, or antimicrobial effects. Monacolins belong to the group of statins, they inhibit the activity of 3-hydroxy-3-methylglutaryl-coenzyme A reductase. HMG-CoA reductase plays a significant role in cholesterol biosynthesis. Mycotoxin citrinin has nephrotoxic and hepatotoxic effects. The use of the genus *Monascus* mainly in the food industry has a large potential, however, the problem with the production of undesirable compounds such as citrinin has to be solved.

Introduction

Monascus fungi are ascomycetes known and used in Asian countries for centuries. In Europe, they were first discovered and described in the 19th century. In European Union, the use of genus *Monascus* is permitted only as a food supplement. The representatives of the genus *Monascus* produce a wide range of secondary metabolites, e.g., *Monascus* azaphilone pigments, monacolins or mycotoxin citrinin. Due to secondary metabolites, *Monascus* fungi and *Monascus*-fermented products possess many biological activities. Monacolins help to control hyperlipidemia and hypercholesterolemia and they are used (mainly monacolin K) as pharmaceutical agents to control normal blood cholesterol levels.

Characterisation of genus *Monascus*

The genus *Monascus* belongs to the kingdom Fungi, phylum Ascomycota, class Eurotiomycetes, order Eurotiales, family Monascaceae[1]. Some authors classified this genus to the family Aspergilaceae[2]. For the first time, the genus *Monascus* was described by the French mycologist Philippe Van Tieghem in the 19th century[3]. However, these fungi are known and used in southeast Asia for centuries[4].

The representatives of the genus *Monascus* are aerobic organisms, and their optimal growth temperature is between 30-38 °C[5]. The reproduction of the fungus Monascus can be either asexual or sexual (Fig. 1). Asexual spores (conidia) are formed at the end of the hyphae, they are single-celled and round[6,7]. Asexual form is also known under the name *Basipetospora*[2]. Sexual spores are oval and are called ascospores. Ascospores are formed in asci, that are grouped in cleisthotecia. Cleisthotecia can differ in size and can also contain different numbers of ascospores[6,7].

More than 20 species were isolated and defined. However, widely accepted is just nine of them; namely *M. ruber*, *M. pilosus*, *M. purpureus*, *M. floridanus*, *M. pallens*, *M. sanguineus*, *M. eremophilus*, *M. lunisporas*, and *M. argentinensis*[8]. The representatives of the genus *Monascus* are usually contaminants of starch-rich foods and food products, mainly rice or cereals. These microorganisms can also occur in agricultural products or wastes. Some representatives were isolated also from soil, river sediment, or plant tissues[9-13].

Use of the genus *Monascus*

The most important and the most common *Monascus*-fermentented product is Red yeast rice, which is also known as Red mold rice, *Monascus*-fermented rice, Hung-Chu, Hong Qu, Ang-kak, Ankak rice or Beni-Koji[14]. Red yeast rice is traditionally used mostly in China, Japan, or South Korea, for food dyeing and preservation[4]. The genus *Monascus* is also traditionally used to produce rice wines and rice vinegars[15,16]. Besides of rice products, there are also other *Monascus*-fermented products, for example, soybean products[17].

In Europe, the only authorized *Monascus*-fermented products are food supplements, which are prepared from RYR fermented by *Monascus purpureus*. For these products, the health claim "Monacolin K from red yeast rice contributes to the maintenance of normal blood cholesterol levels" can be used. The claim may be used only for food which provides a daily intake of 10 mg of monacolin K from red yeast rice as stated by Commission Regulation (EU) No 432/2012[18,19]. Apart from the food industry, the genus *Monascus* and its products are used as a part of traditional Chinese medicine[4].

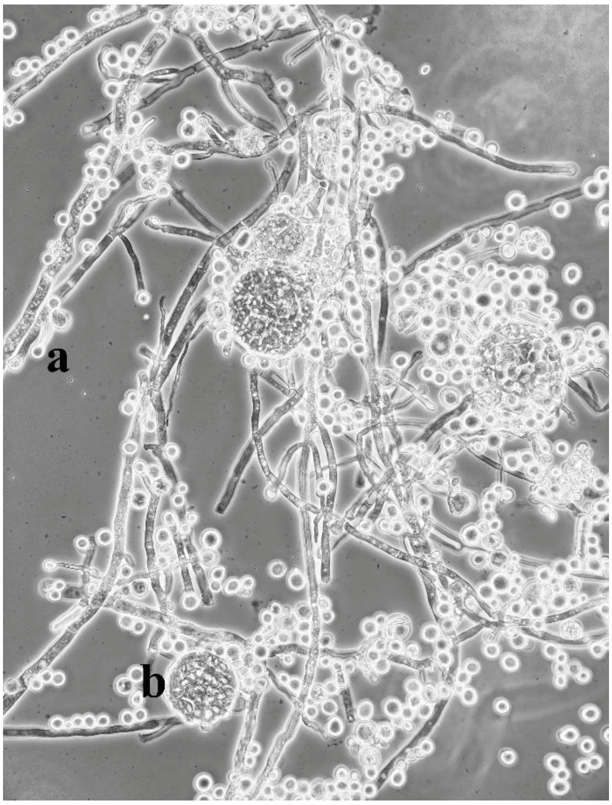

Figure 1. Mycelium, conidia (a), and cleistothecia (b) of *Monascus ruber* DSM 62748 cultivated on Sabouraud agar for 7 days (30 °C)

Metabolites

The fungus *Monascus,* as many other ascomycetes, produces a wide range of secondary metabolites. The most important metabolites are azaphilone pigments, monacolins, and mycotoxin citrinin[20]. These compounds are synthetised by polyketide synthase pathway. Polyketide synthases are widely distributed in bacteria, fungi, and plants, these enzymes are part of the biosynthesis of a remarkable range of natural products[21]. Besides these compounds, the genus *Monascus* produce other significant primary and secondary metabolites, as for example γ-aminobutyric acid, dimerumic acid, and organic acids (succinic, fumaric or malic acid)[4,22-24]. *Monascus* fungi are able to produce ethanol under aerobic conditions in a surplus of a carbon source[25]. Dimerumic acid is a product of siderophore coprogen B breakup. This compound is a stronger natural antioxidant than for example well-known resveratrol or curcumin[24]. γ-aminobutyric acid is non-proteinogenic amino acid, which occurs in microorganism, plants, and animals. It has a role as a signalling molecule, and it is the primary inhibitory neurotransmitter in the mammalian central nervous system with many biological activities[26]. *Monascus* fungi also produce wide range of enzymes, for example amylolytic, proteolytic, and cellulolytic enzymes[20,27].

Pigments

Monascus azaphilone pigments are usually divided into three groups, according to their absorbance maxima (yellow 330-450 nm, orange 460-480 nm, and red 490-530 nm)[28]. At first, there were described the structures of six most abundant pigments, yellow monascin and ankaflavin, orange rubropunctatin and monascorubrin, and red rubropunctamine and monascorubramine. Nowadays, it is identified and described more than 100 *Monascus*-pigments[29]. *Monascus*-pigments are well soluble in water and ethanol and are traditionally used in Asian countries for food dyeing and preservation[28].

In general, *Monascus*-pigments synthase pathway is described as esterification of polyketide chromophore to β-ketoacid (originally form fatty acid synthase pathway) by formation of orange pigments. By the reactions of orange pigments are formed yellow and red pigments, yellow by reduction and red by amination. In the past few years, it was found that yellow unstable reactive intermediates are synthetized by Knoevenagel condensation. From these intermediates are than synthesized yellow and orange pigments, yellow by reduction of double bond and orange by restoring of double bond. Red pigments originated by reaction of orange pigments with amines, especially with amino acids[28].

Monacolins

Monacolins are natural statins. They inhibit the activity of human 3-hydroxy-3-methylglutaryl-CoA reductase enzyme. This enzyme katalyse the main step of cholesterol biosynthesis. The most effective monacolin is Monacolin K, also known as lovastatin or mevinolin. This compound is commercially (e.g., Mevacor®) used to reduce low-density lipoprotein (LDL) cholesterol and total cholesterol levels in blood. The structure of monacolin K is shown in Fig. 2A. It was found that exposure to monacolin K could lead to severe adverse effects on the muscoskeletal system and on the liver. Individual cases have been reported at intake levels as low as 3 mg/day[30].

Mycotoxin citrinin

Citrinin, initially named as monascidin A in *Monascus* fungi[31], is mycotoxin produced by genus *Monascus*, *Aspergillus* or *Penicillium*. It is a yellow crystalline substance with nephrotoxic effects. Furthermore, genotoxic and carcinogenic effects could not be ruled out[32]. In the European Union, there are regulated maximum levels of citrinin in food supplements based on rice fermented with red yeast *Monascus purpureus*. These limits were set by the Commission Regulation (EU) 2019/1901[33] as 100 µg/kg. In some Asian countries, there are maximal levels of citrinin set very similarly (Japan 200 µg/kg[34], South Korea 50 µg/kg[35]). Structure of citrinin is shown in Fig. 2B.

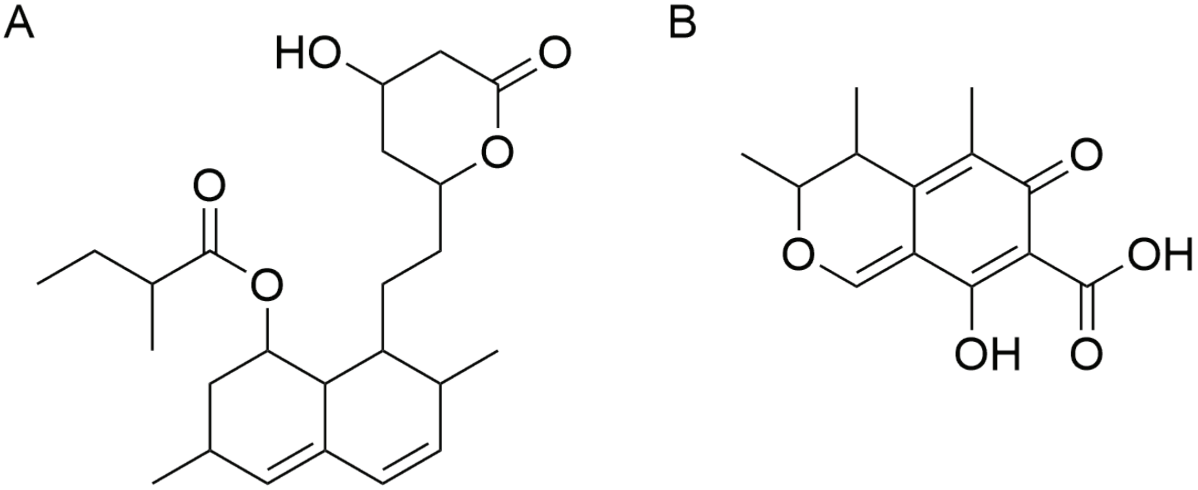

Figure 2. Structures of monacolin K (A) and citrinin (B)

Biological activities

Thu fungus *Monascus* and *Monascus*-fermented products possess a wide range of biological activities. Most important and pharmaceutically used are monacolins. They are used for their inhibition of cholesterol biosynthesis, to control hyperlipidemia and hypercholesterolemia and are authorized for the treatment of those diseases. Monacolins also decrease levels of high-sensitivity C-reactive protein. Lowering cholesterol levels and improving of flow-mediated dilation of blood vessels may help to reduce the risk of atherosclerosis and to prevent cardiovascular diseases[30,36,37].

Monascus-pigments exhibit antimicrobial activity against bacteria, yeast, and fungi, they also suppress the germination of some bacterial spores[38,39]. Derivates of *Monascus*-pigments were identified as potential anti-hepatitis C virus agents, due to their effects on the replication of hepatitis C virus. This activity suggests that a combination of pigment derivates and interferons might offer an alternative strategy for the control of HCV replication[40]. Pigments possess also radical scavenging, antitumor, antiobesity, and anti-inflammatory activity, and can improve the memory and learning ability and suppress Alzheimer disease risk factors[41-44].

The strong natural antioxidant, dimerumic acid, effectively inhibits liver damage and inflammation by attenuating oxidative stress and suppresses cancer cell invasion[24].

γ-aminobutyric acid plays a significant role in human health by exhibiting a wide range of neurological and non-neurological properties. In addition, its physiological role as modulator of neurotransmission, or prevention of insomnia and depression, γ-aminobutyric possesses various pharmaceutical effects on non-neuronal tissues and organs. Especially anti-hypertension, anti-diabetes, anti-cancer, antioxidant, anti-inflammation, antimicrobial, anti-allergy, hepato-protection, reno-protection, and intestinal protection activities were reported[26].

Conclusion

The genus *Monascus* and *Monascus*-fermented products are used in Asia for centuries, not only for food dyeing and preservation, but also as a part of traditional Chinese folk medicine[4]. In the European Union, the use of the genus *Monascus* is permitted only as a food supplement. Wider use of *Monascus*-fermented products and their application in food and pharmaceutical industry is problematic, because of the presence of an undesirable metabolite – mycotoxin citrinin, and also reported severe adverse side effects of monacolin K at low daily doses. These difficulties have to be solved to produce safe and beneficial *Monascus*-fermented products.

Acknowledgement

This work was supported from the grant of Specific university research – grant A2_FPBT_2021_008.

References

1. Geiser, D. M.; Gueidan, C.; Miadlikowska, J.; Lutzoni, F.; Kauff, F.; Valerie, H.; Fraker, E.; Schoch, C. L.; Tibell, L.; Untereiner, W. A.; Aptroot, A.: Mycologia, *98*, 1053 (2006).
2. Houbraken, J.; Kocsube, S.; Visagie, C. M.; Yilmaz, N.; Wang, X. C.; Meijer, M.; Kraak, B.; Hubka, V.; Bensch, K.; Samson, R. A.; Frisvad, J. C.: Stud Mycol, *95*, 5 (2020).
3. van Tieghem, M. P.: Bull Soc Bot France. *31*, 226 (1884).
4. Lin, Y.-L.; Wang, T.-H.; Lee, M.-H.; Su, N.-W.: Appl Microbiol Biotechnol, *77*, 965 (2008).
5. Manandhar, K. L.; Apinis, A. E.: Trans Brit Mycol Soc, *57*, 465 (1971).
6. Young, E. M.: Am J Bot, *18*, 499 (1931).
7. Carels, M.; Shepherd, D.: J Bacteriol, *122*, 288 (1975).
8. Shao, Y.; Lei, M.; Mao, Z.; Zhou, Y.; Chen, F.: Appl Microbiol Biotechnol, *98*, 3911 (2014).
9. Udagawa, S. I.; Baba, H.: Cryptogam Mycol, *19*, 269 (1998).
10. Stchigel, A. M.; Cano, J.; Abdullah, S.; Guarro, J.: Stud Mycol, *50*, 299 (2004).
11. Barnard, E. L.; Cannon, P. F.: Mycologia, *79*, 479 (1987).
12. Barbosa, R. N.; Leong, S. L.; Vinnere-Pettersson, O.; Chen, A. J.; Souza-Motta, C. M.; Frisvad, J. C.; Samson, R. A.; Oliveira, N. T.; Houbraken, J.: Stud Mycol, *86*, 29 (2017).
13. Cannon, P. F.; Abdullah, S. K.; Abbas, B. A.: Mycol Res, *99*, 659 (1995).
14. Zhu, B.; Qi, F.; Wu, J.; Yin, G.; Hua, J.; Zhang, Q.; Qin, L.: Front Pharmacol, *10*, 1449 (2019).
15. Murooka, Y.; Nanda, K.; Yamashita, M.: In Vinegars of the World, Springer, Milano 2009.
16. Huang, Y.-Y.; Liang, Z.-C.; Lin, X.-Z.; He, Z.-G.; Ren, X.-Y.; Li, W.-X.; Molnár, I.: Food Res Int, *141*, 110146 (2021).
17. Lim, J.-Y.; Kim, J. J.; Lee, D. S.; Kim, G. H.; Shim, J.-Y.; Lee, I.; Imm, J.-Y.: Food Chem, 120, 255 (2010).
18. Commission Regulation (EU) No 432/2012.
19. EFSA Panel on Food Additives and Nutrient Sources added to Food (ANS): EFSA J, *9*, 2304 (2011).
20. Patakova, P.; Branska, B.; Patrovsky, M.: In Fungal Metabolites. Springer, Cham 2017.
21. Talapatra, S. K.; Talapatra, B.: In Chemistry of Plant Natural Products: Stereochemistry, Conformation, Synthesis, Biology, and Medicine, Springer, Berlin, Heidelberg 2015.
22. Hajjaj, H.; Blanc, P.; Groussac, E.; Uribelarrea, J.-L.; Goma, G.; Loubiere, P.: Enzyme Microb Technol, *27*, 619 (2000).
23. Lumyong, S.; Tomita, F.: World J Microbiol Biotechnol, *9*, 383 (1993).
24. Lee, B.-H.; Pan, T.-M.: J Funct Foods, *5*, 2 (2013).
25. Chen, M.-H.; Johns, M. R.: Enzyme Microb Technol, *16*, 584 (1994).
26. Ngo, D.-H.; Vo, T. S.: Molecules, *24*, 2678 (2019).
27. Chen, M.; Liu, H.; Zhen, D.; Fang, S. L.: Afr J Biotechnol, *10*, 5166 (2011).
28. Chen, W.; Chen, R.; Liu, Q.; He, Y.; He, K.; Ding, X.; Kang, L.; Guo, X.; Xie, N.; Zhou, Y.; Lu, Y.; Cox, R. J.; Molnár, I.; Li, M.; Shao, Y.; Chen, F.: Chem Sci, *8*, 4917 (2017).
29. Chen, W.; Feng, Y.; Molnár, I.; Chen, F.: Nat Prod Rep, *36*, 561 (2019).
30. EFSA Panel on Food Additives and Nutrient Sources added to Food (ANS): EFSA J; *16*, 05368 (2018).

31. Blanc, P. J.; Laussac, J.; Le Bars, J.; Le Bars, P.; Loret, M.; Pareilleux, A.; Prome, D.; Prome, J.; Santerre, A.; Goma, G.: Int J Food Microbiol, *27*, 201 (1995).
32. EFSA Panel on Contaminants in the Food Chain (CONTAM): EFSA J, *10*, 2605 (2012).
33. Commission Regulation (EU) 2019/1901.
34. Fu, G.; Xu, Y.; Li, Y.; Tan, W., Asia Pac J Clin Nutr, *16*, 137 (2007).
35. Kim, H.-J.; Ji, G. E.; Lee, I.: Food Sci Biotechnol, *16*, 142 (2007).
36. Endo, A.; Hasumi, K.; Negishi, S.: J Antibiot, *38*, 420 (1985).
37. Cicero A. F., Derosa G., Parini A., Maffioli P., D'Addato S., Reggi A., Giovannini M., Borghi C.: Nutr Res, *33*, 622 (2013).
38. Husakova, M.; Plechata, M.; Branska, B.; Patakova, P.: Front Microbiol, *12*, 1254 (2021).8
39. Zhao, G.-P.; Li, Y.-Q.; Yang, J.; Cui, K.-Y.: Czech J Food Sci, *34*, 197 (2016).
40. Sun, J. M.; Kim, S. J.; Kim, G. W.; Rhee, J. K.; Kim, N. D.; Jung, H.; Jeun, J.; Lee, S. H.; Han, S. H.; Shin, C. S.; Oh, J. W.: J Antimicrob Chemother, *67*, 49 (2012).
41. Choe, D.; Lee, J.; Woo, S.; Shin, C. S., Food Chem, *134*, 315 (2012).
42. Lee, C.-L.; Lin, P.-Y.; Hsu, Y.-W.; Pan, T.-M.: J Funct Foods, *18*, 387 (2015).
43. Hsu, L.-C.; Hsu, Y.-W.; Liang, Y.-H.; Kuo, Y.-H.; Pan, T.-M.: J Agric Food Chem, *59*, 1124 (2011).
44. Hsu, L.-C.; Liang, Y.-H.; Hsu, Y.-W.; Kuo, Y.-H.; Pan, T.-M.: J Agric Food Chem, *61*, 2796 (2013).

ANTIMICROBIAL AND ANTIVIRULENCE ACTIVITY OF PTEROSTILBENE, METHOXYLATED DERIVATIVE OF RESVERATROL

Kašparová P.[1], Maťátková O.[1]

[1]Department of Biotechnology, University of Chemistry and Technology in Prague, Technická 5, Prague 6 – Dejvice, 166 28, Czech republic
kasparop@vscht.cz

Abstract

With and increased incidence of antibiotic resistance among pathogenic bacteria and fungi, there is a great pressure on novel drug development. The research is now focused on drugs with potential antivirulence activity rather than traditional antimicrobial substances due to decreased selective pressure on treated pathogen and lower probability of resistance development.

The presented study observed antimicrobial and antibiofilm effect of natural compound pterostilbene compared to traditional macrolide antibiotic – erythromycin on clinically relevant staphylococci.

Pterostilbene was effective against both suspension growth and biofilm formation in contrast to erythromycin. Pterostilbene was found to have bactericidal action on *Staphylococcus aureus* and in combination (49 mg/l) with antibiotic it enhanced erythromycin (5 mg/l) activity and decreased biofilm formation by more than 80% in all studied strains of *Staphylococcus epidermidis*.

Studied stilbene was proved to be a suitable complement of otherwise ineffective antibiotics in treatment of infectious diseases caused by representatives of genus *Staphylococcus*.

Introduction

Antibiotic resistance among microorganisms represents an urgent problem of today clinical practice[1]. With common antibiotics failing to cure infectious diseases caused by resistant pathogens, an alternative strategy for their treatment emerged acting via inhibition of infectious properties of the pathogens rather than their killing[2]. Pterostilbene, a natural antioxidant found in various plants (*Vitis vinifera*, *Vaccinium* spp., *Pterocarpus santalinus*) is a derivative of much more well-known resveratrol (Figure 1). Pterostilbene has a wide spectrum of beneficial pharmacological effects, among which the most outstanding is the antimicrobial activity and ability to enhance antibiotics action[3-5].

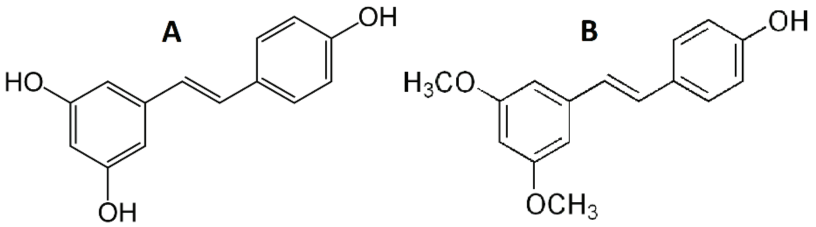

Figure 1. Structural formulae of resveratrol (A) and pterostilbene (B)

Lately, also its antivirulence activity is being observed as some studies reported its effect on hyphae formation in yeast of genus *Candida*[6]. Concerning its mechanism of action, there is little information on the topic with only handful of studies reporting possible cell membrane permeabilizing activity[7]. Beside reports on yeast and fungal pathogens, its great antimicrobial potential is notable especially in the case of gram-positive cocci as was also verified in our previous study[6,8]. Several publications mention pterostilbene and its additive or synergistic action when combined with e.g. oxacillin, vancomycin or gentamicin on suspension growth of *Staphylococcus aureus*[4,5]. In previous research, we have found synergistic action of pterostilbene with tetracycline on *Staphylococcus epidermidis*. In presented paper an antistaphylococcal effect of pterostilbene compared to antibiotic erythromycin was observed and the possible enhancement of antibiotic's action by additions of pterostilbene on biofilm formation of *S. epidermidis* was also studied[8].

S. aureus and *S. epidermidis* belong to a genus of gram-positive bacteria. Both species are greatly pathogenic with variety of virulence factors produced (haemolysins, proteases, lipases, toxins), ability to form thick biofilms on medical implants and great incidence of antibiotic resistance among today population[9,10]. The pathogens can cause wide spectrum of pathological states from sepsis, bacteraemia, endocarditis to chronic states and infectious diseases linked to their biofilm formation or indirect food poisonings due to contaminated food[11,12]. General treatment is provided by aminoglycosides, tetracyclines or macrolides, since β-lactams are mostly ineffective with large prevalence of methicillin-resistant strains of these species[13]. To our best knowledge, there is no report of clinically relevant staphylococci becoming resistant towards natural compounds of stilbene group, which makes these substances especially lucrative for research.

Materials and Methods

Antimicrobial agents

Pterostilbene and erythromycin were provided by Sigma Aldrich (USA). Stock solution of pterostilbene was prepared by dissolving in 100% DMSO (Penta, Czech Republic). Stock solution of erythromycin was prepared by dissolving in Tryptone Soya Broth (TSB) growth medium (Oxoid, Germany) used for cultivation of the studied microorganisms.

Microorganisms

Staphylococcus aureus ATCC 29213, ATCC 12600 (type strain) and ATCC 43300 (methicillin-resistant strain) were obtained from American Type Culture Collection. *Staphylococcus epidermidis* DBM 3179 was kindly provided from Department of Biochemistry and Microbiology of UCT Prague, Czech Republic. *S. epidermidis* ATCC 14990 (type strain) was obtained from American Type Culture Collection. *S. epidermidis* CCM 2343 (an elastase positive strain) was acquired from Czech collection of microorganisms in Brno, Czech Republic. Lastly also two clinical isolates of both microorganisms (*S. aureus* M-2 and *S. epidermidis* M-1) were studied, which originated from joint implant infection and were isolated in Motol Faculty Hospital, Prague, Czech Republic.

Cultivation of suspension cells

The suspension cells (turbidity of OD_{600} = 0.1) were cultured with antimicrobials and TSB in microcultivation device at 37 °C for 24 h as described in Maťátková et al (2017)[14]. Minimum inhibitory concentration (MIC_{80}) was evaluated, as was mentioned in the study, as the lowest concentration of studied substance, which inhibited suspension growth, by 80 %. After cultivation, suspension of treated cells was spotted onto Tryptone Soya Agar plates and cultured for another 24 h at 37 °C to assess minimum bactericidal concentration (MBC). MBC was determined as the lowest concentration of studied substance, which completely supressed any visible growth on plate. Based on MBC/MIC_{80} ratio, an overall bactericidal/bacteriostatic effect of the substance was evaluated according to Ayala-Nunez et al (2009)[15].

Cultivation of biofilm cells

The biofilm formed in presence of antimicrobials was cultured as described before. The suspension of cells (turbidity of OD_{600} = 0.6) were cultivated with antimicrobials and TSB medium as described in Vaňková et al (2020)[6]. After cultivation, the biofilm was rinsed with saline and viability of the biofilm cells was evaluated by resazurin viability assay according to Mariscal et al (2009)[16]. The effect of antimicrobials combined was evaluated according to Mishra and Wang (2017)[17].

Results and Discussion

The effect of antimicrobials on suspension growth of *S. aureus* and *S. epidermidis* is summarized in Table 1. Overall, erythromycin was found to be very effective on suspension growth with the exception of *S. aureus* ATCC 43300, yet MBC determination showed rather bacteriostatic action. Pterostilbene on the other hand although less effective in inhibition of suspension growth, showed bactericidal action in quite low concentrations.

Erythromycin was much less effective on biofilm formation of *S. epidermidis* as shown in Figure 2. It caused maximum 50% inhibition of metabolic activity when used in concentration 100 mg/l. Addition of 32.5 mg/l pterostilbene resulted in significant enhancement of erythromycin action as indicated especially by *S. epidermidis* CCM 2343 (Figure 2C) and clinical isolate M-1 (Figure 2D). The addition of 49 mg/l of pterostilbene to 5 mg/l erythromycin resulted in more than 80% inhibition of metabolic activity of biofilm cells in all studied *S. epidermidis* strains. The mentioned results were partially published in our research paper Kašparová et al (2021)[8].

Table I
Effect of pterostilbene and erythromycin on suspension growth of *Staphylococcus aureus* and *Staphylococcus epidermidis*. MIC$_{80}$ – minimum inhibitory concentration (80% inhibition of growth), MBC – minimum bactericidal concentration (no growth on agar plate)

	Pterostilbene (mg/l)			Erythromycin (mg/l)		
	MIC$_{80}$	MBC	effect	MIC$_{80}$	MBC	effect
S. aureus ATCC 29213	45	80	bactericidal	1	200	bacteriostatic
S. aureus ATCC 12600	30	40	bactericidal	1.5	1.5	bactericidal
S. aureus ATCC 43300	25	70	bactericidal	*	*	none
S. aureus M-2	16	175	bacteriostatic	0.4	50	bacteriostatic
S. epidermidis DBM 3179	37.5	ND	ND	0.75	ND	ND
S. epidermidis ATCC 14990	30	ND	ND	0.75	ND	ND
S. epidermidis CCM 2343	30	ND	ND	0.5	ND	ND
S. epidermidis M-1	25	ND	ND	0.25	ND	ND

*not found in a studied range of concentrations (0.2-400 mg/l)
ND – not determined

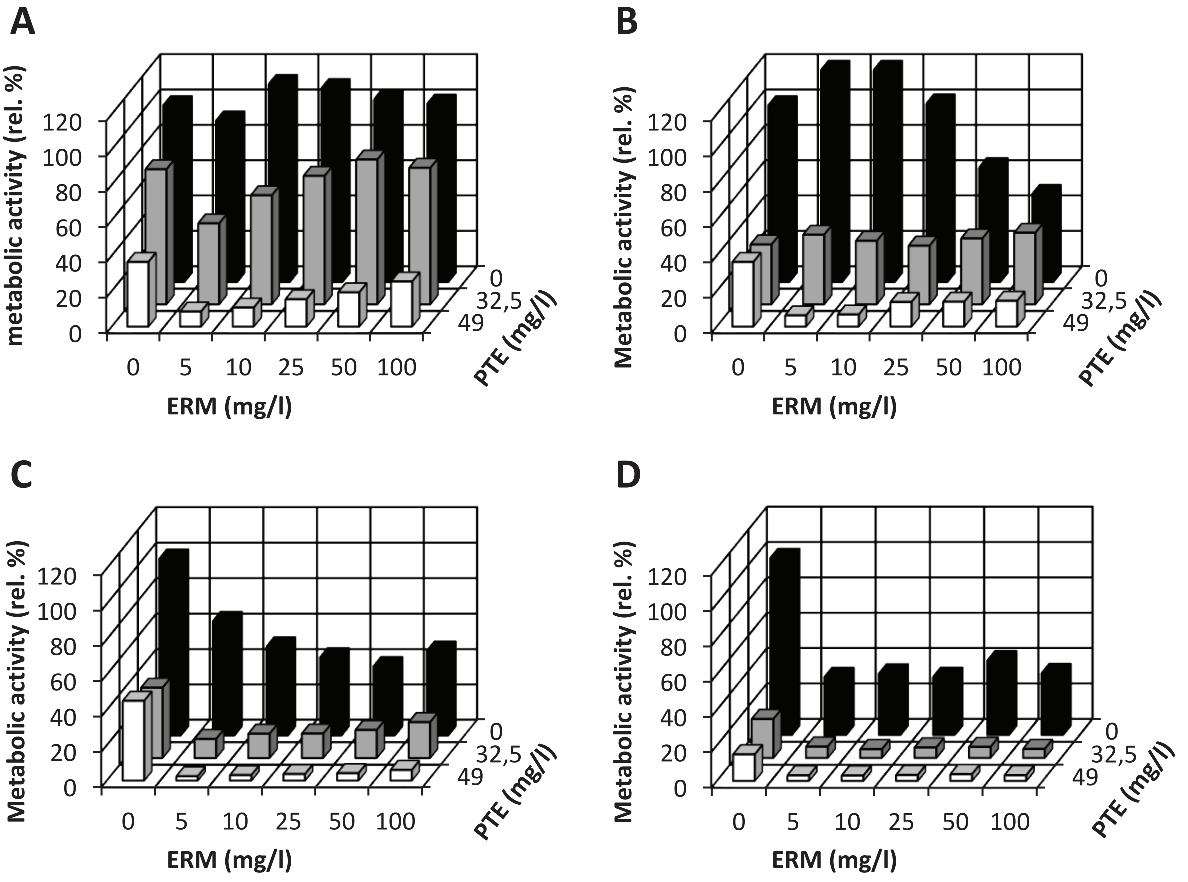

Figure 2. Effect of erythromycin (ERM) when combined with pterostilbene (PTE) on biofilm formation on *Staphylococcus epidermidis*. A – DBM 3179, B – ATCC 14990, C – CCM 2343, D – M-1. Data previously published in our publication Kašparová et al (2021)[8].

Conclusion

Pterostilbene was quite effective on both *S. aureus* and *S. epidermidis* (MIC$_{80}$ 16-45 mg/l) and exerted bactericidal action on *S. aureus*. Erythromycin was very efficient on suspension growth of both staphylococci (MIC$_{80}$ 0.2-1.5 mg/l) but acted bacteriostatically on *S. aureus*. Erythromycin was ineffective towards biofilm formation of *S. epidermidis*, but the addition of 49 mg/l pterostilbene to 5 mg/l erythromycin resulted in more than 80% inhibition in all studied cases. Pterostilbene was thus proved to have antibiotic enhancing activity.

Acknowledgements

This work was supported by the "Operational Programme Prague – Competitiveness" [CZ.2.16/3.1.00/24503]; "National Programme of Sustainability I" [NPU I LO1601] and Czech Science Foundation (GACR) [project 18-26463S].

References

1. Livermore D. M.: Int. J. Antimicrob. Agents, *16*, S3 (2000).
2. Baron C.: Curr. Op. Microbiol., *13*, 100 (2010).
3. Rimando A. M., Cuendet M., Desmarchelier C., Mehta R. G., Pezzuto J. M., Duke S. O.: J. Agr. Food Chem., *50*, 3453 (2002).
4. Ishak S. F., Ghazali A. R., Zin N. M., Basri D. F.: Am. J. Infec. Dis., *12*, 1 (2016).
5. Lee W. X., Basri D. F., Ghazali A. R.: Molecules, *22*, 1 (2017).
6. Vaňková E., Paldrychová M., Kašparová P., Lokočová K., Kodeš Z., Maťátková O., Kolouchová I., Masák J.: World J. Microbiol. Biotech., *30*, 101 (2020).
7. Ren X. Y., An P. P., Zhai X., Wang S., Kong Q. J.: Lwt-Food Sci. Technol., *101*, 1 (2019).
8. Kašparová P., Vaňková E., Brázdová L., Lokočová K., Maťátková O., Masák J.: Microb. Pathogen., *152*, 1 (2021).
9. Cho H. S., Lee J. H., Cho M. H., Lee J.: Biofouling 31, 1 (2015).
10. Tang F., Li L., Meng X. M., Li B., Wang C. Q., Wang S. Q., Wang T. L., Tian Y. M.: Microb. Pathogen., *127*, 85 (2019).
11. Arciola C. R., Campoccia D., Speziale P., Montanaro L., Costerton J. W.: Biomaterials, *33*, 5967 (2012).
12. Enright M. C., Day N. P. J., Davies C. E., Peacock S. J., Spratt B. G.: J. Clin. Microbiol., *38*, 1008 (2000).
13. Cong Y., Yang S., Rao X.: J. Adv. Res., *21*, 169 (2020).
14. Maťátková O., Kolouchová I., Kvasničková E., Ježdík R., Masák J., Čejková A.: Chem. Pap., *71*, 1471 (2017).
15. Ayala-Núñez N. V., Villegas H. H. L., Turrent L. C. I., Padilla C. R.: Nanobiotechnol., *5*, 2 (2009).
16. Mariscal A., Lopez-Gigosos R. M., Carnero-Varo M., Fernandez-Crehuet J.: Appl. Microbiol. Biotech., *82*, 773 (2009).
17. Mishra B., Wang G. S.: Pharmaceuticals, *10*, 1 (2017).

CHITOSAN NANOPARTICLES AS A PROMISSING ANTIMICROBIAL AGENT

Maršík D., Masák J., Ulbrich P.

University of Chemistry and Technology, Prague, Technická 5, 166 28 Praha 6
marsikd@vscht.cz

Abstract

Due to the growing prevalence of highly resistant bacterial strains, there is an increasing need for new treatment approaches that would at least reduce the pressure on the development and use of antibiotics. Very promising is the quorum quenching strategy, which aims primarily to suppress pathogenicity without causing bacteriostatic or bactericidal effects. The principle consists in modulating the communication mechanism of quorum sensing, in which signalling compounds called autoinducers are produced and released in response to fluctuations in cell population density. After reaching a minimal threshold stimulatory concentration, these simple membrane diffusion molecules affect gene expression and phenotype, which are key to the ability of the bacterium to cause serious chronic infections. By finding quorum quenching agents, we could obtain a powerful tool in the treatment of bacterial infection caused by resistant strains.

One of the substances interfering with the bacterial quorum sensing system and antibiofilm activity is chitosan. Compared to chitosan, its nanoparticles have a higher surface charge density, which enhances the antimicrobial effect. Therefore, this work deals with the preparation and stability of chitosan nanoparticles as a promising antimicrobial agent.

Introduction

Chitosan is a natural polysaccharide obtained by deacetylation of chitin. Structurally, it is a copolymer composed of ß-1-4-linked D-glucosamine and *N*-acetyl-D-glucosamine units[1]. The properties of chitosan such as biocompatibility, biodegradability, and antimicrobial activity are used in biotechnology, pharmacy, food, and cosmetics industries[2]. In the form of nanoparticles, chitosan is one of the most studied conventional delivery systems for parenteral, oral ophthalmic drugs, vaccines, and nonviral genes. This system can improve stability or provide controlled release of active substance[3]. In addition to the use of chitosan as a drug carrier, its antimicrobial properties are also very promising. In the case of gram-positive bacteria, chitosan non-covalently interacts with the teichoic acids incorporated in the peptidoglycan, which are important in cell division, among others. In gram-negative bacteria, chitosan chelates bivalent ions of the outer membrane and electrostatically interacts with the anionic part of the lipopolysaccharide[4]. Moreover, chitosan has been reported to interfere with the quorum sensing system of bacteria such as the pathogenic bacterium *Pseudomonas aeruginosa*[5-6]. Since the antimicrobial effect of chitosan is strongly conditioned by the type of chitosan used[4], the nanoparticle form could enhance the antimicrobial effects due to the higher surface charge density[7].

Chitosan nanoparticles can be prepared by ionic gelation method, which is based on the formation of a complex between a positively charged amine group of chitosan and negatively charged polyanion[8]. The average hydrodynamic diameter of the resulting particles is strongly conditioned by the initial concentration and deacetylation degree of chitosan[9] but is also influenced by factors such as the molecular weight of chitosan, temperature, pH, ionic strength of the reaction medium and stirring speed[1]. The disadvantage of colloidal dispersion of chitosan nanoparticles is difficult to predict the system stability, which depends on the repulsive strength of the particles. If the repulsive forces of chitosan nanoparticles are not strong enough, they may form aggregates over time and gradually increase in size[10]. However, destabilization of the nanoparticle system can occur even after transferring the suspension to a culture medium that contains other components and has different properties such as pH, ionic strength, and temperature, which can induce aggregation[11]. The presence of aggregates during the determination of the effect of chitosan nanoparticles on planktonic bacterial growth could increase the optical density values leading to false positive results or affect the resulting antimicrobial effect.

Materials and methods

Materials

Low molecular weight chitosan with 75-85% degree of deacetylation and molecular weight 50-190 kDa (Sigma-Aldrich), sodium tripolyphosphate (Sigma-Aldrich), acetic acid (Penta), sodium acetate (Penta), deionized water.

Synthesis of chitosan/TPP nanoparticles

Chitosan nanoparticles were prepared by ionic gelation according to a modified procedure of Calvo et. al.[12]. Chitosan was first dissolved in 0.05M acetate buffer (pH 5 adjusted by acetic acid) to form a 0.5 mg/ml (w/v) solution. The chitosan solution was magnetically stirred (500 rpm) over night at room temperature. The result solution was then filtered through filter with 0.22 µm pore size to remove insoluble particles. Sodium tripolyphosphate was dissolved in deionized water at a concentration 0.5 mg/ml (w/v) and passed through 0.22 µm pore size filter. Then a TPP solution was added dropwise to a chitosan solution under magnetic stirring (700 rmp) at room temperature followed by 30 min. of continuous stirring (700 rpm). The final volume and optimal ratio of chitosan:TPP mixture were 25 ml and 9:1. The particles were stored at 4 °C under minimal light exposure.

Nanoparticles size, ζ potential and morphology

Mean hydrodynamic diameter, polydispersity index and ζ potential were measured at 25 °C by dynamic light scattering (DLS) on Zetasizer Nano (Malvern Panalytical). Three parallels of nanoparticles samples were measured three times as freshly prepared and after a week and month of storage in 4 °C. Prior to each measurement, the samples were tempered to 25 °C.

The morphological characteristics of the nanoparticles were examined using a transmission electron microscope (100kV JEOL JEM-1010, Japan). Samples were applied on copper carbon-coated electronmicroscopic grid and adhered for several minutes. The excess of solution was removed by tapping the grid on filtration paper and the grid (the adhered sample) was further contrasted by 1% uranyl acetate. The grid was inserted into TEM column and observed at acceleration voltage of 80 kV at various magnifications. Pictures were taken by Olympus SIS MegaView III CCD camera and software Analysis v 2.0.

Results and discussion

In this work, the characteristics and stability of chitosan/TPP nanoparticles prepared under specific conditions were studied. The reaction conditions were chosen with respect to previous works in which the ideal initial concentration of chitosan was in the range of 0.5 to 1 mg/ml[1,13-14]. A chitosan concentration of 0.5 mg/ml has been shown to be suitable for the preparation of stable nanoparticles with a low hydrodynamic diameter and polydispersity index (Table I). The lower concentration of chitosan provides an advantage in increasing intermolecular distance, which leads to a decrease in the intermolecular crosslinking between the chitosan molecules, while the crosslinking density between chitosan and TPP increases[1,15]. The selected reaction volumes of chitosan and TPP were chosen based on the morphology of the nanoparticles observed by SEM microscopy, where the nanoparticles in 9:1 ratio (chitosan:TPP) had a roughly spherical shape and narrow particle size distribution (Figure 1A) compared to a lower ratios leading to crosslinking and enlargement of the chitosan nanoparticles (Figure 1B). The inconsistency in the size values of chitosan nanoparticles between DLS and TEM is probably caused by the fact that the TEM gives the true diameter of the nanoparticles in the dry state while the chitosan nanoparticles swell in water and the DLS determine the hydrodynamic diameter[1]. Although nanoparticles with a ζ potential higher than 30 mV are considered stable colloidal suspension[16], there was no significant change in the properties of the prepared nanoparticles after a month of storage in 4 °C (Table I), which would indicate aggregation. This observation is in line with Jonassen et. al.[10] who reported that the presence of a monovalent salt prolongs the stability of the chitosan/TPP nanoparticles. Overall, these results indicate the suitability of using 0,05M acetate buffer pH 5 as a medium for the preparation of chitosan/TPP nanoparticles.

Table I

The characteristics of chitosan/TPP nanoparticles over time

period	mean hydrodynamic diameter [nm]	polydispersity index	ζ potential [mv]
24 hours	96 ± 4	0.28	22.2 ± 0.9
week	98 ± 5	0.29	23.8 ± 2.3
month	108 ± 7	0.29	24.7 ± 3.1

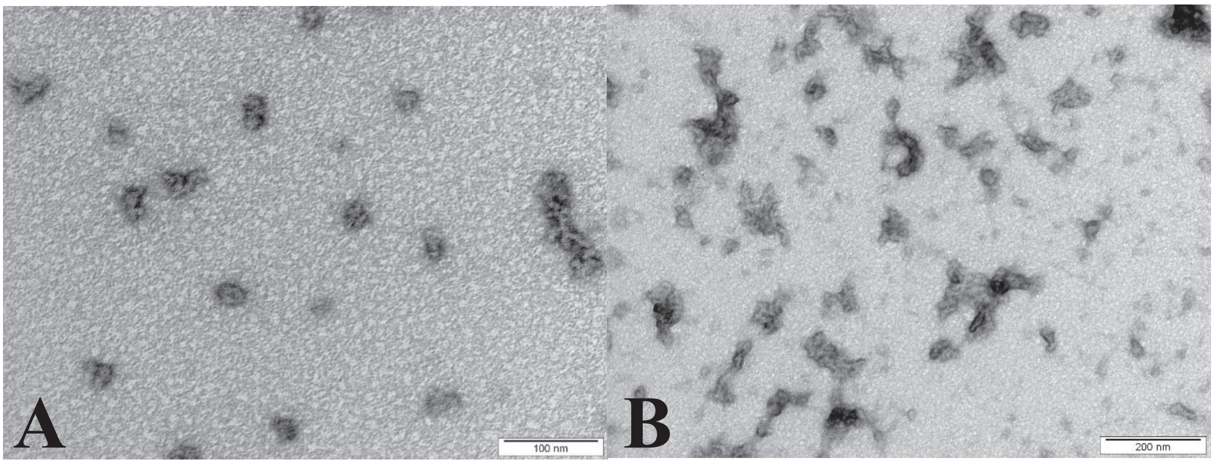

Figure 1. TEM images of chitosan/TPP nanoparticles: 1A – chitosan:TPP ratio 9:1; 1B – chitosan:TPP ratio 4:1.

Conclusion

The selected parameters for preparation of chitosan:TPP nanoparticles lead to the repeatable preparation of stable nanoparticles with mean hydrodynamic diameter of approximately 100 nm. Due to its small size and narrow particle size distribution, it is a suitable system for testing antimicrobial properties of chitosan nanoparticles. However, stability tests in the culture medium are required before the antimicrobial tests themselves.

Acknowledgement

This work was supported from the grant of Specific university research – grant No. A2_FPBT_2021_029 in the project application number from IGA.

References

1. Fan W., Yan W., Xu Z., Ni H.: Colloids and Surfaces B: Biointerfaces *90*, 21 (2012).
2. Raafat D., Sahl H.-G.: Microb Biotechnol *2*, 186 (2009).
3. Nagpal K., Singh S. K., Mishra D. N.: Chemical and Pharmaceutical Bulletin *58*, 1423 (2010).
4. Verlee A., Mincke S., Stevens C. V.: Carbohydrate Polymers *164*, 268 (2017).
5. Muslim S. N., Kadmy I., Ali A. N. M., Salman B. K., Ahmad M., Khazaal S. S., Hussein N. H., Muslim S. N.: International journal of biological macromolecules *107*, 52 (2018).
6. Paldrychová M.: *Dissertation thesis*. University of Chemistry and Technology, Prague 2019.
7. Ibrahim H. M., El-Bisi M. K., Taha G. M., El-Alfy E. A.: Journal of Applied Pharmaceutical Science *5*, 085 (2015).
8. Desai K. G.: Critical Reviews™ in Therapeutic Drug Carrier Systems *33*, (2016).
9. Sreekumar S., Goycoolea F. M., Moerschbacher B. M., Rivera-Rodriguez G. R.: Scientific reports *8*, 1 (2018).
10. Jonassen H., Kjøniksen A.-L., Hiorth M.: Biomacromolecules *13*, 3747 (2012).
11. Ozturk K., Arslan F. B., Tavukcuoglu E., Esendagli G., Calis S.: International journal of pharmaceutics *578*, 119119 (2020).
12. Calvo P., Remuñán-López C., Vila-Jato J. L., Alonso M. J.: Journal of Applied Polymer Science *63*, 125 (1997).
13. Vaezifar S., Razavi S., Golozar M. A., Karbasi S., Morshed M., Kamali M.: Journal of Cluster Science *24*, 891 (2013).
14. Jonassen H., Kjøniksen A.-L., Hiorth M.: Colloid and Polymer Science *290*, 919 (2012).
15. Berger J., Reist M., Mayer J. M., Felt O., Peppas N. A., Gurny R.: European Journal of Pharmaceutics and Biopharmaceutics *57*, 19 (2004).
16. Raval N., Maheshwari R., Kalyane D., Youngren-Ortiz S. R., Chougule M. B., Tekade R. K. *Basic Fundamentals of Drug Delivery,* Academic Press, Cambridge, 2019.

OPERON STRUCTURE INFERENCE IN *CLOSTRIDIUM BEIJERINCKII* NRRL B-589 USING RNA-SEQ

Schwarzerova J.[1], Musilova J.[1], Jureckova K.[1], Branska B.[2], Provaznik I.[1], Patakova P.[2], Sedlar K.[1]

[1]*Department of Biomedical Engineering, Faculty of Electrical Engineering and Communication, Brno University of Technology, Brno, Czechia*

[2]Department of Biotechnology, University of Chemistry and Technology Prague, Prague, Czechia
xschwa16@vutbr.cz

Abstract

Current operon structure inference relies on the utilization of online tools that provide predictions based on knowledge of the intergenic distance of neighboring genes as well as the functional relationships of their protein products. This approach is not sufficient for an accurate inference of operon structure as no information regarding co-expression of genes is considered. Moreover, such predictions are cumbersome in non-model organisms as relationships among their proteins are not known. The combination of wet lab data and data from web services using database searches can, however, greatly improve *in silico* inference of operon structure in individual bacterial or archaeal genomes. Current research in biotechnology is aimed mostly at non-model organisms for their various phenotypic traits. An example can be found in the strain *Clostridium beijerinckii* NRRL B-598, a non-model butanol producer whose phenotype still needs to be explained on the molecular level. We used the complete genome sequence of the strain (available from the NCBI GenBank database under the accession no. CP011966.3) and predicted the operon structure for its 5,442 total genes using the online tool, Operon-mapper. Subsequently, we took 3,351 predicted operons and verified their co-expression using data from our previous transcriptomic studies. These included 36 samples of genome-wide transcriptomes of the strain, under various conditions, gathered using RNA-Seq technology. Finally, we were able to adjust predicted operons according to their co-expression.

Introduction

Clostridium beijerinckii NRRL B-598, has huge potential in solving environmental challenges because it is known as a butanol producer [1]. However, this bacterium belongs to the group of non-model organisms and this strain remains to be described on the molecular level, that is, complex bioinformatics analysis for the inference of an *in silico* model for the bacterium is still unaccounted for. Nevertheless, the genomic sequences for non-model organisms can be determined rapidly at low costs, which is as a result of next-generation sequencing (NGS) technologies. NGS technologies have caused a paradigm shift in molecular biology [2]. This shift in molecular biology is accompanied by research that is focused on understanding *in silico* model functional relationships between individual genes causing the final phenotype.

However, the tools for operon structure inference are usually based only on searching databases and comparing already known operons and genomes derived from model organisms with unknown operons and genomes from non-model organisms. These algorithms [3,4,5] rely on the advanced methodology of machine learning and deep learning, but they do not include any of the gene expression information that is obtainable using RNA-Seq. In this study, we combine the predicted operon, using knowledge about the intergenic distance of neighboring genes as well as the functional relationships of their protein-coding products, through a machine learning approach and information regarding co-expression of genes from RNA-Seq data.

This study presents the operon structure inference in *C. beijerinckii* NRRL B-589 on a genome-wide scale. The operon structure inference in *C. beijerinckii* NRRL B-589 is the next step for final *in silico* model inference because knowledge of operon structures on a genome-wide scale represents indispensable information for understanding gene expression in this bacterium.

Materials and Methods

The co-expression analysis was used to investigate the relationship between two operons. The first operon structure was predicted using the Operon-mapper tool [5] and then gene co-expression information from RNA-Seq was added. Thus, the study allowed us to combine wet-lab experiments studying gene expression and *in silico* analysis for description, prediction, and simulation of operon structure in a genome-wide view. The genome from *C. beijerinckii* NRRL B-589 is available from the NCBI Genbank database under the accession number CP011966.3 [6].

RNA-Seq data

RNA-Seq data were taken from studies by Sedlar et al. [1,6] and Patakova et al. [7]. The RNA-Seq data were obtained from *C. beijerinckii* NRRL B-598 at time points for the purpose of covering the complete cell cycle and both metabolic phases, acidogenesis and solventogenesis of fermentation. Studies by Deslar et. al. [1] and Patakova et. al. [7] describes the standard cultivation transcriptome from *C. beijerinckii* NRRL B-598. Cell samples were taken from each bioreactor for RNA extraction at the selected time points: 3.5 h, 6 h, 8.5 h, 13 h, 18 h, and 23 h. B, C, D and E replicates were sequenced under the same conditions—these replicates represent standard cultivation transcriptomes. However, the B and C replicates [1] were obtained from a different study than the D and E replicates[7]. Replicates F and G represent butanol shock transcriptomes [6]. The sampling time points of butanol shock cultivation were 6 h, 6.5 h, 7 h, 8 h, 10 h, and 12 h. B2, C2, D2, E2, F1, and G1 samples were obtained from three different studies but under the same conditions and, therefore, we could anticipate these samples becoming a cluster.

The samples had been sequenced using Illumina NextSeq 500 technology. The raw sequencing data had been pre-processed using a data analysis pipeline obtained from GitHub – JanaSchwarzerova/Analytical-pipeline-rawRNA-Seq' [8]. To verify the correctness of the pre-processing part, a dimensionality reduction method based on principal component analysis and clustering and relying on the unweighted pair group method with arithmetic mean (UPGMA) was performed (see Figure 1).

Figure 1 shows clusters formed by samples sequenced under the same conditions. Specifically, the B2, C2, D2, E2, F1, and G1 samples formed a single well-distinguished cluster, and this was considered a fulfillment of theoretical prerequisites. The clusters were also visualized using UPGMA clustering methods, as shown in Figure 1 (B).

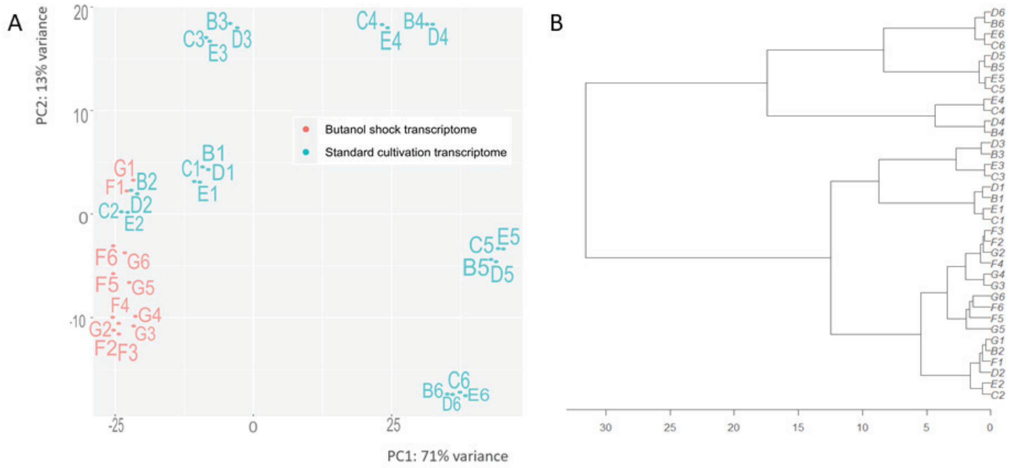

Figure 1. (A) represents principal component (PC) analysis from all time-points (T1-T6) samples of RNA-Seq replicates which have been provided. (B) represents tree clustering structure rely on Euclidean distance between PC1 and PC2. B, C, D, E replicates were sequenced under the same conditions, these replicates represent standard cultivation transcriptomes.

Methodology

This study presents the first overall operon structure in the strain *C. beijerinckii* NRRL B-598 inferred using an advanced methodology that relies on a combination of machine learning and RNA-Seq data processing. The machine learning approach was performed using Operon-mapper [5] and was followed by processing gene expression information obtained from RNA-Seq data.

Figure 2 represents the pipeline of the whole methodology that was implemented for RNA-Seq data from *C. beijerinckii* NRRL B-598. The first section relied on the genome sequence, which was taken as input data for the Operon-mapper tool. The Operon-mapper [5] is an open-source tool in a web server that predicts the operons of any bacterial or archaeal genome sequence. Operon-mapper is based on an artificial neural network (ANN). The Operon-mapper was tested on a set of experimentally defined operons as operons in model organisms, for example*, Escherichia coli* or *Bacillus subtilis*. ANN has inputs that are the intergenic distance of contiguous genes and detect the functional relationships between their protein products. The following implementation, based on the reformatting of the Operon-mapper output to a table, includes serial numbers by operon and gene expression information in *.csv* format. In this step, we found five genes that Operon-mapper excluded from the overall analysis. Specifically, these genes have locus tags X276_26845, X276_26885, X276_26930, X276_26935, and X276_27400. Therefore, these five genes have been marked as operons that include only one specific gene.

The second section of the whole methodology includes adding gene expression information. The study used a principle based on the Operon-expresser algorithm from a study by Schwarzerova [9]. The Operon-expresser algorithm is based on finding the gene expression value of one gene and the gene expression value from the upstream or downstream genes in sequence. The correlation coefficient between these genes is then calculated. If the correlation coefficient exceeds the selected threshold, and the distance between these genes is lower than a defined threshold distance in bp, the algorithm assumes that it is one operon, and these genes are concatenated. However, there are different thresholds to those that were used in the study by Schwarzerova [9]. These thresholds were 5,000 bp for threshold distance and 80% for the correlation coefficient.

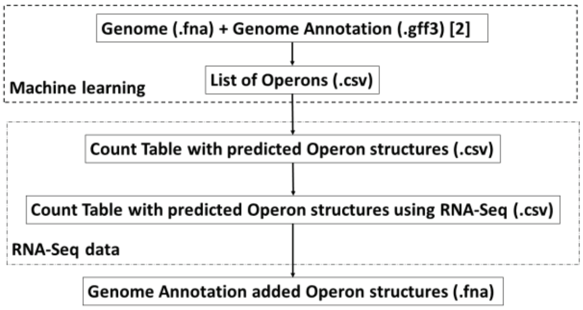

Figure 2. Pipeline of methodology represents step by step pipeline of advanced methodology for inference operon structures.

Figure 2 has the last part of the pipeline represented as a box called genome annotation with added operon structures. This box is the output of the methodology pipeline that represents innovated genome annotation for *C. beijerinckii* NRRL B-598. The genome annotation of *C. beijerinckii* NRRL B-598 contains operon structures and is available from the NCBI Genbank database under the accession number CP011966.3. The results were visualized through interconnected approaches based on the DNAPlotter tool [10], which is included in the Artemis tool, [11] and the Sunburst graph created by R/sunburstR package (see Figure 3).

Results and Discussion

The innovated methodology for genome-wide inference based on RNA-Seq data greatly improves *in silico* inference of operon structure in individual bacterial or archaeal genomes because these data consider information regarding co-expression of the gene. The study used the complete genome sequence of the strain, available from the NCBI GenBank database under accession no. CP011966.3 and predicted the operon structure for its 5,442 total genes using the online tool, Operon-mapper [5]. The operon structure inference by Operon-mapper resulted in 3,351 predicted operons. Significantly, these operon structures do not include any information about genes such as X276_26845, X276_26885, X276_26930, X276_26935, and X276_27400. X276_26845 represents the *ssrA* gene that produces transfer-messenger RNA. X276_26885 and X276_26930 represent the *ssrS* gene that codes 6S RNA, *ssrS*. X276_26935 and X276_27400 are *ffs* genes encoding signal recognition particle sRNA in a large number. All the above-mentioned genes have been marked as operons that include only one specific gene.

Subsequently, we took 3,351 predicted operons and verified their co-expression using data from our previous transcriptomic studies. These include 36 samples of genome-wide transcriptomes of the strain under various conditions, gathered using RNA-Seq technology (see Figure 1). These transcriptomic data had been pre-processed for the purpose of creating a count table, and according to their co-expression had been able to adjust predicted operons.

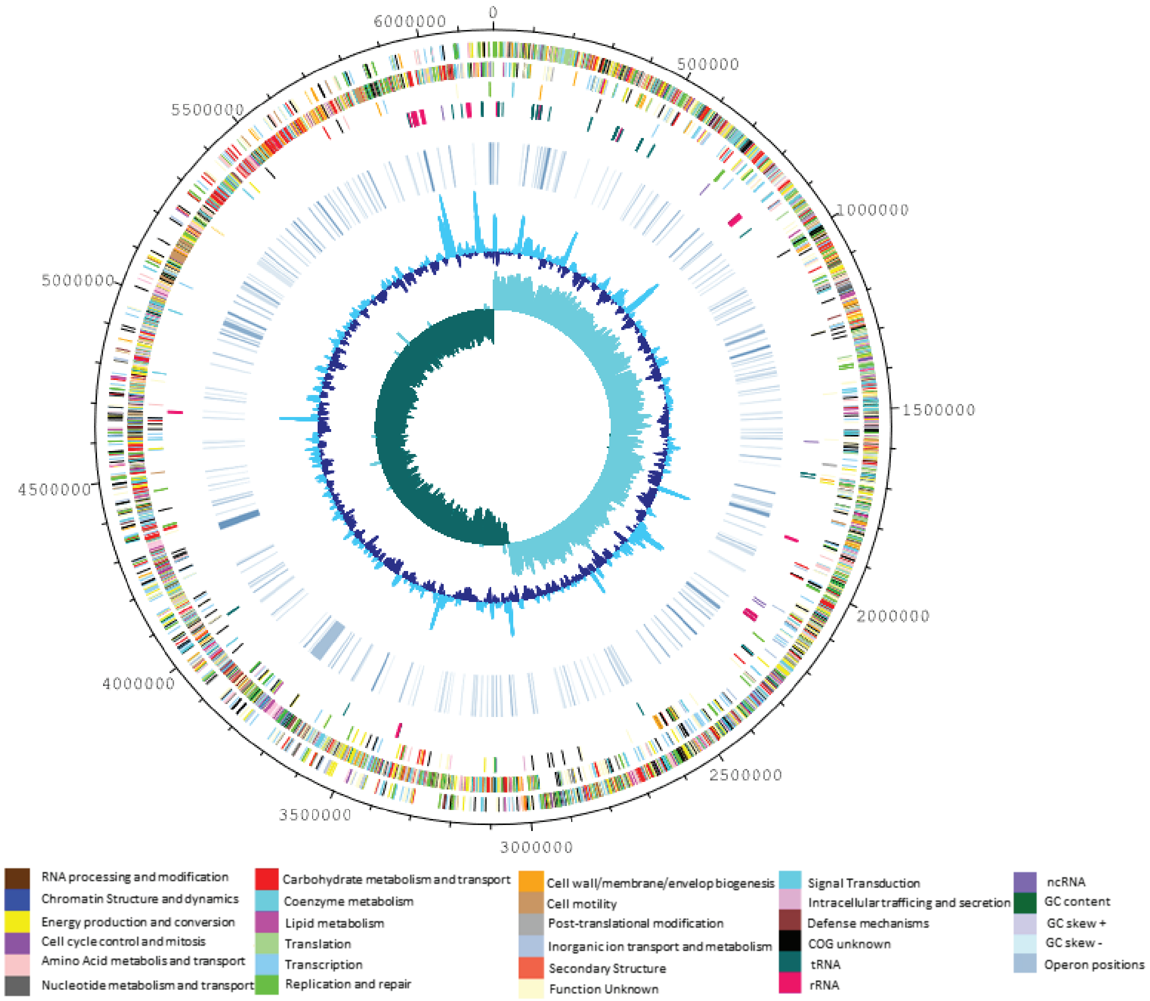

Figure 3. The circular genome of *C. beijerinckii* NRRL B-598 included 5,294 CoDing Sequences (CDSs) represent the protein-coding genes classified to COG into 22 categories. There are also tRNA, rRNA, and ncRNA categories display in the fourth outermost circle. The middle circle marked as Operon positions represent end positions of found operon structures, that are longer than 4,936 bp, created as sunburst graph.

The analysis inferred that the *C. beijerinckii* NRRL B-598 genome consists of 2,752 operons (see Figure 3). Figure 3 shows the position of individual features in the circular genome. In total, 5,294 CDSs represent the protein-coding genes classified, according to the COG database, into 22 categories. RNAs are divided into tRNA, rRNA, and ncRNA categories and displayed in the fourth outermost circle. The dashed middle circle represents the end positions of found operon structures. The visualization of operon structures is filtered for greater informative value. Thus, the dashed middle circle represents operons that are longer than 4,936 bp. The smallest visualized operon is tagged as operon_2720. The operon_2720 includes five protein-coding genes tagged as X276_00370, X276_00365, X276_00360, X276_00355, and X276_00350 and its length is only 4,936 bp. The longer operon is operon_1695, and its length is 47,053 bp. This operon includes 22 protein-coding genes. This circle has been created as a Sunburst graph and connected with Artemis analysis.

The genome-wide operon structure's inference creates new advantages for gene expression analysis. The biggest advantage is the possibility of creating *in silico* models including more specific information about gene expression. Another advantage is the possibility for discussion and analysis of any operon contained in the analyzed genome.

Sol operon

Sol operon was chosen for the verification and demonstration of accuracy because it is the most studied operon in solventogenic clostridia. The structure of sol operon is detected in a range from 4,539,361 bp to 4,542,991 bp. This operon is formed by four genes, and the operon tag is operon_2073. These four genes are *ald, ctfA, ctfB,* and *adc*.

The main property of the operon-expresser algorithm is to divide operons in the absence of linear dependence in added gene expression information. It reflects the specification of the boundaries between the individual operons relying on gene expression information from RNA-Seq. Owing to this, we positively confirmed the position for sol operon in *C. beijerinckii* NRRL B-598, and further evidence has been created for plots to represent gene expression information at individual time points. This can be considered a fulfillment of theoretical prerequisites, connecting with verification of sol operon analysis following gene co-expression (see Figure 4).

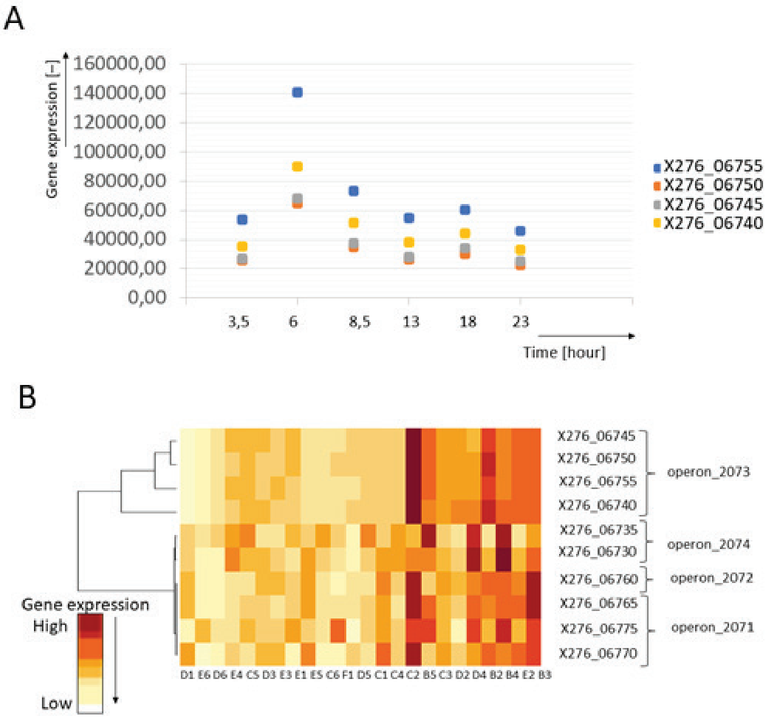

Figure 4. (A) represents gene expression level at individual time-points from standard cultivation. (B) shows heat maps for *sol* operons and its neighbors where it was reconfirmed co-expression gene in *sol* operons, again.

Figure 4 shows four genes tagged as X276_06755, X276_06750 X276_06745, and X276_06740. These tags represent previously mentioned genes in the same order as *ald, crfA, ctfB,* and *adc*. Figure 4 (A) shows that the maximum of gene expression is detected for *ald* and the minimum for *ctfA* and *ctfB*. The subunits *ctfA* and *ctfB* represent enzymes responsible for the re-assimilation of acids that are catalyzed by CoA-transferase. CoA-transferase fulfills the role of transfer CoA from acetoacetyl-CoA to acetate or butyrate.

Conclusion

NGS technologies have caused a paradigm shift in molecular biology and, as a result, research in molecular biology is focused on understanding the use of *in silico* model functional relationships between individual genes causing the final phenotype. However, many microorganisms with huge ecology and biotechnology research potential, such as *C. beijerinckii* NRRL B-598, are not sufficiently described for inferring *in silico* modeling. The correct way for creating an *in silico* model leads over annotated all structures in a genome included gene regulation information. The most important structures are operons that describe gene expression in a genome.

The main benefit of this study is genome-wide inference of operon structure in *C. beijerinckii* NRRL B-598. The operon structure was inferred using advanced tools, through a machine learning approach and considering gene expression information. The results were obtained by this innovative *in silico* tool. The study also contains an analysis of gene expression information in time-series datasets for sol operon tagged as operon_2073, formed by four individual genes. The analysis revealed that the *C. beijerinckii* NRRL B-598 genome consists of 2,752 operons. These operon structures are included in the NCBI Genbank database under the accession number CP011966.3.

Acknowledgement

Computional resources were provided by the CESNET LM2015042 and the CERIT Scientific Cloud LM2015085, provided under the programme "Projects of Large Research, Development, and Innovations Infrastructures

References

1. SEDLAR K, Koscova P, Vasylkivska M, Branska B, Kolek J, Kupkova K, Patakova P, Provaznik I. *Transcription profiling of butanol producer Clostridium beijerinckii NRRL B-598 using RNA-Seq.* 2018.
2. VAN DIJK, Erwin L., Auger H, Jaszczyszyn Y, Thermes C. *Ten years of next-generation sequencing technology*. *Trends in genetics*, 2014, 30.9: 418-426.
3. Assaf, R., Xia, F. & Stevens, R. *Detecting operons in bacterial genomes via visual representation learning*. Sci Rep 11, 2124 (2021). https://doi.org/10.1038/s41598-021-81169-9
4. Huansheng Cao, Qin Ma, Xin Chen, Ying Xu, DOOR: a prokaryotic operon database for genome analyses and functional inference, *Briefings in Bioinformatics*, Volume 20, Issue 4, July 2019
5. TABOADA B, Estrada K, Ciria R, Enrique M. *Operon-mapper: a web server for precise operon identification in bacterial and archaeal genomes*. *Bioinformatics*, 2018, 34.23: 4118-4120.
6. SEDLAR K, Kolek J, Gruber M, Jureckova K, Branska B, Csaba G, Vaslkivska M, Zimmer R, Patakova P, Provaznik I. et al. *A transcriptional response of Clostridium beijerinckii NRRL B-598 to a butanol shock*. 2019.
7. PATAKOVA P, Branska B, Sedlar K, Vasylkivska M, Jureckova K, Kolek J, Koscova P, Provaznik I. *Acidogenesis, solventogenesis, metabolic stress response and life cycle changes in Clostridium beijerinckii NRRL B-598 at the transcriptomic level.* 2019.
8. SCHWARZEROVÁ, J. *Reproducible analytical pipeline for using raw RNA-Seq data from non-model organisms.* Proceedings of the 26th Conference STUDENT EEICT 2020, 2020. ISBN: 978-80-214-5867-3.
9. SCHWARZEROVÁ, J. Operon-expresser: *The innovated gene expression-based algorithm for operon structures inference.* Proceedings of the 27th Conference STUDENT EEICT 2021, 2021. ISBN: 978-80-214-5942-7. (Accepted for publication)
10. CARVER, Tim, Thomson N, Bleasby A, Berriman M, Parkhill J. DNAPlotter: circular and linear interactive genome visualization. *Bioinformatics*, 2009, 25.1: 119-120.
11. RUTHERFORD K, Parkhill J, Crook J, Horsnell T, Rice P, Rajandream M-A, Barrell B. *Artemis: sequence visualization and annotation*. *Bioinformatics*, 2000, 16.10: 944-945.

EFFECTS OF FURAN DERIVATIVES AND PHENOLIC COMPOUNDS ON ABE PRODUCTION BY *CLOSTRIDIUM BEIJERINCKII*

Heřmanová K.[1], Branská B.[1]

[1]*University of Chemistry and Technology Prague, Technická 5, 166 28, Czech Republic*
hermanoe@vscht.cz

Abstract

Solventogenic clostridia can be used in solvent production via the acetone-butanol-ethanol pathway (ABE fermentation) and lignocellulosic biomass (LB) might serve as a cheap and renewable waste substrate for it. However, solvent production from LB is negatively affected by the inhibitory compounds formed during the pretreatment, in particular, furan derivatives and phenolic compounds which are generated during acidic and alkali hydrolysis, respectively. The aim of this study was to determine the effects of furfural, 5-hydroxymethyl furfural, coumaric acid, and ferulic acid on the growth and production of ABE by two different strains of *Clostridium beijerinckii.* The concentrations unambiguously negatively influencing both growth and production of strains were 3 $g.l^{-1}$ for furfural and 5-hydroxymethylfurfural, 1 $g.l^{-1}$ for ferulic acid, and 0.6 $g.l^{-1}$ for coumaric acid. It was also shown that addition of lower concentrations had a stimulating effect, where production or both production and growth were improved comparing to the control experiment.

Introduction

At present, given the global problems related to environmental pollution, there is an increasing interest in searching alternatives to fossil fuels. Particular attention is paid to biobutanol. Butanol is primarily used as a solvent, but has a potential as biofuel[1] or precursor in chemical synthesis. Unfortunately, the “green” technology is still unable to compete with utilization of fossil fuels because of few drawbacks of the process, such as high price of substrates used in microbiological synthesis or energy intensive separation techniques due to low yields of biotechnological production.

Butanol can be produced by microorganisms via fermentation, where butanol is commonly produced together with other two solvents, acetone and ethanol in a process known as ABE fermentation[2]. In this anaerobic process, solventogenic bacteria of the genus *Clostridium* can convert fermentable sugars to acids and then to the solvents. It was shown that solventogenic clostridia are able to utilize various waste materials[3], therefore have a great potential in sustainable chemicals production. The most common waste material which can be used for biobutanol production using species of solventogenic *Clostridium* is lignocellulose biomass (LB). However, LB has very recalcitrant structure that must be released first to enable access of enzymes to its components: cellulose, hemicellulose and lignin. Thus, enzymatic hydrolysis is preceded by pretreatment of lignocellulosic biomass (most often chemical or physical), which is an inevitable step. However, during pretreatment process degradation products are formed - two significant groups of these inhibitors are derived based on type of pretreatment: acidic environment promotes formation of furan derivatives, furfural and hydroxymethyl furfural, and alkali conditions leads predominantly to the formation of phenolic substances such are e.g. ferulic acid, coumaric acid, vanillic acid, syringaldehyde, and many others. Presence of these inhibitors generally reduce the yield of the fermentation process[4] even though in some cases stimulation effect was observed[5,6]. In this work, effect of furan and phenolic inhibitors was studied on growth and production of solvents by two solventogenic clostridial strains, namely *Clostridium beijerinckii* NRRL B598 and *Clostridium beijerinckii* NCIMB 8052.

Materials and methods

Microorganisms and medium

Two solventogenic strains *Clostridium beijerinckii* NCIMB 8052 and *Clostridium beijerinckii* NRRL B-598 were used. Strains were stored in distilled water in a form of spore suspension at 4 °C.

TYA medium, which was used as a fermentation medium, contained: glucose – 20 $g.l^{-1}$, yeast extract – 2 $g.l^{-1}$, tryptone – 6 $g.l^{-1}$, KH_2PO_4 – 0.5 $g.l^{-1}$, ammonium acetate – 3 $g.l^{-1}$, $MgSO_4.7H_2O$ – 0.3 $g.l^{-1}$, $FeSO_4.7H_2O$ – 0.01 $g.l^{-1}$. pH of the medium was adjusted to 6.8 with 1 M NaOH solution. The medium was sterilized in an autoclave for 20 minutes at 121 ° C.

Inoculum preparation

Prior to inoculation, the spore suspension was heated to 80 °C for 2 minutes and vortexed. Subsequently, heat treated spores were transferred to an Erlenmeyer flask with 100 ml of TYA media and culture was cultivated in an anaerobic chamber under a N_2 atmosphere at 37 °C for 24 hours.

Determination of minimum inhibitory concentration

The effect of two furan derivatives (furfural and 5-hydroxymethyl furfural (HMF)) and two phenolic compounds (ferulic acid and coumaric acid) was tested.

The minimum inhibitory concentrations (MIC) of tested inhibitors was determined using microtiter plates; 200 µl TYA medium containing 20 mg.l^{-1} of bromocresol purple, which served as an indicator of acidic metabolites formation, was pipetted to all wells. Then inhibitors (separately for each inhibitor) were added into the wells in increasing concentrations. For furfural and HMF the tested concentration range was 0-6 g.l^{-1}, for ferulic and coumaric acid 0-4 g.l^{-1}. TYA medium without inhibitor was used as a control. Finally, 20 µl of inoculum was pipetted into each well. Microtiter plates were cultivated in an anaerobic chamber under a stable N_2 atmosphere at 37 °C for 24 h. The growth of culture was evaluated based on change in color of bromocresol purple indicator. The color of the medium was purple at the beginning of the cultivation due to the neutral pH of the medium. In the wells where growth of the strain occurred, purple color gradually changed to yellow as a result of pH decrease due to acid production. On the contrary, the wells, which remained purple, indicated inhibition.

Determination of biomass concentration

Concentration of cells was determined as optical density (OD_{600}) of culture broth after fermentation at 600 nm using a Varian Cary 50 spectrophotometer (Agilent, USA). TYA medium was used as a blank.

Analysis of glucose and fermentation products

Samples were centrifuged at 10.000 rpm for 2 minutes and filtered through a 0.2 µm pore size filter into vials prior HPLC analysis. Samples were analyzed on an Agilent Technologies HPLC liquid chromatograph 1200 series (USA) with refractive index detection. The flow rate of the mobile phase was 1 ml.min^{-1}, injection volume was 20 µl and analysis time was 40 minutes. A solution of 5 mM sulfuric acid was used as a mobile phase. A column with stationary phase of Polymer IEX H from 8 µm (Watrex) was used.

Results and discussion

The first experiment was carried out for wider range of concentrations of all inhibitors in order to determine the minimum inhibitory concentrations for both strains and all inhibitors. Concentrations inhibiting fully the growth and metabolite formation are shown in Table I.

Table I

Minimum inhibitory concentrations (MIC) of tested inhibitors

Inhibitor	MIC for *Clostridium beijerinckii* NCIMB 8052 [g.l^{-1}]	MIC for *Clostridium beijerinckii* NRRL B-598 [g.l^{-1}]
Furfural	4.0	3.0
HMF	3.0	4.0
Ferulic acid	1.0	1.0
Coumaric acid	0.6	0.6

Based on the specified MIC values, range of concentrations applied in following experiments was decreased and narrowed. Furan derivatives were tested in the range of 0-4 g.l^{-1} or 0-3 g.l^{-1}. Ferulic acid and coumaric were tested in the range of 0-1 g.l^{-1} and 0-0.6 g.l^{-1} resp., for both strains.

The effect of inhibitors on growth and production of *C. beijerinckii* NRRL B-598 and *C. beijerinckii* NCIMB 8052 was evaluated after 24 h of cultivation. The results for the strain *C. beijerinckii* NCIMB 8052 are shown in the Fig. 1, for the strain *C. beijerinckii* NRRL B-598 in the Fig. 2.

For strain *C. beijerinckii* NCIMB 8052, gradual decrease in optical density was observed for both furfural and HMF comparing to control and with increasing concentration of inhibitors, while the effect on ABE production was apparently different. ABE production was stimulated up to 3 g.l^{-1} for furfural and up to 1 g.l^{-1} for HMF. HMF concentration of 2 g.l^{-1} resulted in comparable production with the control. The similar trend was observed for coumaric acid addition where biomass formation was negatively influenced but low concentration of 0.3 g.l^{-1} coumaric acid stimulated ABE production. In case of ferulic acid a stimulating effect was observed for both cell growth and ABE production at concentrations up to 0.6 $g.l^{-1}$. A significant decrease in optical density and ABE production occurred at 0.6 $g.l^{-1}$ for coumaric acid, for ferulic acid at 1 $g.l^{-1}$, which indicates a lower tolerance of the strain to coumaric acid. Interestingly, the residual glucose concentration does not always correspond to production characteristics which suggest that positive effect of low concentration of furfural, HMF and coumaric acid might be also in increasing a yield of solvents from glucose.

For strain *C. beijerinckii* NRRL B-598 (see Fig. 2), in contrast to the *C. beijerinckii* strain NCIMB 8052, furfural added in low concentrations up to 2 $g.l^{-1}$ (including) stimulated both growth and solvent production. HMF addition inhibited the biomass formation from the lowest tested concentration of 2 $g.l^{-1}$, but ABE production was slightly stimulated at this value. The observed stimulatory effect of furan derivatives at low concentrations is in agreement with previous research with other strains of *Clostridium beijerinckii*[5,7].

Coumaric acid and ferulic acid had a comparable to *C. beijerinckii* NCIMB 8052 effect on the strain *C. beijerinckii* NRRL B-598, even though both strains exhibited stimulated cell growth and solvent production at low concentrations of inhibitors added, coumaric acid also appeared to be more toxic for this strain. These results are in agreement for those obtained in research for *Clostridium saccharoperbutylacetonicum* N1-4[6].

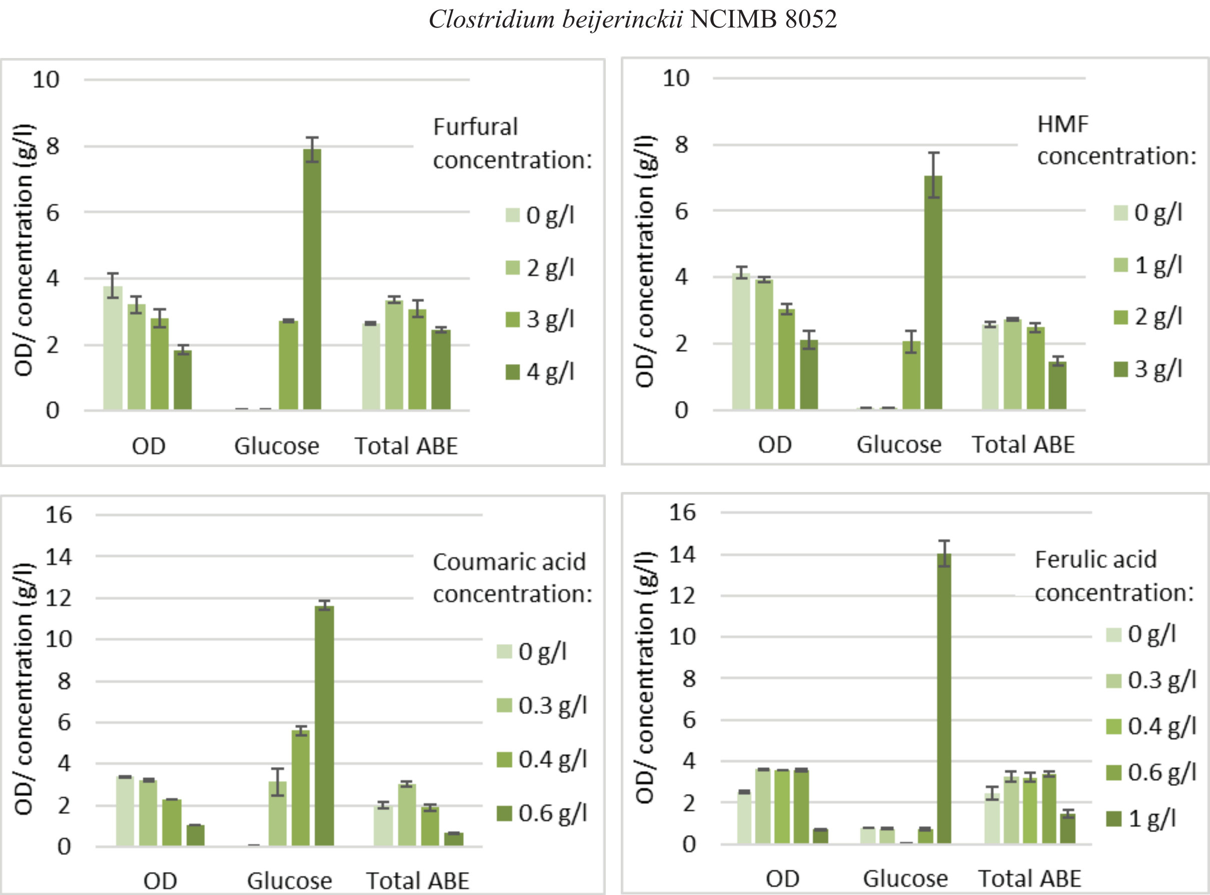

Clostridium beijerinckii NCIMB 8052

Figure 1. Effects of furfural, 5-hydroxymethyl furfural (HMF), coumaric acid and ferulic acid on biomass concentration, glucose consumption and total ABE production (aceton, butanol, ethanol) by C. beijerinckii NCIMB 8052 after 24 h cultivation

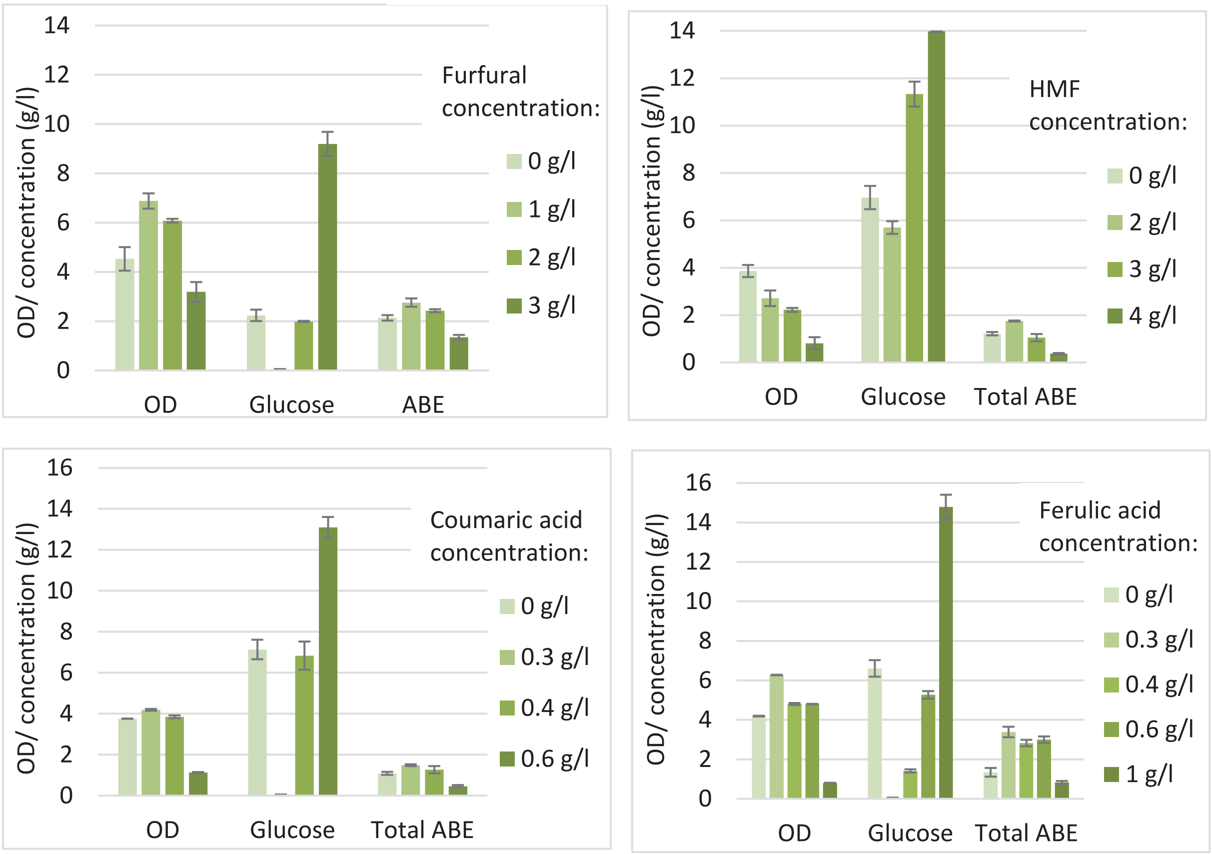

Clostridium beijerinckii NRRL B-598

Figure 2. Effects of furfural, 5-hydroxymethyl furfural (HMF), coumaric acid and ferulic acid on biomass concentration, glucose consumption and total ABE production (aceton, butanol, ethanol) by C. beijerinckii NRRL B-598 after 24 h cultivation

Conclusion

Furfural had an inhibitory effect on cell growth from the lowest tested concentration 2 g.l^{-1} for strain *C. beijerinckii* NCIMB 8052, for strain *C. beijerinckii* NRRL B-598 furfural at low concentrations had an opposite effect. Total ABE production was stimulated by furfural addition at low concentrations in both strains, inhibition occurred at 3-4 g.l^{-1}. 5-hydroxymethyl furfural inhibited the growth of both strains from 2 g.l^{-1} including, ABE production from 3 g.l^{-1} including. Addition of lower concentrations stimulated ABE production in both strains.

The stimulating effect of ferulic and coumaric acid at low concentrations was recorded for both growth and solvent production of both strains. Inhibition of growth and ABE production by coumaric acid was observed at 0.6 g.l^{-1}, ferulic acid had an inhibitory effect on cell growth as well as butanol production from 1 g.l^{-1}.

The observed stimulatory effect of inhibitors is interesting mainly in relation to the potential utilization of lignocellulose hydrolysate prepared under mild conditions. Such conditions might be both environmentally friendly and produce only a low amount of inhibitory substances so that utilization of such hydrolysates might be more beneficial than the use of pure sugar sources. Nevertheless, as was shown in this study the gap between stimulating and negative effects is narrow. Therefore, the stimulating range should be robustly defined especially taking into account that the inhibitory substances in real hydrolysates are present in various combinations, which may have a synergistic effect.

References

1. Vasylkivska M., Patáková P.: J. Biotechnol., *320*, 17 (2020).
2. Jones D.T., Woods D.R.: Microbiol. Rev., *50*, 484 (1986).
3. Branská B., Fořtová L., Dvořáková M., Liu H., Patáková P., Zhang J., Melzoch M.: Renew. Energy, *145*, 1941 (2020).
4. Jonsson L.J., Martin C.: Bioresour. Technol., *199*, 103 (2016).

5. Ezeji T., Qureshi N., Blaschek H.: Biotechnol. Bioeng., *97*, 1460 (2007).
6. Yao D., Dong S., Wang P., Chen T., Wang J., Yue Z-B.: Fuel., *208*, 549 (2017).
7. Qureshi N., Bowman M.J., Saha B.C., Hector R., Berhow M.A., Cotta M.A.: Food Bioprod. Process., *90*, 533 (2012).

BIODIVERSITY OF PROKARYOTES FROM RADON SPRINGS IN JÁCHYMOV

Timkina E.[1], Kolouchová I.[1], Maťátková O.[1]

[1]*UCT in Prague, Czech Republic*
Timkinae@vscht.cz

Abstract

Bacteria and archaea are ubiquitous organisms whose occurrence is limited only by extremely inhospitable conditions. Radon springs are an example of an extreme environment, but their microbiome is poorly studied. Microorganisms in radon springs are exposed to abiotic factors, ie presence of ionizing radiation and heavy metals. Radon springs in Jáchymov are unique with their extremely high radon content. Radon is a source of alpha radiation, which can cause the formation of reactive oxygen species and damage biomacromolecules. Adaptation to stress conditions is essential for the survival of microorganisms in the spring water source environment. In this work, dozens of bacterial isolates were obtained from radon springs in Jáchymov. Ten bacterial isolates were selected for further characterisation. The work with isolates was focused on studying the extent of bacterial strains resistance to ionizing UVC radiation.

Introduction

Wide range of live forms can be found in common habitats which are rich in nutrients and provide optimal growth conditions for numerous bacterial species. Nevertheless, bacterial growth is known to be limited only by some drastic environmental conditions, e. g. extreme pH, temperatures, extremely low water activity or drastically high radiation levels. Taking this into account, we can anticipate finding established bacterial communities even in the most unexpected places [1].

Subterranean water reservoirs represent unique and poorly studied habitats. Up to date, there is not much information available of such subsurface environments and specifically about potential energy and carbon sources in such niches, but scientific interest in the microbiology of subterranean environments has been rising during past decades [2-4]. These subterranean waters often display high mineral concentrations, high temperatures or unique mineral composition. Radon springs are mineral springs with high concentration of dissolved radon. Radon itself is a radioactive element naturally occurring as part of the thorium and uranium decay chains resulting in formation of lead [5]. High levels of ionizing radiation can cause formation of numerous reactive oxygen species formation as well as direct damage to all types of biomolecules [6,7]. Bacteria thriving in localities exposed to ionising radiation are expected to develop adaptation mechanisms helping them to sustain cellular integrity in those conditions [7].

Jachymov, a spa town in the Karlovy Vary Region of the Czech Republic, is known for its radon mineral springs. A cluster of 4 springs with temperatures up to 36 °C provide about 22 m^3 of mineral water per hour. Activities of dissolved radon reach up to 20 kBq/l, making springs in Jachymov one of the top radon springs in the world [2,8,9]. The water of the springs is collected in such a way that nearly no surface water can mix with the spring water, which is distributed to the spa hotels [10]. Nowadays spa is located on the site of former Svornost mine. During the 16th century, the Svornost mine was used for silver mining. From the middle of the 19th century uranium ore became the main mined mineral. The main boom in uranium mining occurred after 1945 and lasted until 1962. As early as the beginning of the 20th century, it was found that some of the underground water springs found in the mine have a high radon content and that they have a positive effect on the treatment of various diseases or injuries. Based on this, the first radon baths were established in 1906 [10].

In this study culture-based methods were used to obtain bacterial isolates from Jachymov water samples. Physiological studies of selected bacterial isolates were conducted to evaluate level of resistance to UV radiation and free radicals. As a possible defence mechanism total antioxidant capacity was evaluated.

Experiment

Collection and Cultivation

Samples were collected from four springs (Agricola, Behounek, C1, and Curie) in Jachymov, Czech Republic. Sterile 50 mL Falcon tubes were used for the sampling. Falcon tubes were prefilled with small amount of LB broth (Luria–Bertani). Water was obtained under sterile conditions as close to the discharge as possible. The samples were then transported back to laboratory and incubated on rotary shakers (150 rpm) at temperatures 30 °C (samples from Agricola, C1 and Curie) or 37 °C (samples from Behounek), the cultivation temperatures were supposed to be matching with the water temperature of the springs. After sufficient cultivation time, samples were inoculated onto different agar plates for isolation. For agar preparation water from the respective spring was used. Agar plates were prepared as follows: agar medium prepared by dissolving glucose (0.2%) and bacteriological agar (2.3%) in filtered spring water; Reasoner's 2A (R2A) agar; lactate (0.5%) agar medium; and pure noble agar (1.8%) medium. The plates were incubated at 30 °C (Agricola, C1, and Curie) or 37 °C (Behounek) for 1 week. Several distinct colonies with different morphologies were transferred from the above agar plates to plate count agar (PCA) plates and incubated at 30 or 37 °C for 24 h for further isolation and purification [11].

Survival of isolates under multiple-stress condition

Ten bacterial isolates were selected for further characterisation. Pure cultures of isolates were obtained after 72 hours cultivation in half diluted TSB broth (tryptone soya) on rotary shakers (150 rpm) at temperatures 30 °C. Cultures were harvested by centrifugation (10000×g, 10 minutes) and washed with physiological solution three times. For the test itself bacterial culture of optical density 0.5 (OD 600_{nm}) in sterile half diluted TSB broth was prepared. Four millilitres of each sample were transferred to a sterile petri dish and were exposed to UV irradiation (254 nm) at 45 cm from a UV-C lamp (OSRAM HNS 30W G13) [12]. Doses of radiation applied were as follows: 7.3 kJ/m^2 (20 minutes), 14.6 kJ/m^2 (40 minutes) and 21.9 kJ/m^2 (60 minutes). After every 20 minutes irradiation was stopped, and samples were shaken to prevent precipitation. Controls were obtained by incubating bacteria without UV radiation (0 minutes). Aliquots of 0,1 ml were transferred to a polystyrene microplate with 0,2 ml of half diluted TSB in each well. Survival rate was evaluated as optical density after 48 h of cultivation in a microplate in each well determined using a microtiter plate reader (TECAN reader).

To study growth in presence of free radicals bacterial samples (0.02 ml) were cultivated in half diluted TSB broth (0.18 ml) supplemented with H_2O_2 to reach 0 – 5 % (equivalent to 0 - 1.46 M). Survival rate was evaluated as optical density after 48 h of cultivation in a microplate [12,13].

Antioxidant capacity

The antioxidant activities were determined using DPPH as a free radical. Isolates were cultivated for 7 days in half diluted TSB broth (tryptone soya) on rotary shakers (150 rpm) at temperatures 30 °C. Afterwards suspensions were centrifugated and supernatants were further analysed. Supernatant (0.2 ml) was added to 0.1 ml DPPH dissolved in methanol (5.2 mg/l). The decrease in absorbance was determined at 515 nm after 15 min incubation in dark [14].

Results and Discussion

Ten bacterial isolates were picked based on colour of colonies at the agar plates. Red and yellow pigmented isolates were preferred due to common train of radiation resistant microorganisms to produce carotenoid pigments as a defence mechanism [15,16]. Studied isolates were obtained in collaboration with doc. Ing. Ondřej Uhlík, Ph.D. and Ing. Gabriela Kapinusová. Following isolates (Table I) were selected for this study:

Table I

Isolates selected for the study

Isolated from spring	Designated number
Agricola Temperature 29 °C	138
	161
	190
Behounek Temperature 36 °C	238
	277
C1 Temperature 29 °C	318 A
	318 B
	370
Curie Temperature 29 °C	402
	4009-2

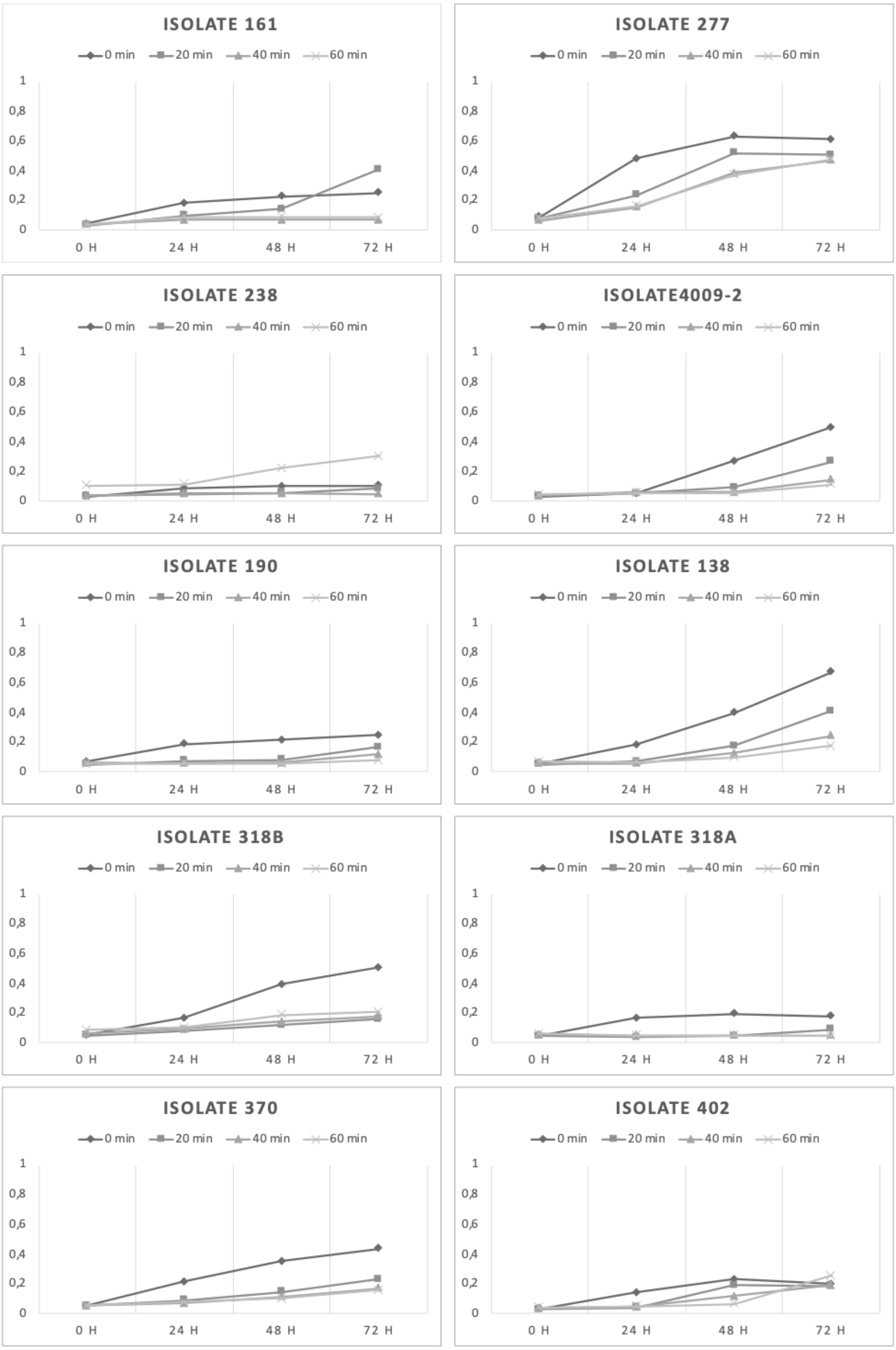

Figure 1. Growth curves of selected isolates exposed to different doses of UV radiation (7.3 kJ/m^2 equal to 20 minutes, 14.6 kJ/m^2 equal to 40 minutes and 21.9 kJ/m^2 equal to 60 minutes). As control not exposed bacteria were incubated (0 minutes).

All selected bacterial isolates were exposed to different doses of UV radiation. Figure 1 show growth curves after UV treatment. Isolate number 277 represent mildly UV resistant bacteria. After 24 hours of incubation growth rate was comparable with the not treated culture. Isolates number 138 and 4009-2 showed resistance up to dose 7.3 kJ/m^2 and nearly zero resistance to higher dosages of UV radiation. The rest of selected isolates showed no resistance to UV irradiation. As a defence mechanism bacteria produce wide board of enzymatic or non-enzymatic antioxidants [7]. In this study DPPH assay was used to evaluate antioxidant capacity. Figure 2 represent level of DPPH degradation as a marker of antioxidant capacity. The higher the level of DPPH degradation, the more antioxidant capacity can be anticipated. Surprisingly the most UV resistant isolate number 277 showed one of the smallest results. This may suggest other defence mechanisms to be key resistance strategies for the studied bacterium.

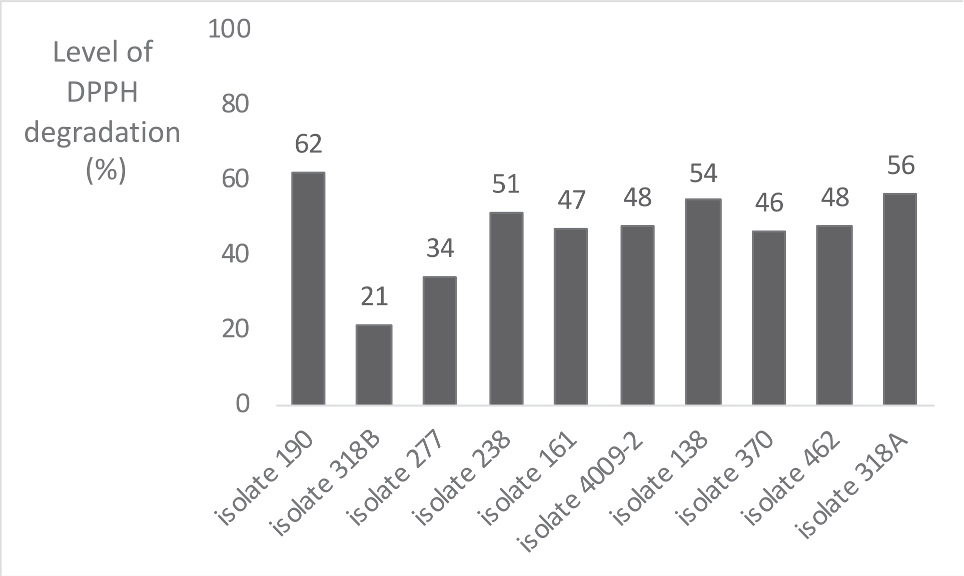

Figure 2. DPPH assay of selected bacterial isolates. The higher the level of DPPH degradation, the more antioxidant capacity can be anticipated.

Conclusion

Jachymov springs are a unique water resource, which bacterial community is not characterized yet. In this study ten bacterial isolates obtained from Jachymov water samples were studied. Three isolates showed moderate UV resistance up to dose 7.3 kJ/m^2 and one of them was able to withstand dose of 21.9 kJ/m^2. Further characterisation of UV resistance extension as well as analysis of possible defence mechanisms will be conducted.

Acknowledgements

1) Financial support was received from research grant GACR 18 - 00036S
2) This work was supported from the grant of Specific university research – grant No. A2_FPBT_2021_027
3) Microbial isolates were obtained in collaboration with doc. Ing. Ondřej Uhlík, Ph.D. and Ing. Gabriela Kapinusová

References

1. Hendry P.: Environ. Chem. *3*, 75 (2006).
2. Weidler G. W., Dornmayr-Pfaffenhuemer M., Gerbl F. W., Heinen W., Stan-Lotter H.: Appl. Environ. Microbiol. *73*, 259 (2007).
3. Gibert J., Deharveng L.: Bioscience *52*, 473 (2002).
4. Pedersen K., Arlinger J., Hallbeck L., Pettersson C.: Mol. Ecol. *5*, 427 (1996).
5. Baskaran M.: *Radon: a Tracer for Geological, Geophysical and Geochemical Studies*. Springer International Publishing AG, Cham, SWITZERLAND 2016.
6. Close D., Nelson W., W. B.: The Journal of Physical Chemistry A *117*, 12608–12615 (2013).
7. Pavlopoulou A., Savva G. D., Louka M., Bagos P. G., Vorgias C. E., Michalopoulos I., Georgakilas A. G.: Mutat. Res.-Rev. Mutat. Res. *767*, 92 (2016).

8. Krejbichova Z.: Czech. J. Phys. *49*, 127 (1999).
9. Anitori R. P., Trott C., Saul D. J., Bergquist P. L., Walter M. R.: Astrobiology *2*, 255 (2002).
10. https://www.laznejachymov.cz/lecive-zdroje/, staženo 1.6.2021.
11. Rezanka T., Gharwalova L., Novakova G., Kolouchova I., Uhlik O., Sigler K.: Lipids *54*, 177 (2019).
12. Gholami M., Etemadifar Z., Bouzari M.: J. Environ. Radioact. *144*, 113 (2015).
13. Shukla M., Chaturvedi R., Tamhane D., Vyas P., Archana G., Apte S., Bandekar J., Desai A.: Curr. Microbiol. *54*, 142 (2007).
14. Brand-Williams W., Cuvelier M. E., Berset C.: Food Sci. Technol.-Lebensm.-Wiss. Technol. *28*, 25 (1995).
15. Samanta A. K., Chaudhuri S., Dutta D.: Mater. Today-Proc. *3*, 3427 (2016).
16. Tian B., Xu Z. J., Sun Z. T., Lin J., Hua Y. J.: Biochim. Biophys. Acta-Gen. Subj. *1770*, 902 (2007).

ISOLATION OF FERULIC ACID FROM WHEAT BRAN USING VARIOUS ADSORBENTS

Nábělek J.[1], Pořízka J.[1], **Diviš, P.**[1]

[1]Brno University of Technology, Faculty of chemistry, Purkyňova 118, 612 00, Brno

divis@fch.vut.cz

Abstract

In this work, four types of adsorbents (activated charcoal, Amberlite XAD16, Amberlyst A21 and IRA-900Cl were tested for isolation purposes of ferulic acid from wheat bran treated with alkaline hydrolysis. The adsorption and desorption efficiency of the materials used were verified in the study. Although the IRA-900Cl sorbent showed the highest adsorption efficiency, the adsorbent Amberlite XAD16 was chosen for further experiments because, despite the lower adsorption efficiency, it showed the most effective desorption efficiency using 0.5 % NaOH solution. The final yield of the optimized isolation process was 0.48 ± 0,02 g of ferulic acid from 1 kg of wheat bran. By FTIR analysis it was confirmed, that proteins reduced the purity of isolated ferulic acid.

Introduction

Wheat, together with maize and rice, accounts for about 90 % of the world's cereal production. Wheat bran, besides other valuable compounds such as wheat germ and parts of the endosperm, remains a major by-product during the milling process[1]. Wheat processing mills can produce up to 50 tons of bran per day. This waste material is suitable for further processing, as it still contains a significant proportion of various usable substances[1]. One of these substances is ferulic acid which is widely used in various industries[2]. Ferulic acid is contained in bran in the form of feruloylated oligosaccharides. In general, feruloylated oligosaccharides are formed of a polymerization of arabinoxylans feruloylated with ferulic acid at the O-5 position of the arabinose units. In addition, the arabinoxylans are composed of a (1–4)-β-D-xylopyranose chain substituted with L-arabinofuranose at the O-2 and/or O-3 position[3]. Ferulic acid can be obtained from feruloylated oligosaccharides after alkaline hydrolysis[4]. However, the purity of obtained ferulic acid is relatively low because hydrolysate after alkaline hydrolysis contains other substances in addition to ferulic acid. Therefore, it is necessary to study the possibilities of separation of ferulic acid from these substances[5].

The aim of this study was to study the usability of various adsorbents for the purpose of separation of ferulic acid from crude wheat bran hydrolysate which would increase the purity of ferulic acid obtained after wheat bran hydrolysis.

Experiment

The wheat bran was provided by Mlyny Vozenilek from Předměřice nad Labem (Czech Republic). Alkaline hydrolysis of wheat bran was performed according to optimised procedure described by Stavova et al.[6]. Briefly, 5 grams of wheat bran was hydrolysed by 150 ml of 0.5 M NaOH (Lachner, Czech Republic) while heating to 50°C for 4 hours. After the hydrolysis, the liquid and remaining solid part were separated using centrifugation at 5000 rpm. Ferulic acid in obtained solution was adsorbed on different adsorbents using batch adsorption. In this study Amberlyte XAD-16 (XAD-16), IRA-900Cl, Amberlyst A21 (A21) and activated charcoal (AU) were tested. All of adsorbents were purchased from Sigma-Aldrich (Germany). One gram of selected adsorbent was added to 10 ml of the solution obtained after alkaline hydrolysis and adjusted to pH in the range of 3-4 using diluted nitric acid (Analytika, Czech Republic). The adsorption proceeded for one hour at room temperature with constant stirring at 150 rpm. At the end of adsorption, the solution was poured through a sieve and the trapped adsorbent was washed by four times the volume of the original solution using water acidified with nitric acid to pH between 3-4. To the washed adsorbent, 10 ml of 0.5 % NaOH was added and the desorption of ferulic acid from the adsorbent proceeded for one hour at room temperature with constant stirring at 150 rpm. After desorption, the obtained solution containing ferulic acid was analysed by HPLC. The HPLC system used for the analysis consisted of an Agilent 1260 Infinity HPLC (Agilent, USA) equipped with diode array detector with 10 mm adsorption cell. Kinetex EVO C18 column (100x3 mm, 2.6 µm particle size) was used as a stationary phase and mixture of acetonitrile (WVR, Germany) and 0.5 % acetic acid (WVR, Germany) (1:9 v/v ratio) was used as a mobile phase during the analysis. The detection of ferulic acid took place at 330 nm. Calibration was done by dissolving different amounts of ferulic acid (Sigma-Aldrich, Germany) in solution with the same composition as the mobile phase. Similar experiment with adsorption and desorption of ferulic acid was carried out with standard solution containing pure ferulic acid. The purity of obtained ferulic acid solution after desorption from adsorbent was tested by measuring FTIR spectra of ferulic acid standard and possible contaminants (carbohydrates and proteins). For this purpose, spectrometer iS50 (Thermofisher Scientifitic) with ATR diamond adapter was used.

Discussion and result analysis

The adsorption efficiency of ferulic acid from solution containing pure ferulic acid ranged from 75 to 98 % (Figure 1). In the solutions obtained after alkaline hydrolysis of wheat bran, the adsorption efficiency was halved. Only IRA-900Cl adsorbent still showed high adsorption efficiency (Figure 2). The reduction of adsorption efficiency may have been due to the interaction of other substances in hydrolysate with the adsorbents used. Stavova et al.[6] in her work quantified a significant amount of sinapic acid in wheat bran hydrolysate. In addition, other phenolic compounds were identified in wheat bran hydrolysate. Other substances that may be present in the hydrolysate and affect the adsorption of ferulic acid may be various carbohydrates or proteins.

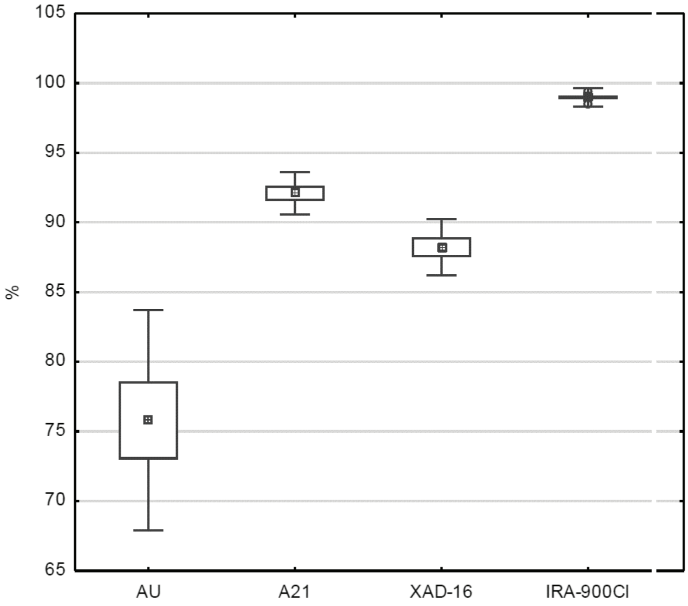

Figure 1. Adsorption efficiency of ferulic acid from ferulic acid standard solution

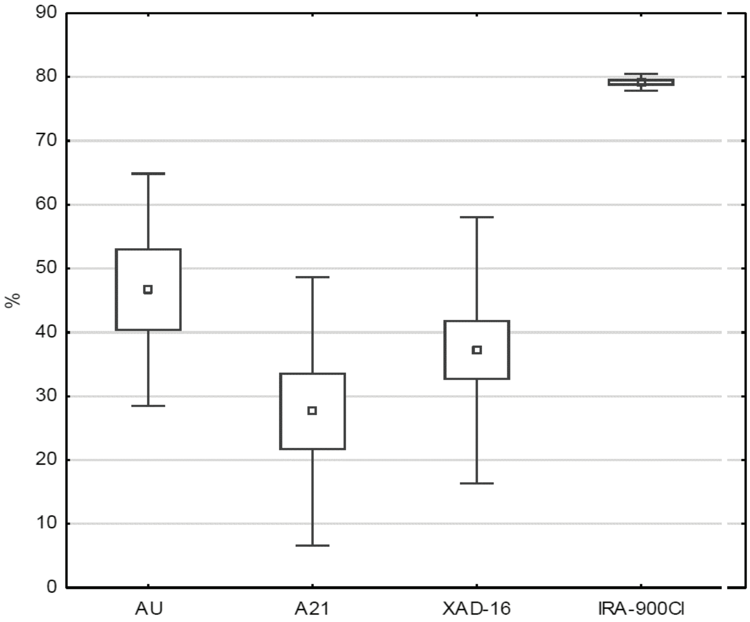

Figure 2. Adsorption efficiency of ferulic acid from the solution obtained after alkaline hydrolysis of wheat bran

Desorption of bound ferulic acid has proven to be problematic in some of tested adsorbents. A very low desorption efficiency was observed when using IRA-900Cl adsorbent (0.3 %). The best desorption efficiency was achieved with Amberlite XAD-16 adsorbent (57 %). The achieved desorption efficiency is lower compared to results published by Gopalan and Madhavan Nampoothiri[7] who used XAD-4 and SRA 400 resins for adsorption of ferulic acid after the hydrolysis of wheat bran, however, in our study we worked with crude untreated hydrolysate. Desorption efficiency using 0.5 % NaOH solution decreased in order Amberlite XAD-16 > Amberlyst A21 > activated charcoal > IRA-900Cl. In the case of IRA-900Cl, other solutions for elution of bound ferulic acid were tested, however, as can be seen in Figure 3, this change did not significantly increased the desorption efficiency.

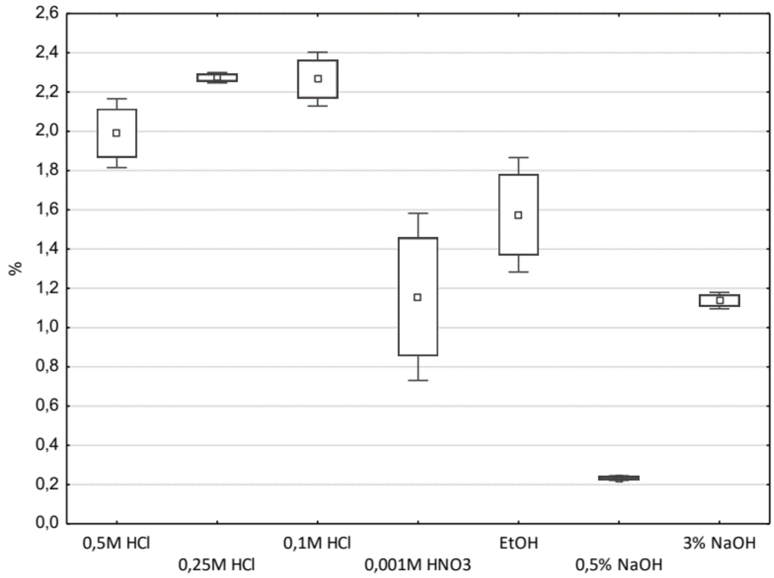

Figure 3. Desorption efficiency of ferulic acid from IRA900Cl using a different solution for elution

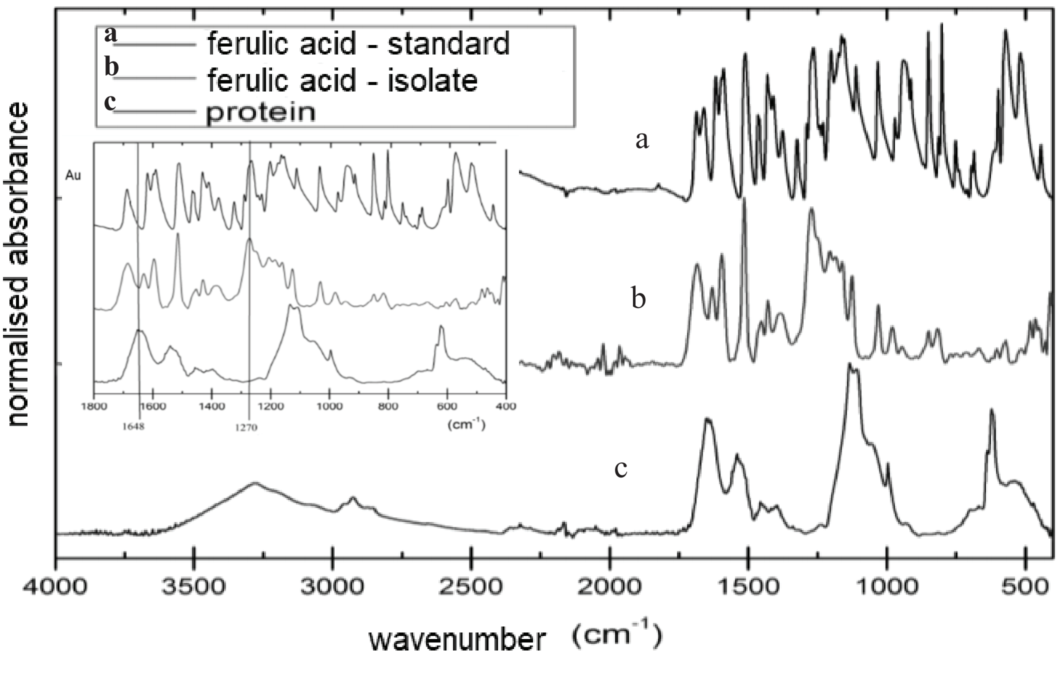

Figure 4. Adsorption efficiency of ferulic acid from the solution obtained after alkaline hydrolysis of wheat bran

The purity of ferulic acid obtained after alkaline hydrolysis of wheat bran and after purification step using batch adsorption experiment was verified by FTIR analysis. Figure 4 shows FTIR spectra of pure ferulic acid, isolated ferulic acid from wheat bran and wheat protein. In the picture wavenumbers 1648 and 1270 cm^{-1} are highlighted. The 1648 cm^{-1} peak is specific for the amine group in proteins, while 1270 cm^{-1} peak represents carbon-carbon stretching vibrations in the aromatic ring of ferulic acid. The FTIR analysis revealed that the isolated ferulic acid was contaminated with proteins. Protein contamination may explain the observed reduced adsorption efficiency of ferulic acid from the solution after wheat bran alkaline hydrolysis (Figure 2).

Conclusion

In this study, it was demonstrated that the wheat bran is a good source of ferulic acid. Separation of ferulic acid from hydrolysed wheat bran is possible using different adsorbents. In the present study, the best adsorbent applicable for separation of ferulic acid from wheat bran hydrolysate was Amberlyt XAD-16. By using this type of adsorbent about 0.5 g of ferulic acid can be obtained after hydrolysis of 1kg of wheat bran. However, elution conditions as well as treatment of the hydrolysate prior to adsorption should be further investigated. Under optimized conditions, the extraction efficiency can be increased, and ferulic acid of higher purity can be obtained.

Acknowledgement

This work was supported by Technology Agency of the Czech Republic, project no. FW02020135, Verification of biorefinery concept for bran processing. The authors would like to thanks Petr Sedlacek for his help with FTIR analysis.

References

1. Pruckler, M., Siebenhandl-Ehn, S., Apprich, S., Holtinger, S., Haas, C., Schmid, E., Kneifel, W. LWT Food Sci. Technol. 211, 56 (2014)
2. Kumar N., Pruthi V., Biotechnol. Rep. 4, 86 (2014)
3. Lin S., Agger J.W., Wilkens C., MeyerA.S. Annu. Rev. Food Sci. Technol. 12, 331 (2021)
4. Buranov A. U., Mazza G. Food Chem. 115, 1542 (2009)
5. Salgado J.M., Max B., Rodrigues-Solana, Dominguez J.M. Ind. Crops Prod. 39, 52 (2012)
6. Stavova E., Porizka J., Stursa V., Enev V., Divis P., Proceedings of 24th international Phd students conference (Mendelnet 2017), 574 (2017).
7. Gopalan N., Madhavan Nampoothiri K. Biocatal. Agric. Biotechnol. 15, 304 (2018)

PRODUCTION AND ANALYSIS OF CRUDE BIOCHAR PRODUCED FROM WHEAT BRAN

Pořízka J.[1], Švec J.[1], Diviš P.[1], Zouharová K.[1], Sedláček P.[1], Enev V.[1], Hajzler J.[1], Mravcová L.[1], Trudičová M.[1]

[1]*Brno University of Technology, Faculty of chemistry, Purkyňova 118, 612 00, Brno, Czech Republic*

porizka@fch.vut.cz

Abstract

Biochar is solid material mainly produced by the pyrolysis of biomass. It is generally a carbonated material with high porosity and a high level of aromatization. Thanks to its properties, biochar is used in various industries, such as power production, agriculture, wastewater treatment, construction, pharmacy and many others. A significant advantage of biochar production is that it is often produced from agricultural and food waste, which corresponds to circular economics's philosophy. The physicochemical properties of biochar strongly depend on the feedstock type. An interesting raw material with potential for the production of biochar is wheat bran, a by-product of milling, which falls into lignocellulosic biomass. The main aspect of this work was developing a pyrolysis procedure and determining the products' physicochemical properties. The pyrolysis was performed in a furnace under an anaerobic nitrogen environment. Three pyrolysis temperatures were tested – 300, 400 and 500°C. Characterization of biochar was proceeded according to the European biochar certificate (EBC), which included size distribution analysis, SEM, BET surface area analysis, elemental analysis, FTIR spectral analysis and analysis of PAHs. FTIR, elemental analysis and SEM proved that 500 °C pyrolysis for 3 hours was optimal to produce well-carbonized biochar with the optimal structure. Yield of the process was 290,2 g of biochar from 1 kg of bran. Biochar contained a significant amount of K (45.7 ± 0.7 µg/g), and P (4.8 ± 0.6 µg/g) and did not exceed the allowed limit of total PAHs (2.28 µg/g) set by European biochar certificate. The surface of the biochar significantly raised with the pyrolysis temperature with 3.4 m^2/g for 500°C. Biochar meets the EBC Class I criteria in terms of the content of potentially toxic metals and PAHs.

Introduction

Biochar is a solid material mainly produced by the pyrolysis of various type of biomass. It is generally a carbonated material with high porosity and a high level of aromatization. Thanks to its properties, biochar is used in various industries, such as power production, agriculture, wastewater treatment, construction, pharmacy and many others. A significant advantage of biochar production is that it is often produced from agricultural and food waste, which corresponds to circular economics's philosophy. The physicochemical properties of biochar strongly depend on the feedstock type. An interesting raw material with potential for the production of biochar is wheat bran, a by-product of milling, which falls into group of lignocellulosic biomasses. Wheat bran consist mostly of non-starch polysaccharides, starch, protein and lignin. Chemical composition of wheat bran corresponds to other plant feedstocks, like wheat straw, rice husk, peanut shell, which are standardly used for biochar production[1,2,3].

The main aspect of this work was developing a pyrolysis procedure and determining the products physicochemical properties. The pyrolysis was performed in a furnace under an anaerobic nitrogen environment. Three pyrolysis temperatures were tested – 300, 400 and 500°C. Characterization of biochar was proceeded according to the European biochar certificate, which included size distribution analysis, SEM, BET surface area analysis, elemental analysis, FTIR spectral analysis and analysis of polyaromatic hydrocarbons.

Experiment

Wheat bran samples for pyrolysis were gathered in milling company Mlýny Voženílek (Czech Republic). Pyrolysis of wheat bran was performed in a furnace under an anaerobic nitrogen environment. Three pyrolysis temperatures were tested – 300, 400 and 500° C with a residence time of 3 hours at the final temperature. Rate of heating was set to 5°C/min.

Different sample preparation methods were used for each biochar analysis. Untreated samples were used for distribution analysis (Retsch AS 200), Scanning electron microscopy (Zeiss EVO 18), BET surface area analysis

(Quantachrome Instruments NOVA 2200e), CHN analysis (Euro-Vector EA 3000) and FTIR spectral analysis (Thermo Nicolet is50).

Microwave digestion (Milestone 1200 mega) was used for the preparation of samples for elemental analysis by ICP-OES (Horiba Jobin Yvonne Ultima 2). Amount of 0.1 g of biochar transferred into PTFE flasks with 5 ml of 65% HNO3 and 1 ml H2O2. Volume of the sample was transferred into 25 ml volumetric flasks after the digestion. Elements Cr, Yn, Cd, Pb, Ni, Co, Mn, Fe, Cu, Al, P, Mg, Ca, Na and K were analysed.

Soxhlet extraction into toluene was used as a sample preparation method for the analysis of PAHs by GC-MS (Thermo TSQ 9000). Amount of 2.5g of sample was transferred into the glass flasks with 150 ml of toluene. Extraction took place for 2.5 hours with final evaporation to 25 ml.

Discussion and result analysis

Yield and size distribution of produced biochar is presented in table I. Temperature of pyrolysis proved to be strongly influential on the yield of biochar. It is mostly connected with fundamental physical changes like release of volatiles, chemically bound moisture and thermal decomposition of biomass[4,5,6]. Yields were comparable with biochar produced from wheat straw and peanut shells[3]. Higher pyrolysis temperature also led to the fusion and melting of multiple particles which resulted in a decrease in the content of the finest particles.

Table I

Yields and size distribution of wheat bran biochar

	Yield (%)	Fractions (%)			
Sample		> 4 mm	2-4 mm	0.5–2 mm	<0.5 mm
Wheat Bran		0	0.11	40.9	59
300 °C	64.9	0.261	3.09	30.8	65.9
400 °C	49.7	2.29	2.62	41.2	53.9
500 °C	29.2	0.121	1.91	67.2	30.7

The carbon content raises from 61.1 % (300°C) to 66.6 % (500°C) (Table II). This corresponds to a higher degree of carbonization at higher temperatures. Carbon content of wheat bran biochar is comparable with another plant base biochar like reed and sawdust. On the contrary, it is richer in carbon than biochar from rice straw[7]. Increasing the pyrolysis temperature further decreased the H/C ratio (table II). Uchimiya et al. (2010) used H/C ratio to predict level of aromaticity and polarity of biochar's[8]. This ratio indicates that wheat bran biochar produced at 500 °C shows higher level of aromaticity. This is supported by the FTIR analysis presented in figure 1. As the pyrolysis temperature increases, the proportion of carbonyl compounds in the material decreases. As the concentration of carbonyl compounds decreases, so does the concentration of carbon bound in aromatic structures. These structures are observable in the spectral region at a wavelength of approximately 1600 cm^{-1}, which is specific for C = C bonds in the aromatic structures. The degree of carbonization can be further observed in the wavelength range 3500 - 2500 cm^{-1}, specific for hydroxyl group bands. This area should be as flat as possible.

Table II

Elemental analysis of wheat bran biochar

	N (%)	C (%)	H (%)	H/C
300 °C	5.38 ± 0.13	61.1 ± 0.4	9.5 ± 0.15	0.155
400 °C	5.3 ± 0.26	65.5 ± 0.7	5.38 ± 0.31	0.082
500 °C	5.42 ± 0.22	66.6 ± 0.7	4.15 ± 0.05	0.062

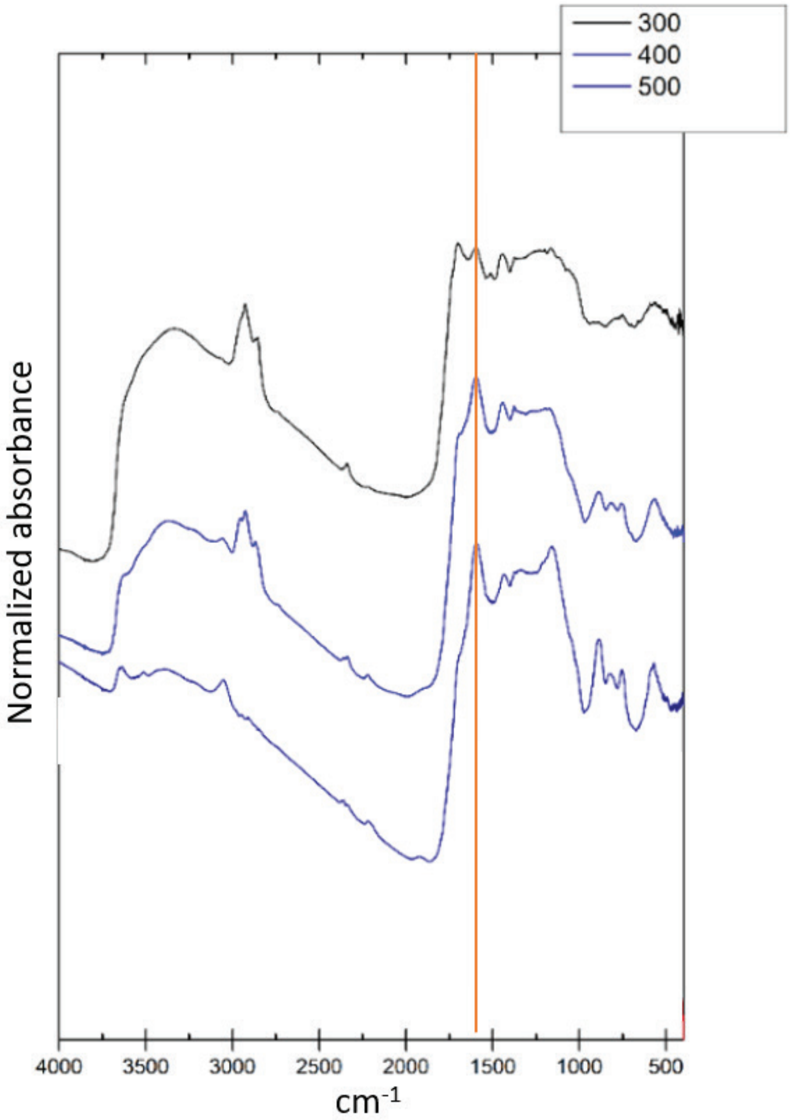

Figure 1. FTIR spectrum of wheat bran biochar produced at different temperatures.

Bet surface area of wheat bran biochar is presented in table III. Specific surface area was significantly influenced by pyrolysis temperature. Wheat bran biochar produced at 500°C showed specific surface 3.4 m^2/g. This is comparable with eggshell (500°C) and grass (400°C) biochar[4,6]. However, the tested crude biochar generally showed a lower specific surface area compared to biochar from other plant materials pyrolyzed at the same temperature like rice straw (34 m^2/g), reed (131.5 m^2/g), sawdust (378.7 m^2/g), oak (370 m^2/g) and pine (475 m^2/g)[3,9]. Crude, not activated biochar from wheat bran thus has a microporous structure, which can be observed in figure 2. This finding corresponds to previous knowledge about the formation of microporous and microporous biochar structure. Pyrolysis of feedstocks rich on lignin, such as bamboo and coconut shell produce biochar with macroporous structure, while feedstocks rich on cellulose, such as husk is suitable to produce microporous structure[10,11]. Wheat bran belongs to this category of materials with approximately 19 % of cellulose and low proportion of lignin[12].

Table III

BET analysis - Specific surface and pore volume of wheat bran biochar

Sample	Specific surface (m^2/g)	Pore volume (cm^3/g)
300 °C	0.604	6.90·10-4
400 °C	2.61	6.38·10-5
500 °C	3.40	3.65·10-3

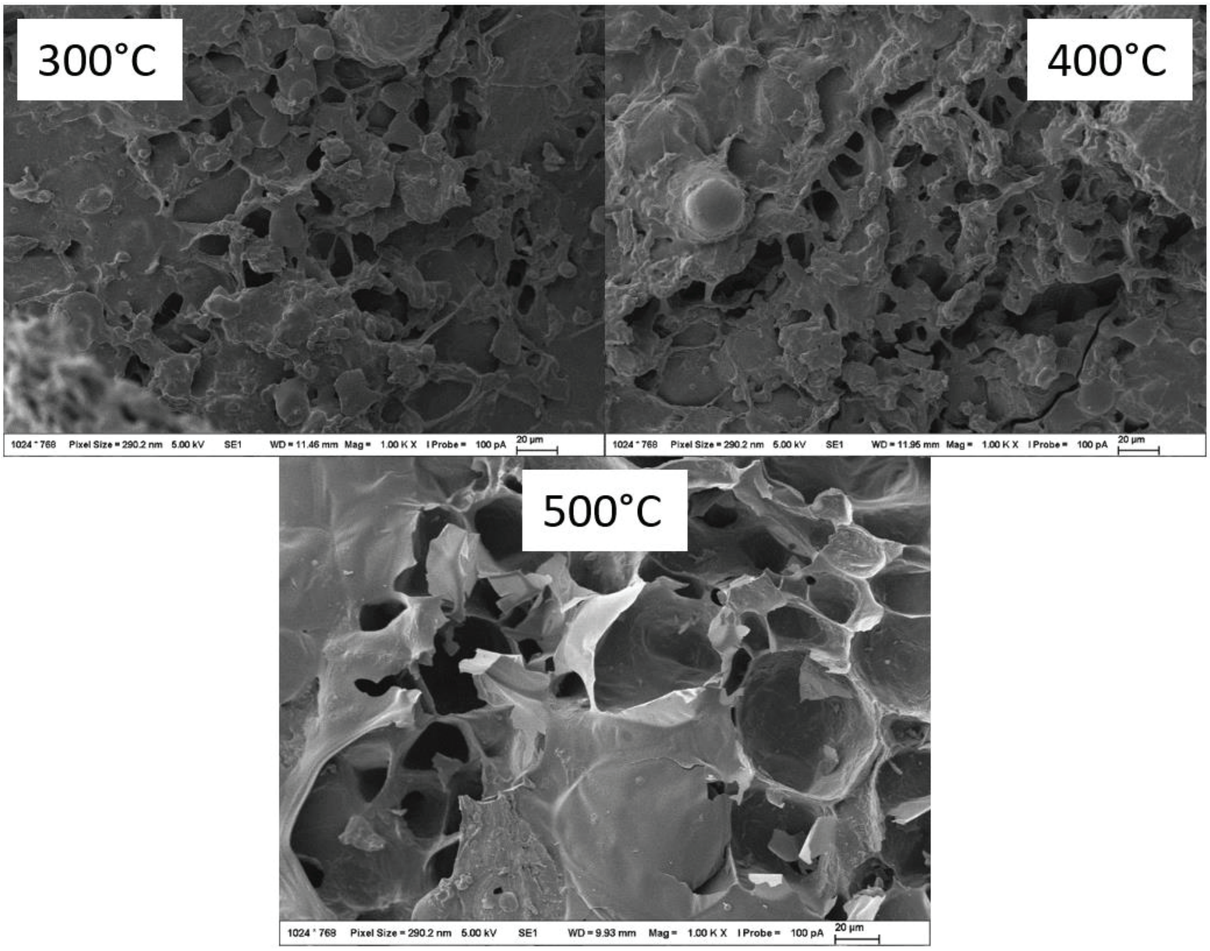

Figure 2. Scanning electron microscopy of wheat bran biochar; magnification 1000x

The produced biochar was further tested for the presence of potentially toxic metals and PAHs. European biochar certificate defines the maximum permissible concentrations for different classes of biochar – Class I Feed, Class II AgroBio, Class III Agro and Class IV Material. The controlled parameters include content of Pb, Cd, Cu, Ni, Hg, Zn, Cr, As, sum of 16 EPA PAHs and specifically content of Benzo[a]pyrene. In the case of wheat bran biochar, these limits were not exceeded in any of the studied parameters. The sum of PAHs concentrations in biochar (500°C) was 2.28 ± 0.1 µg/kg, which ranks this biochar in the most strictly rated Class I. Most abundant PAHs were naphtalene, fenanthrene and pyrene. Biochar also meets the Class I criteria in terms of the content of potentially toxic metals.

Conclusion

Pilot experiments showed that wheat bran proved to be a feedstock suitable for the production of biochar with a microporous structure. Biochar produced by pyrolysis at 500°C showed comparable properties with biochars from feedstocks rich in cellulose. According to European biochar certificate, wheat bran biochar meets requirements for all application classes – Feed, Agrobio, Agro and Material. This creates a good precondition for further development, which should be focus on chemical or physical activation to increase the specific surface area, which is currently the most fundamental weakness.

Acknowledgement

This work was supported by Technology Agency of the Czech Republic, project no. FW02020135, Verification of biorefinery concept for bran processing.

References

1. Weber, K., Quicker P.: Fuel 217 (2018).
2. Bhowmick G. D., Sarmah A. K., Sen R.: Bioresour. Technol. 247 (2018).
3. Fermanelli C.S., Córdoba A, LPierella L.B., Saux C.: Waste Manage. 102 (2020).
4. Sjöström E.: *Wood Chemistry: Fundamentals and applications*. Elsevier, Amsterdam 1993.

5. Antal M.J., Grønli M.: Ind. Eng. Chem. Res 42 (2003).
6. Lua A.C., Yang T., Guo J.: J Anal Appl *Pyrolysis 72 (2004).*
7. *Xu D., Cao J., Li Y., Howard A., Yu K.: Waste Manage. 87 (2019).*
8. *Uchimiya M., Wartelle L.H., Lima I.M., Klasson K.T.: J. Agric. Food Chem. 58 (2010).*
9. *Mukherjee A., Zimmerman A.R., Harris W.: Geoderma 163 (2011).*
10. *Li H.B., Dong X.L., Evando B.S., Letuzia M.O., Chen Y.S., Lena Q.M.: Chemosphere 178 (2017a).*
11. *Li R., Wang J.J., Zhou B., Zhang Z., Liu S., Lei S., Xiao R.: J. Clean Prod. 147 (2017b).*
12. *Merali Z., Collins S.R.A., Elliston A., Wilson D.R., Kasper A., Waldron K.W.: Biotechnol. Biofuels 8:23 (2015).*

CIRCULAR BIODIESEL DOWNSTREAM SIDE-PRODUCTS UTILIZATION FOR UPSTREAM BIODIESEL VALORIZATION

Ondrejíčková P.[1], Kafková V.[1], Holíčková M.[2], Cyprichová V.[2], Gyuranová D.[3], Krasňan V.[3], Rebroš M.[3]

[1]*Association Energy 21, Leopoldov, Slovakia*
[2]*Centre of research and development, s.r.o., Leopoldov, Slovakia*
[3]*The Faculty of Chemical and Food Technology - STU, Bratislava, Slovakia*

Abstract

Post-fermentation corn oil is processed as feedstock in biodiesel production but negatively influencing filterability and cold flow properties of final product. The aim of presented work is to evaluate the steryl glycosides and phytosterols presence in corn oil during the biodiesel process flow and to find the appropriate point of production process where to apply recombinant enzymatic biocatalysts – steryl glycosidases. The enzymes might be produced by microorganisms utilizing glycerol, the side-product of biodiesel production, as carbon source. The closed loop of glycerol industrial application in biofuels processing is the key objective of the presented work, when used as a substrate for high added valuable enzymatic biocatalysts production (whole-cell or enzyme form) to remove existing technological and biodiesel´s quality problems in biorefineries caused by steryl glycosides and phytosterols presented in feedstock oil.

The further research is aimed to obtain representative and comparable data of bio-catalysis high specificity and activity.

Introduction

Biodiesel, or fatty acid methyl esters (FAME), belongs to category of fuel produced from renewable energy sources (mostly with agricultural origin), suitable for diesel (internal combustion) engines. Feedstock composition and FA profile determine the quality of produced biodiesel[1]. The oily raw material used in biodiesel production may contain the components decreasing the quality of biodiesel. These undesirable components with relatively high solidification/crystallization temperature cause several problems manifested especially in transport by pipeline systems or tanks in the winter or at lower temperatures[2]. In the worst scenario, the biodiesel compounds begin to crystallize in the fuel system of cars and can cause fuel filter or nozzles plugging and (temporary) engine dysfunction. There is an effort to eliminate or remove these undesirable components from biodiesel by pre-treatment operations of the raw material or treatment of final biodiesel.

Steryl glycosides (SG) and glycerides have been considered as two main groups of chemicals causing the precipitate formation in biodiesel[3] decreasing the biodiesel stability, deteriorating the quality of produced biodiesel and consequently increasing the operational costs. SGs negatively influences filterability of biodiesel. Precipitate formation in biodiesel depends on the type of vegetable oil, processing method, stirring intensity, temperature and storage time[4,5].

SGs removal from biodiesel or directly from crude oily feedstock using the enzymes seems to be suitable cheap and effective solution while the environmentally friendly approach is still preserved[6]. A. Aquirre et al.[6] used a synthetic codon-optimized version of the lacS gene from *Sulfolobus solfataricus* to treat soybean biodiesel containing 100 ppm of SGs. The lacS gene was expressed by *E. coli* and subsequently purified. The optimal conditions for biodiesel treating were found: pH value 5,5, temperature 87 °C and 0,9 % of the emulsifier polyglycerol polyricinoleate. At these conditions, the total amount of SGs present in biodiesel was reduced by 81 % using the enzyme[6]. A. Peiru et al.[7] research was focused on an enzyme (steryl glycosidases) development. Steryl glycosidases could be used to hydrolyse SGs, producing glucose and sterols soluble in FAME. The produced glucose has been eliminated subsequently during the water-washing after transesterification. The generated products did not have a negative influence on cold flow properties (CP, PP and CFPP value). A steryl glycosidase enzyme from *Thermococcus litoralis* was produced and purified from *E. coli* cultures expressing a synthetic gene, and used to treat the biodiesel. Research also refers to the need for the presence of nutrients for enzymes in biodiesel: a phosphate content of 10 mM and a sodium chloride content of 20 mM, maintaining the ratio and conditions of the experiment (2 hours, 65 °C, 7 μg enzyme/g biodiesel)[7]. Also, it is possible to produce enzymes for SG removal by MO fermentation on additional substrate as carbon source, preferably glycerol, the side-product from biodiesel production. It is possible to produce glycerol in different forms such as crude, neutralized or purified glycerol. F. Eberhardt et al.[8] study was dealing with SGs removal from soybean biodiesel using steryl glycosidases. The enzyme was produced by *E. coli*, which was fermented for 25 h (1300 L fermenter, 37 °C, pH = 6,9, 30 % oxygen saturation) with glycerol (at the concentration of 20 g/L) as the carbon source. The experiment demonstrated that 7 grams of produced steryl glycosidase enzyme can remove on average 100 ppm of SG which means that 1 L of culture is sufficient for SG removal from 1 t of biodiesel[8].

In all these studies, enzymes were applied to treat a final product (biodiesel). Today, enzymatic processes can be used in several stages of the oil processing: extraction, degumming, bleaching, hydrogenation, etc. Therefore, the aim of the first part of the work was to identify phytosterols (mainly steryl glycosides) removal possibilities during the oil refining process and verify enzyme application possibilities in oil refining process. The aim of the second part of this work was to evaluate the growth of *Pichia pastoris* as a recombinant catalyst producer on glycerol in different forms (purified, neutralized and crude glycerol).

Materials and methods

Phytosterols and steryl glycosides analysis

Corn oil used in this work is a liquid side-stream of bioethanol production using non-genetically modified corn (*Zea mays L.*). Distillers corn oil is rich in lipophilic bioactive compounds such as carotenoids, phytosterols, isoprenoids (squalene), tocopherols and further substances. Phytosterol content in individual stages of corn oil refining process was determined. Crude corn oil refining process used in this study is equal to currently implemented industry refining process treating rapeseed oil. The individual stages of refining process include degumming (phosphor content decrease), winterization (waxes content decrease) and distillation, where deodorization takes place, respectively free fatty acids separation run. Total content of phytosterols and individual phytosterols content was determined by internally GC-MS method.

In the second part of the analyzes, the content of steryl glycosides as well as phytosterols and steryl esters in crude corn oil and refined oil (after distillation) were determined. To minimize phytosterols losses associated with other refining steps and to evaluate the impact of distillation conditions on the PE, SG and PS concentration, the crude corn oil was distilled without a prior degumming and winterization step. The SPD unit was used for distillation and three different distillation temperatures (220 °C, 240 °C, 260 °C) were investigated. A lower distillation temperature is preferred to reduce the thermal stress on the phytosterols, higher distillation temperatures improve the FFA and partial glyceride removal from the corn oil. Crude corn oil and refined oil samples were analyzed according to ISO 23349 and values were compared with each other.

Growth on glycerol

The next objective of this work was to investigate the influence of various waste glycerols on the *Pichia pastoris* growth. *P. pastoris* produces recombinant enzymes and is also able to utilize glycerol. Glycerol used in this work is by-product of biodiesel production using rapeseed oil as a feedstock. Prior to testing of *P. pastoris* growth on glycerol, optimization in 96-well microculture plates was performed to determine the optimal culture volume, inoculation percentage, agitation rate, measuring the optical density at 600 nm during the culture period at regular intervals. To determine the optimal conditions, the specific growth rate and the maximum achieved OD_{600} (related to the amount of biomass obtained) were used. The following conditions were determined: culture medium volume in 250 µl well, inoculation percentage 5 %, agitation rate 300 RPM. The culture period suitable for comparing the effect of different conditions was set to 16 hours. For the evaluation, glycerol of two different purities and glycerol with analytical grade of purity were selected. Two different concentrations of glycerol (10 and 40 g/L) and 2 different *P. pastoris* producers were investigated. The mentioned concentrations were used in the inoculation and fermentation medium.

Results and discussion

Phytosterols and steryl glycosides analysis

Corn oil from bioethanol production may be valorized as an oily feedstock for biodiesel production. The corn oil processing into the biodiesel may negatively affect the final biodiesel properties, mainly filterability and cold-flow properties, which could be caused by PS and SG presence.

Initial part of this research work was focused on the PS presence in corn oil during the corn oil refining process and suitable process step identification for recombinant biocatalysts application to remove SG. The objective is to ensure process feasibility and high operational stability and to improve industrial applicability of corn oil. Using the gas chromatography, we determined total sterols and individual sterol content in the individual stages of corn oil refining process. The results are summarized in Table I.

Table I
Results of total sterol content and individual phytosterols content analysis

Sterol content [% of total sterol content]	Rapeseed oil	Crude corn oil	Degummed corn oil	Winterized corn oil	Distilled/Refined corn oil
β-Sitosterol	50.7	48.9	51.5	52.2	49.1
Δ-5 Avenasterol	1.3	19.4	16.1	15.4	19.5
Campesterol	33.4	15.3	15.8	15.9	13.8
Campestanol	0.3	6.1	6.1	6.1	7.4
Stigmasterol	0.4	5.1	5.2	5.2	4.6
Δ-7 Avenasterol	0.1	1.3	1.3	1.3	1.5
Δ-7 Stigmasterol	0.2	1.3	1.4	1.3	1.5
Clerosterol	0.6	0.8	0.9	0.9	0.8
Δ-5, 24 Stigmastadienol	0.3	0.6	0.6	0.6	0.5
24-Methylene-cholesterol	0.5	0.6	0.5	0.5	0.5
Δ-7 Campesterol	0.5	0.5	0.5	0.5	0.6
Cholesterol	0.3	0.1	0.1	0.1	0.2
Brassicasterol	10.6	<0.1	<0.1	<0.1	<0.1
Δ-5, 23 Stigmastadienol	0.3	<0.1	<0.1	<0.1	<0.1
Sitostanol	0.4	< 0.1	< 0.1	< 0.1	< 0.1
Total sterols [ppm]	**8 730**	**19 900**	**19 400**	**19 000**	**15 200**
Total sterols [%]	**0.87%**	**1.99%**	**1.94%**	**1.90%**	**1.52%**

The results show that the total sterols in crude corn oil are more than 2 times higher compared to the rapeseed oil used for industrial biodiesel production. In terms of the percentage of individual phytosterols in crude corn oil, the highest proportion was β-sitosterol (48.9 %, or 9 730 ppm), Δ-5 avenasterol (19,4 %, or 3 860 ppm) and campesterol (15,3 %, or 3 040 ppm). Yang et al. reports the content of mentioned phytosterols as the most abundant phytosterols in corn oil (β-sitosterol 54,5 %, Δ-5 Avenasterol 9,9 % and campesterol 19,9 %)[9]. The crude corn oil analyzed in this study reached the total sterol content of 1,99 %, or 19 900 ppm. Several studies have focused on the total sterol content of corn oil determination, but in these studies the phytosterol content is lower compared to our results. Yang et al. states 9 900 ppm of total sterol content in crude corn oil[9], Verleyen et al. evaluated the total sterol content for crude corn oil at 7 800 – 9 240 ppm and for refined corn oil 6 860 – 7 730 ppm[10]. P.C. Duta reported the level of PS in crude corn oil to be 7800 – 13 900 ppm[11].

The results reported in table 1 proved the expectations, that distillation step has appreciable impact on the phytosterol content decrease in corn oil. The total sterol content was reduced by 24 % compared to the crude corn oil (by 20 % compared to the previous winterization step). The other steps in the corn oil refining process, specifically degumming and winterization step, had a negligible effect on the total sterol content. In both steps, the total sterol content in corn oil was reduced by 4,5 %. Generally, complete refining of vegetable oils results in a variable phytosterol loss ranging between 10 to 70 %, verifying that reduction in the total sterol content is most significant during deodorization step[12,13]. Based on Verleyen et al.[12] analysis, degumming and bleaching barely affected the total sterol content in physical refining of soybean oil (results in 6,7 % and 1,3 % decrease of total sterol content in crude oil). The sterol content was strongly affected by the deodorization process where reduction of sterols was evaluated at 17,3 %[12].

Plant sterols include four types: free sterols, steryl esters, steryl glycosides, and acyl steryl glycosides. Approximately 9 – 37 % of the total sterols in foods are glycosidic sterols[4]. The steryl glycosides content was determined in our study by gas chromatography, but only in crude and distilled corn oil, where we expected the largest difference in the SG content (Table II). The SG content in corn oil was significantly lower compared to phytosterols and steryl esters content reaching the value 114 – 121 ppm in crude corn oil and 102 – 107 ppm in refined oil. There is a little information about SG content in corn oil in publication according to authors best knowledge, but it was found that the SG content is approximately 480 ppm in corn oil-based biodiesel[14], which is more than 4 times higher compared to SG content in refined corn oil analysed in this study. This analysis showed that the distillation step and different distillation temperatures did not significantly affect the SG content

– decrease of SG content in corn oil was 6 – 15,7 %. Increasing the distillation temperature from 220 °C to 260 °C resulted in a gradual reduction of phytosterols and steryl esters content in refined corn oil from 10,4 % to 32,8 %.

Table II
Steryl glycosides and phytosterols and steryl esters analysis

Sample	**Phytosterols & steryl esters [ppm]**	**Steryl glycosides [ppm]**
Crude CO	19 831	114 - 121
Distillated CO (220°C)	17 760	107
Distillated CO (240°C)	14 645	105
Distillated CO (260°C)	13 327	102

Based on these results, we evaluated that the enzymes application to SG removal is possible before or after the distillation step and will depend only on the optimal conditions of application for selected biocatalyst.

Growth on glycerol

In the next part of the research, we investigated the effect of different waste glycerol samples with a concentration of 10 g/L and 40 g/L on the growth of 2 strains of the yeast *P. pastoris*. Glycerol is regularly used as the main initial carbon source in *P. pastoris* fermentations to increase the cell concentration[15]. The reached cell concentration after the culture period of 16 hours (see in the Figure 1 and 2) was very similar for both *P. pastoris* clones. In the case of strain A2, a sample of neutralized glycerol appears to be the most suitable for fermentation – this sample contains higher content of impurities and it has not been additionally purified except for high pH value neutralization. In general, waste glycerol achieves a higher cell concentration compared to purified glycerol, which may be caused by the ability of the yeast to utilize impurities present in glycerol such as fatty acids, vitamins A, E, and K, and trace elements. These compounds are present in the vegetable oils diffusing to the glycerol phase during the biodiesel formation reactions, and thus enriching the glycerol-based cultivation medium[15]. The work carried out confirmed a potential use for crude glycerol, without any further purification. Despite the increasing concentration of glycerol in the medium, the final optical density of both yeasts was similar in this experiment. Thus, the growth of the studied yeast was not inhibited even when a higher concentration of glycerol in the culture medium was used. This was also demonstrated by Tang et al.[16] using initial concentrations of pure glycerol 10 and 70 g/L[16].

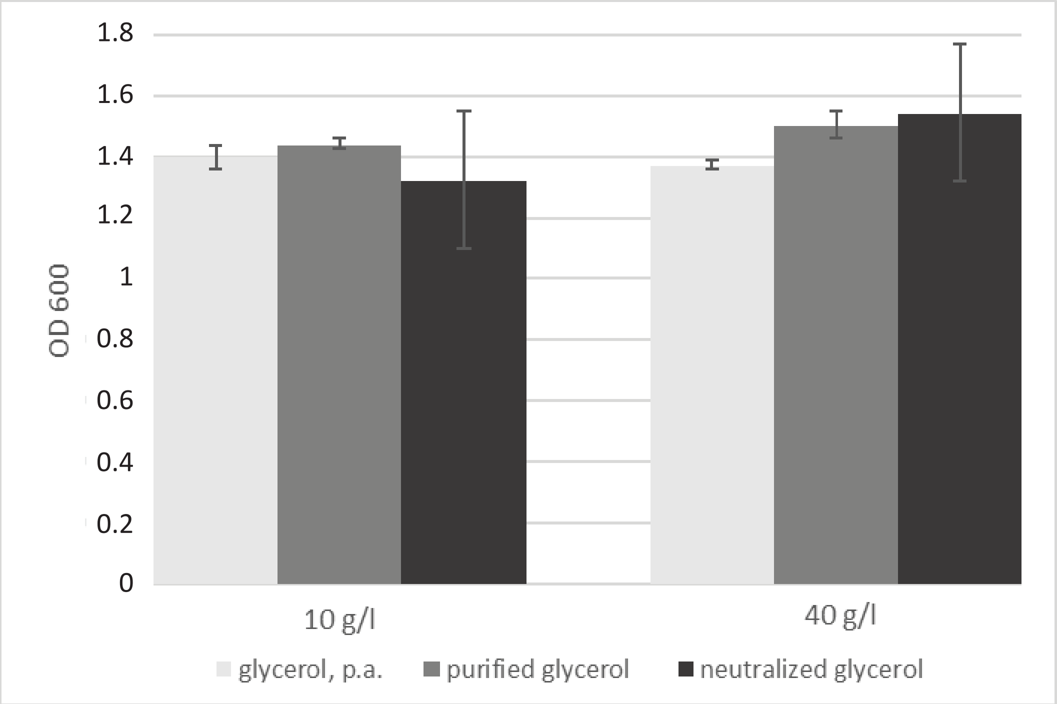

Figure 1. The cell concentration of *P. pastoris* strain A2 after the culture period

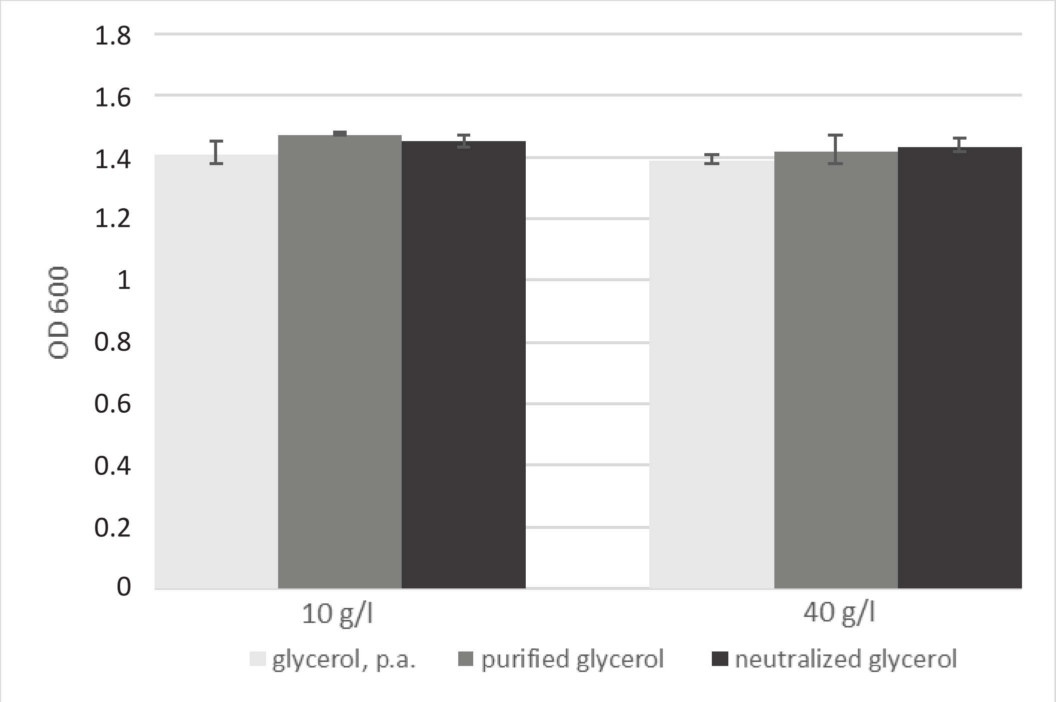

Figure 2. The cell concentration of *P. pastoris* strain E1 after the culture period

Conclusion

The presented work consists of two parts. The aim of the first part was to analyze the sterols in crude corn oil and also to analyze the sterol content during the corn oil refining process. The results showed the phytosterol content is mainly influenced by the distillation step, where the phytosterol content was reduced by 24 % compared to the crude corn oil. The distillation step and different distillation temperatures did not significantly affect the SG content - decrease of SG content in corn oil was 6 - 15,7 %. Based on the obtained results, we evaluated that the enzymes application to SG removal is possible before or after the distillation step and will depend only on the specific conditions for application of the selected biocatalyst.

The second part was focused on verifying the growth ability of *P. pastoris* yeast on different real waste glycerol samples. Both evaluated *P. pastoris* yeast clones were able to utilize glycerol as an additional substrate, achieving comparable amounts of biomass for both clones and tested glycerol concentrations.

The further research will focus on the preparation of recombinant biocatalysts, research on biotransformation processes and subsequent application of selected biocatalytic processes.

Acknowledgement

This work was supported by the Slovak Research and Development Agency under the contract No. APVV-18-0254.

List of Abbreviations

FAME – fatty acid methyl ester
SG/SGs – steryl glycoside/steryl glycosides
PS – phytosterol
SE – steryl ester
FA – fatty acid
CO – corn oil
MO – microorganism
SBO – soybean oil

References

1. Hoekman S., Broch A., Robbins C., Ceniceros E., Natarajan M.: Renew Sustain Energy Rev *16,* 143 (2012).
2. Dunn R. O.: Prog. Energy Combust. Sci. *35*, 481 (2009).
3. Na-Ranong D., Laungthaleongpong P., Khambung S.: Fuel *143*, 229 (2015).
4. Ferrer A., Altabella T., Arró M., Boronat A.: Prog Lipid Res. *67*, 27 (2017).
5. Tang H., Salley O. S., Simon Ng K.Y.: Fuel *87*, 3006 (2008).

6. Aguirre A., Peiru S., Eberhardt F., Vetcher L., Cabrera R., Menzella H.G.: Appl Microbiol Biotechnol. *98 (9)*, 4033 (2014).
7. Peiru S., Aguirre A., Eberhardt F., Braia M., Cabrera R., Menzella H.G.: Biotechnol Biofuels *8*, 223 (2015).
8. Eberhardt F., Aguirre A., Paoletti L., Hails G., Braia M., Ravasi P., Peiru S., Menzella H.G.: Bioprocess Biosyst Eng. *41*, 555 (2017).
9. Yang R., Xue L., Zhang L., Wang X., Qi X., Jiang J., Yu L., Wang X., Zhang W., Zhang Q., Li P.: Foods *8*, 334 (2019)
10. Verleyen T., Forcades M., Verhe R., Dewettinck K., Huyghebaert A., De Greyt W.: J Amer Oil Chem Soc *79*, 117 (2002).
11. Dutta P.C., Phytosterols as Functional Food Components and Nutraceuticals, CRC press, New York (2004).
12. Verleyen T., Sosinska U., Ioannidou S., Verhe R., Dewettinck K., Huyghebaert A., De Greyt W.: J Amer Oil Chem Soc *79*, 947 (2002).
13. Kochhar S.P.: Prog Lipid Res *22*, 161 (1983).
14. Ringwald SC, The 98th AOCS Annual Meeting Abstracts. AOCS Press, Urbana, 15 (2007).
15. Çelik E., Ozbay N., Oktar N., and Çalık P.: Ind. Eng. Chem. Res. *47*, 2985 (2008).
16. Tang S., Boehme L., Lam H., Zhang Z.: Biochem. Eng. J. *43*, 157 (2009)

CHEMICAL PROCESSES AND DEVICES

HOW DOES UNCERTAINTY OF THERMAL CONDUCTIVITY IMPACT MEASUREMENTS OF POOL BOILING HEAT TRANSFER COEFFICIENT?

Vajc V.[1], Dostál M.[1]

[1]Czech Technical University in Prague, Faculty of Mechanical Engineering, Department of Process Engineering, Technická 4, 160 00, Prague 6, Czech Republic
viktor.vajc@fs.cvut.cz

Abstract

This work analyzes how value of thermal conductivity of a tested sample impact pool boiling heat transfer coefficients (HTCs) measured with a common experimental apparatus. A typical measurement of pool boiling HTC is based on 1D conduction in a heated block. Temperature of the boiling surface and heat flux are both calculated from temperature distribution inside the block. Value of thermal conductivity of the block is needed for calculation of heat flux and resulting HTC. Researchers seldom measure thermal conductivity of their samples. A certain value, which corresponds to the material of the investigated sample, is typically adopted from the literature and considered to be independent of temperature. This approach is sometimes criticized as it might lead to significant measurement errors. This contribution quantifies the impact of thermal conductivity and its uncertainty on resulting HTC. For our pool boiling apparatus, it was found out that uncertainty of heat transfer coefficient remains acceptable even when uncertainty of thermal conductivity is purposely overvalued. Furthermore, it was found out that neglecting temperature dependency of thermal conductivity does not lead to substantial errors of resulting HTC.

Introduction

Measurement of pool boiling heat transfer coefficient (HTC) typically involves measurement of temperatures inside a heated metal block. Assuming one-dimensional heat conduction in the block, heat flux is calculated from measured temperatures T_1 and T_2 using Fourier's law

$$q = \lambda \frac{T_2 - T_1}{L_{12}} \tag{1}$$

Temperature of the boiling surface

$$T_\mathrm{w} = T_1 - \frac{T_2 - T_1}{L_{12}} \times L_\mathrm{w} \tag{2}$$

is linearly extrapolated and HTC

$$\alpha = q / (T_\mathrm{w} - T_\mathrm{L}) \tag{3}$$

is calculated. Regarding pool boiling, researchers typically adopt a constant value of thermal conductivity λ from the literature and neglect its temperature dependence. It was pointed out[1] that this might lead to substantial measurement errors in the order of tens of percent.

This work analyses how value of thermal conductivity affects HTCs measured on an experimental apparatus developed at Department of Process Engineering, CTU in Prague. Impact of uncertainty of λ on uncertainty of HTC is investigated and errors in measured HTCs which are caused by assumption of a constant value of λ are evaluated.

Experimental Apparatus

Our pool boiling apparatus shown in Figure 1 employs the standard principle of measurement of saturated pool boiling HTC described above. A copper block heated with five cartridge heaters is inserted into a cut made in a stainless steel bottom. The top face of the block with dimensions of 48 × 48 mm serves as the boiling surface. The block is insulated with cellular glass to reduce heat losses into the surroundings. Six K-type thermocouples are inserted into 1 mm holes with length of 24 mm which were EDM-drilled into the copper block in two lines and three columns. The distance between both lines of thermocouples L_{12} = 24 mm. The distance between the upper line and the boiling surface L_1 = 10 mm. Average temperature in the upper and the lower line of thermocouples is considered as T_1 and T_2, respectively. Temperature of the liquid, which boils inside a glass cylinder with diameter of 300 mm, is measured with two submerged K-type thermocouples. Saturation temperature of the boiling liquid is maintained with a coil-shaped auxiliary heater. To prevent interaction between the auxiliary heater and the boiling surface, both are separated from each other with a stainless steel tube and a funnel roof.

Copper is the most often investigated material in the literature dealing with pool boiling due to its large thermal conductivity around 400 W m^{-1} K^{-1} which provides low temperatures inside the investigated samples and small temperature gradients. This allows investigation of boiling heat transfer at intense heat fluxes without the need for expensive thermoresistant materials. In a typical experimental run performed with our apparatus, maximum investigated heat flux remains below 300 kW m^{-2}, maximum temperatures inside the copper block do not exceed 170 °C and typical temperature gradient inside the block is approximately from 0.4 up to 0.7 °C mm^{-1}.

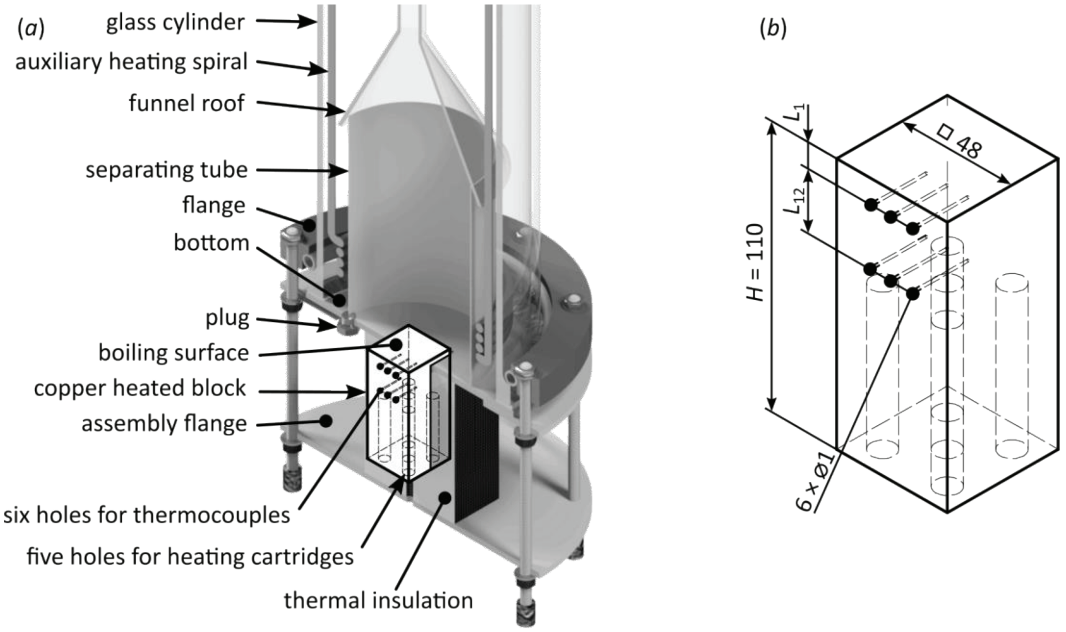

Figure 1. Experimental apparatus for measurement of pool boiling heat transfer coefficient: (*a*) Assembled apparatus before pool boiling experiments; (*b*) Dimensions of the heated copper block.

Results and Discussion

Theory of propagation of uncertainty is used to analyze the impact of uncertainty of thermal conductivity λ on resulting uncertainty of measured HTC. Following assumptions were made:

- Thermal conductivity of copper λ = 400 W m^{-1} K^{-1} is independent of temperature and has a maximum deviation $U_\lambda = \pm 100$ W m^{-1} K^{-1} (the deviation is purposely overestimated).
- Following maximum deviations were assumed for directly measured quantities: for temperature $U_T = \pm 0.5$ °C and for length or distance $U_L = \pm 1.0$ mm.
- All stated deviations have a uniform rectangular distribution and standard deviations $u_i = U_i/\sqrt{3}$.
- Water is the boiling liquid. HTC might be calculated using Rohsenow correlation[2] (this was experimentally verified).

Following equations might be derived for uncertainty of heat flux, wall temperature and HTC (u_q, $u_{T\mathrm{w}}$ and u_α, respectively) by uncertainty analysis of equations (1), (2) and (3)

$$u_q = \sqrt{\left(\frac{T_2 - T_1}{L_{12}}\right)^2 u_\lambda^2 + \left(\frac{\lambda}{L_{12}}\right)^2 \left(u_{T_1}^2 + u_{T_2}^2\right) + \left(\lambda \frac{T_2 - T_1}{L_{12}^2}\right)^2 \left(u_{L_1}^2 + u_{L_2}^2\right)} \tag{4}$$

$$u_{T_\mathrm{w}} = \sqrt{\left(\frac{T_2 - T_1}{L_{12}^2} L_2 - \frac{T_2 - T_1}{L_{12}}\right)^2 u_{L_2}^2 + \left(\frac{T_2 - T_1}{L_{12}^2} L_2\right)^2 u_{L_1}^2 + \left(1 - \frac{L_2}{L_{12}}\right)^2 u_{T_2}^2 + \left(\frac{L_2}{L_{12}}\right)^2 u_{T_1}^2} \tag{5}$$

$$u_\alpha = \sqrt{\left(\frac{1}{T_\mathrm{w} - T_\mathrm{L}}\right)^2 u_q^2 + \left(\frac{q}{(T_\mathrm{w} - T_\mathrm{L})^2}\right)^2 \left(u_{T_\mathrm{w}}^2 + u_{T_\mathrm{L}}^2\right)} \tag{6}$$

where uncertainties u_{T1} and u_{T2} correspond to the average temperature in the upper and lower line of TCs, respectively, and are equal to

$$u_{T_1} = u_{T_2} = u_T/\sqrt{3} \tag{7}$$

Uncertainty of liquid temperature $u_{TL} = u_T$. Symbol L_2 denotes the length between the heating surface and the bottom thermocouple line $L_2 = L_{12} + L_1$. Uncertainties of lengths L_1 and L_2 are equal, i.e., $u_{L1} = u_{L2} = u_L$.

Figure 2 shows resulting relative uncertainties of HTC and its constituents. For very low heat fluxes from 0 to approximately 33 kW m^{-2}, relative uncertainty of α quickly drops to 20%, which is considered to be an acceptable value. For heat fluxes from 33 kW m^{-2} up to 1.3 MW m^{-2}, the uncertainty stays below 20%. In this region, relative uncertainty of heat flux q remains at a constant value of approximately 15% which is caused mainly by the assumed deviation of thermal conductivity λ. Gradual increase of HTC uncertainty is mainly due to rising uncertainty of superheat ($T_w - T_L$) and additionally by increasing uncertainty of extrapolated wall temperature T_w. In region above 1.3 MW m^{-2}, gradual increase of HTC uncertainty continues.

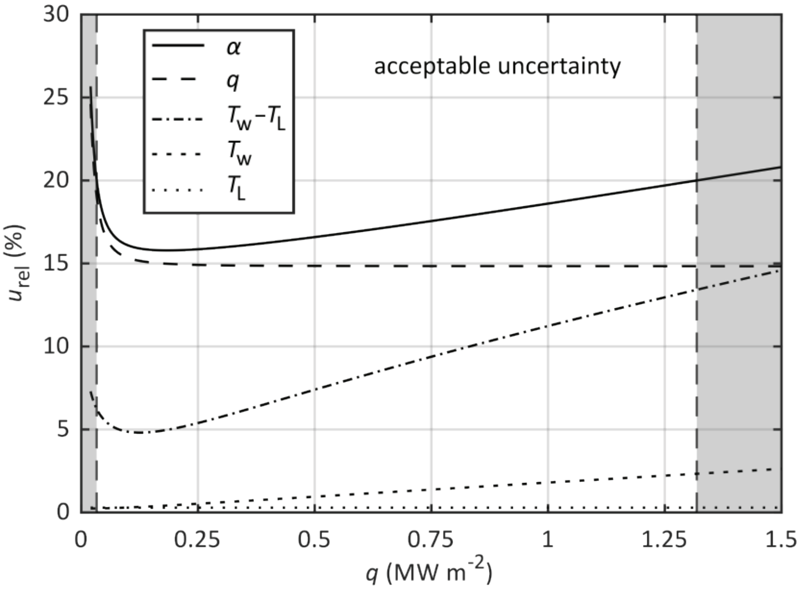

Figure 2. Relative uncertainties of heat transfer coefficient α and its constituents.

Region of acceptable uncertainty from 33 kW m^{-2} to 1.3 MW m^{-2} is much wider than heat flux ranges which we typically study. For instance, during experiments with water–glycerin mixtures[3], we investigated heat fluxes only up to 270 kW m^{-2}. According to Zuber correlation[4], critical heat flux of boiling of water at atmospheric pressure is of about 1.17 MW m^{-2}, which means that the HTC uncertainty would remain acceptable for the entire range of nucleate pool boiling regime.

Next step of our analysis is to evaluate the error caused by the assumption of constant value of thermal conductivity λ independent of temperature. Može et al.[1] obtained temperature dependency of thermal conductivity from laser-flash measurements of thermal diffusivity of copper. They published equation

$$\lambda(T) = 2.83 \times 10^{-4}\, T^2 - 0.165\, T + 378.1 \qquad (8)$$

where T is in (°C). According to Equation (8), thermal conductivity of copper at 20 °C is 375 W m^{-1} K^{-1}. Equation (8) was employed into our calculations. Following iterative algorithm was applied to calculate temperature distribution inside the heated block considering dependency of λ on temperature:

1. Calculate HTC using Rohsenow correlation[2] for investigated heat flux.
2. Calculate wall temperature T_w using Equation (3).
3. Make an initial estimate that average thermal conductivity inside the copper block equals to λ(20°C) = 375 W m^{-1} K^{-1}.
4. Calculate temperatures T_1 and T_2 using Fourier's law of conduction and using the corresponding average thermal conductivities.
5. Calculate average temperatures inside the copper block between the upper line of thermocouples and the heating surface $T_{avg1} = (T_w + T_1) / 2$ and between the bottom line and the heating surface $T_{avg2} = (T_w + T_2) / 2$.
6. Calculate average thermal conductivities between the upper line and the heating surface $\lambda(T_{avg1})$ and between the bottom line and the heating surface $\lambda(T_{avg2})$.
7. Repeat steps 4–6 until the difference between latest and previously calculated values becomes negligible.

Finally, temperatures T_1 and T_2 determined with the algorithm were used to calculate heat flux q, see Equation (1), using a constant value of thermal conductivity $\lambda = 375$ W m^{-1} K^{-1} which corresponds to 20 °C.
Figure 3 shows the difference between Rohsenow correlation and between “as-measured” values of HTCs which were obtained assuming the constant value of thermal conductivity. Neglecting dependency of λ on temperature leads to lower values of “as-measured” HTCs compared with actual HTCs represented by the correlation of Rohsenow. The difference between both values slightly increases for higher heat fluxes.
Figure 4 shows the heat flux dependency of relative difference

$$\delta_\alpha = |\alpha_{\lambda=\text{const.}} - \alpha_{\text{Roh}}| \,/\, \alpha_{\text{Roh}} \tag{9}$$

where $\alpha_{\lambda=\text{const.}}$ stands for HTCs obtained with the assumption of constant thermal conductivity and α_{Roh} are HTCs obtained with Rohsenow correlation. Although relative difference δ_α gets higher with increasing heat flux, it remains below 3.5% for all investigated heat fluxes. Since the obtained differences are significantly lower than the measurement uncertainties, compare with Figure 2, the effect of thermal dependency of thermal conductivity on pool-boiling HTC measurement is considered to be negligible.

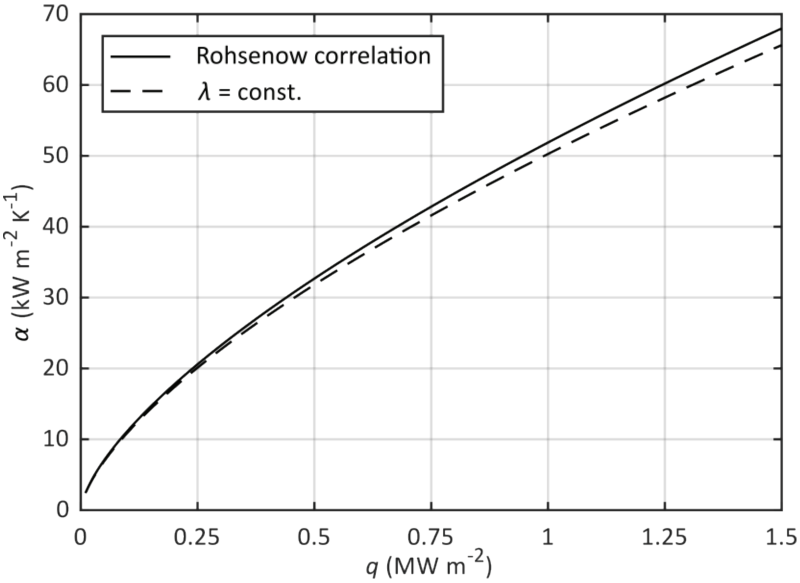

Figure 3. Difference between Rohsenow correlation and “as-measured” HTCs which were obtained assuming a constant value of thermal conductivity λ at 20 °C.

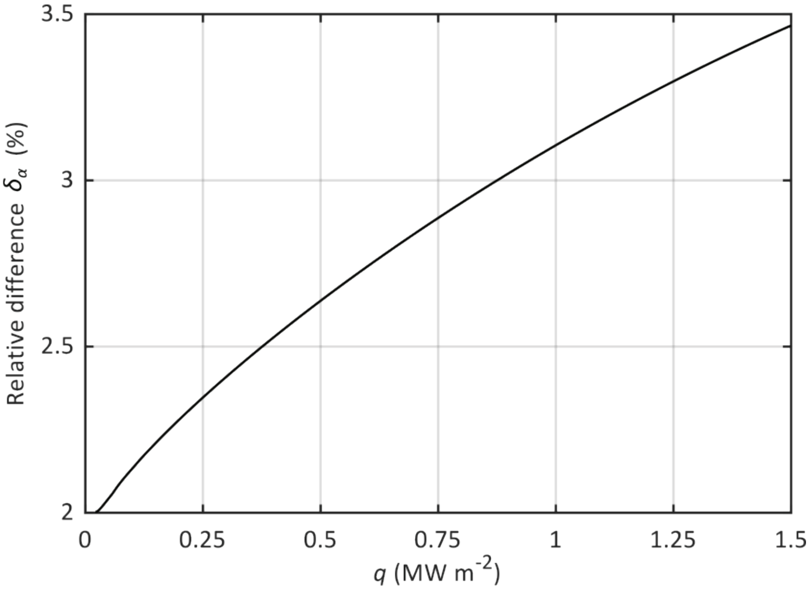

Figure 4. Relative difference, defined by Equation (9), between “as-measured” HTCs and Rohsenow correlation.

Conclusions

Effect of thermal conductivity on nucleate pool boiling heat transfer measurements was studied for a given experimental apparatus. It was found out that uncertainties of measured HTCs are acceptable even for significant uncertainties of thermal conductivity. Higher uncertainties of HTC calculated for more intense heat fluxes are caused by increasing uncertainties of superheat and wall temperature.

Differences were analyzed between HTCs correlated with a verified heat transfer correlation and HTCs which would have been obtained under the assumption of constant thermal conductivity. Differences lower than 3.5% were obtained for a wide range of investigated heat flux from 0 to 1.5 MW m^{-2}. Assumption of constant thermal conductivity is therefore considered to be appropriate for pool boiling heat transfer measurements.

Acknowledgements

This work was supported by the Ministry of Education, Youth and Sports of the Czech Republic under OP RDE grant number CZ.02.1.01/0.0/0.0/16_019/0000753 "Research centre for low-carbon energy technologies" and by the Grant Agency of the Czech Technical University in Prague, grant number SGS20/119/OHK2/2T/12 "Transport Phenomena in Multiphase Systems".

Nomenclature

L	length (m)
q	heat flux (W m^{-2})
T	temperature (°C)
u	uncertainty
U	deviation
α	heat transfer coefficient (W m^{-2} K^{-1})
δ	relative difference (–)
λ	thermal conductivity (W m^{-1} K^{-1})

subscripts:

avg	average
i	ordinal index
L	liquid
rel	relative
Roh	Rohsenow
w	boiling surface (wall)

References

1. Može M., Zupančič M., Golobič I.: Appl. Therm. Eng. *169* (2020).
2. Rohsenow W.M. *A Method of Correlating Heat Transfer Data for Surface Boiling of Liquids*, Tech. Rep., Division of Industrial Cooperation, Heat Tnrasfer Laboratory, Cambridge, MA, USA (1952).
3. Vajc V., Šulc R., Dostál M.: Processes. *9*, 830 (2021).
4. Zuber N., *Hydrodynamic Aspects of Boiling Heat Transfer*, California University and Ramo-Wooldridge Corp., Los Angeles, CA, USA, 1959.

INORGANIC TECHNOLOGY

USE OF THE MSO TECHNOLOGY FOR THE TETRACHLORETHYLENE DISPOSAL

Galek V.[1], Černá A.[1], Pražák P.[1], Hadrava J.[1], Mastný L.[2]

[1]*Research Centre Rez, Husinec-Řež 130, 250 68 Řež, Czech Republic*
[2]*University of Chemistry and Technology, Prague, Technická 5, 166 28 Prague 6 – Dejvice, Czech Republic*
Vojtech.galek@cvrez.cz

Abstract

Currently the use of organic chlorinated substances is constantly increasing and their disposal by conventional methods requires a demanding flue gas cleaning system. Molten Salt Oxidation (MSO) technology is a technology that uses flameless oxidation below the surface of the molten salt. The acidic off-gases are trapped in the molten alkali carbonates with which they react to form respective compounds and thus this system does not require a complex flue gas cleaning. Five experiments were performed on two reactor MSO laboratory apparatus. Pure Na_2CO_3 was used as the alkaline salt in both reactors. The set temperature on both furnaces was 1050 °C. The experiments differed in the amount of C_2Cl_4 dosed and the organic waste dosing rate. The oxidizing air flow was $4.5\ l \cdot min^{-1}$ and was fed to the first reactor. During the experiments, the temperature profile in each reactor was measured, flue gas analysis was performed and at the end of the experiment, samples of the molten salt were taken to determine the content of chlorides. Chlorides were determined by argentometric titration. The efficiency of C_2Cl_4 oxidation was monitored by determining the CO content in the off gases. The whole process was optimized during the experiments and thus the efficiency improved. The formed Cl_2 was captured primarily in the first reactor, where the capture efficiency was around 70%.

Introduction

Every year, more and more hazardous waste is generated in the world. Chlorinated organic solvents, which are widely used in the chemical industry, are one of these hazardous wastes. They are mainly used for heat transfer, as lubricants or for cleaning other organic impurities. The increasing use of these substances leads to a burden on the environment and it is necessary to dispose of these substances effectively. Normally, this waste is disposed of in incinerators, however, this leads to high demands on flue gas cleaning to achieve low emissions of chlorinated substances. Another disadvantage is the faster wear of the metal parts of the reactors. Upon the formation of gaseous Cl_2 or other halogens, reactions with the furnace lining can occur to form halides that are more volatile. (1.2)

To prevent the formation of gaseous halogens, it is necessary to use other methods of disposal. Molten Salt Oxidation (MSO) technology is an alternative to conventional methods. It is a flameless process using high temperatures and alkali salts in molten form. During the process, the waste is dosed together with the oxidizing medium below the surface of the molten salt, where a flameless oxidation takes place. During the disposal of chlorinated waste, a reaction takes place between the halogens and the molten salt to form halides, which are trapped in the molten salt, thus reducing the volume of emissions of chlorinated substances. (2) Other non-combustible inorganic substances, i.e. heavy metals or possibly radionuclides, are trapped in the molten salt and can be easily separated. Capture of Cl_2 gas takes place by a neutralization reaction according to equation (1):

$$C_2Cl_4 + 2Na_2CO_3 + O_2 \rightarrow 4NaCl + 4CO_2 \qquad (1)$$

The MSO process has several advantages over combustion. The operating temperature depends on the used alkali salts, but it is generally lower than in direct combustion. Alkaline carbonates and mixtures thereof have melting points of 400 to 950 °C. The alkaline molten salt also acts as a scrubber for other acidic substances and therefore eliminating the need to use flue gas cleaning system. The molten salt has the function of a stable heat transfer medium which resists thermal shocks and is thus able to maintain rapid process fluctuations. This technology is then also suitable for the disposal of explosive materials, detonators, or other energetic materials. (1,2,3,4)

Despite many advantages the MSO technology has its drawbacks. One of the main disadvantages is the increased economic cost when compared to combustion processes. Another disadvantage is the high corrosivity of the environment. Construction materials do not have a long service life if they are in contact with the molten salts at high temperatures and in an oxidizing environment. (5.6)

Experiment

The experiments were performed on a laboratory apparatus shown on FIG.1, which consisted of several parts. A peristaltic pump with a tank was used to dispense the waste. Tetrachlorethylene was dosed into the injector section, where it was mixed with oxidizing air from a pressure bottle. Through the injector part, the mixture of waste and air was led to the first reactor, which consists of a furnace, a reactor vessel, and a stainless-steel crucible with molten salt. A 2200 g of pure Na_2CO_3 salt was used in the first reactor. The batch in both reactors was used for five experiments. The mixture of the waste and air was passed through an injector below the surface of the molten salt to the bottom of the crucible to ensure the longest possible reaction time between the waste and the molten salt. The C_2Cl4 and Cl_2 were captured during the oxidation process in the form of NaCl. The flue gases from the first reactors were then led to the second reactor, again below the surface level of the molten salt. The second batch of the Na_2CO_3 salt with the same weight as in the first reactor was used in the second reactor. From the second reactor, the flue gases passed into the active air conditioning system through a bubbler with Na_2CO_3 solution for a possible capture of free Cl_2. The concentration of the solution was always 130 $g{\cdot}l^{-1}$. The analysis of the off-gas composition was performed continuously with a portable Testo 350 analyser. A sample of molten salt was taken from each reactor after every experiment. The samples were weighed and dissolved in 100 ml of 20 wt.% HNO_3. The chloride concentration was determined by argentometric titration and then the Cl_2 capture efficiency was calculated.

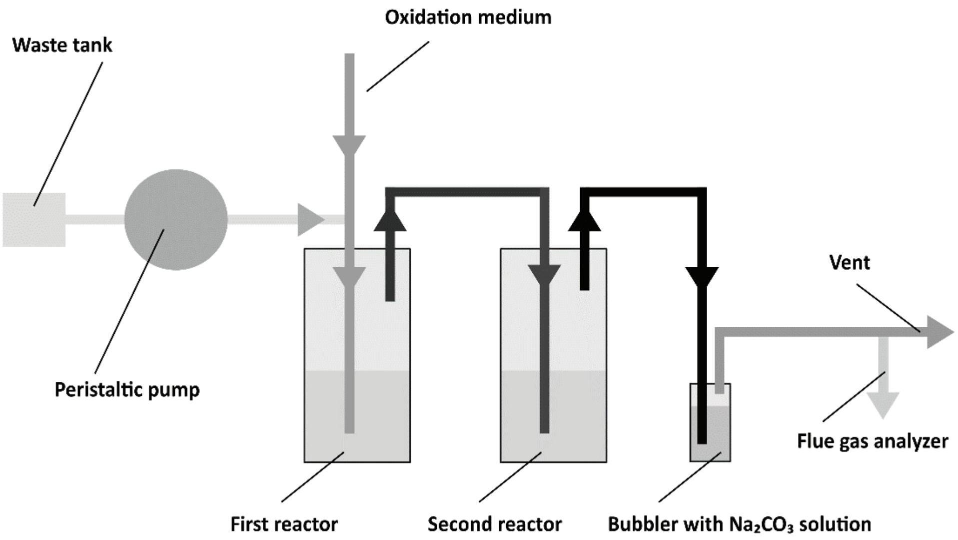

Figure 1. Laboratory apparatus.

The individual experiments were performed at the same temperature 1050 °C in both reactors. The molten salt temperature was continuously measured by thermocouples, which were located at the bottom of the reactor insert, in halfway up the insert and at the reactor lid. The high temperature was set with respect to the problems associated with heating the molten salt. Since the molten salt was placed in the reactor crucible, the measured molten salt temperature at the bottom of the insert was about 100 °C lower than the set temperature. The oxidizing air was led to the first reactor and the same flow rate was set in all experiments at 4.5 $l{\cdot}min^{-1}$. This value was set with respect to the design of the reactor liner to avoid the formation of large bubbles and possible molten salt spray into the reactor vessel itself. The dosing amount of C_2Cl_4 in each experiment is shown in Table I. The reason why the dosing amount differed in the first experiment was to use a new peristaltic pump.

Table I The dosing amount of C2Cl4 in each experiment

Experiment	Set Temperature [°C]	Air flow[$l \cdot min^{-1}$]	Amount of C_2Cl_4 dosed [g]
1	1050	4.5	158.19
2			91.40
3			108.22
4			105.95
5			94.31

Results

The aim of the experiments was to eliminate the organic solvent C_2Cl_4 and at the same time to capture as much of the released Cl_2 as possible in the solid chloride form so that the emissions of gaseous Cl_2 were as low as possible. A total of five experiments on the two-reactor apparatus were performed. In all experiments, air was fed only to the first reactor and the air flow rate did not change. The temperature was set at 1050 °C for all experiments. The experiments differed in the amount of dosed waste. The flue gases composition was analysed to control combustion process. The efficiency of trapping gaseous Cl_2 in solid form in each part of the apparatus is shown on FIG. 2.

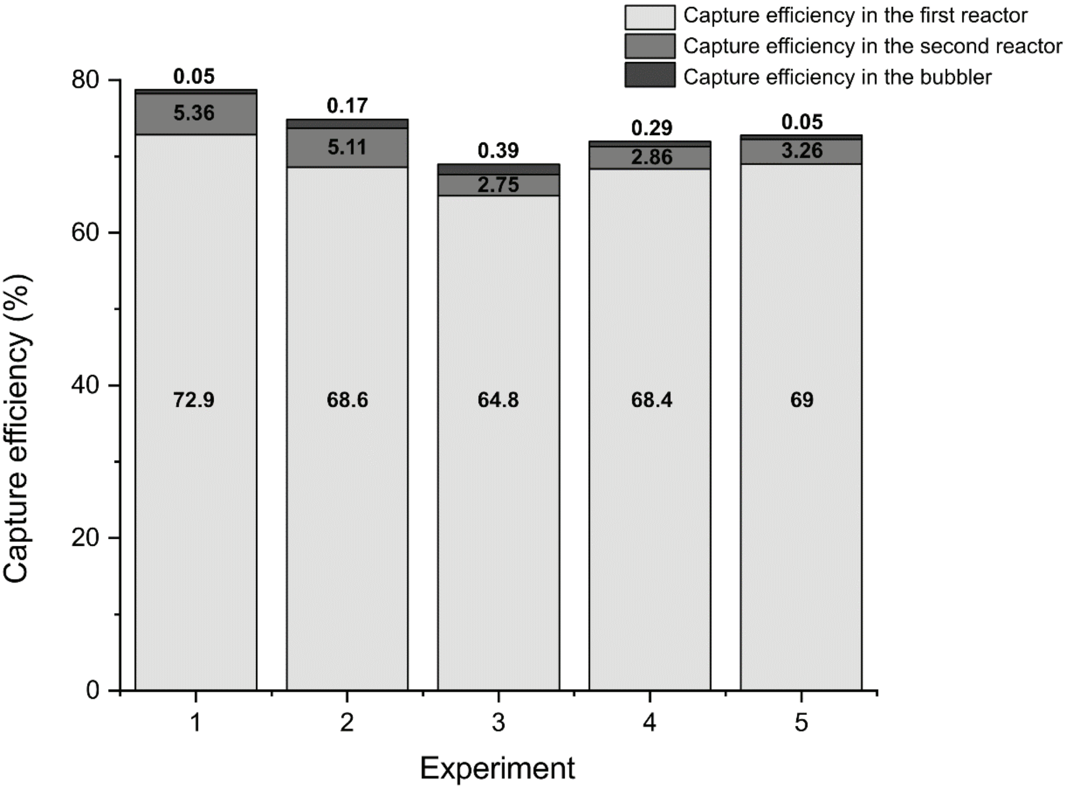

Figure 2. The Cl_2 gas capture efficiency in individual parts of the apparatus.

The total Cl_2 capture into the solid form in the system was approximately 70 %. The capture efficiency was highest in the first reactor, where it ranged from 65 to 73%. The capture efficiency decreased slightly with further experiments. The second reactor served mainly as a safeguard to capture unreacted Cl_2 leaks from the first reactor. The capture there ranged from 2.7% to 5.4%. A bubbler with Na_2CO_3 solution was placed behind the second reactor as a final purification of the flue gassed before entering the ventilation. The analysis shown very small capture of Cl_2 into the Cl^-form in the bubbler.

Lower capture in the molten salt can be caused by several factors. One of the reasons why the capture is not corresponding to equation (1) is the short retention of waste in the molten salt, which may be due to the size of the air bubbles exiting the injector system. The size of the bubbles and their size reduction can be affected by the addition of a stainless-steel sifter to the mouth of the injector system. Another possibility of low capture is the formation of other chlorinated hydrocarbons, which were not trapped in the molten salt and therefore did not have the possibility to react. These alternatives and their possible solutions will be further explored in future experiments.

Conclusions

A total of five C_2Cl_4 combustion experiments in an alkaline molten Na_2CO_3 were performed on two reactor MSO apparatus at the set temperature of 1050 °C. After each experiment, a cooled molten salt sample was taken from each reactor and was subsequently dissolved in HNO_3. The chloride concentration in every sample was determined by argentometric titration.

The efficiency of capturing gaseous Cl_2 into the solid form of NaCl was on average 70%. Compared to data obtained from the literature, the capture efficiency should be approximately 90%. The values obtained by us are lower, however, the efficiency is higher than average. Overall, the results are satisfactory as on the scaled-up pilot plant there are not such high demands on the flue gas cleaning system. Capture can be affected by process parameters such as short retention in the molten salt or a possible decomposition of the waste into other chlorinated hydrocarbons. These options will be further research.

Acknowledgement

This work was supported by TA ČR č. TN01000007 within the National Centre of Competence program - 1. VS.

References

1. Lin, C., Chi, Y., Jin, Y., Jiang, X., Buekens, A., Zhang, Q., & Chen, J. (2018). Molten salt oxidation of organic hazardous waste with high salt content. https://doi.org/10.1177/0734242X17748364
2. Yang, H., Cho, Y., Eun, H., & Kim, E. (2019). Destruction of chlorinated organic solvents in a two-stage molten salt oxidation reactor system, (September 2007). https://doi.org/10.1016/j.ces.2007.01.055
3. Flandinet, L., Tedjar, F., Ghetta, V., & Fouletier, J. (2012). Metals recovering from waste printed circuit boards (WPCBs) using molten salts. Journal of Hazardous Materials, 213–214, 485–490. https://doi.org/10.1016/j.jhazmat.2012.02.037
4. Yao, Z., Li, J., & Zhao, X. (2011). Molten salt oxidation: A versatile and promising technology for the destruction of organic-containing wastes. Chemosphere, 84(9), 1167–1174. https://doi.org/10.1016/j.chemosphere.2011.05.061
5. Volkovich, V. A., Gri, T. R., Fields, M., & Fray, D. J. (1998). Oxidation of ceramic uranium dioxide in alkali metal carbonate-based melts : a study using various oxidants and comparison with UO2 powder. Journal of Nuclear Materials, 256(0022), 131–138.
6. Yang, H., Cho, Y., Eun, H., & Kim, E. (2008). Destruction of chlorobenzene and carbon tetrachloride in a two-stage molten salt oxidation reactor system, 73. https://doi.org/10.1016/j.chemosphere.2008.03.045

GEOPOLYMERS: THE INFLUENCE OF ALKALINE ACTIVATOR CATIONS ON EFFLORESCENCE

Novotná M.[1,2], Polonská A.[1], Šídlová M.[1], Perná I.[2]

[1]*Department of Glass and Ceramics, University of Chemistry and Technology Prague, Technická 5, 166 28, Prague 6*
[2]*Department of Material Structure and Properties, Institute of Rock Structure and Mechanics, Czech Academy of Sciences, V Holešovičkách 41, 182 09, Prague 8*
novotna@irsm.cas.cz

Abstract

This paper describes the effect of the type of cations in the alkaline activator on geopolymer properties and especially on the formation of efflorescence. The susceptibility to the formation of efflorescence is discussed according to the standard ČSN 72 1565-13. Cations in alkaline activators influence the mineralogical type of efflorescence: Li^+ and Na^+ cations form carbonates (Li_2CO_3 and Na_2CO_3, respectively), whereas K^+ cations form sulphate (K_2SO_4). The mechanical properties, workability and pore structure of the geopolymer composites have been determined. Alkaline activators with sodium and potassium ions reach higher mechanical strength than those containing lithium cations. For lithium alkaline activators, there was a noticeable difference in the properties between the SiO_2/Li_2O ratios 1.8 and 2.6. Based on the properties of the mentioned geopolymer composites with various alkaline cations, it is possible to use lithium alkaline activators in geopolymer technology.

Introduction

Due to the efforts of the European Union to reduce emissions (European Green Deal)[1], geopolymer (GP) materials appear to be an advantageous substitute for concrete in some areas of usage. It is stated that the production of ordinary Portland cement (OPC) is responsible for 7–10% of the total CO_2 emissions.[2] The production of GPs thus becomes slightly more advantageous than the production of OPC, although metakaolin is the main raw material for the production.[3] Fortunately, metakaolin can be partially replaced by waste materials with pozzolanic properties, including fly ash or slag,[4,5] and various types of waste or otherwise unsuitable materials, both natural (beach sand, stone dust, etc.) and synthetic (plastic, tyres, fibrous materials, etc.), can be used as fillers.[6,7]

The use of these waste materials affects the properties of GPs. In general, however, GPs are highly heat-resistant and insoluble in water, they can inhibit hazardous materials, and they achieve high strength.[4,8] GPs excel in these properties because of their amorphous polymeric structure, which comprises the bond -Si-O-Al-O-. This structure is formed by the reaction of aluminosilicates with alkaline activators. The aluminium cation is in tetrahedral coordination and the negative charge of this tetrahedron is compensated for by alkali-metal or alkaline-earth cations (Li^+, Na^+, K^+, Ca^{2+}).[8,9,10]

On the contrary, if these cations are not tightly bound in the GP structure, there is a risk of efflorescence, i.e. of their diffusion to the surface and reaction with the surrounding environment to form predominantly white salts.[11,12] Figure 1 illustrates the formation of efflorescence. Not only is the efflorescence unaesthetic, but it can also have a negative impact on the structure and properties of materials.[13]

Therefore, our aims are to examine the effect of efflorescence on geopolymer materials thoroughly and to compare the efflorescence with different cations in alkaline solutions $M^+ = (Li^+, Na^+, K^+)$. The results would contribute to the possible use of geopolymers in common practice. For GP materials, the workability, mechanical properties and pore structure were further compared.

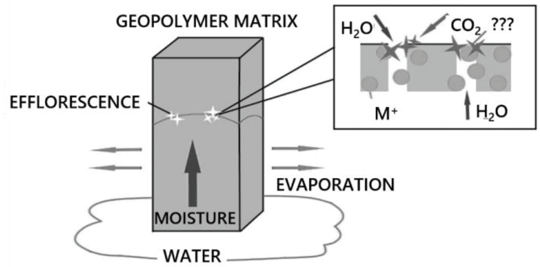

Figure 1. An illustration of the formation of efflorescence.

Experiment

Materials

A metakaolinite-based aluminosilicate has been used as the precursor and chamotte grit as a filler. Both materials are produced by the ČLUZ a. s. (Nové Strašecí, Czech Republic). Activators differ in the type of cations (Li^+, Na^+, K^+) and in the SiO_2/M_2O ratio. Lithium silicates with the molar ratio SiO_2/Li_2O = 1.8 and 2.6 (Li 1.8, Li 2.6) have been supplied by Vodní sklo a. s. (Prague, Czech Republic). Sodium silicate with the molar ratio SiO_2/Na_2O = 1.9 (Na 1.9) and potassium silicate with the molar ratio SiO_2/K_2O = 1.7 (K 1.7) have been supplied by ČLUZ a. s. (Nové Strašecí, Czech Republic). The properties are guaranteed by the producers.

The Preparation of Geopolymers

Geopolymer materials were prepared by a standard procedure according to Table I. The clay precursor was mixed with an alkaline activator for 5 minutes, after which a chamotte filler was added and mixed for another 5 minutes. The mixture was homogenised on a vibrating table and poured into moulds (160 x 20 x 20 mm). The samples were covered with plastic sheets for 7 days. Subsequently, they were demoulded and left in the air at ambient temperature. The prepared and dried samples were used for other measurements and analyses.

Table I
Mix design of geopolymers

Mix designation	Content [g]			SiO_2/Al_2O_3	M_2O/Al_2O_3	H_2O/M_2O	Filling [%]	Water/ Solid
	Si-Al MK	activator	Chamotte					
Na 1.9	100.0	80.0	180.0	3.7	0.6	18.5	58.5	0.2
K 1.7	100.0	90.0	190.0	3.7	0.6	19.2	59.0	0.2
Li 1.8	100.0	80.0	180.0	3.3	0.4	34.8	61.2	0.2
Li 2.6	100.0	80.0	180.0	3.5	0.4	34.1	60.4	0.2

Analyses

The mineralogical composition was measured by the X-ray powder diffraction method (XRD) on a Bruker AXS D8 θ-θ diffractometer (Karlsruhe, Germany) with parafocusing Bragg–Brentano geometry using CoKα radiation (λ = 1.79028 Å, U = 34 kV, I = 20 or 30 mA).

A Spectro IQ analyzer (Kleve, Germany) was used for the analysis of chemical composition by the X-ray fluorescence method (XRF). A milled sample was homogenised with a binding additive and was pressed to a pellet. The pellets were measured in the helium atmosphere with energy ranges of 50.0 and 25.0 keV.

Particle-size distribution was analysed by CILAS 920L (Ariane Group, France). The samples were measured in water suspension by laser-beam reflection and then recalculated.

Mechanical properties were performed according to the standard ČSN EN 12390-312. VEB Thüringer (Industriewerk Rauenstein, Schalkau, Germany) has the following ranges of measurements: 0–2 kN, 0–4 kN, 0–10 kN, 0–20 kN, 0–40 kN and 0–100 kN. Samples of a size of 160 x 20 x 20 mm were measured after 28, 90, 180 and 365 days. On average, the measurements included three samples for flexural strength and six for compressive strength.

Vicat setting times (Matest S. p. A, Treviolo, Italy) for fresh mixtures were tested according to UNI EN 196-3 at laboratory temperature (21 ± 1°C) and relative humidity (35 ± 2%). During the measurement, the samples were covered with a plastic foil.

The susceptibility to the formation of efflorescence was determined according to the standard ČSN 72 1565-13. Specimens were immersed in demineralised water to a height of 1 cm for 7 days and 28 days. Subsequently, they were dried and evaluated, and efflorescence was characterised by the XRD method to identify the mineralogical composition.

Mercury intrusion porosimetry (MIP) was used for the analysis of small fragments and their pore diameter and porosity (Autopore 9500, Micromeritics, USA).

Results and Discussion

The Analyses of Raw Materials

The clay precursor and chamotte filler have been studied by XRF (Table II) and XRD methods. The XRF chemical analysis has shown that both materials are aluminium silicates with a higher content of silica. Interestingly enough, chamotte has a low loss on ignition (0.02 wt. %, see the table) because the raw material is burnt during its production. This corresponds to data from XRD, which show that the major phase in chamotte is mullite. Other phases are two modifications of SiO_2 (quartz and cristobalite). Rutile, anatase and hematite are contained in trace amounts.

The precursor is based on clay pozzolanic materials. The results, as shown in Table II, indicate that the precursor contains a bigger amount of CaO (17.31 wt. %) and MgO (2.96 wt. %). It has a small amount of SO_3 (0.76 wt. %) and Fe_2O_3 (0.73 wt. %) and 2.71 wt. % of loss on ignition (LOI). The XRD indicates that the precursor includes a large amount of amorphous phase (about 80 wt. %) and further crystalline quartz, illite and a minor phase of kaolinite, calcite and mica. Kaolinite remains as a residue after imperfect burning.

Table II
Chemical composition of the raw materials [wt. %]

Sample	Al_2O_3	SiO_2	CaO	Na_2O	K_2O	MgO	Fe_2O_3	SO_3	LOI
precursor	28.68	44.76	17.31	0.11	0.42	2.96	0.73	0.76	2.71
Chamotte	38.65	56.00	0.28	0.11	0.72	0.02	1.86	0.24	0.02

The particle-size distribution shows that the chamotte filler has bigger particles than the precursor. The chamotte filler used has a wide particle-size distribution: D_{10} = 2.62 μm, D_{50} = 24.87 μm and D_{90} = 118.62 μm. The clay precursor has a smaller particle-size distribution: D_{10} = 0.99 μm, D_{50} = 5.29 μm, D_{90} = 17.57 μm. Most of the particles are not bigger than 20 μm. The small particle size (around 2–5 μm) of the clay precursor is necessary for a correct and fast course of the geopolymer reaction.[14]

Workability

Previous works[15,16,17] discussed the influence of the cations used and their size on reactivity and the rate of solidification as well as the preference for the formation of smaller or larger oligomers. To support their suggestions, we performed Vicat setting time. We confirmed that different cation size could affect the chemical reaction and its rate. From the data in Figure 2, the bigger cation, K^+, solidified faster than the smaller cations, Na^+ and Li^+. The most rapidly solidified mixture was K 1.7 (with the initial and final setting time being 1.8/2.1 h, respectively). The next mixture was Na 1.9 with the initial time at 2.3 h and the final time at 3.6 h. The third sample was Li 2.6 (initial: 5.1 h, final: 5.7 h). The hardening time was the longest in the case of Li 1.8, which started to solidify at 69.3 h and was completely hardened after 154.9 h.

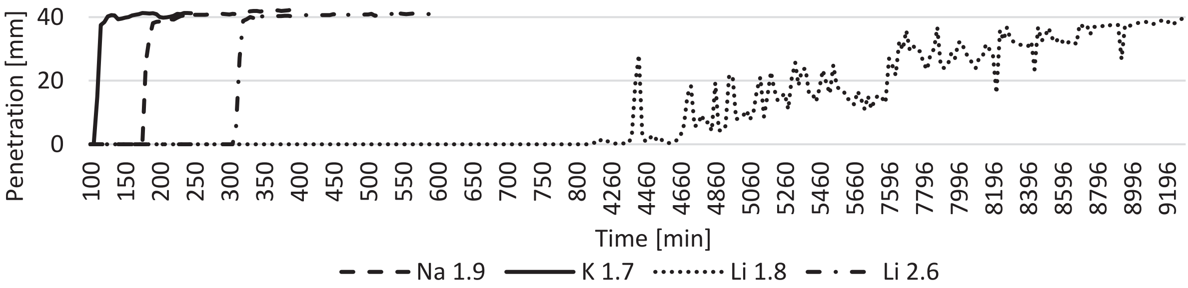

Figure 2. The total solidification time of the geopolymer mixtures.

Mechanical Properties

Flexural and compressive strengths were measured after 28, 90, 180 and 365 days. The results are shown in Figure 3. For Li 2.6, only 28- and 90-day strengths were measured. Nevertheless, it is obvious even from these values that both strengths are lower than those of the sodium- and potassium-cation samples. The highest values of flexural and compressive strengths after 28 days (9.88 and 62.43 MPa, respectively) were observed for Na 1.9 samples. The strengths achieved by the K 1.7 samples after 28 days were lower: the flexural strength of 6.11 MPa and the compressive strength of 48.83 MPa). The specimens with lithium cations had lower strengths than both Na 1.9 and K 1.7. If we compare Li 1.8 and Li 2.6, it is obvious that better flexural and compressive strengths after 28 days were achieved by Li 2.6. The Li 1.8 sample after 28 days had the flexural strength of 1.25 and the compressive strength of 2.82 MPa. The Li 2.6 specimen after 28 days achieved higher flexural and compressive strengths (4.74 and 15.86 MPa, respectively). For these specimens, this strength order was identical after 90, 180 and 365 days.

Therefore, in general, it seems that the reaction of Na^+ cations with smaller oligomers and longer reaction time leads in this case to better bonding of the geopolymer material, which results in higher flexural and compressive strength values. At the same time, there is an effect of the solubility of aluminosilicates: smaller cations (Na^+) attack and better stimulate the dissolution of aluminosilicates, thus enhancing the formation of a better-bonded geopolymer network.[17] On the other hand, lithium cations seem too small, with the compressive strength of the samples not being higher than 15.9 MPa. Unfortunately, there are still many unanswered questions about geopolymer reactions and the effect of lithium silicates.

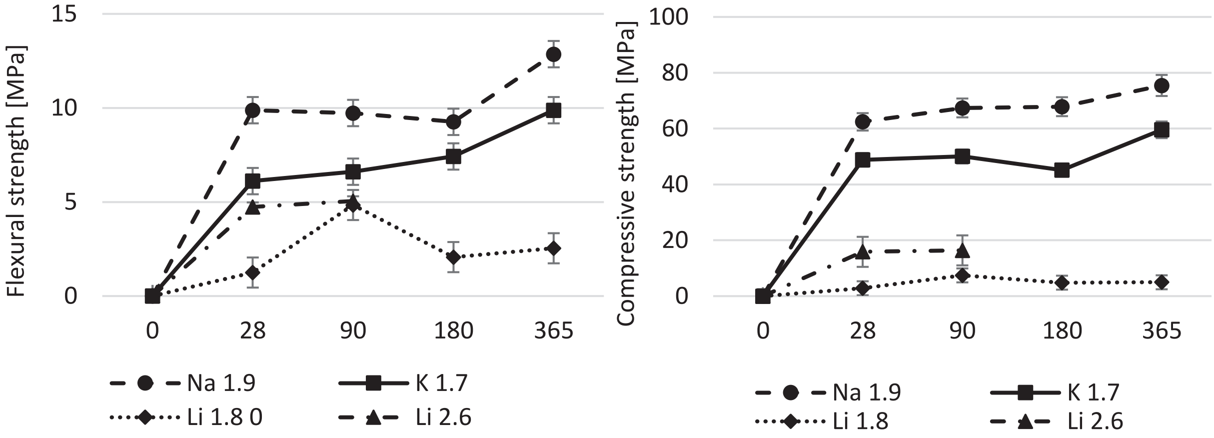

Figure 3. The flexural and compressive strength after 28, 90, 180 and 365 days.

Pore Structure

The pore diameter and porosity are depicted in Figure 4 and Table III, respectively. Based on Figure 4, the pore diameter was in the range of 0.001–1 µm. According to the mechanical-strength (Figure 3) and pore-diameter (Figure 4) tests, the Na 1.9 and K 1.7 geopolymer samples with more pores in the range of 0.001–0.01 µm had higher compressive and flexural strength. The structural stability and mechanical strength of geopolymers were influenced by the pore diameter. The Li 1.8 and Li 2.6 samples had the largest pore-diameter distribution (0.1–1 µm and 0.01–0.1 µm, respectively), which agreed with the lower flexural and compressive strength in Figure 3.

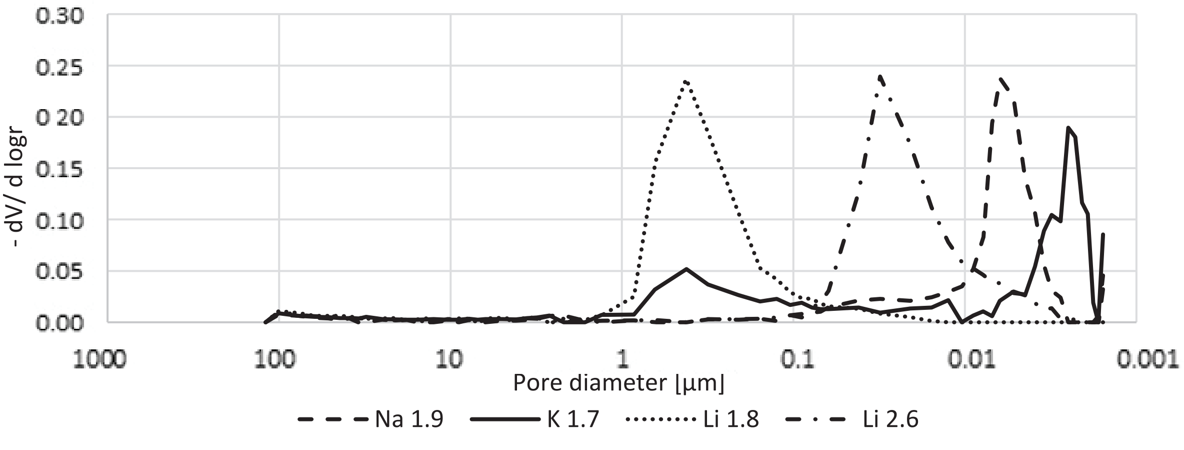

Figure 4. The pore diameter measured by mercury porosimetry.

The results of the porosity are shown in Table III. Na 1.9 and K 1.7 have lower total porosity than samples with lithium cations. The total porosity is 18.83 % for Na 1.9 and 19.33 % for K 1.7. The samples with lithium cations had almost identical porosity, namely 25.46 % for Li 1.8 and 25.45 % for Li 2.6.

Table III
Porosity results measured by mercury porosimetry

	Na 1.9	K 1.7	Li 1.8	Li 2.6
Porosity [%]	18.83	19.33	25.46	25.45

Efflorescence

The determination of visible efflorescence is shown in Table IV. The intensity, colour and location of efflorescence were assessed after 7 and 28 days in distilled water. After 7 days, efflorescence was not visible in the cases of Na 1.9 and Li 2.6, whereas the K 1.7 sample had weak, white efflorescence on the surface and the edge and Li 1.8 exhibited white and yellow efflorescence of medium intensity.

After 28 days, weak efflorescence appeared in the case of Na 1.9 and was visible only on the surface. For K 1.7 and Li 1.8, efflorescence remained the same. The Li 2.6 sample did not achieve any visible efflorescence even after those 28 days. An important role in this case was played by the pore diameter, which influenced the efflorescence. The Li 1.8 had the largest pore diameter (0.1–1 µm) and simultaneously the medium intensity of efflorescence. In comparison, the Li 2.6 had a smaller pore diameter (0.01–0.1 µm) and, as already mentioned above, no efflorescence.

Table IV
Determination of visible efflorescence after 7 and 28 days in distilled water

Sample	After 7 days in distilled water			After 28 days in distilled water		
	Intensity*	Colour	Location**	Intensity*	Colour	Location**
Na 1.9	–	–	–	weak	white	surface
K 1.7	weak	white	surface, edge	weak	white	surface, edge
Li 1.8	medium	white, yellow	surface, edge	medium	white, yellow	surface, edge
Li 2.6	–	–	–	–	–	–

*intensity (none –, weak, medium, large), **location (edge, surface, corner)

The mineralogical composition of efflorescence has been determined using XRD analysis. It has been found that the efflorescence of lithium and sodium cations contains the corresponding carbonate (Li_2CO_3 – zabuyelite, Na_2CO_3 – natrite, respectively). The analysis of the efflorescence of the potassium cation sample K 1.7 has proved the presence of K_2SO_4 (arcanite). The formation of efflorescence is affected by many factors, e.g. the type of cations, permeability, porosity, pH value, redox potential and dissolution.[18]

Figure 5 shows the microscopic images of efflorescence after 28 days in distilled water. The photographs present the differences between particular types of samples. The efflorescence on the Li 2.6 sample was invisible to the naked eye, but it was visible by microscope, which showed small white spots. Other samples (Na 1.9 and K 1.7) had visible fluffy efflorescence. Sample Li 1.8 had a hard crystal structure of efflorescence, coloured white to yellow.

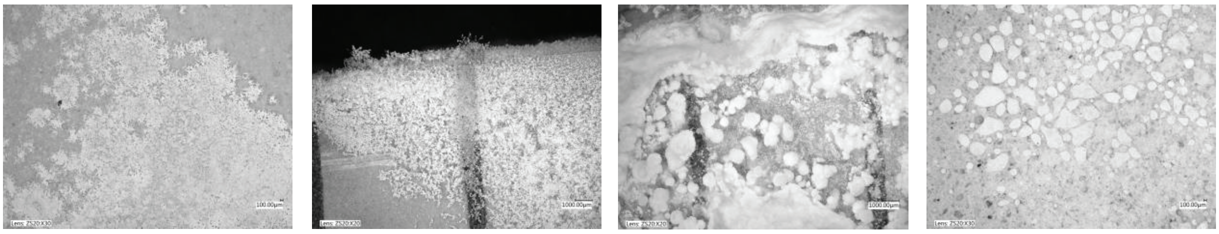

Na 1.9 **K 1.7** **Li 1.8** **Li 2.6**

Figure 5. Microscopic images of efflorescence.

Conclusion

This study has compared three types of cations (Li^+, Na^+ and K^+) in alkaline solution with different SiO_2/M_2O ratios. The experimental results have shown that the samples with lithium ions did not achieve as high compressive and flexural strengths as the samples with sodium and potassium activators. After 28 days, the specimens with Li 1.8, Li 2.6, Na 1.9 and K 1.7 had the flexural strength of 1.25, 4.74, 9.88 and 6.11 MPa and the compressive strength of 2.82, 15.86, 62.43 and 48.83 MPa, respectively. The most rapidly solidified mixture was K 1.7, whereas Li 1.8 required the longest hardening time (with their final setting time being 2.1 h and 154.9 h, respectively). Simultaneously, the specimens with lithium cations had the largest porosity (± 25 %), while the samples with sodium and potassium cations had the porosity of ± 19 %. The results showed an obvious impact of alkaline activator cations on the type and formation of efflorescence. The samples with Li 2.6 do not show the naked-eye-visible efflorescence after 28 days in distilled water. For this reason, it would be appropriate to investigate the influence of cations on geopolymer materials further and to optimise these mixtures to prevent the formation of efflorescence and increase their mechanical resistance. If the efflorescence can be reduced, geopolymer materials could be a suitable OPC replacement in some areas.

Acknowledgement

This work was supported by the grant of Specific University Research – grant No. A1_FCHT_2021_006 and the StrategyAV21, the activity of the Czech Academy of Sciences, the research program VP23 – City as a Laboratory of Change: Historical Heritage and Place for Safe and Quality Life.

References

1. A European Green Deal, available on: https://ec.europa.eu/info/strategy/priorities-2019-2024/european-green-deal_en
2. Miller, S. A., Horvath, A., Monteiro, P. J.: Environ. Res. Lett., 11(7), 074029 (2016).
3. Assi, L. N., Carter, K., Deaver, E., Ziehl, P.: J. Cleaner Prod., 263, 121477 (2020).
4. John, S. K., Nadir, Y., Girija, K.: Constr. Build. Mater., 280, 122443 (2021).
5. Yunsheng, Z., Wei, S., Qianli, C., Lin, C.: J. Hazard. Mater., 143(1-2), 206-213 (2007).
6. Perná, I., Novotná, M., Šupová, M., Hanzlíček, T.: J. Mater. Civ. Eng., 33(4), 04021017 (2021).
7. Novotná, M., Perná, I., Hanzlíček, T.: Waste Forum, 8, 78 (2020).
8. Davidovits J.: Geopolymer Chemistry and Applications. 4th. ed., Institut Géopolymère, Saint-Quentin 2008.
9. Duxson, P., Fernández-Jiménez, A., Provis, J. L., Lukey, G. C., Palomo, A., Van Deventer, J. S.: J. Mater. Sci., 42(9), 2917-2933 (2007).
10. Sazama, P., Bortnovsky, O., Dědeček, J., Tvarůžková, Z., Sobalík, Z.: Catal. Today, 164(1), 92-99 (2011).
11. Lv, X. S., Qin, Y., Lin, Z. X., Tian, Z. K., Cui, X. M.: ACS omega, 5(24), 14822-14830 (2020).
12. Longhi, M. A., Zhang, Z., Rodríguez, E. D., Kirchheim, A. P., Wang, H.: Front. Mater., 6, 89. (2019).
13. Zhang, Z., Provis, J. L., Ma, X., Reid, A., Wang, H.: Cem. Concr. Compos., 92, 165-177 (2018).
14. Hanzlíček, T., Steinerova-Vondrakova, M.: Ceramics-Silikáty, 46(3), 97-103 (2002).
15. Xu, H., Van Deventer, J. S. J.: Int. J. Miner. Process., 59(3), 247-266 (2000).
16. Poulesquen, A., Frizon, F., Lambertin, D.: J. Non-Cryst. Solids, 357(21), 3565-3571. 17 (2011).
17. Okoye, F. N., Durgaprasad, J., Singh, N. B.: Constr. Build. Mater., 98, 685-691 (2015).
18. Gavrunov, A., Mcmillin, T., Mohammed, A. W.: The Green Manufacturing Industrial Consortium (2013).

SUSCHEM

THE ROADMAP OF SUSCHEM CZ IN CONTEXT OF THE NEW EU LEGISLATION

Mlčoch A.[1], **Novák L.[1]**, Šilhan M.[1,2]

[1]Czech technology platform for sustainable chemistry, Rubeška 393/7, 190 00 Praha 9
[2]Research Centre Řež, s.r.o, Hlavní 130, Řež, 250 68 Husinec
ladino@seznam.cz

Abstract

The paper presents the Roadmap of industrial modernisation and implementation of advanced technologies in the chemical industry of the Czech Republic, in context of recent stringent legislative changes and requirements, mainly the European Green Deal (EGD)[1], which is expected to affect a wide range of industries.

Introduction: European Green Deal, expected impacts on chemical and associated industries

Motto: EU GREEN DEAL – green and digital transition

EGD represents a massive and a complex set of over 50 agendas, introduced in December 2019 by the European Commission. EGD goes widely through a wide range of sectors and activities and as a such it will have an effect on EU economy, citizens and public space for several future decades. However, impact studies are lacking, as well as the feedback of that robust agenda package. Generally, its public resonance does not seem to be proper. Ambitions vs. reality in many sectors differ.

EGD is consisting of following strategies, plans and ambitions: Farm-to-Fork Strategy, Biodiversity Strategy, Chemicals Strategy for Sustainability, Renovation Wave EU, Sustainable Finance Agenda, Strategy for Sustainable and Smart Mobility, EU Climate Action &Green Deal, New Circular Economy Action Plan, Europe Fit for the Digital Age, EU Green Deal Initiatives, High Performance Insulation Materials

There are concerns of how much will the implementation of EGD cost and who will pay for it, however, also hopes and challenges for innovative and well performing sectors.

Some relevant areas to the EGD planned story are outlined here, all parts here include chemical industry, which wants to play a significant role.

Energy & Climate

- Couple the higher ambition of the EU 2030 CO2 target with appropriate carbon and investment leakage measures beyond carbon border adjustment mechanisms and without disrupting global trade.
- Remove surcharges/levies for renewable energy electricity for own consumption and generation to enable electrification and shift towards greening chemistry via State Aid rules (EEAG).
- Develop a technology-neutral hydrogen European economy allowing for industrial consumption.
- Support finance for low-carbon process innovations and CO2 abatement technologies.
- Develop a positive approach to Sustainable Finance by providing incentives for all sectors to transform
- Continue to strive for an effective, robust and equitable global CO2 price

Plastics & Circular Economy

- To base product policy on life-cycle thinking and take existing portfolio sustainability assessment schemes into account
- Encourage the use of sustainable, alternative feedstocks in efficient chemical production by supporting the mass balance approach
- Unlock the potential of the bioeconomy by supporting collection, harvest, storage and transport of renewable raw materials
- Consider environmental trade-offs when looking at recyclable packaging
- Ensure that recycling approaches are complementary and technology-neutral to incentivize high-quality mechanical, organic and chemical recycling and higher recycling quotas, also by supporting EU-wide end-of-waste criteria
- Enhance regulatory sandboxing to help speed up transformation
- Ensure a stable legal and political framework for electromobility to further increase circularity in an ecological and economically sound manner

Environmental & Chemicals

- Build on principles of REACH[2] as the world's most advanced chemical legislation to improve chemicals management globally based on the risk principle
- Establish sustainability rating considering the application of the chemicals
- Consider "use" conditions as an essential element of chemical safety management based on scientific evidence and the risk principle
- Respect confidential business information as crucial for the competitiveness of the EU chemical industry
- Consider impacts on the entire value chain including downstream industries
- Maintain alignment of global classification and labelling

Sustainable Agriculture

- Develop objective metrics to help set achievable targets and measure progress toward agricultural sustainability
- Develop legislation based on scientific evidence and use of sustainability metrics which are applied in a consistent way across the various policy options
- Analyse trade-offs resulting from proposed policy measures, including ex-ante and ex-post impact assessment of agricultural sustainability, productivity, food security and profitability
- Recognize and encourage the contribution innovation can make toward achieving the objectives of the Farm to Fork Strategy, including seed breeding, chemical and biological crop protection, digital and precision agriculture, and sustainability performance measurement
- Involve and engage the agri-food chain and encourage collaboration among all stakeholders to drive sustainable strategies forward

Construction

- Ensure that the Renovation Wave initiative delivers on its ambition and remains technology and material-neutral and focuses on the building envelope
- Adopt a performance-based, material-neutral and life-cycle approach to the environmental performance of buildings
- Progressively widen the use of Environmental Product Declarations (EPDs) via the Construction Product Regulation
- Maintain and strengthen an efficient single market for construction products, including efficient market surveillance

Megatrends, identified by SUSCHEM CZ

Czech technology platform for sustainable chemistry (SUSCHEM CZ) identified following megatrends for chemical industry in the Czech Republic (CR)

- EGD
- Low-carbon economy
- Hydrogen strategy
- Chemicals Strategy for Sustainability Towards a Toxic-Free Environment (COM(2020) 667 final)
- Intelligent specialization
- Circular economy
- Industry 4.0
- Water management

The ability of the CR to influence these megatrends is limited, however, the impact of the megatrends is significant. CR ranks among the most industrialised countries in the world, about 35 % of GNP is industry-based.

Roadmap of SUSCHEM CZ

The Roadmap of industrial modernisation and implementation of advanced technologies in the chemical industry of the Czech Republic ("Roadmap")[3] identifies the needs for creation of a sustainable, innovative and competitive development of the chemical industry and its role for realization of different challenges. The Roadmap includes different visionary elements, research and development requirements beyond the current technology status, barriers to the desired development and pathway for a further interdisciplinary industrial cooperation.

The requirements on chemical industry rise, as the world becomes more and more digital and strives for sustainability. The products complement digitally, linear supply chains become complex economic networks, materials recycling and molecular handling become important. Chemistry 4.0 requires digitalisation development, but also new trade models.

The Roadmap was worked out with accent on future needs of chemical and subsequent industries. The roadmap deals with ideas in industrial chemistry, advanced process technologies, advanced materials, nanotechnology and industrial biotechnologies. The strategy in the roadmap brings up new ideas for cooperation within European research area, but also innovation proposals for small and medium-sized enterprises. The chemical recycling is also an issue of rising importance.

The full version of the roadmap is available on www.suschem.cz.

SUSCHEM CZ outlook for next years

- Finishing the current SUSCHEM IV, the work will involve the update of Strategic Research Agenda, finalizing the Roadmap and linking the final version to the EGD provisions
- Submitting national and international projects,
- Ongoing cooperation with the SUSCHEM EU with a particular focus on commonly initiated and submitted projects mainly in the framework of Horizon EU.
- Participation in the Governmental Council for Strategic Technologies and Products (since 2020) and in stipulating strategic materials (example: Hydrogen Strategy) with a particular focus on all steps linked to the EGD.
- Cooperation with other Czech technology platforms to maintain competitiveness for represented areas
- Cooperation with Association of Chemical Industry of the Czech Republic on „The 2050 Vision of the Chemical Industry in the Czech Republic“ document.

Acknowledgement

This work was supported by Ministry of Industry and Trade No. CZ.01.1.02/0.0/0.0/17_105/0018878/2020/002/POST CZ.01.1.02/0.0/0.0/17_105/0018878

References

1. COMMUNICATION FROM THE COMMISSION TO THE EUROPEAN PARLIAMENT, THE EUROPEAN COUNCIL, THE COUNCIL, THE EUROPEAN ECONOMIC AND SOCIAL COMMITTEE AND THE COMMITTEE OF THE REGIONS , COM (2019) 640 final
2. REGULATION (EC) No 1907/2006 OF THE EUROPEAN PARLIAMENT AND OF THE COUNCIL of 18 December 2006 concerning the Registration, Evaluation, Authorisation and Restriction of Chemicals (REACH), establishing a European Chemicals Agency
3. Mlčoch A., Novák L., Šilhan M.: Chem. Listy 115, 205−211 (2021)